

Geosynthetics 2007

January 16-17, 2007 • Washington, D.C.

ENVIRONMENTAL
CONFERENCE
PROCEEDINGS



SPONSORED BY



SOLMAX

Table of Contents

Environmental Technical Session Papers
Geosynthetics 2007 Conference
January 16-19, 2007
Washington D.C.

Containment/CQA/CQC

- Image Analysis for QC/QA of Geosynthetic Deformation during Wide Width Tensile Testing, Ahmet Aydilek, Assistant Professor of Civil and Environmental Engineering, University of Maryland
- Spark Testing of a Conductive Liner - Liner Vs. Underneath the Weld Flap, Jimmy Youngblood, Product Manager, GSE Lining Technology
- Enhanced Geomembrane CQA Through Proper Application of Geomembrane Leak Location Surveys, Bradford Smith, Associate, Stearns & Wheeler, LLC
- What IAGI Approved Installation Contractor Program Can Do For You, Laurie Honnigford, Managing Director, International Association of Geosynthetic Installers
- Infrared Thermography: A nondestructive technique for assessing geomembrane seam bond strength; Ian D. Peggs, I-corp International, Inc.
- A Contaminant Migration Equivalency Assessment for a Municipal Solid Waste Landfill, Craig Lake, PhD, Dalhousie University

Drainage and Filtration

- Proposed Design Criteria for Geotextile Biofilters, Cevat Yaman, PhD, RT Environmental Services Inc.
- A Strength-Based Design Method for Drainage Geocomposites, Dhani Narejo, PhD, PE Caro Consultants, Inc.
- Measuring the Strand Inclination Angle of Bi-Planar Geonets, Sam Allen, vice president, TRI/Environmental, Inc.

Research

- Secondary Containment Applications: Long Term Behaviour of Geomembranes Exposed to Diesel Fuel, Daniele Cazzuffi, PhD, CESI S.p.A.
- Diffusive Migration of Gas-Phase Volatile Organic Compounds through PVC Geomembranes, Rebecca McWatters, PhD Candidate, GeoEngineering Centre at Queen's University-RMC
- Use of Geosynthetics at The Cleveland Hopkins International Airport Deicing Facility, Chris Athanassopoulos, P.E., CETCO
- Temperature of Secondary Liners In Municipal Solid Waste Landfills, R. Kerry Rowe, Professor/Vice Principal, Research, GeoEngineering Centre at Queen's University-RMC
- Influence of leachate chemical composition on the depletion of antioxidant from HDPE geomembrane, R. Kerry Rowe, PhD, Vice-Principal (Research) and

Professor of Civil Engineering, Queen's University; M.Z. Islam, GeoEngineering Centre at Queen's-RMC

- Influence of Strain Gage Adhesive's Stress-Strain Behavior on PVC Geomembrane Tensile Test, Laura Hannum, Graduate Research Assistant, Lehigh University
- Alternative Gripping Systems for GCL Internal Shear and Interface Friction Testing, John Allen, Director Geosynthetic Interaction Laboratory, TRI/Environmental; Patrick Fox, Department of Civil Engineering & Geodetic Science
- Cyclic Shear Strength of a Needle-Punched GCL, Patrick Fox, PhD, Ohio State University; Christopher Nye, OSU; Jim Olsta, CETCO

Exposed Geomembranes

- Holding Your Liquor - Exposed Synthetic Liners in Wastewater Applications, Jack Hinshelwood, Vice President, Olver Inc.
- Finalizing Exposed Geomembrane Covers for Landfills, Donald Hullings, Research Engineer, Jones Edmunds
- Appropriate Final Cover Design for Optimal Landfill Airspace, Mickey Pollman, Geotechnical Designer, Jones Edmunds and Associates Inc.

Special Applications

- MSW Final Closures Incorporating Structured or Embossed Geomembranes, Ronald Frobel, Owner/Principal, R. K. Frobel & Associates
- Design Method for Utilizing Geosynthetic Clay Liners as Puncture Protection Materials, Dhani Narejo, PhD, PE, Caro Consultants Inc.
- Restoration of Distressed Secondary Monitoring System at A Hazardous Waste Landfill, James J. Parsons, Principal Engineer, NTH Consultants, LTD
- Understanding and Minimizing Uncertainty in Geosynthetic Testing, Rich Lacey, Laboratory Director, Geotechnics
- Defining the Transmissivity Testing Requirements for Geonets and Composite Drainage Nets, Robert Mackey, Principal Engineer, S2L Incorporated

NAGS Student Paper Competition

- Development of Low Altitude Aerial Photometry Techniques to Quantify Geomembrane Wrinkles, Melissa Chappel, Graduate Student, R. W. I. Brachman and W. A. Take, GeoEngineering Centre at Queen's-RMC
- Effect of Wet-Dry Cycles on Capillary Break Formation in Geosynthetic Drainage Layers, John McCartney, Doctoral Candidate, University of Texas at Austin
- Assessment of Geotextile Filament Properties and Size Variation During Interface Shearing, Duhwan Kim, Graduate Research Assistant, Georgia Institute of Technology

Containment/CQA/CQC

IMAGE ANALYSIS FOR QC/QA of GEOTEXTILE DEFORMATION DURING WIDE TENSILE TESTING

Ahmet H. Aydilek, Assistant Professor, and former Undergraduate Research Assistant, M. Emin Kutay, Members ASCE, Rita Sparacino, and Hiruy Dafla

ABSTRACT

A laboratory testing program was undertaken to evaluate the feasibility of using digital image analysis technique to track deformation of geosynthetics during tensile testing. The techniques developed in this study offer great potential to identify localized deformations in geosynthetics. The technique can be used in understanding the grip efficiency, quality control of manufactured products or determination of boundary conditions in geosynthetics under tensile loads, which may further be used in development of constitutive models.

INTRODUCTION AND EXPERIMENTAL PROGRAM

Geosynthetics are expected to offer certain mechanical properties that will provide satisfactory performance when exposed to field conditions. Among various properties, strength is one of the most important ones in reinforcement applications, and wide-width tensile test is commonly used to determine strength (Koerner 1997). Primarily, the stress-strain behavior and strength properties determined from this test are defined at a particular strain or elongation level and strains are usually calculated on average basis for the entire specimen. The accurate determination of the deformation (therefore strain) zones is necessary particularly for quality control/quality assurance (QC/QA) evaluation of these materials. Due to limitations in the current test methodologies, these zones usually remain undetected in the wide-width tensile testing which results in incomplete characterization of mechanical performance.

There are various methods used to measure strains, i.e., extensometers, strain gages, laser beam and infrared sensors, but with certain shortcomings as they cannot accurately define complete strain fields. Disruption of yarns or filaments on a geotextile by use of extensometers and strain gages is common, while all devices including the laser beam and infrared sensors, give only average strain along a selected gage length on specimen surface. Image-based methods, often termed as optical flow or particle tracking techniques, have the potential to define the strain zones in a geosynthetic during the tensile testing. As these techniques are non-invasive, they do not suffer from the shortcomings of the existing strain determination methods and do not disturb the specimen. Moreover, once the image-based method is developed, the model has the potential to be used as a QC/QA tool during geotextile manufacturing and beyond.

A laboratory test program was employed in the current study to make automated image-based measurements of strain in geosynthetics during wide width tensile testing. Specimens were tested using both roller and pneumatic grips to identify the effects of clamping. The testing plan included one nonwoven, two low strength woven, and five high strength woven geotextiles. The woven geotextiles had a range of manufacturing styles including monofilament, multifilament and yarn filaments (Table 1). The dimensions of the specimens were selected in accordance with the ASTM D 4595. The selected strain rate was 11%/min for specimens tested in the hydraulic grips. A strain rate of 12%/min was utilized for the specimens, when roller grips were used for

clamping. During testing, a monochrome camera was mounted apart from the test setup and simultaneously captured digital pictures of the test specimens at 2 or 5 seconds intervals depending on the rate of displacement applied during testing. The image frames

Table 1. Properties of geosynthetic specimens tested

Type	Geotextile ID	Polymer Structure	Mass per unit area (g/m ²)	Wide Width Tensile Strength (kN/m)	
				At 5% strain	Ultimate
Nonwoven Geotextile	NW	NP, PP	278	NA	NA
Low Strength Woven Geotextiles	W1	MF, PP	190	11.4	39.5
	W2	MF, PP	250	13.2	47.4
High Strength Woven Geotextiles	HW1	FY, PP	284	19.8	47.3
	HW2	MU, PET	290	15.8	70
	HW3	FY, PP	490	35.1	70.2
	HW4	FY, PP	578	43.9	105.1
	HW5	MU, PET	1907	316.0	632

Note: NW = Nonwoven geotextile, W = Low strength woven geotextile, HW = High strength woven geotextile, NP= Needle-punched, PP = polypropylene, PET = polyester, MF = monofilament, MU = multifilament, FY = fibrillated yarn, NA = Not analyzed.

were saved onto the hard disk and subsequently used for image analysis of strain distributions developed within the specimens. Two image-based particle tracking methods, BMAD and normalized cross-correlation (NCC), were employed to define the time-dependent axial and lateral strains in geosynthetics. Kutay et al. (2006) describes the detailing of the testing procedure and image analysis methodology.

RESULTS

Preliminary investigations indicated that both algorithms provided highly comparable results with cross-head displacements (Figure 1). This was highly encouraging. As the displacements measured by both algorithms were also comparable, BMAD was used for remainder of the tests.

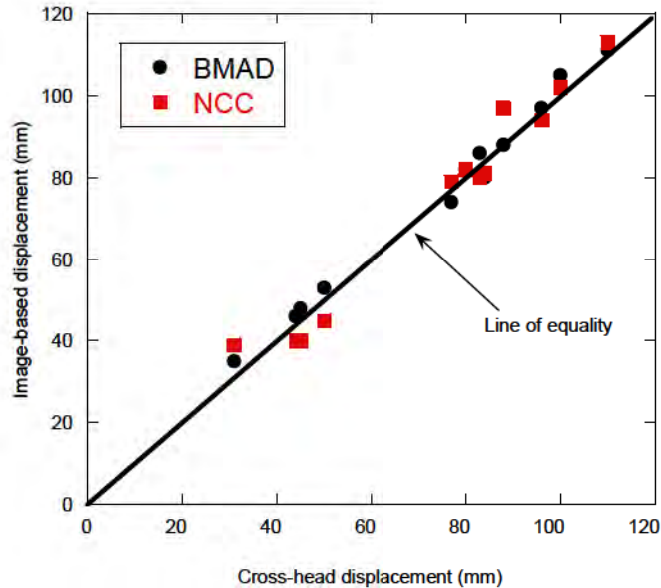


Figure 1 Image-based versus cross-head displacements

The image based analysis successfully identified localized strains in geosynthetics. One primary advantage of the image-based methodology was to define the axial as well as lateral strains. This is obviously not available through cross-head displacement determination method generally used in wide-width testing. Figure 2 presents the lateral versus axial strains in selected geotextiles. The clear advantage is that an estimate of lateral strain in a geotextile at a given axial strain (e.g. design strain) can be made through these plots. These lateral strains can be significant in testing of some geotextile, such as nonwovens. Figure 3 presents the observed strains as well as displacements for the nonwoven tested in this study.

CONCLUSIONS

Two-image-based particle tracking techniques were developed to analyze the strain distribution in geosynthetics. The technique was used in testing of eight geosynthetics. Lateral strains as well as the local weak zones in a geosynthetic were easily identified using the image-based approach. Overall, the image analysis provided a quick and accurate approach in defining the

strain zones and identifying anomalies in a geosynthetic specimen. The methodology developed herein has the potential for utilization as a QC/QA tool in geosynthetics industry.

REFERENCES

Koerner, R.M. (1997). "Designing with Geosynthetics", 4th edition, Prentice Hall, Englewood Cliffs, New Jersey, USA, 761 p.

Kutay, M.E., Guler, M., and Aydilek, A.H. (2006). "Analysis of Factors Affecting Strain Distribution in Geosynthetics", *Journal of Geotechnical and Geoenvironmental Engineering*, ASCE, Vol. 132, No. 1, pp. 1-11.

CONTACT:

Ahmet Aydilek
Assistant Professor
University of Maryland
1163 Martin Hall
College Park, MD 20742
Phone:301-314-2692
Email: aydilek@eng.umd.edu

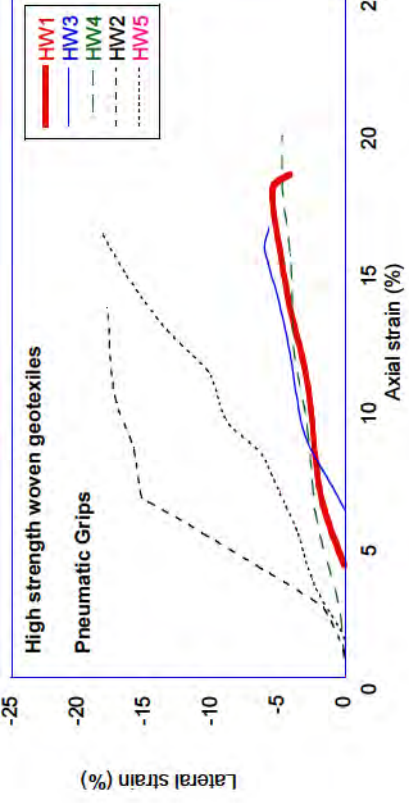
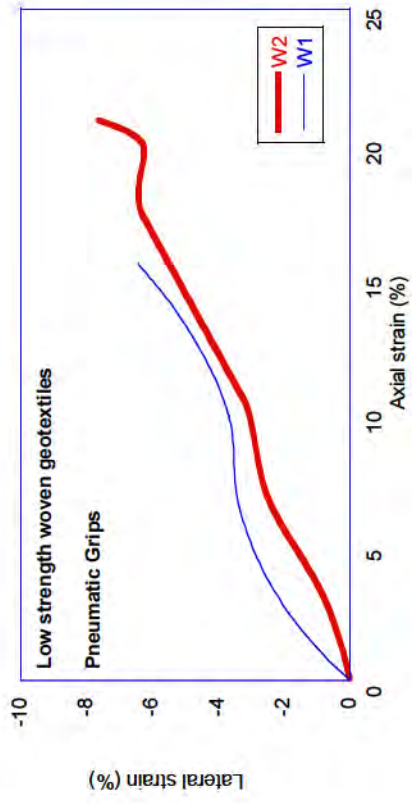
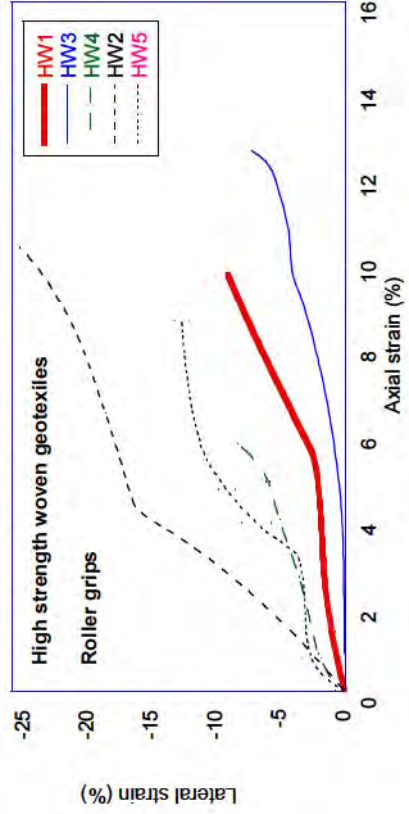
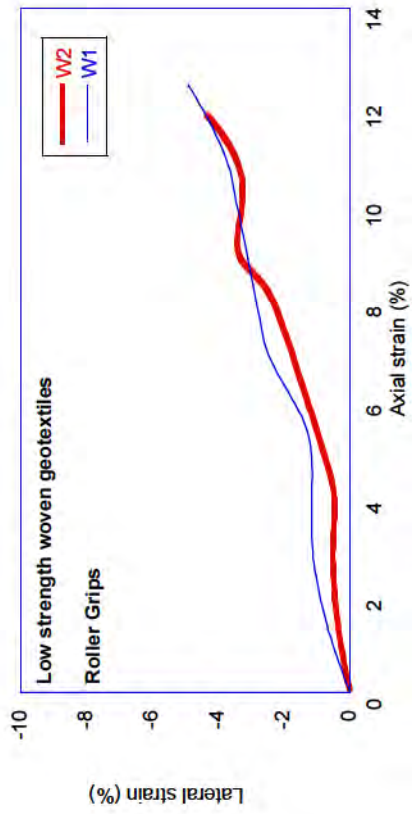
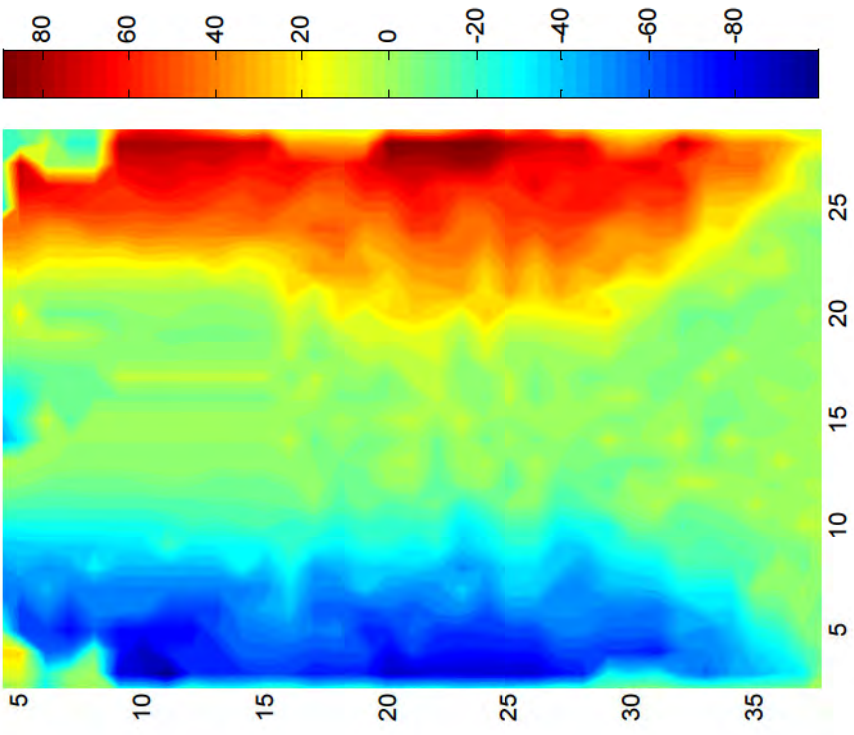
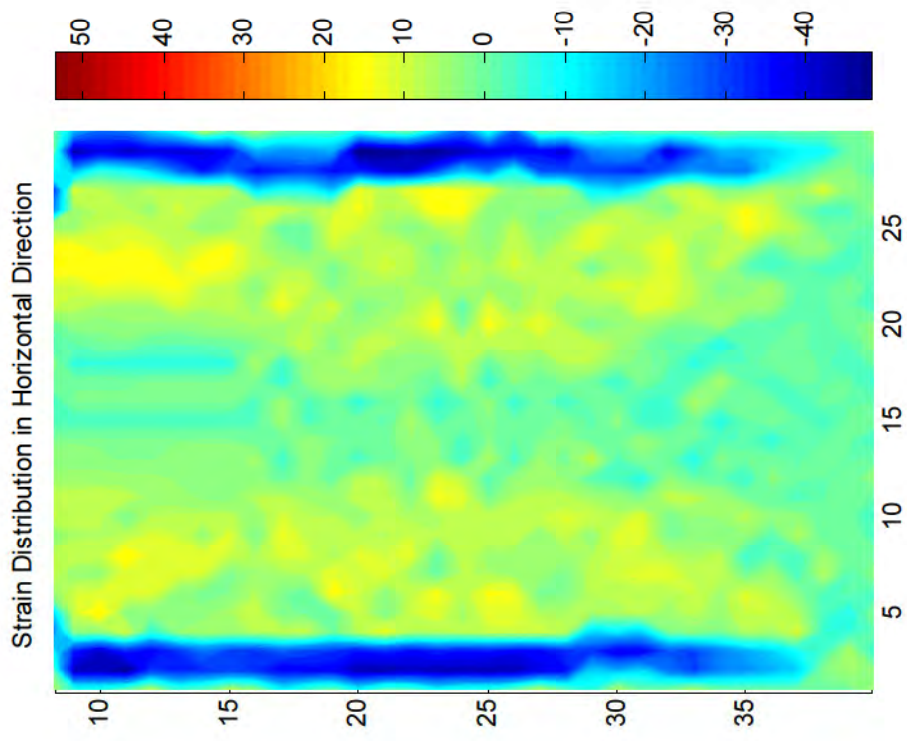


Figure 2 Lateral versus axial strains in selected geotextiles





(a) *Strain in horizontal direction in nonwoven geotextile NW.* (b) *displacement.* (b) *strain*

The Technical Background and Successful Field Experience of Spark Testing a Conductive Liner

J. Youngblood, Geomembrane Product Manager, GSE Lining Technology; B. Ward, Chief Engineer, Pipeline Inspection Co., Ltd.

ABSTRACT

Construction Quality Assurance (CQA) plays an important role in producing a quality containment system. Electrical Leak Surveys are CQA non-destructive tests that help locate leaks/defects after the installation of the geomembrane is completed. Spark testing of an insulating geomembrane with an underlying conductive layer is the electrical leak survey method in which this paper will be focused. Conductive Geomembranes typically include a 2 to 3 mil thick coextruded layer of polyethylene containing a conductive carbon black on the bottom surface of an insulating geomembrane which allows it to be spark tested for defects. The advantage of the conductive geomembrane in regards to spark testing is that the conductive layer is in intimate contact with the geomembrane, and it allows the geomembrane to be 100% spark tested in the field per ASTM D7240 (*Standard Practice for Leak Location using Geomembranes with an Insulating Layer in Intimate Contact with a Conductive Layer via Electrical Capacitance Technique*). This paper is intended to discuss the intricacies of field spark testing a conductive geomembrane. It will include the equipment used and the calibration of the equipment for site specific conditions. It will also discuss the process in spark testing the geomembrane and spark testing underneath the weld flap.

INTRODUCTION

The purpose of geomembranes is to be containment barriers for liquids and/or gases in environmental and industrial applications. The design engineer of a project uses the physical and/or chemical properties of a specific geomembrane to determine if it is appropriate for use in their specific application. Geomembranes can be damaged during shipping, handling, poor subgrade conditions, installation, traffic, and cover material. This may alter the material from the prime material manufacturing state. Thus, engineers rely on or should rely on good CQA to alleviate and/or detect any damage to the geomembrane and to provide a quality installed geomembrane containment system.

The objective of CQA is to ensure that the liner is built according to the project specifications, with the best possible workmanship, and within the constraints of the budget and schedule. CQA does not ensure a perfect lining system. If the liner is poorly designed, CQA will ensure that that poorly designed liner is properly installed. There are several different methods to incorporate CQA in to the post installation of a project to assure the quality of the geomembrane system in an application. Visual inspection, destructive testing of seams, non-destructive testing of seams, leak location using electrical potential which is performed with water/soil on top of geomembrane, and the spark testing of a conductive geomembrane which is performed on an exposed conductive geomembrane are some different techniques used as CQA of geomembrane systems. This paper examines the CQA technique of spark testing a conductive geomembrane using the capacitance effect on the geomembrane panels and the conductive geomembrane underneath the fusion weld flap.

CONDUCTIVE GEOMBRANE

Spark (Holiday) testing was originally developed to inspect coatings on steel pipe. A high electrical potential (voltage) of negative polarity (ground) is applied to the metal pipe to be tested. An electrode (wand or brush) of opposite (positive) polarity is passed over the coating. Any voids in the coating will establish electrical continuity and allow a spark to pass between the metal pipe and the electrode.

Geomembrane manufacturers use this type of electrical spark testing of synthetic polyethylene geomembranes for defects during the manufacturing process. The next logical step was to then take this proven technology from the factory to the field. This move was accomplished with the development of a specialty coextruded geomembrane with an integral outer layer of conductive material. A conductive geomembrane typically comprises of a 2 to 3 mil layer of a special conductive carbon black (Figure 1) which provides the geomembrane with an intimate conductive layer.

Figure 1: Coextruded Conductive Geomembrane Cross-section

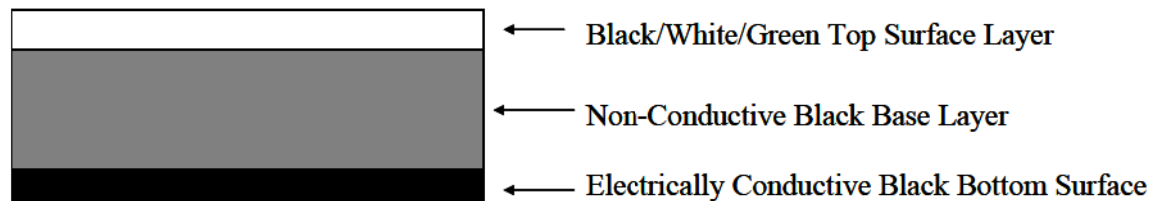


Figure 1: Coextruded Conductive Geomembrane Cross-section

SPARK TESTING

The electrical leak location test using the spark test of a conductive geomembrane containment system can involve the spark test of two areas of the installed geomembrane system. The first area is the spark test of each individual geomembrane panel between the fusion welded seams, and the second area is the spark test underneath the fusion weld flap. The spark tests on each of these areas are similar, but each test should be setup and calibrated separately. The spark test on the wide geomembrane panel is typically done with brass brush electrode (Figure 2) that is typically 4 foot wide. The spark test performed on the conductive layer on bottom of the fusion weld flap is typically done with a conductive neoprene electrode (Figure 3) which is usually flat so that it can slide underneath the flap.

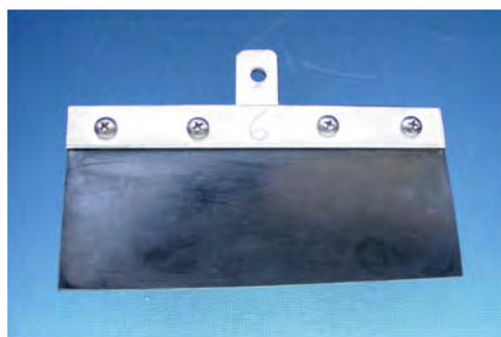
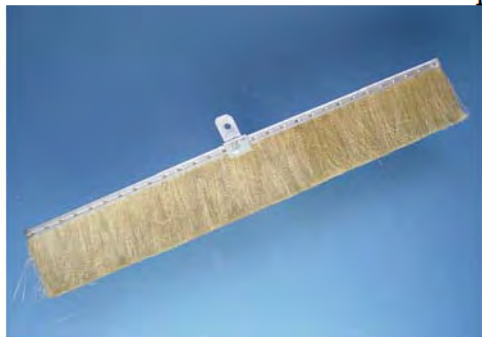


Figure 2 – Brass Brush Electrode

Figure 3 – Neoprene Electrode

The spark testing of a conductive geomembrane typically utilizes a high voltage spark tester “Holiday Detectors” – typically those over 5KV – these operate by generating a narrow pulse of high voltage. These pulses occur between 30 and 150 times per second. Any holes (or holidays) in the material being tested will allow this high voltage to arc across to the ground side of the circuit. This current flow is detected and indicated (by visual and audible signals typically). While this pulse of voltage does not “alternate”, it does act like an AC voltage in many respects. One of these is that the material being tested – in this case a conductive geomembrane – acts like a capacitor. A capacitor is an electrical device in which two electrically conductive materials are separated by an insulating layer (Figure 4). By moving a conductive rubber ground pad with the spark test electrode, the electrode acts like one side of the capacitor, the grounding pad-to-liner-to-electrode acts like the insulator of the capacitor, and the ground pad is the opposing side of the capacitor. A small current will pass through this “capacitor” even when no defect is present in the geomembrane. This allows the use of a ground pad with a short cable to detect any defects in the liner material. The spark testers used for leak location on conductive geomembranes typically range from 15,000 volts to 35,000 volts with a sensitivity adjustment (Figure 5). The range in voltage and sensitivity allows the operator to adjust the spark tester for the site specific material and conditions.

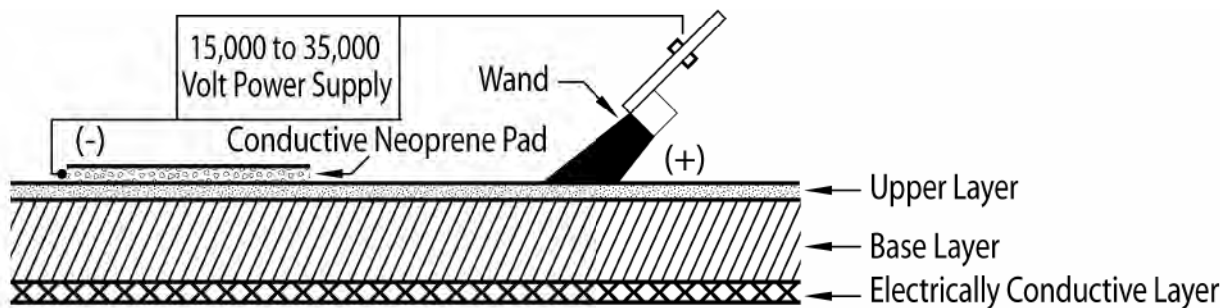


Figure 4 – Capacitance Display

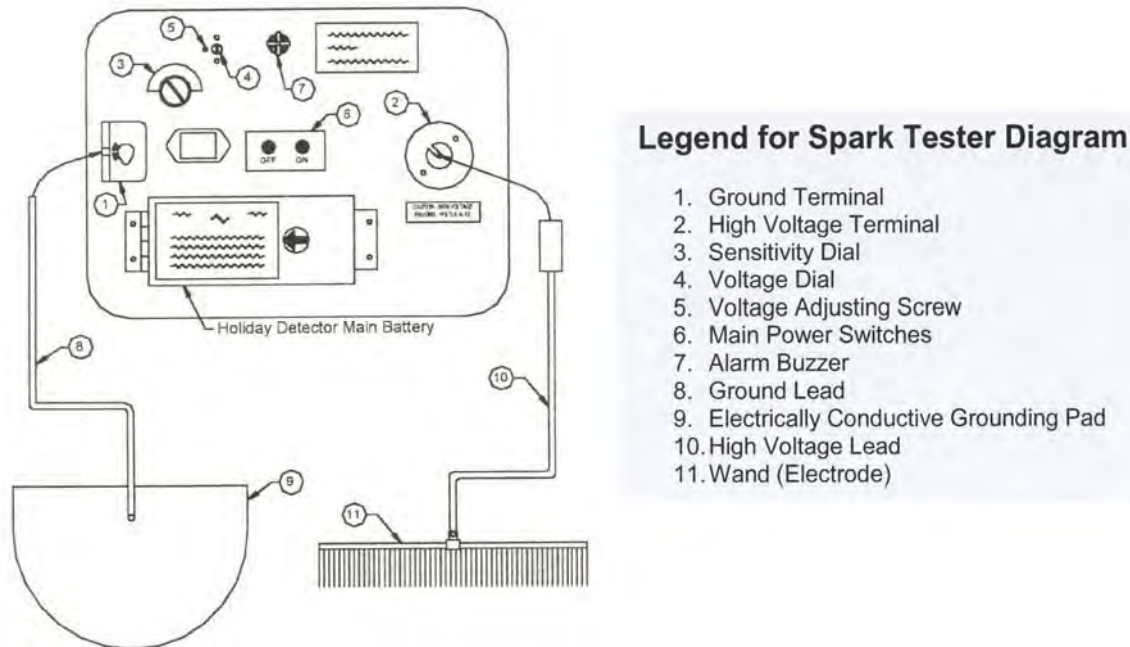


Figure 5 – Typical High Voltage Spark Tester

The procedure for spark testing starts by determining a grid pattern that the technician will follow during testing the individual geomembrane panels. The technician begins the survey with the test wand contacting the surface of the geomembrane, and he continues until the entire surface of the geomembrane panel has been spark tested. Sometimes engineers are concerned with potential flaws that may occur underneath the fusion weld flaps where two different panels have been seamed. Unless the operator is able to get the electrode within a few millimeters of the flaw it will not be detected. The GSE conductive layer on the bottom of the flap solves this problem by propagating the high voltage along the conductive layer beyond just the area directly touched by the electrode. Because there is a loss in the conductive layer adjusting the sensitivity of the Holiday Detector will allow the Holiday Detector to detect any flaw as far away as a few meters or as closely as a few centimeters.

Pipeline Inspection Company’s Holiday Detectors, when used with a GSE conductive liner, are typically adjusted to maximum voltage (about 35KV) and the sensitivity is adjusted such that when the electrode is touched to the underside of the top layer of a seam (the flap) a brief “holiday detected” signal may be received. This is due to the “capacitor” becoming charged, thus more current is flowing. Once this effect is over the “holiday detected” signal goes off. The operator now moves the electrode along the flap. As they get near a flaw the “holiday detected” signal sounds. Once they have moved beyond this flaw some distance the signal goes off. Midway between the signal first sounding and then end of it is the location of the flaw. If this distance is too large to identify the exact location of the flaw, then the sensitivity adjustment may be turned down (less sensitive) and the area probed again try to find the exact location, or the operator may just look under flap for a visual detection.

FIELD TESTING OF A BRINE POND

Spark testing of a conductive geomembrane was performed on a 20 acre, 30 foot deep Brine Pond in Texas. The pond containment system consisted of a secondary 40 mil GSE conductive geomembrane, geonet, and a primary 60 mil GSE conductive geomembrane with a protective geotextile between the subgrade and secondary liner on a portion of the project. A Pipeline Inspection Company Ltd. Spark tester Model Number(s) 735 and 790 with sensitivity adjustments were used for spark testing the conductive geomembrane on this project. A field technician of EnviroCon Systems, Inc. performed the spark testing with a third party inspector overseeing the leak detection testing. The entire secondary and primary liners were spark tested during the construction phase, and the primary liner was spark tested a second time after all construction was completed. The electrical spark testing of the pond located approximately 6 to 7 defects per acre in the double lined brine pond. The defects were primarily on the secondary 40 mil conductive layer.

Spark testing of the individual geomembrane panels was performed using a grid system agreed upon by the installer and third party CQA representative. Approximately 70% of defects detected were on the individual panels that were due to dragging 40 mil conductive liner over subgrade with gravel embedded into the subgrade. As the geomembrane rolls were dragged over subgrade, the gravel would come loose and introduce indentations in the geomembrane. These indentations were slightly thinner and would trigger the spark tester audio alarm indicating a potential defect. About half way during installation of the secondary liner, a protective geotextile was installed underneath the secondary liner to solve this problem.

Spark testing of the conductive geomembrane underneath the fusion weld flap was performed. Approximately 30% of the defects were located under the fusion weld flap, and the defects were due to weld heat separation of the bottom overlap during welding of the seams. The spark testing underneath the flaps located these defects.

One hurdle to overcome was the continuous false audio alarms that were triggered by the spark testers on one end of the pond during spark testing underneath the weld flap. Investigation was performed on the sensitivity adjustment of the spark tester at different locations throughout the pond. The author noticed that on one end of the pond, the spark testing underneath the fusion weld flap worked without false alarms at a specific sensitivity adjustment. However, the author noticed when we got to the north end side of the pond the spark tester started producing false audio alarms, and we had to adjust the sensitivity of the spark tester to successfully take out the false alarms. The only explanation that was determined for the increase in sensitivity was the near location of a high voltage power lines running parallel within 100 feet of the north end side of the pond (See Figure 6). The conductive geomembrane was successfully installed and spark tested and after one month of filling the pond with brine at level of 20 feet, no leakage has been observed in the leak detection layer of this brine pond.



Figure 6 – Brine Pond with High Power lines

CONCLUSION

Geomembranes are exposed to all types of external forces during the construction phase of a project. Therefore, a good CQA program is crucial to the successful installation of a quality geomembrane system, and Electrical Leak Surveys have become valuable CQA post installation tests that help engineers achieve their goal of a leak free geomembrane barrier system. The experience with the brine pond project mentioned above and numerous other projects have shown that spark testing of a conductive geomembrane is a proven, successful technique for the location of defects on exposed geomembranes. Based on field experience, the author believes that this procedure should be considered by designers for all critical containment applications where leak free construction is important.

REFERENCES

ASTM D7240 Standard Practice for Leak Location using Geomembranes with an Insulating Layer in Intimate Contact with a Conductive Layer via Electrical Capacitance Technique (Conductive Geomembrane Spark Test)

CONTACT:

Jimmy Youngblood

Project Manager

GSE Lining Technology

19103 Gundle Road

Houston, TX 77073

Phone: 281-230-2523

Email: jyoungblood@gseworld.com

Enhanced Geomembrane CQA Through Proper Application of Geomembrane Leak Location Surveys

Bradford L. Smith, P.E., BCEE, Stearns & Wheeler, LLC; Glenn T. Darilek, P.E, Leak Location Services, Inc.; Daren L. Laine, Leak Location Services, Inc.

ABSTRACT

Historically, geomembrane construction quality assurance (CQA) has focused on destructive testing of welded seams to verify seam strength and integrity. Paradoxically, seams are not subject to significant stress and practically never fail in service, while holes and construction damage in the geomembrane are a much more widespread problem. The historical approach fails to evaluate how well the geomembrane performs in providing a liquid barrier, which is the primary function of a geomembrane. More recently, CQA efforts have focused on verifying liquid barrier performance using electrical leak location surveys. Engineers, installers, regulators, and owners are starting to rely on these surveys to evaluate geomembrane performance. The only function of a geomembrane is to prevent liquid flow. It is certainly prudent to spend a fraction of a percent of the construction cost of a landfill to test the performance of the geomembrane. So now a total approach is needed that incorporates a sound design that considers the most relevant and cost-effective CQA requirements, construction monitoring and testing, proper preparations for leak location surveys, and effective geomembrane leak location surveys.

Geomembrane leak location surveys using electrical methods have been used commercially for more than 20 years. Leak location surveys are conducted on bare geomembranes, geomembranes covered with soil, and geomembranes covered with water. Industry standards have been developed for all the major electrical methods. Optimum leak detection sensitivity depends not only on the proper performance of the survey itself, but also on the design of the liner system and the proper preparation of the liner system prior to testing. The electrical method is used to detect electrical current flowing through holes in the geomembrane. The liner system design and leak location preparations should take this into consideration. Certain landfill liner designs can reduce leak detection sensitivity and hinder the detection of holes. At the same time, the detection of smaller holes requires special preparations and considerations. This paper discusses a total approach to geomembrane CQA from design to pre-construction preparation to leak location field surveys, and makes specific recommendations for enhanced geomembrane leak detection performance.

GEOMEMBRANE CQA PROBLEM ANALYSIS

More than fifteen years ago, geomembrane construction quality assurance guidelines were written to perform tests of the material suitability and physical properties of the geomembrane and to perform destructive testing of geomembrane field seams. These guidelines were incorporated into regulatory requirements, and the geomembrane industry had their “marching orders.” Soon after that, the industry realized that landfill leachate had negligible effect on the

most popular geomembrane materials, and the geomembranes rarely failed the physical tests. At the same time, with the introduction of the double wedge fusion welder, with a testable air channel, seam strength was no longer an issue. Many in the geomembrane industry feel that the current protocol of destructive testing of seams actually does more harm than good because each destructive seam test removes 1 to 1.5 meters (3 to 5 feet) of double wedge weld and requires a patch using 3.5 to 4.5 meters (12 to 15 feet) of inferior manual extrusion welding.

The only function of a geomembrane is to prevent liquid flow to the environment. Therefore, the quintessential approach should be to test for liquid leakage. Although seam strength and material suitability are factors to consider, the CQA guidelines have completely disregarded the problem of holes in the geomembrane. Holes in installed geomembranes have always been a problem. Geomembrane leak location contractors have found tens of thousands of leaks in geomembranes, and the contractors have typically tested only a very small percentage of the geomembrane being installed. Landfills with regulatory CQA had 4.2% of the leachate leaking through the primary geomembrane before the leachate could be pumped off the geomembrane (Tedder). Construction damage while emplacing protective earth materials on the geomembranes is the major quality problem. One leak location contractor reported that 73% of the leaks were caused by construction activities (Nosko). A momentous consideration for installations where an underlying geosynthetic clay liner (GCL) is used instead of a thick compacted clay liner is that construction damage that causes damage to a geomembrane will most likely also breach the GCL.

Electrical leak location surveys have been used for more than two decades on a variety of single and double lined facilities – from farm ponds to hazardous waste landfills. The methodology and results of the methods have been described in the technical literature including Laine (1989), Laine (1993), and Rollin. The number of leaks found using electrical leak location methods, and the characteristics of these leaks have been documented in many publications. Colucci reported a leak density of 15.31 leaks per hectare (6.20 leaks per acre) for geomembranes in Italian landfills. Laine (1993) reported 22.5 leaks per hectare (9.11 leaks per acre) for impoundments filled with water in the United States. Rollin reported 2.03 leaks per hectare (0.82 leaks per acre) for bare geomembranes in Canada and France. These statistics do not convey the variability of the density of leaks found using electrical leak location methods. No leaks are found during some leak location surveys, while some surveys find literally hundreds of leaks in a single facility.

Design engineers have been aware of the availability of the technology for use in the event that problems arise during construction. The experience of the primary author is that electrical leak location surveys are most common with double lined or double composite lined landfills, where a defect in the primary geomembrane may readily result in an unacceptable action leakage rate detected in the secondary collection system. The design of these facilities, while still meeting federal and state criteria, can be optimized to produce highly sensitive, and therefore accurate, leak location surveys. As more state regulatory agencies require electrical leak location in their regulations or as a standard permit condition for lined landfill facilities, the need to design the multiple-component liner systems to compliment the performance of the electrical leak location survey becomes more important.

The technical guidelines for geomembrane CQA promulgated years ago were intended as a starting point, and were never intended to be permanent. Nonetheless, they have been adopted

into the regulations for every state in the United States, and similar measures were adopted throughout the world. It is time to reexamine geomembrane CQA practices and update historical practices with productive measures that test the true function of the geomembrane. Revised CQA guidelines can then be adopted by the regulatory agencies and the geomembrane industry.

COMMON SENSE TESTING OF A GEOMEMBRANE

The overall goal of geomembrane construction quality assurance (CQA) should be to provide a geomembrane system that has no leaks and has very low potential for developing leaks during the lifetime of the lined facility. The best approach to improving our ability to detect defects in the geomembrane liner is to implement a total approach that incorporates design, construction, and CQA components.

After two decades of emphasis on destructive testing of seams, the industry has learned that seams are generally quite reliable; however seams are an ineffective measure of geomembrane performance. Most protocols for destructive testing of seams may result in more harm than good (Kerkes) (Koerner) (Theil). Recent suggestions to reduce seam testing based on improved liner installation performance, while a step in the right direction, still ignores testing the fundamental function of the geomembrane. Some destructive testing of seams will always be needed to verify that seaming machines are operating properly and to compel quality workmanship. Making use of the essentially nondestructive pressure testing of double welded seams is a very effective measure to test seams for defects. But it does not make sense to spend project resources testing a problem that rarely arises while ignoring a problem that exists with practically every geomembrane installation. The emphasis on destructive seam testing has focused attention away from the most significant problem, which is liquid leakage through holes in the geomembrane liner.

Within the last few years, regulators and the industry are realizing the need for more effective geomembrane CQA (Phaneuf). Almost no one is challenging the need to reduce destructive testing. Many engineers and regulators are realizing that the most relevant test for a component whose function is to prevent leakage is to test for leaks. Leak location testing technology using electrical methods was developed at Southwest Research Institute in San Antonio, Texas under cooperative contracts with the U.S. Environmental Protection Agency. Commercial geomembrane leak location services using those methods have been available for more than 20 years.

Several states have adopted regulations or guidelines that require electrical leak location testing, and several other states are considering that measure. Presently there are at least 14 companies in the United States that offer electrical leak location surveys, and at least that number more internationally. The typical construction cost for a double composite landfill liner system is USD\$108 per square meter (\$10 per square foot), of which \$22 per square meter (\$2 per square foot) is spent for CQA (Duffy). It does not make sense to skip a electrical leak location survey which typically costs less than \$0.65 per square meter (\$0.06 per square foot).

DESIGN AND CONSTRUCTION PREPARATIONS FOR ELECTRICAL LEAK LOCATION TESTING

The goals of a total approach to geomembrane CQA are:

- * Provide a sound design that will facilitate and enhance CQA;
- * Specify the measures to properly implement the design;
- * Monitor the construction to be sure the facility is constructed as designed; and
- * Implement relevant testing to verify that the facility will perform as designed.

An essential part of this total approach to CQA is to perform relevant destructive and non-destructive testing of the geomembrane liner. This testing includes performing an electrical leak location survey of the installed geomembrane. Therefore, the design and the construction of the geomembrane lined facility must take into account the guidelines for best performing this type of test. This will improve the quality of the electrical leak signal, the leak detection sensitivity, and the efficiency of the electrical leak location survey. By accomplishing these goals, we can enhance the results of the electrical leak location survey and obtain the best value for the CQA investment.

The design of the geomembrane-lined facility should be considered to facilitate and enhance electrical leak location surveys to be consistent with the improving performance of the liner system. In order for electrical current to flow through the leaks, electrical continuity must exist from the material above the geomembrane, through the leaks, and to a return electrode in contact with the conducting material below the geomembrane. Therefore, there should not be an electrically-insulating layer above or below the geomembrane and the defect must have some conductive material in it. Likewise, the geomembrane must provide an electrically insulating layer with no electrical conduction paths through the seams or around the geomembrane.

The following factors provide some general guidelines for enhancing the leak detection process. In many cases it is not necessary to require the most optimal design in order to successfully perform a electrical leak location survey. In less than optimal designs, leak detection sensitivity might be decreased, but in most cases, larger leaks and construction damage caused by heavy equipment will be detected. It is important to realize that just because every small leak may not be found, that does not mean that one does not want to find any leaks. Small leaks are anticipated, as evidenced by an allowable leakage rate in regulations.

Layers and Conduction

The basic design concept behind a composite liner section consists of a drainage layer overlying a barrier layer. The barrier layer is further divided into geosynthetic barrier component overlying a soil barrier component. For double composite liner systems the design of the primary and secondary composite liner are usually different. In order to enhance the geomembrane CQA process, the selection of each of these components must keep in mind the conditions required to improve electrical leak location survey sensitivity.

Barrier Layer. The soil component of the barrier layer of a composite liner system typically consists of low permeability soil or a geosynthetic clay liner. Either material can successfully be used in a composite liner system and provide the electrical continuity required. Earth materials generally meet these requirements if they have some moisture, and some fines or moisture content above field capacity to enter the defects in the geomembrane. One can imagine that

large, dry gravel could bridge smaller defects in the geomembrane and prevent electrical current from flowing through the defect to create a leak. This would not be a problem if water or rainfall wets the gravel to field capacity or if sufficient fines with some moisture fill the defect to create continuity (a leak).

If the manufacturers' recommended minimum moisture level is maintained, geosynthetic clay liners have sufficient moisture for performing electrical leak location surveys of an overlying geomembrane. Exceptions include instances when the GCL is installed in an arid environment, and the moisture is evaporated before the GCL can be covered with geomembrane and there has been no rainfall on the geomembrane or water percolating through the cover materials. In these cases, the bare geomembrane or material-covered geomembrane must have water added to allow moisture to penetrate through the leaks. The moisture will penetrate the geotextile component and hydrate the clay component. The hydrated clay swells into the leak and also provides a larger contact area with the clay layer to establish sufficient electrical conductivity.

GCLs that include a geomembrane substrate can hinder leak detection. Construction damage (larger defects) to the geomembrane will most likely also breach the GCL, but smaller holes caused by small rock punctures or installation activities are more difficult to detect. To a lesser degree, the woven geotextile side of some GCLs can also insulate a smaller leak. If possible, the nonwoven side of the GCL should be installed away from the geomembrane if the design will permit.

Drainage Layer. The drainage component of the liner system provides the greatest variety in materials of construction and the greatest potential impact to the quality of electrical leak location surveys. In order to detect a leak, some moisture must be present in the layers above and below the geomembrane, and within the defect itself. One way to enhance these conditions is to have water present on the geomembrane surface, creating a small hydrostatic head that allows water flow through the defects to the layers below. The design intent of drainage layers is to remove water from above the liner system, reducing the head on the liner and therefore reducing the action leakage rate. However, with proper design and proper preparations, both functions can be implemented.

The primary component of many drainage layers is sand or gravel. Although coarse sands may meet most minimum permeability requirements of 1×10^{-3} cm/sec, many designs utilize an even higher permeability of up to 1 cm/sec. This permeability can only be met with clean gravel. Shredded tire material can also be used, but they are a special situation. Gravel in direct contact with geomembrane might lead directly to holes in the geomembrane. Therefore, a geotextile cushion layer is often used immediately above the geomembrane to protect it from installation damage. This cushion geotextile can provide enough water holding capacity to create the small head required to create the electrical conduit necessary to enhance geomembrane CQA. Geotextiles are usually installed dry, and if covered with dry earth materials will also create an insulating layer. Therefore, if rainfall does not wet the geotextile, the geotextile or material above the geotextile (or both) should be pre-wetted with water to provide electrical continuity through the smaller defects. Construction damage will likely force earth materials through the leak, so larger leaks would be detected without the need for added water.

Geocomposites provide another potential for creating an electrically insulating layer above the geomembrane. Some designs use a geosynthetic drainage composite immediately above the geomembrane to increase the lateral flow capacity above the geomembrane and to reduce the water head on the liner, thus reducing action leakage rates. The geonet component of a geocomposite does not, by itself, usually retain sufficient moisture. For this design approach the drainage composite should include a geotextile on the bottom of the composite, adjacent to the geomembrane, to provide the electrical continuity required for enhanced electrical leak location testing if the design allows. For optimum results, measures should be taken to maintain adequate moisture in the geotextile components.

While geomembrane leaks can be detected under geocomposites, the conditions must be controlled. Another approach for designs with a thin insulating layer above the geomembrane is to conduct an initial electrical leak location survey on the bare geomembrane to detect small leaks caused during installation, followed by a second survey with earth materials covering the geomembrane and the thin insulating layer. Construction damage to the geomembrane would also breach the thin insulating layer. This approach has also been used for landfills in arid areas to enhance CQA.

Because slopes drain more quickly than flatter surfaces, the hydrostatic head on slopes cannot be maintained as well. Therefore, extra measures should be taken to provide moisture on the side slopes. Fortunately, smaller leaks are not as prevalent on the side slopes because there is less construction traffic and fewer seaming details on the side slopes. The primary area of concern with side slopes is near the bottom of the slope where it is difficult for equipment operators to judge where the geomembrane transitions from the flat floor to the slope. However, damage in these areas is typically more significant and can be detected without the need for additional moisture.

Leak Detection Layer. Often in a double-geomembrane system, there is only a geonet leak detection layer placed between the geomembranes. For these installations, the layer between the geomembranes is typically flooded with water during electrical leak location surveys. However, a GCL, a sand layer, or other conductive layer will facilitate the leak location survey without having to flood the leak detection zone with water. Consideration can be given to using the proprietary conductive geomembrane with the conductive side up for the secondary geomembrane to create a suitable electrical environment. EPDM geomembranes are electrically conductive, and they could be used as the secondary geomembrane if otherwise suitable. Conductive geotextile has been used between geomembranes to provide a conductive layer, but their cost has been about three times the cost of the leak location survey and is not justified if a geotextile is not otherwise needed. Conductive foil with a substrate such as that used for a radiant barrier has been used in some installations to provide the electrical path. Measures must be taken to ensure the conductive sheets are connected together.

If flooding the leak detection layer with water is required, this approach can be facilitated through proper design. For the case of a water-covered geomembrane, flooding the geomembrane is routine. Measures should be taken to ensure the water level in the leak detection layer is slightly lower than the water in the impoundment to prevent the geomembrane from floating. However for the case of a soil-covered geomembrane, the water head pressure in the

leak detection layer must be less than the pressure of the soil on the geomembrane to keep it from floating. Water can be added above the primary geomembrane to provide additional downward pressure.

As an example, assume the geomembrane is covered with 600 mm (2 feet) of earth materials that have a relative density of 1.6 Mg/m^3 (100 pcf). When the water level in the leak detection layer reaches an elevation of 960 mm (3.2 feet) above the lowest point on the geomembrane the geomembrane will just begin to float. Therefore, the primary geomembrane up to an elevation of 960 mm (3.2 feet) could be surveyed. To test above that elevation, an equivalent level of water must be added above and below the primary geomembrane. Because of the amount of water that is needed to flood the leak detection zone and counter balance the effects of liner uplift, only the floor is surveyed in these situations. Testing this system would be routine if the floor had only 960 mm (3.2 feet) of slope. So reducing the amount of slope on the floor would facilitate leak location surveys. There are minimum slopes that are required for proper drainage. However, the total amount of elevation difference on the floor can be minimized if:

- * Leak detection sumps are located in the middle of the facility, if feasible;
- * The leak detection sumps are located on the longer axis of the facility; and
- * Multiple leak detection and leachate collection sumps are used.

When the leak location survey is completed, the water between the geomembranes should be removed first to prevent floating the geomembrane. This procedure also minimizes “squeeze-out”, which is the flow of residual water into the leak detection sump.

There have been a few liner installations where the leaks were so numerous and closely spaced that the signals from the individual leaks could not be differentiated. A leak signal occurs over a distance of several times the depth of the overburden. Therefore, if there are multiple closely-spaced leaks, the superimposed signals from offset leaks will augment and cancel each other to produce a signal that cannot be easily recognized as a leak signal. The combined leak signals can appear to be background noise. Only the signals from the largest leaks can be differentiated from the mixed signal background. Good practice dictates isolating the leaks that are found and performing additional surveys to determine if other leaks are nearby. However, if the additional leaks are numerous, the process must be repeated many times and individual, small leaks may not be recognized. When there are that many leaks, it is usually more economical and sound practice to replace the geomembrane and correct the conditions that caused the numerous leaks.

Extraneous Conduction Paths

Darilek (1989), Peggs (1999) and Peggs (2006) described many other design factors to facilitate electrical leak location surveys. In order to provide electrical continuity through any holes, the use of geomembrane rub sheets and protective sheets installed on the geomembrane should be avoided. If there is a leak under the rub or protective sheet, one might detect signals around the edges of the sheet where electrical current is flowing under the sheet, but the actual leak could not be located. A geotextile rub sheet can help avoid this problem because it is porous.

In addition, electrical isolation should exist between the conducting materials above and below the geomembrane. The electrical leak location method detects electrical current flowing through defects in the geomembrane. Other conduction paths will also conduct electrical current and provide a large signal that will prevent the detection of smaller leaks in their vicinity, and may decrease the leak detection sensitivity to some degree throughout. Therefore, the design should consider this wherever practical.

In the case of single geomembranes, grounded structures through the geomembrane should be avoided, such as the use of metal pipe penetrations. Plastic pipe can be used, but one must also consider that the water in the plastic pipe may be grounded at a grounded metal valve or pump. Plastic pipes can be isolated using a non-conducting plug or by draining the water from behind a partly-conductive plug.

For lined concrete structures, battens should be covered with geomembrane or cast-in embedment strips can be used. Columns or stanchions or any other conductive structures should be booted with geomembrane to a level above the water or earth material. If a leak detection or leachate collection pipe drains to a wet well, the design should consider how to isolate the water in the pipe from earth ground. An isolation valve or plug can be incorporated. Underwater conductive structures such as metal grates or screens should be avoided, if possible.

In the case of a single geomembrane with earth materials placed on the geomembrane, the earth materials on the geomembrane should be isolated from earth ground by leaving a narrow width of the geomembrane exposed around the perimeter of the cell during the leak location survey. This can be accomplished by delaying the complete backfilling of the anchor trenches or leaving a strip of geomembrane exposed at the inside edge of the trench. Haul roads or earthen ramps should be designed to allow temporary isolation during the leak location survey. Otherwise, the road will provide a large interfering signal. To electrically isolate the ramp, a trench can be excavated down to the bare geomembrane to expose the bare liner. Typically, a geotextile covered with plywood is placed on the bare liner to protect the liner during the excavation process. Another approach is to have a vertical flap of sacrificial geomembrane placed on the bare geomembrane and designed to protrude from the road. The edge of the flap would need to be excavated and exposed during the leak location survey, or the flap can be welded to a length of plastic pipe that barely protrudes from the road.

Floating aerators, pumps, or suction barges in water-filled installations must be removed or insulated from earth ground. Electrical lines and conducting pipes must be disconnected. Nonconductive mooring lines can be used for electrical isolation in some cases, but if a towed probe is used to survey the geomembrane covered with deep water, the mooring lines will probably interfere with the survey.

For double-lined systems, the leak detection sump and layer between the geomembranes should be electrically isolated from the material on the primary geomembrane. If the materials between the geomembranes are effectively insulated from earth ground, then the edges of the primary geomembrane can be covered with earth materials during the leak location survey. The primary and secondary geomembranes should be welded together, or carefully buried in close contact with each other, with no GCL or other material between the geomembranes.

Means must be provided to isolate leak detection pumps and instrumentation lines from earth ground. In some cases, temporarily removing the pump is the easiest method. In other cases, disconnecting the grounding wire is sufficient, but the power conductors should be also disconnected for safety. Metal cables used for pump retrieval and leachate line camera inspection should also be isolated from ground during the leak location survey.

Wherever practical, for the water puddle method, the edges of the geomembrane should be propped up to prevent a signal when the water puddle overflows the edge of the geomembrane to earth ground. Likewise, grounded battens can be encapsulated with geomembrane, or a flexible flap can be installed under the batten to form an isolating barrier to allow a leak location survey up to the very edge of the geomembrane.

Other Factors

Electrical current cannot flow through the air. The quality of the survey will be impacted if the subgrade has voids or the geomembrane is bridging at the bottom of the slope. Tire ruts or track ruts placed in a wet subgrade can also result in air voids under the geomembrane. Therefore, the subgrade should be smoothly graded to eliminate air gaps.

Water puddle surveys should be conducted with the geomembrane lying flat on the conducting substrate. In particular, wrinkles are to be avoided during the survey. Wrinkles not only create an air gap but, depending on their size, may also prevent water from puddling on them. Often the flexible geomembranes can be flattened during the survey, but stiffer geomembranes, such as high density polyethylene, cannot be easily flattened. Therefore, water puddle surveys should be accomplished in the night or early morning before wrinkles form. On the other extreme, water puddle testing on bridging geomembranes should not be attempted.

For large cells, installing a suitable current electrode between double geomembranes will enhance the sensitivity of electrical leak location surveys. The number and placement of the electrodes depends on the design. A qualified leak location contractor should be consulted. The ends of the wires to the electrodes must remain exposed, and should be protected from burial or damage. A good design will have the ends of the wires permanently available in case subsequent operations damage the geomembrane and another leak location survey is needed.

Sandbags, scraps of geosynthetics, and other large debris should be removed from impoundments for surveys in deep water to allow a probe to be towed across the bottom with no obstructions. Scraps of metal, particularly wires, can provide false signals that may not be discerned, particularly in deep water. Vegetation and thatch should be managed to allow measurements to be made on the underlying earth materials.

The final factor involves project planning. Electrical leak location surveys cannot be conducted if the water or soil is frozen.

Again, these factors provide for enhanced electrical leak locations surveys. However, one need not forego a electrical leak location survey because one or more of these recommendations cannot be implemented. If these recommendations can be implemented in the design and construction stages then the sensitivity of the leak location survey will be increased. However, successful leak locations survey results have been obtained under less than ideal conditions. For example, excellent results have been obtained at large single-geomembrane installations and landfill caps where none of the edges of the geomembrane were isolated.

EFFECTIVE ELECTRICAL LEAK LOCATION SURVEYS

Specifications

Obviously, as with any technology, perfection can seldom be obtained. It is naïve to specify that the leakage through a primary liner system be zero. Fortunately, the regulations recognize that and define acceptable performance of the liner system in terms of allowable leakage rates. If we specify leak detection sensitivity for holes that are too large, the number of smaller defects that are missed may impact performance. If action leakage rates obtained after the completion of the electrical leak location are unacceptable, our CQA work becomes largely ineffective, and must be corrected. The overriding goal of the total approach is to balance the electrical leak location survey design to focus on the goals of the project.

Leak location surveys must be performed effectively and in accordance with the project specifications by a qualified electrical leak location contractor. Fortunately, the industry has established ASTM standards for the various electrical leak location methods. ASTM Standard Guide D 6747 describes the various implementations and applications of the methods. ASTM D 7002 is a standard practice for leak surveys on bare geomembranes. ASTM D7007 includes standard practices for leak location surveys with water on the geomembrane and with earth materials on the geomembrane.

The ASTM standards are performance-based standards that specify leak detection performance. Artificial or actual leaks are used to verify the leak detection sensitivity of the equipment and field procedures. Leak detection sensitivity is defined as the smallest leak that the leak location equipment can detect. It is not sufficient to be able to detect the leak when the measurements are made directly on or over the leak. The field procedures must be tailored to meet the leak detection sensitivity under worst-case measurement spacing conditions. The ASTM standards recommend leak detection sensitivities that usually can be economically met. When considering the smallest size leak that one wants to find, the obvious answer is every hole, no matter how small. While properly performed electrical leak location surveys can produce impressive results, one must temper the requirements to be realistic, attainable, and economical. Specifying the ultimate in leak detection sensitivity will require that the site conditions be near perfect and that the leak location measurements be made at closely-spaced intervals. This mentality will greatly increase the time for and cost of locating and repairing leaks that may not significantly improve the performance of the lining system.

Contracting

The owner and design engineer have two primary options available for implementing the geomembrane CQA process. The geomembrane CQA firm can be retained by the contractor through the contract documents or they can be retained by the engineer or owner directly. Both approaches have advantages and disadvantages. Regardless of approach, it has been theorized that by knowing that geomembrane CQA will be required on the project the contractors are more careful and perform better. It has been shown that knowing that electrical leak location survey will be required on the project, contractors are more careful and perform better (Darilek 1995). Better performance of the liner system should be the goal of everyone on the team.

Having the contractor retain the geomembrane CQA and leak location firms has the disadvantage of loss of control over qualifications. The construction bidding process typically places a premium on cost and the lowest cost usually wins. This may result in some contractors searching out lower cost, but less experienced geomembrane CQA providers. There have been at least 34 companies that have performed electrical leak location surveys in the United States. Twenty of these no longer offer leak location services or are no longer in existence. Selecting a leak location contractor with experience in successful geomembrane leak location surveys is important. The results, performance, and time required to perform a leak location survey is highly operator dependent and less experienced providers may not produce the same quality field data. This may result in more time and cost, and damaged reputations in the long run.

Another potential disadvantage of this contractual relationship is that there may be the appearance of a conflict of interest because the CQA and leak location firms are paid by the contractor and are therefore not entirely independent. At the same time, by having the contractor responsible for the entire geomembrane CQA process, the owner and engineer remove themselves from having to coordinate the process with ongoing construction activities. This is even more important if both the secondary and primary geomembranes are to be tested.

Having the geomembrane CQA implemented though either the engineer or directly by the owner under the guidance of the engineer allows a more selective process that focuses on experience and quality. This follows a quality based selection process similar to that used to select engineering firms. By selecting a geomembrane CQA firm prior to construction, specific design and construction requirements can be incorporated during the design process, thus improving the quality of the electrical leak location survey. However, any components of the electrical leak location system that are required by the geomembrane CQA firm to be installed during construction must be properly incorporated into the contract documents. The engineer's field representative must make sure that electrical leak location system preparations are properly performed during construction. And, most importantly, the owner and engineer assume the responsibility for coordinating their subconsultant with the construction activities of the contractor. Without proper communication and coordination, the contractor may be entitled to delay claims if the CQA and leak location requirements are not properly incorporated into the project schedule. Properly specifying the contractor's obligations and the time allowances during the geomembrane CQA and the electrical leak location survey should alleviate these problems.

Having the owner/engineer contract the geomembrane CQA firms directly appears to be the best approach to ensure that there is no conflict of interest and that the design and specification process incorporates the electrical leak location components to enhance geomembrane CQA.

Construction Requirements

Regardless of who retains the geomembrane CQA firm, there should be several field requirements specified by the geomembrane CQA firm. These include:

- * The number and location of electrodes (location both in plan and within the liner system);
- * Routing of electrical lines to the perimeter of the cell for future electrical leak location survey connections;
- * The level of assistance from the general contractor in establishing field control and other related tasks;
- * The need for additional water to wet the liner surface. If the geomembrane and layers above the geomembrane have not had sufficient rain, one can assume that water will be needed;
- * Whether the leak detection system will need water added to it to improve continuity below the liner system; and
- * Whether the geomembrane installer should be on site during the electrical leak location survey so that repairs can be immediately made and retested.

Electrical Leak Location Field Survey Criteria

Because the most significant geomembrane damage is caused by construction machinery while placing earth materials on the geomembrane, it is most important to conduct a leak location survey after earth material is placed on the geomembrane. If more than one layer of earth materials is placed on the geomembrane, it is technically better to perform the leak location survey after the first layer is installed. However, the moderate gain in the leak detection capability is usually negated by scheduling requirements. To be efficient, contractors overlap the installation of multiple layers. Therefore, to perform the leak location survey on the first layer would require the leak location contractor to be on site longer, and at least a part of the leak location survey to be in the critical path of the project schedule.

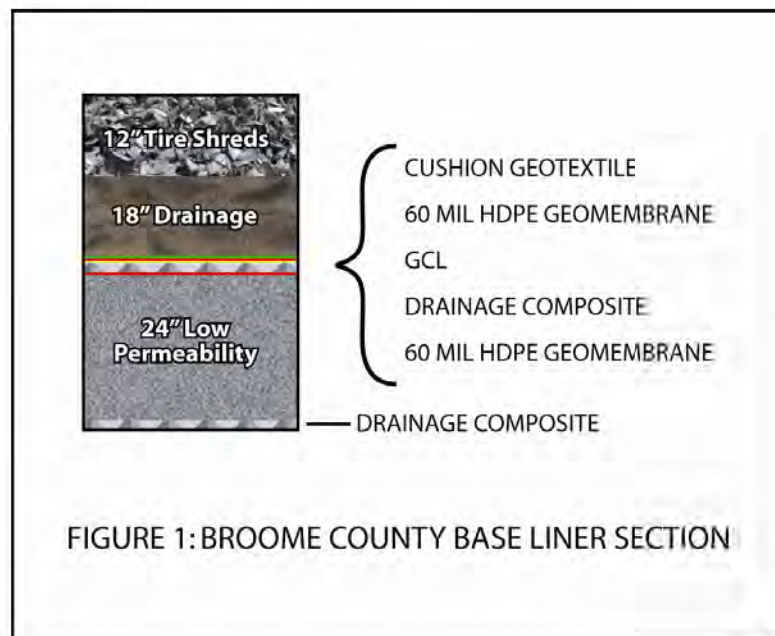
As previously mentioned, particularly for installations with a geocomposite above the geomembrane and at arid sites, the most thorough rationale is to perform a leak location survey of the bare geomembrane to detect smaller leaks, and then perform a leak location survey after the earth materials are installed to detect construction damage. The water puddle method must be performed on the bare geomembrane. The geomembrane must remain exposed with no cushion geotextile, drainage composite, etc. installed. This approach also allows for quick repair of

defects as the geomembrane is already exposed. Covered liners require the careful excavation of soil and the removal of geosynthetics prior to making repairs.

Some designs now include the use of shredded tires to provide some or all of the drainage capacity, physical separation between waste and the liner system, and frost protection in colder climates. While the shredded tire insulates the liner system from cold temperatures, they also insulate the liner system from the electrical signal that we are trying to measure. Therefore, unless extraordinary measures are attempted, testing must be performed prior to placing the shredded tires. Some designs have a final filter geotextile installed on the uppermost earth material layer. Electrical leak location surveys should be conducted before the geotextile is installed. This sequencing also facilitates repair of the leaks.

CASE HISTORY

The Broome County, New York Section IV Landfill Expansion provided an excellent example of using a total approach to enhance geomembrane CQA (Smith). The Broome County Section IV expansion consisted of approximately 4.8 hectares (12 acres) of double composite liner, 4 hectares (10 acres) of which comprised the floor of the cell. The base liner section is depicted in Figure 1.



The entire cell drains by gravity through a single, HDPE pipe penetration. The owner-engineer agreement specified that the engineer would retain the geomembrane CQA firm. Qualifications and quotes were solicited and the engineer worked directly with the selected geomembrane CQA firm during design of the cell. The contract documents specified that geomembrane CQA, including an electrical leak location survey, would be performed on the primary liner and also incorporated installation of required electrical leak location system components as part of the contract. The contractor was diligent while placing the drainage material, using a minimum of 0.9-meter (3-foot) thick haul roads for truck traffic and placing material in the morning. The

contractor also used an excavator to place the drainage material instead of pushing the material with low ground pressure bulldozers and risking the possibility of creating wrinkles in the liner system (even though this approach was not specified in the contract documents). Communication was maintained with both the contractor and the geomembrane CQA firm. The contractor provided laborers to assist the CQA firm with establishing field control and with adding water to the liner system ahead of testing. The electrical leak location results identified a total of 8 leaks in the liner system or less than 0.4 leaks per hectare (< 1 leak per acre), which is much better than previously reported data. All of the leaks were smaller than 6 mm (0.25 inches) and were the result of construction activities. One leak was a scratch that was most likely caused by a dropped piece of geomembrane installation equipment. One leak, although identified by the electrical leak location survey and checked twice during the survey process, was never visually identified. This may have been a broken needle in the underlying GCL penetrating the geomembrane from below. Even though this signal may have been weak, it could be detected because a total approach was used to enhance geomembrane CQA.

The action leakage rate for the primary liner system has been less than 1 liter/hectare/day (less than 0.1 gallons/acre/day.) The only time that higher leakage rates were observed was when the liner was purposely flooded with 1.5 to 1.8 meters (5 to 6 feet) of water at the pipe penetration, even though it is highly unlikely that the leachate head during operations would ever reach this level. There was a minor defect in the pipe boot, which was repaired, and the system has performed as designed and well below regulatory limits since.

CONCLUSIONS

The primary function of a geomembrane is as a liquid barrier. Historic CQA practices have focused on testing geomembrane seams rather than detecting leaks in the sheet. Electrical leak location surveys are the only commercially proven method to detect leaks through geomembranes. It is time to adopt a total approach to enhancing geomembrane CQA.

A total approach to geomembrane CQA should include electrical leak location surveys and the process should incorporate liner system design, contracting, leak location survey specifications, survey system preparation during construction, and the performance of the survey. Specific measures can be taken to enhance the electrical leak location signal and improve the quality of the survey. Electrical leak location surveys should be required after the placement of the overlying earth materials for the primary geomembranes of all landfills. Consideration should also be given to testing the secondary geomembranes for leaks. In dry areas and for certain designs, the primary geomembrane should be tested before and after earth materials are emplaced. Both geomembranes of liquid impoundments should be tested for leaks using electrical methods.

Several other factors should be considered during the total approach to enhance geomembrane CQA. These factors are intended to improve leak signal sensitivity so that smaller defects can be more readily and cost effectively detected. However, regardless of the number of these factors that can be incorporated into a given design, the benefits of an electrical leak location survey make it a prudent step for any geomembrane installation.

REFERENCES

ASTM D 6747 Guide for Selection of Techniques for Electrical Detection of Potential Leak Paths in Geomembranes

ASTM D 7002 Standard Practices for Leak Location on Exposed Geomembranes Using the Water Puddle System

ASTM D 7007 Standard Practices for Electrical Methods for Locating Leaks in Geomembranes Covered with Water or Earth Materials

Colucci, P., and Lavagnolo, M.C., "Three Years Field Experience in Electrical Control of Synthetic Landfill Liners," Proceedings of the Fifth International Landfill Symposium, Sardinia, Italy, October 2 – 6, 1995, pp. 437 – 451.

Darilek, G.T., Laine (1989) "Understanding Electrical Leak Location Surveys of Geomembrane Liners and Avoiding Specification Pitfalls," D.L., Proceedings of the 10th National Conference, Superfund '89, Washington, D.C., U.S.A., Nov. 27-29, 1989.

Darilek, G.T., Menzel, R., Johnson, A., (1995), "Minimizing Geomembrane Liner Damage While Emplacing Protective Soil," Geosynthetics '95 Conference Proceedings, Nashville, Tennessee, U.S.A., Feb. 21 - 23, 1995.

Duffy, D.P., "Landfill Economics, Part II, Getting Down to Business," MSW Management, Forester Communications, Vol. 15, No. 4, July/August 2005, pp 68-74

International Association of Geosynthetic Installers White Paper, "Improving Geomembrane Installations," IAGI, St. Paul, MN, Jan. 30, 2004

Kerkes, David, J., "Geomembrane Weld Specifications Are Too Conservative," Geotechnical Fabrics Report (now Geosynthetics), IFAI, Roseville, MN, Vol. 13, No. 6, August 1995, pp 33-36.

Koerner, Robert, M. and Koerner, George R., "Providing Flexibility in Destructive Seam Sampling/Testing," GRI White Paper #3, Geosynthetic Institute, Folsom, PA, Feb. 13, 2003.

Laine, D.L., Miklas, M.P. (1989) Detection and Location of Leaks in Geomembrane Liners Using an Electrical Method: Case Histories," Proceedings of the 10th National Conference, Superfund '89, Washington, D.C., U.S.A., Nov. 27-29, 1989.

Laine, D.L., Darilek, G.T. (1993), "Locating Leaks in Geomembrane Liners of Landfills Covered With a Protective Soil," Geosynthetics '93 Conference Proceedings, Vancouver, British Columbia, Canada, March 30 - April 1, 1993, pp 1403-1412.

Nosko, V., Andrezal, T., Gregor, T., Ganier, P., "SENSOR Damage Detection System (DDS) - The Unique Geomembrane Testing Method." Geosynthetics: Applications, Designs and Construction. Proceedings of the First European Geosynthetics Conference, EuroGeo 1. Rotterdam, Netherlands. 743-748.

Peggs, I.D., (1999) Mobile Geoelectric Liner Integrity Surveys: Planning Ahead, Proceedings of Geosynthetics '99 Conference Proceedings, IFAI, Roseville, MN, pp 627 – 634.

Peggs, I.D., (2006) Designing For Geoelectrical Liner Integrity and Leak-Location Surveys, Geosynthetics, IFAI, Roseville, MN, August – September, 2006, pp 44 - 45.

Phaneuf, R. and Peggs, I.D., Landfill Construction Quality: Lessons Learned from Electrical Resistivity Testing of Geomembrane Liners, Geotechnical Fabrics Report (now Geosynthetics) vol. 19, no. 3, April, 2001, pp 28-35.

Rollin, A.L., Marcotte, T., Forget, B., Saunier, P. Leak Location in Exposed Geomembrane Liners Using an Electrical Leak Detection Technique, Proceedings of Geosynthetics '99, Boston, pp 615-626.

Smith, B., Phaneuf, R., and Roche, K., The Evolution of a Better Landfill Liner System, Geotechnical Fabrics Report (now Geosynthetics), IFAI, Vol. 22, no. 6, August, 2004, pp. 20-27.

Tedder, R., "Evaluating the Performance of Florida Double-Lined Landfills," Geosynthetics '97 Conference Proceedings, Vol. 1, IFAI, Long Beach California, March 1997, pp 425-438.

Theil, R., Darilek, G., and Laine, D., "Cutting Holes for Testing vs. Testing for Holes," Geotechnical Fabrics Report (now Geosynthetics), IFAI, Roseville, MN, Vol. 21, No. 5, June/July 2003, pp. 20-23.

CONTACT:

Mr. Bradford Smith, PE, BCEE

Stearns & Wheeler, LLC

One Remington Park Drive

Cazenovia, NY 13035

Phone: 315-655-8161

Email: blsmith@stearnswheler.com

What the IAGI Approved Installation Contractor Can Do for You

Laurie Honningford, International Association of Geosynthetic Installers; David McLaury; Brian McKeown

ABSTRACT

The International Association of Geosynthetic Installers (IAGI) has developed two programs designed to assist engineers, owners and regulators in improving geosynthetic installations on their job sites. The purpose of the proposed paper is to inform users about the Certified Welding Technician and the Approved Installation Contractor programs developed by IAGI to raise the level of professionalism and improve the quality of geosynthetic installations. IAGI's goal is for engineers and regulators who work with geosynthetic installers on their job sites to embrace this program and require that Approved Contractors be used on their job sites. This paper and presentation will discuss the specifics of each program. IAGI's Certified Welding Technicians program tests the skills and knowledge of the geomembrane welders who put liner into landfills, landfill caps and wastewater treatment facilities. The second program, currently being launched by IAGI, is the Approved Installation Contractor program. This voluntary program sets a minimum level of standards that installation companies must meet to become an Approved Installer. The purpose of this paper is to inform engineers, owners and regulators about the advantages of requiring that the contractors who work on the landfill sites employ Certified Welding Technicians and participate in the Approved Installation Contractor program. The International Association of Geosynthetic Installers is a group of geosynthetic installers dedicated to advancing the state of the practice in the industry. We welcome all stake holders as members of our organization.

OVERVIEW

More than 10 years ago a group of geosynthetic installers got together in Nashville, Tenn. to form what became the International Association of Geosynthetic Installers (IAGI). The purpose of IAGI was to advance the state of the practice in the geosynthetic installation community. Their first project was to write an installation guideline that IAGI continues to use to this day. Another project was to test the welding technicians in the field to determine if they are qualified to do the job. The Certified Welding Technicians program was launched in 1999. The IAGI Board of Directors then took up the issue of recognizing companies that meet a minimum level of professionalism in the field. Discussions about defining this program took more than four years to refine. In May of 2006 the Approved Installation Contractor (AIC) program was launched.

BACKGROUND

Based upon dialogs with member installers, member suppliers, outside experts in the containment field, and government officials involved in the geomembrane business, the International Association of Geosynthetic Installers (IAGI) began developing a new standard of performance – the Approved Installation Contractor Program (AIC). Industry professionals involved in AIC program planning had a specific task in mind – to establish a benchmark for installation contractors.

The mission of the AIC program is to establish criteria for recognizing geosynthetic installation companies that meet a minimum level of professionalism, experience and business practices. The goal is to promote growth in the geomembrane installation industry and promote better quality workmanship.

Installation companies that participate:

- Show a commitment to being a professional in the geomembrane installation industry.
- Differentiate their company from other companies that do not employ the basic business practices required by IAGI's AIC program.
- Control their own destiny – installers have determined what the industry standard practices should be before it is imposed upon the installers by outside organizations and regulatory bodies.

Companies achieving AIC status prove that they have made a commitment to implementing a business strategy that strives to get the job done right the first time – from experienced personnel to training programs for their field and supervisory personnel, to having the financial backing to overcome the daily challenges that happen on most construction sites. With any construction site comes Murphy and Mother Nature and they typically have a different set of plans for your job site than those nice ones drawn up and stamped. The experienced contractor knows how to handle those challenges – because they have done it many times before.

Why does the AIC program benefit engineers and owners?

- It gives the user community tools to select experienced professionals for their projects. In all project specifications, engineers and owners can require installation companies to have AIC status.
- It helps get the best installations completed on projects.
- It raises the level of professionalism for installation companies.

REQUIREMENTS

AIC applicants must meet requirements in the following areas: corporate history and business practices, insurance verification, safety training, and professional competence and experience. Below is a list of information required on the AIC submittal form:

- Company history and information
- Minimum 500,000 square feet installed annually
- Ability to be bonded
- General liability insurance
- Worker Compensation insurance
- Automobile liability
- Safety Training
- Health and safety orientation program
- Drug-free work program
- Professional competence/experience
- Certified Welding Technicians (CWT) required (CWT is an official IAGI certification program for welders.)

All of the above information is reviewed and verified by IAGI's third party reviewer, Sims & Company CPAs. Applicants also must submit for verification written references from the following industry professionals: engineers; contractors/owners; and geosynthetic manufacturers. Each of the items submitted are reviewed and verified by Sims & Company CPAs. This entire process must be repeated annually.

Each company must provide Company information and history for the AIC form. General company information is provided including a listing of offices, contacts, company incorporation and registration information.

IAGI recognizes that for people who deal primarily in landfills, 500,000 square feet isn't a large amount of liner. IAGI is comprised of many different types of liner installers, some of whom are small specialty contractors. This square footage requirement was established so these specialty contractors, many of whom are excellent in their own market segment, could also get the AIC designation. So if an engineer's job requirements dictate the need for more square footage of experience, the engineer's specification may have to read something like "An IAGI Approved Installation Contractor – with more than 1,000,000 square feet of annual material installation," or what requirement is for the job being conducted.

In relation to the bonding requirements, AIC designated companies do not have to own a bond at the time of AIC is granted, but they must have a company who is willing to issue a bond to them. The bond company will do due diligence on the company's financial status. Those companies who may be unable to complete a job will not be able to get a bonding letter. This is the financial component of the AIC designation. Owners and/or engineers may have a minimum level of bonding needed so they might want to designate an AIC company with a minimum bonding capability that meets their internal or their client's minimum standards.

For many owners the idea that some installers would not carry minimal levels of insurance covering their company seems elementary for anyone running a business. The sad fact is that some "low bidders" do not carry this minimum type of insurance. The AIC Company must provide evidence of general liability insurance, worker's compensation and automobile liability insurance. The information that is provided is verified by the accounting firm.

CWT REQUIREMENT

The Certified Welding Program along with safety training requirements is the training component of the AIC program. The CWT program was designed to test the skill and training of those welders who work on geomembrane installations. There are hundreds of CWTs in the industry. Engineers and owners should feel confident specifying that CWTs be on their job site.

Dr. Robert Koerner did a lot of work early on to qualify and quantify what a good geomembrane material would look like. Once industry professionals had good material in the field and a way to determine what was good and what wasn't – the natural progression was to next determine whether this excellent material was properly installed.

Dr. Koerner also used to say: “the weakest link in any installation is the seams,” hence much work was done to define what constitutes a good seam. GM-19 is the industry standard that most industry professions refer to today.

IAGI first tackled the welder – the person in the field who can make or break your job. The material can be lovely, the project perfectly designed, the site nicely prepared, but if the person running the welder doesn’t know what he or she is doing – all of the work that went before it is wasted.

The CWT test consists of two components, a written exam and hands on welding exam. The hands on component require that the welder test a variety of geomembranes. The welds are sent to third party labs to be tested. The test results are then sent to IAGI’s office for grading. The written exam is 77 multiple choice questions.

Laurie Honnigford, IAGI’s managing director, is often asked if the CWT test is easy – and her answer is always the same. “IF you have a person who knows what he or she is doing in the field, has experience welding, understands the parameters that can influence the quality of the seam and cares about his or her work – the test will not be difficult for the welder. If you have someone who doesn’t meet the above parameters – he or she will likely fail.” IAGI has set up guidelines for administering the tests verbally if reading is problematic for the welder. The CWT test is currently available in Spanish, English and French. IAGI has begun working with contacts in Asian countries to get the test translated into other languages.

Early in this program, some geomembrane installers were naturally concerned about spending lots of money to get their welders tested due to the transient nature of some of the crews. It is an expensive proposition to accomplish this certification. These companies figured they would send their supervisors to get their CWT and the companies then could represent that a CWT was on the job site. Over time, IAGI has learned that the group of people most often failing this test is the supervisors. Supervisors tend to pass the written portion of the test with no problem. However, generally they cannot get through the challenges of the hands on component. The practice of testing only supervisors largely has ended – it became too expensive to test folks who weren’t going to make the grade.

MEETING ALL REQUIREMENTS

Independently, just one of the above requirements alone does not make an installer a good one, but when taken together, they are the basis for a company who strives to complete a job on time, accurately and with superior quality as demanded by the engineer or designer. A company can claim to have installed 500,000 square feet, but this claim doesn’t clarify whether the material was installed well. Each required component of the AIC program serves as a check on another. When a company meets all of the parameters of the AIC program, the industry can be sure that this company is committed to doing a good job – in every aspect of its business.

WHAT AIC IS NOT

IAGI’s AIC is not a certification program, and it is not a substitute for engineers and owners doing their own due diligence. The AIC program gives engineers and owners the ability to specify companies that meet and exceed requirements set by the program, thus ensuring an

installation job well done. IAGI encourages those who specify the AIC designation to familiarize themselves with the requirements of the AIC program and to require standards above the minimum designations if that is part of their internal requirements.

Contact

Laurie Honnigford

International Association of Geosynthetic Installers

Phone : +1-651-554-1895

e-mail iagi@iagi.com

DEVELOPMENTS IN USING INFRARED THERMOGRAPHY FOR THE NONDESTRUCTIVE MEASUREMENT OF GEOMEMBRANE SEAM BOND STRENGTH

Ian D. Peggs, I-CORP INTERNATIONAL, Inc.; Thabet Tolaymat, USEPA – Office of Research and Development

EXTENDED ABSTRACT

It does not make sense to cut holes in geomembrane seams every 150 m so that destructive tests can be performed to ensure there are no holes in the seams! In 1994 Peggs et al reported on work funded by the Electric Power Research Institute on the use of infrared thermography (IRT) for the nondestructive evaluation of seam bond quality every millimeter lengthwise and widthwise of both extrusion and fusion seams, and with the ability to make a hard copy of the data. This preliminary work has recently been renewed with the financial support of the USEPA Office of Research and Development.

Six test welds, some with intended flaws, were made with 1.5 mm thick smooth HDPE geomembrane as follows:

1. “Good” extrusion seam
2. “Good” fusion seam
3. Fusion seam made at speeds of 8.5 fpm, 14 fpm, then 8.5 fpm
4. Fusion seam with water, soil, water, soil sections before welding
5. Extrusion seam with water, soil, moisture, soil sections before welding
6. Fusion seam made at “high” roll pressure.

These samples were subjected to an instantaneous flash of thermal energy using a halogen flash tube which raised the surface temperature about 10°C. The surface temperature along 180 mm of seam was then monitored for up to 30 seconds by an indium/antimony IR camera and analysed using EchoTherm™ software (Shepard, 2006). At locations where the thermal energy could diffuse through the top geomembrane or weld bead and across a well-bonded weld interface the surface temperature dropped significantly. When the weld interface was not well bonded, or when there were voids or particulates on the interface that would provide resistance to heat flow, the surface temperature remained high. Thus, the thermal contours along and across the weld reflect the quality of the weld bead and interface at that location.

Pinholes at the edge of a weld, voids in the weld bead and on the weld interface, dirt in the interface, cuts along the edge of the weld in the bottom liner, and sections removed from the bottom edge flap, could all be seen on the thermogram. Many of these features were marked on the seams for subsequent evaluation by conventional peel testing and cross-sectional microscopy.

Although there were variations and discrete features in the thermograms of both “good” welds none of the peel specimens showed any separation. And even though the welds made at different speeds generated significantly different thermograms there were no differences in peel

behavior except for one of the higher speed specimens that showed a little peel separation. Thus conventional peel testing did not reflect the differences shown by the thermograms.

The soil and wet areas of the fusion seams showed no differences in peel performance but there was also little difference in the thermograms at these locations. However, the major differences in thermograms of the soil and moisture regions of the extrusion seam were well-reflected by the peel behavior, the worst areas completely separating.

Thus extreme differences in the thermograms are reflected in peel performance, but smaller differences that are quite clear in the thermograms are not necessarily matched by conventional peel testing. Therefore IRT facilitates a more sensitive assessment of seam quality.

When the “good” seams that did not peel were sectioned at thermogram locations that implied lower weld quality (white areas), there were particulates on the interface to a degree that was consistent with the size and whiteness of the area on the thermogram. It was noted that the weld bead was not centered over the edge of the top sheet which was possibly reflected in the thermogram. A gap between the two geomembranes at the edge of the upper sheet was evident in the thermogram compared to adjacent areas where the two surfaces were in contact (but not welded).

Lighter and darker areas in the thermograms could be related to differences in the width and intensity of the weld interface and heat-affected zones in thin slice microsections viewed by light transmission microscopy. This was evident in both the “good” fusion weld and the welds performed at different speeds. The faster speed appeared to generate a better looking weld, but this is a little inconsistent with the thermograms and peel performance. A more comprehensive study is required. It would be expected that a weld that is less well-defined and that blends smoothly into the two geomembrane microstructures would be the better weld.

A very small but discrete spot was sectioned but no flaw could at first be found. The microtome was progressively advanced until a small oval pocket of dirt (about 1 mm by 0.3 mm) was found on the interface.

It is clear that IRT will nondestructively provide detailed information on the nature and quality of both extrusion and fusion welds, including information that may not impact the ability of the weld to practically perform its function. Work still remains to relate thermogram features to microstructural characteristics of the welds and to identify those microstructural characteristics that critically affect the mechanical performance of the weld, for all flaws will not be critical.

There is no question that IRT has the potential to nondestructively confirm or deny the acceptance of extrusion and fusion geomembrane welds. It remains to properly evaluate the thermograms generated.

REFERENCES

Shepard, S. "Understanding Flash Thermography", *Materials Evaluation*, May 2006, pp 460-464.

Peggs, I.D., Miceli, G.F., McLearn, M.E., "Infrared Thermographic Nondestructive Testing of HDPE Geomembranes Seams: A Feasibility Study", 5th International Conference on Geotextiles, Geomembranes and Related Products, Singapore, September 1994, pp 941 - 944.

CONTACT:

Ian Peggs
I-Corp International
6072 N. Ocean Blvd
Ocean Ridge, FL 33435
Phone: 561 369 0795
Email: icorp@geosynthetic.com

A CONTAMINANT MIGRATION EQUIVALENCY ASSESSMENT FOR THE QUEENS MUNICIPALITY WASTE MANAGEMENT FACILITY IN NOVA SCOTIA, CANADA

Craig B. Lake, Assistant Professor, Department of Civil Engineering, Dalhousie University, Halifax, Nova Scotia; Gordon Balcombe, Senior Environmental Engineer, ABL Environmental Limited, Dartmouth, Nova Scotia; Tom Austin, Senior Environmental Engineer, ABL Environmental Limited, Dartmouth, Nova Scotia

ABSTRACT

Several publications have addressed equivalency assessments for geosynthetic clay liners (GCLs) utilized in basal liner systems for municipal solid waste landfills. This paper examines a case history of utilizing one such equivalency assessment to justify the implementation of a geosynthetic clay liner into the basal liner system of the Region of Queens Municipality Waste Management Facility in Nova Scotia, Canada. Existing site soils near the landfill consist of silty sand to sandy silt with compacted hydraulic conductivity values well in excess of regulatory requirements for the primary compacted liner system. To avoid excessive costs of importing compacted clay or constructing a sand-bentonite liner system, a geomembrane/GCL/compacted silty sand primary liner system was proposed. Contaminant migration equivalency assessment results are presented in the paper to justify the equivalency of the proposed barrier system to the regulatory primary liner system.

1. INTRODUCTION

The Region of Queens Municipality (RQM) Waste Management Facility was commissioned in 1989 to provide municipal solid waste disposal service to the residents of Queens County, Nova Scotia and the Town of Liverpool, Nova Scotia. The facility provides management and disposal of municipal solid wastes, construction demolition waste, septic lagoons and transfer for compost wastes. The facility also accepts ash from a nearby pulp and paper mill. Until January 2006, the facility was operated as a first generation landfill, with no engineered liner system. The change to a second generation landfill was initiated by changes to provincial guidelines in 1997 that required all landfills in the province to abide by "second generation" landfill guidelines (as will be discussed in the next section) before January 2006. In 2004, work began on designing such a facility adjacent to the existing operating landfill.

The RQM Waste Management Facility is situated over a silty sand to sandy silt (interspersed with gravel, cobble and boulder sized material) glacial till deposit, varying in thickness from approximately 3m to 20m. This surficial soil is underlain by fractured quartzite bedrock. Based on the hydrogeological study performed for the landfill (AMEC, 2005), it was established that a continuous groundwater surface exists approximately 3 m below the ground surface. Subsequent test-pit excavations and borehole investigations performed to evaluate borrow material for the construction of the barrier system established laboratory hydraulic conductivities of the compacted material could range from 5×10^{-7} m/s to 1×10^{-8} m/s. As will be discussed in a later section, these values are well in excess of the 1×10^{-9} m/s specification established by provincial environmental guidelines (NSDEL, 1997). For this particular landfill, the lack of economically available clay in the area presented only two feasible

options for constructing the low hydraulic conductivity barrier materials; geosynthetic clay liners (GCLs) or sand bentonite liners (SBLs). Based on previous economic information available for a SBL system in the province, it was deemed that use of a GCL in combination with site soils could result in excess of \$3,000,000 in savings to the municipality over a 30 year time period). The purpose of this paper is to describe the type of GCL “equivalency” assessment that was performed to justify to the regulator the use of a combination of GCL and site soils for the primary barrier system.

2. BACKGROUND

Existing municipal solid waste landfill guidelines in Nova Scotia (NSDEL, 1997) require the base of landfills to be lined with a double liner system, as shown in Figure 1. The double liner system consists of a primary leachate collection system overlying a primary GM/CCL composite system, a secondary leachate collection system and secondary geomembrane. Geotextiles are to be used as required for protection of the geomembranes placed in the landfill. As stated in the regulations, “all of the components of the landfill should be designed to function over the lifespan of the facility” (NSDEL, 1997). Lifespan is defined in the guidelines as “the period of time in which a facility will produce contaminants at levels which could have an adverse effect if discharged to the surrounding environment”. This design philosophy is similar to the contaminating lifespan concept discussed by Rowe et al (2004) and Ontario provincial municipal solid waste guidelines (MOE, 1998).

In the Nova Scotia guidelines, the CCL used as part of the primary composite liner system must be a minimum of 1 m thick with a hydraulic conductivity of less than 1×10^{-9} m/s. “Alternate technologies”, such as low hydraulic conductivity geosynthetic clay liners (GCLs) or sand-bentonite liners (SBLs) can be proposed within the framework of the guidelines to achieve an “equivalent” barrier system to that specified. As discussed in the Nova Scotia regulatory documents, it is the duty of the designer to demonstrate that the proposed alternate system is “equivalent” to the low hydraulic conductivity (1×10^{-9} m/s) CCL it is replacing. “Equivalency” with respect to GCLs is a topic that has been discussed from several different viewpoints in the technical literature (Koerner and Daniel, 1993; Rowe, 1998; Foote et al. 1999). However, since the primary function of a bottom liner system is to mitigate contaminant migration from the landfill, equivalency comparisons should, as a minimum, include a contaminant migration assessment. As discussed by Rowe et al (1997b) and Rowe (1998) a proper equivalency assessment of a bottom liner system should include all relevant factors influencing contaminant migration through the barrier system such as diffusion, advection (including leakage between the geomembrane and liner contact), sorption (if present), biodegradation (if present), and finite service lives of engineered components. When each of these factors are considered in conjunction with the landfill characteristics (i.e. size and leachate characteristics) and the hydrogeological setting, a proper comparison of equivalency between a CCL and GCL barrier system can be made.

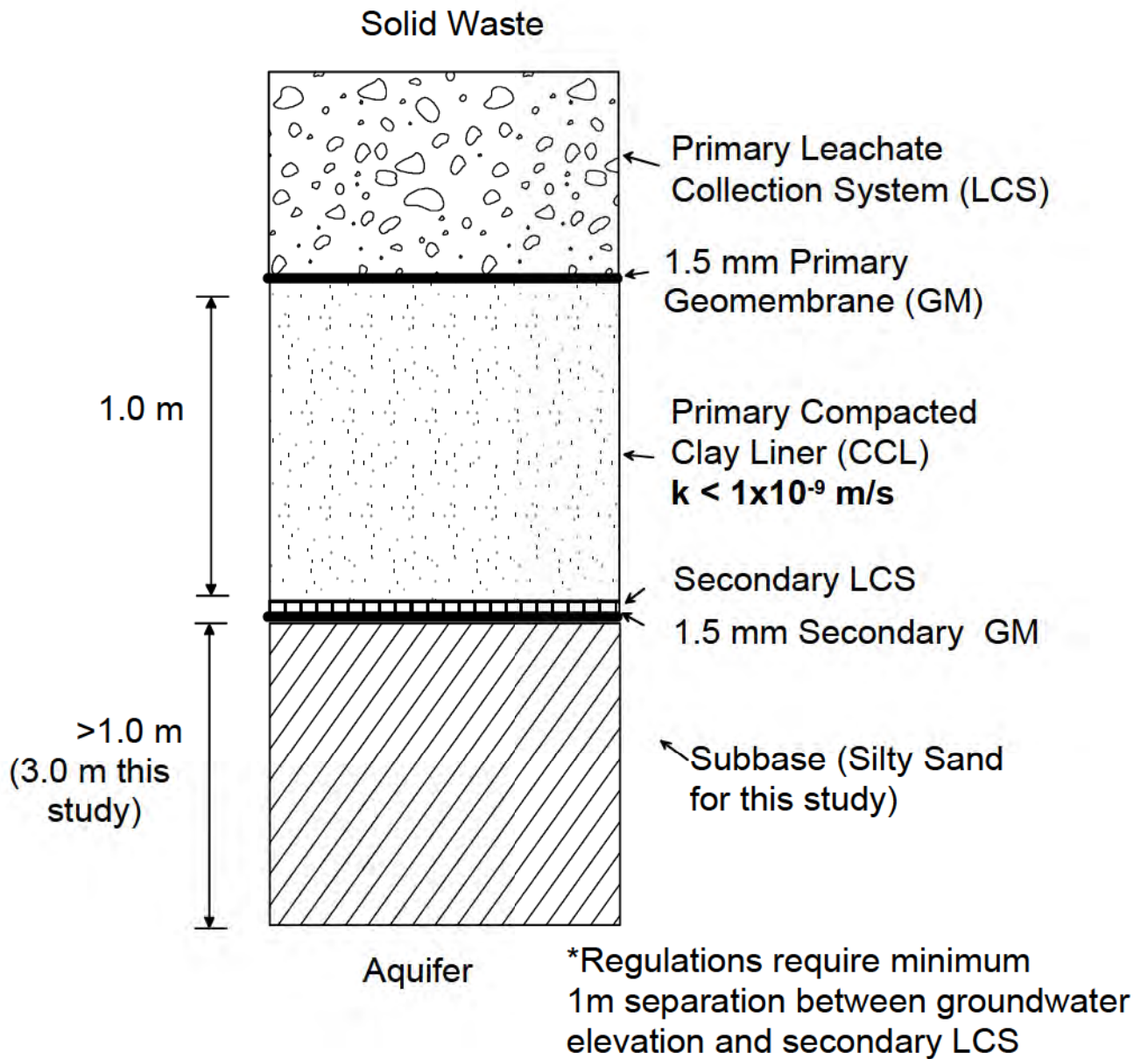


Figure 1. Schematic of Regulated Municipal Solid Waste Landfill Liner System for Nova Scotia (modified from NSDEL, 1997) (*some layers have been left out of schematic for clarity).

3. GCL EQUIVALENCY ASSESSMENT

In the case of the RQM Waste Management Facility, the intention during design was not to substitute the 1m thick primary compacted clay liner shown in Figure 1 with a 0.01m thick GCL, but to use a combination of GCL and a 1.0 m thick compacted soil liner (CSL) constructed of the silty sand/sandy silt site borrow material. In essence, the thickness of the primary barrier system remained the same as the regulated system, as shown in Figure 2. The function of the 1m thick GCL/CSL was to not only act as a hydraulic barrier, but also to act as a diffusion barrier. For design purposes, a conservative value of “exceeded” hydraulic conductivity of 1×10^{-6} m/s was chosen for the CSL. GCLs have shown in the literature to exhibit hydraulic conductivities of less than 1×10^{-10} m/s, even when exposed to various municipal solid waste leachates (Petrov and Rowe, 1997).

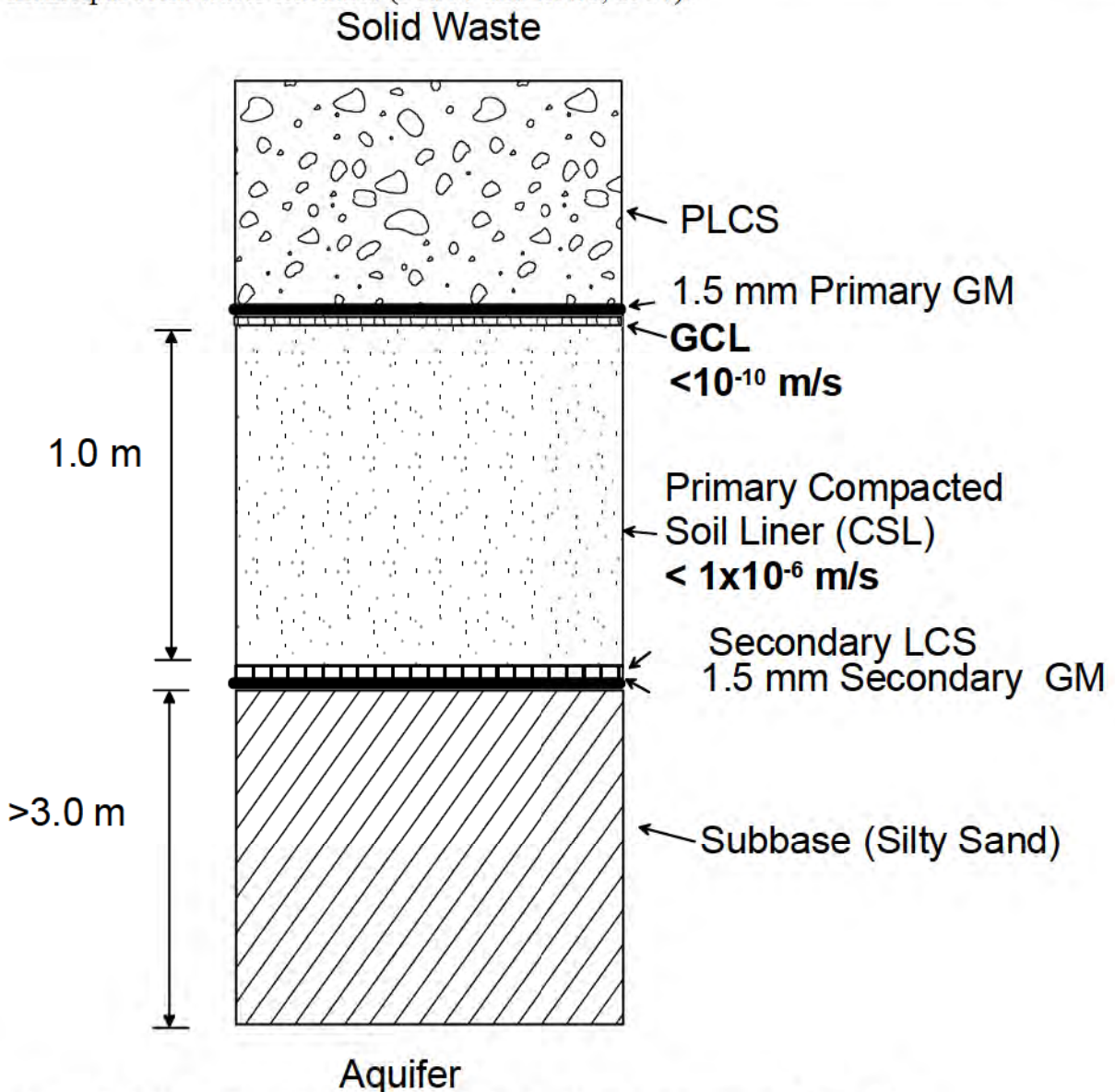


Figure 2. Schematic of GCL alternate technology for proposed landfill.

To assess the “performance” of the barrier system proposed in Figure 2, contaminant transport analyses were performed with the computer program, POLLUTE (Rowe and Booker, 1999). POLLUTE has been used to back-calculate diffusion coefficients for various field containment liner systems (e.g. Lake and Rowe, 2005). This program is specified for use when assessing “alternate technologies” for landfill liner barrier systems as requested in section 3.3(e), subsection 2 of the guidelines (NSDEL, 1997). To facilitate the comparison, the GCL based alternative was compared to the landfill liner standard specified by section 3.3(d) of the guidelines, as shown in Figure 1. The Nova Scotia guidelines do not provide any specific parameters or methodologies to be utilized for the contaminant transport analyses and hence to perform a rationale assessment, general recommendations set forth by the Ministry of Environment of Ontario (MOE, 1998) were used in this contaminant transport assessment. Other parameters necessary for modelling were obtained from the noted literature sources of Table 1.

Two different contaminants were examined in the assessment; chloride and dichloromethane (DCM). Chloride is a relatively conservative contaminant while DCM is an organic contaminant that has been found in low concentrations in MSW leachate (Rowe, 1995). These two contaminants are also suggested critical contaminants to examine for barrier assessments, as specified by the Ministry of Environment of Ontario (MOE, 1998). As shown in Table 1, the DCM half-life in the leachate was assumed to be 10 years. A conservative DCM half-life of 50 years was assumed for the soil based on the results of Rowe et al (1997a). No sorption of DCM to the soil layers was considered in the analysis (a conservative assumption). Other pertinent parameters for the GMs, CCLs, GCL, and site soils are provided in Table 2.

For this equivalency assessment, finite service lives were considered in the contaminant transport modelling to reflect failure of engineered components of the landfill barrier system (see Table 3). It was assumed that the primary leachate collection system was functioning as designed (design leachate level of 0.3 m) and removing leachate for a period of 60 years. At this time, the primary leachate collection system underwent a gradual “failure”; a leachate mound instantaneously developed above the primary liner system to 50% of its maximum height (5 m). At 70 years, it reached its maximum height of 10 m (this is a conservative assumption). At 150 years, the primary geomembrane was assumed to instantaneously fail, causing the leachate mound height to decrease to the point where all infiltration coming into the landfill was migrating through the primary liner system. At 350 years, the secondary geomembrane and secondary leachate collection system was assumed to undergo instantaneous “failure” and all infiltration coming into the landfill (0.15 m/a) was being transferred into the underlying hydrogeological system. A summary of the leakage rates (calculated using the methods outlined by Rowe, 1998) for the three cases considered is shown in Table 3. These times to failure were selected based on suggested service lives of primary and secondary geomembranes put forth by the Ministry of Environment of Ontario (MOE, 1998). The province of Nova Scotia does not provide such recommendations in the provincial guidelines. Although there may be some debate as to actual service lives of geomembrane components, Rowe (2005) suggests that primary geomembranes may last for as long as 160 years and secondary geomembranes as long as 600 years. However, it was decided to be consistent with the Ontario guidelines for the purposes of the regulatory

process. It should be noted that the main issue related with performing the contaminant transport equivalency assessment is consistency in assumptions between the two different systems evaluated.

Table 1. Barrier parameters used in contaminant migration assessment.

Parameter	Units	Value
Length (in direction of groundwater flow)	m	300
Mass of waste per unit area	t/m ²	12
Proportion of chloride in waste	mg/kg	1800
Proportion of DCM in waste	mg/kg	2.3
Initial chloride concentration in leachate	mg/l	2500
Initial DCM concentration in leachate	mg/l	3.3
Percolation rate through waste	m/yr	0.15
Half life of chloride in landfill	yr	∞
Half life of DCM in landfill	yr	10
Aquifer thickness	m	3
Aquifer porosity	-	0.05
Base Darcy Flux (horizontal)	m/yr	1

References: Rowe (1998), Lake and Rowe (2000), Lake and Rowe (2004), Ontario Ministry of Environment (1998)

Table 2. Landfill layer properties.

Parameter	Units	GMs	CCL (NSDEL)	CSL (Site Soil)	GCL	Subbase
Thickness	m	0.0015	1.0	1.0	0.01	3.0
Diffusion Coefficient Chloride	m ² /s	1x10 ⁻¹³	6x10 ⁻¹⁰	7x10 ⁻¹⁰	2x10 ⁻¹⁰	9x10 ⁻¹⁰
Diffusion Coefficient DCM	m ² /s	1x10 ⁻¹²	6x10 ⁻¹⁰	7x10 ⁻¹⁰	2x10 ⁻¹⁰	9x10 ⁻¹⁰
Henry's Coefficient Chloride	-	8x10 ⁻⁴	-	-	-	-
Henry's Coefficient DCM	-	2.3	-	-	-	-
Hydraulic Conductivity	m/s	-	1x10 ⁻⁹	1x10 ⁻⁶	1x10 ⁻¹⁰	1x10 ⁻⁶
Geomembrane-Soil Transmissivity	m ² /s	-	1.6x10 ⁻⁸	7.3x10 ⁻⁸	2x10 ⁻¹⁰	1x10 ⁻⁵
Sorption	-	-	0	0	0	0
Porosity	-	-	0.35	0.35	0.7	0.3

Table 3. Leakage rates for systems considered.

Time Period	Leakage Through Primary Liner [m/yr]	Leakage Through Secondary Liner [m/yr]
-------------	---	---

	<u>NSDEL</u> <u>Standard</u>	<u>GCL/CSL</u>	<u>NSDEL</u> <u>Standard</u>	<u>GCL/CSL</u>
0 to 60 years	4.7×10^{-5}	1.4×10^{-6}	4.7×10^{-5}	1.4×10^{-6}
60 to 70 years	6.4×10^{-4}	1.7×10^{-5}	6.4×10^{-4}	1.7×10^{-5}
70 to 150 years	1.2×10^{-3}	3.2×10^{-5}	1.2×10^{-3}	3.2×10^{-5}
150 to 350 years	0.15	0.15	1.5×10^{-3}	1.5×10^{-3}
350 to 450 years	0.15	0.15	0.15	0.15

4. RESULTS AND DISCUSSION

4.1 Chloride Modelling

Figure 3 shows modelling results of the regulated barrier system compared to the proposed barrier system for chloride. It is interesting to note that the results of the two cases for chloride are essentially indistinguishable from each other (i.e. the graphs of the NSDEL regulated case and the GCL/CSL alternative plot on top of each other). Chloride is a conservative inorganic contaminant, since it is assumed that it undergoes no sorption/degradation in the landfill or the soil during its migration through the landfill barrier system. For the two different barrier systems examined, aquifer chloride concentrations are well below the typical chloride drinking water objective of 250 mg/L for the size of the landfill considered. This is not surprising for a high density polyethylene (HDPE) geomembrane double-lined barrier system. HDPE geomembranes have been shown to be excellent diffusive barriers to ionic compounds such as chloride (Rowe et al., 1995). As discussed by Lake and Rowe (1999), mass transport of inorganic contaminants such as chloride across HDPE geomembranes will be governed by leakage through a few small holes in the geomembrane. This concept is illustrated by the results shown in Figure 3, where even for a 10 m high leachate mound above the barrier systems examined, the chloride impact in the aquifer prior to 350 years (secondary geomembrane failure) was approximately zero for each of the three cases. After secondary geomembrane “failure”, flushing of leachate from the landfill occurs, causing a maximum chloride aquifer concentration of approximately 4 mg/L for each case to occur at approximately 360 years. Based on the results shown for chloride, it appears as if for the conditions examined herein, the proposed GCL/CSL proposed alternative to the regulatory specified liner system is equivalent.

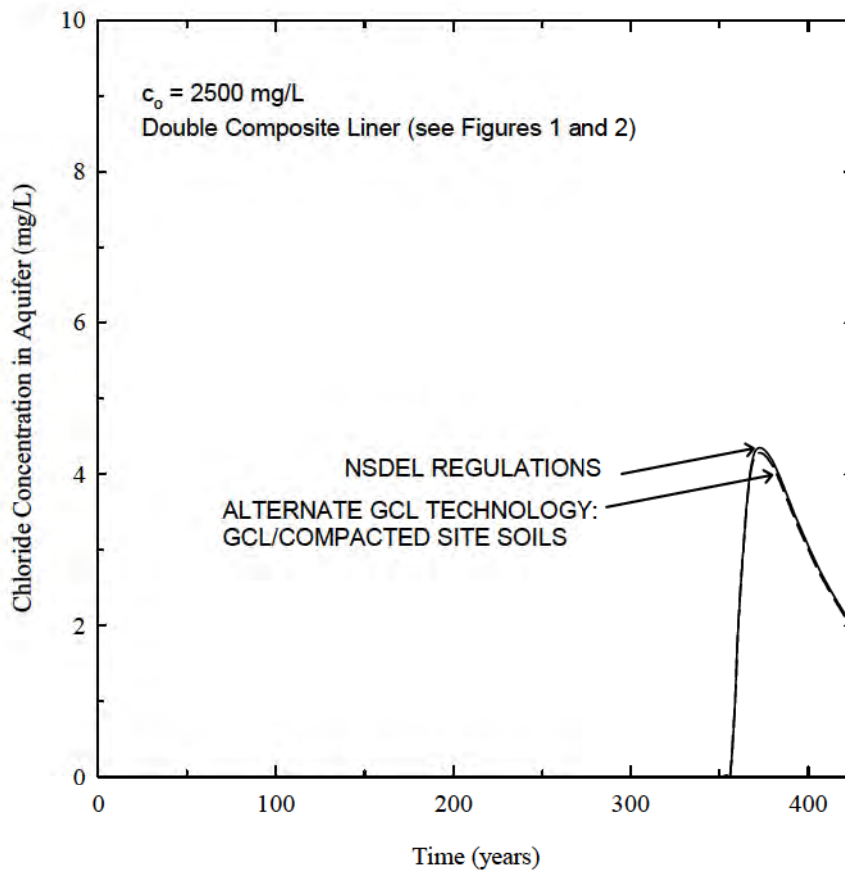


Figure 3. Chloride modelling results, GCL/CSL liner system compared to Nova Scotia regulatory liner system.

4.2 Dichloromethane (DCM) Modelling

Volatile organic compounds such as DCM are often present at low levels in municipal solid waste leachate (Rowe, 1995). Small VOC molecules such as DCM will migrate more readily through HDPE GMs than chloride (Sangam & Rowe, 2001) and hence are important to consider for design of municipal solid waste barrier systems. Contaminant migration of DCM through the double lined systems of the cases considered in Figures 1 and 2 will not be controlled by leakage through GMs, as for chloride, but by diffusion and degradation of the compound as it migrates through the barrier system (Lake and Rowe, 1999).

Figure 4 shows results for DCM. Relative to the chloride results in Figure 3, it can be seen that peak DCM impact in the aquifer occurs relatively quickly (approximately 100 years) for each case examined. The regulated barrier system results in DCM peak concentrations of 10 ug/L, which are much lower than the typical Maximum Acceptable Concentration (MAC) value of 50 ug/L specified by many drinking water guidelines. Figure 4 also shows the GCL/CSL system performs slightly better than the regulated system, indicating that for all practical purposes, the alternative GCL lined barrier system is equivalent to that of the regulated case for DCM (and chloride).

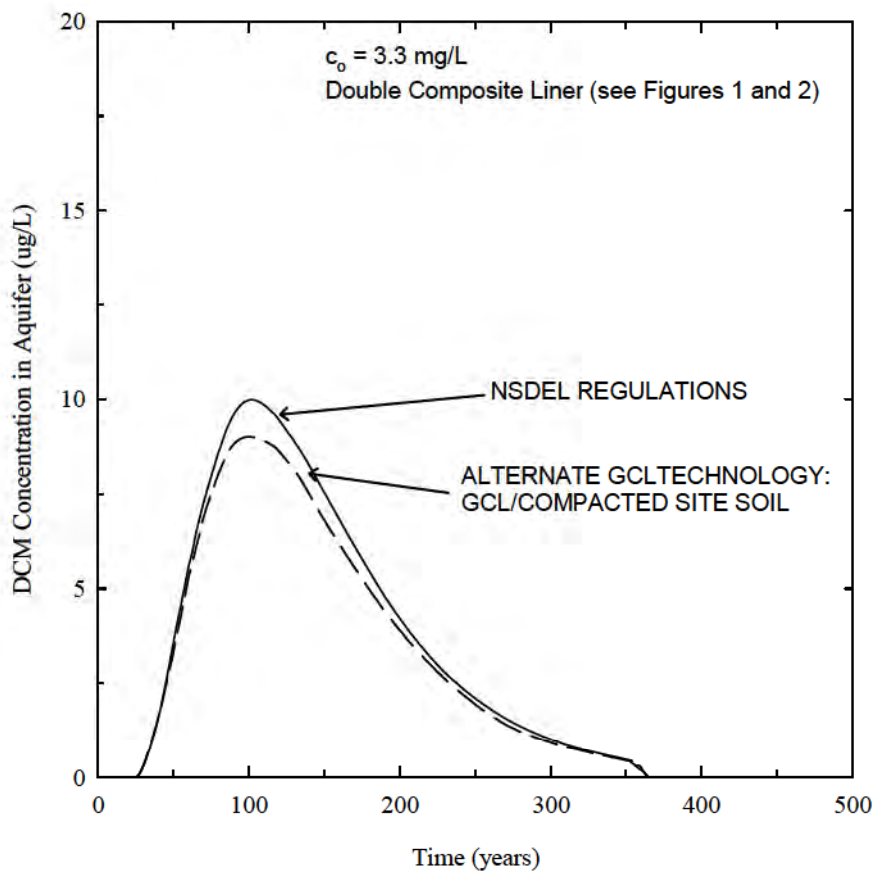


Figure 4. DCM modelling results, GCL/CSL liner system compared to Nova Scotia regulatory liner system.

The main reason for similar DCM aquifer concentrations for the two different liner systems is that the total thickness of the double lined system is the same. Although there are variations in the two liner contaminant transport properties, the diffusion and degradation of DCM by the total soil thickness is essentially controlling the contaminant migration through the liner system. The majority of its migration is controlled by the soil thickness separating the landfill from the aquifer. If the thickness of the primary CSL was reduced to 0.7 m, there would be more diffusive flux through the liner and less biodegradation in the soil. Practically speaking, even though chloride results would suggest a thinner barrier system (lower cost) would be adequate at preventing chloride impacts, the same hypothesis will not hold true for DCM.

It is important to recognise that the theoretical aquifer concentrations shown in Figures 3 and 4 represent concentrations at the down-gradient edge of the landfill. Since the down-gradient edge of the landfill will be at least 100 m away from the property boundary, further attenuation of concentration levels in the aquifer due to other physical, chemical and biological processes will most likely occur.

5. APPROVAL AND CONSTRUCTION OF THE GCL/CSL LINER SYSTEM

The full equivalency assessment performed for the project was submitted to the Nova Scotia Department of Environment and Labour for review in early 2005. There were no issues or concerns posed by the regulators regarding the assessment performed and along with other design documents, was given approval in mid 2005. The RQM Waste Management Facility is one of seven second generation landfills in the province of Nova Scotia that resulted from the “new” guidelines. Of these seven landfills, five landfills utilize GCLs as part of the primary base liner system. This is one reason for the relatively “smooth” approval process. The only main difference between the RQM facility and that of the other landfills utilizing GCLs in the base is the lack of any clay fraction as part of the primary compacted soil layer.

Construction began in mid 2005 of the liner system. The RQM public works staff acted as general earthworks contractor for the project, with Atlantic Poly Liners Inc. acting as a subcontractor to install the GCL, geomembranes, geotextiles, and geonet components of the barrier system. Construction proceeded well, with only “typical” problems associated with wet weather delaying the projects at various points in time. Most of the delays involved anticipated problems associated with the silty compacted soil liner (CSL) during wet weather events.

6. SUMMARY AND CONCLUSIONS

Based on the assumptions adopted for this comparison, a GCL/CSL system was shown to provide similar protection to that specified by the NSDEL regulated liner system, albeit at an estimated cost savings in excess of \$3,000,000 over a 30 year period. Concentrations of chloride and DCM at the downgradient edge of the aquifer were below typical drinking water guidelines throughout the contaminating lifespan of the proposed landfill. For practical purposes, it could be said that the two liner systems examined are “equivalent” with respect to contaminant transport. Additional analyses performed using the methods described in this paper can also assess other alternative liner systems provided sufficient information is available for modelling the systems.

7. ACKNOWLEDGEMENTS

The authors would like to acknowledge Mr. Brad Rowter, P. Eng., Director of Engineering and Works for the Region of Queens Municipality for permission to publish this paper. It should be noted that the entire analysis performed for regulatory approval has not been presented in the present paper. Other factors such as sensitivity of parameters and hydrogeological conditions were also considered for the original study.

8. REFERENCES

AMEC, 2005. Internal hydrogeological report to Region of Queens Municipality.

Foose, G.J., Benson, C.H. and Edil, T.B. 1999. Equivalency of composite geosynthetic clay liners as a barrier to volatile organic compounds, Geosynthetics 99 proceedings, pp.321-334.

Koerner, R.M. and Daniel, D.E. 1993. Technical equivalency of GCLs to CCLs, Proceedings 7th GRI seminar, Geosynthetics Research Institute, Drexel University, Philadelphia, pp. 255-275.

Lake, C.B. and Rowe, R.K. 1999. The role of contaminant transport in two different geomembrane/geosynthetic clay liner composite liner designs. Proceeding of Geosynthetics '99. pp. 661-670.

Lake, C.B. and Rowe, R.K. 2000. Diffusion of sodium and chloride through geosynthetic clay liners. Geotextiles and Geomembranes, Vol 18, pp.103-131.

Lake, C.B. and Rowe, R.K. 2004. Volatile Organic Compound Diffusion and Sorption Coefficients for a Needle-punched GCL. Geosynthetics International (Special Issue on GCLs), Vol. 11(4), 257-272.

Lake, C.B. and Rowe, R.K. 2005. The 14-Year Performance of a Compacted Clay Liner Used as Part of a Composite Liner System for a Leachate Lagoon. Journal of Geotechnical and Geological Engineering, Vol 23(6).

MOE, Ministry of the Environment, Ontario, Canada, 1998. Landfill standards - a guideline on the regulatory and approval requirements for new or expanding landfilling sites, Queens Printer for Ontario.

NSDEL, Nova Scotia Department of Environment and Labour, 1997. Municipal solid waste guidelines, Government of Nova Scotia, Canada. Available from http://www.gov.ns.ca/enla/waste/docs/Municipal_Solid_Waste_Landfill_Guidelines.pdf (last accessed November 10, 2006).

Petrov, R.J. and Rowe, R.K. 1997. "Geosynthetic clay liner compatibility by hydraulic conductivity testing: Factors impacting performance", Canadian Geotechnical Journal, Vol. 34, No. 6, pp 863-885.

Rowe, R.K., 1995. Leachate characterization For MSW landfills, Proceedings Sardinia 95, Fifth International Landfill Symposium, S. Margherita di Pula, Cagliari, Italy, Vol. 2, pp. 327-344.

Rowe, R.K. 1998. Geosynthetics and the minimization of contaminant migration through barrier systems beneath solid waste, Keynote Lecture, Proceedings of the Sixth International

Conference on Geosynthetics, Atlanta, March, Vol. 1, pp. 27-103, Industrial Fabrics Association International, St .Paul. MN

Rowe, R.K. 2005. Long term performance of contaminant barrier systems. *Geotechnique* Vol. 55, No. 9, 631–678.

Rowe, R.K. and Booker, J.R. 1999. POLLUTE 1-D pollutant migration through a non-homogeneous soil. Distributed by GAEA Environmental Engineering Ltd.

Rowe, R.K., Hrapovic, L. and Kosaric, N. 1995. Diffusion of chloride and dichloromethane through an HDPE geomembrane, *Geosynthetics International*, Vol. 2, No. 3, pp. 507-536.

Rowe, R.K., Hrapovic, L., Kosaric, N. and Cullimore, D.R. 1997a Anaerobic degradation of dichloromethane diffusing through clay", *ASCE Journal of Geotechnical and Geoenvironmental Engineering*, Vol. 123, No. 12, pp. 1085-1095.

Rowe, R.K., Lake, C., von Maubeuge, K. & Stewart, D. 1997b Implications of diffusion of chloride through geosynthetic clay liners, *Geoenvironment '97*, Melbourne, Australia, November: pp. 295-300.

Rowe, R.K., Quigley, R.M., Brachman, R.W.I. and Booker, J.R. 2004. Barrier systems for waste disposal facilities," E & FN Spon (Chapman & Hall), London.

Sangam, H.P. and Rowe, R.K (2001) "Migration of dilute aqueous organic pollutants through HDPE geomembranes", *Geotextiles and Geomembranes*, 19(6): 329-356): 329-357.

CONTACT:

Dr. Craig Lake
Assistant Professor
Dalhousie University
1360 Barrington Street, Room D215
Halifax, NS
CANADA B3J1Z1
Phone: 902-494-3220
Email: craig.lake@dal.ca

Drainage and Filtration

Proposed Design Criteria for Geotextile Biofilters

Dr. Cevat Yaman, RT Environmental Services Inc; Eyup Nazfiz Korkut, PhD, Istanbul Metropolitan Municipality

ABSTRACT

In this paper, the design of layered geotextile filters for biological treatment of septic tank effluent was presented. The goal was to provide design criteria for geotextile biofilters used for septic tank effluent treatment. The important design parameters are hydraulic loading rate (HLR), local temperature, five-day biochemical oxygen demand (BOD₅), NH₃ and TSS (total suspended solids) concentrations, and, most importantly, selected geotextile properties such as AOS (Apparent Opening Size), fabric weight, and the geotextile type, woven or nonwoven.

1. INTRODUCTION

In a laboratory study by using nonwoven geotextile filters, over 90% of TSS, BOD₅ and NH₃ were removed from a wastewater sample (Yaman, 2003), in which HLR of 365 L/m²/day (9.0 gal/ft²/day) was applied in dose and drain cycles to the geotextile biofilter. The result was a little loss in permeability, and ammonia (NH₃) and nitrate (NO₃⁻) concentrations in the effluent were reduced to below 5 mg/l and 10 mg/l, respectively.

2. BACKGROUND

Individual home systems generally treat less than 1000 gallon/day. The smaller the source flow, the higher the fluctuation in flow rate is. Therefore, various daily flow predictive methods are in use for onsite systems. In many states, a lumped 150 gallon/day/bedroom is used, even though the bedrooms themselves don't generate wastewater. This design standard is implicitly based on peak flow per capita (Tchobanoglous, 2003).

Septic systems are, of course, also used by commercial and institutional sources located outside of sewer areas. Unit generation rates are also used. For example "dry" commercial establishments such as retail outlets where wastewater generation is incidental to the operation may be of the form such as 0.125 gallon/day/ft² (Tchobanoglous, 1998). Hence, prescriptive septic system design and review by a local agency would apply for a storm of 10,000 ft², whereas a major retailer with 60,000 ft² under roof would use community scale design and require an NPDES permit.

The premise of this study was that the common observation that microorganisms colonize geotextiles in subsurface drain filters presented an opportunity for treatment. The goal was to develop a compact system with a high sustainable hydraulic capacity that would produce effluent suitable for groundwater discharge. One likely application is to onsite wastewater treatment and disposal systems, which serve about 25% of the nation.

3. CONVENTIONAL SEPTIC SYSTEMS

Sewer systems and treatment plants serve most large communities. However, more than 60 million residents, 25% of the U.S. population, live in homes that are not connected to sewers. Geographical and economic constraints prevent service to most of them. Thus, onsite treatment and disposal is the only available solution, producing more “non-point” pollution sources. Suburban expansion (“sprawl”) often extends beyond practical reach of sewer systems, increasing the number of unsewered homes and other occupied sites. Consequently, the projected need for improved wastewater treatment techniques is now directed to single houses and small communities. As a class, this is now called decentralized wastewater management (DWM), the collection, treatment, and disposal/reuse of wastewater from single houses, groups of homes, and industries, commercial facilities and institutions (Tchobanoglous, 1998). The flow rate determines the appropriate type of treatment system, including decisions on mechanical complexity, operator attention, and detention time and space requirements. The objectives of improved small treatment facilities are to protect public health and receiving environments, and to reduce the costs of treatment. Many existing onsite wastewater disposal systems now perform poorly for one or both of two basic reasons:

- 1- Inadequate hydraulic capacity, often a result of increased living standards and water use
- 2- Incomplete treatment and resulting surface or groundwater pollution

Regulatory standards are increasingly more stringent to address both problems. A high-sustained hydraulic loading rate, the primary interest of the owner, is no longer the sole design criteria. It is increasingly required that the quality of the effluent that reaches the water table not degrade the community water resource. The key issues are NH_3 , NO_3^- and, more recently, viruses. Because the practical amount and sophistication of testing and analysis is limited on the onsite scale compared to community level projects, even dilution usually cannot be demonstrated. Hence, regulations include assuring a 4 ft unsaturated treatment zone above the seasonal high water table, and often, a clay content in the subgrade or sand filter to assist denitrification.

Many sophisticated onsite treatment and disposal systems have been developed, but the standard, from the viewpoint of user economy, is the basic septic system. The two basic components are shown on Figure 1 along with other features; a septic tank and soil absorption or leaching field or bed. A rectangular infiltration bed is shown, but trench systems are also used (Yaman et al, 2005). Gravity flow is used where topography and water table depth allow.

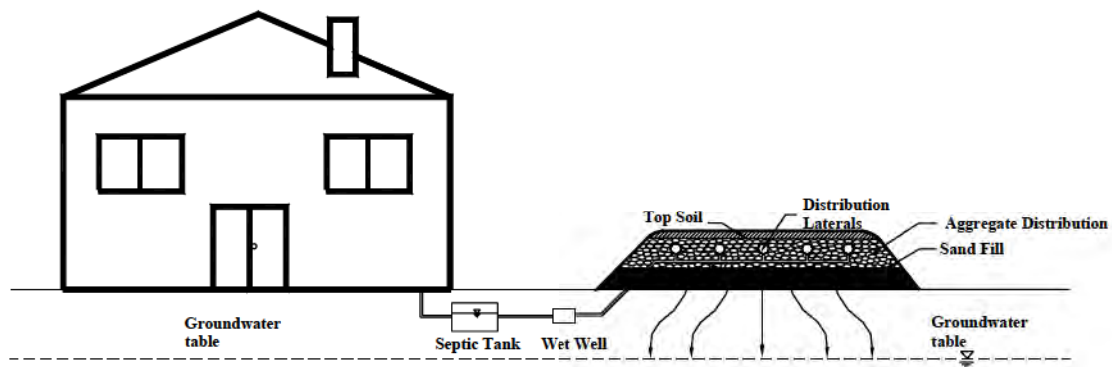


Figure 1 Mounded Septic System

4. PROCESS ANALYSIS

Figure 1 also shows the increasingly more common situation where effluent is pumped up to the infiltration surface to provide the required water table clearance. The additional components are a pump placed in a wetwell that accumulates tank effluent between pump cycles. The pumping system is often designed to distribute effluent in controlled volumes that not only assure uniform distribution, but also flood the coarse aggregate distribution layer to a known depth in each dose. This forces substrate and biomass to distribute vertically, and draws air into the subgrade at each drainage cycle, i.e., a pressure dosing system.

Septic tank effluent has low dissolved oxygen (DO). Thus, it is difficult to reach secondary treatment levels in the leaching field unless the HLR is low and oxygen can be supplied. With continuous flow, the model for a gravity septic system, the subgrade below the infiltration system re-aerates only by diffusion. This requires that the soil be unsaturated and have access to the atmosphere. In buried filters, the covering topsoil can reduce air diffusion into the aggregate layer, especially during wet or freezing weather conditions. Filter surfaces exposed to air circulation, as in buried chambers, offer better oxygen supply. However, when flooding continues for several hours, air diffusion stops (Schwager et al, 1997). Allowable flow rates and application intervals are thus limited to maintain a low degree of saturation under the infiltration surface. When the subgrade has high capillary retention (i.e., “field capacity”), or where a higher strength effluent would overload biological treatment capacity, an intermittent sand filter may be inserted between the septic tank and the infiltration surface. Thus, when an elevated surface such as that in Figure 1 is required, the infiltration bed is usually constructed as a sand bed anyway.

As self cleaning (sludge digestion) biological treatment units, as opposed to just being a means to dispose of liquid by infiltration, the organic loading rate is as important as the hydraulic loading rate. Increasingly, septic systems are being designed and installed as intermittent sand filters. A

study by Buuren et al. (1999), indicated that they can provide removal efficiencies of 90 % COD, 95 % BOD₅, 30 % TN, 40 % TP and 99.9 % fecal coliform at maximum BOD₅ loadings of 10 g/m²/day and hydraulic loading rates of 5-10 cm/day. The organic loading rate can be increased by better aeration and using multilayer filters.

The effective particle size in the top layer of a filter influences the likelihood of clogging. As the TSS concentration decreases, the period between filter cleanings increases as well. The maximum TSS loads at which clogging is prevented are approximately 4, 10 and 13 g TSS / m²/day at surface layer grain sizes of 0.17, 0.40 and 0.68 mm, respectively. Assuming a TSS concentration of 260 mg/L in the wastewater delivered to the septic tank, and 40% TSS removal in the septic tank, the tank effluent would have a TSS = 156 mg/L. This is actually well above the average for modern tanks. Adopting 13 g SS/m²/day as a maximum load, the maximum hydraulic loading rate on the filter would be 83 L/m²/day (8.3 cm/day). As noted earlier, intermittent loading provides better oxygen transfer than continuous loading. Boller (1997) calculated a maximum O₂ flux into the filter of 55 g O₂/m²/day for a sand of 0.85 mm effective size. USEPA recommends a maximum organic load on sand filters of 24 g BOD₅/m²/day. Assuming typical BOD₅ and TKN concentrations (Leak et al., 1981) in primary effluent of 270 mg/L and 60 mg/L, respectively, the total oxygen demand (TOD) can be calculated as:

$$\text{TOD} = (\text{BOD}_5) + 4.5 (\text{TKN})$$

Therefore, the TOD value would be around 540 mg/L. Considering a maximum oxygenation capacity of 55 g O₂/m²/day, the maximum hydraulic loading rate would be around 100 L/m²/day (10 cm/day).

The two issues that will confront any effluent recharge system in the future are nitrogenous materials and viruses.

Luanmanee et al. (2001) investigated the use of a multi soil layering system for treatment of domestic wastewater treatment. The multi soil layering (MSL) system enhanced the natural subgrade soil's performance in wastewater treatment. The efficiency of MSL system varies with the operational parameters. For example, aeration can enhance BOD₅, COD, TSS, TN, and TP removal rates. Special materials may be added to accelerate treatment processes, such as zeolite for NH₄ adsorption, organic material as a denitrification process carbon source, and iron particles for phosphate fixation/adsorption.

Reliance on downstream aquifer processes to provide biological denitrification is referred to a soil-aquifer treatment (SAT). Such systems require anaerobic conditions and an organic carbon source for growth of the denitrifying microorganisms. This amount is about 2.5 mg/L BOD for each mg/L of NO₃⁻ removed. Most secondary effluents have 15 to 20 mg/L nitrogen, mostly as NH₃. Pressure dosing in septic systems uses hydraulic control, i.e., dose and drain, to cycle between aerobic and anaerobic conditions to encourage nitrification/denitrification. However, removals above 50% cannot generally be assured. Converting NH₃ to NO₃⁻, and then N₂ gas may require several cycles. The point of the pressure dosing is to create a thin biofilm, which rapidly degrades organics. Intermediate decomposition products such as NO₃⁻ can be washed out of the upper layers. However, the flooding that delivers fresh NH₃ temporarily depletes oxygen and encourages NH₃ sorption on any clay particles that are present. As the percolate drains, air enters

the soil to restore aerobic conditions for nitrification of adsorbed NH_3 . The next flooding dose re-creates the anaerobic conditions for denitrification to N_2 gas. Thus, permeable soils that have a finite clay content (loamy sands and sandy loams) to detain the nitrogenous constituents are desired.

Yamaguchi et al. (1996) investigated nitrification during unsaturated leaching at a constant flow rate. Nitrification is highly temperature dependent, so the transformation was complete after 3-5 days at 30°C but it took about 50 days at 10°C . It was suggested that a large soil-air ratio is also needed, with the minimum recommended for rapid infiltration (RI) systems of more than $0.10 \text{ cm}^3 \text{ air/cm}^3$ soils. This study suggested a potential for using RI porous media reactors for nitrification of NH_3 concentrations between 20 and 80 mg/L.

5. MICORBIAL ISSUES

Bacterial populations in effluent have both positive (treatment) and negative (pathogens) implications. Craun (1985) reported that contaminated groundwater causes almost half of the recorded waterborne disease outbreaks, often by subsurface cross-connections between onsite wastewater disposal and wells. Pell et al (1989) monitored the development of bacterial populations in a sand-filter system using a three-chambered septic tank, a sand filter, and eight columns. After steady state conditions were reached, it was found that the wastewater contained over two orders of magnitude higher more aerobic bacteria in the third chamber compared to the first chamber of the septic tank. On the 10th day, the bacterial population on the surface of the sand filter increased significantly, and reached a peak on day 24. As anaerobic conditions developed, the number of aerobic bacteria decreased and sulfate-reducing bacteria increased. In the sand filter surface layer both aerobic and denitrifying bacteria increased in numbers until days 65 to 75, thereafter remaining in a steady state at around 10^8 bacteria/gr-dry sand. The populations of NH_4 and NO_2^- oxidizing bacteria both started at low levels, but increased to 10^5 to 10^7 /gr-dry sand until days 70 to 95. At steady state, the bacterial population occupied 8 % of the pore volume in the sand surface layer.

Pathogens in the wastewater are degraded or scavenged by naturally occurring soil microorganisms (Kadlec et al, 1996). Scandura et al (1997) studied the survival and transport of a model enterovirus (BE-1) and fecal coliform bacteria in the sandy soils treating effluent from four septic treatment systems. The systems were seeded seasonally with known amounts of BE-1. The fate of BE-1, fecal coliform and other wastewater parameters were monitored for three months in the seeded wastewaters and groundwater monitoring wells. BE-1 levels in seeded wastewater decreased exponentially with a 3-day hydraulic residence time, but it was detected in monitoring wells as early as 1 day after seeding, persisting for two months. Virus detection was higher in winter than in summer. It was associated with soils having the lowest clay content, elevated groundwater pH and shallower vadose zone. Under optimum conditions, virus reductions were as high as 9 log₁₀, but in systems with the most coarse (sand) soils and higher water tables (most shallow vadose zones); there was extensive groundwater contamination by viruses and other wastewater parameters.

Ausland et al. (2002) monitored the removal of fecal coliforms and fecal streptococci over a period of 13 months in 14 buried pilot scale filters that treated septic tank effluent. The effects of

grain size, hydraulic loading rate and wastewater distribution method were investigated. Two natural sands and two lightweight aggregates were used. Intermittent doses ranging from 20 to 80 mm/day in 12 doses per day were applied to the filters by uniform pressure distribution or by point application in gravity dosing. The removal rates of fecal coliform were three orders of magnitude higher in the media with the finest grain sizes as compared to the coarsest media under the same conditions. Higher removal rates of fecal streptococci were observed in pressure-dosed filters than in gravity dosed filters. As the hydraulic loading rate increased, the removal rates of fecal coliform and fecal streptococci decreased. At retention times lower than about 50 hours, there was a correlation of 0.96 between retention time and removal of fecal coliforms. Retention times longer than 50 h produced almost complete removal of fecal coliforms.

6. DESIGN OF THE GEOTEXTILE BIOFILTER

This section provides information on design criteria if the geotextile biofilters were used to treat septic effluent of a single house with three bedrooms. The design flowrate for septic effluents is based on either the number of people living in the house or the number of bedrooms. As described earlier, in most states it is common to use a design flowrate of 150 gal/day/bedroom. Therefore, a design flowrate of 450 gal/day/bedroom will be selected. The geotextile treatment unit for this single house will resemble Figures 2, 3, 4, 5, and 6, which show different details of a mounded geotextile septic system. The reasons for using a mounded system can be explained as follows:

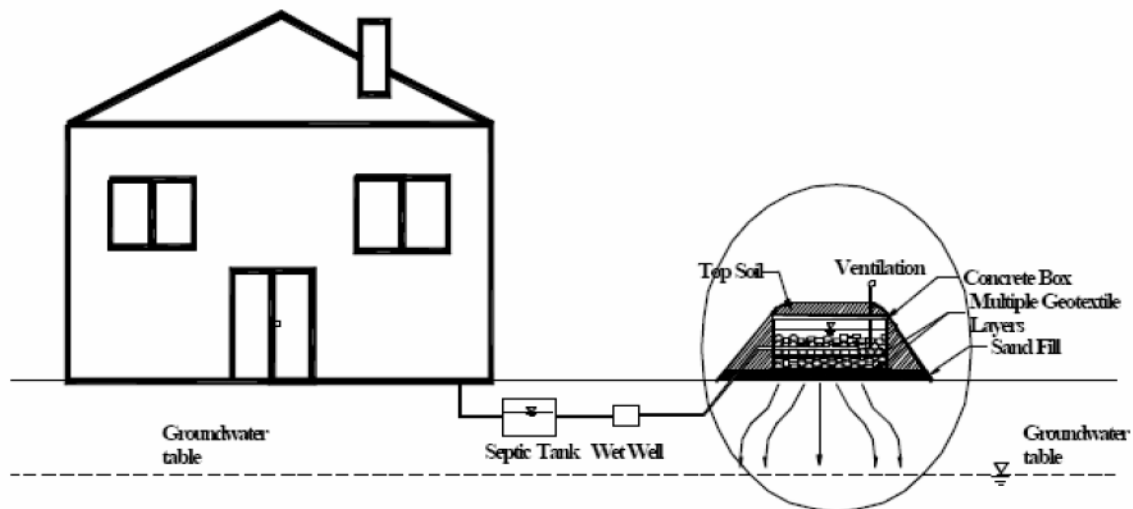


Figure 2 Cross Section of a Mounded Geotextile Septic System

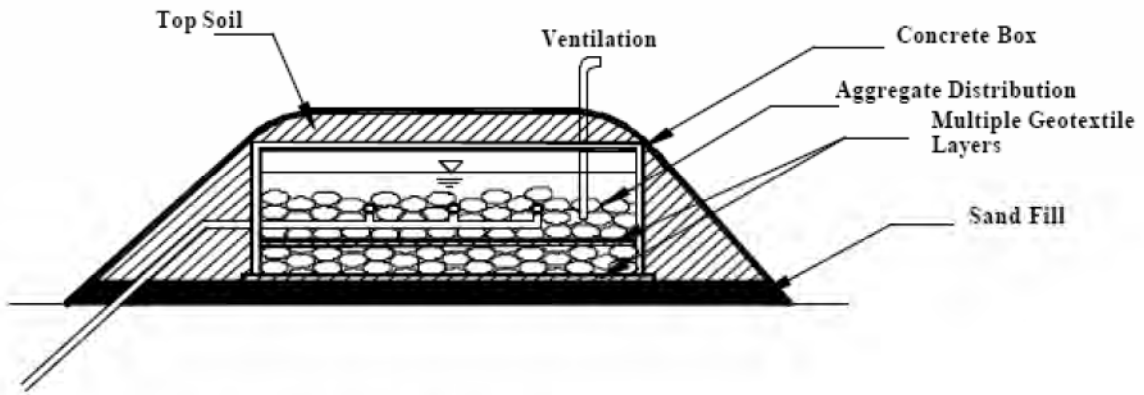


Figure 3 Geotextile Biofilter for Septic System

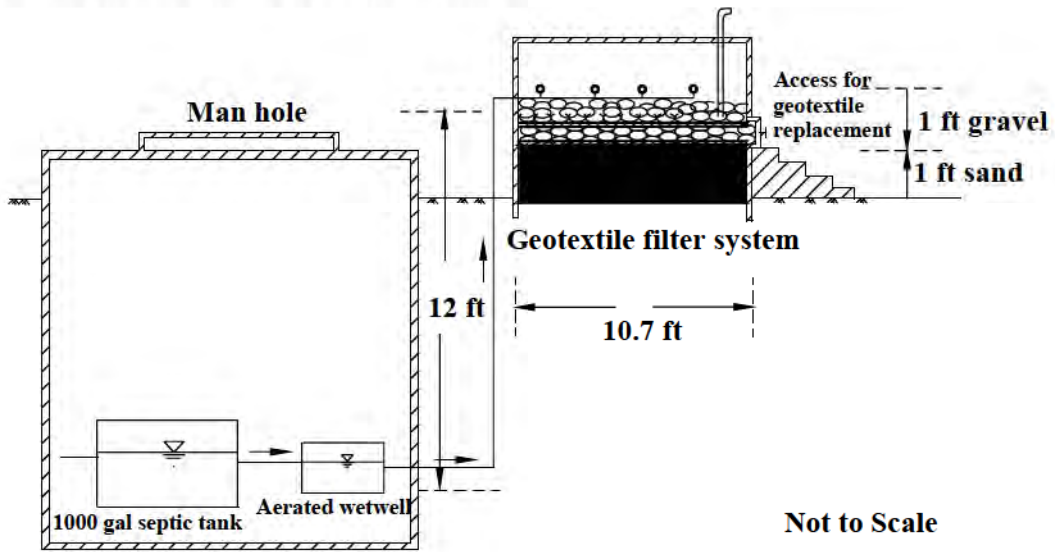


Figure 4 Schematics of Septic Tank, Aerated Wetwell, and Mounded Geotextile Biofilter

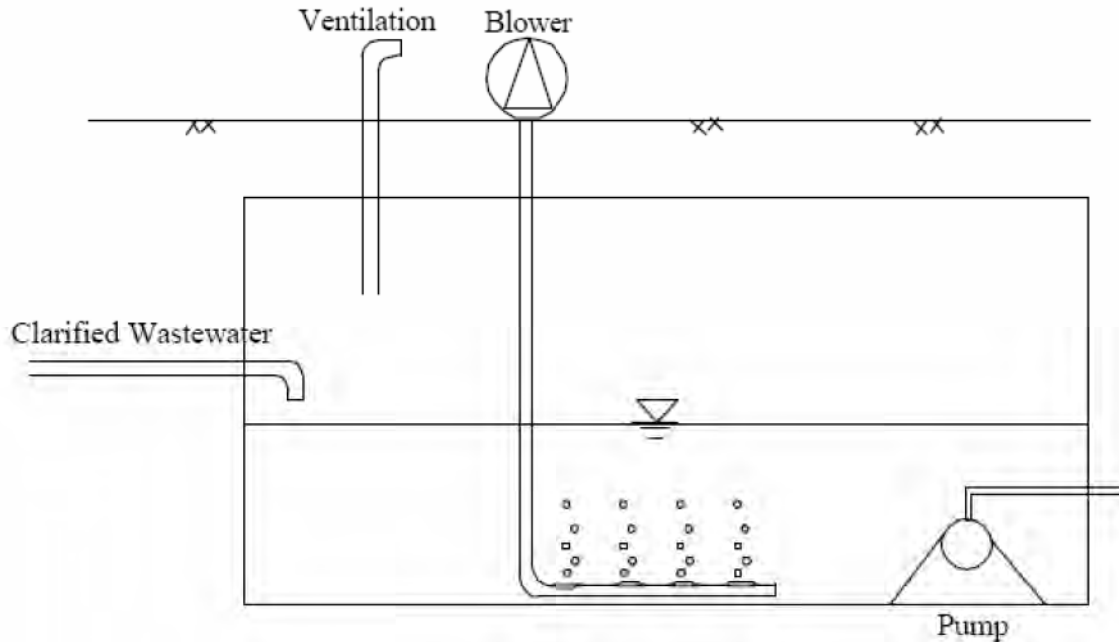


Figure 5 Aeration Wetwell for Geotextile Biofilter

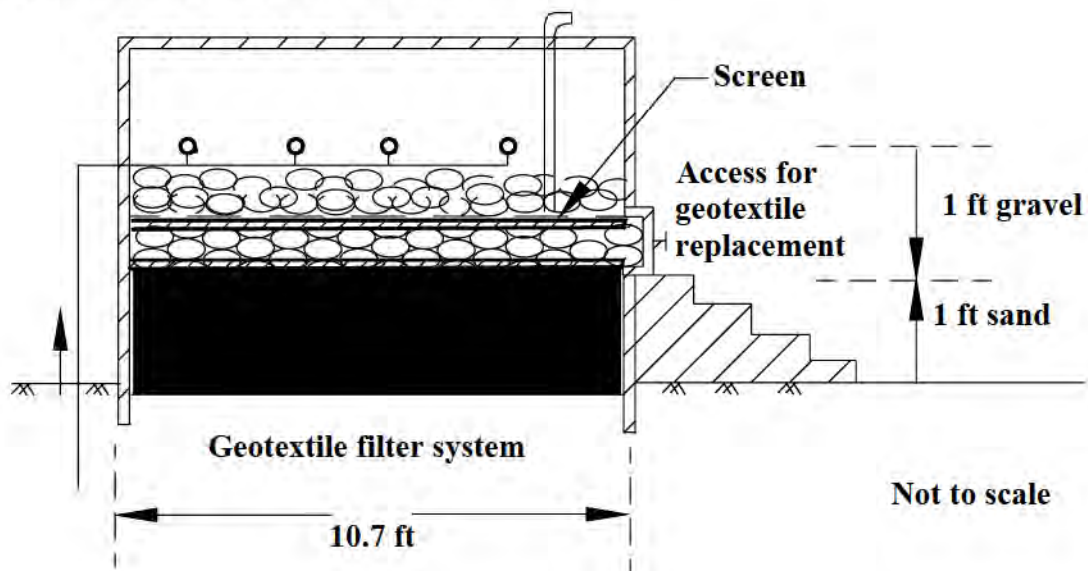


Figure 6 Detailed Profile of Geotextile Biofilter

1-groundwater level is assumed to be close to the surface, and

2-easy access to the treatment unit if geotextile replacement is needed

Total thickness of 24 inches (2 ft) treatment unit will include two layers of geotextile placed in 12 inches (1 ft) fine gravel layer with 12 inches (1 ft) coarse sand beneath the lower geotextile. The gravel layer provides even wastewater distribution over geotextile and captures coarse

particles. The coarse sand layer beneath the lower geotextile is assumed to be permeable enough to distribute the effluent to groundwater without causing any mounding.

Table 1 Typical Composition of Septic Tank Effluent with Kitchen Grinder (Tchobanoglous, 1998)

Parameter	Without Tank Effluent Filter Concentration (mg/L)	With Tank Effluent Filter Concentration (mg/L)
BOD ₅	190	140
COD	400	300
TSS	85	30
NH ₃	35	35
TKN	31	31
Organic N	66	66
Total P	16	16
Oil and Grease	30	20

Table 1 shows typical parameters for septic tank effluent with and without effluent filter. As shown, the septic tank effluent filter provides 25 % reduction in BOD₅ and 65 % in TSS. However, dissolved parameters such as NH₄, organic N and total P are not reduced with the use of septic tank effluent filter. Typical BOD₅ value of the septic tank with effluent filter is 140 mg/l. In order to achieve good BOD₅ removal, a HLR of 5 gallon/day/ft² would be used. This HLR value is still much higher than the HLR values used in typical septic sand filters. The minimum HLR used in Yaman's (2003) laboratory study was 9 gallon/day/ft² (365 l/m²/day). Reducing the HLR in half would eliminate the problem that higher BOD₅ (140 mg/l) would create. The effluent filter is designed mainly to capture the particles and delay the clogging in the septic sand filter. It is also assumed that a kitchen food-waste grinder is installed to the sink. The influent concentrations for the geotextile biofilter are taken from Table 1. The design parameters are selected as follows:

$$Q \text{ (flow rate)} = 450 \text{ gal/day}$$

$$\text{BOD}_5 = 140 \text{ mg/l}$$

$$\text{TSS} = 30 \text{ mg/l}$$

$$\text{NH}_3 = 35 \text{ mg/l}$$

$$\text{Organic N} = 31 \text{ mg/l}$$

$$\text{TKN} = 66 \text{ mg/l}$$

$$\text{Oil and grease} = 20 \text{ mg/l}$$

$$\text{HLR} = 5 \text{ gallon/day/ft}^2$$

$$\text{Dosing cycle} = 4 \text{ dose/day}$$

$$Q \text{ for each dose} = 450/4 = 112.5 \text{ gal/dose}$$

$$\text{Pump capacity (PC)} = 100 \text{ gal/min (Tchobanoglous, 2003)}$$

$$\text{Dosing duration} = 112.5 \text{ gal/dose} / 100 \text{ gal/min} = 1.125 \text{ minutes (The pump will work for 1.125 minutes to carry 112.5 gal wastewater to the geotextile filter for each dose)}$$

$$\text{Total head for the pump (TH)} = 12 \text{ ft}$$

$$\begin{aligned} \text{Pump capacity} &= \text{TH (ft)} \cdot \text{PC (gal/min)} \cdot \delta_{\text{water}} \text{ (lb/ft}^3\text{)} \cdot 1 \text{ ft}^3/7.48 \text{ gal} \\ &= 12 \text{ ft} \cdot 100 \text{ gal/day} \cdot 62.43 \text{ lb/ft}^3 \cdot 1 \text{ ft}^3/7.48 \text{ gal} \end{aligned}$$

= 10,015.5 lb-ft/min

1 Horse power = 33,000 lb-ft/min

Pump capacity in Horse Power = $10,015.5 / 33,000 = 0.30$ HP (The pump capacity needed)

Cross sectional area required $A = Q / \text{HLR} = 450 / 5 = 90 \text{ ft}^2$

$90 = \pi \cdot D^2 / 4 = D = 10.7 \text{ ft}$

Gravel thickness = 12 inch (1 ft)

Sand thickness = 12 inch (1 ft)

The maximum removal rates for BOD₅, TSS and NH₃ in Yaman's study (2003) were 97, 95, and 90%, respectively. If these values were taken as removal rates, the final effluent concentrations for this system would be as follows:

BOD₅ initial = 140 mg/l

BOD₅ final = 4.2 mg/l

97 % removal

TSS initial = 30 mg/l

TSS final = 1.5 mg/l

95 % removal

NH₃ initial = 44 mg/l

NH₃ final = 4.4 mg/l

90 % removal

These values are below the discharge standards for surface and groundwater. However, NO₃⁻ that is produced from nitrification in the geotextile biofilter has to be handled in an anaerobic denitrification system. Therefore, it is suggested that a proper amount of carbon source along with sufficient detention time have to be maintained in order to have complete nitrogen removal.

7. PROPERTIES OF GEOTEXTILES SELECTED

Geotextiles are manufactured from polypropylene (PP) or polyester (PET) in many types (woven, needle punched, heat set, etc.) to serve filtration, separation, transmission and reinforcement functions in infrastructure projects (Koerner, 2005). One method of designing with geosynthetics involves determining the product characteristics required for that function. In addition to having measurable hydraulic and mechanical properties that are used in analytical expressions, available products have internal structures and surface textures that have been empirically correlated with behavior in service.

Design of a geotextile biofilter illustrates the sequence of analysis and product specification. Geotextile biofilters are developed based on the findings of a study by G. R. Koerner (1993), which investigated landfill filter clogging using many leachate sources, geotextile types, and test conditions. Leachate was percolated through columns packed with alternating layers of gravel, geotextile, and sand. The filters appeared to provide habitat for what might be called a "planar ecosystem". The premise that geotextiles attract microorganism attachment was implicitly supported by Corcoran and Bhatia (1996). In 1993, they exhumed samples installed in 1988 at

the Fresh Kills landfill in New York City, one of the first uses of geotextile as leachate system filters. The nonwoven geotextiles protected the aggregate drains in trenches excavated in a fine-grained subgrade. Only on the top did leachate permeate the filter directly from the source waste. On the other three sides, the geotextiles were conventional soil filters, retaining the fine-grained soil in place while accommodating the limited flow of leachate percolating through the subgrade. Hence, most contact between the filter and leachate was tangential rather than transverse, i.e., flow along the path where the geotextile was effectively the boundary of the drain channel. Even so, bacteria grew within the fibers of the non-woven geotextile and formed a biofilm that decreased sidewall permittivity.

The intent in Yaman's study (2003) was to take advantage of microorganisms' attraction to geotextile. What is a problem in soil and landfill drainage is an opportunity to protect receiving waters from pollution discharges. However, the feasibility of using geotextile filters to treat wastewater or weather generated flows requires high hydraulic capacity.

Unlike conventional sand filters, which eventually clog and are then replaced, a geotextile biofilter must remain permeable. The clogging potential of the geotextile filter must be carefully evaluated. Then the hydraulic function must be satisfied by selecting a geotextile filter that provides the required cross- plane permeability or permittivity.

An abridged list of the properties reported by manufacturers of the geotextiles used is shown in Table 2. While it is customary to use permeability or hydraulic conductivity (k , in cm/sec), as the property characterizing the fluid flow resistance of a porous media to flow, it is customary to use permittivity (in sec⁻¹ units) in geotextiles.

In Yaman's study (2003), nonwoven geotextiles, NWGT3, NWGT4 and NWGT5, demonstrated the best results compared to woven geotextiles, WGT1 and WGT2. They rapidly formed and retained biomass without dramatic change in permeability. These results were attributed to the products having an interior porosity. NWGT3 and NWGT4 were each made by a different manufacturer, with similar permittivity and AOS, as indicated in Table 2, but different surface textures as a result of the fabrication method (stapled fiber vs. continuous filament).

As noted earlier, Koerner (1993) also showed that needle-punched nonwoven geotextiles displayed the highest residual permeability, whereas heat-bonded nonwoven geotextiles displayed the lowest, and wovens were intermediate.

Table 2 Published Properties of the Geotextiles Studied

Product, Polymer, Type	Apparent Opening Size (AOS), mm	Permittivity, s ⁻¹	Puncture Resistance, kN (lbs)	Trapezoid Tear Strength, kN (lbs)
WGT1 PP	0.600	0.05	0.28 (65)	0.28 (65)
WGT2 PP	0.212	0.28	0.60	0.45

			(135)	(100)
NWGT3 PET Continuous Filament	0.149 – 0.210	2.01	0.50 (115)	0.47 (105)
NWGT4 PP Stapled Fiber	0.212	2.10	0.24 (55)	0.17 (40)
NWGT5 PP Continuous Filament	0.120 – 0.180	1.60	0.53 (120)	0.45 (100)

8. DISCUSSION

Biological activity in this proposed geotextile biofilter can be affected by several environmental factors such as temperature and oxygen supply. Most biological wastewater treatment systems operate in the temperature range of 20-40°C. The rate of biological activity doubles for every 10-15°C temperature rise (Tchobanoglous, 2003). Therefore, the temperature effect on microbial activity is of concern. The geotextile biofilter system must be insulated to minimize the low temperature effects on biological activity.

The proposed geotextile biofilter focused on a pattern of dose and drain methods for numerous reasons. One of which was the need to provide opportunities for air to reach the biomass and prevent the system from going anaerobic. Therefore, to increase the biological activity of the geotextile biofilter, the influent wastewater needs to be aerated in the wetwell (Figure 5).

It is also suggested that periodic filter performance should be monitored by performing permeability tests on the geotextile biofilter. If the residual permeability of the system indicates severe clogging, the geotextile should be either replaced with a fresh one or the system should be backwashed.

Tests were run with successively more favorable operating conditions in terms of producing the desired effluent quality and minimizing the potential for clogging by biomass accumulation. In effect, the latter involves finding the substrate (food) to biomass ratio (F/M ratio) that would maintain active microorganisms in an endogenous, near starvation condition, and thus minimize accumulation of undecomposed organic material. The geotextile biofilter design, shown in Figure 6, is such that it is very easy to replace the geotextile filter if it fails to perform in the system. As mentioned above, another alternative for clogged geotextile biofilters is to backwash the system.

The geotextile biofilter system can also be modified to investigate the alternative operating modes. For instance, the geotextile treatment unit can be dosed continuously rather than intermittently. In both cases, continuous and dose and drain modes, the influent wastewater should be aerated before application to the treatment unit. Further research is needed to investigate the possible modifications of the geotextile treatment system.

9. CONCLUSIONS

Infiltration of septic effluents generally produces some degree of clogging due to growth of biomass. Therefore, groundwater protection and hydraulic performance should be improved by removal of biodegradable constituents before reaching the soil infiltration surface. The premise of this investigation is that geotextiles developed for other purposes can host a treating biomass while maintaining acceptable permeability of the filter itself. A hydraulic loading 205 L/m²/day (5 gallon/ft²/day) would bring TSS, BOD₅, and NH₃ concentrations to secondary treatment limits. This value is much greater than the customary regulatory restriction of 41 L/m²/day (1.0 gallon/ft²/day).

LIST OF ABBREVIATIONS

HLR	Hydraulic Loading Rate
BOD ₅	5-day Biochemical Oxygen Demand
TSS	Total Suspended Solids
AOS	Apparent Opening Size
NPDES	National Pollutant Discharge Elimination System
DWM	Decentralized Wastewater Management
DO	Dissolved Oxygen
COD	Chemical Oxygen Demand
TN	Total Nitrogen
TP	Total Phosphorous
SS	Suspended Solids
USEPA	United State Environmental Protection Agency
TKN	Total Kjeldahl Nitrogen
TOD	Total Oxygen Demand
MSL	Multi Soil Layering
SAT	Soil Aquifer Treatment
RI	Rapid Infiltration
PP	Polypropylene
PET	Polyester
GT	Geotextile
NW	Nonwoven
W	Woven

REFERENCES

Yaman, C. (2003), Geotextiles as Biofilters in Wastewater Treatment,” *A Ph.D. Thesis at Drexel University*, Philadelphia, PA

Yaman, C., Martin, J. P., and Korkut, E. (2005), “Use of Layered Geotextiles to Provide a Substrate for Biomass Development in Treatment of Septic Tank Effluent Prior to Ground Infiltration,” *Journal of Environmental Engineering*, ASCE, Volume 131, Issue 12, pp. 1667-1675

- Tchobanoglous G. (2003), *Wastewater Engineering*, Metcalf & Eddy, Mc Graw Hill
- Tchobanoglous, G. (1998), "Small and Decentralized Wastewater Management Systems," *Mc-Graw-Hill Series in Water Resources and Environmental Engineering*
- Schwager, A. and Boller, M. (1997), "Transport Phenomena in Intermittent Filters," *Water Science and Technology*, Vol.35, No.6, pp. 13-20, 1997
- Buuren, J. C. L., Abusam, A., Zeeman, G., and Lettinga, G. (1999), "Primary Effluent Filtration in Small-scale Installations," *Water Science and Technology*, Vol.39, No.5, pp. 195-202
- Boller, M. (1997), "Small Wastewater Treatment Plants-A Challenge to Wastewater Engineers," *Water Science and Technology*, Vol.35, No.6, pp. 1-12
- Leak, R., Parase, M. A., and Costello, R. (1981), "Denitrification of Black Water with Grey Water," *Journal of Environmental Engineering Div.*, Vol.107, pp. 581-590
- Luanmanee, S., Attanandana, T., Masunaga, T., and Wakatsuki, T. (2001), "The Efficiency of a Multi-layering System on Domestic Wastewater Treatment during the Ninth and Tenth Years of Operation," *Ecological Engineering*, Vol.18, pp. 185-199
- Yamaguchi, T., Moldrup, P., Rolston, S. I., and Tearnishi, S. (1996), "Nitrification in Porous Media during Rapid, Unsaturated Water Flow," *Water Research*, Vol.30, No.3, pp. 531-540
- Craun, G.F. (1985), "A Summary of Waterborne Illness Transmitted through Contaminated Groundwater," *Journal of Environmental Health*, Vol.48:122-7
- Pell, M. and Nyberg, F. (1985), "Infiltration of Wastewater in a newly Started Pilot Sand Filter System: II, Development and Distribution of the Bacterial Populations," *Journal of Environmental Quality*, Vol.18, pp. 457-462
- Kadlec, R. H. and Knight, R. I. (1996), *Treatment Wetlands*, Lewis Publishers, New York, NY
- Scandura, J. E. and Sobsey, M. D. (1997), "Viral and bacterial Contamination of Groundwater from On-site Sewage Treatment Systems," *Water Science and Technology*, Vol.35, No.11-12, pp. 141-146
- Ausland, G., Stevik, T.K., Hanssen, J. F., Kohler, J. C., and Jenssen, P. D. (2001), "Intermittent Filtration of Wastewater-Removal of Fecal Coliforms and Fecal Streptococci," *Water Research*
- Koerner G.R. (1993), "Performance Evaluation of Geotextile Filters used in Leachate Collection Systems of Solid Waste Landfills", *A Ph.D. Thesis at Drexel University*, Philadelphia, PA

Corcoran B. W. and Bhatia S. K. (Bhatia S. K. and David S. L. Eds.) (1996), "Evaluation of Geotextile Filter in a Collection System at Fresh Kills Landfill", *Recent Developments in Geotextile Filters and Prefabricated Drainage Geocomposites*, ASTM STP 1281, ASTM

Koerner, R.M. (2005), *Designing with Geosynthetics*, Prentice Hall, 5th Edition

CONTACT:

Dr. Cevat Yaman

RT Environmental Services Inc

215 W. Church Rd.

King of Prussia, PA 19406

Phone: 484-716-5207

E-Mail: jyaman@rtenv.com

Design Strength for Geonet Geocomposites

Dhani Narejo, Caro Consultants, LLC

ABSTRACT

A very important property of drainage geocomposites is compression strength, which is the stress at which the core of a geocomposite collapses. The transmissivity of drainage geocomposites decreases significantly beyond compression strength, in some cases by as much as two orders of magnitude. Current design methods based on transmissivity - even if the testing is carried out to 100 hours as required by GRI GC-8 and even when a reduction factor for creep is used - do not fully capture the time-dependent behavior of geocomposites. In fact, the GRI procedure GC-8 is invalid at certain stresses as related to compression strength of geocomposites. This paper presents a design method that explicitly considers compression strength and creep failure, i.e., time-dependent failure, of geocomposites. When used in conjunction with current methods of hydraulic design, the suggested design method ensures that the geocomposite would not fail throughout the design life of a project. Because the current design methods do not accomplish this very important design objective, the proposed design method is a significant improvement over the current state of practice. The design method proposes the following equation:

Where FS_{str} is factor of safety for strength, s is compression strength and p is overburden pressure.

An important contribution of this paper is the use of creep data in the derivation of a factor of safety of 2 in the above equation. The author purports to demonstrate that when geocomposites are loaded beyond 50% of their compression strength (i.e., when the above equation is violated), a material failure in compression mode invariably follows. As creep reduction factors in GRI GC-8 are based on a linear relationship between thickness and time, it is shown that the use of GRI GC8 is inappropriate at stresses below a factor of safety of 2 in the above equation.

1. INTRODUCTION

Drainage geocomposites consist of a polymeric core to which a geotextile is bonded on one or both sides. The polymeric core forms the main liquid transmission medium while the geotextile, depending on the boundary conditions, acts as a filter or a friction layer. The flow rate or transmissivity of the geocomposite depends primarily on the polymeric core, with a relatively limited influence of other factors, including geotextile and manufacturing process. Two types of geonet drainage cores are used in landfills in the US: biplanar and triplanar. Figure 1 shows a photograph of a typical biplanar geonet. There are four major manufacturers of biplanar geonets in the US with the same overall structure as indicated in Figure 1. The details of the ribs, such as rib shape, junction, spacing and orientation vary from manufacturer to manufacturer, and therefore, no two products have exactly the same performance.

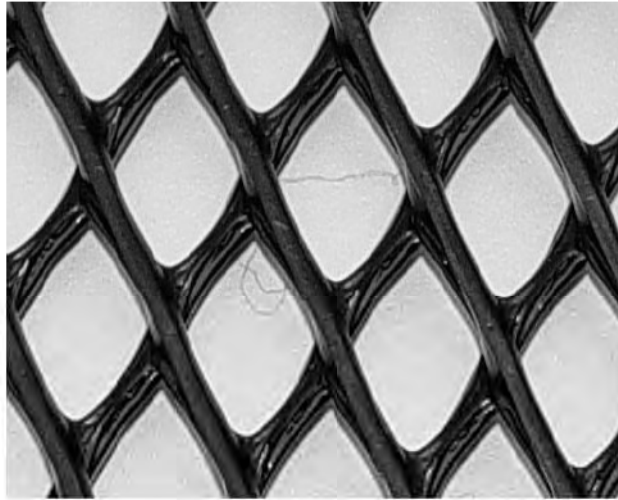


Figure 1 – The Overall Structure of Biplanar Geonets.

The site overburden or compressive stress on a drainage geocomposite depends on the application and varies from project to project. For example, for landfill caps, the overburden stress on the geocomposite is typically due to less than one meter of cover soil. Most commercially available products have strengths much higher than stress imposed by a landfill cover. As such, the strength of drainage geocomposites for landfill covers is rarely a concern. On the other hand, the depth of waste over a landfill leachate collection layer at the base of a landfill can be as high as 150 meters (500 ft.) with a much higher compressive stress. At such stresses, the long-term structural integrity of the core of the drainage geocomposite can be a concern. Many types of geonets can have strengths lower than overburden stress in some of the landfills.

The selection of geocomposite drainage layers is currently based entirely on hydraulic requirements expressed in GRI procedure GC8 as:

$$\theta_{all} = \frac{\theta_{100}}{RF_{cr} \times RF_{cc} \times RF_{bc}} \quad (1)$$

$$FS = \frac{\theta_{all}}{\theta_{req}} \quad (2)$$

where:

- θ_{100} = 100-hour transmissivity from a lab test
- RF_{cr} = reduction factor for creep
- RF_{cc} = reduction factor for chemical clogging
- RF_{bc} = reduction factor for biological clogging
- θ_{all} = allowable transmissivity
- θ_{req} = required transmissivity
- FS = factor of safety for drainage

Although two of the variables in the above equations – θ_{100} and RF_{cr} – do depend on stress, the GRI procedure GC8 does not explicitly account for the strength of the geonet in a geocomposite. The purpose of this paper is to propose a companion design procedure that can be used to calculate the required compressive strength of geonets.

2. DATA AND ANALYSIS:

The compression strength of the core of a geocomposite can be obtained from ASTM test method D 1621. This test method requires applying compressive stress on a circular or square specimen at the rate of 2.5 mm/minute. The result for a typical biplanar geonet is a curve of the type presented in Figure 2. The curves indicate a peak value for each of the products after which there is stress-softening in the material. The peak value is referred to as compression strength or lay-over strength of the geonet.

Geonets are polymeric, and hence, visco-elastic in their compressive mechanical behavior. The values of crush strength indicated would change depending on the rate of application of the compressive stress – being higher for higher rate and lower for the lower rate. One way to consider the effect of time on compression strength of a geonet is to perform compression creep tests. The first step in performing a compression creep test is to obtain compression strength of the geonet according to ASTM D 1621. For example, products A, B, C and D in Figure 2 have compression strengths of approximately 18000 psf, 20000 psf, 31000 psf and 40000 psf, respectively. Obviously, different geonet would have different types of stress-strain behavior and the test must be performed on a representative sample of the product which is to be tested for compressive creep.

Detailed description of compression creep tests on geonets have been provided by Thornton, et. al. (2000) and Narejo & Allen (2004). The tests are performed in a controlled environment at ambient or elevated temperature. When performed at elevated temperature, the tests are referred to as “accelerated creep tests”, of which stepped isothermal method (SIM) is but one variety. A contact stress, equal to a certain fraction of compression strength, say 25%, 50% or 75%, is applied on a test specimen and maintained over a desired time. During this time, the thickness of the specimen is recorded at regular intervals while ensuring that the temperature remains constant. Whether a conventional creep test is used or an accelerated one, the final output of the test is a plot of change in thickness, or thickness retained, with time. Such a plot of a product with a compressive strength of 10,000 psf (478 kPa) is provided in Figure 3. The reader may note that the rate of decrease of thickness (i.e., decrease in thickness per unit time) increases as stress on the specimen is increased. At 1000 psf (47.9 kPa), which is equal to about 10% of strength, the decrease in thickness is the least and the relationship between retained thickness and time is linear. This linear behavior can be extrapolated to obtain thickness at desired project life, say 30 years. The next stress increment shown in the figure is 5000 psf (239 kPa), which equals to 50% of short term strength of the geonet. Again, the response with time is linear. However, at a stress of 7500 psf (359 kPa), the response is linear up to a certain time at which the specimen fails, as indicated by sudden drop in the curve. There is a significant scatter in the data at 7500 psf indicating variability in the material among different test specimen. The material represented in Figure 3, with a compressive strength of 10,000 psf, is not capable of sustaining stress beyond

5000 psf for any significant amount of time. Thus, for all practical purposes, 50% of strength seems to be the upper limit of stress that can be placed on this material.

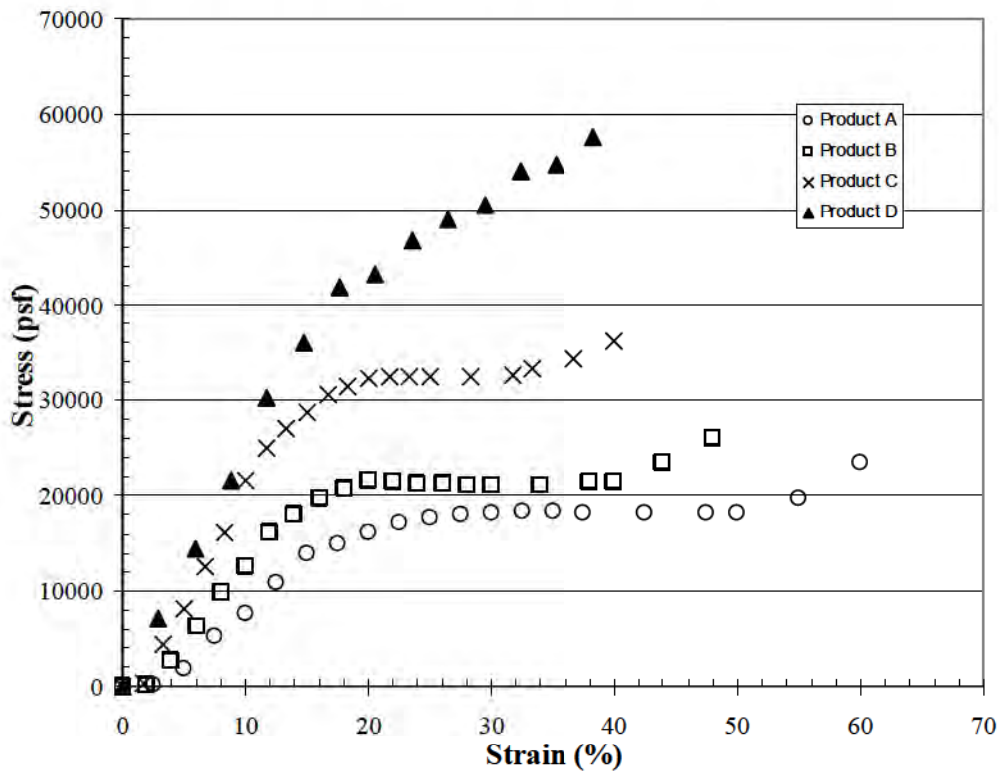


Figure 2 – Compressive Stress-Strain Behavior of Geonets.

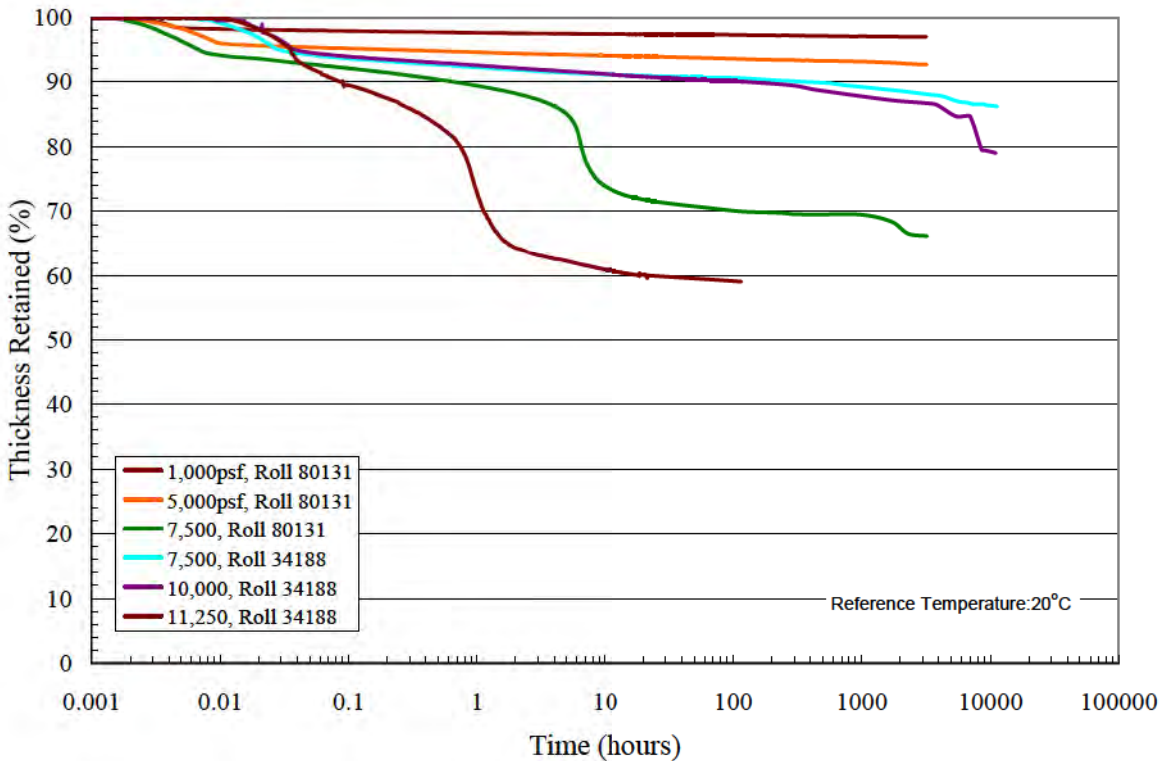


Figure 3 – Compression Creep Response of a Geonet with a Nominal Compression Strength of 10,000 psf (478 kPa).

The creep curves of the type shown in Figure 3 were developed for products with compression strengths ranging from 10,000 psf (478 kPa) to 50,000 psf (2394 kPa). These plots are generally of the type indicated in Figure 3 with the response being linear up to a certain stress beyond which the material failure takes place at some time before 10,000 hours. All tests show that the response between thickness retained and time is linear as long as stress is kept below 50% of strength. However, as soon as the 50% stress limit is exceeded, the geonet fails by creep at some time between the start of the test and 10,000 hours.

A plot of failure time vs. stress as a percentage of strength is presented in Figure 4 based on tests performed on many biplanar geonets. The plot shows the curve becoming asymptotic to the x-axis at a stress of approximately 50% of strength below which failure time can be very long (i.e., much longer than the scale on x-axis). There is a considerable scatter in the data which can be attributed to the nature of the compression tests and variability of the test specimen. Certainly, more testing is necessary to obtain a better representation of this very important relationship.

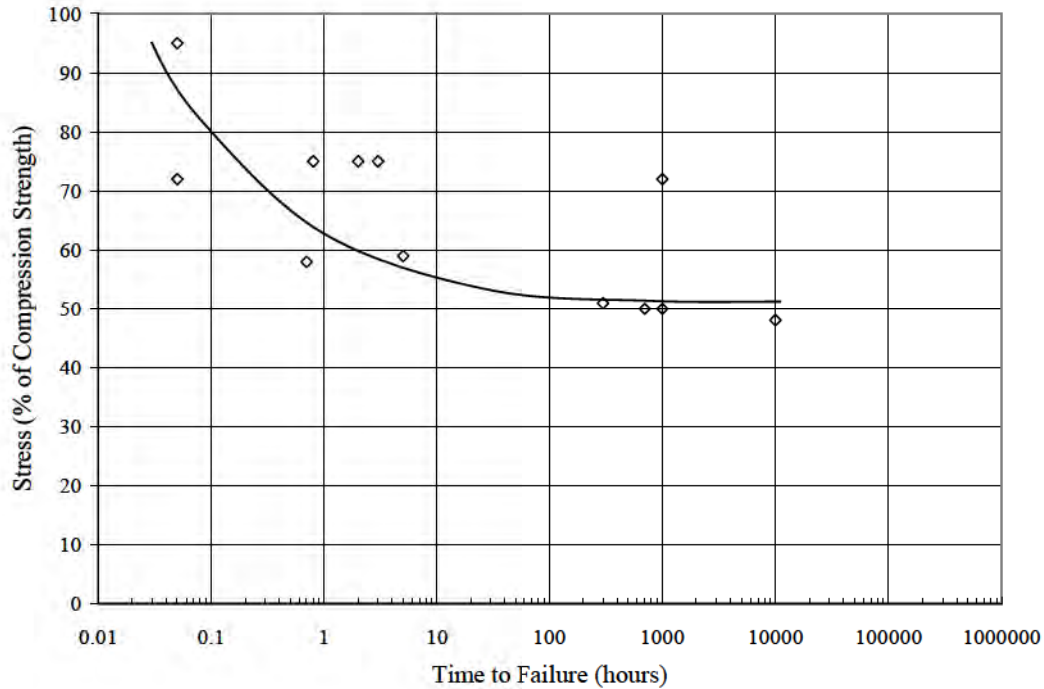


Figure 3 – Relationship between Applied Stress and Failure Time of Biplanar Geonets.

3. DESIGN METHOD

The test data shown graphically in Figure 2 and Figure 3, and supported by similar results from other tests, can be presented in the form of an empirical relationship as follows:

$$FS_{str} = \frac{S}{P} > 2 \quad (3)$$

Where, FS_{str} = factor of safety for strength of geonets, S = compression strength of geonets (ASTM D 1621) and P is stress on a geocomposite in the field. For a landfill leachate collection layer, $P = \gamma h$, where γ = density of waste and h is the height of waste over a liner system.

Equation 3 can have significant implications for the design and selection of drainage geocomposites. It states that the geonet must have compression strength of more than twice the stress it is expected to resist in the field. For example, for a landfill with overburden stress of 10,000 psf over the liner system, the geonet must have compression strength of 20,000 psf. That certainly makes sense based on our understanding of other visco-elastic materials such as geogrids. These materials are never used close to their strength since that would indicate failure due to creep rupture within a short time after construction.

The above design method for strength can be used in association with hydraulic design of drainage geocomposites, according to GRI method GC8, to select a geocomposite for a project. Many different types of geonet cores are available from manufacturers and the one that has

adequate compression strength -- i.e., results in a factor of safety of at least 2 according to Equation 3 -- can be selected as the first step in design. Once the geonet core is decided upon, the next step is to ensure that the geocomposite meets the hydraulic requirements. The material aspect of the hydraulic design is expressed by equations (1) and (2) above from GRI procedure GC8. In addition to other information (refer to the GRI procedure for further details) the procedure requires a reduction factor for creep for the core. This must be obtained for the actual site stress for the exact product being considered for use. For example, if a project has an overburden stress of 5000 psf, then a creep curve at 5000 psf must be obtained from actual creep tests. Alternatively, the manufacturer of the material can be requested to provide the data. Once a creep curve is available, one can calculate creep reduction factors as detailed in the GRI procedure.

4. BENEFITS TO THE END USER

Geocomposite Manufacturers – Drainage geocomposite manufacturers currently price their products according to weight, i.e., the amount of polymer used in a product per unit area. Thus, a product having strength of 50,000 psf is sold at the same price per unit weight as the one that has strength of 10,000 psf. That said, manufacturers do not see the benefit of putting in the extra time and cost into producing high strength materials. A geonet that has a better structural performance, i.e., one that can withstand a higher load can and should be sold at a higher price than the one that can be used at a relatively lower stress. Since the structural performance depends on the manufacturing process, including die design and manufacturing process speed, a premium is justified for products that require more investment in the manufacturing process. The design method proposed in this paper offers a basis for specifying strength of geonets. Manufacturers can use this basis to price their products differently as is done currently, for example, for plastic pipe.

Engineers and Owners – The overriding concern for engineers and owners is to ensure that the geonet will perform its intended function over the life of a project. The design method presented in this paper ensures that the selected product would be structurally adequate throughout the life of a project. In the absence of the proposed method, engineers and owners currently rely on the hydraulic design of geocomposite. Although important in its own right, this does not prevent the failure of the geonet due to crushing from overburden stress. Using the approach presented in this paper, owners can demonstrate adequate long-term performance of their proposed design and gain regulatory approval relatively quickly.

Regulators – The structural integrity of drainage geocomposites is often questioned by regulators during the design approval phase. Using this approach, regulators can ascertain whether the geocomposite being proposed for project does indeed have adequate strength to provide the required hydraulic performance over the life of a project. In the absence of this approach, one has to guess or rely on “fudge factors” to ensure that the geonet has sufficient strength. This approach provides a logical basis for comparing alternative materials being proposed for approval. In certain cases, it can reduce cost to the taxpayer by showing acceptable products from more than one manufacturer.

5. SUMMARY

A method was proposed in this paper that can be used in association with the hydraulic design to ensure that a geocomposite has adequate structural strength against creep-related failure. The method was derived from creep tests on several different geonets. It is seen that a geonet must have compression strength of at least twice the overburden stress to prevent time-dependent failure. The method needs to be developed further by expanding the number of tests and type of materials.

6. REFERENCES

Narejo, D. & Allen, S., 2004. Using the Stepped Isothermal Method for Geonet Creep Evaluation. EuroGeo '3, Third European Geosynthetics Conference, Munich, 01-04 March, 2004.

Thornton, J., Allen, S., Siebken, J. 2000. Long Term Compression Creep of High Density Polyethylene Geonet, Proceedings of EuroGeo 2, 2nd European Geosynthetics Conference.

CONTACT:

Dhani Narejo
Caro Engineering
Senior Engineer
10695 Meachen Meadows Trail
Conroe, TX 77302
Phone: 936-321-1956
Email: dnarejo@caroeng.com

Measuring the Strand Inclination Angle of a Bi-Planar Geonet

Sam Allen, Vice President, TRI/Environmental, Inc.; Jarrett Nelson, Special Projects Manager, TRI/Environmental, Inc.; Dhani Narejo, PhD, Product Manager, GSE Lining Technology, Inc.

ABSTRACT

Understanding the planar flow properties of geonets and geocomposites is critical to drainage designs and applications. While transmissivity testing is the standard test procedure for measuring planar flow performance, the procedure often involves a minimum of 100 hours of test duration, eliminating the ability for immediate and final performance evaluation. In addition to transmissivity testing, several other product properties are relevant to subsequent performance including strand inclination, thickness, density, short-term compression strength and long-term creep properties.

While it is generally recognized that a geonet's structure is related to its performance, certain structural features such as strand inclination are generally not measured or specified. Yet, it is this structure, or geometry, that gives a drainage product its performance capacity and limitations, contributing to both time-dependent response under compressive load and related flow properties. Of specific importance is the nature of the junction between the upper and lower planar ribs in the geonet structure. The angle of inclination of individual strands as well as the relative angle between the upper and lower ribs may be measured.

INTRODUCTION

The measurement of planar flow is a standardized test procedure. Transmissivity testing per ASTM D 4716, *Test Method for Determining the (In-plane) Flow Rate per Unit Width and Hydraulic Transmissivity of a Geosynthetic Using a Constant Head*, specifies a number of test parameters including the requirement for a minimum number of test specimens. For geonets and geocomposites, a minimum of two specimens is required, with allowances for a user defined reduction or increase in the number of specimens for performance oriented tests.

With new awareness of the time dependency of planar flow, and increased use of GRI Standard – GC8, *Determination of the Allowable Flow Rate of a Drainage Geocomposite*, construction projects are incorporating an increasing number of performance oriented 100 hour transmissivity tests for geosynthetic drains. This time requirement has been challenging to accommodate when manufacturing, shipping, and material approval test schedules have been compressed to assure timely project construction. In addition to the time requirement for performance of this test, site specific materials are often required for use during performance tests. These project-specific superstratum and substratum may involve typical landfill construction materials such as compacted clay, cover soils, geomembranes and GCLs. Test specimens as part of designed drainage profiles, increased costs for longer term flow testing and the increased time requirement for final results, have often resulted in reduced test specimens used to secure a measurement of flow. Many performance tests are performed using only a single test specimen, usually secured from the center of the roll width.

These abbreviated test populations born of concern for time and economy are often problematic in their relevancy. Apparent product failures defined by single test specimens are often challenged with regard to their limited representation. This criticism is especially appropriate given variability of the test and material performance. ASTM related round robin test efforts have revealed inter-laboratory reproducibility of up to 40 percent. In addition, the difference between product conformance and failure can sometimes be related to which part of the product roll width the test specimen is selected from. The results of many testing programs seem to suggest challenges with single specimen tests.

These challenges of time duration, specimen number and representation all argue for finding a way to predict product performance in the shorter term. There has been an ongoing effort to find shorter term indicators of expected flow that lend themselves to confident acceptance/rejection criteria. Various attempts and associated challenges in this regard have focused on short-term transmissivity testing, thickness-dependent transmissivity testing, compression strength and strain, and accelerated (SIM) creep testing.

Short-Term Transmissivity Testing

When a history of product testing has suggested a consistent flow vs. time relationship, the testing community has often used early flow measurements to predict longer term flow results. Indeed, because of the immediate nature of primary compression response, early flow tests at 1 to 24 hours can often serve to identify a poor or compliant product with regard to the required flow.

The challenge in this approach is the still cumbersome requirement of setting up a transmissivity test even when a product is failing in the early response. In addition, the flow vs time relationship is not always consistent and can be changed by manufacturing processes, related structural differences, adjacent site-specific materials used during transmissivity testing, etc.

Thickness-Dependent Transmissivity Testing

If a strong thickness vs time relationship is known, it has been suggested that accelerated transmissivity testing may be accomplished through the immediate compression of a planar drain to an agreed upon retained thickness corresponding to a desired time (ex. 100 hours). Immediate flow testing can commence to affect the equivalent of a time dependent flow test (Allen, 2000).

The challenges with this approach are numerous in that one must be confident that “crushing” a drain to a desired thickness yields the same result as a time dependent process. One must also know what the thickness of the drain is throughout loading and testing and this is quite difficult when the drain is surrounded by project specific materials including soils that contribute significantly to total realized system compression. Finally, the uncertainty associated with product thickness vs time behavior requires establishing this relationship for each product style if not each product roll tested.

Compression Strength and Strain

Parallel plate compression testing, as outlined in ASTM D 6364, *Standard Test Method for Determining the Short-Term Compression Behavior of Geosynthetics*, serves to define compression behavior as the drain is loaded. The strain behavior, and strength at specific strains, observed over numerous test specimens may sometimes be excellent predictors of related variability in flow. If a planar drain does not reach the same level of vertical strain, or percent thickness retained, when simply loaded between two loading platens, then differences in planar flow would be reasonable to expect. The figure below shows an example of a simple biplanar HDPE geonet undergoing three modified compression tests under the same load to realize a controlled loading followed by a load dwell at 720 kPa normal stress. These tests are similar to short term compression creep tests and are called ramp and hold compression tests, the purpose of which are to identify the average starting strain of a primary compressive creep curve. The curves suggest a variability of 5% strain after about 15 minutes of loading.

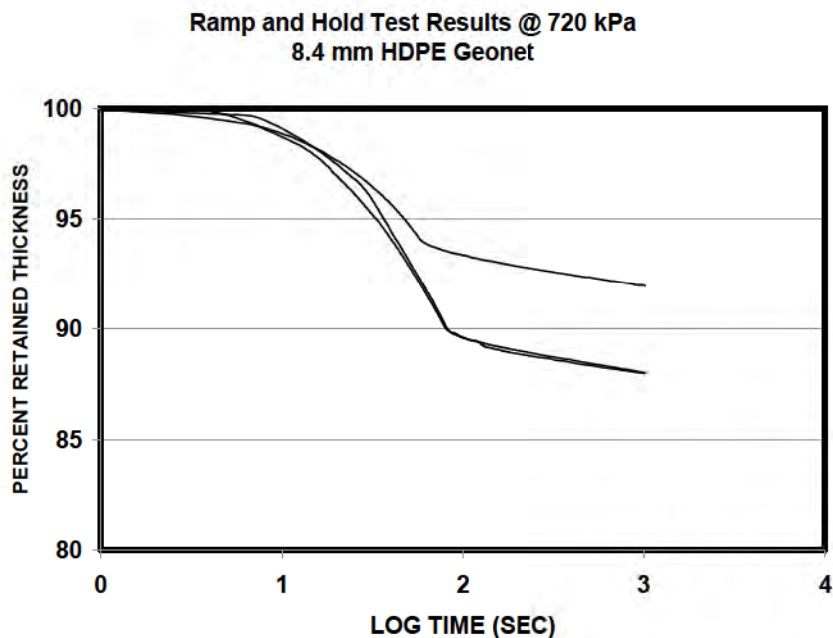


Figure 1: Ramp and Hold Compression Tests at 720 kPa Compressive Load

While this test is believed to be valuable, it is currently rarely observed as part of product acceptance testing. Early implementation may be challenged by lack of data. Still, while not directly measuring flow, the test may be a good indicator of product behavior.

Accelerated (SIM) Creep Testing

The variability suggested in short term compression tests may also be expected in the longer term and measured via longer term creep tests. Although conventional creep tests are not reasonable to perform during construction related material verification efforts, accelerated testing via the Stepped Isothermal Method (SIM) may be. This test may predict a final product

thickness and porosity, and resulting creep reduction factor to assist in approving product performance (Thornton, 2000, Allen 2005).

While this test has been used successfully, it is not, along with its conventional compressive creep method (at 20C), yet standardized. The drainage product manufacturing industry has been the traditional resource for measuring creep reduction factors, although this phenomenon has been relatively recent in the life of our industry, and has generally relied upon a limited number of measurements to support characterization of a product style. Still, conventional and accelerated (via SIM) creep testing has suggested variability of the onset of creep sometimes leading to very different results for creep reduction factors, an important feature of design flow of planar drains.

While the approaches above have not yet answered the call for quick and ready measures of product performance, they have served to define and investigate sources of observed variability. Observations of product features have led to a new effort of define the governing structures of planar drains.

IN SEARCH OF STRUCTURE

Though not always measured, it has long been recognized that several structural and physical properties of geonets contribute to flow capacity and thus performance. Among these are geonet density, height and width of ribs, rib junction integrity, load supporting surface area, aperture dimensions and corner angles. All these parameters vary during geonet production and can impact resulting performance.

One new approach to defining the governing structure was developed through two key observations. The first dealt with the substantial variability associated with short term ramp and hold strain responses between products, even when they represented the same style. The second observation related to the observed structural differences in geonet structures. While geonets are routinely described by thickness and mass per unit area, no standardized procedure for describing the structural details yet exists. Yet, we routinely see differences in the curve and orientation of planar strands, the magnitude of the junction between the upper and lower geonet strands, and the shape of the apertures. While we understand that these structural features contribute and affect resulting product performance, we do not, as an industry, specify them nor do we have experience and vocabulary for describing them.

Typical compressive strength testing looks for a feature in the resulting load vs. displacement curve that corresponds to a transition. Typical transitions relate to the geonet structure assuming more load through increased strain rather than load resistance. Well pronounced features meeting these criteria are called yield points and often correspond to what we term “roll-over” strength or compressive strength of the product.

Under increasing compressive load, a geonet may crush or “pancake” with the top strand driven into and crushed on top of the bottom strand. Or, typically, it yields by displacing the upper strand downward and to the sides of the bottom strands, referred to as “roll-over” behavior.

Either of these events in the load displacement curve corresponds to the yield or compression strength.

This shape under load of the yielded geonet has been captured and photographed by various experimenters by first loading geosynthetic drains, then waiting for resulting compressive creep, and finally locking in the resulting shape by flooding the loaded drain with epoxy to capture the new compressed condition.

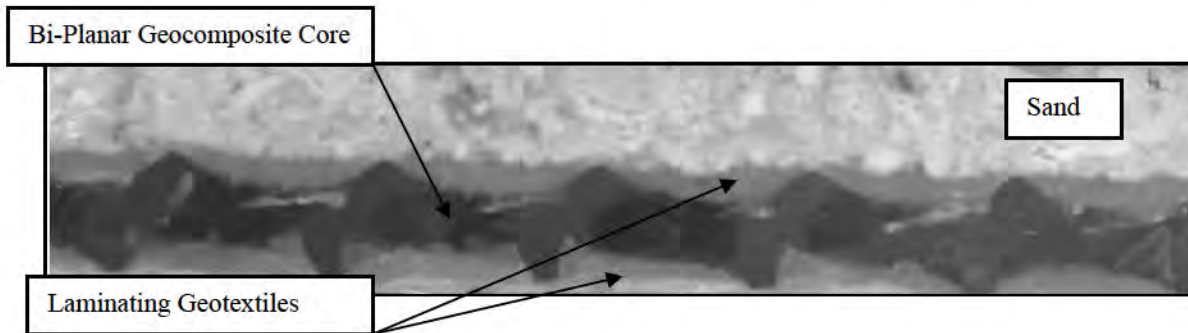


Figure 2: Bi-planar geocomposite, with sand cover, under 720 kPa normal load

STRAND INCLINATION ANGLE

One additional product construction feature observed to be variable between products and sometimes between different lots of the same product is the orientation the upper and lower geonet strands have by themselves, and relative to each other. This orientation relates the strands to an assigned plane positioned parallel to the intersection of the strands. It was hypothesized that a lower angle of inclination for a geonet structure would correlate to that structure more easily yielding its thickness when placed under the same compressive loading; or yielding at earlier load or strain than a product having higher angles of strand inclination. This strand inclination angle is a feature of every geonet, and may have a maximum value of 90 degrees for an upper geonet strand positioned directly above a lower geonet strand.

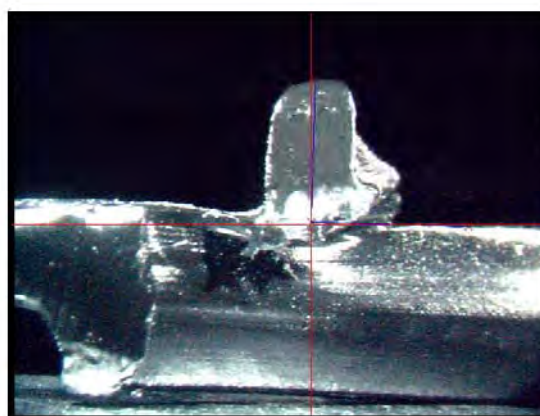
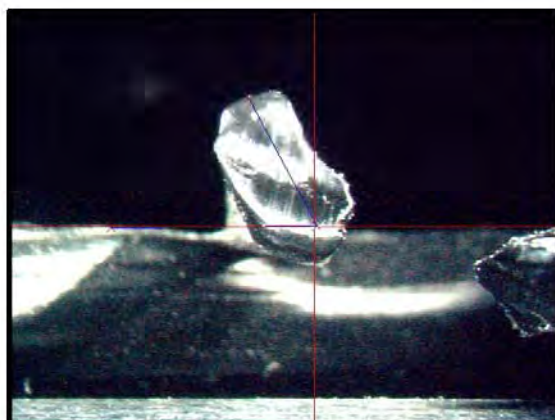


Figure 3: Examples of strand inclination angle of upper strand

A testing program was initiated to accomplish the following.

- 1) Develop specimen preparation and measurement procedures to determine the strand inclination angle.
- 2) Determine the optimal product location to sample and measure the strand inclination angle
- 3) Determine the relevancy to strand inclination angle to product performance.

A high density polyethylene biplanar geonet, was evaluated for strand inclination angle. The product was tested for physical properties.

Feature	Test Method	Result
Density	ASTM D 1505	0.954 g/cm ³
Mass per Unit Area	ASTM D 5261	0.89 kg/m ²
Thickness	ASTM D 5199	5.95 mm

The product roll width was divided into five equivalent widths excluding the outer 300 mm edge. Next, a single 300 mm square specimen was cut from the center of each width for measurement of strand inclination angles.

Strand inclination angles were measured using a CalTex System 3D Digital Video Inspection Measurement System equipped with AVM1 Version 3.00 data acquisition software. This same equipment is sometimes used to measure the critical angle between liquids and test surfaces to determine the surface tension of materials.

The equipment allows a relatively large specimen to be gripped and stabilized while the camera is positioned to observe a profile defined by the angle of interest. It is important that the entire specimen is large enough to maintain stability, and thus inherent structural angles, during measurements. Specimens of insufficient size are prone to relax or destabilize and thereby change the inherent structure. After unsuccessfully using small (< 2500 mm²), a specimen having 230 cm² was observed to have sufficient stability for measurement.

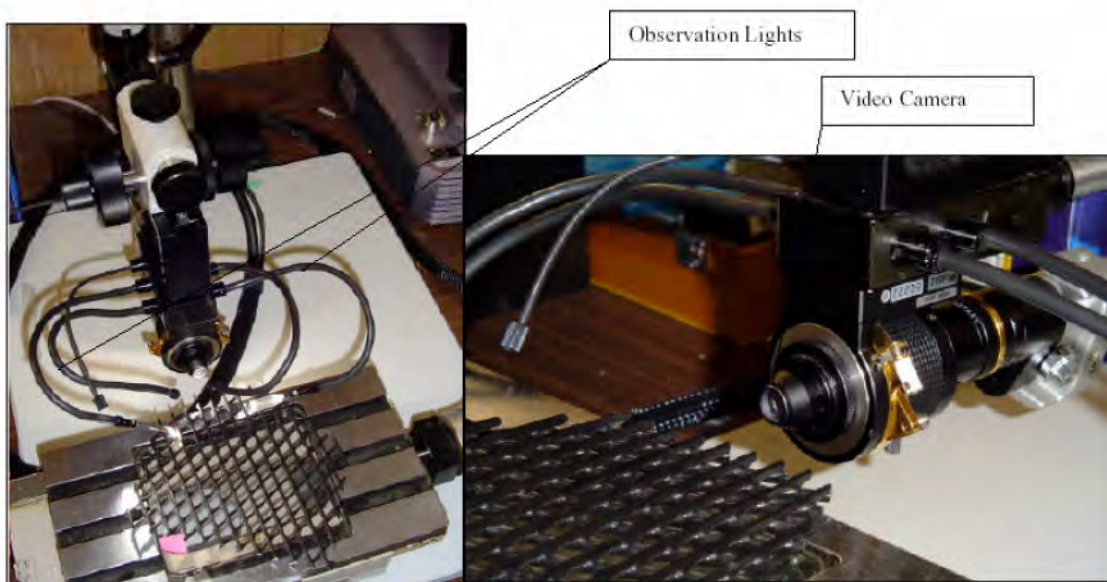


Figure 4:
Strand
Inclination
Angle
Measurement
Equipment

The
specimen

was mounted, lit with ancillary lights and positioned for focused observation and video recording under magnification. After the streaming video is observed, an image is photographed and angle measurements are performed. Each geonet specimen was measured for strand inclination angle at four locations:

- 1) lower strand at middle of aperture,
- 2) upper strand at middle of aperture,
- 3) strand intersection defined by mid-plane and upper strand, and
- 4) strand intersection defined by mid-plane and lower strand.

Each specimen was cut at the location of measurement using a sharp cutting blade. The inclination angles defined by the lower of the measured 1) and 2), and 3) and 4), were recorded. That is, the lower of the upper and lower strand related angles was recorded for each specimen. Poor images and associated ambiguous angle measurements were rejected. The following presents the measured inclination angles.

Width Section 1				Width Section 2				Width Section 3			
Top Strand		Bottom Strand		Top Strand		Bottom Strand		Top Strand		Bottom Strand	
Angle	Location	Angle	Location	Angle	Location	Angle	Location	Angle	Location	Angle	Location
78.2	Intersection	79.8	Intersection	87.1	Intersection	80.7	Intersection	72.5	Intersection	79.1	Intersection
75.2	Intersection	86.8	Intersection	75.2	Intersection	82.5	Intersection	79.9	Intersection	88	Intersection
80.1	Intersection	86.3	Intersection	74.4	Intersection	84	Intersection	87.6	Aperature	89.4	Intersection
80.8	Intersection	80.3	Intersection	76.9	Intersection	85.5	Intersection	86.8	Aperature	88.4	Intersection
80.4	Intersection	89.4	Intersection	79.8	Intersection	87.8	Aperature	83.3	Aperature	89.9	Intersection
78.2	Intersection	88.9	Intersection	86.2	Aperature	83.7	Aperature	89.4	Aperature	86.5	Intersection
74.2	Intersection	88.4	Intersection	78.2	Aperature	66.1	Aperature	82.4	Aperature	87.3	Intersection
73.3	Intersection	84	Aperature	74.1	Aperature	80.7	Aperature	88	Aperature	87.1	Aperature
76.2	Aperature	87.3	Aperature	76.2	Aperature	87.1	Aperature	88	Aperature	84.1	Aperature
76.4	Aperature	86.2	Aperature	86.5	Aperature	85.3	Aperature	86.8	Aperature	85.7	Aperature
79.6	Aperature	88.4	Aperature	88.4	Aperature			83.5	Aperature	80.8	Aperature
89.6	Aperature	82.5	Aperature	87	Aperature			80.3	Aperature	87	Aperature
78.2	Aperature	85.4	Aperature								
75.1	Aperature	86.5	Aperature								
86.2	Aperature										

Width Section 4				Width Section 5			
Top Strand		Bottom Strand		Top Strand		Bottom Strand	
Angle	Location	Angle	Location	Angle	Location	Angle	Location
76.4	Intersection	85.1	Intersection	80.4	Intersection	87.4	Intersection
70.3	Intersection	86.6	Intersection	82	Intersection	88.6	Intersection
73	Intersection	87.9	Intersection	83	Intersection	89.8	Intersection
75.6	Intersection	87.4	Intersection	82.3	Intersection	84.6	Aperature
79.1	Intersection	88.7	Aperature	73.5	Intersection	88.8	Aperature
86.9	Intersection	89.3	Aperature	74.8	Intersection	87.4	Aperature
77.3	Intersection	86.8	Aperature	79.5	Aperature	83.4	Aperature
85.7	Aperature			76.9	Aperature	87.2	Aperature
85.2	Aperature			86.6	Aperature	88.4	Aperature
85.6	Aperature			87.8	Aperature	88.5	Aperature
84.6	Aperature						
83.4	Aperature						
77.9	Aperature						

Table 1: Strand Inclination

Each product roll width section was tested for compressive strength in accordance with ASTM D 6364, mass per unit area in accordance with ASTM D 5261, and thickness in accordance with ASTM D 5199. The results were as follows.

Width Section	Thickness (mm)	Mass/Unit Area (kg/m ²)	Compressive Strength (kPa)
1	5.99	0.952	648
2	6.02	0.942	666
3	5.89	0.825	561
4	5.89	0.820	615
5	5.94	0.918	700

Table 2: Section physical and mechanical properties

The average and minimum strand inclination angle measurements were determined and plotted vs the measured compression strength. Finally, the mass per unit area and thickness of each width were plotted vs. compression strength. The relevant results of these determinations and associated plots are presented in the following table and plots.

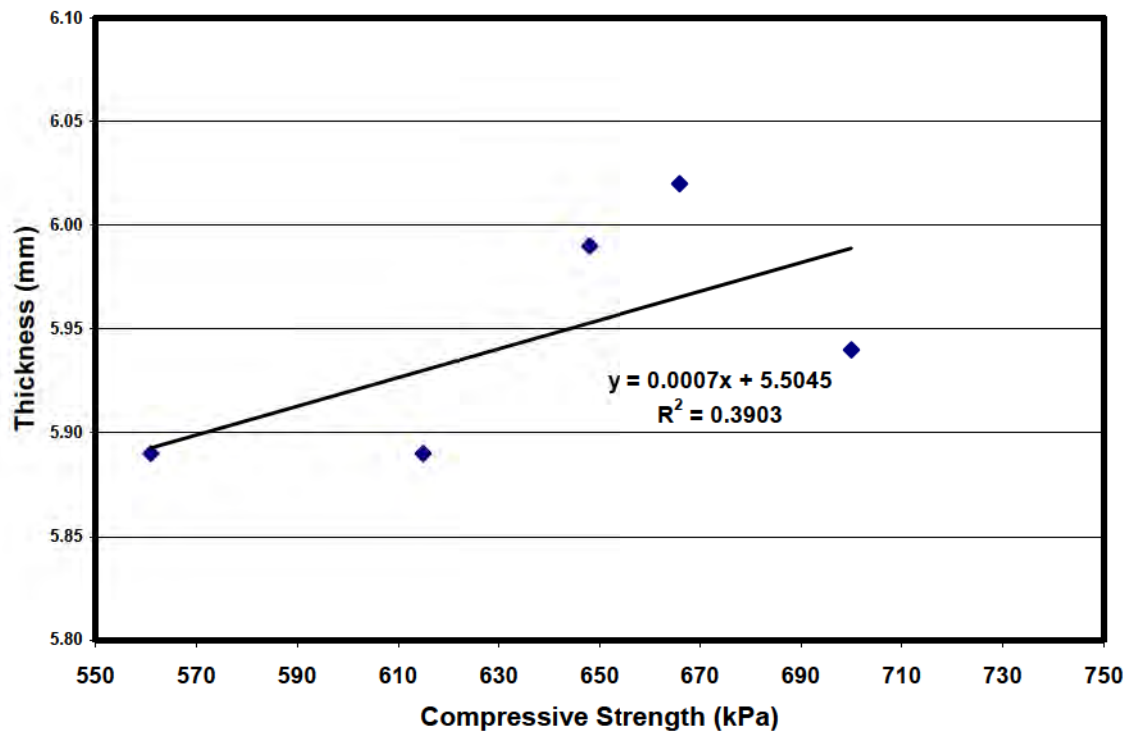


Figure 5: Compressive Strength vs. Thickness

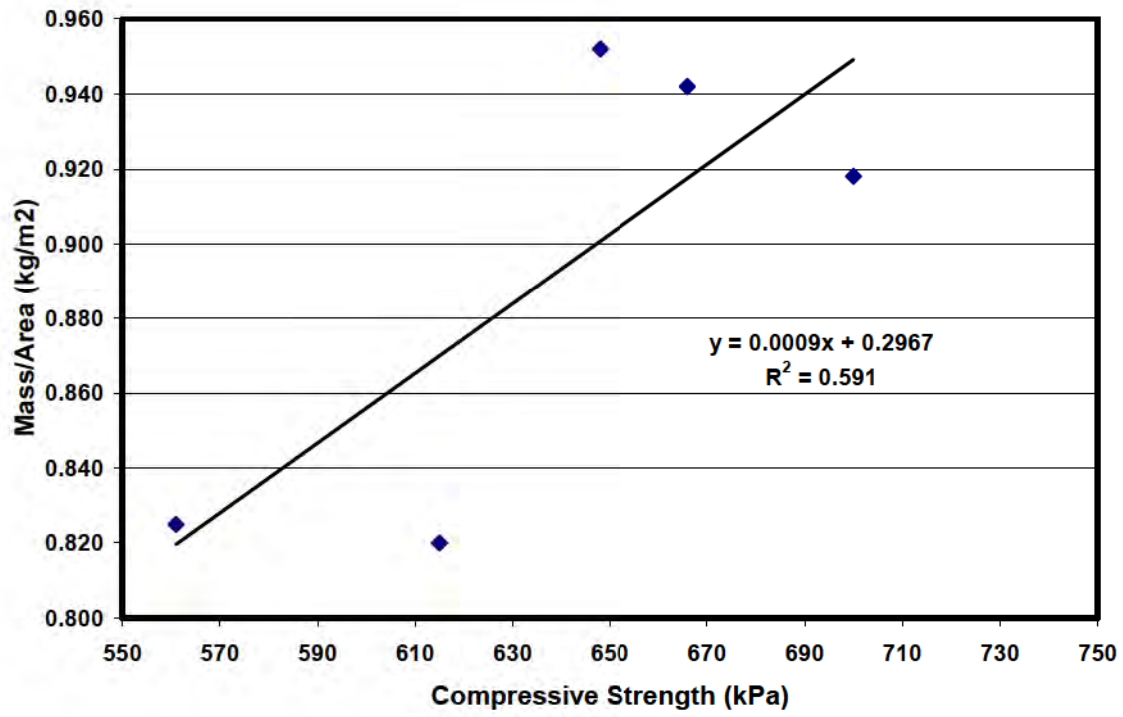


Figure 6: Compressive Strength vs. Mass/Unit Area

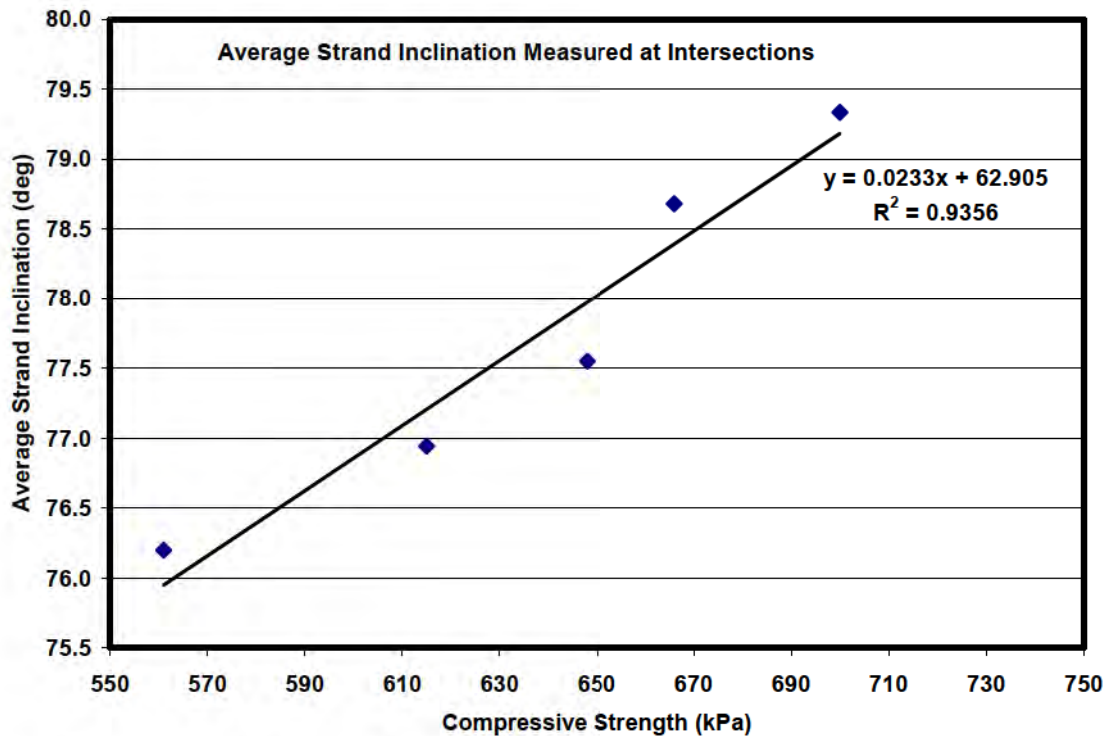


Figure 7: Compressive Strength vs. Average Strand Inclination (at Intersections)

OBSERVATIONS

- While variability in strand inclinations on a single product roll was observed, strand inclination angle test populations all demonstrated a coefficient of variation less than 10 percent.
- The correlation between all measured mid-aperture angles and the corresponding compressive strengths were not well defined. This was attributed to a belief that the apertures did not govern compression behavior.
- The correlation between all minimum angles measured and the corresponding compressive strengths were not well defined. It is believed that low strand inclination angles, while present, do not represent a given sample accurately. A non-representative single specimen is not uncommon for most geosynthetic test populations.
- It was believed that thicker, heavier zones in a product roll width would exhibit increased resistance to loading. This was not the case, demonstrated by the poorly defined correlation between mass per unit area, thickness and compressive strength. This re-emphasizes the need for additional tools for short term test measurements that are relevant to performance.
- The correlation between average intersection strand inclination angles and corresponding compression strengths was excellent demonstrating a regression coefficient of 0.936. This strong correlation was attributed to the significance of the intersection between upper and

lower strands. The orientation of these strands is believed to be relevant to eventual geonet performance under load. In the context of short-term compression strength, this appears to be true.

- The correlation between average intersection strand inclination angles and corresponding compression strengths suggest a valid research area with regard to the structural orientation and load bearing behavior of individual rib cross sections. It is reasonable to anticipate that the kern of a rib cross section could be evaluated to demonstrate how active normal compressive loads result in axial and flexural stresses within the body of the geonet structure, leading to increased or decreased flow performance.

CONCLUSION

It is acknowledged that while geonet manufacturers control various processing parameters that impact geonet angles and other structural features, the authors are not aware that current processing technologies are always able to directly control the actual features. Thus, there is much more work to accomplish both in measurement and processing before one could attempt to specify or establish limits for these important features.

Still, the work described in this paper suggests that a procedure to determine a geonet's strand inclination angle is possible and may lead to a predictive tool for studying performance under load. The measurement presents an opportunity to develop protocols for describing visually observed features of geonets, and a reasonable candidate for future specification. While correlation to compression strength was established for only a limited use of strand inclination angle measurement, the authors believe that increases in specimen populations may prove additional correlation is possible. Further, additional work is needed to refine the procedure, employ the test on a variety of materials and expand correlation efforts to short term flow and long term compression results. Work continues in this regard.

REFERENCES

ASTM D4716-04, Test Method for Determining the (In-plane) Flow Rate Unit Width and Hydraulic Transmissivity of a Geosynthetic Using a Constant Head, ASTM International, 100 Barr Harbor Drive, PO Box C700, West Conshohocken, PA 19428

GRI Standard – GC8 (2001), Determination of the Allowable Flow Rate of a Drainage Geocomposite, Geosynthetic Research Institute, <http://www.geosynthetic-institute.org/grispecs/gc8.pdf>

Allen S. (2000), Issues Regarding the Measurement of the Planar Flow of Geocomposite Drains used in Waste Containment Applications, Proceedings from the 5th Annual Landfill Symposium, Solid Waste Association of North America, Austin, Texas, June 2000

Thornton, J., Allen, S., Siebken, J. 2000: Long Term Compressive Creep of High Density Polyethylene Geonet, Proceedings of EuroGeo 2

Allen, S.R., (2005), The Use of an Accelerated Test Procedure to Determine the Creep Reduction Factors of a Geosynthetic Drain, Geo-Frontiers 2005 Conference Proceedings Published by: ASCE, ISBN Number: 078440769X

ASTM D 6364, Standard Test Method for Determining the Short-Term Compression Behavior of Geosynthetics, ASTM International, 100 Barr Harbor Drive, PO Box C700, West Conshohocken, PA 19428

CONTACT:

Sam Allen

TRI/Environmental Inc.

9063 bee caves road

Austin, TX 78733

Phone: 512-263-2101

Email: sallen@tri-env.com

Research

Secondary Containment Applications: Long Term Behaviour of Geomembranes Exposed to Diesel Fuel

Dr. Daniele Cazzuffi & Elisa Cantarelli, CESI S.p.A

ABSTRACT

In the last years, geomembranes have been often used in secondary containment, with barrier function. Secondary containment could be defined as a means of surrounding, permanently or temporarily, one or more primary storage containers or articles to collect any hazardous material spillage, in the event of loss of integrity or container failure. Examples of hazardous materials are oil-filled equipment, chemicals, and hazardous wastes. So, when selecting the type of geomembrane to use as secondary containment, the compatibility with the type of the material or waste to be contained is one of the most important aspects to consider. The Geosynthetics and Environmental Geotechnics Laboratory of CESI in Milano carried out an experimental activity to study the behaviour, when in presence of diesel fuel, of different types of geomembranes usually applied with barrier function. Laboratory tests were performed on the virgin material samples and on the different samples respectively after one, two, four and eight months of contact with diesel fuel, aiming at determining the chemical-physical, mechanical and hydraulic properties of the different types of geomembranes and their evolution vs. time. The results of the tests allowed to establish some preliminary conclusions on the long-time behaviour of the different types of geomembranes in direct contact with diesel fuel.

INTRODUCTION

A major component in minimising pollution sources is in providing proper liquid waste collection and disposal facilities. Secondary containment is defined as a means of surrounding one or more primary storage containers or articles, providing additional storage capacity to collect any hazardous material spillage in the event of loss of integrity or container failure (SLAC, 1997). The leakage of potentially harmful liquids, like oil-filled equipment, chemicals and hazardous wastes, could due also to overfilling or improper draining of the primary storage. Therefore, to prevent any release to the environment, all containers used to store waste oils and other such potentially dangerous substances should have a form of secondary containment, which provides an essential line of defence in the event of a failure of a primary containment (such as a bulk storage container, a mobile or portable container, pipes or flow-lines, or other oil-filled operational equipment). The system provides temporary containment of spilled oil until the appropriate response actions are taken to abate the source of the discharge and remove oil from areas where it has accumulated before the oil reaches the surrounding environment (EPA, 2005). Secondary

containment systems may be either permanent or temporary. Permanent containment systems are generally made of reinforced cement concrete or bituminous concrete revetments on the upstream face of an embankment, with a geomembrane applied as the external layer, i.e. in direct contact with oil in case of failure of the primary containment. Also temporary secondary containment systems, based on the use of geomembranes with barrier function, are diffused.

An example of the use of geomembranes as permanent secondary containment liners is the rehabilitation carried out in 1997 of the fuel tanks of the Craney Island Fuel Terminal in Portsmouth, VA, USA (Shehane, 2001). A reinforced 0,8 mm thick geomembrane, with resistance to all grades of jet fuel, was installed on about 80,000 m² of the dike liners and left exposed, also to eliminate the need for maintenance crews to cut the grass and to reduce the clean-up costs in case of a fuel spill (no expense for removal of contaminated soil). Another example of permanent secondary containment with geomembrane liners is given by the concrete walls and containment area floors of the Denver International Airport tank farm, that were overlaid with about 50,000 m² of reinforced ethylene copolymer alloy geomembrane. This type of geomembrane was previously tested in constant contact with Jet A (commercial jet fuel) for six-and-a-half years, with no substantial damage or loss of strength (www.xr-5.com).

The purpose of the experimental activity developed at CESI in Milano and presented in this paper is to study the behaviour of different types of geomembranes, commonly available on the European market, when in contact with diesel fuel for a prolonged period of time.

design of a geomembrane liner for secondary containment

As already described above, geomembranes are flexible membranes extensively used as secondary containment as spill protection on chemical storage tanks surrounding areas. Geomembranes are made by combining one or more thermoplastic polymers with additives, like plasticizers, carbon black, processing aids, anti-oxidants. A wide range of thermoplastics resins are used for geomembranes, including high density polyethylene (HDPE), very low density polyethylene geomembrane (VLDPE), polyvinyl chloride (PVC), polypropylene (PP).

First of all, when selecting the type of secondary containment to use, it should be considered the compatibility with the type of substance or waste to be contained, its durability and resistance to fire, heat and sunlight. Therefore mechanical properties (as tensile behaviour and tear resistance) and durability properties (as heat resistance) are properties of the geomembranes that should be examined to determine the most appropriate material in relation to the final use. The tensile properties refer to the tensile strength of a geomembrane and to the ability to elongate under stress and must be sufficient to satisfy the stresses (for example self-weight) and the strains (for example not exceeding the yield strain for HDPE) anticipated during its service life. Geomembrane liners can also be subjected to tearing during installation due to high winds or handling. Exposure to atmosphere and temperature changes can cause degradation in the geomembrane if it is exposed for a prolonged period of time. Not only the geomembrane capacity to withstand long term contact with whatever the secondary containment hold must be investigated, but also the capacity to meet the

requirements typical of a barrier system, for the entire life of the storage tanks. Finally, probable risk and severity of potential spills, cost and ease of installation have to be taken into account. Among the different types of oils to be stored in secondary containment systems, for the experimental activity presented in this paper it was considered important to evaluate the behaviour of geomembranes in presence of diesel fuel. In fact, diesel fuel has to be stored at burner facilities and it may be also present in the sanitary landfills, due to disposal of transportation related substances and diesel-contaminated media or diesel-powered engine parts. The selected diesel fuel was the diesel fuel commonly used in Italy for cars and trucks.

EXPERIMENTAL STUDY

The experimental activity described in this paper interested seven types of geomembranes that were exposed to diesel fuel for eight months. The selected geomembranes, of different types and made of different polymers, were the following:

HDPE-1 and HDPE-2 (high density polyethylene, manufactured by two different companies);

CHD (modified high density polyethylene);

MP-G (modified polyethylene reinforced with glass fibres);

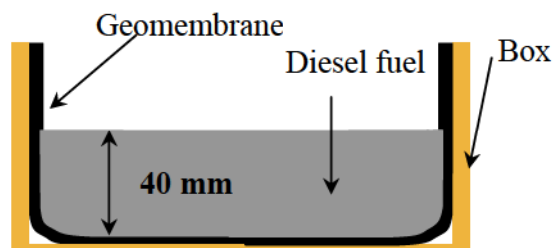
VLDPE (very low density polyethylene);

PVC (polyvinylchloride);

PVC-P (plasticised polyvinylchloride).

All the considered geomembranes were 2.00 mm in nominal thickness, with the exclusion of the two made of PVC, that were 1.50 mm in nominal thickness.

Different specimens of 700 mm x 700 mm were cut from the seven geomembrane samples subjected to the experimental activity at the Geosynthetics and Environmental Geotechnics Laboratory at CESI in Milano. The edges of the specimens were wrapped in such a manner to obtain containers in which the diesel fuel was poured and then retained without leakages (Figure 1). The geomembrane specimens were left in contact with the diesel fuel at 20 °C for a maximum of eight months and, during this time period, the level of the diesel fuel was kept equal to 40 mm: therefore, regular additions were made in order to compensate the lowering of the diesel fuel level due to evaporation. No agitation was foreseen in the immersion tank.



Laboratory tests were performed on the virgin material samples and on the different samples respectively after one, two, four and eight months of contact with diesel fuel, aiming at determining the chemical-physical, mechanical and hydraulic properties of the geomembranes and their evolution with time. The following tests were performed: nominal thickness (ASTM D 5199), thermo-gravimetric analysis (ASTM E 1131), density (ISO 1183), Shore A hardness (ISO 868), tensile stress and strain (ASTM D 638), tear strength (ASTM D 1004), cold bending (ASTM D 2136), dimensional stability (ASTM D 1204), water vapour permeability (ASTM E 96).

The selected tests above mentioned allow in fact a direct comparison among all seven types of geomembranes; therefore, specific tests valid only for some types of geomembranes, as HP-OIT tests for PE materials and plasticizer content for PVC materials, were not performed in this study. The results of the following tests are illustrated: nominal thickness, thermo-gravimetric analysis, tensile stress and strain, tear strength. In fact, as far as the chemical-physical properties are concerned, density and cold bending of all tested materials don't effectively change. Moreover, the Shore A hardness related to all types of geomembranes decreases, if compared to the virgin sample value, more quickly during the first two months, more slowly later; in particular, after eight months of exposure to diesel fuel, the VLDPE geomembrane is subjected to the highest decrease (about 16%), while the hardness of the other six types of geomembranes decreases in the range of 10%.

As far as thickness behaviour is concerned, Figure 2 illustrates the percent variation of nominal thickness vs. exposure time to diesel fuel. As it can be seen, HDPE 2 maintains the same thickness after eight months and PVC, PVC-P and HDPE 1 are subjected to an increase of about 3-4%, while CHD, VLDPE and MP-G seem the most affected by a prolonged contact with diesel fuel, because their thickness increase of about 10%, 18% and 20% respectively: these ranges of increase are already evident after two months of exposure.

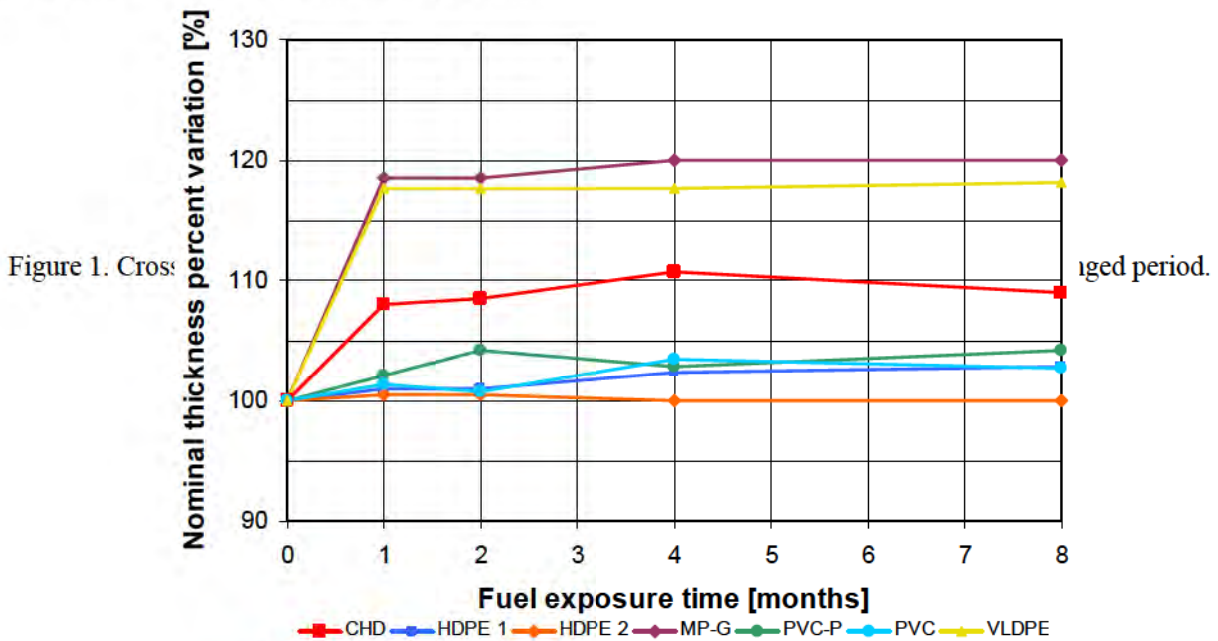
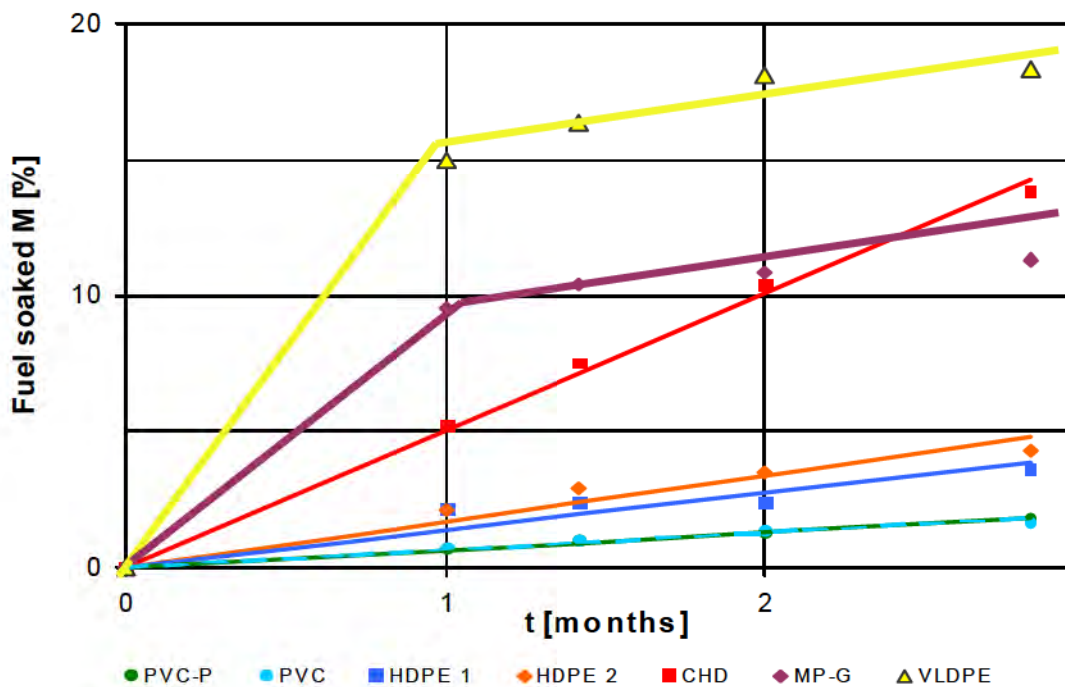


Figure 2. Percent variation of nominal thickness vs. exposure time.

The increase in nominal thickness is surely connected to a diesel fuel absorption. The thermogravimetric analysis allowed to calculate the quantity of fuel soaked by geomembranes and the results are represented in Figure 3. The very low density polyethylene geomembrane (VLDPE) soaks up more diesel fuel than the other types: in fact, the VLDPE geomembrane soaks up about 18%, while the modified polyethylene glass fibres reinforced geomembrane (MP-G) and the modified high density polyethylene geomembrane (CHD) absorb in the range between 10% and 15%. On the contrary, the high density polyethylene geomembranes (HDPE 1 and 2), the polyvinylchloride geomembrane (PVC) and the flexible polyvinylchloride geomembrane (PVC-P) soak up a minimal amount of diesel fuel (about 4.5% for HDPE and about 2% for PVC). In fact, MP-G, VLDPE and CHD geomembranes are subjected to higher increases in thickness, if compared to HDPE and PVC geomembranes: this correspond to a larger quantity of diesel fuel absorbed. The structure of the polymer matrix could explain the behaviour of the different polymers in presence of solvents. Polymers are large molecules built through addition (polymerisation) of small repetitive molecules called monomers. A small amount of unfilled volume is associated with the end of polymer chain.



This volume is called the “free volume” (Figure 4) and its amount for a given mass of polymer depends on the number of chain ends, hence the number of chain and the degree of polymerisation. Using this interpretation, solvents, like diesel fuel, can permeate the polymers (the absorption phenomenon observed) thanks to the volume of the polymer mass not actually occupied by molecules.



Figure 4. Free volume associated to the end of polymer chain...
 Free volume
 1 chain

Thus,

Figure 3. Fuel soaked (M) vs. square root of the exposure time (\sqrt{t})

the solvent molecules,

when penetrate into the material through the free volume, break weak inter-chain interactions, increasing the distance between polymer chains and reducing their cohesion: this typically leads to an increase in dimensions (swell) and to a loss of stiffness, as described by Kay et al., 2004.

As illustrated in Figure 3, where the fuel soaked percentage M is plotted vs. the square root of the time, data related to all geomembranes, except CHD and VLDPE, fit a linear interpolation of the Fick's law, as suggested by Weitsman (1986):

$$M(t) \div \sqrt{\frac{D \cdot t}{\pi}} \quad (1)$$

where:

M= fuel soaked; t = exposure time; D = diffusivity coefficient.

If we assumed D as a constant, the relationship (1) becomes a line crossing the axes origin, as it appears clear for HDPE, CHD and PVC. On the contrary, the Fick's law can not be applied to MP-G and VLDPE geomembranes. In both cases, it should be said that the diffusivity coefficient isn't constant. MP-G is a modified polyethylene reinforced with glass fibres geomembranes : the presence of the reinforcement explains why the diffusivity coefficient isn't constant and consequently justifies the anomalous absorption of diesel fuel of MP-G illustrated in Figure 3. In fact, after the first month of contact, the data related to MP-G can be interpolated by a line with the same slope as both HDPE 1 or HDPE 2, as if the effect of the diesel fuel on the polymeric matrix prevails after the first month, while in the first thirty days the absorption through the reinforcement dominates. An explanation of the VLDPE behaviour in terms of diesel fuel soaked seems more difficult, because this type of geomembrane has not a reinforcement.

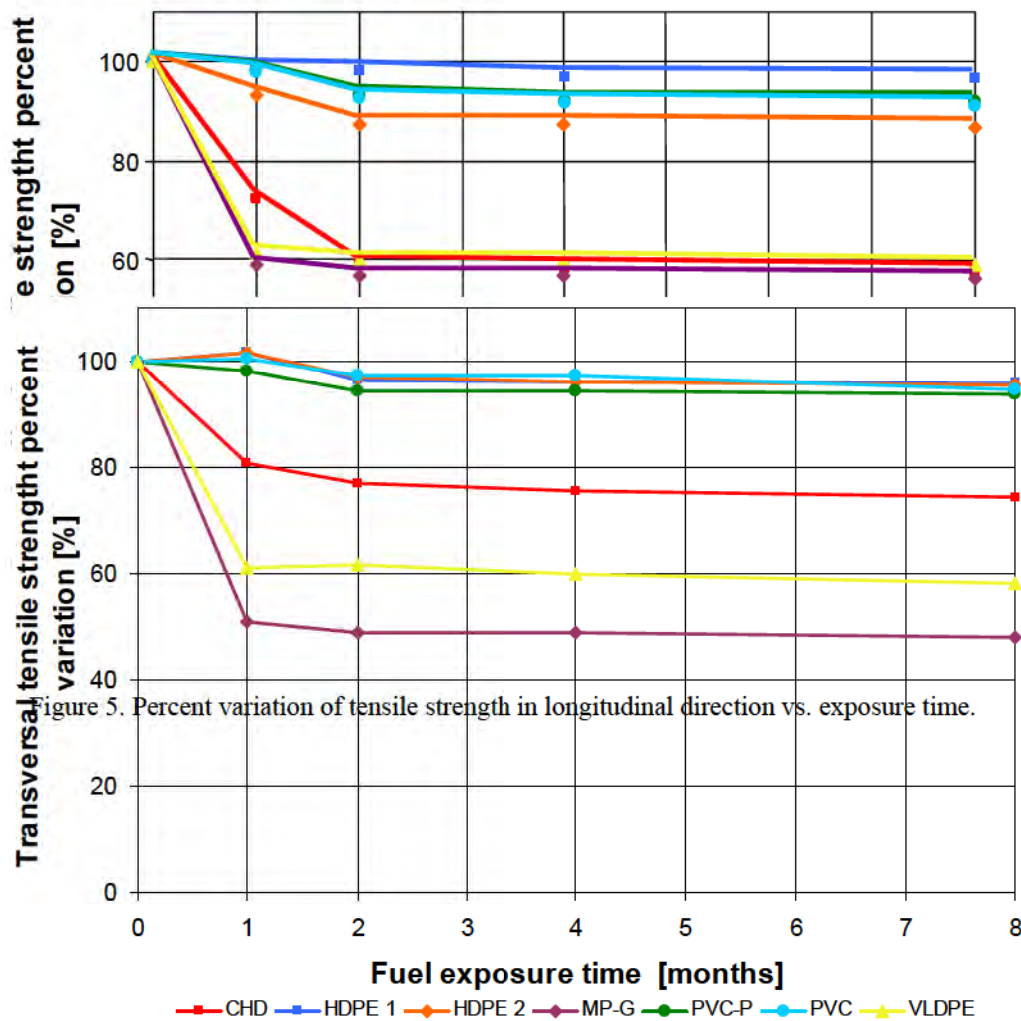


Figure 5. Percent variation of tensile strength in longitudinal direction vs. exposure time.

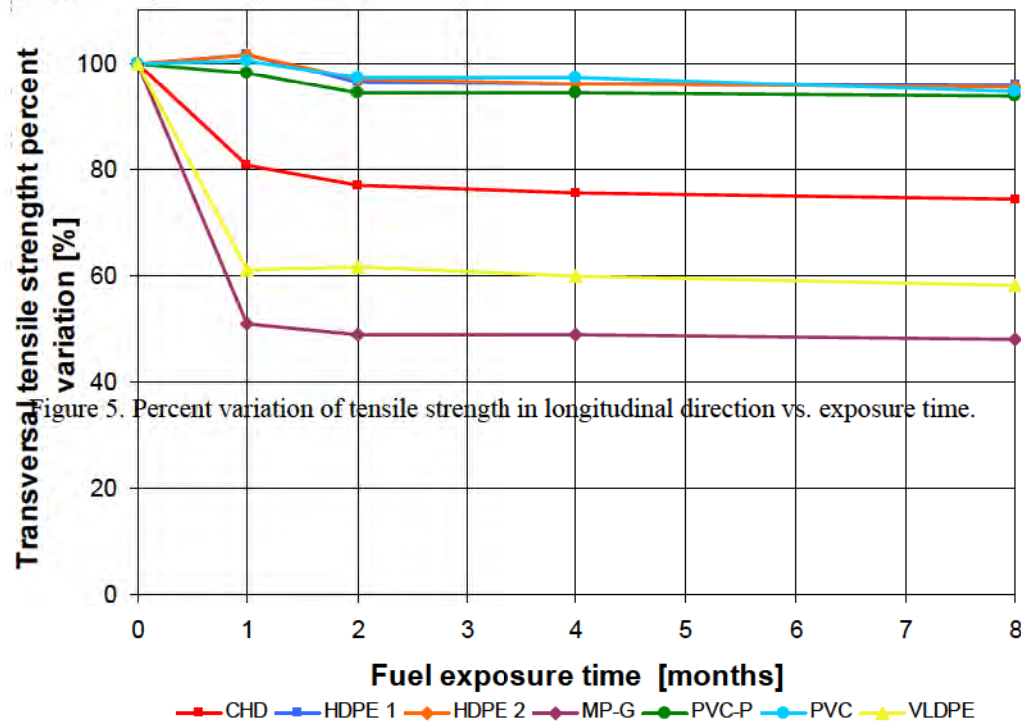


Figure 6. Percent variation of tensile strength in transversal direction vs. exposure time.

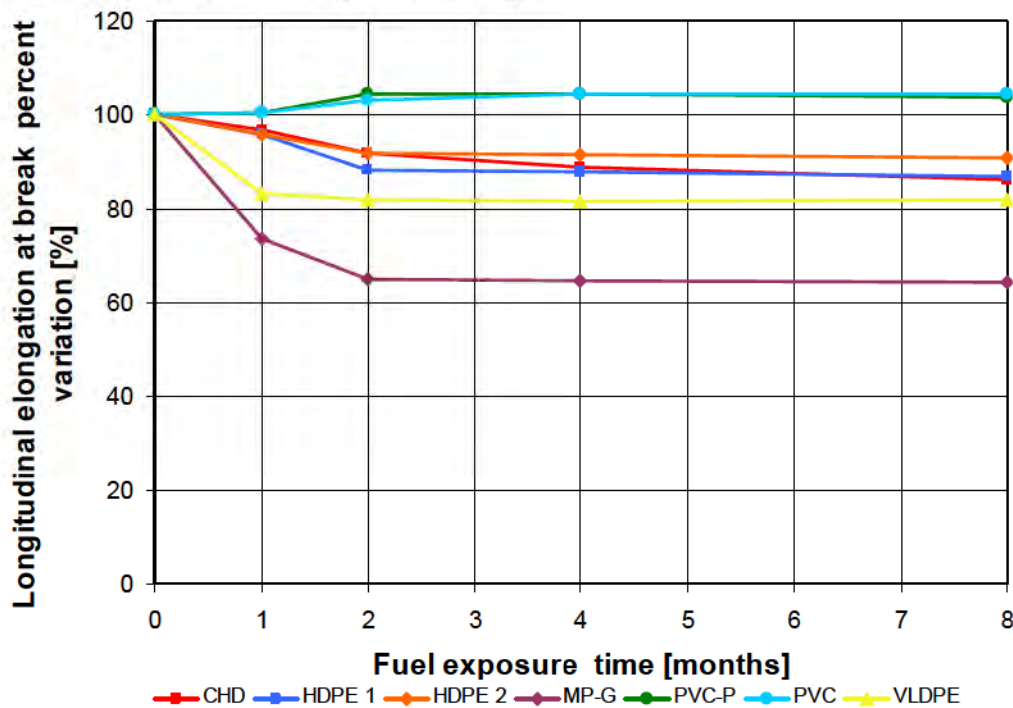
In Figures 5 and 6 the percent variations of tensile strength in longitudinal and transversal directions are illustrated, while in Figures 7 and 8 the percent variations of tensile elongation at break in longitudinal and transversal directions are shown. The geomembranes can be subdivided in two

groups in terms of tensile behaviour: HDPE 1, HDPE 2, PVC and PVC-P in the first group, CHD, MP-G and VLDPE in the second one. In fact, the tensile strength in longitudinal direction (Figure 5) decreases less than 15% after eight months for the first group, while about 40% for the second one.

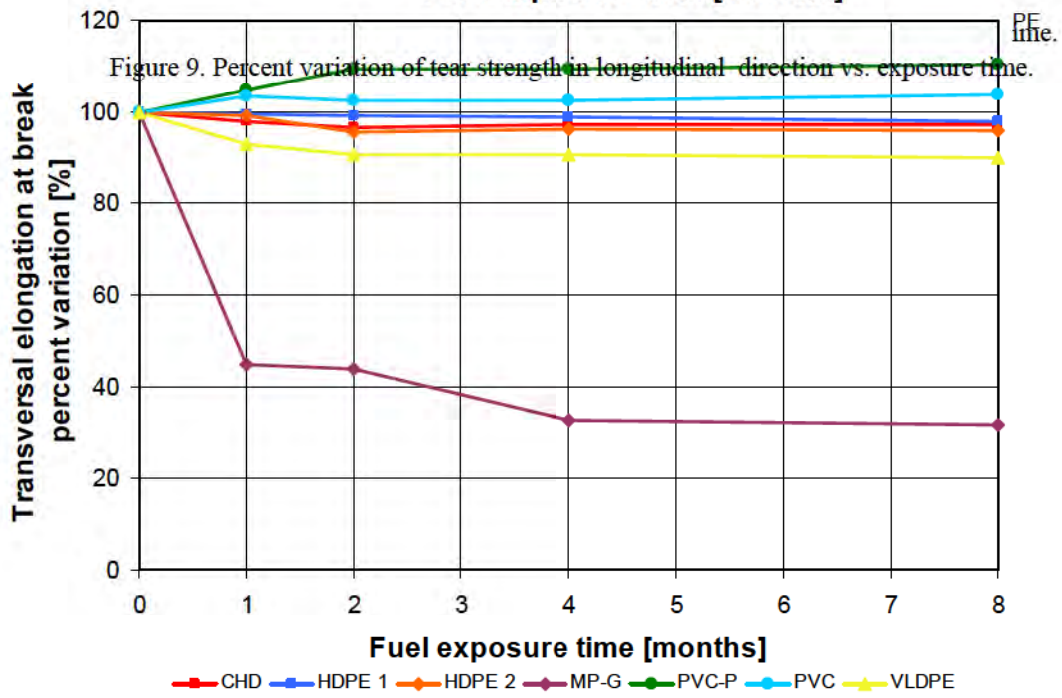
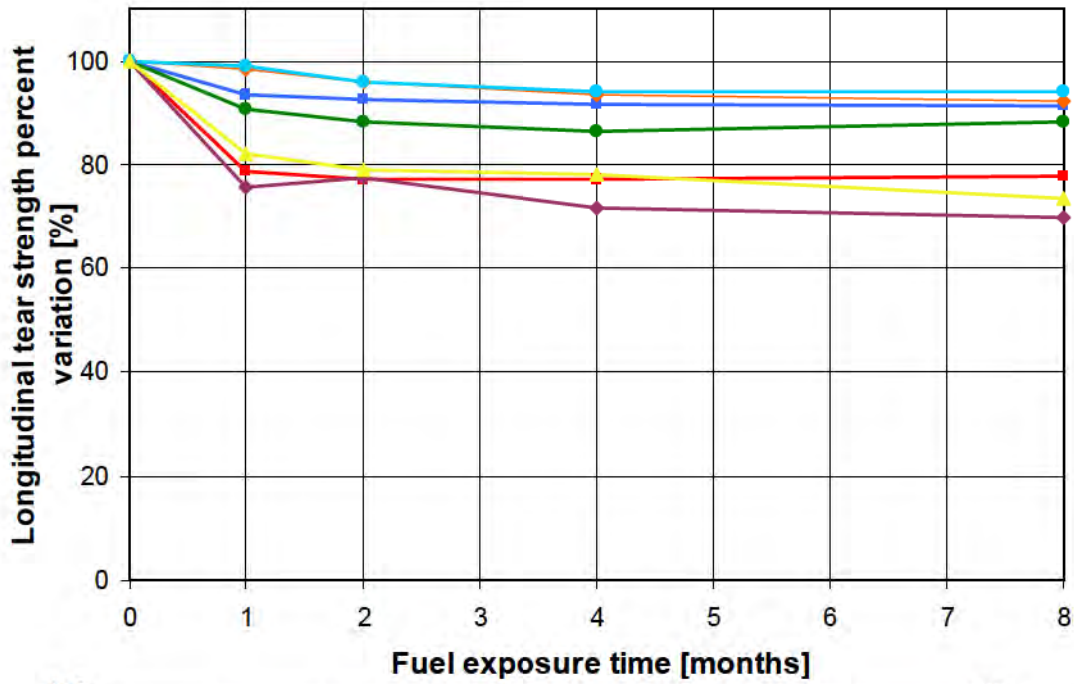
In terms of tensile strength behaviour in transversal direction (Figure 6), the geomembranes belonging to the first group exhibit percent variation less than 10% after eight months, while CHD, VLDPE and MP-G percent variation differ one from each other in a more marked way and ranging from 25% to about 52%. In particular, MP-G retains less than 50% of tensile strength after eight months of contact with diesel fuel. Variations in tensile strength occur within the first two months of contact with diesel fuel, as it is the case also of the tensile elongation at break, both in longitudinal direction (Figure 7) and in transversal direction (Figure 8). As it was expected (Kay et al., 2004), all types of geomembranes exhibit a decrease in the stiffness values, due to the penetration of solvent molecules into the material.

In particular, both types of PVC geomembranes exhibit a reduction in stiffness values due to a reduction in the tensile strength and to a contemporary increment in the strain. On the contrary, the other types of geomembranes show a decrease in the stiffness values, due to the combined effect of a reduction in the tensile strength and of a corresponding smaller reduction in the tensile strain.

Figures 9 and 10 show tear strength behaviour in longitudinal and transversal directions respectively. Also in the case of tear, as for tensile tests, the geomembranes can be subdivided in two groups: HDPE 1, HDPE 2, PVC and PVC-P in the first group, CHD, MP-G and VLDPE in the second one. Again MP-G is subject to the higher decrease of tear strength (about 30% in both



directions). Figure 7. Percent variation of elongation at break in longitudinal direction vs. exposure time.



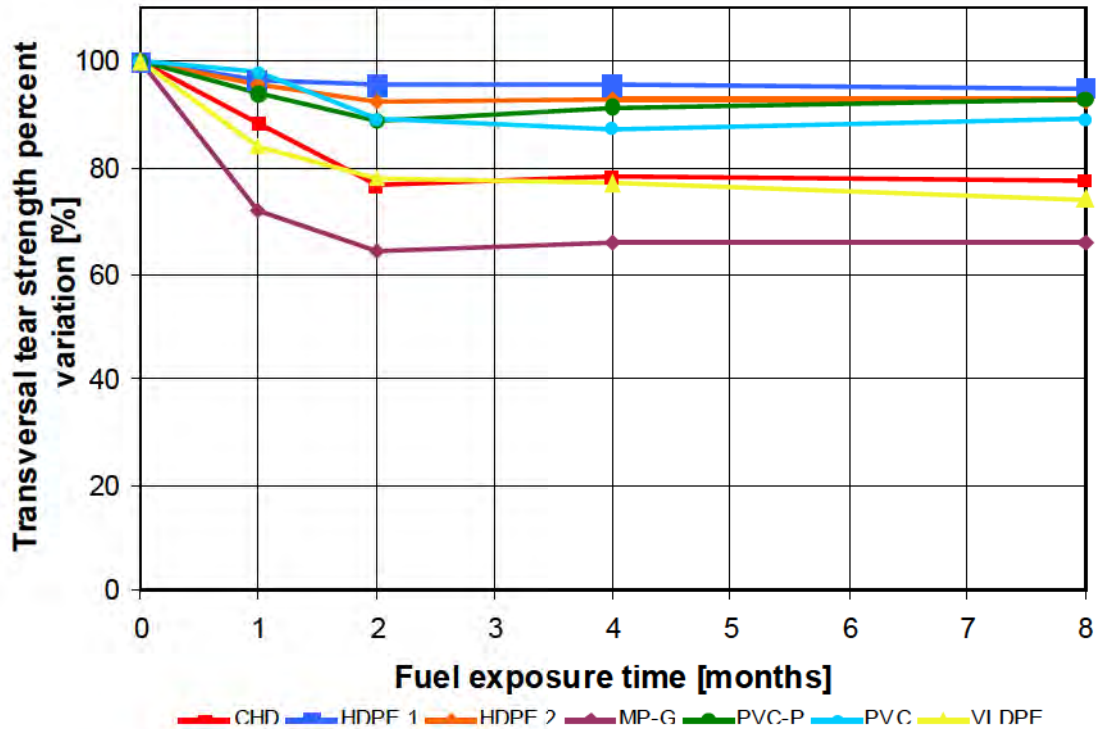


Figure 10. Percent variation of tear strength in transversal direction vs. exposure time.

CONCLUSIONS

In order to determine the evolution vs. time of chemical-physical, mechanical and hydraulic properties of seven different types of geomembranes, different samples of HDPE, PVC, PVC-P, CHD, MP-G and VLDPE were kept in contact with diesel fuel for a maximum term of eight months. Laboratory tests were performed on the virgin material samples and on the samples respectively after one, two, four and eight months of contact with diesel fuel. The obtained results allow to define how diesel fuel affects the geomembrane behaviour; in particular, the following considerations could be settled:

the increase in nominal thickness, due to a swelling of the geomembranes in consequence of a diesel fuel adsorption, is particularly relevant (about 20%) for MP-G and VLDPE geomembranes and important (about 10%) for CHD geomembranes, while it is almost negligible (less than 5%) for high density polyethylene (HDPE) and polyvinylchloride (PVC) geomembranes; correspondingly, the action of the diesel fuel on high density polyethylene (HDPE) and polyvinylchloride (PVC) causes negligible alterations of mechanical properties both in tensile and tear tests, while the tensile and tear characteristics of CHD, VLDPE and MP-G geomembranes are subjected to a more marked reduction.

According to the obtained results it can be said that MP-G, VLDPE and CHD geomembranes are the most affected by a prolonged contact with diesel fuel.

Figure 10. Percent variation of tear strength in transversal direction vs. exposure time.

Finally, the greatest variations of all considered properties were registered within the first two months, whereas after this period they remain substantially unchanged.

It must be considered that a secondary containment system provides an essential line of defence in the event of a failure of the primary containment such as oil containers and bulk storage containers: this system provides temporary containment of spilled oil until the appropriate response actions are taken to abate the source of the discharge and remove oil from areas where it has accumulated before the oil reaches the soil, rivers, lakes, wetlands etc..

In general terms, it could be expected that geomembranes will be directly exposed to oil for a short period of time, i.e. during cleaning-up and reparation operations.

Therefore the good compatibility between geomembranes and diesel fuel should be assured primarily in the short term: from the obtained results, considering the tests performed after one and two months of exposure, PVC and HDPE geomembranes appear to be the most suitable for the considered application.

However, it should be considered also the long term behaviour of geomembranes permanently installed as secondary containment. In fact geomembranes should be chosen based on their capacity to withstand working conditions even in the long term: therefore the selected geomembranes should exhibit not only good compatibility with diesel fuel, but also resistance to UV degradation (in particular for exposed working conditions), excellent behaviour vs. puncture, hold up to thermal expansion and contraction, resistance to environmental stress cracking (for PE materials) and finally withstand long term contact with whatever the tanks hold, from unrefined oil to jet fuel.

REFERENCES

EPA (2005): Spill Prevention Control and Countermeasures Guidance for Regional Inspectors, Office of Emergency Management EPA 550-B-05-001, U.S. Environmental Protection Agency, Washington, DC, USA.

Kay, D., Blond, E., Mlynarek, J. (2004): Geosynthetics durability: a polymer chemistry issue, Proceedings of the 57th Canadian Geotechnical Conference, Quebec City, Canada.

Shehane, W. (2001): Updated containment on Craney Island, Geotechnical Fabrics Report, Volume 19, Number 6, August, pp.36-37.

SLAC (1997): Secondary Containment Technical Basis Document, SLAC-I-750-0A16E-001, Stanford Linear Accelerator Centre, Menlo Park, CA, USA.

Weitsman, Y. (1986): Moisture in composites: sorption and damage, Technical Report Mechanics and Materials Centre, Texas A&M University, College Station, TX, USA.

www.xr-5.com : XR-5 lines jet fuel tank farm at Denver Airport, Case histories, Case study 2.

CONTACT:

Dr. Daniele Cazzuffi, PhD

CESI S.p.A.

Milano, ITALY

Phone: +39 02 2125 5375

Email: cazzuffi@cesi.it

Diffusive Migration of Volatile Organic Compounds through PVC Geomembranes.

Rebecca S. McWatters, PhD Candidate, GeoEngineering Centre at Queen's-RMC; R. Kerry Rowe, GeoEngineering Centre at Queen's-RMC

ABSTRACT

Geomembranes are often used in municipal solid waste landfill final cover systems to minimize the release of landfill gases to the atmosphere. This paper examines the diffusive migration of four volatile organic compounds (benzene, toluene, ethylbenzene and xylenes) through samples of a 0.76 mm (30 mil) thick flexible PVC geomembrane. Sorption and diffusion tests were performed to estimate the parameters controlling diffusive migration, including the partitioning, diffusion and permeation coefficients of the geomembrane.

INTRODUCTION

Volatile organic compounds (VOCs) found in landfill gas can contribute to contamination of both the air and groundwater in the vicinity of a municipal solid waste (MSW) landfill. Migration of landfill leachate through the composite liner system has been the primary focus of past research into contaminant transport of VOCs. However, migration of VOCs through the landfill cover and around the barrier system can also contribute to both atmospheric and groundwater contamination.

Depending on the local regulations, landfill covers may include a geomembrane, geosynthetic clay liner (GCL) or compacted clay liner (or some combination of these as a composite liner) as the primary barrier to the infiltration of water into the landfill and the escape of landfill gas from the landfill. In cases where the geomembrane rests directly on an underlying foundation layer, the degree of saturation may be high enough that the air voids in the soil are not continuous. In this case VOCs in underlying landfill gas will dissolve in the pore of the foundation layer and diffuse upward to the overlying geomembrane. They will diffuse through the geomembrane and any surface film of moisture above the geomembrane or the pore fluid of soil above the geomembrane until it encounters a continuous air phase at which point the VOCs will exsolve and be released to the atmosphere. Under these circumstances the diffusion of the VOCs will be from the dissolved phase in water into and through the geomembrane and the question arises as to what resistance the geomembrane will provide to this diffusion. To answer that question one requires an estimate of the sorption and diffusion of VOCs for the particular geomembrane. Thus this paper focuses on assessing the diffusion characteristics poly-vinyl chloride (PVC) geomembranes with respect to VOCs dissolved in water. The alternative case of diffusion from gas phase through the geomembrane will be considered in a subsequent paper.

BACKGROUND

Landfill gas is generated by the biochemical degradation of solid waste, typically by anaerobic bacteria (Prosser and Janecek, 1995). The average large landfill produces 50 Mg of gas emissions per year. Methane typically comprises 45% to 58% of the landfill gas volume. Carbon dioxide is usually 32% to 45% of the landfill gas volume. VOCs contribute only a small fraction to landfill gas composition, ranging from 0% to 0.1% by volume (Soltani-Ahmandi, 2000). However, even in low concentrations, VOCs can pose significant health risks. 30 organic landfill gas constituents are classified as Hazardous Air Pollutants (HAP) by the US Environmental Protection Agency (EPA).

Typical concentrations of compounds found in landfill gas, compiled from 9 different sites, are listed in Table 1 along with the lowest and highest concentrations reported. The most common VOCs found in the gaseous phase in landfills are BTEXs: benzene, toluene, ethyl benzene and xylenes and are known HAPs (U.S. EPA, 2003). They volatilize quickly, but resist degradation in the environment. Often, the concentrations of organic contaminants found in landfill gas exceed the Ambient Air Quality Guidelines set by the Ontario Ministry of the Environment in Regulation 346, Schedule 2 (MOE, 2004). Contaminants that migrate out of the landfill can be potential risks to human health and the environment. Thus it is critical to understand the extent of potential transport of these VOCs from the gas and through the liners in an overlying cover system.

There are two transport mechanisms: advective and diffusive flow. A pressure gradient arising from a build up of pressure in the landfill provides the driving force for advective flow through tears or holes in the geomembrane (Stark and Choi, 2005). Contaminants are carried or moved with the flowing medium (Benson, 2000). Proper installation of the final cover system minimizes defects in the liner. However, even if the geomembrane is free from defects, contaminants can migrate through the non-porous membrane by molecular diffusion (Haxo, 1990.)

For a well constructed geomembrane with minimal holes, diffusion is the dominate mode of transport for organic contaminants, including VOCs (Edil, 2003, Rowe, 2005). Research has shown that VOCs can diffuse through high-density polyethylene (HDPE) geomembranes (Park and Nibras, 1993; Mueller et al., 1998; Sangam and Rowe, 2001b). There is also been one study of sorption and permeation of organic contaminants through poly-vinyl chloride (PVC) geomembranes (Xiao et al., 1997). Further research is needed to examine diffusive migration through PVC geomembranes.

Diffusion of vapour or liquid permeants through geomembranes occurs in three steps; adsorption, diffusion and desorption. This has been examined for dilute organic contamination in aqueous solutions (Park and Nibras, 1993; Prasad *et al.* 1994; Sangam and Rowe, 2001). Several researchers (Pierson and Barroso, 2002 Stark and Choi, 2005) have reported that the transport of gases and vapours through non-porous geomembranes can also be estimated by this three step mechanism.

Table 1
Typical concentrations of compounds found in landfill gas at different sites^a.

Compounds	Average Concentration (ppmv)	Minimum Concentration (ppmv)	Maximum Concentration (ppmv)
Benzene	2.34	0.002	52.2
Chlorobenzene	0.34	0.002	7.6
1,2-Dichlorobenzene	0.82	0.002	1.6
1,1-Dichloroethane	1.95	0.002	19.5
1,2-Dichloroethane (EDC)	0.84	0.001	30.1
1,2-Dichloroethene	1.90	0.003	84.7
DCM	13.33	0.003	620.0
Ethylbenzene	14.52	0.001	428.0
Styrenes	1.50	0.002	87.0
Tetrachloroethene (PCE)	4.07	0.002	180.0
Toluene	44.66	0.005	758.0
Trichloroethene (TCE)	3.16	0.003	34.0
Vinyl chloride	4.52	0.051	48.1
Xylenes	64.13	0.002	664.0

^aCompiled by the author from different landfill sites: Challa *et al.* (1997); Hodgson (1992); Lee and Jones-Lee (1994); Soltani-Ahmadi (2000); Tchobanoglous *et al.* (1993).

Firstly, the contaminant partitions between the source medium and adjacent surface of the geomembrane. Secondly, the compound diffuses through the geomembrane driven by chemical potential. Finally, the compound partitions between the outer geomembrane surface and the receiving medium (Sangam and Rowe, 2001). After a period of time, equilibrium is reached between the concentration in the geomembrane and the concentration in either the source or receptor media (Rowe, 1998). The equilibrium between geomembrane and the source medium can be related by Henry's Law:

$$c_g = S_{gf}c_f, \quad (1)$$

where c_g is the concentration in the geomembrane [ML^{-3}], c_f is the concentration in the source fluid (either gas or liquid) [ML^{-3}], and S_{gf} is the partitioning coefficient [-].

In the second step, the diffusion of the penetrant through the geomembrane is described by Fick's first law:

$$f = -D_g \frac{dc_g}{dz}, \quad (2)$$

where f is the mass flux [$\text{ML}^{-2}\text{T}^{-1}$]. The diffusion coefficient, D_g [L^2T^{-1}] is specific to the geomembrane and contaminant of interest. c_g is the concentration of the compound in the geomembrane [ML^{-3}] and z represents the distance parallel to the direction of transport. When the diffusion coefficient is constant, the change in penetrant concentration in the geomembrane with time t , is expressed by Fick's second law:

$$\frac{\partial c_g}{\partial t} = D_g \frac{\partial^2 c_g}{\partial z^2} \quad (3)$$

The final step is also described by Henry's Law:

$$c'_g = S'_{gf} c_f, \quad (4)$$

Often the partitioning coefficient into the geomembrane is assumed to be equal to the partitioning coefficient out of the geomembrane ($S_{gf}=S'_{gf}$). This is especially true when the source and receptor fluid are the same (Sangam, 2001).

It is very difficult to measure the concentration of contaminant inside the geomembrane. Instead Equations 1 and 3 are rearranged to give a relationship for the change in concentration in the geomembrane. When the source and receptor media are alike the relationship is as follows:

$$f = -D_g \frac{dc_g}{dz} = -S_{gf} D_g \frac{dc_f}{dz}, \quad (5)$$

The equation can further be simplified in terms of a permeation coefficient, P_g [L^2T^{-1}], which represents the mass transfer across the boundaries (Sangam and Rowe, 2001), where:

$$P_g = S_{gf} D_g \quad (6)$$

This paper focuses on the transport of VOC contaminants in dilute aqueous concentrations through PVC geomembranes exposed to water above and below the liner. Geomembranes in direct contact with contaminants from landfill gas in the vapour phase is addressed in a subsequent paper.

EXPERIMENTAL INVESTIGATIONS

3.1 Material and Methods

The study examined a 0.76 mm (30 mil) thick flexible polyvinyl chloride (PVC) geomembrane supplied by Canadian General-Tower Limited (Cambridge, Ontario, Canada). Table 2 summarizes its relevant properties. Four aromatic hydrocarbons (benzene, toluene, ethylbenzene and xylenes) that are common volatile organic compounds existing in landfill leachate and gases were examined (U.S. EPA, 2003). The significant properties of these laboratory grade chemicals (purchased from Sigma-Aldrich, Mississauga, Ontario, Canada and Chromatographic Specialties Inc, Brockville, Ontario, Canada.) are presented in Table 3.

Tests were carried out using purchased BTEX standards and injecting known amounts into vials and cells filled with organic-free distilled deionized water (DD water). Care was taken to ensure that VOCs from the testing environment did not contaminate the water source. Concentrations in cells reflected typical levels of VOCs found in landfill gas.

Table 2
Properties of PVC geomembranes

Properties	Methods (ASTM)	Units	Values
Thickness	D5199	mm (min)	0.72
Breaking factor	D882	kN/m ² (min)	13100 x 11721
Elongation at break	D882	% (min)	500 x 500
Tear resistance	D1004	N (min)	27 x 22
Low temperature	D2136	°C	-30
Dimensional stability	D1204	% (max)	5.0
Water Extraction	D1239	% (max)	0.25
Volatile Loss	D1203	% (max)	1.0

Table 3
Selected properties^a of organic contaminants tested

Chemicals	Molar weight (g/mole)	Density (g/cm ³)	Aqueous Solubility ^b (mg/l)	Log K _{ow}	Henry's Constant ^c (L _{water} /L _{air})
Benzene	78.11	0.8765	1780	2.13	0.200
Toluene	92.14	0.8669	515	2.79	0.234
Ethylbenzene	106.17	0.8670	152	3.13	0.273
<i>m</i> -Xylene	106.17	0.8642	161.9	3.20	0.254
<i>p</i> -Xylene	106.17	0.8811	156	3.13	0.265
<i>o</i> -Xylene	106.17	0.8802	152	3.18	0.180

^aFrom Montgomery and Welkom (1990).

^bAt 20°C.

^cFrom U.S. EPA (2001). At 22°C.

From the sorption and control cell vials, 5 ml liquid samples were taken using a 5ml Purge & Trap syringe. In diffusion tests, 100 µl liquid samples were taken using gas tight syringes and directly injected into the 5 ml Purge & Trap syringe filled with DD water. For all tests, 10 µl of 20 µg/ml surrogates fluorobenzene and 1,4-dichlorobenzene were added.

3.2 Analytical Methods

Samples were analyzed by Purge and Trap Gas Chromatography/Mass Spectrometer (P&T)-GC/MS. The procedure used a Hewlett Packard 5890 GC with a P&T unit and 5972 mass selective detector (MS). Samples purged for 11 minutes with helium carrier gas at a flow rate of 0.9 m/min. The temperature was then raised to 225°C for the baking step. The VOCs were desorbed off the VOCARB trap inside the Purge and Trap apparatus for 4 minutes. Desorbed compounds travel to the VOCOL column (60 m x 0.32 mm x 2.0 µl) in the GC. Chromatographs were quantified using selective ion monitoring (SIM). This method is based on EPA method 8240.

A certified BTEX reference standard of known concentration was analyzed regularly throughout the testing. Sample concentrations were quantified based on this standard's area. The efficiency was calculated by using the recovery of the surrogate. Samples were rejected if the efficiency was outside the 80-120% range. The efficiency was predominantly between 95-100%

throughout the testing period. Concentrations were corrected for the recovery of the surrogate. Duplicate and triplicate samples from the cells were often analyzed. Blanks, spikes and quality control samples were run at a frequency of approximately 10%. Quality control samples were prepared from a separate BTEX standard source. The GC/MS had a detection limit of 1 µg/l, established prior to testing.

3.3 Procedures

3.3.1 Control tests

Control tests were performed to establish the mass losses of contaminants due to sampling procedures, leaks in the cells, or sorption to the cell materials: stainless steel, glass, viton o-rings. Control tests were performed in both the 40 ml glass serum vials used for sorption testing and stainless steel double compartment diffusion cells (Fig. 1). In the sorption vials, BTEX concentrations were prepared using a high concentration standard diluted in DD water. Vials were sampled in duplicate throughout the sorption testing period.

Control tests in the diffusion cells did not contain geomembrane samples. However, the viton o-rings and septums were used to mimic the diffusion cell tests. The source and receptor compartments were filled with DD water and sealed. Chemical were added to the source water to create concentrations similar to those in the diffusion tests. Samples were taken from the source and receptor at regular intervals during the diffusion cell testing period.

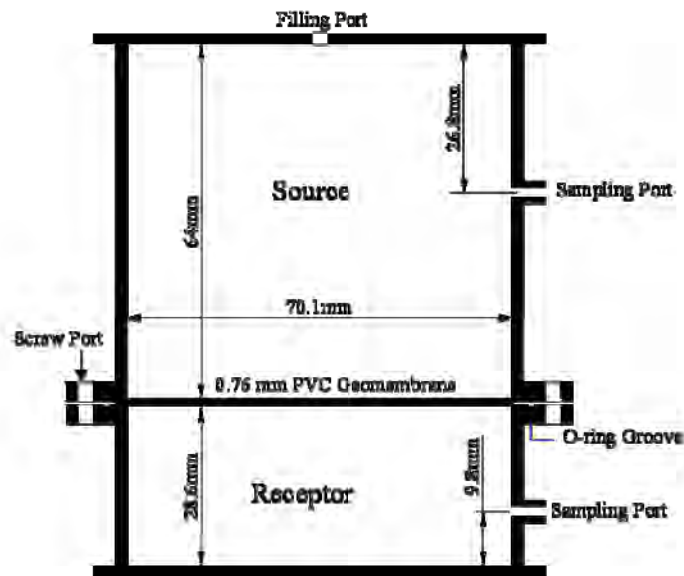


Fig. 1. Schematic of Diffusion Cell

3.3.2 Sorption tests

For sorption tests, after recording the initial masses of geomembrane samples, they were immersed in 40 ml glass serum vials filled with DD water. The same concentrations of BTEX as the control cells were prepared. Samples were agitated in rotating box, moving at 30 ± 2 rpm, to achieve maximum sorption of chemicals into the geomembranes, following the USEPA Method 1311. Vials were sampled in duplicate. Contaminant concentrations were evaluated over time until equilibrium was reached. The partitioning coefficient for each compound was calculated using the following equations derived from the contaminant mass balance at equilibrium. The mass balance Eq. 7 is listed:

$$M_{s0} = M_{sF} + M_{gF}, \quad (7)$$

where M_{s0} is the initial mass of the contaminant in solution [M]; M_{sF} is the final mass of the contaminant in solution [M] and M_{gF} is the mass contained in the geomembrane [M]. When the Eq. 6 is rearranged in terms of concentrations and volumes, it becomes:

$$c_{f0}V_{f0} = c_{fF}V_{fF} + \frac{M_g}{\rho_g} c_{gF}, \quad (8)$$

where c_{f0} is the initial contaminant concentration in solution [ML^{-3}]; V_{f0} is the initial solution volume [L^3]; c_{fF} is the final contaminant concentration in solution [ML^{-3}]; V_{fF} is the final solution volume [L^3]; M_g is the initial mass of the geomembrane sample [M]; ρ_g is the geomembrane density [ML^{-3}] and c_{gF} is the final concentration of the contaminant in the geomembrane at equilibrium [ML^{-3}]. The partitioning equation can be expressed by substituting Eq. 8 into Eq. 1 as shown below:

$$S_{gf} = \frac{[c_{f0}V_{f0} - c_{fF}V_{fF}] \rho_g}{M_g c_{fF}} \quad (9)$$

3.3.3 Diffusion tests

In the diffusion tests, a stainless steel double compartment cell (source and receptor) were divided by a 30 mil PVC geomembrane sample. The receptor cell was filled with DD water. The source cell was filled with a dilute aqueous chemical solution at concentrations levels similar to contaminant concentrations in landfill leachate. The liquid phase was sampled to measure the initial concentration in the source. Diffusion cells were maintained at a constant temperature of 22°C . Samples were taken from the source and receptor at regular time intervals. The concentrations in the source and receptor were plotted as normalized concentrations relative to the initial concentration in the source.

The experiments used concepts and theory developed by Rowe et al. (1998) for clayey soils and by Rowe et al. (1995, 1996) for geomembranes. Sangam and Rowe (2001) reported diffusion and partition coefficients for dilute organic contaminants in the liquid phase through high-density polyethylene geomembranes using this approach.

A finite mass boundary exists within the closed system. Therefore, the mass of contaminants in the source at a given time is equal to the initial mass minus the mass diffused through the geomembrane. The equation for the concentration in the source at time t is written as:

$$c_{ss}(t) = c_{s0} - \frac{1}{H_{ss}} \int_0^t f_{ss}(\tau) d\tau \quad (10)$$

where $c_{ss}(t)$ is the contaminant concentration in the source at time t [ML^{-3}]; c_{s0} is the initial contaminant concentration in the source [ML^{-3}]; H_{ss} is the reference height of the source reservoir [L]; $f_{ss}(\tau)$ is the mass flux of contaminant into the geomembrane with time τ [$\text{ML}^{-2}\text{T}^{-1}$]. The decrease in contaminant concentrations in the source are modeled using Eq (10). To model the increase in concentrations in the receptor as contaminants partition out of the geomembrane, a similar equation is used:

$$c_{rs}(t) = c_{r0} + \frac{1}{H_{rs}} \int_0^t f_{rs}(\tau) d\tau \quad (11)$$

where $c_{rs}(t)$ is the contaminant concentration in the receptor at time t [ML^{-3}]; c_{r0} is the initial contaminant concentration in the receptor [ML^{-3}]; H_{rs} is the reference height of the receptor solution [L]; $f_{rs}(\tau)$ is the mass flux of contaminant into the geomembrane with time τ [$\text{ML}^{-2}\text{T}^{-1}$].

The diffusion (D_g), partition (S_{gf}) and permeation (P_g) coefficients of contaminants through PVC geomembranes were inferred by fitting theoretical results of the diffusion equations to the source and receptor concentration data from diffusion tests. The boundary conditions given by Eq. 10 and Eq. 11 were used. Analysis of experimental data followed the procedure outlined by Rowe et al. (1995) using the finite layer analysis program POLLUTE[®] v.7 (Rowe and Booker, 2004).

RESULTS AND DISCUSSIONS

4.1 Control tests

Results of the sorption control tests are shown in Fig. 2. Benzene did not experience any significant mass loss as the concentration decreased 0.6% from the initial concentration. The decrease in concentration of toluene, ethylbenzene, m&p-xylenes and o-xylenes from the initial concentration were 6.7, 10, 12 and 9.0% respectively. The decrease in concentration may be attributed to their sorption onto the walls of the glass vials. Since there was no significant change in the concentration of benzene, losses associated with sampling events can be considered negligible. Therefore, the dominant form of mass loss of the other contaminants is sorption to the testing material. Analysis of the sorption and diffusion tests using the geomembrane takes into consideration the mass loss of contaminants due to sorption onto the testing material (glass vials or cells).

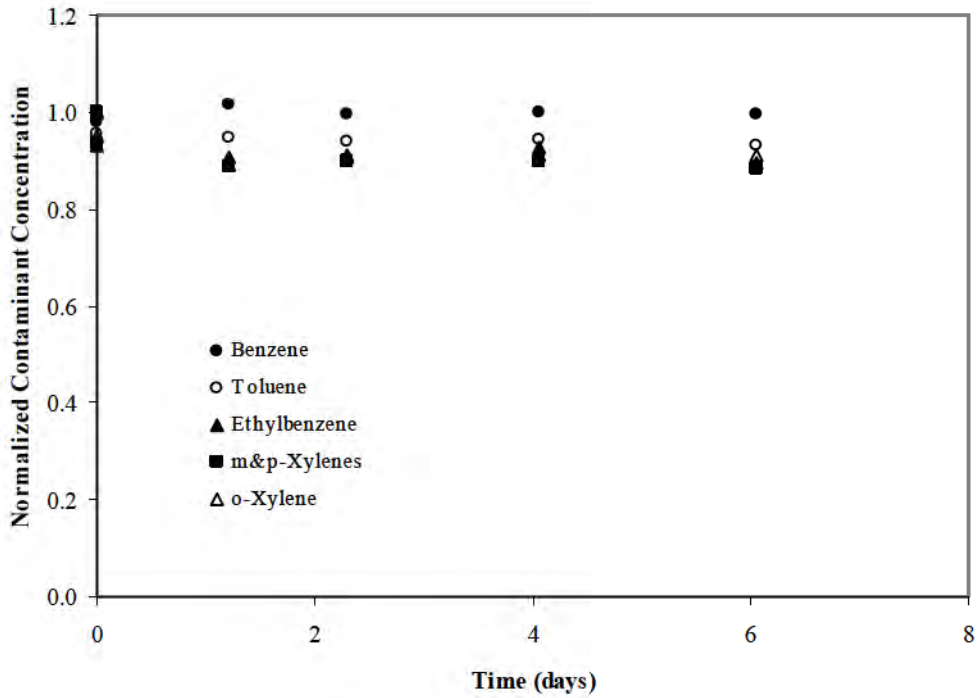


Fig 2. Measured concentrations of contaminants in sorption control cells.

4.2 Sorption tests

Fig. 3 shows the decrease in contaminant concentrations in the solution during the sorption tests using PVC geomembrane samples. The changes in concentration are plotted as normalized concentrations relative to the initial concentration. The equilibrium concentration was reached after 2 days. Benzene concentrations decreased by 79% of the initial concentration. The decrease in initial contaminant concentration was much higher for the other contaminants. Ethylbenzene and xylenes showed the greatest decrease of 97%, while toluene had a concentration decrease of 93%.

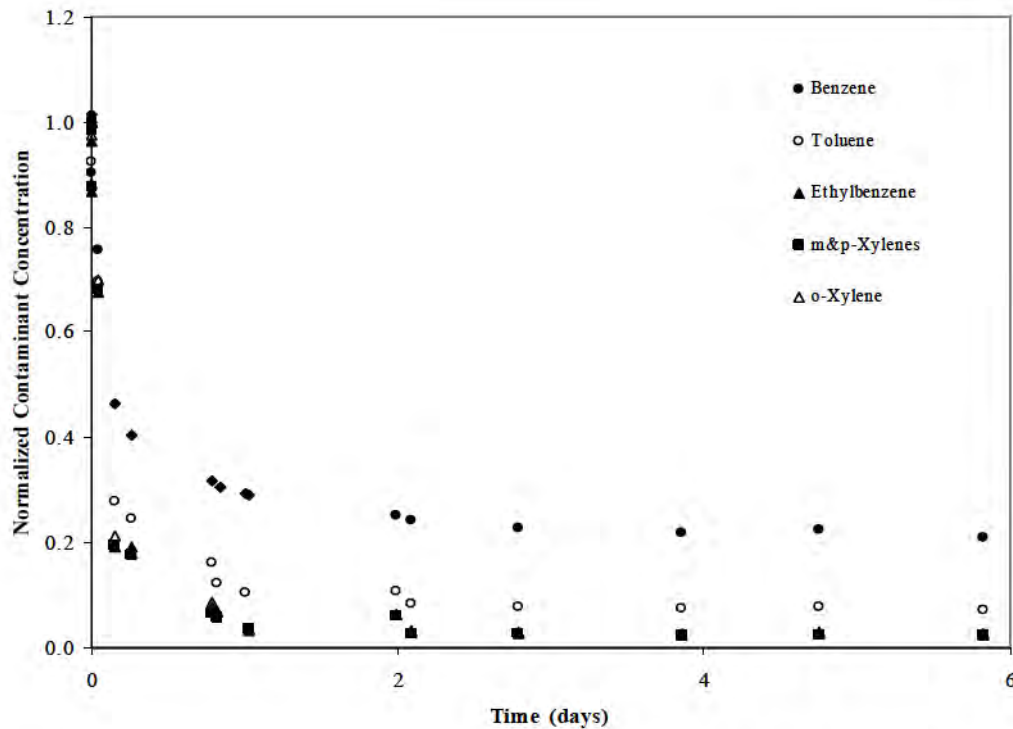


Fig. 3. Measured concentrations of contaminants during sorption test with PVC geomembrane.

The partitioning coefficients S_{gf} for the geomembrane were calculated using Eq. 9 and are presented in Table 4. A non-corrected S_{gf} was calculated assuming that there was no significant mass loss of contaminants. This case assumes that the sorption of contaminants to the testing material (glass vials or cells) is negligible in comparison to their attraction to the geomembrane. The corrected S_{gf} took into consideration the mass loss of contaminants to the testing material even in the presence of the geomembrane. The extent of mass loss of contaminants was approximated using results from the control tests. The actual values for the partitioning coefficients are expected to lie between the non-corrected and corrected values.

The highest non-corrected S_{gf} =1536 for the geomembrane was *m&p*-xylenes, followed by *o*-xylene (S_{gf} =1425), ethylbenzene (S_{gf} =1335), toluene (S_{gf} =450) and benzene (S_{gf} =135).

Table 4
Estimated partitioning coefficients from sorption tests

Contaminants	PVC Geomembrane	
	Non-corrected S_{gf}	Corrected S_{gf}
Benzene	134.3	133.4
Toluene	450.3	417.8
Ethylbenzene	1335	1191
<i>m&p</i> -Xylenes	1536	1349
<i>o</i> -xylenes	1425	1295

4.3 Diffusion tests

Throughout diffusion tests, contaminant concentrations in the source and receptor were monitored with time until equilibrium was reached. In repeated tests, equilibrium was reached after 7-8 days. The normalized concentrations in the source and receptor are presented in Fig. 4 and Fig. 5, respectively. Both of these values were normalized relative to the initial concentration of contaminants in the source reservoir.

Concentrations in the source decreased with time as the contaminants diffused through the geomembrane. Concentrations for *m&p*-xylenes in the source decreased the greatest. The partitioning coefficient controls the decrease in source concentration; therefore the higher values of S_{gf} for *m&p*-xylenes would predict this trend. Following *m&p*-xylenes, *o*-xylene concentrations decreased the greatest in the source, followed by ethylbenzene, toluene and benzene. Benzene had the fastest rate and amount of increase in the receptor, followed by toluene. Ethylbenzene, *m&p*-xylenes and *o*-xylene increased at slower rates. The increase in contaminant concentration in the receptor is controlled by the permeation coefficient.

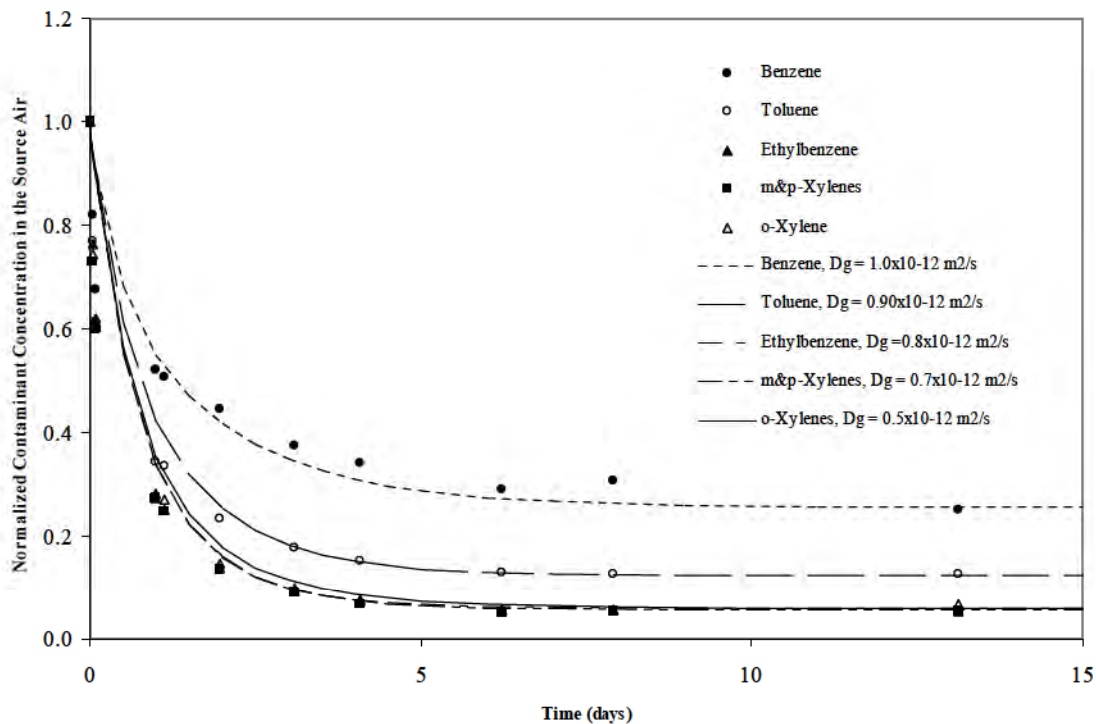


Fig. 4. Contaminant concentration changes in the source with time during diffusion tests using 30 mil PVC geomembrane.

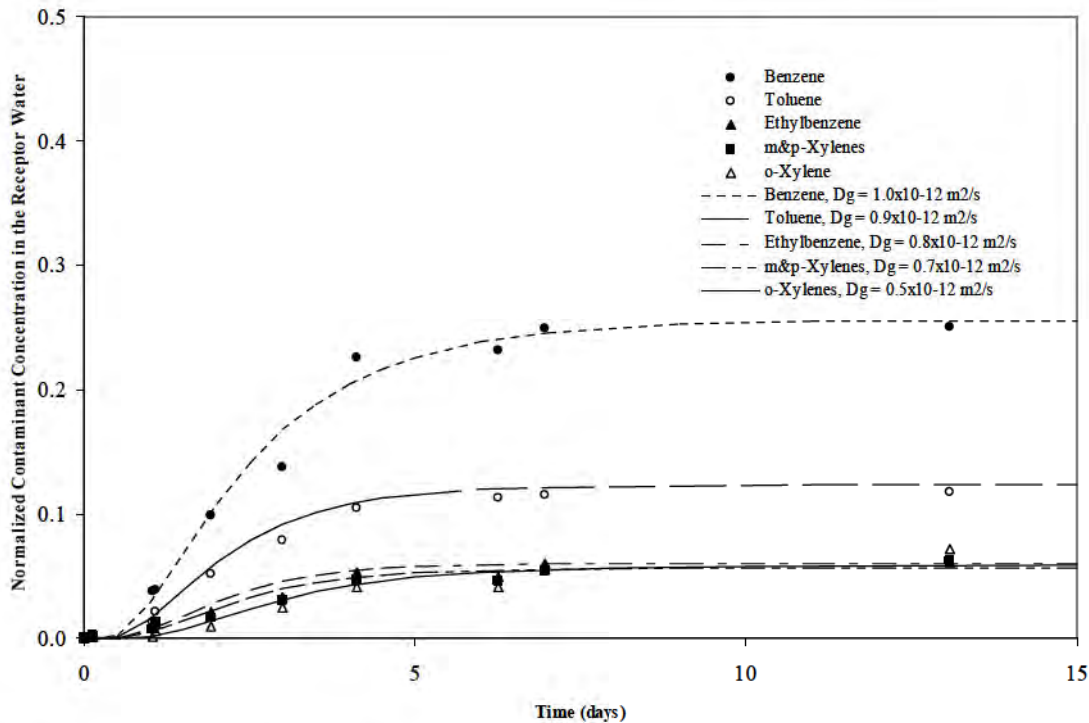


Fig. 5. Contaminant concentration changes in the receptor with time during diffusion tests using 30 mil PVC geomembrane.

Theoretical curves obtained with POLLUTEV7 are shown in Fig. 4 and 5. The permeation coefficient for each contaminant was calculated from these curves and the S_{gf} measured in sorption tests. All three diffusive migration parameters: D_g , S_{gf} and P_g , are presented in Table 5. They are compared with the S_{gf} and D_g values for HDPE geomembranes from literature.

Table 5

Inferred partitioning, diffusion and permeation coefficients of PVC geomembranes from diffusion tests and of HDPE geomembranes from Literature^a.

Contaminants	PVC Geomembrane			HDPE Geomembranes		
	S_{gf} (-)	D_g ($-10^{13} \text{ m}^2 \text{ s}^{-1}$)	P_g ($-10^{10} \text{ m}^2 \text{ s}^{-1}$)	S_{gf} (-)	D_g ($-10^{13} \text{ m}^2 \text{ s}^{-1}$)	P_g ($-10^{10} \text{ m}^2 \text{ s}^{-1}$)
Benzene	200	10.0	2.00	30-32	1.2-3.5	0.4-1.1
Toluene	550	9.3	5.12	65-100	1.2-3.0	0.8-3.0
Ethylbenzene	1250	8.0	10.0	285	1.8	0.5
<i>m&p</i> -Xylenes	1350	7.0	9.45	205-347	0.6-1.7	0.1-0.6
<i>o</i> -xylenes	1300	5.0	6.50	180-240	0.4-1.5	0.1-0.4

^aFrom Rowe et al. (2004).

CONCLUSIONS

The success of a landfill is dependant on the barrier system's ability to minimize the migration of contaminants into the surrounding environment. Specifically, the effectiveness of the primary cover material, PVC geomembranes, as a barrier to the diffusion of VOC contaminants has been measured. From theoretical modeling using POLLUTE[®], curves were fit to results from laboratory studies carried out on 0.76 mm PVC geomembrane samples. The diffusion coefficients were found to be between 5×10^{-13} - 1×10^{-12} $\text{m}^2 \text{s}^{-1}$. The partitioning coefficients were ascertained from laboratory sorption tests. It was found that S_{gf} was higher for xylenes and ethylbenzene than toluene and benzene. Results from this study can be used to predict the rates of diffusion of gas-phase VOC contaminants through the final covers in landfills.

ACKNOWLEDGEMENTS

The study was financially supported by PGI and Canadian General-Tower Limited. The authors are also grateful to the Analytical Services Unit of Queen's University, Kingston, Canada for their support and use of their laboratory facilities.

REFERENCES

- Benson, C.H., 2000. "Liners and Covers for Waste Containment", *Proceedings of Fouth Kansai International Geotechnical Forum, Creation of a New Geo-Environmental*, Japanese Geotechnical Society, Kyoto, Japan, May 2000, 1-40.
- Challa, J., Skoff, D. and Quirus, F.J. 1997. "Landfill Gas as Source of VOCs in Ground Water". *Practice Periodical of Hazardous, Toxic, and Radioactive Waste Management*. 1 (2): 61-75.
- Edil, Tuncer, B. 2003. "A Review of Aqueous-phase VOC Transport in Modern Landfill Liners". *Waste Management*. (23): 561-571.
- Eiswirth, M., 1999. "Gas Transport and Contaminant Movement in the Unsaturated Zone and Groundwater". *Gambling with Groundwater-Physical, Chemical and Biological Aspects of Aquifer-stream Relations*, Ed. Brahana *et al.*, Karlsruhe, Germany, 433-438.
- Haxo, H.E., 1990. "Determining the transport through geomembranes of various permeant in different applications". *Geosynthetic Testing for Waste Containment Applications*, STP 1081, Koerner, R.M., Editor, ASTM International, West Conshohocken, PA, USA, 75-94.
- Hodgson, A., Garbesi, K., Sextro, R. and Daisey, J., 1992. "Soil-Gas Contamination and Entry of Volatile Organic Compounds into a House Near a Landfill". *Air and Waste Management*. (42): 277-283.
- Kraemer, T.A., Marshall, M. and Hartley, J., 1998. "Developing Strategy for Establishing Landfill Gas as Cause of Ground-Water Contamination". *Practice Periodical of Hazardous, Toxic, and Radioactive Waste Management*. 2 (4): 150-153.
- Lee, G.F. and Jones-Lee, A, 1994. "Impact of Municipal and Industrial Non-Hazardous Waste Landfills on Public Health and the Environment: An Overview" *Prepared for California EPA Comparative Risk Project*. Sacramento, CA.
- Ministry of the Environment (MOE), 2004. "Ambient Air Quality Criteria: Regulation 346". Ontario, Canada.

- Mueller, W., Jakob, I., Tatzky-Gerth, R. and August, H., 1998. "Solubilities, Diffusion and Partition Coefficients of Organic Pollutants in HDPE Geomembranes: Experimental Results and Calculations", *Proceedings from the 6th International Conference on Geosynthetics*, Federal Institute for Materials Research and Testing, BAM, Berlin, Germany, 239-248.
- Park, J. K., Nibras, M., 1993. "Mass Flux of Organic Chemicals Through Polyethylene Geomembranes". *Water Environment Research*, (65): 227-237.
- Pierson, P. and Barroso, M., 2002. "A Pouch Test for Characterizing Gas Permeability of Geomembranes." *Geosynthetics International Journal*, 9 (4):345-372.
- Prosser, R. and Janecek, A., 1995. "Landfill Gas and Groundwater Contamination". *Proceedings of 1995 American Society of Civil Engineers (ASCE) Convention*, GC Environmental, Inc., October 1995.
- Rowe, R.K., Quigley, R.M. and Booker, J.R., 1995a. "Clayey Barrier Systems for Waste Disposal Facilities", E& FN Spon (Chapman & Hall), London, Ontario, Canada, 390.
- Rowe, R.K., Hrapovic, L and Kosaric, N., 1995b. "Diffusion of Chloride and DCM through HDPE Geomembrane", *Geosynthetics International*, 2 (3): 507-535.
- Rowe, R.K., 1998. "Geosynthetics and the Minimization of Contaminant Migration through Barrier Systems Beneath Solid Waste," Geotechnical Research Report GROT-2-98, Geotechnical Research Centre, University of Western Ontario, London, Ontario, Canada.
- Rowe, R.K. and Booker, J.R., 2004. POLLUTE v.7- 1D Pollutant Migration Through a Non-Homogeneous Soil, © 1983, 1990, 1994, 1997, 1998, 2004. Distributed by GAEA Environmental Engineering Ltd.
- Rowe, R.K., Quigley, R.M., Brachman, R.W.I. and Booker, J.R., 2004. *Barrier Systems for Waste Disposal Facilities*, 2nd Ed. Spon Press.
- Rowe, R.K., 2005. "Long-term Performance of Barrier Systems." *Geotechnique*, 55 (9): 631-678.
- Sangam, H.P., 2001. "Performance of HDPE Geomembrane Liners in Landfill Applications", Thesis for Doctor of Engineering Science, University of Western Ontario, London, Ontario, Canada.
- Sangam, H. P. and Rowe, R. K., 2001. "Migration of Dilute Aqueous Organic Pollutants Through HDPE Geomembranes". *Geotextiles and Geomembranes*, 19 (6): 329-357.
- Soltani-Ahmadi, H., 2000. "A Review of the Literature Regarding Non-Methane and Volatile Organic Compounds in Municipal Solid Waste Landfill Gas", *Department of Civil Environmental Engineering, University of Delaware*.
- Stark, T. D. and Choi, H., 2005. "Methane Gas Migration Through Geomembranes". *Geosynthetics International*, 12 (2): 120-126.
- Staudinger and Roberts, 1996. "A Critical Review of Henry's Law Constants for Environmental Applications" *Critical Reviews in Environmental Science and Technology*, 26 (3): 205-297.
- Tchobanoglous, G., Theisen, H. and Vigil, S., 1993. *Integrated Solid Waste Management Engineering Principles and Management Issues*. McGraw-Hill, New York.
- United States Environmental Protection Agency (USEPA), 1992. Method 1311: Toxicity Characteristic Leaching Procedure. USEPA.
- United States Environmental Protection Agency (USEPA), 1996. Method 8260: Volatile Organic Compounds by Gas Chromatography/Mass Spectrometry (GC/MS). USEPA.
- United States Environmental Protection Agency (USEPA), 2003. "Hazardous Landfill Gas". *Federal Register: Rules and Regulations*. 68 (11): 2227-2242.
- Washington, J., 1996. "Gas partitioning of dissolved volatile organic compounds in the vadose zone: Principles, temperature effects and literature review" *Ground Water*, 34 (4): 709-718.

Xiao, S., Moresoli, C., Bolvenkamp, J., and De Kee, D., 1997. "Sorption and Permeation of Organic Environmental Contaminants Through PVC Geomembranes". *Journal of Applied Polymer Science*, 63 (9): 1189-1197.

CONTACT:

Rebecca S. Mc Watters
GeoEngineering Centre at Queen's-RMC
Department of Civil Engineering Queen's University
Kingston, Ontario
Canada K7L 3N6
rebecca@civil.queensu.ca
Phone:613-572-2325

USE OF GEOSYNTHETICS AT THE CLEVELAND HOPKINS INTERNATIONAL AIRPORT DEICING FACILITY

Daniel A. Petno, P.E., R.W. Armstrong and Associates, Cleveland, Ohio; Chris Athanassopoulos, P.E., Colloid Environmental Technologies, Arlington Heights, Illinois

ABSTRACT

The design and construction of the new deicing facility at the Cleveland Hopkins International Airport involves several innovative geosynthetic applications. Historically, airplane deicing operations at the airport have taken place at the individual airline gates, resulting in an increased potential for uncontrolled releases of aircraft deicing fluids, such as propylene glycol. In response to the threat of discharges to the nearby Rocky River and its tributary, Abram Creek, the Ohio EPA mandated a new centralized deicing facility, where deicing fluid could be applied and collected in a fully controlled manner. The new deicing facility, which covers approximately 40 acres, was sized to allow deicing fluid to be applied to eight airplanes at one time, allowing up to 30 aircraft depart in each peak operation, thus minimizing departure delays. The 38-inch pavement section at the facility consists of (from top to bottom): 16 inches of Portland Cement Concrete; 8 inches of econocrete; 8 inches of crushed aggregate; a hydraulic barrier layer; 6 inches of aggregate-filled geoweb; and existing subgrade. To control the deicing fluids, a geosynthetic clay liner (GCL) was selected as the barrier layer, the most critical environmental component of the design. A plastic-laminated GCL was selected to mimic a composite liner design. A geoweb with aggregate infill was placed beneath the GCL to provide a drainage layer, frost protection, and structural support. To provide separation and filtration in the underdrain system, nonwoven geotextiles were incorporated into the design. The facility design also includes a 1.6 million gallon pre-cast concrete underground storage tank, 4 million gallons of aboveground spent deicing fluid storage, a pump station, an elaborate system of flow diversion valves, and over fifty-seven thousand feet of welded HDPE pipe, up to 54 inches in diameter. Construction of the new deicing facility began in the autumn of 2005, and was completed in September 2006.

INTRODUCTION

The design and construction of a new centralized deicing facility at the Cleveland Hopkins International Airport (CLE) involved several geosynthetic applications, including a plastic-laminated geosynthetic clay liner (GCL), a cellular confinement system (geoweb), nonwoven geotextiles, and HDPE pipe. This paper presents a discussion of the project background, design, and construction, with a particular focus on the geosynthetic elements. To the authors' knowledge, this is the first use of either GCLs or geoweb materials at an airport deicing facility.

BACKGROUND

Ice, frost, or snow present significant concerns for airports in temperate and cold-weather climates. Even small amounts of these materials on aircraft surfaces can pose serious safety concerns. To address this concern, deicing fluids (such as ethylene glycol, propylene glycol, and urea) are typically sprayed on aircraft before takeoff. Historically, airplane deicing operations at CLE have taken place at the individual airline gates (Photograph 1). In the past, individual planes were sprayed with deicing fluids while passengers were boarding, with any drippings and overspray collected by vacuum trucks. For the 2004 to 2005 deicing season, a total of

approximately 1.1 million gallons of concentrated deicing fluid (applied as a 50:50 propylene glycol/water solution) were handled in this manner at CLE. While this deicing approach minimizes departure delays – particularly at a hub airport where many flights depart at one time – it also results in an increased potential for uncontrolled releases of propylene glycol. Although propylene glycol is not as toxic as ethylene glycol, it does have a high biochemical oxygen demand (BOD), driving down dissolved oxygen levels in receiving waters, and potentially impacting aquatic organisms.

In response to past glycol releases to nearby Abram and Silver Creeks (both tributaries of the Rocky River, which empties into Lake Erie), the Ohio EPA mandated a centralized deicing operations at CLE, where deicing fluid could be applied and collected in a fully controlled manner. The City of Cleveland Department of Port Control contracted R.W. Armstrong and Associates, Inc. to design a new centralized deicing facility and oversee its construction. The design is discussed in the following section.

DESIGN OVERVIEW

The CLE centralized aircraft deicing facility (CDF) covers a total area of 76 acres, which includes Deice Pad 1, Deice Pad 2, associated taxiways, Site A and Site B (Figure 1). Since the primary deicing operations will take place at the two CDF Pads and their associated taxiways, these areas were sized to allow deicing fluid to be applied to eight commercial airplanes at one time (30 planes/hub movement). Site A will provide a staging and storage area for deicing applicator equipment, while Site B will contain two 2-million gallon aboveground storage tanks for either onsite recycling or discharge to the Northeast Ohio Regional Sewer District (NEORS) sanitary system.

As shown in Figure 2, the typical 38 inch thick CDF pavement cross-section consists of (from top to bottom): 16 inches of Portland Cement Concrete; 8 inches of econcrete; 8 inches of crushed aggregate; a hydraulic barrier layer; 6 inches of aggregate-filled geoweb; and existing subgrade. The geoweb with aggregate infill was placed beneath the GCL to provide drainage, frost protection, and structural support. Nonwoven geotextiles were provided below the geoweb for subgrade separation and on top of the geoweb to cushion the hydraulic barrier above. Nonwoven geotextiles were also incorporated into the underdrain system to provide separation and filtration.

The CDF has a total fluid capture capacity of 5.6 million gallons – 4.0 million in two aboveground storage tanks (ASTs) at Site B, and 1.6 million in an underground storage tank (UST) beneath Site A. The underground tank was constructed using pre-cast concrete arch top structural sections – the first of its kind for this type of application. A GCL was installed beneath the UST as secondary containment in case of tank leakage, with a separate underdrain system installed between the tank bottom and the GCL. A network of HDPE pipes will collect runoff from the pads and transport it by gravity to the UST for retention, then either directly to the stormwater system (clean run-off from the entire airport during the summer), or to the collection system (glycol-laden water during the winter). Based on the glycol concentrations, runoff will be segregated and managed through the use of five diversion vaults. One of the vaults will divert the highest concentration flows from the primary glycol application area to an isolated section of the UST. High concentrate runoff that accumulates in this 150,000 gallon vault will be pumped into trucks for further processing, recycling, or off-site disposal. The

remaining four diversion vaults will route runoff to either the storm sewer or to the low concentration section of the UST. From here, the glycol-impacted water will flow over 3,500 feet through a sealed pipe system to a deep wet well. A 10 cfs pump station will transfer glycol-laden runoff to the aboveground tanks located outside the airfield fence at Site B. From there, fluids will be metered into a gravity sanitary sewer line connecting the aboveground tanks to the NEORS D sanitary sewer system. In-line measurements and telemetry reporting will be used to ensure that the NEORS D influent limits (summarized in Table 1) are not exceeded. These limits were established to prevent excessive BOD/COD loads associated with propylene glycol from overwhelming the processing capabilities of the sewer treatment plant.

TABLE 1 - NEORS D DISCHARGE LIMITS

Parameter	Daily Maximum	<i>Daily Loading</i>
COD	650 mg/L	21,150 lb/day
BOD	406 mg/L	13,200 lb/day
Ammonia	72 mg/L	600 lb/day
Flow	2,700 gpm	3.9 MGD

The specific geosynthetic elements of the CDF design, which are critical to this project’s success, are discussed in the following section.

GEOSYNTHETIC ELEMENTS

Geosynthetic Clay Liner

Successful completion of the CLE deicing facility project involved contributions from several civil engineering specializations (transportation, structural, hydraulics, and environmental). Since the major design objective is to prevent leakage of deicing fluids, the most critical environmental component of the project is the pavement’s hydraulic barrier layer. A needlepunch reinforced, plastic-laminated GCL was selected as the hydraulic barrier layer. Over 2.1 million square feet of GCL were used to line the deicing pads, associated taxiways, and Sites A and B. The GCL consisted of 0.75 lbs/ft² of sodium bentonite encapsulated between woven and nonwoven geotextiles. A 4-mil HDPE plastic geofilm was laminated to the nonwoven geotextile for improved hydraulic performance and chemical resistance. An additional nonwoven geotextile was laminated to the HDPE geofilm to provide increased durability and puncture protection. The GCL was selected for the following reasons:

- **Low hydraulic conductivity.** The plastic-laminated GCL product is certified by the manufacturer to have a maximum hydraulic conductivity of 5×10^{-10} cm/sec when permeated with distilled water. Because the plastic geofilm is virtually impermeable, the actual hydraulic conductivity of the plastic-laminated GCL is expected to be lower.

- **Compatibility with deicing fluids.** Past testing performed by the manufacturer (summarized in Figure 3) showed that, when permeated with a 50:50 solution of ethylene glycol, a standard GCL (without any plastic backing) exhibited a long-term hydraulic conductivity of 7.0×10^{-10} cm/sec. The manufacturer test results are consistent with past findings in the literature. Petrov et al. (1997) found that GCLs are compatible with nonpolar, miscible organic compounds, provided that the organic concentration is less than 60 percent.
- **Bentonite self-healing characteristics.** The potential for punctures was another consideration in selecting a GCL as the hydraulic barrier layer. The swelling and sealing properties of bentonite give a GCL the unique ability to recover from punctures. Studies performed by Shan and Daniel (1991) on GCL samples that were deliberately punctured found that the GCL was able to self-heal holes up to 1 inch in diameter, and still maintain a low hydraulic conductivity. This self-sealing ability allowed for rapid installation around penetrations, such as inlet structures, pipes, and manholes.
- **Protection against ion exchange.** Since the CDF pavement includes crushed limestone aggregate (AASHTO #57 stone), a plastic laminate was incorporated into the GCL to reduce the risk of ion exchange in the sodium bentonite posed by dissolved calcium leaching from the aggregate.
- **Schedule.** A major project driver was schedule – the Ohio EPA had mandated that the new facility be operational by the Fall of 2006. Due to the amount of time involved in getting funding in place, agreement from the airlines, and receiving OEPA approval of the Permit To Install, the construction duration was compressed to one year. This aggressive schedule required construction through the winter months of late-2005 and early-2006. After evaluating various materials, the decision was made to install GCL in lieu of geomembrane or compacted clay. At low ambient temperatures, it would have been extremely difficult to control clay temperature, moisture content, and hydraulic conductivity. Geomembrane panels should only be installed and seamed when ambient temperatures are greater than 40° F, while GCLs have been successfully installed in many cold weather settings. Cold weather delays related to either geomembrane or clay could have pushed the project completion date into 2007, resulting in significant fines.
- **Simplicity of installation.** Another benefit of using a GCL as the hydraulic barrier is ease of installation. While geomembranes require thermal seaming methods, GCLs are seamed by overlapping adjacent panels and applying supplemental granular bentonite to the overlap area. In addition, a pneumatically-powered geosynthetic installation device was used to deploy the GCL. The installation device was mounted on a large-capacity tractor, as shown in Photograph 2. As the tractor operator drove forward, a ground operator used a control cable to unroll the GCL onto flat panels. Using this equipment, several acres of GCL per day were deployed, accelerating the installation.

Deicing fluid collection system (HDPE Pipe)

Another critical environmental component of the CDF design is the liquid collection system. The collection/drainage system consists of over fifty-seven thousand feet (almost 11 miles) of HDPE pipe and underdrains. (Photograph 3). Reinforced concrete pipe (RCP) is typically used for airport drainage applications. However, RCP systems can allow significant infiltration if not installed correctly and can degrade over time. Both possibilities were unacceptable – particularly when repairs would impact airfield operations. HDPE pipe with fusion welded connections, which is compatible with glycol, was selected instead of RCP, to limit glycol exfiltration and groundwater infiltration potential. The HDPE collection system for all anticipated glycol flows was provided from the inlets, through the diversion valves, and downstream to the disposal facilities. The pipe diameters range from 24 to 54 inches, with motor-actuated gate valves. Because of their size, both the piping and valves were specially fabricated for this project, and required a long lead time (the lead time and pipe cost unexpectedly escalated in the fall of 2005 due to the Hurricane Katrina's impact on manufacturing plants along the Gulf Coast). The collection pipes draining the CDF area were sized to accommodate a 10-year summer storm event. To evaluate expected winter flows and storage requirements, a model was developed using the past 50 years of rainfall data, the existing fleet of aircraft, assumed glycol application rates, and estimates of glycol drippage and overspray. This resulted in sizing the total project storage at 5.6 million gallons – consisting of the ASTs, the UST, and storage in the pipe system. The designers also worked with the HDPE pipe manufacturer to determine the minimum pipe thicknesses needed to withstand the expected loading associated with the pavement and the design aircraft.

Drainage Layer/Underdrain System

The native soils at CLE consist of glacial tills (primarily silts and clays), with highly variable geotechnical properties. The 38-inch thick pavement section has been designed based on a subgrade California Bearing Ratio (CBR) of four. Typically, when existing conditions are encountered with CBR values under four, the subgrade needs to be improved by disk and dry; adding cement or lime treatment; or removal of the yielding soil and replacement with stabilization aggregate. However, even when adequate subgrade conditions were present during construction, the relatively shallow water table in the vicinity of the site presented an increased likelihood of saturated soils, which would further reduce the soil's strength and bearing capacity. The water table has been found to rise up to within a couple of feet of the ground surface during the wet seasons in northeast Ohio. To address these subgrade limitations, a 6-inch drainage layer was incorporated into the pavement design. The drainage layer was placed directly on subgrade which was sloped to allow groundwater to move up into the drainage layer and flow to the perforated underdrain system that runs along all edges of the airfield pavement. The intent of the drainage layer and underdrain is to collect shallow groundwater, thus preventing saturated soil conditions, as well as providing structural support and frost heave protection. The underdrain system includes two geosynthetic components: a geoweb and nonwoven geotextiles.

In addition to the “standard” groundwater underdrain system addressed above, the CDF also must provide a drainage path for the glycol-laden water that makes its way down through the top

of the pavement and is blocked by the clay liner. To capture this fluid and keep it from saturating the pavement section over time, a second perforated underdrain system was constructed above the liner. This system is assumed to collect glycol-impacted water for 12 months of the year. Therefore, the outlet pipe cannot be tied into the storm drain system, but will flow by gravity to the pump station for disposal to the sanitary sewer. The entire glycol underdrain system is composed of welded HDPE pipe.

Geoweb

As discussed previously, the glacial till soils present on the CLE airfield are subject to great variability. While the soil typically performs well when near optimum moisture levels, saturated soils are not satisfactory for pavement subgrade. This problem was exacerbated when working during the winter months. In order to bridge some of the softer areas of subgrade, a flexible, three-dimensional polyethylene cellular confinement system (also known as a geoweb) was placed over the subgrade. The geoweb used at CLE is shown in Photograph 4 - over 1.3 million square feet of geoweb were used.

Historically, the drainage layer design consisted of combining a poorly graded aggregate (AASHTO #57 stone) with an asphalt or concrete binder. The layer would then be placed on subgrade with an asphalt or concrete paver. After hardening, the drainage course would form a porous and flexible slab. However, since asphalt plants are not in operation during the winter, and cold winter temperatures would prevent cure of cement binder, a geoweb was chosen to bridge the soft spots as the drainage course. A secondary benefit was that the geoweb drainage layer became a structural layer. During design it was determined that the 6 inch geoweb layer would improve subgrade soils with a CBR value of two, up to the required design CBR of four. The aggregate-filled geoweb produced a stable structural base that distributed loads laterally, and reduced subgrade contact pressures. This was not only beneficial in terms of the overall pavement stability, but also in terms of a stable interim construction platform. By spanning weak soils that would otherwise need to be dug up and moisture conditioned, construction was allowed to proceed uninterrupted through the winter months.

Geotextiles

Since the geoweb was placed directly on top of fine-grained soils, an 8 oz/yd² nonwoven polypropylene geotextile was used as a separation layer between the two distinct soil types. Separation was needed in this application to prevent contamination of the granular infill (and consequently, loss of shear strength) and to prevent punching or migration of the infill material into the subgrade. An additional 8 oz/yd² nonwoven geotextile was placed between the top of the geoweb and the bottom of the GCL for puncture protection. The puncture risks posed by both the aggregate-filled geoweb (below the GCL) and the crushed aggregate concrete subbase (above the GCL) were evaluated during the early stages of construction by building a field test pad. The test pad was constructed using 8 oz/yd² nonwoven geotextiles on either side of the geoweb. Various heavy construction vehicles (loaded dump trucks, graders, etc.) were driven repeatedly across the pad, simulating worst-case construction conditions. The GCL was then exposed and inspected for signs of damage. Since no significant damage was observed in the

test pad samples, the 8 oz/yd² nonwoven geotextile beneath the GCL and the 3.2 oz/yd² nonwoven geotextile laminated to the top of the GCL were deemed adequate for puncture protection. The favorable test pad results indicated that there would be little concern regarding swelling GCL under the rigid pavement or above the geoweb. As a constructability issue, the contractor took due care to make sure the GCL did not sit unconfined for a long period such that it would hydrate. As a practical matter, the needlepunch-reinforced proved quite able to withstand the construction process without issue.

CONCLUSION

The design and construction of the new centralized deicing facility at Cleveland Hopkins International airport involved several innovative uses of geosynthetics. In response to historical glycol releases to nearby streams, Ohio EPA mandated that a new centralized deicing facility be built within one year to capture and control airplane deicing fluids. The design of the deicing facility had to meet these regulatory requirements, while at the same time, minimize departure delays. Geosynthetics were critical in successful completion of a project with such strict regulatory constraints and customer expectations. The overall project, which had a budgeted cost of \$46.89 million, was constructed within budget and within the EPA-mandated schedule of one year. Because of the tight deadlines, much of the construction activities took place during the winter months in late-2005 and early-2006. The cost of the construction effort was borne by the airlines, and will ultimately be recovered from airline customers, through a Passenger Facility Charge added to the price of each ticket.

REFERENCES

1. CETCO. (2000) "Technical Reference 109 - GCL Compatibility with Airport Deicing Fluid".
2. Giroud, J.P. (1997) "Equations for Calculating the Rate of Liquid Migration Through Composite Liners Due to Geomembrane Defects", *Geosynthetics International*, Vol. 4, Nos. 3-4, pp. 335-348.
3. Ohio EPA. (2004) "Report on a Permit to Install Application and Detail Plans for the Cleveland Hopkins International Airport Centralized Deicing Facility."
4. Petrov, R.J. et al. (1997), "Selected Factors Influencing GCL Hydraulic Conductivity", *ASCE Journal of Geotechnical and Geoenvironmental Engineering*, Vol. 123, No. 8, pp. 683-695.
5. Shan, H.Y., and Daniel, D. (1991) "Results of Laboratory Tests on a Geotextile/Bentonite Liner Material." Presented at *Geosynthetics '91*, Atlanta, Georgia.
6. Draft 2006 - 2007 Aircraft Anti-icing/De-icing and Discharge Management Plan, Cleveland Hopkins International Airport.

FIGURE 1 – CLE CENTRALIZED DEICING FACILITY

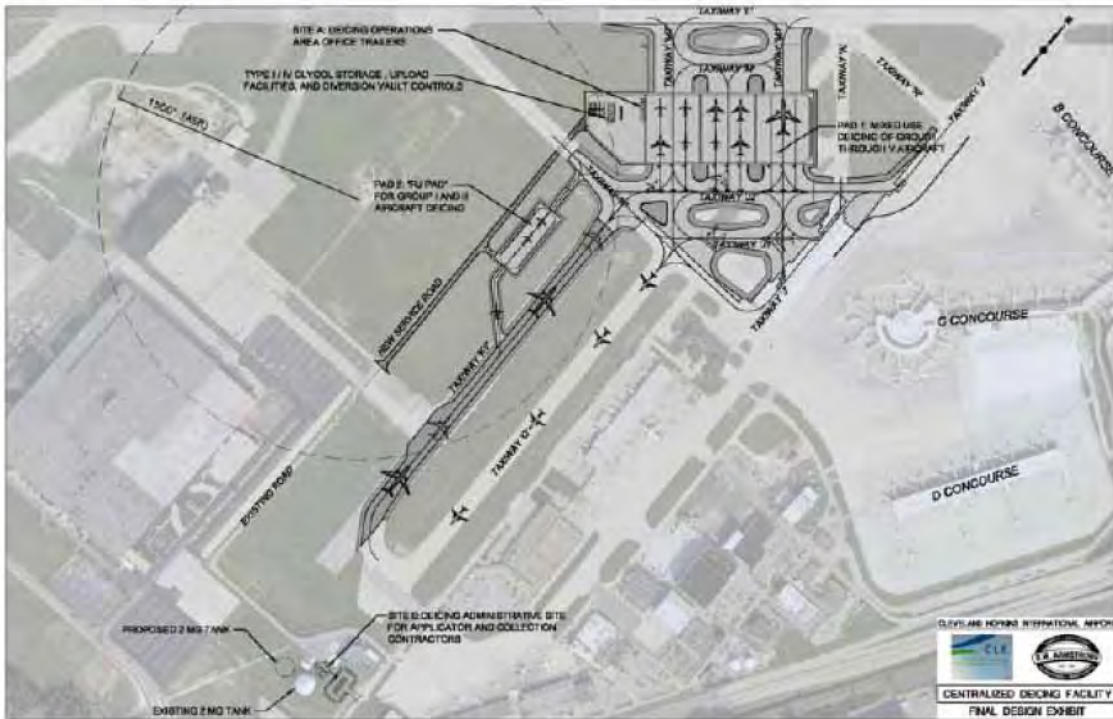


FIGURE 2 – TYPICAL CDF PAVEMENT CROSS-SECTION

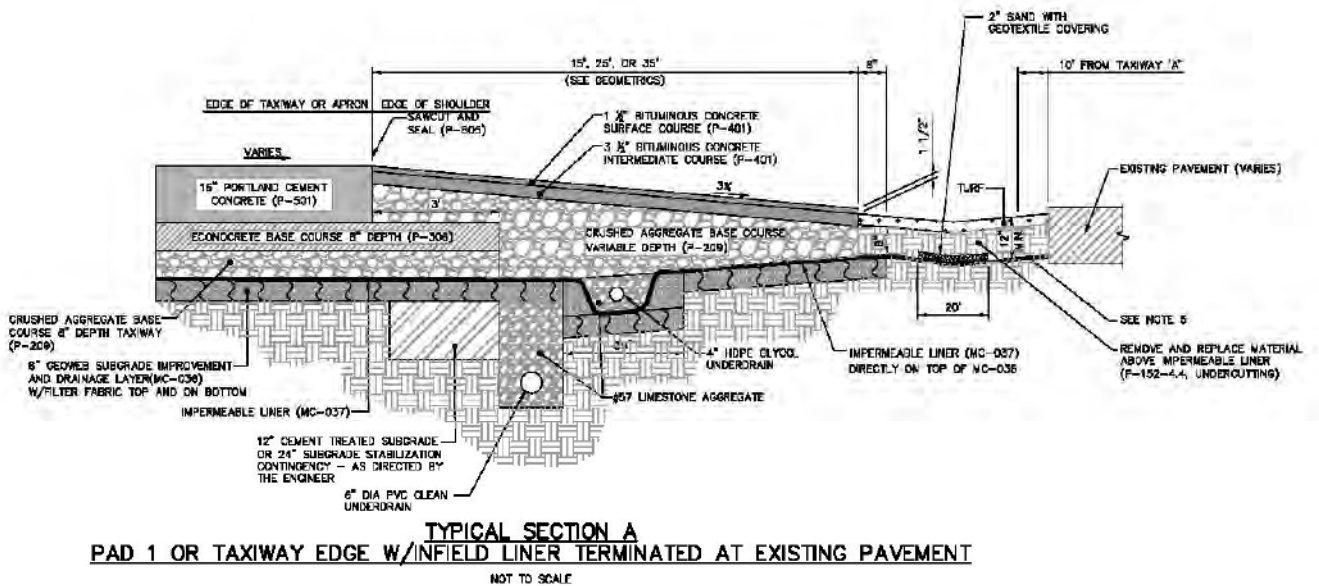
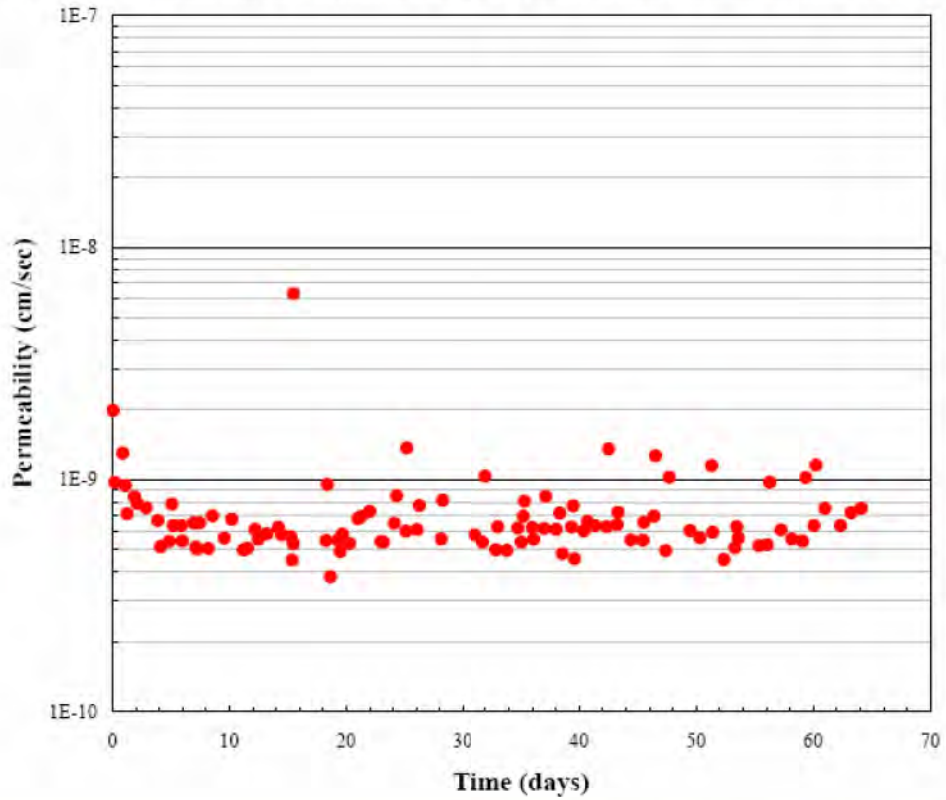


FIGURE 3 - GCL COMPATIBILITY WITH AIRPLANE DEICING FLUID



PHOTOGRAPH 1 - AIRPLANE DEICING OPERATIONS



PHOTOGRAPH 2 – GCL INSTALLATION



PHOTOGRAPH 3 – HDPE PIPE INSTALLATION



PHOTOGRAPH 4 – GEOWEB INSTALLATION



CONTACT:

Chris Athanassopoulos, PE

CETCO

1500 West Shure Drive, 5th floor

Arlington Heights, IL 60004

Phone: 847-818-7945

Email: catha@cetco.com

TEMPERATURE OF SECONDARY LINERS IN MUNICIPAL SOLID WASTE LANDFILLS

R. Kerry Rowe, GeoEngineering Centre at Queen's-RMC, Department of Civil Engineering, Queen's University, Canada; A. Hoor, GeoEngineering Centre at Queen's-RMC, Department of Civil Engineering, Queen's University, Canada

ABSTRACT

Heat generated by biodegradation of waste and by other chemical processes can potentially affect the long-term performance of liner system by causing desiccation of clay liner and rapid aging of geomembranes. Recognizing that primary liners are susceptible to the effects of elevated temperature the question then arises as to how much less susceptible is the secondary liner to temperature? This paper examines heat flow in the barrier system below municipal solid waste (MSW) and examines the likely temperature of the secondary liner for a number of different liner configurations and modes of landfill operation. It is shown that the temperature on the secondary liner may be significantly elevated and suggested that this should be considered in design.

INTRODUCTION

Modern landfill barriers systems are expected to control contaminant migration into the surrounding ground and surface water systems for decades to centuries. Often these systems involve a double composite liner comprised of a primary geomembrane and either compacted clay liner (CCL) or geosynthetic clay liner (GCL), a leak detection/ secondary leachate collection system and a secondary geomembrane and CCL or GCL. The geomembrane provides the main resistance to leakage while the CCL or GCL reduces the potential for leakage through holes in the geomembrane. In order to provide good long-term protection the geomembrane (especially the secondary geomembrane) will need to have a long service life and the CCL or GCL should not desiccate.

Heat is generated in landfills as a result of biodegradation of waste and hydration of ash (Rowe 2005). High temperatures are reported in the body of landfill and in landfill liners. At the base of landfills temperatures up to 50°C to 60°C have been reported (Collins 1993; Yoshida et al. 1997) for cases where there is no leachate collection system. With an operating collection systems temperatures of 30-40°C have been reported (Rowe 2005) and with the operation of the landfill as a bio-reactor temperatures of 45°C have been reported (Koerner and Koerner 2006). The temperature of an underlying aquifer is typically in the range 5 to 20°C. Thus there will usually be a temperature gradient between the base of the waste down to the aquifer. This temperature gradient can cause water vapor to flow from the base of landfill to underlying layers. There can also be a counteracting movement of water due to the development of high matric suction in the upper, dryer soil. The net effect of these mechanisms may be desiccation of the clay liner. In addition the higher the temperature of the geomembrane, the shorter will be its service life (Hsuan and Koerner, 1998; Rowe and Sangam 2002; Rowe 2005).

Hanson et al. (2005) performed numerical studies and field measurements to examine the temperature profile in a landfill liner. A landfill with single composite liner system was studied

and the effect of seasonal variations of temperature before and after waste placement was investigated.

The potential for desiccation cracking of clay liners due to thermal gradients has attracted a limited amount of attention. Holzlohner (1990), Gottheil and Brauns (1995) and Philip et al. (2002) performed experimental studies on clay liners in basal lining systems. These studies focused on thermally induced moisture movement in liners. These tests have also been numerically simulated by several investigators (Döll 1997; Zhou and Rowe 2003). Similarly Southen (2005) and Southen and Rowe (2004, 2005a and 2005b) examined composite liners with a GCL and reported both experimental studies from small scale and large scale laboratory tests as well as the results of numerical simulations of coupled heat and moisture transfer in single liner landfill barriers.

Although, as noted above, there has now been a modest amount of research dealing with the temperature, and effects of temperature for primary liners, there is a paucity of data relating to secondary liners. Thus the objective of this paper is to report on a preliminary examination of the potential temperature on secondary liners for different liner configurations and different modes of landfill operation.

HEAT CONDUCTION

Fourier's law gives the basic equation for defining heat transfer under steady condition:

$$q = -\lambda \nabla T \quad (1)$$

where q is heat flux, λ is thermal conductivity, and ∇T is temperature gradient in the direction of heat flow.

Transient heat conduction can be derived by performing energy balance for a control volume and, for a heterogeneous material, is given by:

$$\lambda_x \frac{\partial^2 T}{\partial x^2} + \lambda_y \frac{\partial^2 T}{\partial y^2} + \lambda_z \frac{\partial^2 T}{\partial z^2} + \dot{q} = \rho c \frac{\partial T}{\partial t} \quad (2)$$

where λ_x , λ_y and λ_z are thermal conductivity in x, y and z directions. In this equation \dot{q} is volume energy addition, ρ is density of the material, c is specific heat (the product ρc is called heat capacity) and t is time.

Assuming that the problem is one-dimensional and no energy is added or taken out of the system, equation 2 can be rewritten as:

$$\lambda \frac{\partial^2 T}{\partial x^2} = \rho c \frac{\partial T}{\partial t} \quad (3)$$

or, on rearranging terms, as:

$$\frac{\lambda}{\rho c} \frac{\partial^2 T}{\partial x^2} = \frac{\partial T}{\partial t} \quad (4)$$

where the term $\frac{\lambda}{\rho c}$ is called thermal diffusivity and denoted by α .

MODEL PARAMETERS AND MODELING PROCEDURE

In order to model heat transfer in barrier system, thermal properties of soil and geosynthetic materials are required. Typically one requires the thermal conductivity, thermal diffusivity and/or the heat capacity (when any two of these parameters are defined, the third one can be calculated) to model heat conduction. In this study the thermal properties of soil were selected based on data published in the literature.

The thermal conductivity of soil depends on many parameters. The soil structure and the number and nature of contacts between soil particles play a key role in thermal conductivity values (Farouki 1981). The dry density and porosity of soil are also important factors affecting thermal conductivity. An increase in porosity results in a decrease in density. In dry soils this means that there is more air in the soil. Therefore thermal conductivity of dry soil decreases with an increase in porosity. However in wet soils the relationship between thermal conductivity and porosity is more complex. In a saturated soil, the thermal conductivity decreases with an increase in porosity only if thermal conductivity of soil particles is greater than that of water (Farouki 1981). The soil moisture content has a great impact on thermal conductivity. An increase in moisture content results in increase in thermal conductivity (Salomone et al. 1984a, 1984b, 1989; Becker et al. 1992). The mineral composition of the soil is another important factor with quartz based soils having a higher thermal conductivity than soils comprised of other minerals. Particle shape and grain-size distribution may also affect thermal conductivity. Figure 1 shows the typical range of thermal conductivities for different types of soil based on published data.

A few researchers have measured specific heat of soil (e.g. Kersten 1949; Ghuman and Lal 1985; Bilskie 1994). However, most investigators have assumed that heat capacity of soil is the weighted sum of heat capacities of soil constituents (i.e. soil grains, water and air). This latter method is used for calculating heat capacity herein.

A number of studies have measured thermal diffusivity (Mickley 1951; Ghuman and Lal 1985; Hopmans and Dane 1986; Bilskie 1994). Thermal diffusivity usually increases with water content, however experimental studies carried out by Ghuman and Lal (1985) suggested that in some types of soil (sandy and loamy soils in these tests) the thermal diffusivity reached a peak at a moisture content below saturation and decreased for higher water contents .

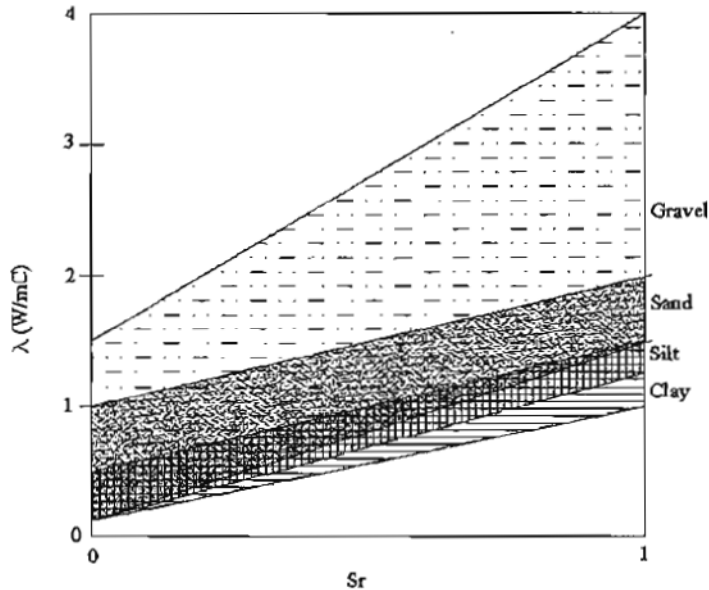


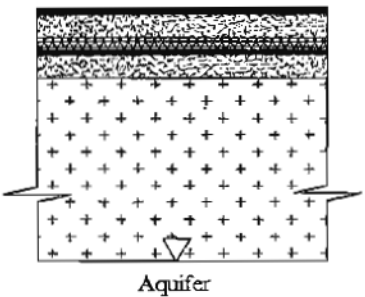

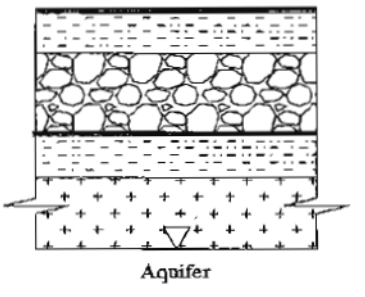
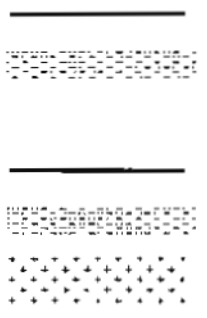
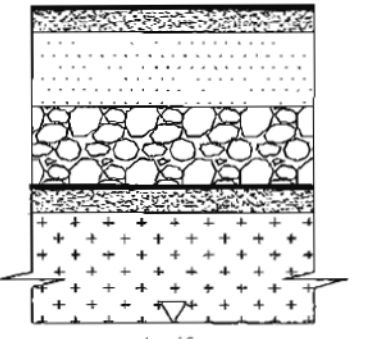
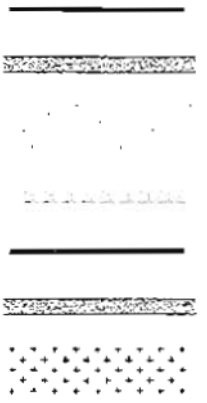
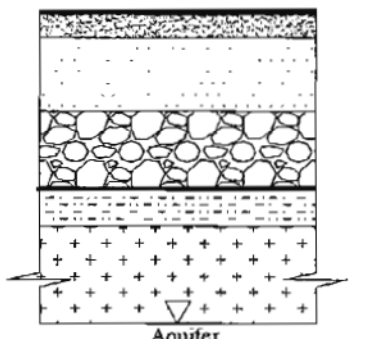
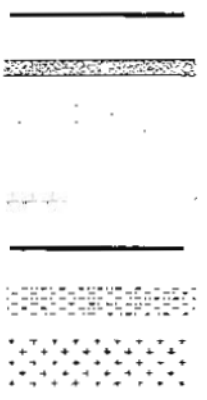
Figure 1 - Thermal conductivity, λ , of soils versus degree of saturation, S_r (Data is collected from: TM 5-852-6/ AFR 88-19; Sepaskhah and Boersma 1979; McInnes 1981; Ghuman and Lal 1985; Hopmans and Dane 1986; Sorour et al. 1990; Bristow 1998; Tarnawski et al. 2000; Tarnawski and Leong 2000; Ochsner et al. 2001; Bristow et al. 2001; Coté and Konard 2005a, 2005b)

There is a paucity of data regarding the thermal properties of geosynthetic materials. Thus for this paper, the thermal conductivity and heat capacity of the geosynthetics of interest are calculated based on their components. Since high density polyethylene (HDPE) geomembranes are primarily comprised (~97%) of HDPE, the thermal properties of geomembranes were taken to be within the range of thermal properties of HDPE. The same approach was used for geotextiles. For GCLs the properties were calculated based on the properties of a layer of clay (the bentonite) and two layers of geotextile.

Given the large area of a barrier system compared with its thickness, a one-dimensional model was adopted to simulate heat flow in the vertical direction. Heat conduction can be modeled either by equation 1 (steady state) or equation 4 (transient). In this paper, the computer program POLLUTE v.7 was used to solve equation 4. The barrier system was modeled as several layers of materials with different thermal properties. The temperature was specified at the upper boundary (top of top liner) and lower boundary (top of aquifer).

Different liner configurations were modeled to estimate the likely temperature of the secondary liner. Table 1 shows different liner configurations simulated in this study. The distance from the thermal boundaries to the secondary liner may be an important factor influencing the secondary liner temperature. Thus the distance between primary and secondary geomembrane (i.e. thickness of the primary CCL or foundation layer below a primary GCL and the thickness of the leak detection/ secondary leachate collection system) and the distance between the bottom of the secondary liner and the aquifer (i.e. thickness of the attenuation layer) was examined for second, third and fourth barrier systems.

Table 1- Configurations of barrier systems examined (* base case; see text for other cases examined)

	Barrier System	Layers	Thickness (mm)
1	 <p>Aquifer</p>	 <p>Geomembrane GCL Geonet Geomembrane GCL Attenuation Layer</p>	<p>2 14 5 2 14 3000</p>
2	 <p>Aquifer</p>	 <p>Geomembrane CCL Gravel Geomembrane CCL Attenuation Layer</p>	<p>2 750* 300 2 750 3000</p>
3	 <p>Aquifer</p>	 <p>Geomembrane GCL Foundation Layer Gravel Geomembrane GCL Attenuation Layer</p>	<p>2 14 500* 300 2 14 3750</p>
4	 <p>Aquifer</p>	 <p>Geomembrane GCL Foundation Layer Gravel Geomembrane CCL Attenuation Layer</p>	<p>2 14 500 300 2 750 1000*</p>

RESULTS

As a base case, consideration was given to a 40°C difference in temperature between the aquifer and the top of uppermost geomembrane (e.g. an aquifer temperature of 10 °C and top of liner temperature of 50°C) and the increase in temperature throughout the profile was calculated relative to the aquifer temperature. For a given profile the problem is linear with respect to temperature and thus the results for an increase in temperature could be used to calculate the increase in temperature for any combination of aquifer and top liner temperature combination. For example, if the aquifer temperature were really 10 °C and the top liner was 40 °C giving a temperature difference of 30 °C, the increase in temperature at any point would be $30/40=0.75$ times that shown below for a 40 °C difference.

Given that there is variability in the published thermal properties being used for the layers of soil and geosynthetics an initial series of analyses were performed to examine the sensitivity of the results to these properties. Figures 2 and 3 show the temperature profile for the first barrier system (all geosynthetic above the attenuation layer). In these simulations the thermal diffusivity (α) of the geosynthetic and soil layers was chosen to be at the upper end of the published range for one case (denoted "maximum α ") and at the lower end of the published range (denoted "minimum α "). Given the thin profile of this "all geosynthetic" barrier system, Figure 2 is dominated by the temperature gradient in the soil attenuation layer. Figure 3 therefore focuses on the temperature changes within the geosynthetic components of the barrier system.

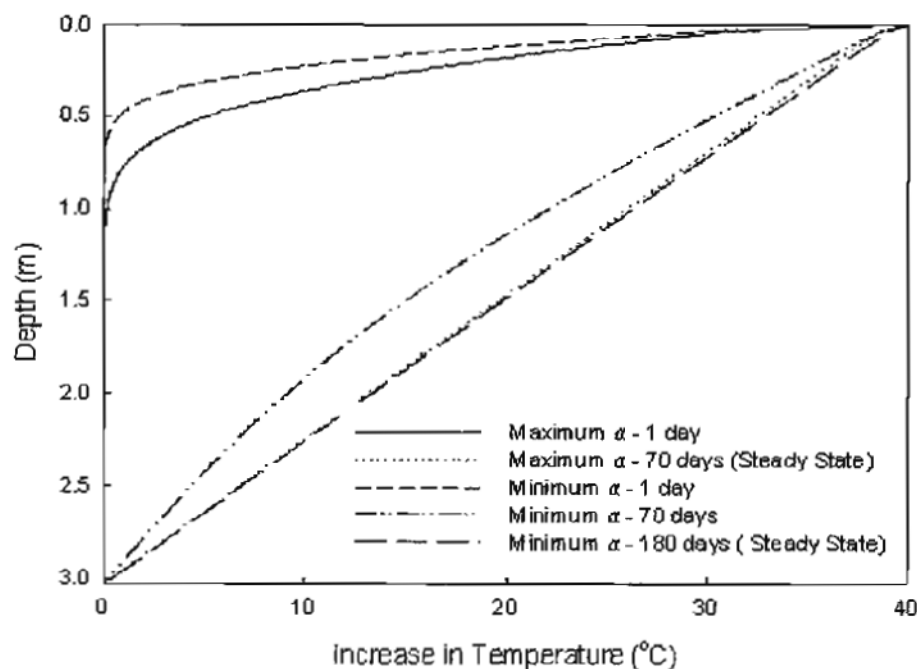


Figure 2- Effect of thermal diffusivity on temperature profile- 1st barrier system shown in Table 1 (geonet is used for leak detection/secondary leachate collection system)

Figures 2 and 3 show that while an increase in thermal diffusivity affects the time it takes to reach the steady state temperature profile, it does not significantly affect the final profile. This is because the thermal properties of liner materials do not differ from each other sufficiently to

have a significant effect on final heat flow. For the range of thermal diffusivities considered, it only takes between 70 and 180 days to come to a thermal equilibrium. These times are quite short. It is also noted that at equilibrium the temperature of the secondary geomembrane is within 1oC of that of the primary geomembrane. This is consistent with the (albeit very limited) field data (Rowe 2005). Thus while the secondary geomembrane has the advantage of not being directly exposed to leachate (which should increase the service life of the geomembrane) the similarity in temperature will mean that the service life of the secondary geomembrane is likely to be of a similar order of magnitude as the primary geomembrane (see Rowe 2005).

Figure 4 provides a similar examination of the effect of uncertainty regarding the thermal properties of the geosynthetics and soil for the second barrier system shown in Table 1. In this case the GCL has been replaced by 0.75m thick compacted clay liners and 0.3m of gravel is used for the leak detection/ secondary leachate collection system. For this thicker profile it took between 200-550 days to reach steady state depending on the parameters.

Figure 5 shows calculated increase in temperature versus time at the secondary geomembrane for both barrier systems examined above (Systems 1 and 2 in Table 1). It can be seen that uncertainty regarding thermal properties does not have a significant effect on the result but that the geometry of the barrier system does. At steady state, for a 40°C increase in temperature on the primary geomembrane, there would be a 30.2°C to 39.4°C increase on the secondary liner for systems 2 and 1 respectively (for maximum α). This difference is significant since a 0.6oC difference between primary and secondary will have little effect on service life but a 9.8oC difference could have a significant effect on the difference in service life of the primary and secondary geomembrane.

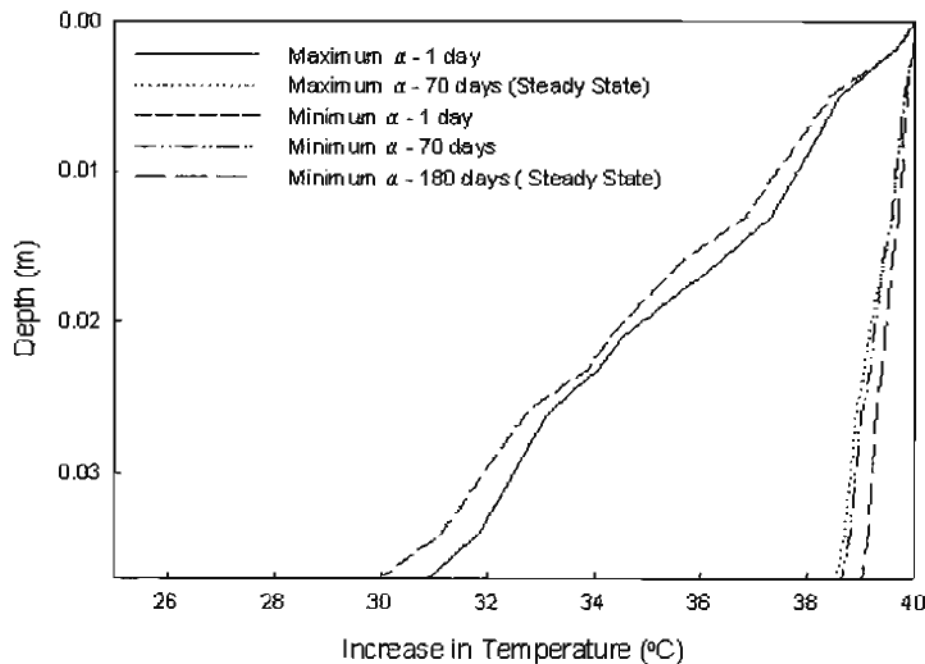


Figure 3- Temperature profile within the geosynthetic components of Figure 2

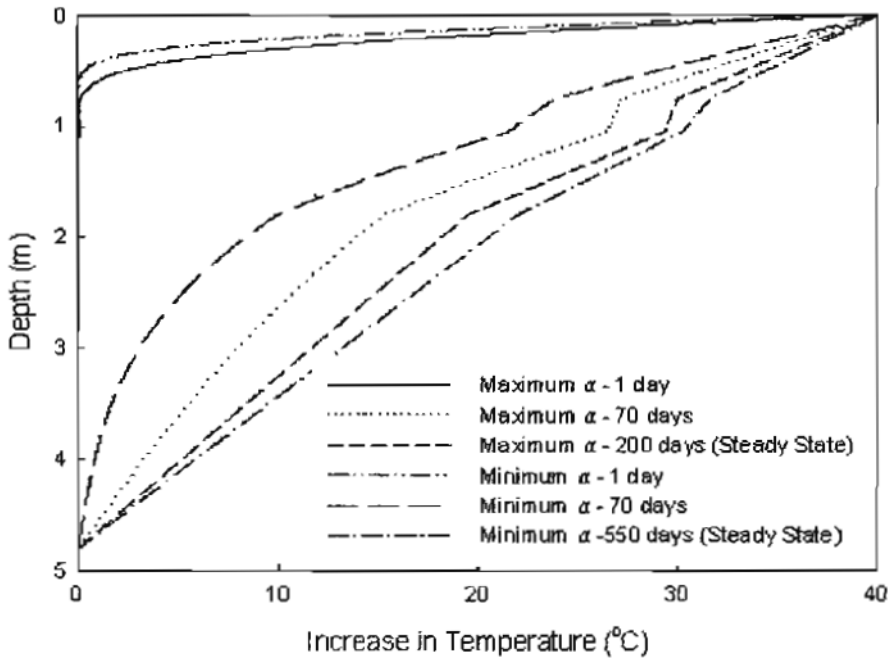


Figure 4- Effect of thermal diffusivity on temperature profile- 2nd barrier system (gravel is used for leak detection/secondary leachate collection system)

Recognizing the important role played by the primary compacted clay liner and gravel leak secondary leachate collection system on the increase in temperature on the secondary geomembrane for in the comparison of barrier systems 1 and 2 above, the effect of varying the thickness of CCL underlying primary geomembrane was examined. Figure 6 shows results for CCLs with thicknesses of 0.5, 0.75 and 1 m (all other parameters held constant, minimum thermal diffusivity was used). The increase in temperature in secondary geomembrane for CCL thicknesses of 0.5, 0.75 and 1 m was 32.5, 30.2 and 28.1, respectively. Figure 7 shows a similar examination of the effect of the foundation thickness for the third barrier system shown in Table 1, where as primary liner a GCL is combined with a soil foundation layer assumed to be 0.5, 0.75, 1 m thick and the increase in temperature in the second geomembrane is 31.7, 29.3 and 27.2, respectively. Both Figures 6 and 7 show that the thicker the CCL or GCL and foundation layer, the lower the temperature in secondary liner.

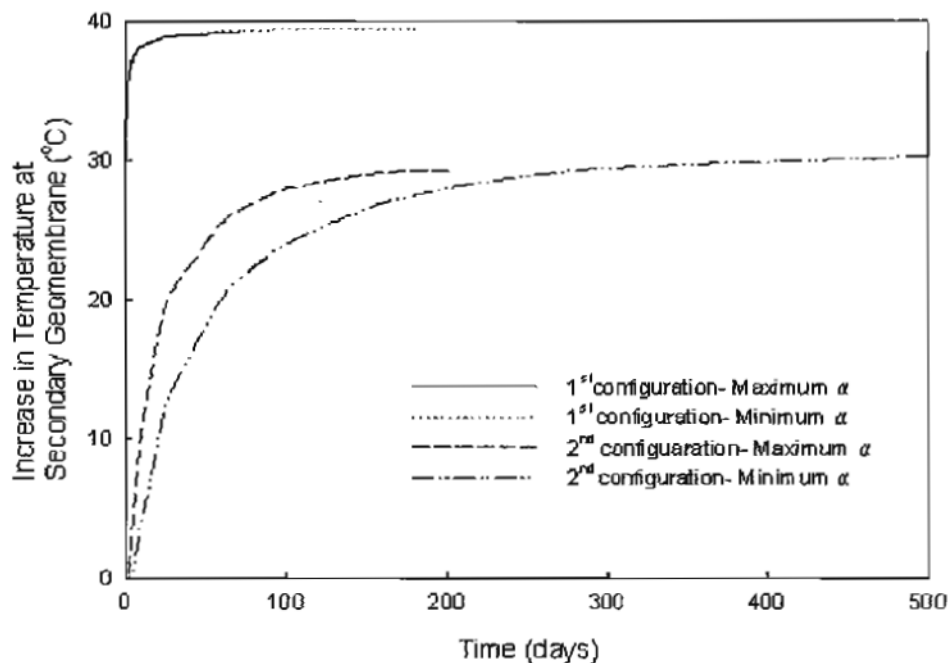


Figure 5 - Effect of thermal diffusivity on temperature in secondary liner

The distance to the aquifer can also have an impact on the increase in temperature at the secondary geomembrane and the thermal gradient through the liner system. To illustrate this, calculations were performed for barrier system 4 in Table 1 considering attenuation layer thicknesses of 1, 1.75, 3.75 and 10 m. The results are shown in Figure 8. The increase in temperature on the secondary geomembrane was 22.1, 25, 29.5, and 34.6 for attenuation layer thicknesses of 1, 1.75, 3.75 and 10 m respectively. Thus the hydrogeology of the site can have an impact on the liner temperatures and consequently on the service life of liners.

To illustrate the effect of the barrier system for a number of different temperature on the primary geomembrane, analyses were performed for barrier systems 1 and 2 (Table 1) assuming an aquifer temperature of 10°C and top of primary liner temperature of 30, 40 and 50°C. The results are given in Figures 9 and 10 for the first and the second barrier systems respectively. It can be seen that for the fully geosynthetic system the temperature on the secondary geomembrane is very close to that of the primary liner for a typical system. For the system with CCLs (and similar results could be obtained for a GCL and foundation layer of similar total thickness as the CCL) the temperature on the secondary geomembrane is 5-10 °C less than on the primary liner – and this could have a significant impact on the service life of the secondary geomembrane relative to the primary. This also highlights the importance of the design of the barrier system to accommodate temperature if the landfill is to be operated as a bioreactor.

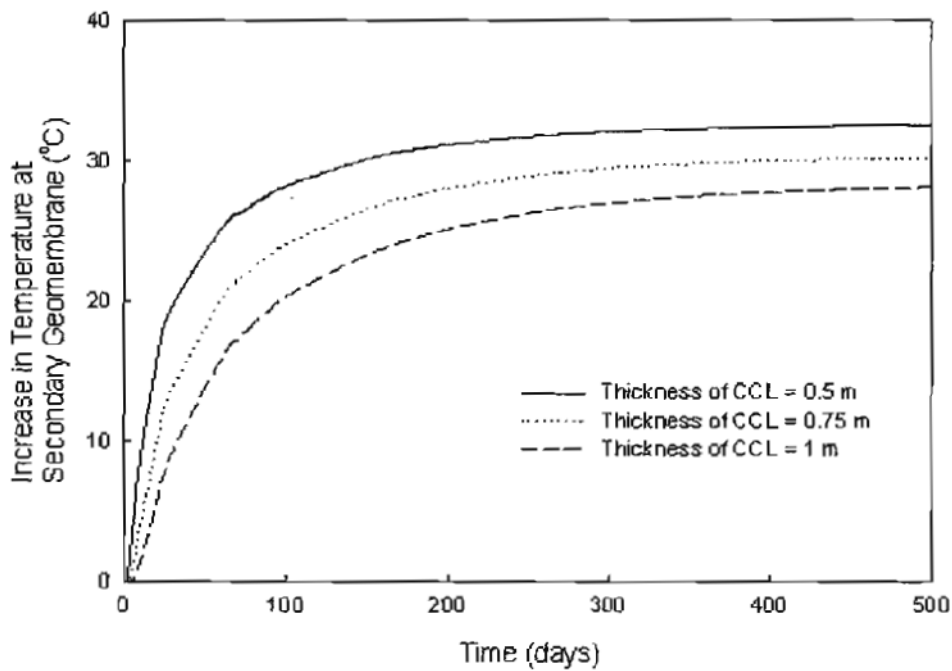


Figure 6- Effect of foundation layer on temperature in secondary liner- 2nd barrier system in Table 1

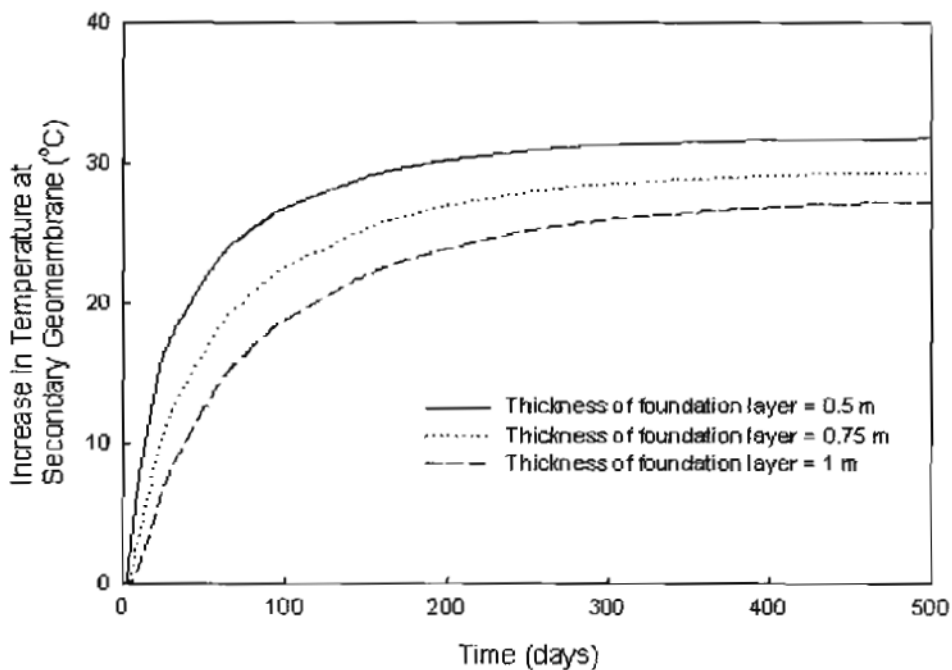


Figure 7- Effect of foundation layer on temperature in secondary liner- 3rd barrier system in Table 1

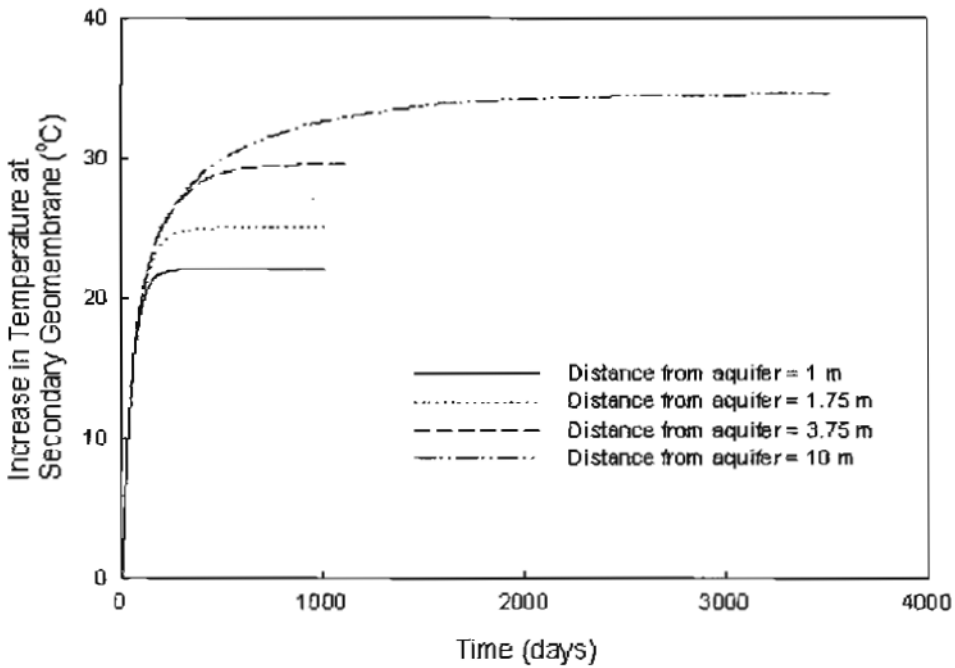


Figure 8- Effect of distance from aquifer (thickness of attenuation layer) on temperature in secondary liner- 4th barrier system in Table 1

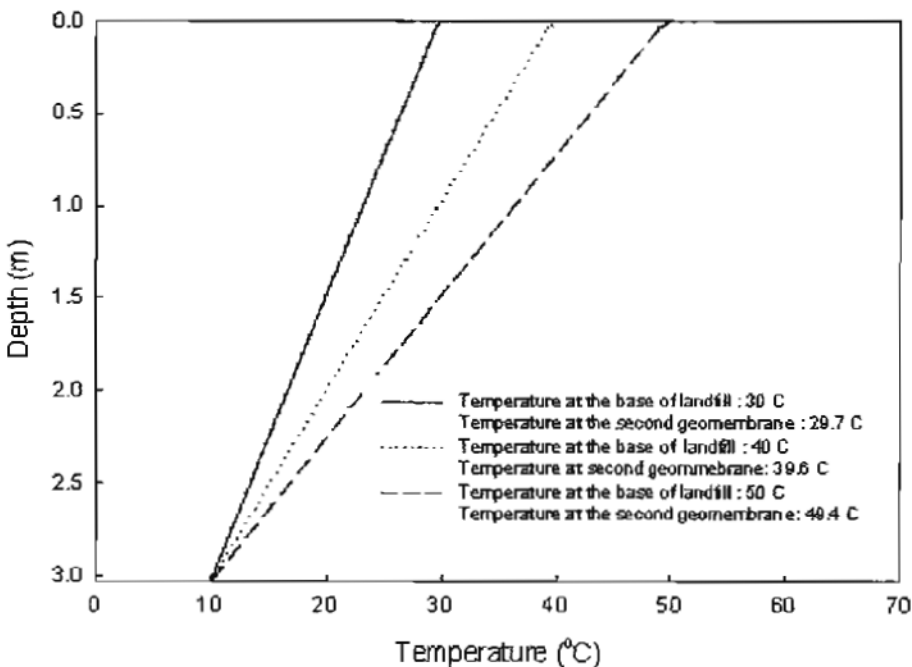


Figure 9- Temperature at second geomembrane for different modes of operation- 1st barrier system in Table 1

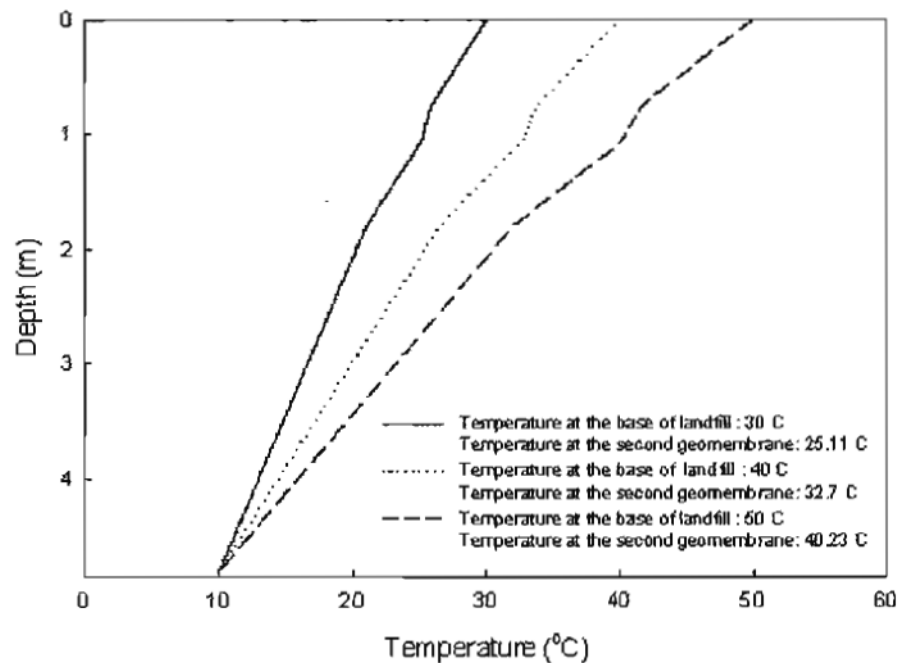


Figure 10- Temperature at second geomembrane for different modes of operation- 2nd barrier system in Table 1

CONCLUSION

The effect of geometry and material properties of barrier system on temperature at secondary liner has been examined. For the cases considered, the following may be concluded: Since thermal properties of liner materials do not significantly vary from each other, they did not significantly influence final temperature profile. However, thermal diffusivity affected the time required to reach steady state.

The temperature at secondary geomembrane liner for the all geosynthetic barrier systems was higher than in systems involving both soil and geosynthetic materials. Moreover, the thicker the primary liner the lower the temperature in the secondary geomembrane.

The hydrogeology of the site (depth of the aquifer layer) influences the liner temperature and its service life.

The studies presented in this paper give some insight into temperatures that might be expected on a secondary line in a double lined landfill. It is shown that temperature in secondary liner is high enough to impact on the service life of the secondary liner for typical liner configurations and this should be considered in the design of these facilities.

ACKNOWLEDGEMENTS

The research reported in this paper was supported by the Natural Sciences and Engineering Research Council of Canada (NSERC).

REFERENCES

- Becker, B. R., Misra, A., Fricke, B. A. (1992). "Development of correlations for soil thermal conductivity", *Int. Commun. Heat Mass Transfer*, 19(1): 59-68.
- Bilskie, J. R. (1994). "Dual probe methods for determining soil thermal properties: Numerical and laboratory study", Ph. D. Dissertation. Iowa State University.
- Bristow, K. L. (1998). "Measurement of thermal properties and water content of unsaturated sandy soil using dual-probe heat-pulse probes", *Agricultural and Forest Meteorology*, 89(2): 75-84.
- Bristow, K. L., Kluitenberg, G. J., Goding, C. J., Fitzgerald, T. S. (2001). "A small multi-needle probe for measuring soil thermal properties, water content and electrical conductivity", *Computers and Electronics in Agriculture*, 31(3): 265-280.
- Collins, H. J. (1993). "Impact of the temperature inside the landfill on the behaviour of barrier systems", *Proc. 4th. Int. Landfill Sym., Cagliari, Italy*, 417-432.
- Cote, J., Konrad, J. (2005a). "A generalized thermal conductivity model for soils and construction materials", *Canadian Geotechnical Journal*, 42(2): 443-458.
- Cote, J., Konrad, J. (2005b). "Thermal conductivity of base-course materials", *Canadian Geotechnical Journal*, 42(1): 61-78.
- Doll, P. (1997). "Desiccation of mineral liners below landfills with heat generation", *Journal of Geotechnical and Geoenvironmental Engineering, ASCE*, 123(11): 1001-1009.
- Farouki, O. T. (1981). "Thermal properties of soils", US Army Corps of Engineers, Cold Regions research and Engineering Laboratory, Hanover, N. H. CRREL Monograph 81-1.
- Ghuman, B. S., Lal, R. (1985). "Thermal conductivity, thermal diffusivity, and thermal capacity of some Nigerian soils", *Soil Sci.*, 139: 74-80.
- Gottheil, K.M., Brauns, J. (1994). "Das Austrocknungsverhalten von mineralischen Dichtungsschichten unter Kunststoffdichtungsbahnen bei erhöhten Temperaturen", In, H. Prühs (ed), *Geotechnische probleme bei bau von abfalldeponien*, 1994, 10. Nürnberger Deponieseminar. Eigenverlag LGA Nürnberg, 299-306.
- Hanson, J. L., Yesiller, N., Swarbrick, G. E. (2005). "Thermal Analysis of GCLs at a Municipal Solid Waste Landfill", *Geotechnical Special Publication, Geo-Frontiers 2005*, n 130-142, 3269-3283.
- Holzlöchner, U. (1990). "Langzeitverhalten von mineralischen Abdichtungsschichten", in *Deponieabdichtungen hinsichtlich Austrocknung und Rißbildung. Bundesanstalt f. Materialforschung und -prüfung, Berlin, Forschungsbericht 10203412, Teil III.*
- Hopmans, J. W., Dane, J. H. (1986). "Thermal conductivity of two porous media as a function of water content, temperature, and density", *Soil Sci.*, 142: 187- 195.
- Hsuan, Y.G. and Koerner, R.M., 1998. "Antioxidant depletion lifetime in high density polyethylene geomembranes", *Journal of Geotechnical and Geoenvironmental Engineering ASCE*, 124(6): 532-541.
- Kersten, M. S. (1949), "Thermal properties of soil", University of Minnesota, Eng. Exp. Station Bull. No. 28. Univ. of Minnesota Inst. of Technol. Eng. Exp. Station, Minneapolis, MN.
- Koerner, G. R., Koerner R. M., (2006). "Long-term temperature monitoring of geomembranes at dry and wet landfills", *Geotextiles and Geomembranes*, 24(1): 72-77.
- McInnes, K. (1981). "Thermal conductivities of soils from dryland wheat regions in eastern Washington", M. Sc. Thesis, Washington State University.

- Mickley, A. S. (1951). "The thermal conductivity of moist soil" *Am. Inst. Elec. Eng. Trans.*, 70:1789-1797.
- Ochsner, T. E., Horton, R., Ren, T. (2001). "A new perspective on soil thermal properties", *Soil Science Society of America Journal*, 65(6): 1641.
- Philip, L. K., Shimell, H., Hewitt, P. J., Ellard, H. T. (2002), "A field-based test cell examining clay desiccation in landfill liners", *Quarterly Journal of Engineering Geology and Hydrogeology*, 35: 345-354.
- Rowe, R.K. (2005) "Long-Term Performance of Contaminant Barrier Systems", 45th Rankine Lecture, *Geotechnique*, 55 (9): 631-678.
- Salomone, L.A., Marlow, J.I. (1989). "Soil rock classification according to thermal conductivity", EP.RI CU-6482, Electric Power Research Institute, Palo Alto, CA.
- Salomone, L.A., Kovacs, W. D. (1984a). "Thermal resistivity of soils", *Journal of Geotechnical Engineering, ASCE*, 110 (3): 375-389.
- Salomone, L.A., Kovacs, W. D., Kusuda, T. (1984b). "Thermal performance of fine-grained soils", *Journal of Geotechnical Engineering, ASCE*, 110 (3): 359-374.
- Sangam, H.P. and Rowe, R.K., (2002) "Effects of exposure conditions on the depletion of antioxidants from high-density polyethylene (HDPE) geomembranes", *Canadian Geotechnical Journal*, 30: 1221-1230.
- Sepaskhah, A. R., Boersma, L. (1979). "Thermal conductivity of soils as a function of temperature and water content", *Soil Science Society American Journal*, 43(3): 439-444.
- Sorour, M. M., Saleh, M. M., Mahmoud, R. A. (1990). "Thermal conductivity and diffusivity of soil", *International Communications in Heat and Mass Transfer*, 17(2): 189- 199.
- Southen, J. M., Rowe, R. K. (2004). "Investigation of the behavior of geosynthetic clay liners subjected to thermal gradients in basal liner applications", *Journal of ASTM international*, 1 (2), ID JA11 1470, Online; Available: www.astm.org; 13p.
- Southen, J. M. (2005). "Thermally driven moisture movement within and beneath geosynthetic clay liners", PhD thesis, University of Western Ontario, Canada.
- Southen, J. M., Rowe, R. K. (2005a). "Laboratory investigation of geosynthetic clay liner desiccation in a composite liner subjected to thermal gradients", *Journal of Geotechnical and Geoenvironmental Engineering*, 131(7): 925-935.
- Southen, J. M., Rowe, R. K. (2005b). "Modeling of thermally induced desiccation of geosynthetic clay liners", *Geotextiles and Geomembranes*, 23(5): 425.
- Tarnawski, V. R., Leong, W. H. (2000). "Thermal conductivity of soils at very low moisture content and moderate temperatures", *Transport in Porous Media*, 41(2): 137- 147.
- Tarnawski, V. R., Leong, W. H., Bristow, K. L. (2000). "Developing a temperature-dependent Kersten function for soil thermal conductivity", *International Journal of Energy Research*, 24(15): 1335-1350.
- TM 5-852-6/ AFR 88-19, Volume 6.

Zhou, Y., Rowe, R. K. (2003). "Development of a technique for modeling clay liner desiccation", *International Journal for Numerical and Analytical Methods in Geomechanics*, 27(6): 473-493.

Yoshida, H., Tanaka, N., Hozumi, H. (1997). "Theoretical study on heat transport phenomena in a sanitary landfill", *Proc. 6th. Int. Landfill Sym., Cagliari, Italy*, 109-120.

Yoshida, H., Rowe, R. K. (2003). "Consideration of landfill liner temperature", *Proc. 9th. Int. Landfill Sym., Cagliari, Italy* (CD-ROM).

CONTACT:

Professor R. Kerry Rowe
GeoEngineering Centre at Queen's-RMC
Department of Civil Engineering Queen's University
Ellis Hall
Kingston, Ontario
Canada K7L 3N6
Phone: +1 613 533 6934
Email: kerry@civil.queensu.ca

Leachate composition and antioxidant depletion from HDPE geomembranes.

M. Z. Islam, GeoEngineering Centre at Queen's-RMC, Department of Civil Engineering, Queen's University, Canada; R. Kerry Rowe, GeoEngineering Centre at Queen's-RMC, Department of Civil Engineering, Queen's University, Canada

ABSTRACT

The results of an accelerated ageing laboratory test program examining the influence of leachate chemical composition on the depletion of antioxidant from 1.5mm thick high density polyethylene (HDPE) geomembranes are reported. Results are presented for geomembrane immersed in four different synthetic leachates involving different combinations of volatile fatty acids, inorganic nutrients, trace metal solution, and surfactant. The depletion of OIT followed a first-order degradation pattern. The activation energy of the antioxidant depletion mechanism in all four leachates was calculated using Arrhenius model and found to be between 61 and 64 kJ/mol. This indicates that the four leachates are very similar in term of OIT depletion. The lowest antioxidant depletion time was observed for the simplest leachate (#2 which consisted of trace metal solution and surfactant). Given the uncertainty regarding actual leachate compositions in the field, it would appear that this leachate could reasonable and conservatively used for assessing potential depletion rates of different geomembranes and exposure conditions.

1. INTRODUCTION

High density polyethylene (HDPE) geomembranes have been extensively used as barrier materials in waste containment facilities (e.g., landfills and leachate lagoons) because of their excellent resistance to a wide range of chemicals. However, geomembranes are expected to experience ageing during their service life as a landfill barrier due to the adverse chemical effects of leachate, high physical stresses from waste loads, and elevated operating temperatures (Hsuan and Koerner, 1998). Ageing is defined as a slow and irreversible evolution of material properties under environmental stresses (Verdu, 1984). Evaluation of ageing characteristics under field condition is extremely time consuming and therefore accelerated ageing tests are conducted in the laboratory at elevated temperatures.

Sangam & Rowe (2002) performed accelerated ageing test at temperatures between 22 and 850C to investigate the depletion of antioxidant in synthetic municipal solid waste (MSW) leachate, water, and air. Their results revealed that antioxidant depletion rate was much faster in synthetic leachate than in water and air. The slowest depletion rate was observed in air aged samples. Hsuan and Koerner (1998) conducted antioxidant depletion studies on geomembranes fully immersed in water without stress and water saturated on one-side (saturated sand above and dry sand below) with 260 kPa applied normal stress at four elevated temperatures (55 - 850C). Testing results showed that the antioxidant depletion rate was faster for the water immersed samples than for samples with one-sided exposure to water.

Müller and Jacob (2003) studied accelerated ageing test of nine commercially available 2.5mm thick HDPE geomembranes at 800C by immersing in hot water and hanging up in a forced air oven. Results showed that OIT decreased at a faster rate in water than in air as had been previously observed by Sangam and Rowe (2002) for 2mm thick geomembrane. They noted that

the oxidation of the geomembrane starts only after complete depletion of the antioxidant. They also concluded that the service life of a HDPE geomembrane is controlled by the slow loss of stabilizers.

Gulec et al. (2004) conducted degradation tests on 1.5mm thick HDPE geomembrane in three immersion mediums: synthetic acid mine drainage (AMD), acidic water having pH of 2, and deionized water at 20, 40, and 60°C. OIT test results showed that antioxidant depleted at a faster rate in AMD followed by acidic water and deionized water.

From the investigations described above, it is clear that antioxidants deplete at a faster rate in liquid immersion tests compared to forced-air oven. It also appears the depletion rate is faster for synthetic municipal solid waste (MSW) leachate than for AMD, acidic water, or water alone (deionized or distilled). MSW leachate typically contains volatile fatty acids, inorganic ions, trace metals, and surfactant. However it is not clear as to whether one needs to full leachate chemistry or if a simplified leachate can be used in geomembrane ageing experiments to simulate MSW landfill leachate. Thus the objective of this paper is to examine the hypothesis that a leachate comprised of the trace metals and surfactant would provide results sufficiently close to that for full leachate that it could be used in ageing experiments instead of the full leachate.

2. BACKGROUND

2.1. Ageing Mechanisms

Various ageing and degradation mechanisms can take place in geosynthetics depending on the type of polymer and environmental exposure. The degradation mechanisms include: chemical degradation, ultraviolet degradation, biological degradation, degradation by swelling, degradation by extraction, thermal degradation and oxidative degradation (Haxo and Nelson, 1984 and Koerner et al., 1990). Among these degradation processes, oxidative degradation is considered to be the most harmful for high density polyethylene geomembranes (Hawkins, 1984). However, more than one degradation mechanism occurs in the HDPE GM that creates synergistic effects and eventually the overall HDPE geomembrane degradation process accelerates. Due to the degradation of the polymer, the following changes take place in the geomembranes: gain or reduction of molecular weight, formation of free radicals, brittleness, loss of additives and plasticizers (Kulshershta, 1992).

2.2. Oxidation of Polymers

Oxidation in polymeric materials (e.g. HDPE geomembrane) is associated with the formation of free radicals or auto-oxidation chain mechanism (Kelen, 1983). The auto oxidation chain mechanism has two interacting cyclical processes: cycle A and cycle B as shown in Figure 1 (Grassie and Scott, 1985). In cycle A, hydroperoxide (ROOH) and free radicals are formed due to alkyl/alkylperoxyl chain reactions whereas in cycle B, homolysis of hydroperoxide occurred and more free radicals are formed. Geomembranes which experience a decreased molecular weight due to the chain scission eventually become more susceptible to environmental stress cracking (Tisinger and Giroud, 1993). As described by Grassie and Scott (1985), Equations (1) to (6) describe the oxidative degradation process in polymers. The oxidative reaction initiates by forming a free radical ($R\bullet$) from the polymer chain (RH) under the influence of energy or catalyst residues in the polymer:



Once a free radical is formed it reacts with oxygen and to produce a peroxy radical ($ROO\bullet$) (Cycle A, Figure 1).



A hydrogen atom from the surrounding polymer reacts with the peroxy radical (ROO•) and forms hydroperoxide (ROOH) and another free radical (Fay and King, 1994).



The breakdown of hydroperoxide initiates when a significant concentration of ROOH accumulates (Cycle B, Figure 1).



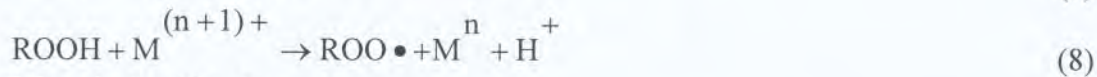
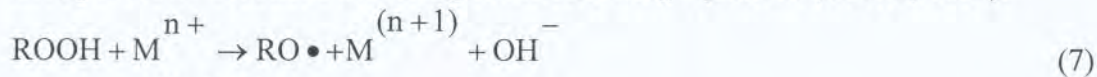
More free radicals form due to the decomposition of ROOH which eventually attacks the polymer chain to form more free radicals and alcohol (ROH).



Simultaneously, there are reactions between the OH• radical and the polymer chain which yield free radicals and water.



Oxidative degradation is known to be accelerated by the presence of transition metals (Osawa and Ishizuka, 1973). More free radicals are formed when metal ions react with hydroperoxide through 'redox' reactions according to the following equations (Osawa, 1992):



2.3. Antioxidants

Antioxidants are normally added to polymeric materials to retard the oxidative reactions and to extend the induction period (Grassie and Scott, 1985 and Al-Malaika, 1998). Antioxidants break the links in the auto-oxidation chains as shown by letters (a) – (d) in Figure 1. Various factors affect the effectiveness of antioxidants: temperature, type of antioxidant, amount of antioxidant, and the combination of antioxidants used. There are four different antioxidants that are commonly used in the formulation of polyethylene geomembranes: hindered phenols, hindered amines, phosphites, and thiosynergists (Fay and King, 1994). Antioxidants can also be divided into two categories: primary (hindered amines and hindered phenol) and secondary antioxidants (phosphates, thiosynergists, and hindered amines). Primary antioxidants react with free radical either by accepting or donating an electron and form a stable polymer chain. Secondary antioxidants interfere the formation of free radical by decomposing hydroperoxides into stable alcohols. The selection of antioxidant should be such that they can withstand the manufacturing temperatures (2000C and 2800C) as well as service temperatures (Gulec et al., 2004). More than one antioxidant is generally used by the manufacturers to provide greater stability to the geomembrane.

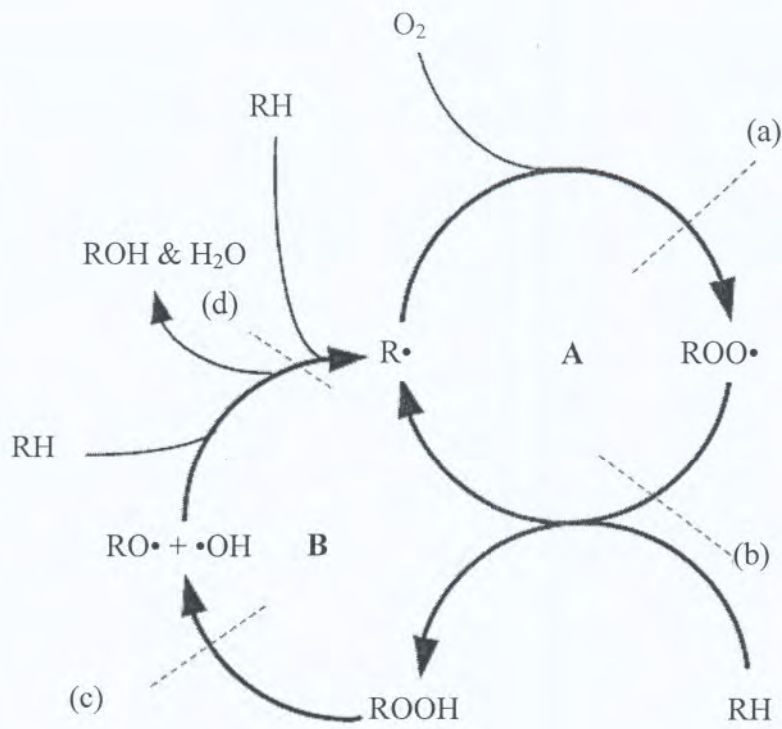


Figure 1. Auto-oxidation chain reaction cycles in polyethylene (adapted from Grassie and Scott, 1985)

Antioxidants are depleted from polymeric materials due to the chemical reactions with oxygen, free radicals, and hydroperoxide; and/or to their physical loss by diffusion, extraction or volatilization (Gedde et al., 1994; Hsuan and Koerner, 1998; and Sangam and Rowe 2002). Since the typical operating temperature for HDPE geomembrane is below 600C, volatilization is not a major concern for HDPE geomembranes (Hsuan and Koerner, 1998). Loss due to extraction is significant in controlling the life time prediction of antioxidant. Tests conducted by Smith et al. (1992) on medium density polyethylene pipes exposed to water inside and air outside have shown a 75% reduction in antioxidants due to extraction.

3. EXPERIMENTAL PROCEDURES

3.1. Materials

In this study a 1.5 mm thick high density polyethylene geomembrane was used. The geomembrane was manufactured by GSE Lining Technology Inc., Houston, TX and was supplied by Terrafix Geosynthetics Inc., Toronto. The initial OIT (ASTM D3895) and the density (ASTM D792) of the geomembrane were 174 min and 0.946 gm/cm³ respectively.

3.2. Exposure Conditions:

Geomembrane samples were cut into small coupons (190mm by 100mm) and immersed in four different synthetic leachates at 22, 40, 55, 70, and 850C. To avoid the effects of leachate interaction with the container material, 4 liter glass jars with Teflon lined lids were used. As many as 16 geomembrane coupons were put in a glass jar for each specific temperature and leachate type. The coupons were separated by 2mm glass rods to ensure that there was leachate

in contact with all surfaces. Synthetic leachates were produced by mixing different combinations of volatile fatty acids, inorganic nutrients, trace metals, and surfactant with distilled water (Tables 1 and 2) and were changed every two weeks. Surfactants arise in landfill leachate due, inter alia, to the disposal of detergents in the waste stream. Several researchers observed surfactants in different MSW landfills (e.g., Maisonneuve et al., 97; Hrapovic, 2001; Kjeldsen et al., 2002; Borghi et al., 2003 etc.). A representative surfactant, Igepal® CA 720 was chosen in this study to simulate the landfill leachate condition. The chemistry of synthetic leachate -1 was based on average data for leachate from the Keele Valley Landfill, Ontario.

Table 1. Composition of synthetic leachates

COMPONENT	Concentration, mg/L (except where noted)			
	Leachate-1a	Leachate-2	Leachate-3	Leachate-4
Volatile Fatty Acids				
Acetic Acid (mL/L)	7	---	---	7
Propionic Acid (mL/L)	5	---	---	5
Butyric Acid (mL/L)	1	---	---	1
Inorganic Nutrients				
NaHCO ₃	3012	---	3012	---
CaCl ₂	2882	---	2882	---
MgCl ₂ •6H ₂ O	3114	---	3114	---
MgSO ₄ •7H ₂ O	319	---	319	---
NH ₄ HCO ₃	2439	---	2439	---
CO(NH ₂) ₂	695	---	695	---
NaNO ₃	50	---	50	---
K ₂ CO ₃	324	---	324	---
KHCO ₃	312	---	312	---
K ₂ HPO ₄	30	---	30	---
Trace Metal Solution (mL/L)	1	1	1	1
Others				
Surfactant, Igepal® CA720 (mL/L)	5	5	5	5
pH (adjusted by adding either NaOH or H ₂ SO ₄) (-)	6	6	6	6
Eh (adjusted by adding 3% w/v Na ₂ S•9H ₂ O) (mV)	-120	---	-120	-120

a based on Hrapovic (2001)

Table 2. Composition of trace metal solution (modified from Hrapovic, 2001)

COMPONENT	Formula	mg/L(except where noted)
Ferrous Sulfate	FeSO ₄ •7H ₂ O	2000
Boric Acid	H ₃ BO ₃	50
Zinc Sulfate Heptahydrate	ZnSO ₄ •7H ₂ O	50
Cupric Sulfate Pentahydrate	CuSO ₄ •5H ₂ O	40
Manganous Sulfate Monohydrate	MnSO ₄ •H ₂ O	500
Ammonium Molybdate Tetrahydrate	(NH ₄) ₆ Mo ₇ O ₂₄ •4H ₂ O	50
Aluminum Sulphate 16-Hydrate	Al ₂ (SO ₄) ₃ •16H ₂ O	30
Cobaltous Sulphate Heptahydrate	CoSO ₄ •7H ₂ O	150
Nickel (II) Sulfate	NiSO ₄ •6H ₂ O	500
Sulfuric Acid (mL)	H ₂ SO ₄	1

3.3. Oxidative Induction Time (OIT) by Differential Scanning Calorimeter (DSC)

The amount of antioxidant present in the geomembrane was assessed according to ASTM D3895 in terms of the oxidative induction time (OIT) obtained using a Q-100 series differential scanning calorimeter (DSC). The OIT deduced using this technique is useful in monitoring the relative oxidative resistance of the GM (Tisinger, 1989; Dudzik and Tisinger, 1990; Surman et al., 1995; Hsuan and Koerner, 1995, 1998; Maisonneuve et al., 1997; Sangam and Rowe, 2002; Gulec et al., 2004; and Rimal et al., 2004). For each specimen, at least five replicate samples were tested and the average used for each data point.

4. RESULTS AND DISCUSSIONS

4.1. Antioxidant Depletion

Figure 2 shows the variation in logarithm of OIT (ln OIT) with time for geomembranes immersed in leachate-1 at different temperatures. The standard deviation of each data point is represented by the vertical bars. The linear relationship between ln(OIT) and time represents the first-order decay law for antioxidant depletion. The slope of the line, *s*, represents antioxidant depletion rate. The depletion rate increases with increasing temperature indicating that OIT depleted at a faster rate with higher temperature, as has been observed by other researchers (Hsuan and Koerner, 1995 and 1998; Hsuan and Guan, 1998; Sangam and Rowe, 2002; and Gulec et al., 2004). At 850C and 700C, OIT depleted completely after around 4.5 and 20 months respectively. For all other temperatures OIT has not been depleted completely within the testing period (20 months). Similar trends were observed for all other leachates. Since, OIT was depleted after 4.5 months at 850C, the data points after that time are not included in establishing the regression line.

The depletion of OIT in four different leachates at all testing temperatures are shown in Figures 3-4. There was no statistically significant difference between the OIT data points for samples immersed in leachate-1 and leachate-4 which both contained fatty acids. There were some (albeit small) differences between leachate-1 and leachate-3; between leachate-1 and leachate-2; between leachate-2 and leachate-3; and between leachate -2 and leachate-4. The highest depletion rate was observed for samples immersed in leachate-2, which only contained trace metals and surfactant. Although the same amount of trace metals and surfactant was added to all four leachates, it appears that the presence of either fatty acids or inorganic nutrients, or both,

may have reduced the antioxidant depletion rate although the effect is small enough that it may not be real. The significance of this is discussed below.

Although there is some variability in OIT data, there appeared to be a trend with the OIT depletion rates following the order (highest to lowest): leachate-2 (trace metals and surfactant only) > leachate-3 (same as 2 plus inorganic ions) > leachate-4 (same as 2 plus VFAs) > leachate-1 (full leachate). The reason for the highest depletion rate being for the simplest leachate (leachate-2) is not yet known and further research is needed to understand this phenomenon.

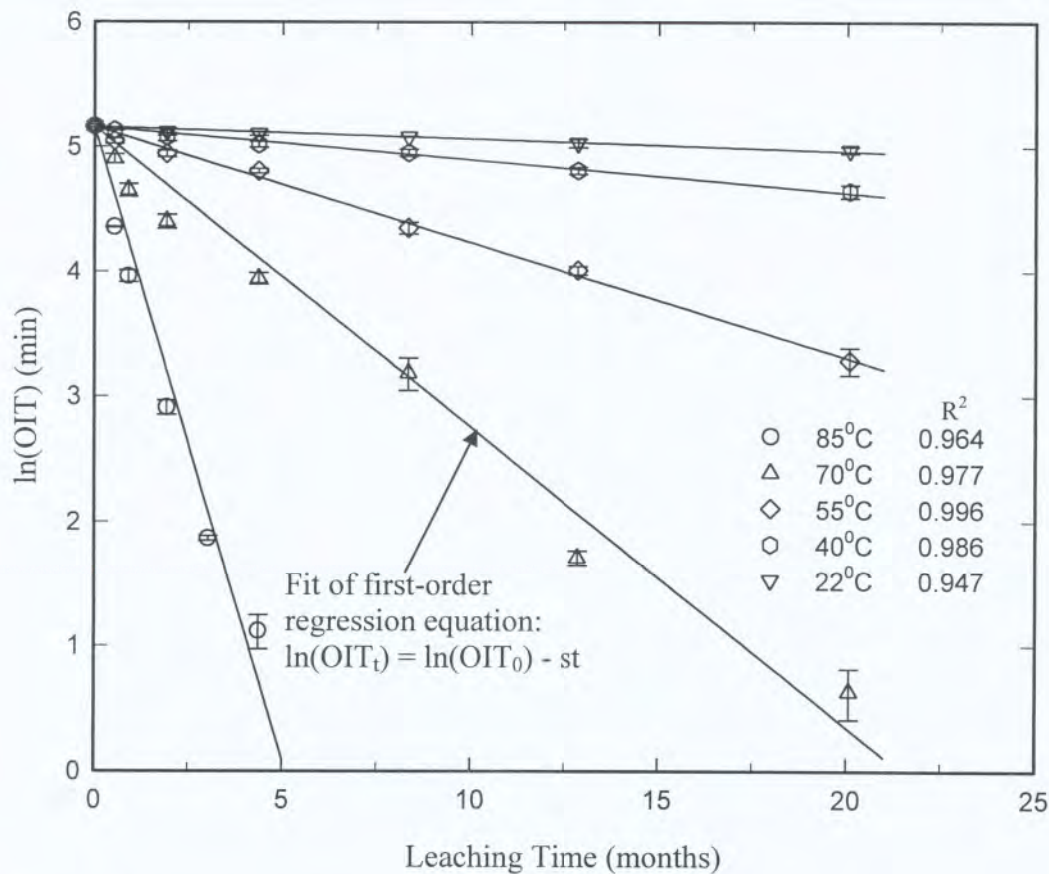


Figure 2. Variation in ln(OIT) with time at different temperatures in Leachate -1. OIT₀ is the initial OIT and OIT_t is the OIT at time t (month), s is the antioxidant depletion rate (month⁻¹).

4.2. Prediction of Antioxidant Depletion Time

The antioxidant depletion time at a temperature of interest (e.g. at expected field temperature) is usually predicted using the Arrhenius equation which describes the relationship between reaction rate and temperature (Hsuan and Koerner, 1998). The Arrhenius equation can be expressed as:

$$s = Ae^{-(E_a/RT)} \quad (9)$$

where s is the antioxidant depletion rate, A is a constant often called as collision factor, R is the universal gas constant (8.314 J/(mol K)), E_a is the activation energy of the depletion process

(J/mol), T is the absolute temperature (K). Equation (9) can also be written as follows by taking natural logarithm on both sides:

$$\ln(s) = \ln(A) - \left(\frac{E_a}{R}\right)\left(\frac{1}{T}\right) \quad (10)$$

Plotting the variation in $\ln(s)$ with the inverse of absolute temperature ($1/T$) one can then get the best fit for equation (10) as shown in Figure 5 and tabulated in Table 3. The activation energy, E_a , varied between 61 and 64 kJ/mol for the four leachate immersed conditions. The lowest activation was energy observed for leachate-2 (trace metal and surfactant only) and the highest for leachate 1 (full leachate) immersed samples. However the relatively small difference in activation energies suggests that all leachates have a similar effect on antioxidant depletion.

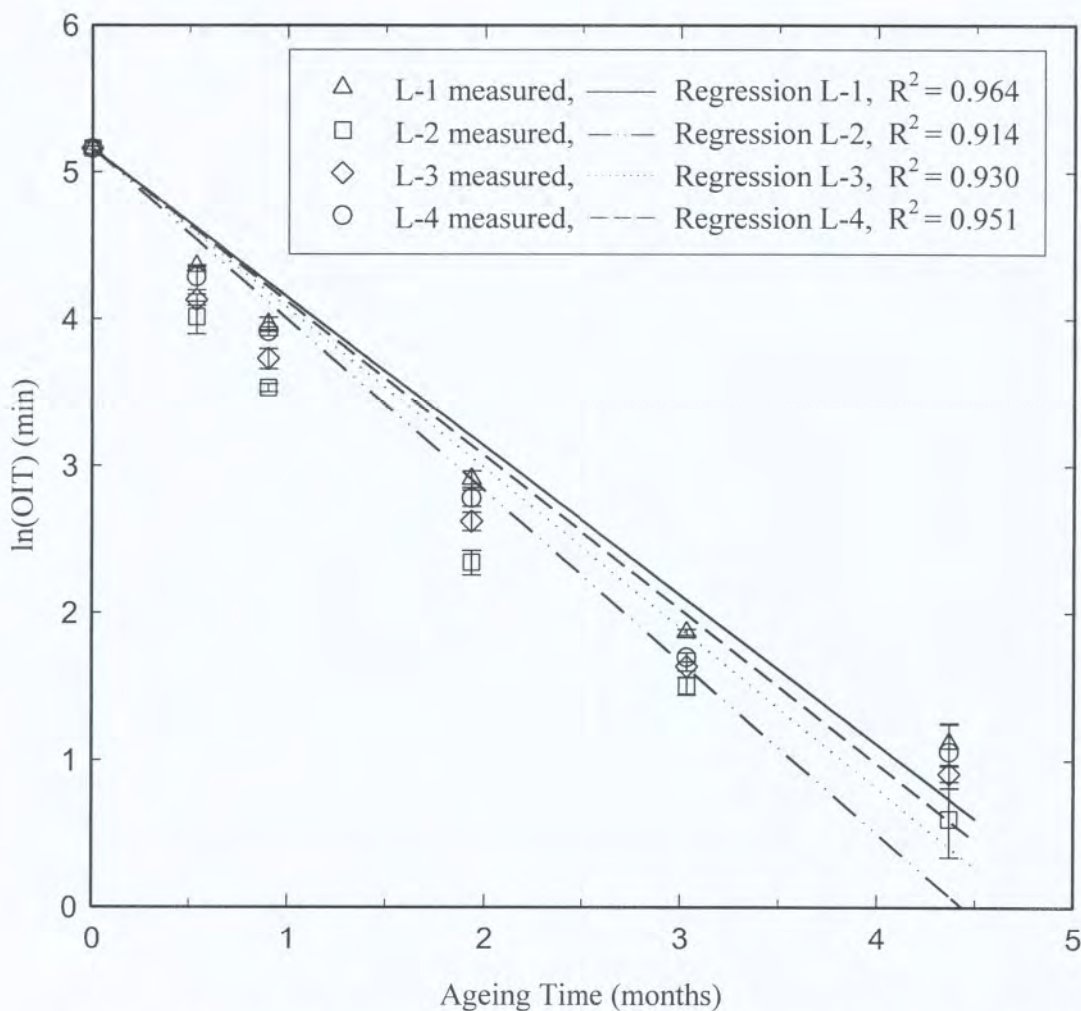


Figure 3. Variation in $\ln(\text{OIT})$ with time at 85°C in four different leachates.

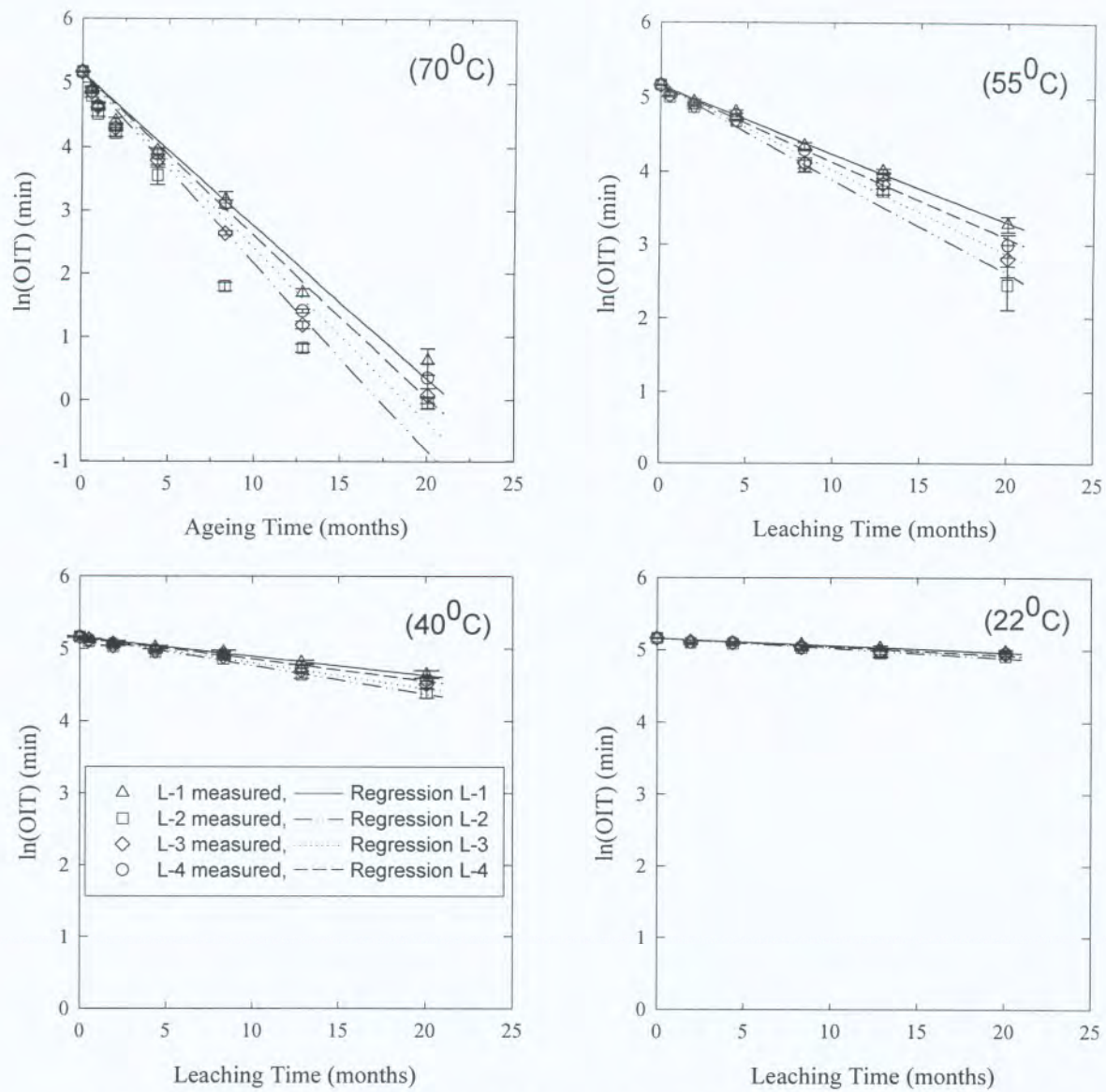


Figure 4. Variation in $\ln(\text{OIT})$ with time at 22, 40, 55, and 70°C in four different leachates.

Table 3. Activation energy and Arrhenius equation for four different leachates. (TM & S = trace metals and surfactant; II = inorganics; VFA = volatile fatty acids; Full = TM & S + II+VFA)

Leachate Type		Activation Energy,	Arrhenius Equation	R2
Leachate - 1	Full	64.02	$\ln(s) = 21.216 - 7700/T$	0.9793
Leachate - 2	TM & S	60.81	$\ln(s) = 20.319 - 7315/T$	0.9839
Leachate - 3	TM&S + II	61.91	$\ln(s) = 20.617 - 7447/T$	0.9836
Leachate - 4	TM&S + VFA	61.84	$\ln(s) = 20.519 - 7438/T$	0.9784

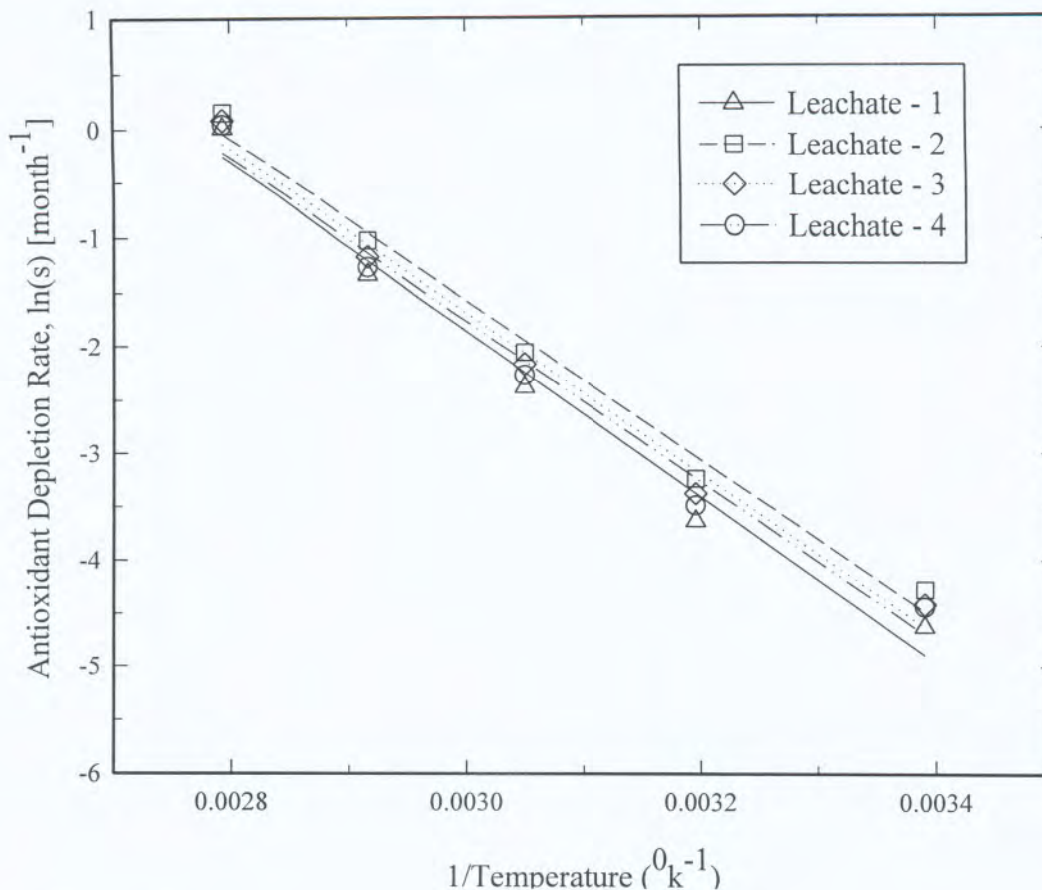


Figure 5. Arrhenius plot of antioxidant depletion in four different leachates.

The temperature at the base of the landfill depends on various factors such as waste types, age of the landfill, geologic conditions, performance of leachate collection systems etc. (Rowe, 2005). A wide range of temperature at the base of the landfill has been reported in the literature. Koerner and Koerner (2006) monitored the temperature of the geomembrane at two different cells (e.g., dry and wet cells) in the same MSW landfill in Philadelphia, USA. In the dry cell, where liquid was reduced intentionally, the temperature was 200C for the first 5.5 years and after that it rapidly increased to an average value of 320C. For the wet cell, where liquid was added at a constant rate, the average initial temperature was 250C and this then increased to between 41 and 460C over the next 3.7 years of monitoring. Rowe (2005) reported a temperature of 30-400C at the base of the Keel Valley Landfill in Ontario, Canada. Tokyo Fort Landfill in Japan had a temperature of 500C for the first 7-10 years of Landfilling (Yoshida and Rowe, 2003). The probable upper end of primary liner temperature may be anticipated to 600C where there is a significant leachate mound (Rowe, 2005). Considering the wide variations in landfill base temperature, antioxidant depletion time is predicted for three hypothetical base temperatures (e.g., 20, 40, and 600 C) in Table 4. It can be seen that the difference between antioxidant depletion times is not significant at 600C, however at lower temperatures the difference is as much as 25 years. As mentioned earlier, there is no statistically significant difference between OIT data values for Leachate 1 and 4 immersed samples. However, the difference in antioxidant depletion time based on the best fits to the data at 200C is 10 years (Table 4). This shows that when extrapolating over a wide range of temperatures the predictions based on the Arrhenius plot are

sensitive to some natural variability in the data and thus while they indicate the relative magnitude of the depletion time, based on this data, any resolution beyond ± 5 years can not be justified at 20oC. Clearly the sensitivity decrease as the temperature increases. Therefore, reasonable assumption and care should be taken in predicting antioxidant depletion time using an Arrhenius relationship. Given the uncertainties regarding actual leachate composition in the field it can be seen the simplest leachate (#2) provides conservative, but reasonable predictions. It should be noted that a similar Arrhenius modelling based on tests with leachate #1 reported by Rowe (2005, Table 5) for a different geomembrane gave a depletion time of 25 years at 200C. Rowe's paper also makes the point that while ageing in leachate is good for assessing the relative performance of different geomembranes and effects of different leachates, it is a very severe test and the in-service life is likely to be much longer than predicted based on the immersion test and the interested reader is referred to Rowe (2005) for more details.

Table 4. Predicted antioxidant depletion times for different leachates at different temperatures.

Temp (0C)	Antioxidant depletion time (yrs)			
	Leachate-1	Leachate-2	Leachate-3	Leachate-4
20	75	50	60	65
40	15	10	10	15
60	3.3	2.5	2.8	3.0

5. CONCLUSIONS

An experimental investigation on the depletion of antioxidant from HDPE geomembrane immersed in four synthetic leachates at five different temperatures (22-850C) is described in this paper. Results of immersion test showed that the difference of activation energies in four leachates were quite small (61 and 64 kJ/mol). This indicates that the four leachates were very similar in term of OIT depletion. The lowest antioxidant depletion time was observed for the simplest leachate (#2 which consisted of trace metal solution and surfactant). Given the uncertainty regarding actual leachate compositions in the field, it would appear that this leachate could reasonable and conservatively used for assessing potential depletion rates of different geomembranes and exposure conditions.

Acknowledgements

This study was financed by the Natural Sciences and Engineering Research Council of Canada (NSERC). The authors are grateful to Terrafix Geosynthetics Inc., Toronto for donating the geomembrane used in this study.

REFERENCES

- Al-Malaika, S., 1998. Antioxidants: an overview. Plastic additives: An A-Z Reference, Pritchard, G., Editor, Chapman and Hill, London, pp55-72.
- ASTM D3895-95. Standard Test Method for Oxidative-induction Time of Polyolefins by Differential Scanning Calorimetry. Annual Book of ASTM Standards, Philadelphia, USA, Vol. 08.02. pp. 539-544.
- ASTM D792. Standard Test Methods for Density and Specific Gravity of Plastics by Displacement. American Society for Testing and Materials, 1986.

- Borghi, A.D., Binaghi, L., Converti, A, and Borghi, M.D., 2003. Combined treatment of leachate from sanitary landfill and municipal wastewater by activated sludge. *Chem. Biochem. Eng. Q.*, Vol. 17, No. 4, pp. 277-283.
- Dudzik, B. and Tisinger, L., 1990. An evaluation of chemical compatibility test results of HDPE geomembrane exposed to industrial waste leachate. *Geosynthetic testing for waste containment applications*, STP 1081, Koerner, R., Editor, ASTM, West Conshohocken, PA, pp. 37-54.
- Fay J.J. and King, R.E., 1994. Antioxidants for Geosynthetic Resins and Applications. In *Geosynthetic Resins, Formulations and Manufacturing*, Edited by Hsuan, Y.G. and Koerner, R.M., GRI Conference Series Published by IFIA, St Paul, MN, U.S.A., pp. 77-96.
- Gedde, U. W., Viebke, J., Leijstrom, H. & Ifwarson, M., 1994. Long-term properties of hot-water polyolefin pipes: a review. *Polymer Engineering and Science*, 24 (34): 1773–1787.
- Grassie, N. and Scott, G., 1985. *Polymer Degradation and Stabilization*. Cambridge University Press, New York, USA, 222p.
- Gulec, S.B., Edil, T.B., and Benson, C.H., 2004. Effect of acidic mine drainage on the polymer properties of an HDPE geomembrane. *Geosynthetics International*, 2(11): 60-72.
- Hawkins W.L., 1984. *Polymer Degradation and Stabilization, Polymer/Properties and Applications 8*, H.J. Harwood, Ed. Springer-Verlag Berlin Heidelberg, Germany, 119p.
- Haxo, H.E. and Nelson, N.A., 1984. Factors in the durability of polymeric membrane liners. *Proceedings of the International Conference on Geomembranes*, Vol. II, Denver, CO. IFAI Publishers, St. Paul, MN, pp. 287–292.
- Hrapovic, L., 2001. *Laboratory Study of Intrinsic Degradation of Organic Pollutants in Compacted Clayey Soil*. Ph.D. Thesis, The University of Western Ontario, 300p.
- Hsuan, Y. G., and Guan, Z., 1998. Antioxidant depletion during thermal oxidation of high density polyethylene geomembranes. *Proceedings of the Sixth International Conference on Geosynthetics*, Atlanta, Georgia, 1: 375-380.
- Hsuan, Y. and Koerner, R., 1995. Long-term Durability of HDPE Geomembrane. Part 1: Depletion of Antioxidant, GRI Report 16, 35p.
- Hsuan, Y.G. and Koerner, R.M., 1998. Antioxidant depletion lifetime in high density polyethylene geomembranes. *Journal of Geotechnical and Geoenvironmental Engineering ASCE*, 124(6): 532–541.
- Kelen, T., 1983. *Polymer Degradation*. Van Nostrand Reinhold, New York, NY, 211p.
- Kjeldsen, P., Barlaz, M.A., Rooker, A.P., Baun, A., Ledin, A., and Christensen, T.H., 2002. Present and Long-Term Composition of MSW Landfill Leachate: A Review, *Critical Reviews in Environmental Science and Technology*, 32(4):297–336.
- Koerner, G.R. and Koerner, R.M., 2006. long-term temperature monitoring of geomembranes at dry and wet landfills. *Geotextile and Geomembranes*, 24(1): 72-77.
- Koerner, R.M., Halse, Y.H., and Lord Jr., A.E., 1990. Long-term durability and aging of geomembrane. In: Bonaparte, R.(Ed.), *Waste Containment Systems: Construction, Regulation, and Performance*. ASCE Geotechnical Special Publication No.26, New York, pp. 106–134.
- Kulshershta, A., 1992. Chemical degradation. *Handbook of Polymer Degradation*, Hamid, S.H., amin, M.B., and Madhah, A.G., Editors, Marcel Dekker, New York, pp.55-95.
- Maisonneuve, C., Pierson, P., Duquenois, C., and Morin, A., 1997. Accelerated Aging Tests For Geomembranes Used in Landfills, *Proceedings of the 6th International Landfill Symposium, Sardinia'97*, Cagliari, Italy, 3: 207-216.
- Müller, W. and Jacob, I., 2003. Oxidative resistance of high density polyethylene geomembranes. *Polymer Degradation and Stability*, 79: 161–172.

- Osawa Z., 1992. Photo-induced Degradation of Polymers, In Handbook of Polymer Degradation, A.H. Hamid, M.B. Amin and A. G. Maadhah Eds., Marcel Dekker Inc., pp. 169-217.
- Osawa Z. and Ishizuka T., 1973. Catalytic Action of Metal Salts in Autoxidation and Polymerization (X) – The Effect of Various Methyl Stearates on the Thermal Oxidation of 2,6,10,14-Tetramethylpentadecane, Journal of applied Polymer Science, 17: 2897-2907.
- Rimal, S., Rowe, R.K., and Hansen, S., 2004. Durability of geomembrane exposed to jet fuel a-1. 57th Canadian Geotechnical Conference, Quebec City, October, Section 5D: pp13-19
- Rowe, R. K., 2005. Long-term performance of contaminant barrier systems. Géotechnique, 55(9): pp. 631–678.
- Sangam, H.P. and Rowe, R.K., 2002. Effects of exposure conditions on the depletion of antioxidants from high-density polyethylene (HDPE) geomembranes. Canadian Geotechnical Journal, 30 : 1221-1230.
- Smith, G., Karlsson, K., and Gedde, U., 1992. Modeling of antioxidant loss from polyolefins in hot-water applications. Polymer Engineering and Science, 32(4): 655–667.
- Surmann, R., Pierson, P., and Cottour, P., 1995. Geomembrane liner performance and long term durability. Proceedings 4th International Landfill Symposium, Sardinia 95, Christensen, T., Cossu, R., and Stegmann, R., Editors, S. Margherita di pula, Cagliari, Italy, 3: 405–414.
- Tisinger, L., 1989. Chemical compatibility testing: a typical program. Geotechnical Fabrics Report, 3: 22–25.
- Tisinger L.G. and Giroud, J.P., 1993. The Durability of HDPE Geomembranes. Geotechnical Fabrics Report, 11(6): 4-8.
- Verdu, J., 1984. Vieillissement des plastiques, AFNOR Techniques.
- Yoshida, H., Hozumi, H., and Tanaka, N., 1996. Theoretical study on temperature distribution in a sanitary landfill. Proceeding of the 2nd International Congress on Environmental Geotechnics, Osaka 1: 323–328.
- Yoshida, H. and Rowe, R. K., 2003. Consideration of landfill liner temperature. Proceedings of the 8th International Waste Management and Landfill Symposium. Cagliari (CD-ROM).

CONTACT

Mr. M.Z. Islam
Queen's University
GeoEngineering Centre at Queen's-RMC
Ellis Hall
Kingston, ON
CANADA
Phone: (613) 533-6933
Email: mislam@civil.queensu.ca

Influence of Strain Gage Adhesive's Stress-Strain Behavior on PVC Geomembrane Tensile Test

Laura M. Hannum, Department of Civil and Environmental Engineering, Lehigh University

ABSTRACT

Geotechnical instrumentation for monitoring the field performance of geosynthetics is often achieved by affixing electrical resistance strain gages to the material to measure the deformation of the geosynthetic under applied loading. To consider the effects of adhesive properties on an axially loaded geomembrane, the stress-strain behavior of a polyvinyl chloride (PVC) geomembrane with three different strain gage adhesives applied was analyzed. The samples were tested using a modified strip tensile test (ASTM D882), and a comparison was made between the actual strain and that measured by the gage.

It was determined from the study that silicone rubber based adhesives which exhibited a secant modulus of elasticity at 10% strain similar to that of the geomembrane were the most accurate in modeling the entire stress-strain behavior of the geosynthetic and less prone to adhesive failure. Additionally, it was demonstrated that adhesives which contained less of the cross-linking polymer agent methyltrimethoxysilane retained their bonds to the geomembrane for higher strain values, even up to nearly 12% engineering strain.

INTRODUCTION

Geomembranes are essentially plastic sheets which act as impermeable layers in a system. The primary purpose of geomembranes is to serve as a barrier to contain liquids or gases. Failure of the geomembrane may lead to contamination of groundwater with leachate from landfills or pollution of the atmosphere. Additionally, geomembranes are used to contain hazardous waste; therefore, the integrity of the geosynthetic is critical for the safety of the public, wildlife, and environment.

Advances have been made in leakage detection of geomembranes such that if the geomembrane is damaged in a way as to allow contamination outside of the containment area, field technicians will be alerted to the problem and can take steps to quarantine the cell and repair or replace the failed geomembrane. Such leak detection methods include the installation of electrically conductive wires placed in a grid pattern beneath the geomembrane and the use of double lined systems.

Typically, electrical resistance strain gages are bonded directly to the geomembrane using adhesives. These gages are used to monitor the deformation of the geomembrane throughout its design life. However, the attachment of the strain gage to the geomembrane is critical to ensure that the strain gage is accurately measuring the deformation in the geosynthetic and not in the adhesive and that the adhesion to the geomembrane does not fail. This task can be challenging due to the non-rigid surface of the geomembrane and the need to waterproof the strain gage and its bond. Additionally, previous studies have shown experimentally that PVC geomembranes tend to exhibit small, closely spaced wrinkles when exposed to UV radiation. The wrinkle height has been shown to be a function of the elastic modulus of the PVC polymer rather than of the coefficient of thermal expansion. Therefore, while these wrinkles can be minimized by using a lower modulus PVC or manipulated by using high density polyethylene (HDPE), which will result in larger wrinkles spaced farther apart, the problem remains that the uneven surface will

make strain gage instrumentation even more challenging (1). As a result, the proper application of a strain gage to a geosynthetic sample has become a rapidly growing research area, as demonstrated by the use of digital photography and image analysis to analyze strain gages and strain distribution in geosynthetics (2, 3).

BACKGROUND AND INVESTIGATION

Tensile Strength. The tensile strength of a geomembrane sample is usually determined via a tensile test, such as ASTM test method D882 for PVC, which was used for this study. The test is performed by applying an increasing axial load to the sample and measuring the resulting strain from axial elongation.

The axial deformation of the geomembrane sample is typically measured with a strain gage. However, while the gage provides information on the strain experienced by the material, it does not account for changes in the cross-sectional area. Therefore, the strain which is computed and plotted is the engineering strain, ϵ , rather than the true strain.

The engineering strain is the percentage increase from the original length, L_0 , and is computed as shown in equation (1), where ΔL , is the change in length.

$$\epsilon(\%) = \frac{\Delta L}{L_0} \times 100 \quad (1)$$

The stress, σ , in the geomembrane sample is calculated as the load applied, P , divided by the cross-sectional area, A , of the sample as shown by equation (2).

$$\sigma = \frac{P}{A} \quad (2)$$

PVC was used in this experiment due to its fairly predictable stress-strain behavior, low cost, and routine use in the field.

Molecular Properties of PVC. The molecules in polymers are sometimes called macromolecules due to the fact that each polymer molecule contains atoms bounded together by covalent inter-atomic bonds. For PVC, these molecules form long, flexible chains, each with a carbon atom backbone. This linear polymer structure is represented schematically in Figure 1. A mer unit is defined as the repeating group of elements which connect to form the larger polymer molecule's chemical structure, as shown in the figure. Under tensile stress, the tangled molecular chains stretch with total percent elongation of the geomembrane ranging from 20 - 40% elongation (4). PVC is widely used as a geomembrane material because it is chemically inert, tough and dent-resistant, has water, corrosion, and weather resistance, and a relatively high strength-to-weight ratio. The workability, flexibility, tensile strength, elongation, and puncture and abrasion resistance can be further improved with the aid of additives such as plasticizers. Plasticizers are generally liquids with low vapor pressures and low molecular weights. PVC is intrinsically brittle by nature at room temperature and very hard and stiff. When a plasticizer is added, the small plasticizer molecules occupy positions between the relatively large polymer chains to improve ductility (4). Most PVC sheets produced in roll form contain 25 - 35% of one or more plasticizers. Chemical stabilizers may also be added to improve the ultraviolet (UV) radiation resistance of the material. Stabilizers are used to counteract the deteriorative process in which UV radiation severs the covalent bonds in the PVC polymer chain (4). PVC liner materials typically contain 1 - 5% of chemical stabilizers.

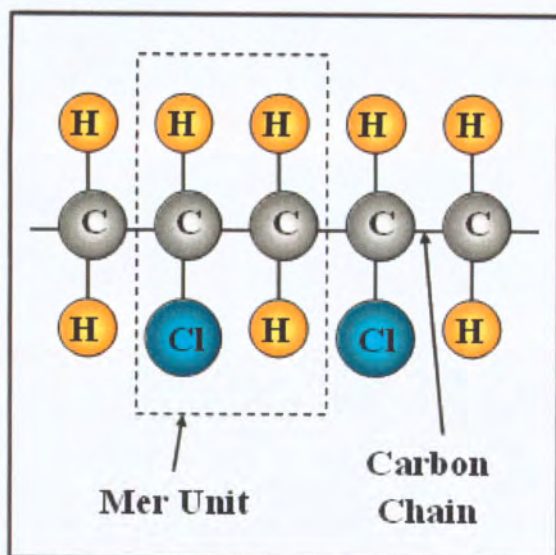


FIGURE 1: PVC mer structure

Molecular Properties of Adhesives. The three adhesives used in this study were one-part, room-temperature-vulcanizing (RTV), silicone rubber based adhesives. These types of adhesives cure to a durable, rubber adhesive-sealant via a condensation reaction with moisture in the air. The active ingredient in the three adhesives used in this study is methyltrimethoxysilane. The empirical formula of the chemical compound is $C_4H_{12}O_3Si$ and the linear formula is $CH_3Si(OCH_3)_3$. The chemical structure is shown in Figure 2.

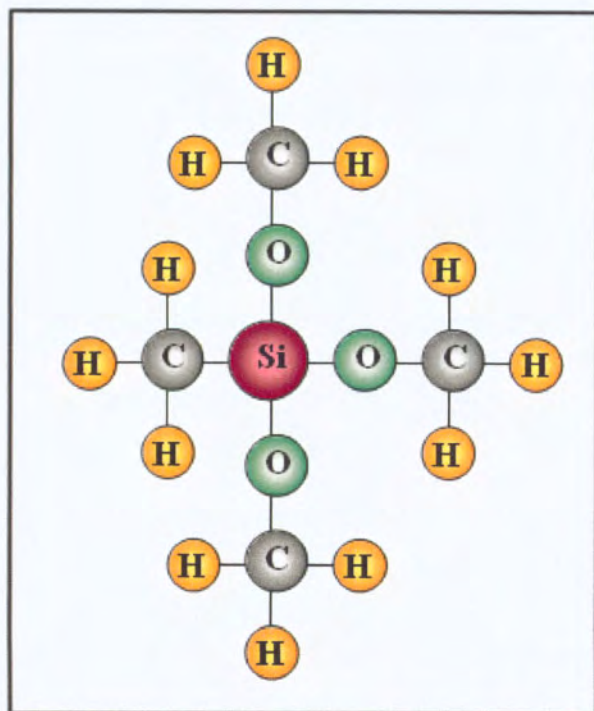


FIGURE 2: Methyltrimethoxysilane chemical structure

The purpose of methyltrimethoxysilane is that it acts as a cross-linking agent for room temperature cured silicone rubber (5). Unlinked polymer chains are more elastic because the chains are able to slide past each other under applied stress. By adding a chemical which creates links between polymer chains, the result is a more rigid material (4).

Due to the silicone in the adhesive, the one-component adhesive types are highly permeable to moisture vapor and, as a result, typically cure at a rate of 0.3 cm/day, which is faster than non-silicone based rubber adhesives. A further advantage of these RTV silicone rubber based adhesives is that the saturated inorganic Si-O-Si polymer backbone enhances the flexibility, durability, and UV resistance of the adhesive. Additionally, the silicone in the adhesives tends to enhance the water, thermal, and oxidative resistances of the hardened adhesive (5). Therefore, these types of adhesives possess properties that are very favorable to strain gage instrumentation of geosynthetics.

The failure mechanism observed in this study was the loss of adhesion to the PVC geomembrane under increasing applied axial loading. Loss of adhesion is primarily associated with either the formation of a weak boundary layer or breaking of the silicone-substrate chemical bonds. If there is a weak boundary layer, typically there exists a cohesively weak region at the adhesive-substrate interface. As a result, weaker bonds are formed or the adhesive preferentially forms bonds with a secondary boundary layer rather than the PVC surface. The causes of a weak boundary layer are usually the presence of contaminants on the surface or migration of additives from the PVC to the silicone-substrate interface. Additionally, molecular components from the adhesive can diffuse to the interface and form a weak boundary layer as well. In the case of failure being caused by the breaking of the silicone-substrate chemical bonds, this failure typically occurs due to water vapor, which is required for the condensation reaction, permeating through the silicone adhesive to the interface and interfering with hydrogen bonding and thus weakening the adhesion (6).

EXPERIMENTAL PROGRAM

A modified strip tensile test was performed based upon ASTM test method D882. The geomembrane used in this experiment was 40 mil (1 mm thick) dark gray PVC. The sample was originally 1067 mm long and 69.0 mm wide. Three different types of adhesives were applied to the geomembrane.

The adhesives used were silicone rubber based adhesives obtained from the Dow Corning Corporation. The first is a translucent adhesive, product number 3145 RTV MIL-A-46146 Adhesive/Sealant, as shown in Figure 3 (a). It is made of 7.0 – 13.0% methyltrimethoxysilane by weight. The glue is non-corrosive and has a high tensile strength of 940 psi and high elongation at 660% before breaking. The specific gravity is 1.10 and the extrusion rate is 110 g/min when measured at 90 psi through a 1/8" (3.18 mm) orifice. It also contains a UV indicator for automated inspection.

The second of the silicone rubber based adhesives is product number 739 Plastic Adhesive. It is an opaque white, non-corrosive, general purpose adhesive, as shown in Figure 3 (b). It is made of 1.0 – 5.0% methyltrimethoxysilane by weight, which is less than the 3145 adhesive. The adhesive has a tensile strength of 200 psi, overlap shear strength of 140 psi, and elongation of 500%. The specific gravity is 1.40.

The third of the rubber based adhesives is product number 839 Silicone Adhesive/Sealant. It is a translucent blue, non-corrosive, general purpose adhesive, as shown in Figure 3 (c). The adhesive is a mix of three active ingredients: greater than 60% dimethyl siloxane, 5.0 – 10.0%

methyltrimethoxysilane, and 1.0 – 5.0% diisopropoxy di(ethoxyacetoacetyl) titanate by weight. The adhesive has a tensile strength of 250 psi, overlap shear strength of 140 psi, and elongation of 350%. It has an extrusion rate of 220 g/min when measured at 90 psi through a 1/8" (3.18 mm) orifice. The specific gravity is 1.02.

All three of the adhesives cure at room temperature and are nonflow pastes applied with a brush or metal spatula. During the curing process, methyltrimethoxysilane can generate flammable methyl alcohol. Therefore, for safety purposes, the glues were applied within a vapor hood to provide adequate ventilation.

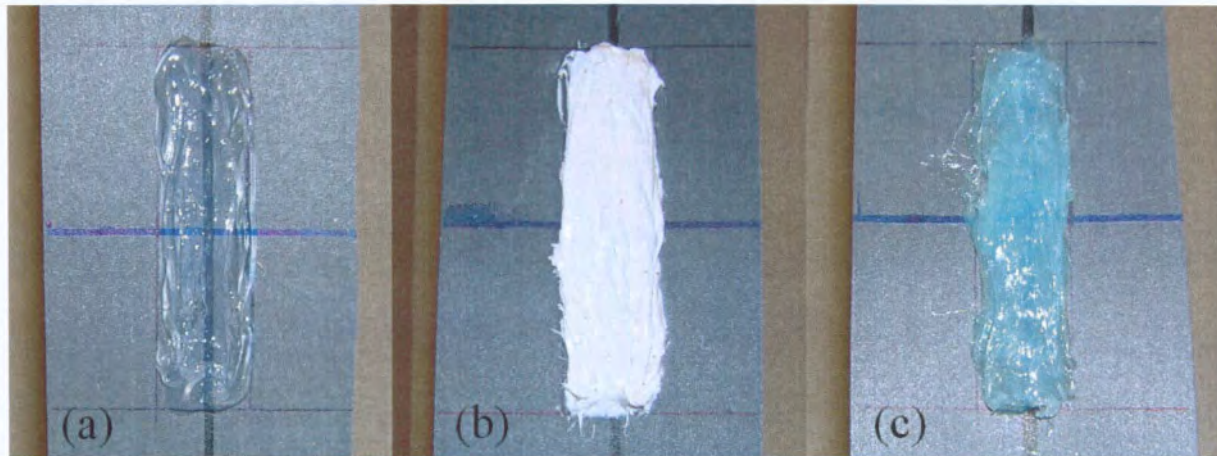


FIGURE 3: Adhesives applied to PVC geomembrane (a) Translucent silicone adhesive-sealant 3145 RTV MIL-A-46146, (b) White plastic adhesive 739, (c) Translucent blue silicone adhesive 839

PROCEDURE

Sample Preparation

The PVC geomembrane was cleaned with cotton gauze pads dipped in 70% ethyl alcohol. The three adhesives were applied in 8 cm long, 2 cm wide, and 3 mm thick strips on the geomembrane and allowed to cure for 5 days, which is two days longer than the minimum required time of 72 hours to ensure full hardening.

The geomembrane was then attached to a metal frame using metal clamps and hung vertically. While previous studies have shown that roller-type gripping mechanisms are the most reliable for high-strength geosynthetics to prevent slippage, the geomembrane was assumed to be of moderate strength and such a measure was decided to be unnecessary (7). A metal clamp was also attached to the bottom of the geomembrane and below it an ELE 88-4100 mechanical dial strain gage was set up. Masses were hung from the bottom metal clamp and the elongation in the sample was measured by the dial gage.

Testing

The original dimensions of the geomembrane strip and all three adhesives were measured prior to any load application. Then, an increasing mass was applied axially to the geomembrane in increments of 1.0 kg from 1.0 kg to 9.0 kg. Time was allowed for the geomembrane and

adhesives to complete deformation prior to measurements. Dial gage movement was monitored over this time, and final measurement was taken when the dial movement settled over a set period of time of 15 minutes. The geomembrane deformation for each applied mass was measured using the dial strain gage. The change in length in the adhesives was determined using an engineering scale. A strain gage could not be used for the adhesive measurements due to the fact that the strain gage measurements may not be accurate if the adhesives' elastic moduli are significantly different than that of the geomembrane's elastic modulus. As this was one of the objectives of the study, error could have been introduced if strain gages had been used for the adhesives' measurements. Taking direct physical measurements yielded actual changes in the lengths of the adhesives.

RESULTS AND DISCUSSIONS

Stress-strain behavior of geomembrane. The axially loaded geomembrane underwent a total elongation of 122.3 mm, resulting in an engineering strain of 11.5%. This elongation did not result in plastic yielding of the membrane because after unloading, the geomembrane strip recovered back to its original length of 1067 mm. The experimental stress-strain results are shown in Figure 4. Superimposed on the plot is the maximum tensile strength of the geomembrane sample predicted as 1268 kPa at the strain level of 13.5%. This strain corresponds to a total elongation of the sample of 144.0 mm.

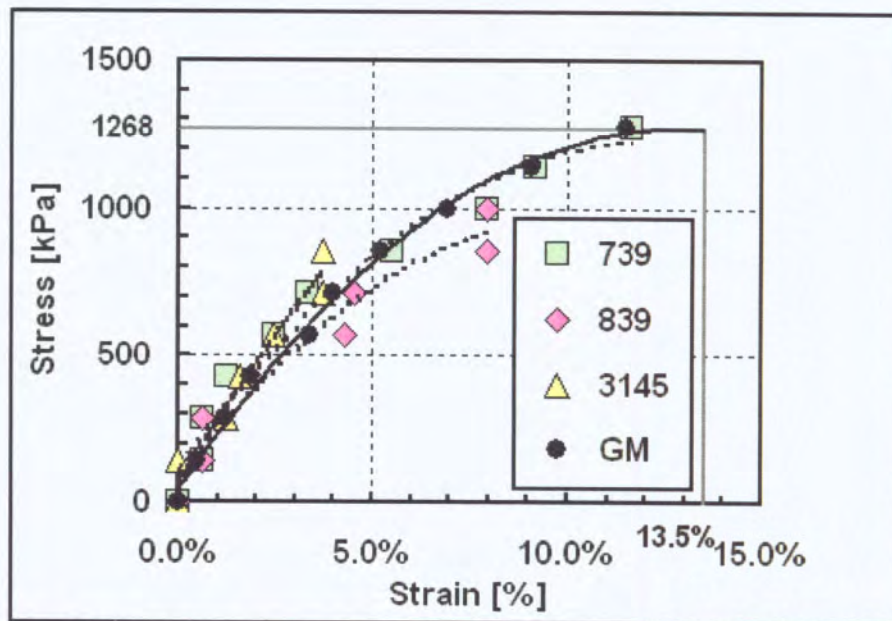


FIGURE 4: Stress-strain relationships of geomembrane and adhesives

The polynomial trendline that best fits the geomembrane data is given by equation (3).

$$\sigma = -74,311\epsilon^2 + 19,076\epsilon + 47.382 \quad (3)$$

The modulus of elasticity, E , is the slope of a line drawn tangent to the initial portion of the stress-strain curve. This method assumes that for relatively small deformations at room temperature, the polymer behaves elastically and obeys Hooke's Law, as shown by equation (4).

$$\sigma = E\epsilon \quad (4)$$

The secant modulus is determined for a specific percent strain, typically 10%, by drawing a straight line from the origin to that strain level on the stress-strain curve (8). Hence, the initial tangent modulus of elasticity is determined to be 24,000 kPa and the secant modulus of elasticity at 10% strain, E_{s10} , is 12,120 kPa for the PVC geomembrane strip used in this experiment. These values comply well with strength reported for PVC membranes. For example, for 30 mil PVC geomembranes, the initial tangent modulus of elasticity is typically 31,000 kPa (8). Stress-strain behavior of adhesives. The three adhesives exhibited varying stress-strain behaviors. The 3145 silicone rubber based adhesive lost its bond to the PVC at stresses above 853 kPa. Therefore, at adhesive strains beyond 3.7%, the strain gage adhered to the geosynthetic using the 3145 silicon rubber would no longer be measuring the geosynthetic deformation. The E for the adhesive was determined to be 19,300 kPa. The 839 silicone rubber based adhesive lost its bond to the PVC at stresses above 995 kPa. The E for the adhesive was determined to be 32,500 kPa. The 739 plastic adhesive never lost its bond to the PVC over the course of the experiment, even up to 12% strain. The E and E_{s10} values were determined to be 36,400 and 12,000 kPa, respectively.

Discussion of results

The 739 plastic adhesive was the only specimen not to lose its adhesion to the geomembrane. The E_{s10} value of 12,000 kPa of this adhesive yielded a percent difference of only 1.0% from the geomembrane value of 12,120 kPa. Therefore, while secant elastic modulus appears to be a reasonable indicator of how durable a bond will be to PVC in the field, it is important to note that using only E would have been misleading. If only the initial tangent results had been used, the 3145 silicone rubber based adhesive would have been recommended for this application because its E value is the closest to the geomembrane value at 19,300 kPa. However, the 3145 adhesive was the first of the three adhesives to lose its bond. Therefore, E values can be insufficient when choosing adhesives for strain gage instrumentation. E_{s10} values give a much more accurate representation of how effective the adhesive will be.

Additionally, the performance of the adhesives is directly proportional to the percentage by weight of methyltrimethoxysilane, the active ingredient, they contain as shown by Figure 5. Adhesives with low percentages by weight of the cross-linking agent achieved greater stresses without losing the bond to the geomembrane.

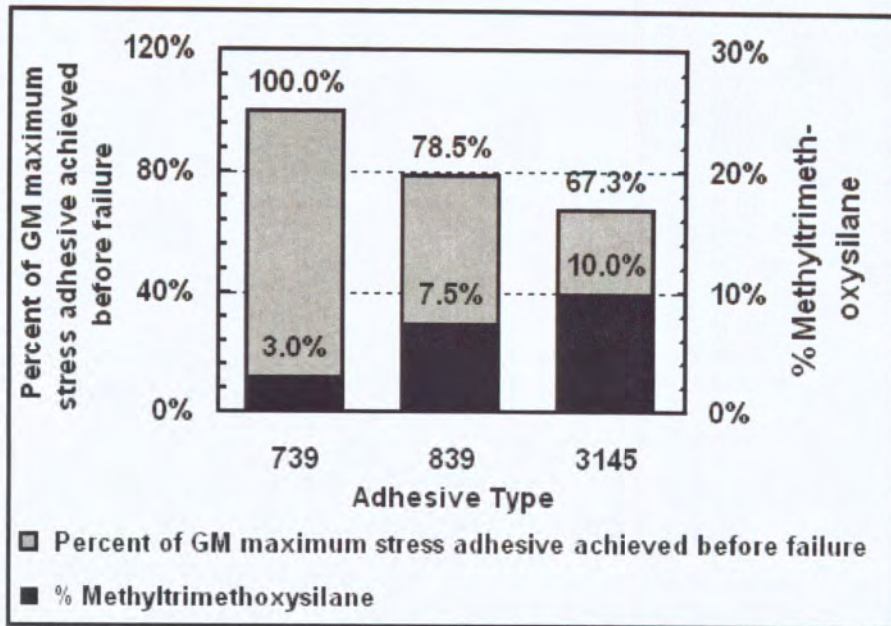


FIGURE 5: Maximum adhesive stress relationship to methyltrimethoxysilane content

Similarly, the maximum stress obtained prior to adhesion failure increases linearly with decreasing values of methyltrimethoxysilane, as shown by Figure 6. A linear function fits the data points exceedingly well, with a regression coefficient value of 1.000. While a linear relationship was found between maximum adhesive stress and percent methyltrimethoxysilane, a non-linear relationship was found for adhesive strain, as shown by Figure 7.

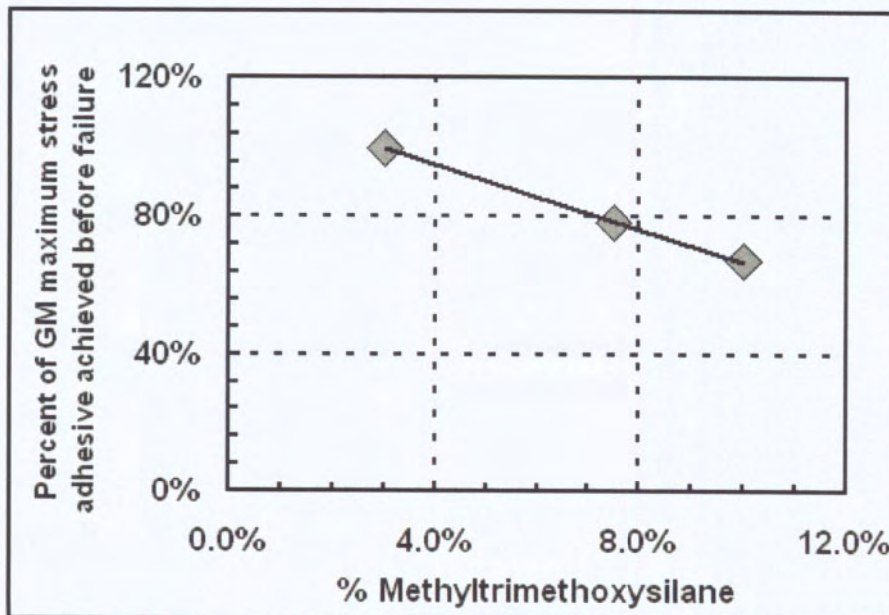


FIGURE 6: Maximum stress achieved as a function of percentage of methyltrimethoxysilane

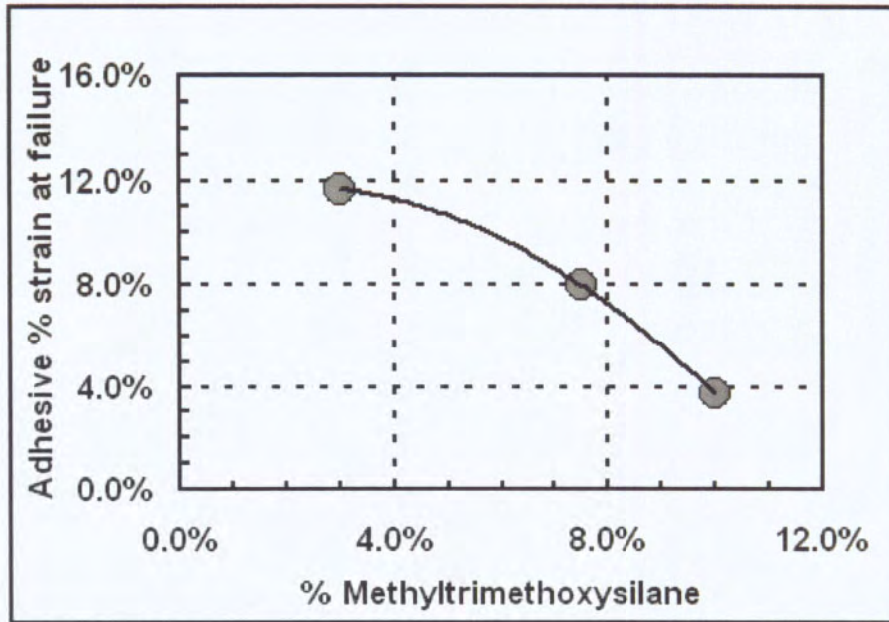


FIGURE 7: Maximum adhesive strain achieved as a function of percentage of methyltrimethoxysilane

The equation of the polynomial function is given by equation (5).

$$\varepsilon_{\max} = -12.724(\%MTES)^2 + 0.5181(\%MTES) + 0.1125 \quad (5)$$

where $\%MTES$ = percentage of methyltrimethoxysilane by weight in the adhesives.

Once again, the function fits the data extremely well, with a regression coefficient value of 1.000. By taking the derivative of the equation and setting it equal to zero, the strain can be maximized and the corresponding percentage of methyltrimethoxysilane is found to be 2.0%. Therefore, the theoretical maximum strain that can be achieved by manipulating the percent of methyltrimethoxysilane is when the percent content by weight is 2.0% or less. This value corresponds to a maximum strain of 11.7%. As shown by Figure 4, the 739 plastic adhesive was the only adhesive tested which was able to achieve 11.7% strain without losing its bond to the geomembrane. It is also contains the lowest percent of methyltrimethoxysilane of the adhesives tested.

The data obtained from strain gage instrumentation of geosynthetics in the field is only useful when the strain measurements pertain to the geosynthetics rather than to the adhesives.

Therefore, it is a necessary requirement of the adhesive that it has an inherent stress-strain behavior similar to that of the geosynthetic to which it is attached.

Additionally, adhesives which can attain relatively large deformations without losing their bond to the geosynthetic will be the more useful choices. Methyltrimethoxysilane acts as a cross-linking agent by creating covalent bonds between the polymer chains of the adhesives. The cross-linking agent improves the tensile strength and abrasion resistance of the adhesive.

Cohesion failure, in which a silicone network depolymerizes and the adhesive tears apart, is less likely to occur with increasing methyltrimethoxysilane content (6). The more bonds that are formed, the more rigid the hardened adhesive will be. However, the adhesive will not deform as easily under tensile stress, as demonstrated by this study. Hence, the adhesives with greater concentrations of methyltrimethoxysilane are more resistant to deformation, and subsequently more likely to lose their bonds to the geomembrane. Due to the fact that adhesives used in

geosynthetic applications are more susceptible to adhesion failure rather than cohesion failure, the percent of methyltrimethoxysilane by weight used should be minimized.

CONCLUSIONS

This study demonstrated that initial tangent modulus of elasticity values can be misleading when choosing adhesives for the strain gage instrumentation. While the goal in strain gage instrumentation is to choose an elastic adhesive with a stress-strain relationship similar to that of the geomembrane, secant modulus of elasticity values at 10% strain provide a much more accurate representation of how durable the adhesive's bond will be. Additionally, adhesives which contained low amounts, on the order of 1.0 – 5.0% by weight, of methyltrimethoxysilane, the cross-linking polymer agent, adhered to the geomembrane surface the most successfully while undergoing relatively high strains, even up to nearly 12% strain.

The limitation of this study is that it was assumed that the geomembrane sample experienced uniform axial tensile strain throughout the duration of the experiment. However, as shown by previous studies using image-based analysis on geotextiles and geogrids, localized strain can vary throughout the sample (3). Additionally, it is recommended that a more stable gripping system be developed as the current use of a metal clamp may cause slippage at stresses above 1268 kPa. Roller-type grips have been recommended in previous studies for higher strength geosynthetics (7). Finally, analysis of moisture effects and geomembrane wrinkles on the adhesive bond durability is also of interest to future research.

REFERENCES

- (1) Giroud, J.P. (2005). "Quantification of Geosynthetic Behavior." *Geosynthetics International*, Special Issue on the Giroud Lectures, 12, No. 1, 2-27.
- (2) Warren, Kimberly A., Howard, Isaac L., and Brooks, Jeremy A. (2006). "Use of Digital Photography to Analyze Foil Strain Gages in Geosynthetics." *GeoCongress 2006*, Geo-Institute of the American Society of Civil Engineers, Atlanta, GA.
- (3) Aydilek, Ahmet H., Guler, Murat, and Edil, Tuncer B. (2004). "Use of Image Analysis in Determination of Strain Distribution During Geosynthetic Tensile Testing." *Journal of Computing in Civil Engineering*, ASCE, 18:1(65).
- (4) Callister, William D. Jr. (2003). *Materials Science and Engineering*. John Wiley & Sons, Inc., New York, NY, 454, 457.
- (5) Lower, Loren D. and Klosowski, Jerome M. (2003). *Handbook of Adhesive Technology*. 2nd ed. Pizzi, A. and Mittal, K.L., eds., Marcel Dekker, Inc., New York, 813-821.
- (6) Parbhoo, B., O'Hare, L.-A., and Leadley, S.R. (2002). *Surfaces, Chemistry & Applications*, Chaudhury, M. and Pocius, A.V., eds, Elsevier, Boston, 2, 639, 697-699.
- (7) Kutay, M. Emin, Guler, Murat, and Aydilek, Ahmet H. (2006). "Analysis of Factors Affecting Strain Distribution in Geosynthetics." *Journal of Geotechnical and Geoenvironmental Engineering*, ASCE, 132:1(1).
- (8) Koerner, Robert M. (2005). *Designing with Geosynthetics*. Pearson Prentice Hall, Upper Saddle River, NJ, 110, 439-443.

Key words: Geosynthetic instrumentation, geomembrane, adhesive, polyvinyl chloride, methyltrimethoxysilane.

CONTACT:

Laura Hannum

Graduate Research Assistant

Department of Civil and Environmental Engineering Lehigh University

Bethlehem, PA, 18015

Phone: 484-241-7405

Email: lmh7@lehigh.edu

PYRAMID-TOOTH GRIPPING SURFACE FOR GCL SHEAR TESTING

John M. Allen, Director, Geosynthetic Interaction Laboratory, TRI/Environmental; Patrick J. Fox, Professor, Department of Civil & Environmental Engineering & Geodetic Science, Ohio State University

ABSTRACT

A new gripping surface, called the “pyramid-tooth gripping surface”, for shear strength testing of geosynthetic clay liners (GCLs) is presented. Each pyramid-tooth gripping plate is machined from a single piece of stainless steel stock and therefore has excellent strength and durability. The teeth have the shape of a truncated pyramid with a vertical flat face on one side that is capable of biting into the woven or non-woven geotextile of a GCL. A large number of drainage holes and channels also provide a GCL specimen with free access to water during hydration, consolidation, and shear. Compared to a conventional truss plate surface and the GRI-GCL4 surface, the pyramid-tooth gripping surface produced the highest peak shear strengths and lowest displacements at peak over a wide range of normal stress. However, the pyramid-tooth surface was not capable of internally shearing GCL specimens at a normal stress of 9.6 kPa.

INTRODUCTION

The internal shear strength of geosynthetic clay liners (GCLs) can be influenced by many factors, including product type, manufacturing conditions, hydration conditions, consolidation procedures, shear displacement rate, and gripping/clamping system (Fox and Stark 2004). The gripping surface is the rough surface that covers the shearing blocks and transfers shear stress to the test specimen. The key components of a gripping surface are teeth that engage the specimen and provide resistance to slippage during shear and drainage holes that provide the specimen with free access to water. Gripping surfaces still vary widely among laboratories and the preferred surface remains a topic of debate in the GCL testing community. Several authors have demonstrated success using a variety different gripping surfaces (Fox et al. 1997, Pavlik 1997, Trauger et al. 1997, Fox et al. 1998, Zanzinger and Alexiew 2000, Olsta and Swan 2001, Triplett and Fox 2001, Koerner and Lacy 2005, and Fox et al. 2006). In 2006, the Geosynthetic Research Institute published a guide for a standardized GCL gripping surface (GRI-GCL4 2006) that makes use of the “truss plates” developed by Fox et al. (1997). Although significant efforts have been made to introduce gripping surfaces that can consistently shear GCL specimens at low normal stress levels, no one surface has yet been universally adopted by the community of commercial and research testing laboratories.

Although recent attempts have been made to standardize GCL gripping surfaces for internal and interface shear testing, the need remains to improve certain aspects of these surfaces. Currently, laboratories and research centers use a variety of gripping surfaces that range from steel truss plates attached to plywood to the new GRI-GCL4 gripping plates that consist of machined PVC plates and milled truss plates. Sandpaper, wood, wood rasps, and coarse soil have also been used historically. Koerner and Lacy (2005) designed a gripping surface that was able to internally

shear a woven/non-woven (W/NW) GCL under a normal stress of 47.8 kPa, which led to the GRI-GCL4 standard. The need for a new gripping surface is driven by manufacturer requirements that GCLs exceed a specified minimum internal shear strength under even lower nominal stress levels (9.6 kPa). This becomes progressively more difficult with the continuing development of stronger reinforced GCL products.

The objective of this paper is to introduce a new "pyramid-tooth" gripping surface that provides superior gripping over a wide range of normal stress while maintaining free access to water. Replicate shear tests were performed on a hydrated needle-punched GCL using this new surface and two other common gripping surfaces. This paper presents and discusses the results of these tests.

EQUIPMENT

A gripping surface for GCL internal and interface shear testing should be aggressive enough to hold a woven or non-woven geotextile during shear without slippage, but not so aggressive that the teeth bind or otherwise interfere with the shearing process. It should also allow the GCL to have free access to water during hydration, consolidation, and shear. The teeth are a key component in a successful gripping surface. Tooth height varies depending on normal stress conditions, with reported values generally varying from 1.0 to 2.5 mm. The teeth are typically made from screws, nails, wood rasps or truss plates used in wood truss construction, and may be shaped to a variety of configurations. For example, truss plates may be milled flat or at an angle, or have the tooth height reduced by a spacer material. If the tooth height is too large for the applied normal stress, the gripping plates will bind with each other and not shear the specimen properly. If the tooth height is too small, the specimen may slip during shear and start to roll up or bind between the shearing surfaces. Either case will produce unreliable test data.

This study evaluated the shear strength of a needle-punched GCL using three gripping surfaces: 1) a plywood and truss plate (i.e., "conventional") grip, 2) the GRI-GCL4 grip, and 3) the newly developed pyramid-tooth grip. The conventional grip consists of a 19.5 mm-thick sheet of plywood with truss plates screwed to one side. To reduce the height of the teeth, a 7 mm-thick spacer (another piece of plywood) is pressed over the truss plates. The resulting product is a gripping plate with sharp pointed teeth that are 1-2 mm in height. The teeth become bent and dull over time, which results in unwanted variation of gripping capacity. The plywood is also subject to deterioration in the wet environment. Such deterioration can be rapid if holes are drilled through the plywood to allow free water access to the GCL specimen.

The GRI-GCL4 gripping plates are made from a 25.4 mm-thick PVC plate that has been machined to allow free access to water. A truss plate with gripping teeth milled flat to 1.5 mm in height is then screwed to the PVC plate. GCL specimens are trimmed so that excess geotextiles are wrapped around their respective shearing blocks. Fox et al. (1997) and Fox et al. (1998) first proposed the use of truss plates for GCL gripping surfaces. In those studies, however, the teeth were not milled flat but were cut at an angle to have a triangular cross-section that would more effectively bite into the GCL geotextiles.

The pyramid-tooth gripping surface is shown in Figure 1. Schematic diagrams of the plates and their detailed geometry are shown in Figures 2 and 3. Each plate was machined from a single

piece of 12.5 mm-thick stainless steel stock. One side of the plate has a 2.0 mm-deep slotted grid pattern to allow water to flow underneath. A 3.1 mm-diameter drainage hole was drilled at each slot intersection (20.3 mm on center) to allow water to move through the plate from the slotted side to the gripping side. The drainage holes give the GCL specimen free access to water during hydration, consolidation, and shear. The gripping surface consists of 870 pyramid-shaped teeth with one side of each pyramid cut vertically to create a flat sharp face. The flat faces are oriented in the same direction such that the teeth can bite into the geotextiles

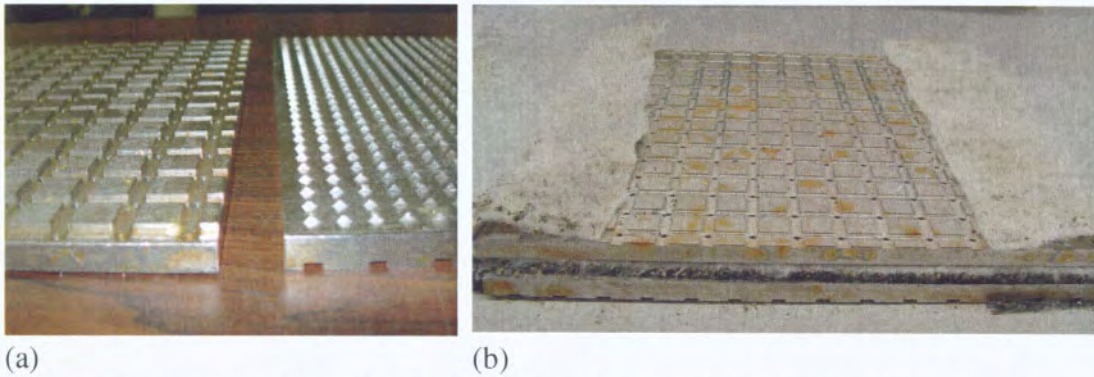


Figure 1. (a) Two pyramid-tooth gripping plates showing the drainage grid (left) and gripping teeth (right), and (b) an assembled GCL specimen ready for mounting in the shear box.

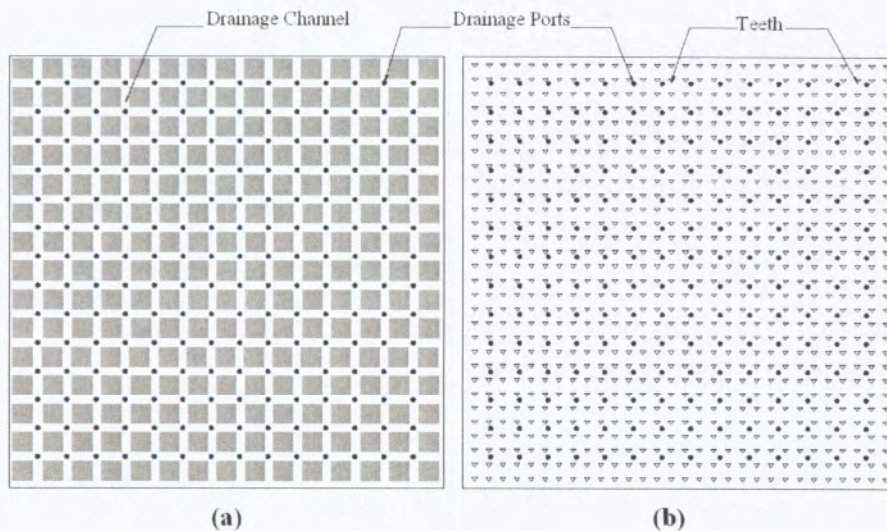


Figure 2. (a) Drainage Channel and (b) Teeth. front side.

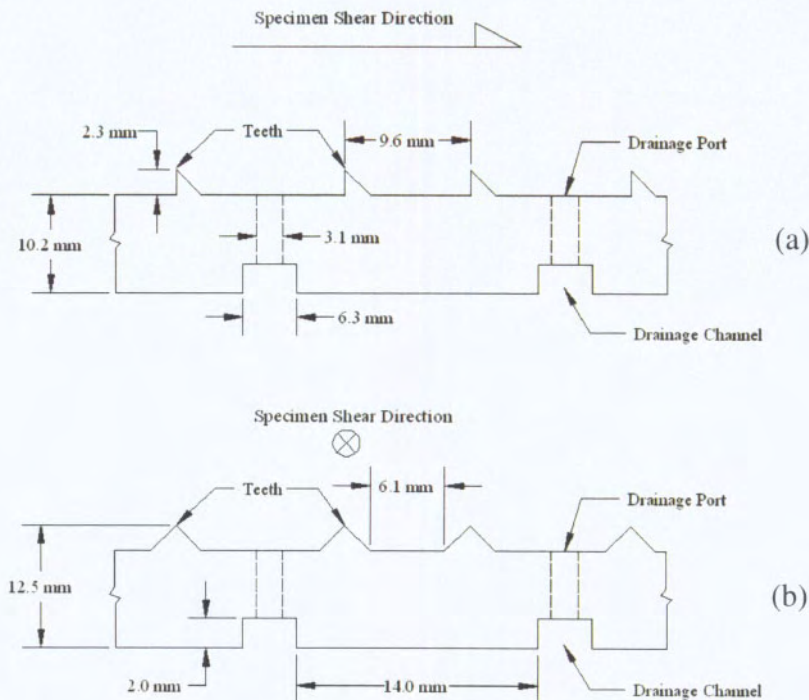


Figure 3. Detail section view of pyramid-tooth plate geometry: (a) in the direction of shearing, and (b) normal to the direction of shearing.

when normal stress is applied and provide a passive resistance to sliding of the geotextile during shear. A tooth height of 2.3 mm was used to shear specimens for normal stresses less than 50 kPa and a tooth height of 1 mm was used for normal stresses greater than 450 kPa. The GCL specimen is placed between two gripping plates with the vertical flat faces aligned in opposite directions and the geosynthetics are wrapped around the ends (Figure 1b). Each set of gripping plates were machined for less than \$500.

GCL MATERIAL AND TEST PROCEDURES

Direct shear tests were conducted at TRI/Environmental on a non-commercial grade W/NW needle-punched GCL with an average peel strength of 458 N/m. GCL specimens were cut to 305 × 457 mm and the woven and non-woven geotextiles were separated by hand so that an area of 305 × 305 mm of intact reinforcement remained. The specimens were then hydrated and sheared using a Durham Geo model LG-115 large-scale direct shear box. In all cases, the non-woven geotextile was placed against the upper fixed shear box and the woven geotextile was attached to the lower traveling shear box. Specimens were hydrated with tap water under a normal stress of 9.6 kPa for a minimum of 24 hours prior to mounting in the shear box. The gap for the shear box was set so that shear would occur between the geotextiles of each GCL specimen.

Mounting of the GCL specimens followed specific protocols associated with each gripping surface. GCL specimens sheared with the conventional gripping surface were clamped outside of the shearing area using bar clamps. Specimens tested with the GRI-GCL4 gripping surface had their excess geotextiles wrapped around the gripping plates and held in place using hot glue (GRI 2006). Specimens sheared with the pyramid-tooth gripping surface were mounted in the shear box in a similar fashion as described in the GRI-GCL4 procedure with the lower and upper plates oriented such that the flat faces of the pyramid teeth were facing toward one another. GCL specimens were sheared using each gripping surface at initial (i.e., nominal) normal stress $\sigma_n = 9.6, 47.9, \text{ and } 478.8 \text{ kPa}$, giving a total of nine shear tests. The 9.6 kPa value was selected because it is the lowest value for which GCL manufacturers provide minimum internal shear strengths. The other two values were selected because they cover a typical range for GCLs. For the two higher stress levels, each specimen was hydration at 9.6 kPa and then consolidated by incremental loading with a load-increment-ratio of one (i.e., doubling the load each time). The minimum duration of each load increment was four hours. The final normal stress remained on the GCL specimens for a minimum of 12 hours prior to shearing. The displacement rate used for all shear tests was 0.1 mm/min, as recommended by Fox et al. (2004), to minimize the effects of shear-induced excess pore pressures. Specimens were sheared to a final displacement of approximately 88 mm.

RESULTS AND DISCUSSION

Shear stress data was corrected for bearing slide resistance and an area correction was applied to both normal and shear stresses. The shear stress vs. displacement relationships are presented in Figures 4–6 for the high, medium, and low normal stress levels, respectively. Thus, each plot gives a direct comparison of shear strength data obtained using the conventional, GRI-GCL4, and pyramid-tooth gripping surfaces. Results from the testing program are summarized in Table 1.

At the highest normal stress level ($\sigma_n = 478.8 \text{ kPa}$), all three gripping surfaces sheared the GCL specimens internally. This was clear during examination of the failed specimens and can be inferred from the shear stress vs. displacement relationships in Figure 4. When a reinforced GCL specimen shears internally, measured shear stress rises rapidly and often reaches a peak value at a displacement of 30 mm or less. Shear strength then decreases rapidly and approaches a residual condition. Fox et al. (2004) provides examples and additional discussion of good- and poor-quality internal shear test data. In this study, Figure 4 shows that the pyramid-tooth

gripping surface produced the highest peak shear strength at $\sigma_n = 478.8 \text{ kPa}$, followed by the conventional surface and the GRI-GCL4 surface.

Shear stress vs. displacement curves for the different gripping surfaces at the medium normal stress level ($\sigma_n = 47.9 \text{ kPa}$) display more pronounced differences than at the high normal stress (Figure 5). The pyramid-tooth gripping surface sheared the GCL specimen internally, whereas the conventional and GRI-GCL4 surfaces allowed their specimens to slip during shear. This is also implied from the stress-displacement curves. The pyramid-tooth surface produced a high tight peak and the other surfaces produced irregular curves with broad peaks. Post-test examinations of the conventional and GRI-GCL4 specimens showed areas of intact needle-

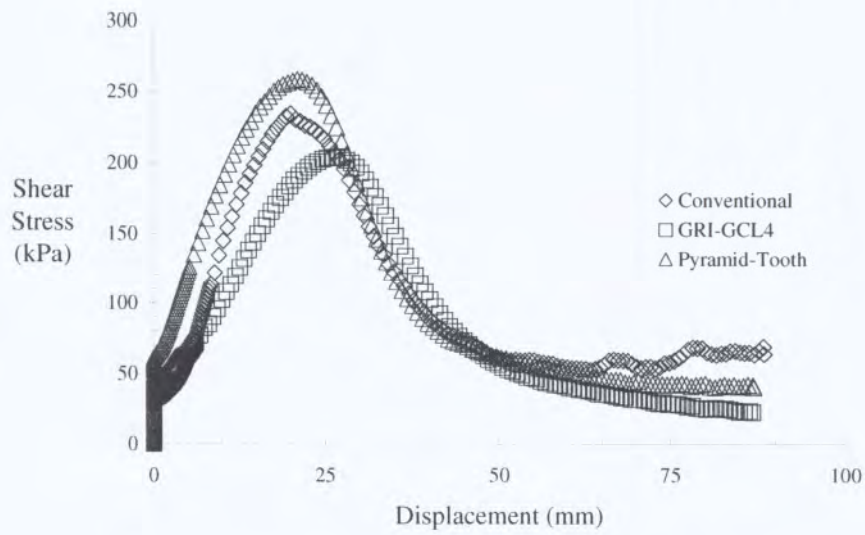


Figure 4. Effect of different gripping surfaces for three internal shear tests at $\sigma_n = 478.8$ kPa.

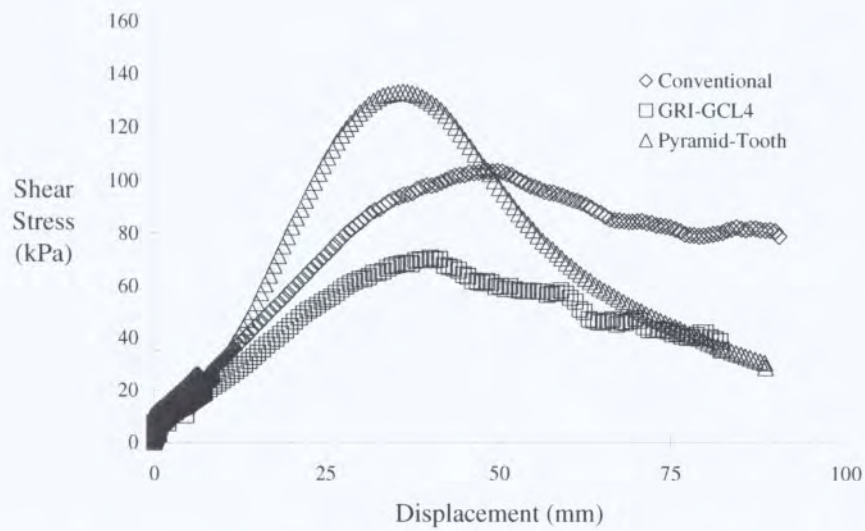


Figure 5. Effect of different gripping surfaces for three internal shear tests at $\sigma_n = 47.9$ kPa.

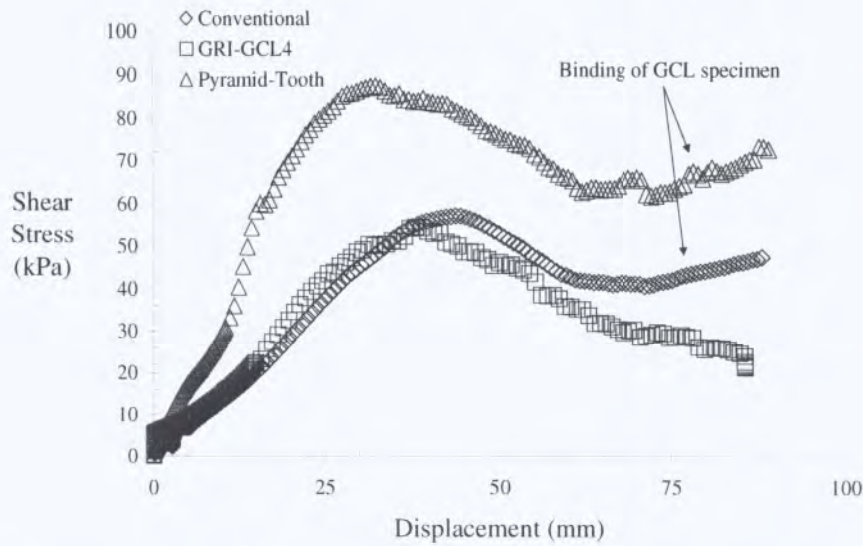


Figure 6. Effect of different gripping surfaces for three internal shear tests at $\sigma_n = 9.6$ kPa.

Table 1. Summary of results for testing program.

Gripping Surface	Initial Normal Stress, (kPa)	Peak				Large Displacement (80 mm)		
		Displacement At Peak, (mm)	Corrected Shear Stress, (kPa)	Corrected Normal Stress, (kPa)	Secant Friction Angle, ($^{\circ}$)	Corrected Shear Stress, (kPa)	Corrected Normal Stress, (kPa)	Secant Friction Angle, ($^{\circ}$)
Conventional	9.6	43.8	57.1	11.2	78.9	44.2	13.0	73.6
	47.9	49.7	102.3	57.2	60.8	79.1	64.4	50.8
	478.8	20.1	233.4	512.6	24.5	64.6	649.9	5.7
GRI-GCL4	9.6	37.2	54.4	10.9	78.7	25.7	13.0	63.2
	47.9	39.9	70.7	55.1	52.1	41.9	64.9	32.8
	478.8	26.6	203.6	524.5	21.2	24.4	649.7	2.2
Pyramid-Tooth	9.6	32.4	87.3	10.7	83.0	67.3	13.0	79.1
	47.9	36.0	133.1	54.3	67.8	38.1	65.0	30.4
	478.8	21.0	258.3	514.2	26.7	42.7	649.3	3.8

punching that did not shear. Similar areas were not observed for the failed pyramid-tooth GCL specimen.

All shear stress vs. displacement curves at the lowest normal stress ($\sigma_n = 9.6$ kPa) display irregularities because none of the three surfaces provided adequate gripping of the GCL (Figure

6). In each case, the woven side of the GCL slipped on the gripping surface. A rise in shear strength at large displacement (> 70 mm) for the conventional and pyramid-tooth surfaces resulted from the GCL binding in the shear box. Post-test inspections of the specimens showed that internal shearing did not occur for the conventional and GRI-GCL4 surfaces. Some local shearing of the GCL occurred for the pyramid-tooth surface, which indicates that the new grips did work to some extent. None of the test specimens showed slippage of the non-woven geotextile on any of the gripping surfaces.

Taken together, Figs. 4–6 show some interesting trends. In each case, the pyramid-tooth gripping surface gave the highest peak shear strength and the smallest (or nearly smallest) displacement at peak. This suggests that the pyramid-tooth surface was the most effective in preventing slippage and introduced the least amount of progressive failure of the GCL specimens during shear (Fox and Kim 2007). It is also observed that the displacement at peak generally increases as σ_n decreases, which is likely due to increasing slippage that occurs for each gripping surface. The GRI-GCL4 surface produced the lowest peak shear strength at each normal stress.

The pyramid-tooth gripping surface was more effective in this study because the teeth were better able to engage the geotextiles of the GCL. The sharp point of each pyramid-tooth allows it to puncture the woven and non-woven geotextiles as the normal stress is applied. Once shearing begins, the tooth engages the fibers of the geotextiles and holds them, thus forcing the GCL to shear internally. In this study, the flat tooth of the GRI-GCL4 plate was probably too wide to puncture the geotextiles as effectively for $\sigma_n < 50$ kPa. Thus, once shearing began, the woven geotextile was able to more easily slide over the GRI-GCL4 tooth. The pyramid-tooth gripping surface also failed to completely engage the woven geotextile at $\sigma_n = 9.6$ kPa.

The pyramid-tooth surface described in this paper has the same general triangular profile (Figure 3a) as the teeth described by Fox et al. (1997). That surface was also highly effective in gripping geotextiles and was able to shear needle-punched GCLs at normal stresses as low as 37.8 kPa without end-clamping of the geosynthetics (Fox et al. 1998). Thus, it appears that a triangular tooth that can punch into a geotextile and lock to the fibers is perhaps the most effective type of gripping surface. The pyramid-tooth surface in this paper has the advantage of being made of stainless steel, whereas the Fox et al. (1997) modified truss plates are made of galvanized steel and will deteriorate over time.

CONCLUSIONS

This paper has presented internal shear strength data that was obtained for a non-commercial grade W/NW needle-punched geosynthetic clay liner (GCL) using three different gripping surfaces: a conventional truss plate gripping surface, the GRI-GCL4 gripping surface, and the new pyramid-tooth gripping surface. In replicate internal shear tests, the pyramid-tooth surface produced the highest peak shear strengths and lowest displacements at peak over a wide range of normal stress levels. Each pyramid-tooth gripping plate is machined from a single piece of stainless steel stock and therefore has excellent strength and durability. The teeth have the shape of a truncated pyramid with a vertical flat face on one side that is capable of punching into the geotextiles of a GCL. A large number of drainage holes and channels also provide the GCL with free access to water during hydration, consolidation, and shear.

The pyramid-tooth gripping surface was capable of internally shearing GCL specimens at normal stresses of 478.8 and 47.9 kPa, but not at 9.6 kPa. The other two gripping surfaces were capable of producing internal shear failures only at the highest normal stress (478.8 kPa). A more aggressive pyramid-tooth gripping plate with a larger number of teeth could be developed but was outside the budget for this study. By increasing the number of teeth it may be possible to shear specimens internally at 9.6 kPa. Thus, although a number of studies have reported variable success for internal shear of GCLs, it appears that no gripping surface to date can produce a clean internal shear failure for a needle-punched GCL specimen under loads typical of landfill cover systems (approx. 10 kPa).

REFERENCES

- ASTM, Standard D 6243, "Standard Test Method for Determining the Internal and Interface Shear Resistance of Geosynthetic Clay Liner by the Direct Shear Method," Annual Book of ASTM Standards, Vol. 04.13, ASTM International, West Conshohocken, Pa.
- Fox, P. J. and Kim, R. H. (2007). "Effect of progressive failure on measured shear strength of geomembrane/GCL interface," *Journal of Geotechnical and Geoenvironmental Engineering*, in review.
- Fox, P. J. and Stark, T. D. (2004). "State-of-the-art report: GCL shear strength and its measurement," *Geosynthetics International*, 11(3), 141-175.
- Fox, P. J., Rowland, M. G., Scheithe, J. R., Davis, K. L., Supple, M. R., and Crow, C. C. (1997). "Design and evaluation of a large direct shear machine for geosynthetic clay liners," *Geotechnical Testing Journal*, 20(3), 279-288.
- Fox, P. J., Rowland, M. G., and Scheithe, J. R. (1998). "Internal shear strength of three geosynthetic clay liners," *Journal of Geotechnical and Geoenvironmental Engineering*, 124(10), 933-944.
- Fox, P. J., Stark, T. D., and Swan, R. H. Jr. (2004). "Laboratory measurement of GCL shear strength," *Advances in Geosynthetic Clay Liner Technology: 2nd Symposium*, STP 1456, R. E. Mackey and K. von Maubeuge, eds., ASTM International, West Conshohocken, Pa., 92-109.
- Fox, P. J., Nye, C. J., Morrison, T. C., Hunter, J. G., and Olsta, J. T. (2006). "Large dynamic direct shear machine for geosynthetic clay liners," *Geotechnical Testing Journal*, 29(5), 392-400.
- Geosynthetic Research Institute (2006). "GRI-GCL4 Gripping of Reinforced GCLs to End Platens During Direct (Interface) Shear Testing," Folsom, Pa.
- Lacey, R. and Koerner, G. R. (2005). "Clamping/gripping of geosynthetic clay liners for mid-plane shear strength testing," *Proceedings, GRI-18 Conference at GeoFrontiers*, ASCE, Austin, Tex. (CD-ROM).
- Olsta, J. T. and Swan, R. H. Jr. (2001). "Internal shear strength of a geosynthetic clay liner at high normal loads," *Proceedings, Tailings and Mine Wastes '01*, Fort Collins, Co., 197-200.
- Pavlik, K. L. (1997). "Corps of Engineers geosynthetic clay liner interface test program," *Proceedings, Geosynthetics '97*, IFAI, Long Beach, Ca., 2, 877-884.
- Trauger, R. J., Swan, R. H. Jr., and Yuan, Z. (1997). "Long-term shear strength behavior of a needlepunched geosynthetic clay liner," *Testing and Acceptance Criteria for Geosynthetic Clay Liners*, STP 1308, L. W. Well, ed., ASTM International, West Conshohocken, Pa., 103-120.
- Triplett, E. J. and Fox, P. J. (2001). "Shear strength of HDPE geomembrane/ geosynthetic clay liner interfaces," *Journal of Geotechnical and Geoenvironmental Engineering*, 127(6), 543-552.

Zanzinger, H. and Alexiew, N. (2000). "Prediction of long term shear strength of geosynthetic clay liners with shear creep tests," Proceedings, 2nd European Geosynthetic Conference, Bologna, Patron Editore, 2, 567-571.

CONTACT

John M. Allen

Director, Geosynthetic Interaction Laboratory

TRI/Environmental

9063 Bee Caves Road

Austin, TX

Phone : 512-262-2101

email: jallen@tri-env.com

DYNAMIC SHEAR TESTING OF A NEEDLE-PUNCHED GCL

Christopher J. Nye, Graduate Research Assistant, Ohio State University; Patrick J. Fox, Professor, Ohio State University

ABSTRACT

Dynamic shear strength data for a needle-punched geosynthetic clay liner (GCL) is presented, including both monotonic and cyclic test results. The data illustrate the effect of displacement rate and displacement amplitude on material response. Monotonic tests indicate that peak shear strength first increased and then decreased with increasing displacement rate. Cyclic test results are used to construct backbone curves at various numbers of cycles from which values of secant shear stiffness and damping ratio are obtained. Shear stiffness decreased with increasing displacement amplitude, whereas damping ratio first decreased and then increased as failure was approached. Post-cyclic static shear tests indicate that peak shear strengths decreased with increasing cyclic displacement amplitude and residual shear strengths were unaffected by previous cyclic loading.

INTRODUCTION

Geosynthetic liner systems are often utilized in seismic regions and, as such, characterization of the dynamic shear behavior of these materials is important for the prediction of long-term performance. Conventional static shear tests provide insight into shear strength behavior under slow, monotonic displacement rates. However, static tests do not provide information on dynamic response, such as cyclic stress ratio vs. number of cycles to failure and post-cyclic static shear strength. Static shear tests also cannot provide relationships for shear stiffness and damping ratio that are needed for ground response analyses. Dynamic shear tests must be performed in order to obtain this information.

Several studies have been conducted on the dynamic shear response of geosynthetic interfaces, including geotextile/geomembrane, geonet/geomembrane, geonet/geotextile, and geomembrane/geomembrane (Yegian and Lahlaf 1992, Yegian et al. 1995, De and Zimmie 1998, Yegian and Kadakal 1998, Kim et al. 2005). Much of this data was obtained using shake table shear tests at low normal stress levels, often 15 kPa or less. Despite these efforts, relatively little data are available for shear strength of geosynthetics and geosynthetic interfaces under dynamic loading conditions, especially for high normal stresses. For example, only one investigation has studied the dynamic internal shear strength (Lai et al. 1998) and two investigations have studied the dynamic interface shear strength (Lo Grasso et al. 2002, Kim et al. 2005) of geosynthetic clay liners (GCLs).

Lai et al. (1998) tested small specimens (diameter = 80 mm) of an unreinforced geomembrane-supported GCL using a direct simple shear device. These specimens were subjected to sinusoidal excitations and sheared to small displacements for a normal stress range of 36 – 69 kPa. The dry specimens showed a slight strength increase under cyclic loading due to bentonite densification. When hydrated, GCL shear strength decreased under cyclic loading. Similar to natural clays, the number of cycles required to cause failure decreased with increasing cyclic

stress ratio. Lo Grasso et al. (2002) conducted shake table shear tests on GCL/geomembrane interfaces at a normal stress of 0.82 kPa using both sinusoidal and seismic loading conditions. The tests revealed that the dynamic interface friction angle increased with excitation frequency. Information on the type of GCL and hydration/consolidation conditions used in the study was not provided. Kim et al. (2005) conducted shake table shear tests on a double-nonwoven needle-punched GCL/smooth HDPE geomembrane interface to investigate the effect of displacement rate. Cyclic triangular waveform tests were conducted at varying displacement rates and amplitudes on dry and submerged specimens at normal stress levels of 10.9 and 22.5 kPa. Large-displacement shear strengths of the dry specimens increased slightly with increasing displacement rate, whereas values for the submerged specimens were relatively insensitive to displacement rate.

OBJECTIVES

In response to the above need, a laboratory research program is in progress at Ohio State University to investigate the shear behavior of GCLs and GCL interfaces under dynamic loading conditions. The full testing program is described by Fox et al. (2005). Dynamic shear tests are being conducted using a new dynamic direct shear machine that was designed and constructed for the project. An initial data set presented by Nye and Fox (2007) has provided first insights to the internal shear behavior of a needle-punched GCL under cyclic loading. This paper presents more recent data, including the results of tests performed at higher normal stress levels.

PROCEDURES

The dynamic direct shear machine, shown in Fig. 1, is described in detail by Fox et al. (2006). The main features of this device include a large specimen size (305 × 1067 mm), large normal stress range (2000 kPa maximum), capacity for large shear displacement (254 mm maximum), large range of displacement rate (0.01 to 60,000 mm/min for zero load), negligible machine friction, and the capability to measure specimen volume change. A GCL specimen is sheared between the underside of a horizontal pullout plate and the floor of the test chamber, each of which is covered with an aggressive gripping surface (truss plates). The gripping surfaces permit drainage of the specimen on both sides and are sufficiently rough that end-clamping of the geosynthetics is not required. This allows a specimen to fail along the weakest surface and avoids possible progressive failure effects (Fox and Stark 2004, Fox and Kim 2007). The shearing system is powered by a 245 kN hydraulic actuator that can impart bidirectional (i.e., back-and-forth) motion to the pullout plate. The maximum frequency for sinusoidal loading with a displacement amplitude of 25 mm is 4 Hz. Normal stress is provided by two bellowed air bags that rest on an overlying stationary load plate. Between the load plate and the pullout plate, a layer of 517 free-rolling stainless steel balls reduce the shear stress due to friction to 0.27% of the applied normal stress. Vertical displacement of the load plate due to specimen volume change is continuously monitored during hydration and shearing using a linear variable displacement transducer (LVDT). GCL specimens are hydrated from a water reservoir at the rear of the machine through a network of drainage channels in both shearing surfaces. The

system has an automated digital servocontroller that provides full control over machine operation and data collection.

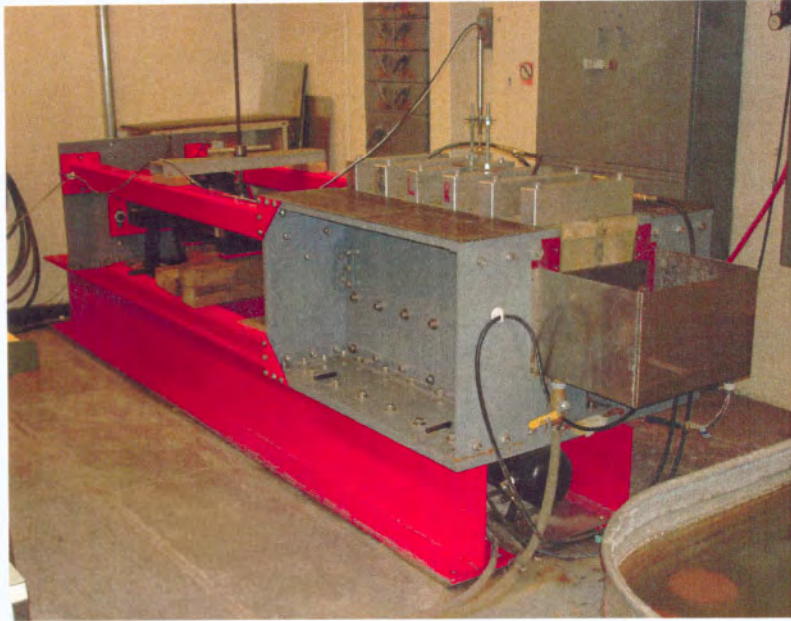


Figure 1. Dynamic direct shear machine.

Dynamic shear tests were performed on Bentomat ST, a woven/nonwoven (W/NW) needle-punched (NP) GCL with no thermal bonding manufactured by CETCO (Arlington Heights, Illinois). The average peel strength of the material (ASTM D 6496) was 1580 N/m. Specimens were hydrated using the two-stage procedure described by Fox et al. (1998). Following hydration, ten GCL specimens were subjected to displacement-controlled monotonic (i.e., single direction) shear tests to evaluate the effect of shear displacement rate R on peak and residual dynamic shear strengths. These tests were performed at a shearing normal stress $\sigma_{n,s} = 348$ kPa with displacement rates ranging from 0.1 to 28,000 mm/min (the maximum limit of the machine for these loads). Six additional specimens were subjected to 50 cycles of displacement-controlled cyclic (i.e., sinusoidal) shearing with displacement amplitudes $\Delta_a = 2, 5, 10, 15, 20$ and 25 mm. The normal stress for these cyclic tests was 141 kPa and the frequency was 1 Hz. Following each cyclic test, the pullout plate was disconnected from the actuator and the specimen was permitted to rest under the same normal stress and zero shear stress for 24 h. The specimen had free access to water during this time and could consolidate or swell as needed. After the 24 h rest period, each specimen was sheared at $R = 0.1$ mm/min (constant) to obtain the post-cyclic peak and residual static shear strengths. An additional static shear test was performed on a fresh specimen at the same normal stress (141 kPa) for comparison with the cyclic and post-cyclic shear data.

RESULTS

Monotonic Shear Tests

Representative relationships obtained from the monotonic shear tests for shear stress τ versus shear displacement Δ are shown in Fig. 2. The curves are generally similar in shape, with well-defined peak shear strengths and large post-peak strength reductions due to failure of the reinforcement. Values of peak and residual shear strengths are shown in Fig. 3 as a function of displacement rate. A static peak shear strength of 216 kPa was measured for $R = 0.1$ mm/min. With increasing displacement rate, the average peak strength increased to 268 kPa at $R = 1000$ mm/min and then decreased to 239 kPa at $R = 28,000$ mm/min. Thus, peak strength increased to a maximum of 24% above the static value; however, this increase was not sustainable at the highest values of R . Residual shear strengths were relatively constant at 23 kPa for $R \leq 10$ mm/min and then increased to 48 kPa at $R = 28,000$ mm/min. Displacements at peak strength, also show in Fig. 3, were approximately 23 mm at the slow rates and progressively decreased to 16 mm at the highest rate.

Figure 3 also includes data from Nye and Fox (2007) for monotonic shear tests performed on the same GCL material at $\sigma_{n,s} = 141$ kPa. The observed trend in peak strengths was attributed to increasing and then decreasing resistance of reinforcing fibers at faster displacement rates, and the increase in residual strength to rate-dependent shear resistance of the hydrated bentonite. Trends for peak and residual shear strengths in the current study are consistent with those presented by Nye and Fox. As expected, both peak and residual strengths increased at the higher normal stress. Displacements at peak strength decreased with increasing normal stress; however, both data sets show a similar trend with increasing displacement rate.

Cyclic Shear Tests

The general shear behavior of a W/NW NP GCL under displacement-controlled cyclic loading was presented by Fox et al. (2006) and Nye and Fox (2007). These studies indicated that shear strength decreased nonlinearly with increasing number of cycles N and that excitation frequency and waveform had little effect on cyclic shear behavior or post-cyclic static shear strengths. $N \geq 10$ also had little effect on post-cyclic static shear strengths. The tests conducted in this study were generally consistent with the earlier results. The shear stress vs. displacement relationships for the first cycle of each cyclic test are compared in Fig. 4. The curves are quite similar for the first quarter cycle, with slight deviations attributed to material variability and displacement rate effects. Also included in Fig. 4 is the initial portion of the static shear test conducted on a fresh GCL specimen with no prior cyclic loading. This figure shows that static shear data provides a reasonable approximation for the initial dynamic response until displacement reversal occurs. Cyclic shear stresses exceed corresponding static values at each displacement, which is apparently due to displacement rate effects.

Following each cyclic test and the 24 h rest period, a static shear test was conducted on the GCL specimen at $R = 0.1$ mm/min. The τ vs. Δ relationships are shown in Fig. 5 along with the corresponding relationship from the static shear test with no prior cyclic loading ($\Delta_a = 0$). Peak and residual shear strengths are plotted in Fig. 6. These figures clearly show that increasing

cyclic displacement amplitude yielded progressively lower post-cyclic static peak strengths, which is due to greater levels of damage to the needle-punched reinforcement. Post-cyclic

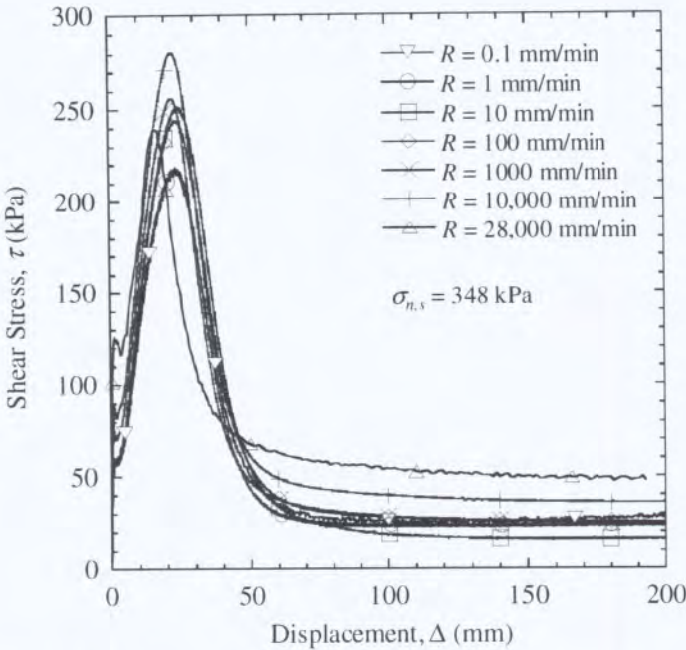


Figure 2. Shear stress-displacement relationships for seven monotonic shear tests.

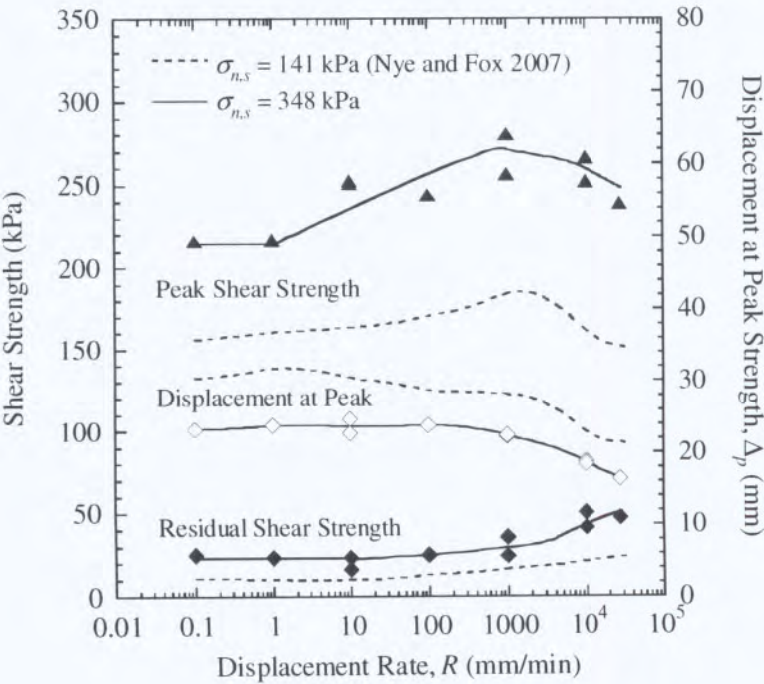


Figure 3. Effect of displacement rate on peak and residual shear strengths and displacement at peak for monotonic shear.

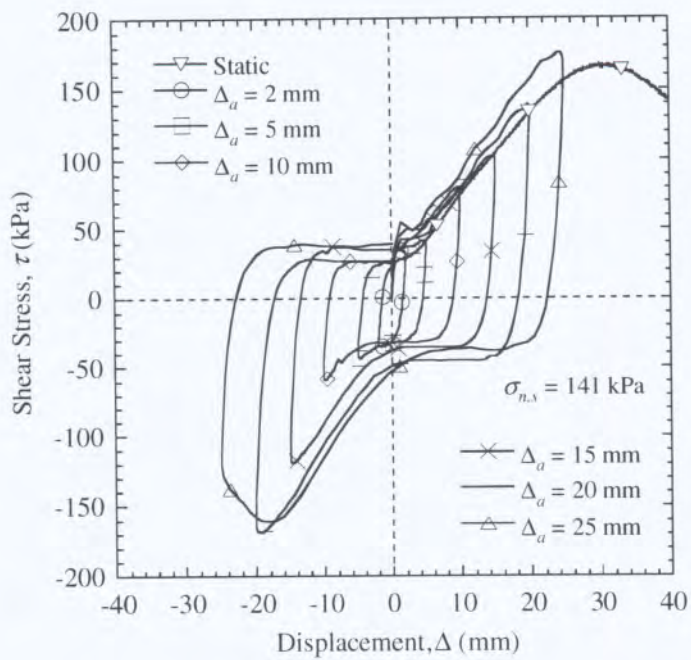


Figure 4. Shear stress-displacement curves for one static shear test and the first cycle of six cyclic shear tests with varying displacement amplitude.

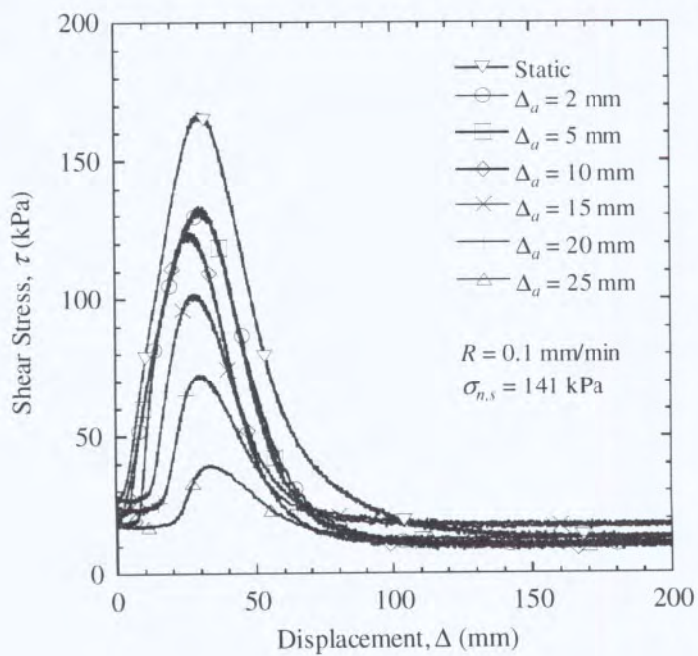


Figure 5. Effect of cyclic displacement amplitude on post-cyclic static shear behavior.

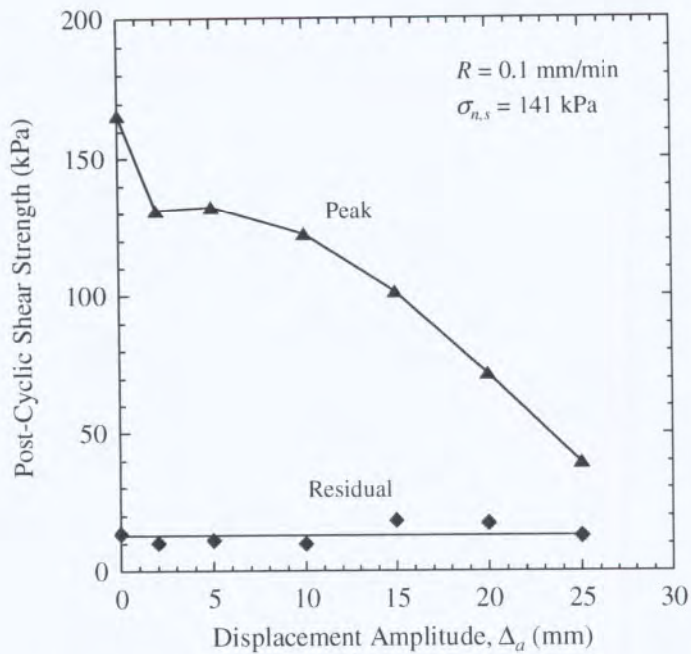


Figure 6. Post-cyclic peak and residual static shear strengths.

residual shear strengths were unaffected by previous cyclic loading and yield a secant residual friction angle of 5.2° .

An effective means to characterize general shear stiffness and energy dissipation in natural soils under dynamic loading is through the secant shear modulus and damping ratio, as typically used in equivalent linear ground motion analyses (Idriss and Seed 1968). This method was modified for a sand/concrete interface by Desai et al. (1985) and applied to a smooth geomembrane/geotextile interface by Yegian et al. (1998). Similarly, we define a secant shear stiffness K (shear stress per unit displacement) as,

$$K = \frac{K_1 + K_2}{2} = \frac{\tau_{m,1} + \tau_{m,2}}{2\Delta_d} \quad (1)$$

where K_1 and $\tau_{m,1}$ are average shear stiffness and maximum shear stress for the first half-cycle, respectively, and K_2 and $\tau_{m,2}$ are corresponding values for the second half-cycle (Fig. 7). Secant shear stiffness for the entire cycle is taken as the average of two half-cycle values in Eq. (1) to account for asymmetry in the hysteresis loop. Likewise, damping ratio β is defined as,

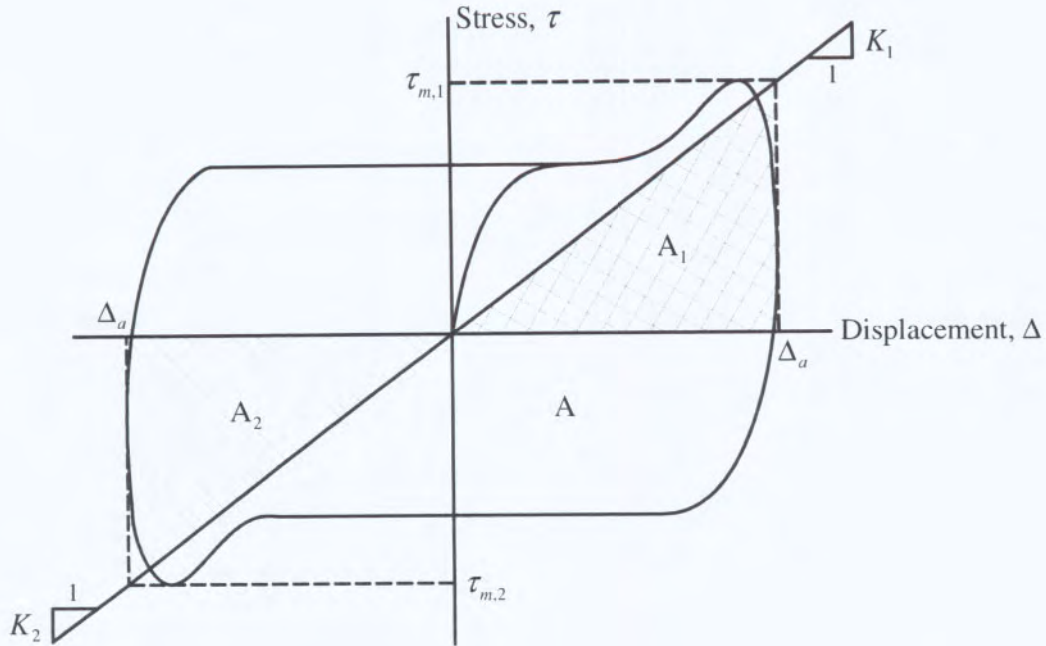


Figure 7. Calculation of secant shear stiffness and damping ratio from hysteresis loop.

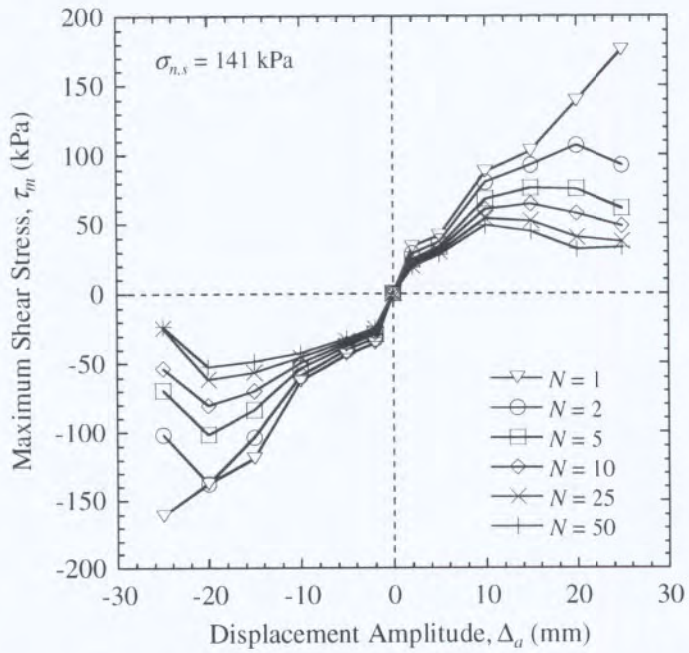


Figure 8. Backbone curves for six cyclic shear tests.

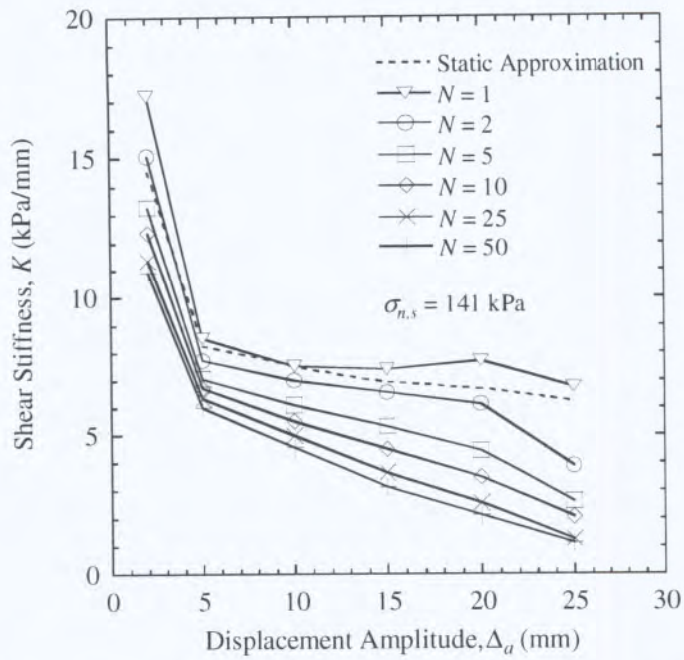


Figure 9. Shear stiffness reduction curves for six cyclic shear tests.

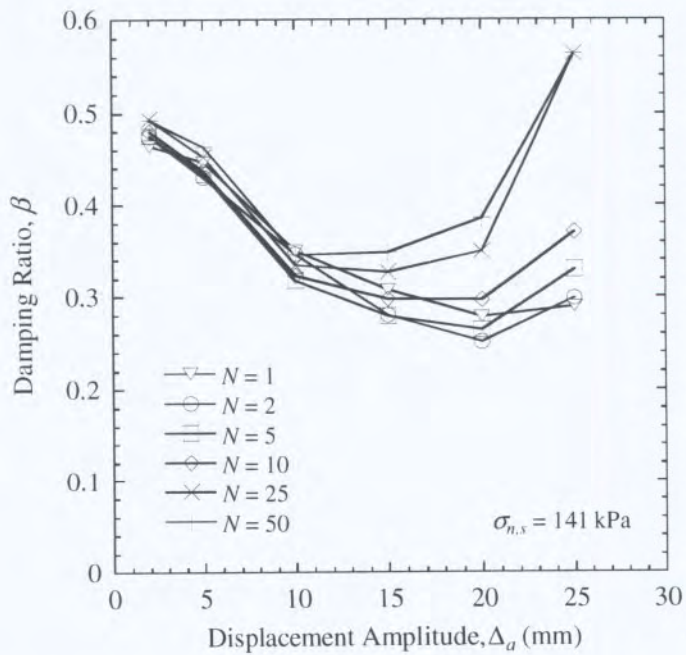


Figure 10. Damping ratio for six cyclic shear tests.

$$\beta = \frac{\beta_1 + \beta_2}{2} = \frac{1}{2} \left(\frac{A}{4\pi A_1} + \frac{A}{4\pi A_2} \right) = \frac{A}{4\pi \Delta_a} \left(\frac{1}{\tau_{m,1}} + \frac{1}{\tau_{m,2}} \right) \quad (2)$$

where β_1 and β_2 are damping ratios for the first and second half-cycles, respectively, A is the total area enclosed by the loop, and A_1 and A_2 are the areas defined in Fig. 7. Figure 8 is a plot of maximum shear stress vs. displacement amplitude – the so-called “backbone curve” – for the cyclic shear tests at various N values. These curves are approximately symmetric about the origin but display some asymmetries due to material variability and reinforcement damage. Corresponding values of shear stiffness K , plotted in Fig. 9, indicate strong stiffness reduction with increasing displacement amplitude and stiffness degradation with continued cycling. Figure 9 also contains a plot of secant shear stiffness obtained directly from the static shear test (Fig. 4). This curve is a reasonable first approximation to that obtained from cyclic testing for $N = 1$. Values of damping ratio β , presented in Fig. 10, showed little change with N for $\Delta_a \leq 10$ mm but then increased with increasing N at larger Δ_a . Higher values of damping ratio at larger displacement amplitudes also reflect increasing amounts of reinforcement damage to the GCL.

CONCLUSIONS

A research program is currently in progress to investigate the shear strength behavior of geosynthetic clay liners (GCLs) and GCL interfaces under dynamic loading conditions. This paper presents data obtained on the dynamic internal shear strength of a hydrated needle-punched GCL with no thermal bonding. A series of displacement-controlled monotonic shear tests were conducted with displacement rates ranging from 0.1 to 28,000 mm/min. These tests show that peak shear strengths first increased and then decreased with increasing displacement rate. Residual shear strengths more than doubled from the slowest to the fastest displacement rate.

A series of displacement-controlled cyclic shear tests were conducted with displacement amplitudes ranging from 2 to 25 mm. Increasing cyclic displacement amplitude resulted in progressively lower post-cyclic static peak strengths due to greater levels of GCL reinforcement damage. Post-cyclic static residual strengths were unaffected by prior cyclic loading. Secant shear stiffness showed strong reduction with increasing displacement amplitude and degradation with continued cycling. Static shear data yielded a stiffness reduction curve that is a reasonable first approximation to that obtained from cyclic testing. Damping ratio was essentially independent of number of cycles for low displacement amplitudes and increased with increasing number of cycles for larger displacement amplitudes.

ACKNOWLEDGEMENTS

Financial support for this work was provided by a grant from CETCO of Arlington Heights, Illinois, and a University Fellowship from Ohio State University for the first author. This support is gratefully acknowledged. The writers thank Joseph Sura, a senior at Ohio State

University, and Janguen Lee, a doctoral candidate at Ohio State University, who assisted with the experimental work presented in this paper.

REFERENCES

- ASTM D 6496, "Standard Test Method for Determining Average Bonding Peel Strength Between the Top and Bottom Layers of Needle-Punched Geosynthetic Clay Liners," ASTM International, West Conshohocken, Pennsylvania, USA.
- De, A. and Zimmie, T. F. (1998). "Estimation of dynamic interfacial properties of geosynthetics," *Geosynthetics International*, 5(1-2), 17-39.
- Desai, C. S., Drumm, E. C. and Zaman, M. M. (1985). "Cyclic testing and modeling of interfaces," *Journal of Geotechnical Engineering*, 111(6), 793-815.
- Fox, P. J. and Stark, T. D. (2004). "State-of-the-art report: GCL shear strength and its measurement," *Geosynthetics International*, 11(3), 141-175.
- Fox, P. J. and Kim, R. H. (2007). "Effect of progressive failure on measured shear strength of geomembrane/GCL interface," *Journal of Geotechnical and Geoenvironmental Engineering*, in review.
- Fox, P. J., Rowland, M. G. and Scheithe, J. R. (1998). "Internal shear strength of three geosynthetic clay liners," *Journal of Geotechnical and Geoenvironmental Engineering*, 124(10), 933-944.
- Fox, P. J., Morrison, T. C., Nye, C. J., Hunter, J. G. and Olsta, J. T. (2005). "Current research on dynamic shear behavior of needle-punched geosynthetic clay liners," *Proceedings, Geosynthetics '05*, North American Geosynthetics Society, Las Vegas (CD-ROM).
- Fox, P. J., Nye, C. J., Morrison, T. C., Hunter, J. G. and Olsta, J. T. (2006). "Large dynamic direct shear machine for geosynthetic clay liners," *Geotechnical Testing Journal*, 29(5), 392-400.
- Idriss, I. M. and Seed, H. B. (1968). "Seismic response of horizontal soil layers," *Journal of the Soil Mechanics and Foundations Division*, 94(SM4), 1003-1031.
- Kim, J., Riemer, M. and Bray, J. D. (2005). "Dynamic properties of geosynthetic interfaces," *Geotechnical Testing Journal*, 28(3), 1-9.
- Lai, J., Daniel, D. E. and Wright, S. G. (1998). "Effects of cyclic loading on internal shear strength of unreinforced geosynthetic clay liner," *Journal of Geotechnical and Geoenvironmental Engineering*, 124(1), 45-52.
- Lo Grasso, S. A., Massimino, M. R. and Maugeri, M. (2002). "Dynamic analysis of geosynthetic interfaces by shaking table tests," *Proceedings, 7th International Conference on Geosynthetics*, P. Delmas and J. P. Gourc, eds., Nice, 4, 1335-1338.
- Nye, C. J. and Fox, P. J. (2007). "Dynamic shear behavior of a needle-punched geosynthetic clay liner," *Journal of Geotechnical and Geoenvironmental Engineering*, in press.
- Yegian, M. K. and Kadakal, U. (1998). "Geosynthetic interface behavior under dynamic loading," *Geosynthetics International*, 5(1-2), 1-16.
- Yegian, M. K. and Lahlaf, A. M. (1992). "Dynamic interface shear strength properties of geomembranes and geotextiles," *Journal of Geotechnical and Geoenvironmental Engineering*, 118(5), 760-779.
- Yegian, M. K., Yee, Z. Y. and Harb, J. N. (1995). "Seismic response of geosynthetic/soil systems," *Geoenvironment 2000*, Y. B. Acar and D. E. Daniel, eds., *Geotechnical Special Publication No. 46*, ASCE, 2, 1113-1125.
- Yegian, M. K., Harb, J. N. and Kadakal, U. (1998). "Dynamic response analysis procedure for landfills with geosynthetic liners," *Journal of Geotechnical and Geoenvironmental Engineering*, 124(10), 1027-1033.

CONTACT:

Christopher J. Nye, Graduate Research Assistant, Ohio State University, Columbus, OH USA
Patrick J. Fox, Professor, Ohio State University, Columbus, OH USA

Exposed Geomembranes

Holding Your Liquor - Exposed Synthetic Liners in Wastewater Applications

Hinshelwood, J.S., Olver Incorporated

1. INTRODUCTION

Synthetic liners for wastewater applications face demanding conditions that pose unique challenges for designers, installers and maintenance personnel. Those challenges can be especially significant when the application requires long term exposure of the synthetic membrane to the elements. In particular, careful consideration in the design and installation process must be given to wind and sunlight effects to ensure that the material can withstand the associated stresses.

This paper discusses the design, installation and recommended maintenance of a 1.5 mm thick HDPE synthetic liner for a 1.13 hectare, 22.7 million liter domestic wastewater equalization basin for the Henry County Public Service Authority (HCPSA) in southwest Virginia. Since during dry weather the basin might be empty for long periods, the liner had to be designed as though it was permanently exposed and fluids could not be relied on to hold the liner in place. In addition, the HCPSA requested that the finished surface be smooth and free of surface obstructions to facilitate cleaning. To satisfy these criteria, an anchorage method was devised that presented a smooth surface to the wastewater and avoided inducing stress at the welds. The liner anchors were designed to withstand significant wind uplift forces (based on analysis methods by J.P. Giroud *et al.* 1995) but allow enough slack in the liner to avoid contraction stresses during cold weather.

The installation required the contractor to methodically sequence the liner placement in order to establish the liner anchorages and to avoid any operation of equipment on the liner. The equalization basin has been in operation since September 2005 and the HCPSA is following guidelines for inspection and maintenance of the liner that minimize the need for personnel or equipment of any kind to come in contact with the liner.

2. SYSTEM DESCRIPTION

The basin was constructed by retrofitting an existing but unused aeration basin identical to the basin shown in Figure 1. As shown in Figure 2, the basin is 125 meters long, 91 meters wide and 4.3 meters deep. It has a 1.2 meter high center ridge running widthwise which allows one sided operation during low flow events. The side slopes are 3:1 (horizontal to vertical). When the wastewater flow rate to the site pump station exceeds the 15,000 kiloliters per day (kl/d) permitted pumping limit, the excess is pumped to the basin through a 41 centimeter diameter wastewater pipe discharging at one corner of the basin. When the flow drops back down below 15,000 kl/d, wastewater stored in the basin can be drained through the two sump drains back to the site pump station by opening a valve on the basin discharge line. Lining the basin with a geomembrane minimizes the risk of ground water contamination from waste water that would seep into the ground through a soil liner.



Figure 1
Existing Aeration Basin

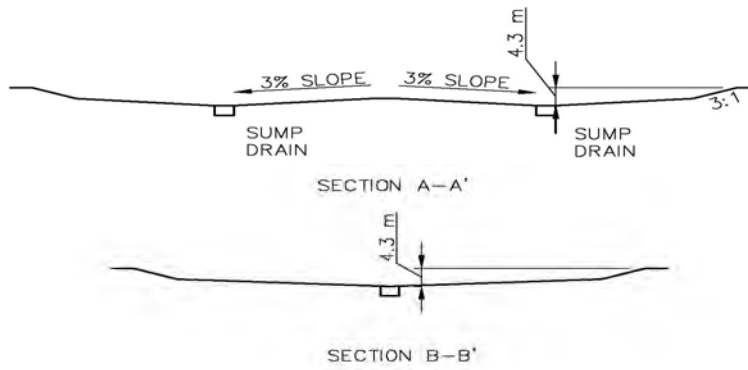
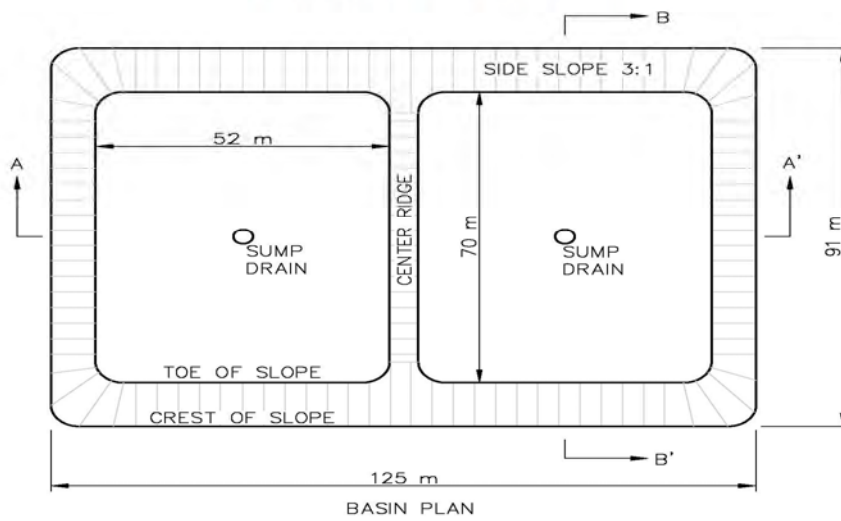


Figure 2
Basin Dimensions

3. LINER MATERIAL SELECTION

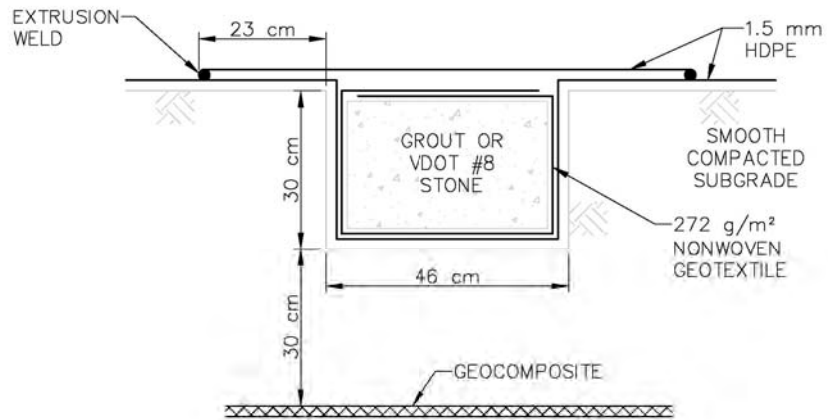
The liner material was required to have a service life of at least 20 years in an exposed condition and had to be resistant to ultraviolet rays and freeze thaw cycles. Henry County experiences an annual average low temperature of 5.5° C, an annual average high temperature of 20° C, and averages 59 sunny days per year. HDPE was selected for the liner material based on its ability to resist ultraviolet degradation and evidence that it could withstand exposure to the elements over the required 20 year service life.

Three types of HDPE materials were specified including standard black liner, a co-extruded liner with a white surface, and a liner with an electrically conductive bottom surface. With a white surfaced liner, pinholes or tears will expose the underlying black HDPE, providing a more visible indication of damage during construction as well as during the service life of the basin. The white surface of the liner also stays cooler than black HDPE, reducing wrinkles in the liner. Liner material that has a bottom layer of electrically conductive HDPE offers enhanced detection of liner defects through spark testing with an electric current. All three types of liner were included in the project bid documents. Primarily for budget reasons, the less expensive standard black HDPE liner was ultimately selected by the HCPSA.

4. LINER SYSTEM DESIGN

In order to accommodate the HCPSA's request for a cleanable finished surface, the liner anchorage was designed as shown in Figure 3. The liner anchor trench is sealed over with a welded HDPE cap strip to present a smooth surface that prevents the anchor trench from snagging or accumulating solids. The cap strip was designed to be wider than the anchor trench so that the welds for the cap strips would not be located at the points of maximum tension near the edge of the anchor trench. At the request of the construction contractor, the anchor trench was filled with gravel-sized stone in lieu of the originally specified grout. The contractor was able to sequence the geomembrane installation so that stone could be placed in the anchor trenches without having to put equipment on the liner. The geocomposite below the anchor trench in Figure 3 was installed to provide an outlet for ground water below the liner.

Henry County is located in the foothills of Virginia's Piedmont physiographic region, an area that is less exposed to the extreme wind conditions sometimes encountered along the Virginia coastline. However, the area is subjected to occasional high winds from the remnants of passing hurricanes and infrequent tornado activity. Based on the characteristic intensity and duration of winds in the area, a Category 3 hurricane maximum wind speed (Saffir-Simpson Scale) of 209 kilometers per hour was selected as an appropriate design criterion for the exposed liner.



ANCHOR TRENCH DETAIL

Figure 3
Anchor Trench Detail



Figure 4
Anchor Trench Construction

The required geomembrane anchorage to withstand wind uplift forces was determined using the design methodology developed by Giroud *et al.* (1995). This methodology is based on wind tunnel research conducted by Dedrick (1975) to measure wind forces on small scale reservoir structures. Figure 5 illustrates the various pressure conditions on the reservoir bottom, leeward and windward slopes as wind blows across the reservoir.

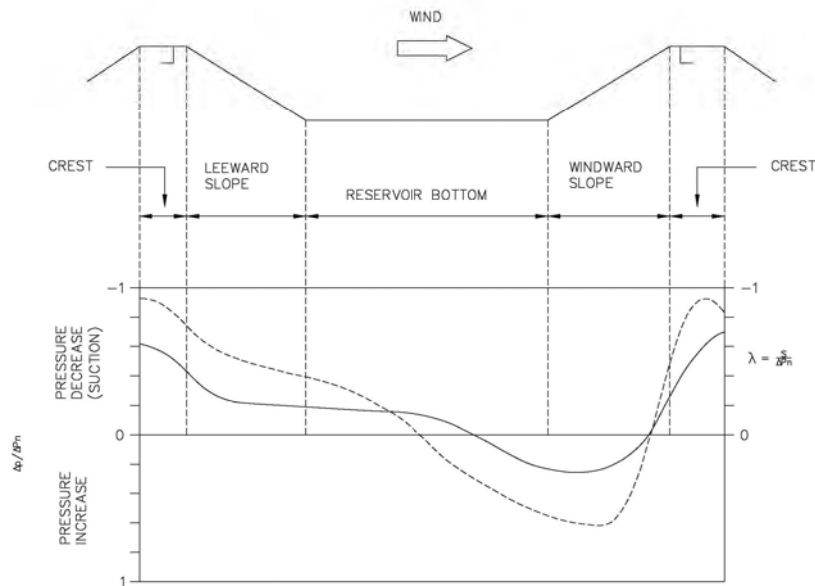


Figure 5
Reservoir Wind Pressure
(Courtesy of J.P. Giroud)

A portion of the windward slope and a portion of the reservoir bottom nearest the windward slope are actually subjected to increased pressure forcing the geomembrane down onto the subgrade. The rest of the reservoir experiences negative pressure tending to lift the geomembrane off the subgrade. To accommodate shifting wind direction, the entire basin must be designed so that each slope can withstand the wind uplift loads associated with leeward slopes.

Noting the variation in pressures in a leeward slope, Giroud *et al.* (1995) developed suction factors corresponding to the bottom, side, and crest of a slope as shown in Figure 6. At the crest of the slope, where the maximum suction pressure is located, the suction factor, λ is equal to 1.00. At the bottom of the slope, where the suction pressure is lower, the suction factor is 0.40. In the calculation of wind uplift forces, applying the suction factor will appropriately decrease those forces as one moves from the crest of the slope down.

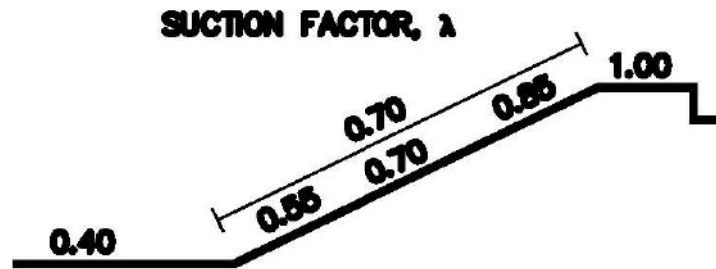


Figure 6
Reservoir Wind Suction Factors
(Courtesy of J.P. Giroud)

For the HCPSA equalization basin side slopes, the wind uplift on a 1.5 mm thick HDPE geomembrane is calculated as:

$$S_e = 0.05 \lambda V^2 e^{-(1.252 \times 1.0E-04) Z} - 9.81 \mu_{gm} \cos \beta \quad (1)$$

where: S_e = Effective Suction (N/m^2)

λ = Suction Factor = 0.7

β = slope angle = 18.4° (3:1)

V = wind velocity = 209 km/h (Category 3 hurricane)

μ_{gm} = geomembrane mass per unit area = 1.41 kg/m^2

Z = Elevation above mean sea level = 219 meters

Inserting site specific values in equation (1) yields:

$$S_e = (0.05)(0.7)(209)^2 e^{-(1.252 \times 1.0E-04)(219)} - 9.81 (1.41) \cos 18.4$$

$$S_e = 1,474 \text{ N/m}^2$$

The next step in the design is to calculate the normalized allowable tension, which is defined as:

$$\tau_{all}' = \tau_{all} / (S_e L) \quad (2)$$

where τ_{all} is the allowable tension for the selected geomembrane based on its tension-strain curve and L is the length of the geomembrane between anchor points. The tension-strain curve for the 1.5 mm thick HDPE liner used in the HCPSA basin is shown in Figure 7, and indicates that the stress at an acceptable 13% strain is 1,910 psi ($13,169 \text{ kN/m}^2$). Multiplying by the geomembrane thickness (0.0015 m) converts this value to the allowable tension per meter:

$$\tau_{all} = 13,169 \times 0.0015 = 19.75 \text{ kN/m}$$

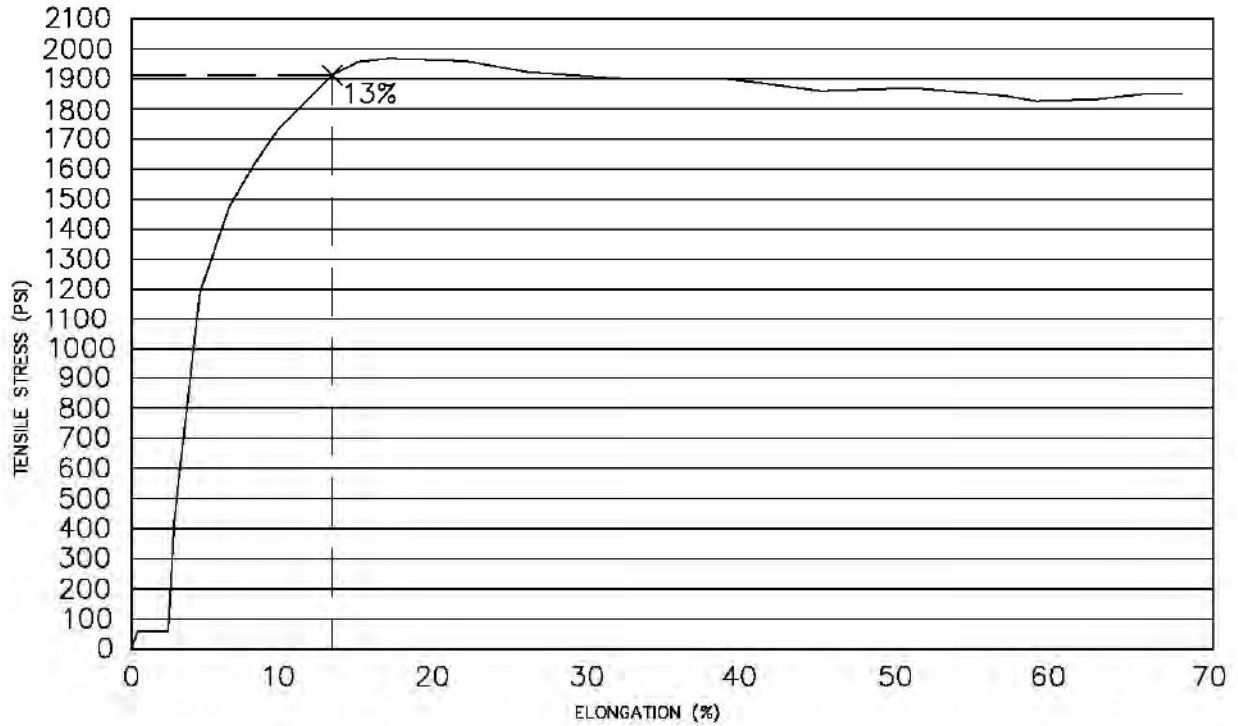


Figure 7
HDPE Liner Material Stress-Strain Curve

Inserting this result into equation (2) and multiplying by 1,000 to convert kN to N, allows the normalized allowable tension in the geomembrane on the 9.144 meter long slope to be calculated as follows:

$$\tau_{all}' = 19.75 \times (1,000) / (1474 \times 9.144) = 1.47 \text{ (unitless)}$$

The final step is to compare τ_{all}' to the corresponding normalized tension value in Table 1. If the normalized allowable tension, τ_{all}' in the geomembrane is greater than the normalized tension value from Table 1, then the selected geomembrane is acceptable for the design conditions. From Table 1 for a strain value $\epsilon = 13\%$, the normalized tension value, $T/(S_e L) = 0.67$. Since $\tau_{all}' = 1.47$ is greater than 0.67, the selected geomembrane is considered acceptable and provides a factor of safety of 2.19 ($1.47/0.67$). Giroud *et al.* (1995) provides an explanation of the derivation of Table 1 values which are based on a free-body diagram analysis of the wind forces acting to lift the geomembrane off the subgrade. The Table 1 values are also represented graphically in Figure 8.

Table 1

Geomembrane Strain ϵ (%)	Normalized Tension $T/(S_e L)$
10.00	0.73
10.35	0.73
11.00	0.71
11.37	0.70
12.00	0.69
12.44	0.68
13.00	0.67
13.56	0.66
14.00	0.65

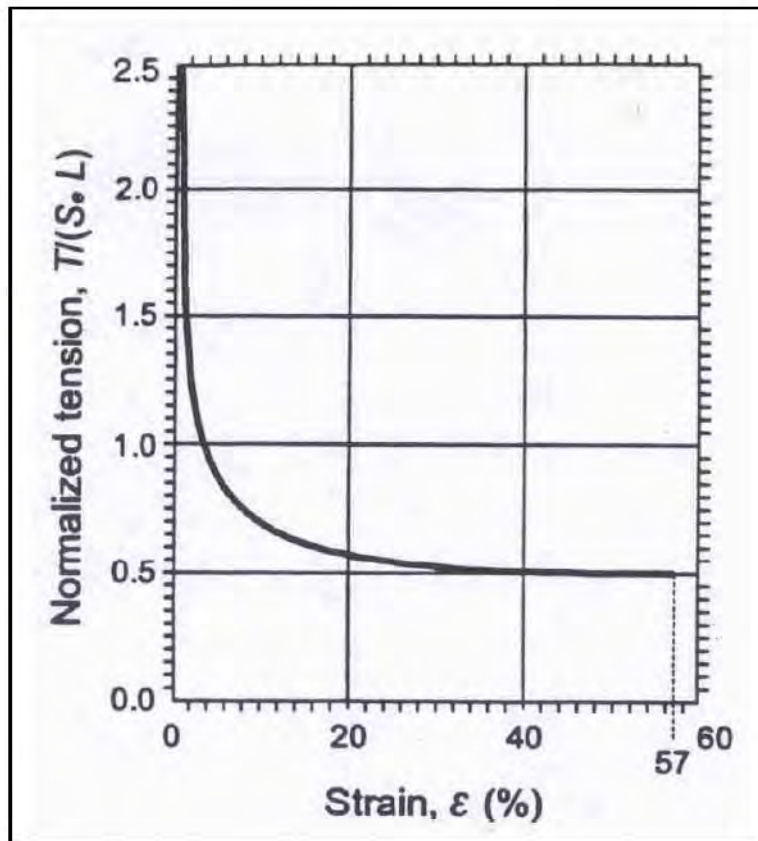


Figure 8
Relationship of Strain and Normalized Tension
(Courtesy of J.P. Giroud)

A similar analysis was used for the bottom of the basin where the distance between anchor points was selected through an iterative process to achieve an acceptable factor of safety. A summary of the wind uplift analyses for the side slopes and the liner bottom is provided in Table 2.

Table 2
Summary of Wind Uplift Analyses

Side Slope	Value	Comment
Side Slope Angle (degrees)	18.4	3:1
Slope Length Between Anchors (m)	9.144	Anchor trenches at the toe & crest only
Elevation at mid slope (m)	219.5	
Suction Factor, λ	0.7	
Wind Speed (km/h)	209.2	Full Strength Category 3 Hurricane
Geomembrane Thickness (mm)	1.5	
Geomembrane mass per unit area (kg/m^2)	1.41	
Allowable Tension, τ_{all}' (kN/m)	20.17	Calculated from the Stress Strain curve for the selected material
Strain at Allowable Tension (%)	13	Per Stress Strain curve for selected material
Effective Suction, S_e (N/m^2)	1474	
Effective Suction At Length, S_eL (kN/m)	13.5	
Normalized Allowable Tension, τ_{all}'	1.47	
Normalized Tension Value	0.67	From Table 1
Is $\tau_{all}' >$ Normalized Tension Value?	Yes	OK
Factor of Safety	2.19	OK
Bottom Area		
Distance Between Anchors (m)	22.86	
Average Bottom Elevation (m)	217.6	
Suction Factor, λ	0.5	
Wind Speed (km/h)	209.2	Full Strength Category 3 Hurricane
Geomembrane Thickness (mm)	1.5	
Geomembrane mass per unit area (kg/m^2)	1.41	
Allowable Tension, τ_{all}' (kN/m)	20.17	Calculated from the Stress Strain curve for the selected material
Strain at Allowable Tension (%)	13	Per Stress Strain curve for selected material
Effective Suction, S_e (N/m^2)	1051	
Effective Suction At Length, S_eL (kN/m)	24.0	
Normalized Allowable Tension, τ_{all}'	0.82	
Normalized Tension Value	0.67	From Table 1
Is $\tau_{all}' >$ Normalized Tension Value?	Yes	OK
Factor of Safety	1.22	OK

The resulting anchor plan for the basin liner is shown in Figure 9, and includes anchor trenches at the crest and toe of the side slopes and four anchor trenches in the basin bottom. The maximum separation distance between any two anchor trenches is 22.86 meters, thereby achieving at least the designed 1.22 factor of safety. Figure 10 is a photograph of the completed basin liner installation.

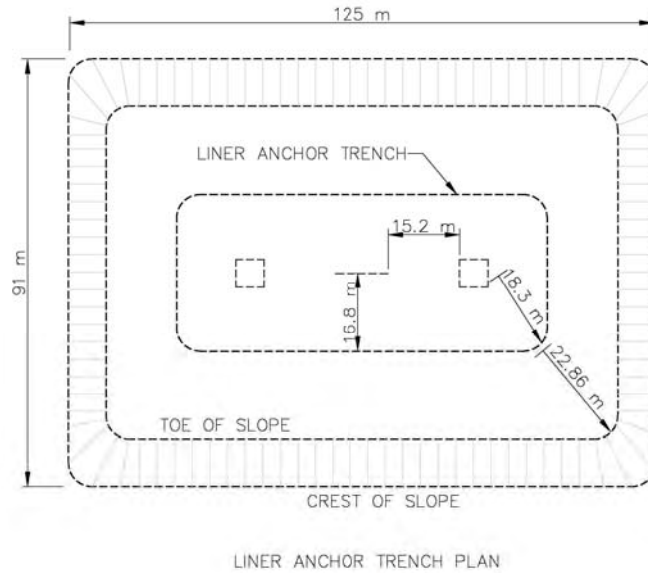


Figure 9
Liner Anchor Trench Plan



Figure 10
Completed Basin

5. LINER MAINTENANCE

In order to minimize traffic on the exposed liner, the guidelines in Table 3 were developed for use by maintenance personnel for cleaning and inspecting the liner. The basin bottom slopes are relatively flat (3%), so some accumulation of solids does occur near the sump drains as evidenced by the two soil colored squares in the basin bottom in Figure 10. Cleaning of solids after each basin use is recommended before the solids harden and become more difficult to remove and to prevent excessive buildup of solids in the basin. A lightweight all terrain rubber-tired vehicle with a rubber-tired trailer attachment may also be used to load out solids from the basin without causing undue stress on the geomembrane. The liner is inspected regularly for damage and the inspections may be conducted by walking inside the basin or with binoculars to avoid foot traffic on the geomembrane.

Table 3
Liner Protection Guidelines

- Avoid walking or putting vehicles on the liner as much as possible.
- If walking on the liner is necessary, do so only with soft soled shoes that are free of mud, dirt and debris. The ramp at the southwest corner should be used for entry and exit.
- Only lightweight vehicles (an all terrain vehicle for example) with large rubber tires should ever be allowed on the liner and as infrequently as possible. If such a vehicle is driven down into the lagoon, the tires must be free of all mud, dirt and debris and the liner surface must be checked to make sure it is clean of all debris where the vehicle will travel. The vehicle should enter and exit the lagoon via the ramp in the southwest corner. The vehicle must be operated at slow speeds and avoiding any sharp or sudden turns.
- A protective mat should be placed over the liner in any area where work or maintenance is conducted.
- If the grates in the sump manholes are removed, care should be taken to avoid damaging the liner with the grates.
- During cold weather the liner will be in tension in some areas and especially vulnerable to puncture damage. Getting out on the liner (even walking) should be avoided when the liner is tight during cold weather.
- Liner inspections can be effectively conducted using binoculars to avoid traffic on the liner.

6. CONCLUSION

As of September 2006, the HCPSA equalization basin has been used for wastewater storage an estimated 6 times over its one year service life and the basin has been filled to near capacity 3 times. Winds speeds are not recorded at the site, however wind speed records from the nearby Martinsville, Virginia airport (3.5-4.5 kilometers from the site) indicate that the area has experienced sustained winds of 58 kilometers per hour with gusts to 103 kilometers per hour since the basin was placed in service. Inspections have not revealed any leaks or damage to the geomembrane and indicate that the liner is functioning as intended.

ACKNOWLEDGEMENTS

The author is grateful to J.P. Giroud for permission to use information from the referenced papers and for development of the methodologies that allowed for a practical and systematic approach to the design of the project. Appreciation is also extended to Mike Ward of the HCPSA for his support of this paper and the information he provided.

REFERENCES

Giroud, J.P., Wallace, R.B., and Castro, C.J., 2006, "Improved Methodology for Geomembrane Wind Uplift Design", *Geosynthetics*, Publication pending.

Zornberg, J.G. and Giroud, J.P., 1997, "Uplift of Geomembranes by Wind – Extension of Equations", *Geosynthetics International*, Vol. 4, No. 2, pp. 187-207.

Giroud, J.P., Pelte, T., and Bathurst, R.J., 1995, "Uplift of Geomembranes by Wind", *Geosynthetics International*, Vol. 2, No. 6, pp. 897-952.

Dedrick, A.R., 1975. "Air Pressures Over Surfaces Exposed to Wind. –II. Reservoirs," *Transactions of ASAE*, Vol. 18, No.3.

CONTACT:

Jack Hinshelwood, P.E
Vice President
Olver Incorporated
1116 South Main St.
Blacksburg, Virginia, 24060,
Telephone: 540 552-5548
E-mail: jhinshelwood@olver.com

Finalizing Exposed Geomembrane Covers for Landfills

Donald E. Hullings, P.E., Jones Edmunds & Associates, Inc.

ABSTRACT

While exposed geomembrane covers (EGCs) have been used for intermediate landfill covers at several sites, EGCs are now being seriously considered for final cover applications. Prescriptive landfill covers containing a geomembrane have inherent problems with the overlying protective soil layer. A relatively weak interface shear strength between the soil cover and underlying geosynthetics and the build-up of seepage forces or gas pressures have led to veneer slope stability failures at a number of landfills. Even soil layers that remain “stable” slowly slough and erode away, creating long-term maintenance issues and potential corrective action. EGCs have no overlying soil; therefore, stability and erosion problems do not exist. In addition, EGCs have the benefits of lower construction costs; improved water quality (clean run-off); and easier quality control, inspection, and maintenance. The absence of soil cover, however, does present new design concerns, including protecting the geomembrane from mechanical and ultraviolet light degradation and restraining the cover against wind loads and landfill gas build-up.

EGCs for intermediate landfill covers have an excellent track record to date. Applications have survived hurricane-force winds, have not presented problems from landfill gas build-up, and have largely retained their original mechanical properties over a number of years. In moving forward, the solid waste industry needs to take advantage of lessons learned while keeping an eye on long-term performance. This paper focuses on how design considerations specific to EGCs are addressed, what lessons can be learned from existing applications, and how issues raised during the permit process of several final cover applications are being addressed.

INTRODUCTION

Geomembranes without an overlying layer of soil have been used successfully as “temporary” landfill covers in certain situations, typically bioreactors. Owners and operators of landfills from Delaware to Florida have used EGCs and have quickly become advocates for extending the use to final cover applications. Conversations with regulators in Florida in this regard have been positive and the regulatory community is now open to the concept. The process of moving forward, however, must be a team effort that includes several groups:

- Regulators who are open-minded and understand the intent of regulations.
- Owners and operators who recognize the advantages of EGCs and are willing to pursue the opportunity by presenting project-specific proposals to the regulators.
- Engineers who can identify the unique design aspects of EGCs and provide the appropriate supporting calculations and details.

- Manufacturers prepared to stand behind their products and develop improved geomembranes specifically formulated for EGCs.

In Florida, representations from all of these groups are being assembled to gain approval of EGC as final covers.

REGULATORS

Gaining approval for new technology has always been a problem in the solid waste industry. Subtitle D regulations, which took effect in 1993, made a great leap in eliminating “dumps” and creating sanitary solid waste landfills. These regulations, the basis for all state regulations, are predicated on technology from the 1980s, however, and do not reflect advances made over the subsequent two decades. Concepts such as the dry tomb are being challenged by bioreactors, as are the prescriptive landfill cover with evaporative soil covers and now EGCs.

With some foresight, many State regulations include provisions for alternatives to the prescriptive standard. The State of Florida, for example, allows for alternative procedures that demonstrate an equal degree of protection for the public and the environment (FAC Section 62-701.310). More specific passages, such as FAC 62-701.600(5)(g) that requires alternatives to have substantially equivalent rates of storm water infiltration, are also written into the regulations. California requires a demonstration that the prescriptive standards are unnecessarily burdensome and New York is revising its regulations to allow for temporary cover applications. While regulations vary, most will allow for alternatives and more specific provisions are being added as regulations are periodically reviewed and updated.

The most difficult task is to convince the specific regulator responsible for a project to be the first to allow an alternative. Understandably, most regulators would be more comfortable with citing a precedent when approving an alternative procedure. Many regulators have been generally positive, but they cannot issue a “blanket” approval and must judge each project on its specific merits. Their concerns—predominantly long-term performance, repair, and maintenance—must be addressed. Each project seeking to incorporate an alternative procedure must, therefore, make a formal request and demonstrate equal protection.

OWNERS AND OPERATORS

We are currently discussing alternative procedures with owners in three Florida districts. In each case, the owner recognizes the success of previous “temporary” applications and advantages to be gained from EGCs in final cover applications.

CURRENT APPLICATIONS

Current applications of EGCs are limited, but they have proven successful (Table 1). The EGC constructed by the Delaware Solid Waste Authority (DSWA) in 1997 was one of the first and nearly a decade later the system has withstood wind gusts exceeding 100 mph and is still performing as designed (Vasuki, 2006). The three EGCs constructed in central and north-central Florida have been performing beyond expectations (Figure 1). The EGC at Polk County

Landfill, for example, survived three hurricanes in one season with sustained winds of 75 to 90 mph and wind gusts of 115 mph. Routine inspections have revealed little damage and annual testing on exposed geomembrane coupons indicates little discernable loss of mechanical properties.

Table 1 – Sampling of Current Applications

Site	Location	Year	Material	Status
SSWMC Cells 1 and 2	Delaware	1997	40-mil green reinforced polypropylene	Approaching 10-year permit review
Sabine Parish Phases I and III	Louisiana	1999	60-mil green textured HDPE	Approved as final cover.
Polk County Phase 1	Florida	2001	60-mil green textured HDPE	Performing well
New River Cells 1 and 2	Florida	2001	White textured LLDPE	Performing well
Marion Cell III-C	Florida	2002	White textured LLDPE	Performing well



Figure 1

A quick survey of actual EGC applications supports the argument that these systems are able to perform over several years, but geomembranes have actually been used in exposed applications for decades. An HDPE geomembrane used in a pond liner showed no significant reduction in primary physical properties after 20 years (Ivy, 2002). Oxidative induction times (OIT), a measure of how well anti-oxidants are working to ward off degradation, were about half the likely original value, which indicates that antioxidants are depleted but still seemingly working after two decades. An exposed 80-mil-thick textured HDPE canal liner appears to be in excellent condition after 10 years (Bureau of Reclamation, 2000). Testing indicated that OIT was down 30 percent, but a life of 20 to 25 years was predicted. Keep in mind that these polyethylenes were formulated at least 15 years ago and that advancements in polymer science should extend the service life of today's geomembranes even farther.

Advantages

The move to permit EGCs is the result of the distinct advantages they offer over traditional soil-covered geomembranes.

Construction Cost Savings. Saving money is a sensitive topic when seeking an alternative to prescriptive standards and usually discussed briefly, if at all. It is, however, a major driver in seeking an EGC and should be discussed openly. The money saved from not covering the geomembrane with soil and vegetation is more than enough to pay for other methods of restraint and increased stormwater controls (as discussed later). Depending largely on the availability of soil, net savings of \$20,000 to \$60,000 per acre can be achieved. These savings can be used to provide enhanced post-closure care and even future replacement of the EGC.

Soil Erosion. No soil cover means no erosion issues: no regrading, no revegetation, no maintenance and clean-out of storm water control structure, and no turbid stormwater runoff.

Slope stability. Covering geomembrane slopes with soil can be a problem, as evidenced by numerous cover failures. Low interface shear strengths inherent in geosynthetic systems, along with the build-up of seepage forces, pose a geotechnical challenge. EGCs simply avoid this problem.

Repairs and Maintenance. Damage to an EGC may be more likely than for prescriptive covers, but the damage is also easily seen and repaired. Routine inspection and repair is less expensive than mowing, re-grading, vegetating, and maintaining the stormwater control system.

Flexibility. EGCs allow for more flexibility in operating the landfill in the future, including landfill mining, cover replacement, and possible cover removal and post-closure development once the landfill is determined not to pose a threat to the environment.

Savvy owners are aware of these precedents and advantages and are ready to move forward.

ENGINEERS

While the advantages are the impetus for moving forward, the engineer must be prepared for the unique design challenges. A review of the literature (Thiel, 2003; Gleason, 1998; Richardson, 1994) on previous designs and our experiences in Florida reveal the following potential disadvantages with leaving the landfill final cover geomembrane exposed:

- Damage due to uplift forces resulting from wind or landfill gas.
- Damage from falling objects including hail.
- Increased volume and velocity of stormwater runoff.
- Limited roadway access.
- Vectors and vandalism.
- Poor aesthetics.
- Limited design life.
- Limited regulatory approval.

As we move forward with EGCs as final cover alternatives, these potential disadvantages must be addressed.

Damage Due to Uplift

Design methodologies for providing resistance against wind and landfill gas build-up are readily available. Procedures based on Giroud (1995) were used to design the anchorage system at the Polk North Central Landfill to resist 80-mph winds. Three significant hurricanes materialized soon after construction, undoubtedly to test design procedures. Hurricane Charlie, passing within 25 miles of the landfill, was the worst with sustained winds of 75 to 90 mph and wind gusts of 115 mph. Although the landfill required substantial clean-up, the EGC escaped unscathed. Design procedures for landfill gas pressure and collection design are also available (Thiel, 1999), and although applications based on these methods have not been tested as dramatically, they are functioning well.

A wind-resistant EGC design must include restraints of some kind that fall into one of the following categories (illustrated in Figure 2):

1. Overburden Pressure. While soil cover is the traditional overburden of choice, sand bags, tires, and other weights can be placed over the geomembrane. The amount of weight can be determined from the design procedures. Weights tend to move around and usually need to be constrained with ropes (Figure 2.a) or enveloped in the geomembrane (Figure 2.b). Since many weights are usually needed, this choice often supplements anchors.

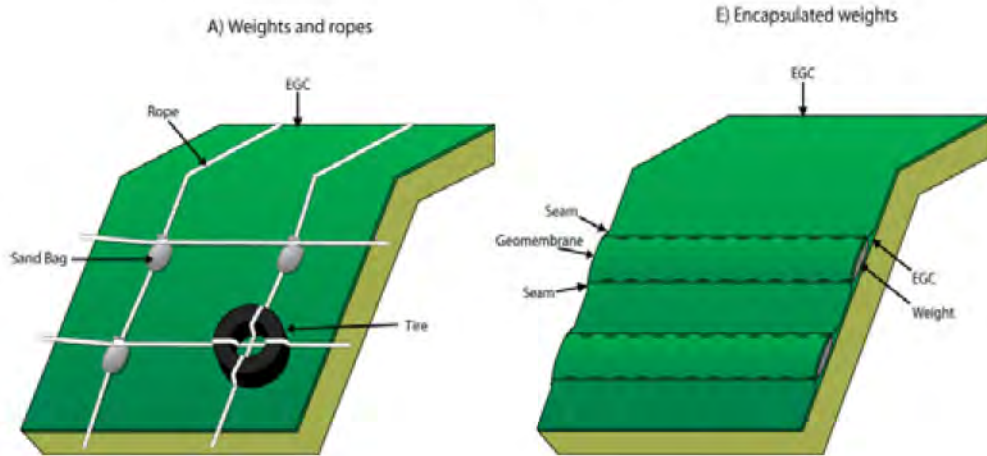


Figure 2.a

Figure 2.b

2. Anchors. Anchorage is usually provided by anchor trenches. While others have placed anchor trenches at the crest and toe slopes (Figure 2.c), Jones Edmunds developed a system of trenching up and down the slope (Figure 2.d) which performed well at Polk County and resists downward creep of the geomembrane. Screw anchors (Figure 2.e)

have been proposed (Richardson, 1994), but to the author's knowledge have not been applied.

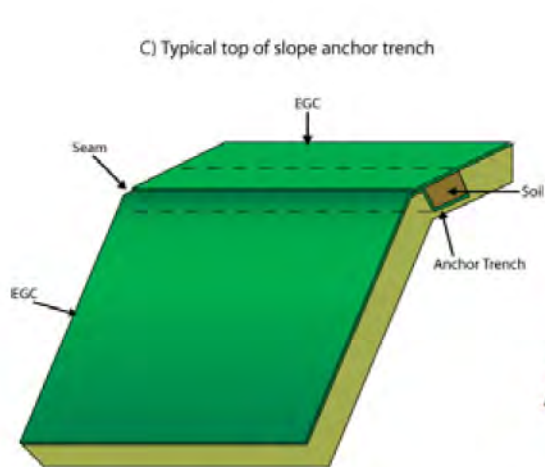


Figure 2.c

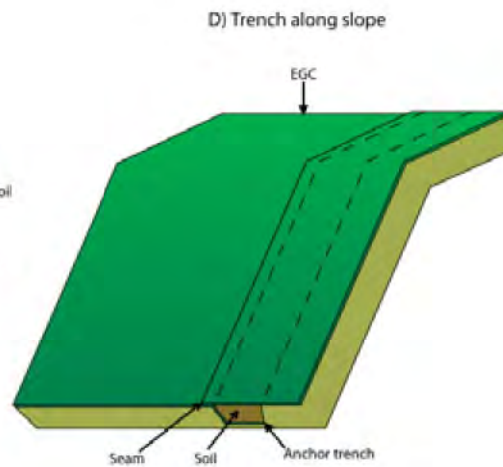


Figure 2.d

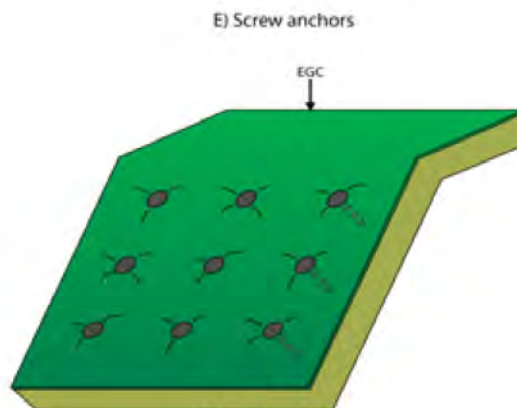


Figure 2.e

3. Vacuum. Jones Edmunds used a teed pipe to partially offset the pressure caused by high winds (Figure 2.f). Sites with active landfill gas collection systems may also take advantage of a vacuum under the geomembrane to counteract wind loads.

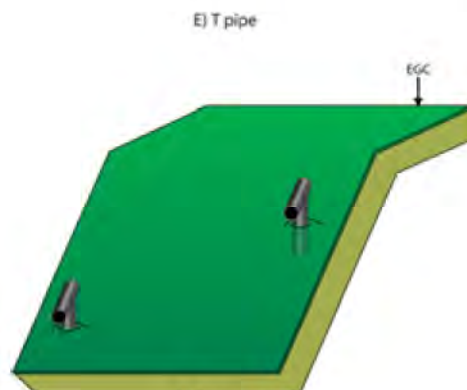


Figure 2.f

Damage from Falling Objects

A design methodology for hail damage was developed and applied originally to the Delaware facility (Gleason, 1998). Using this methodology, designs in Florida (where the potential for hail storms is surprisingly high) have a factor of safety against hail damage in excess of 3.0. Damage from other falling objects, from windblown vegetation to chicken bones dropped by seagulls, is unlikely to be any worse than hail but can be accounted for in like manner. No damage resulting from falling objects has been recorded at any existing EGC included in our survey.

Increased Volume and Velocity of Stormwater Runoff

Calculating potential stormwater runoff from an EGC is a very simple process. Conservatively assuming 100-percent runoff and instantaneous time of concentration, runoff is basically equal to the design storm. Without the concern of soil erosion, sheet flow is suggested so downdrains and bench drains are not required. Perimeter drainage channels will be larger, with capacities of about 50 percent more than a typical cover, but do not have to be designed to accept flow from downdrains. Depending on the channel design, energy dissipators may be required at the toe of slope, but sites in Florida are operating well simply with properly sized perimeter channels. In short, increased stormwater flows are easily designed for with minimal increase (about 20 percent more for stormwater improvements) to the overall closure cost.

Limited Roadway Access

Vehicles cannot drive over the exposed geomembrane so traffic is limited to an access road constructed over the landfill. As with traditional landfills, the access road can be constructed along a ramp formed as part of the original solid waste fill. A typical paved road with asphalt over aggregate can be constructed as long as sufficient protection (typically layers of geosynthetics) is first placed over the EGC. A stable road over moderate (less than 10-percent slopes) can be built if textured geomembrane is used as the EGC. Textured geomembrane also allows for better traction for those who must walk over the EGC. While access roads can be constructed over EGC, the limited access must be considered during construction and for long-term maintenance.

Vectors and Vandalism

Without soil cover, the geomembrane is susceptible to damage from a variety of animals. Vandalism from the human population is controllable by limiting site access, which is already a condition for landfills. Accidental damage is also something to consider, but this is no different than accidental damage to gas wells or piezometers which seem to be targets at most landfills. Thiel (2003) reports birds being a nuisance at the Yolo County facility in California as they seem to like picking at the ends of seams, but no such damage has been recorded at Florida sites. Birds picking at the scrim reinforcement in the EGC have also been noted in Delaware (Vasuki, 2006). On the positive side, burrowing animals and root penetration, potential problems for soil-covered geomembranes, are not a concern for EGCs.

Poor Aesthetics

A large mound covered by a black sheet may not be seen as aesthetically pleasing. Colored geomembrane may be a better option for aesthetics (although not as good for long-term performance), but not many people will confuse a green geomembrane-covered landfill with a grassy knoll. If the reactions of neighbors are a concern, EGCs may simply not be the best choice. Some more creative people, however, may consider the geomembrane a large blank canvas ready to become a work of art. The more business-inclined may see the largest billboard ever built. How the EGC is viewed is certainly a site-specific consideration.

Limited Design Life

While geomembranes in any application have a limited design life, exposed applications have a shorter life because of exposure to the elements. Susceptibility to falling objects is one aspect, but limited design life usually refers to the deterioration of properties as the result of ultraviolet light degradation. Geomembranes typically contain additives such as carbon black and antioxidants to combat degradation, but the amount of antioxidants is finite and they will eventually become depleted.

Design life is not strictly defined, but is generally considered to occur when antioxidants are depleted and physical properties (elongation at break, tensile strength) have changed more than 50 percent. For geomembrane final covers, covered geomembranes are assumed to last through the post-closure period (30 years or more), while typical polyethylene geomembranes are thought to last 15 to 20 years while exposed. Molecular weight (HDPE is better than LLDPE), color (black is best), and the additive package (a propriety blend of antioxidants and processing aids) all have major impacts on design life.

MANUFACTURERS

EGC applications have been either polyethylene or a reinforced polypropylene. Polyethylene was not initially the material of choice because of its high thermal expansion, creep properties, lower modulus, and tensile strength. Reinforced polypropylene addresses these issues and seemed to be well positioned for this application. However, experience with unreinforced polyethylene in landfill applications and its lower costs led to its use in some EGCs, and polyethylene proved successful. Tensile strength can be handled by placing more restraints and a system of vertical trenches seems to have alleviated the concerns with downward creep. HDPE does require specialized seaming equipment and more extrusion welding than is normally required for a cover, not only because of pipe penetrations typical in bioreactor covers but also because of the various methods of restraint.

Other materials may still play a significant role. Higher-strength geomembranes are generally more expensive but can reduce the number of restraints. A cost-benefit analysis is certainly warranted here. An odd concern with reinforced geomembranes has arisen; birds seem to find the woven scrim particularly attractive and tend to pick at the geomembrane.

Ideally we are looking for the following properties in geomembranes for EGC applications:

- Long life in exposed environment
- High strength to resist wind loads
- Flexibility to resist settlement
- Low thermal expansion coefficient to reduce wrinkling and downslope creep
- Ease of installation and repair
- Competitive cost
- An extended warranty

Manufacturers can recognize and address the shorter design life and other issues in a number of ways by working with engineers to:

- Predict design life using methods based on measurable chemical properties such as oxidative induction time.
- Establish a testing program for exposed samples of the geomembrane to monitor changes in chemical and physical properties.
- Establish an inspection and maintenance program as part of post-closure.
- Promote research and development of geomembranes for this application.
- Provide an extended warranty.

The manufacturer providing the best combination of properties and research will be well positioned in an emerging application.

MOVING FORWARD

With the positive experiences to date, the solid waste industry is ready to move forward with EGCs. Regulators are open to considering the possibilities and owners, who see the advantages, are ready to present site-specific requests for alternatives. Tested design procedures are in place and successful applications can be cited. With the opportunity at hand, it is now time for the manufacturers to step up with geomembranes specifically intended for EGC applications.

REFERENCES

Gleason, M.H., Houlihan, M.F., and Giroud, J.P., 1998, "An Exposed Geomembrane Cover System for a Landfill," Sixth International Conference on Geosynthetics Proceedings, pp 211-218.

Paredes-Bonilla, Valerie, 2002, "Exposed Geomembrane Caps," Master Thesis, University of Florida.

Thiel, R., Purdy, S., and Yazdani, R., 2003, "Case History of Exposed Geomembrane Cover for Bioreactor Landfill, Proceedings for Sardinia '03 Ninth International Landfill Symposium, Oct.

Roberts, M., Bonilla, V., Kelner, R, and Choate, A, 2005, "The EGC Takes on Three Hurricanes in Polk County," MSW Management, March/April.

Ivy, N., 2002, "HDPE geomembrane after 20 years of service," Geotechnical Fabrics Report, June/July.

Richardson, G.N., Peggs, I.D., Barton, B. 1994, "30 Year Exposed Geomembrane Landfill Cover: Performance, Material & Design Criteria," Fifth International Conference on Geotextiles, Geomembranes, and Related Products, Singapore, September, pp. 1097-1100.

Thiel, R.S. 1999. "Design of a Gas Pressure Relief Layer Below a Geomembrane Cover to Improve Slope Stability," Geosynthetics '99, Boston, April.

Bureau of Reclamation. 2000. "Canal-Lining Demonstration Report – 2000 Supplemental Report," January.

Vasuki, N.C, 2006. personal conversations.

Giroud, J.P, Pelte, T., and Bathurst, R.J. 1995, "Uplift of Geomembranes by Wind," Geosynthetics International, Vol. 2, No. 6, pp 897-952.

CONTACT:

Donald E. Hullings, P.E.
Director of Solid Waste
Jones Edmunds & Associates, Inc.
730 NE Waldo Road
Gainesville, Florida 32641
Phone: 352-377-5821
Email: dhullings@jonesedmunds.com

Appropriate Final Cover Design for Optimal Landfill Airspace

Mickey Pollman, Jones Edmunds and Associates Inc.; Don Hullings, Jones Edmunds and Associates Inc.

ABSTRACT

As solid waste professionals our goal is to optimize landfill airspace to maximize the amount of waste disposed of within a landfill's footprint. This often means lengthening (e.g removing benches) and steepening exterior waste slopes. The final cover system must then have sufficient drainage to reduce seepage forces and sufficient interface shear strength capabilities to provide a stable cover system. An integrated drainage "net" and textured geomembrane product may be able to do both. One particular product has been successfully used on over a dozen final cover projects where its textured underside provides interface shear strength with the underlying soil or GCL and studded top surface (when covered with a geotextile) provides the necessary drainage layer.

Jones Edmunds designed and permitted a final cover system for the Astatula Phase II Landfill in Lake County, Florida using the integrated drainage net and textured geomembrane product. The modified closure design included: increasing side slopes to 3:1, removing the side slope stormwater benches, and reducing the thickness of the final cover materials. The result was a cost-effective final cover design that provided a 30-percent increase in the available airspace within the current landfill footprint and gave Lake County 1.5 years of additional lifespan.

This paper / presentation will provide valuable information for solid waste professionals on methods and geosynthetic materials available for optimizing available air space by increasing side slopes. This paper / presentation will provide practical details regarding minimum requirements for geosynthetics used for landfill final covers and demonstrate the effectiveness of a integrated drainage net and geombrane cover system.

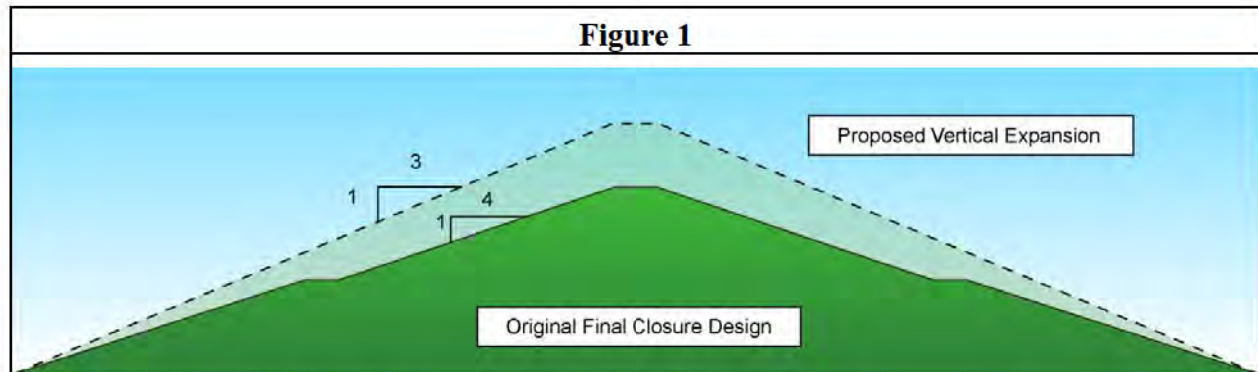
INTRODUCTION

Our client in central Florida was in immediate need of additional landfill airspace within the current landfill footprint while the owner was in the process of designing and permitting a new landfill. Jones Edmunds' proposal included steepening the side slopes and removing the proposed stormwater benches. These approaches introduce stability issues, in particular a reduction of the veneer slope stability. Jones Edmunds investigated various landfill cover materials and found a product that provides an effective barrier layer with sufficient veneer stability and drainage capabilities.

This paper will present the proposed design for the landfill vertical expansion, the results of the stability analyses showing the minimum requirements for the cover materials, and interviews with owners and engineers describing the successful use of this product in the final cover design.

LANDFILL VERTICAL EXPANSION

The proposed vertical expansion of a Florida landfill will increase the maximum height of the landfill by 27 feet. The vertical expansion will be accomplished by eliminating the stormwater benches and increasing the side slopes to 3 horizontal to 1 vertical (3:1). Thus, the final closure side slopes will be constructed continuously over approximately 85 vertical feet. Figure 1 shows a cross section of the original final closure design, and the proposed final closure design. The vertical expansion results in an approximately 30% increase in available landfill airspace.



VENEER SLOPE STABILITY

The steepened slopes and the removal of the benches decreases the factor of safety against veneer slope failure. The factor of safety against veneer slope failure is calculated using an infinite slope method presented by Giroud, Bacchus, and Bonaparte (1995). The infinite slope method is appropriate because cover soil veneer is so thin compared to the long continuous 3:1 slopes so that there is little influence from the toe buttress, and the cover soil is modeled as a purely frictional material. The proposed cover soil for this landfill will be sandy soil, which is readily available on-site.

We looked at the minimum interface friction requirements for the barrier layer for conditions without seepage forces and with seepage forces. The method for calculating the factor of safety against veneer slope failure without seepage forces is the simplified infinite slope equation. The method for calculating the factor of safety against veneer slope failure with seepage forces is the infinite slope equation, but including seepage forces. Both methods are based on Giroud, Bacchus, and Bonaparte (1995).

Infinite Slope Without Seepage Forces

The simplified infinite slope method used for calculating the factor of safety against veneer slope failure without seepage forces is shown in Figure 2.

The Factor of Safety (FS) for the simplified infinite slope method is calculated:

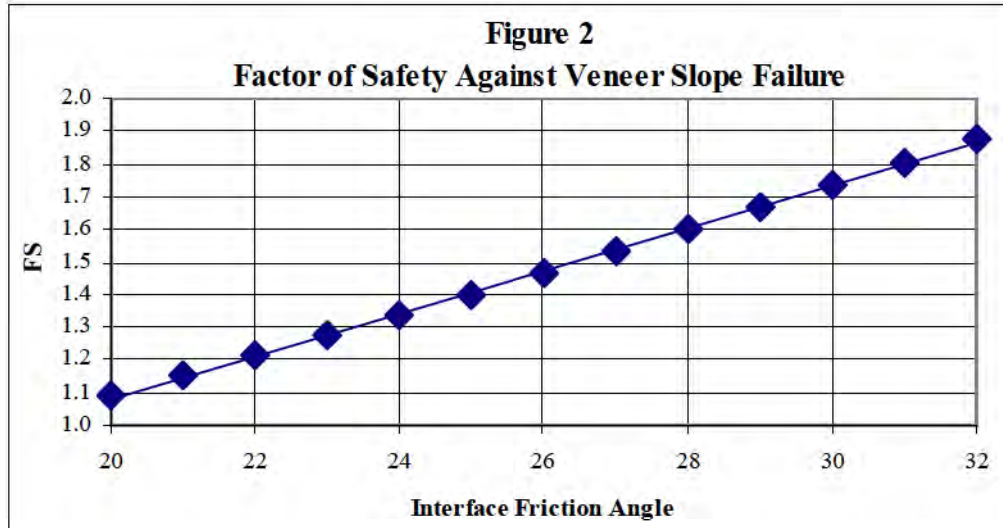
$$FS = \tan(\delta) / \tan(\beta)$$

Where:

δ = Interface friction angle between the barrier layer and the cover soil or subgrade soil.

β = Slope Angle = 18.4° for 3:1 slope.

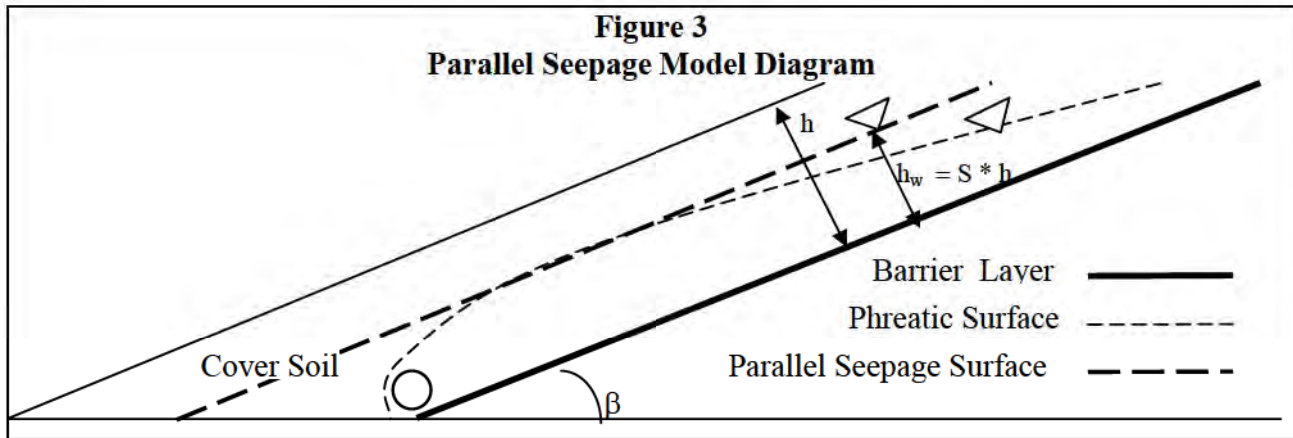
Figure 2 shows that the factor of safety increases as the barrier layer interface friction angle increases.



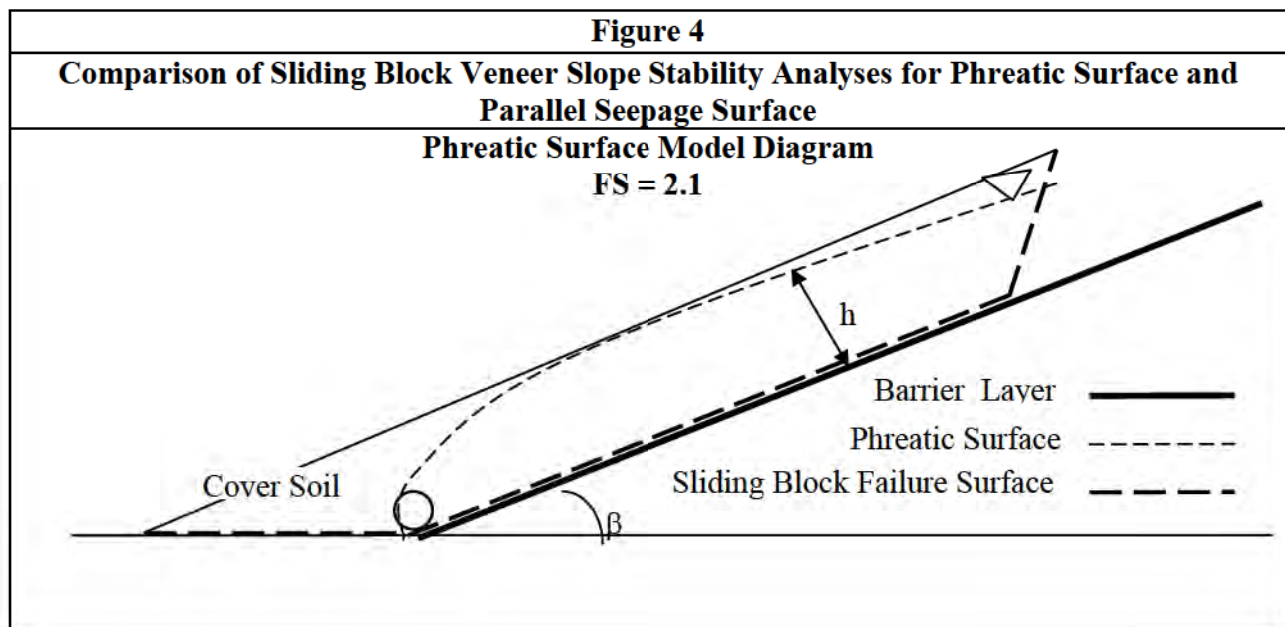
This analysis applies to the interface above the barrier layer (cover soil to the barrier layer) and below the barrier layer (subgrade soil to barrier layer), not including seepage forces.

Infinite Slope With Seepage Forces

If we include seepage forces due to stormwater infiltration, we use an infinite slope model that with seepage forces parallel to the barrier layer. A diagram of the cover soil and the model of the parallel seepage forces is shown in Figure 3. In Figure 3, as in the calculation of the seepage forces, the total height of the cover soil is represented by 'h', and the height of the zone of saturated soil is represented by 'h_w'. The actual phreatic surface in the cover soil (shown as the thinner dashed line in Figure 3) is not uniform, but increases in height toward the toe of the slope (Giroud, Bacchus, and Bonaparte, 1995). A parallel seepage model is a conservative approximation, where the height of the saturated soil (h_w) is approximately the height of the phreatic surface.



To check this assumption, we analyzed the veneer slope stability of a 3:1 slope using the block failure method for both a phreatic surface and a parallel seepage surface. The sliding block analysis including a phreatic surface resulted in a factor of safety greater than the analysis with a parallel seepage surface. Thus, the parallel seepage model results in a lower factor of safety, and is more conservative. Figure 4 presents the results and a diagram of the failure surface.



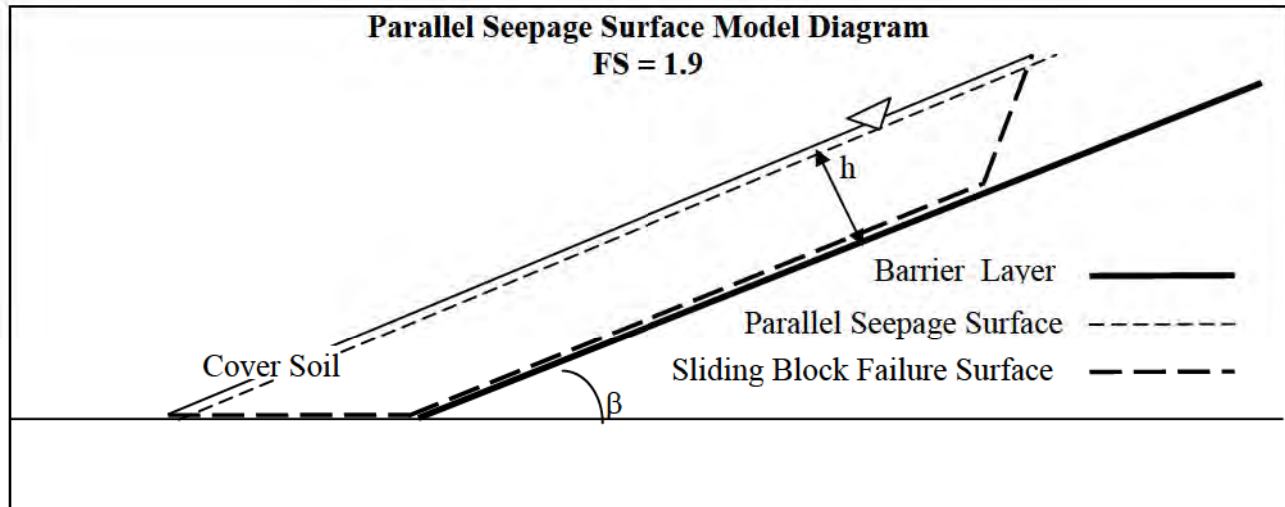


Figure 5 shows the relationship between the factor of safety against veneer slope failure and the interface friction angle between the cover soil and the barrier layer for various thicknesses of the saturated soil (or varying average height of the phreatic surface). This calculation is based on an infinite slope with seepage forces parallel to the cover soil and barrier layer interface, as presented by Giroud, Bacchus, and Bonaparte (1995). Note that the seepage forces are modeled in the cover soil above the barrier layer. There are no seepage forces below the barrier layer.

The Factor of Safety (FS) for the parallel seepage infinite slope method is calculated:

$$FS = \frac{\gamma(h-h_w) + \gamma_b h_w}{\gamma(h-h_w) + \gamma_{sat} h_w} \times \frac{\tan \delta}{\tan \beta}$$

Where:

γ = In-place unit weight of soil (pcf)

γ_b = Bouyant unit weight of soil (pcf) ($\gamma_{sat} - 62.4$ pcf (unit weight of water)).

γ_{sat} = Saturated unit weight of soil (pcf).

h = Height of cover soil above barrier layer (feet).

h_w = Height of saturated soil above barrier layer = $S * h$ (feet).

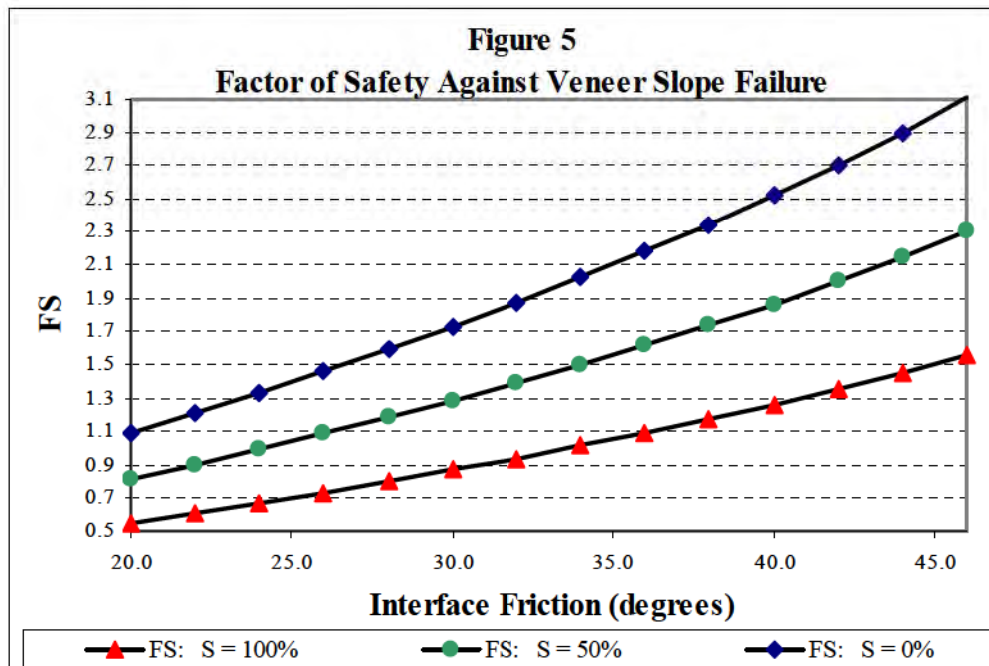
S = Percentage of soil that is saturated (%).

δ = Interface friction angle between the cover soil and barrier layer (degrees).

β = Slope Angle = 18.4° for 3:1 slope.

The parallel seepage forces are calculated based on thickness of the saturated soil above the barrier layer, conservatively modeled as a constant thickness above the barrier layer. The saturated soil thickness is shown as $h_w = S * h$. 'S' equals the percentage of the cover soil that is saturated, and 'h' equals the total height of the cover soil (see Figure 3). $S = 100\%$ for a saturated soil thickness equal to the total thickness of the cover soil, $S = 50\%$ for the saturated soil thickness equal to half of the total thickness of the cover soil, and $S = 0\%$ for no seepage

forces. As shown in Figure 5, the factor of safety decreases with increasing thickness of saturated soil.



Please note that the calculations shown here are for purely frictional barrier layer and cover soil and do not include an interface adhesion. The use of an adhesion term will increase the factor of safety relative to the assumed percentage of soil saturation. The applicability of the use of an adhesion term is an important topic that has been addressed by others. We do not use adhesion unless there is a compelling physical reason.

Also note that the interface friction angle for the barrier layer is determined by laboratory direct shear tests, and is highly dependent on testing method and the cover soil materials. Thus, establishing the interface shear strength for a final cover design should be based on laboratory tests using materials and loads comparable to those specific to the design.

REQUIRED MINIMUM INTERFACE FRICTION ANGLE

The purpose of the veneer slope stability analyses is to determine the required minimum interface friction angle for the final cover design. The required minimum interface friction angle will be used to evaluate an appropriate final cover design. The required minimum interface friction angle for our 3:1 slopes is dependent on the required (1) factor of safety and (2) the assumed percentage of saturated cover soil.

To establish the required factor of safety we need to consider the failure mode and the interface that is being evaluated. For a final cover system, not all modes of failures are equal. In a very simple final cover design consisting of a barrier layer over compacted subgrade and protective cover soil over the barrier layer, two distinct failure interfaces should be evaluated:

- Barrier layer sliding over the subgrade.
- Protective cover soil sliding over the barrier layer.

The geomembrane to subgrade is the more critical interface since failure will result in removal of the barrier layer and protective cover soil. Failure at this interface will be the most costly to repair. A higher factor of safety should be required for this surface. Working in its favor, this interface will tend to have a higher factor of safety because the underside of the barrier layer will not be subject to seepage forces. Although, the effects of landfill gas pressure should be evaluated.

The protective cover soil to geomembrane interface is less critical since failure will result only in sloughing of the cover soil, and will not directly impact the barrier layer. The cover soil can be repaired and replaced more easily than the barrier layer. A lower factor of safety should be required for this interface, which will help because seepage forces acting on top of the barrier layer can significantly reduce the factor of safety.

Establishing the required factor of safety must also take into consideration the seepage forces acting on the interface. The required factor of safety is also dependent on the seepage forces used to calculate the required minimum interface friction angle for that interface.

Based on these arguments, we are looking for a factor of safety against veneer slope failure of 1.5 for the interface below the barrier layer – which does not include seepage forces. This factor of safety is established based on recommended minimum values (Duncan and Wright, 2005) and local permitting requirements. Figure 2 and Figure 5 indicate that a factor of safety of 1.5 is achievable with an interface friction angle of 27 degrees.

The interface above the barrier layer is dependent on the saturation of the cover soil. If the full thickness of the cover soil is saturated ($S = 100\%$ and $h_w = h$), to achieve a factor of safety of 1.5, the interface friction angle of the cover soil and barrier layer must be at least 45° . This interface friction angle is not realistic for typical final cover designs. Consider also that a factor of safety of 1.5 may not be appropriate for saturated soil conditions since this is a temporary condition, and a factor of safety of 1.0 or 1.05 may be more appropriate. For our final cover design, we established a required factor of safety of 1.0 for the interface above the barrier layer with fully saturated cover soil. Table 1 lists the required minimum factor of safety and the established conditions required for the specified factor of safety.

Table 1 – Required Minimum Interface Friction Angle			
Required Minimum Interface Friction Angle	Conditions		
	Interface	Required Factor of Safety	Saturation
27°	Below the Barrier Layer	1.5	0%
34°	Above the Barrier Layer	1.0	100%
34°	Above the Barrier Layer	1.5	50%

Using a factor of safety of 1.0 for the condition with 100% saturated cover soil is appropriate because the infinite slope model is conservative, and thus, has some built-in factor of safety.

Using a factor of safety of 1.0 for 100% saturated slopes begs the question whether 100% saturated slopes are possible. During 2004 Florida experienced four hurricanes within a few months. Astatula Landfill experienced record rainfall with over 19 inches of rain over 50 days. Part of the north end of the landfill has a well vegetated final cover on a 4:1 slope. A small amount of damage due to erosion did occur – but no sloughing of the cover soil was observed. Even with this period of very heavy rainfall, it is unknown if the final cover reached full saturation.

If 50% of the soil is saturated, a factor of safety of 1.5 is achievable with an interface friction angle of approximately 34° (Figure 5). A factor of safety of 1.5 is appropriate for 50% of the soil saturated. Figure 5 also shows that with 50% of the soil saturated, a factor of safety of 1.3 is achievable with an interface friction angle of 30°. This interface friction angle is more typical of conventional final cover designs.

Thus, if we are to achieve a factor of safety against veneer slope failure of 1.5 with 50% of the cover soil saturated, our interface friction angle between the cover soil and the barrier layer should be 34°, and the interface between the subgrade soil and the barrier layer should be 27°.

FINAL COVER ALTERNATIVES

The traditional final cover alternatives we investigated are:

- Compacted clay
- Textured 40-mil High Density Polyethylene (HDPE) geomembrane
- Geosynthetic Clay Liner (GCL)
- Textured 40-mil HDPE geomembrane with double-sided geocomposite

The interface friction shear strengths of these materials were investigated and the results are shown in Table 2.

Final Cover Alternative	Interface Friction Angle	Factor of Safety 100% Saturated ¹	Factor of Safety 50% Saturated ¹
Compacted clay ¹	28°	0.8	1.2
Textured 40-mil HDPE geomembrane ²	28°	0.8	1.2
Textured 40-mil HDPE geomembrane with double-sided geocomposite ³	21°	0.6	0.8
GCL ⁴	34°	1.0	1.5

1 – The height of the saturated soil h_w is reduced by a factor of 3, resulting in a much lower equivalent saturation.

2 – Interface shear test with Ottawa Sand reported by Poly-Flex.(1996)

3 – Interface shear test reported by Tenax (2003)

4 – Internal shear strength of reinforced Bentomat SDN reported by CETCO (2005)

Compacted clay can vary greatly in shear strength properties and is a cohesive material that does not strictly apply to the infinite slope models. As shown here, using the internal shear strength alone does not achieve an adequate factor of safety. Another consideration for the compacted

clay is that clay soils are not readily available in our landfill area and can be price prohibitive. Thus, compacted clay was not considered for this final closure design.

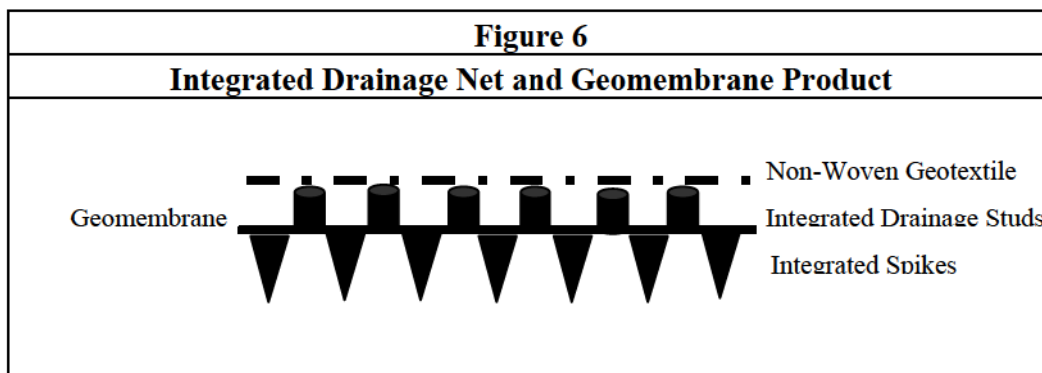
The textured 40-mil HDPE geomembrane alone against a sandy cover soil does not meet the interface friction requirements based on laboratory direct shear tests. Laboratory direct shear tests with textured geomembrane will vary greatly, and may result in higher interface shear strengths than the reported value shown here. Although, a compilation of direct shear test results is beyond the scope of this paper. Because of the low reported interface friction angle, the textured geomembrane was not considered for this final closure design.

Placement of a double-sided geocomposite over the textured geomembrane to reduce the seepage forces was considered. However, the interface between the texture geomembrane and the geotextile of the double-sided geocomposite did not meet the minimum interface shear strength required by the infinite slope model. Thus, the textured geomembrane with a double-sided geocomposite was not considered for this final closure design.

The GCL meets the minimum interface friction requirements. The GCL was investigated further, and the material was found to be incompatible with the waste. The waste at this landfill includes 70% waste-to-energy bottom ash commingled with the municipal solid waste. A swell test was performed using the leachate from the site and the GCL did not meet minimum free swell requirements. A soil buffer between the waste and the GCL was considered to prevent any possible contact with the leachate, but this would further reduce the valuable landfill air space. Thus, the GCL was not considered for this final closure design.

INTEGRATED DRAINAGE NET AND GEOMEMBRANE PRODUCT

An innovative barrier layer was proposed that includes a textured 40-mil LLDPE geomembrane with integrated drainage net studs above the geomembrane and integrated bottom spikes for increased friction. The drainage net studs are covered with a non-woven geotextile to create an integrated drainage net and geomembrane barrier material. A diagram of the product cross-section is shown in Figure 6.



Laboratory shear strength tests on this product resulted in high interface shear strengths of 35° between the saturated cover soil and the non-woven geotextile and 36° between the bottom spikes and the underlying subgrade soil (TRI, 2006). In-plane flow rate of the integrated

drainage net and geomembrane product has been reported to be approximately 3 times greater than a sand cover soil (SGI, 2005). Thus, the height of the saturated soil can be reduced for the infinite veneer slope stability model. Table 3 lists the Factor of Safety against veneer slope failure for the integrated drainage layer and geomembrane barrier layer material.

Interface	Interface Friction Angle	Factor of Safety 100% Saturated ¹	Factor of Safety 50% Saturated ¹	Factor of Safety 0% Saturated ¹
Cover soil to geotextile to integrated drainage net/geomembrane ²	35°	1.7	1.9	2.1
Integrated drainage net/geomembrane and subgrade soil ³	36°	1.8	2.0	2.2

1 – The height of the saturated soil h_w is reduced by a factor of 3, because of the increased drainage through the drainage net, resulting in a much lower equivalent saturation.

2 – Laboratory direct shear tests reported by TRI (2006) on site specific material for the three layers of material (1) cover soil, (2) geotextile, and (3) integrated drainage net and geomembrane product.

3 - Laboratory direct shear tests reported by TRI (2006) on site specific material for the two layers of material (1) subgrade soil, and (2) integrated drainage net and geomembrane product with bottom spikes up into soil.

Our analyses show that the integrated drainage net and geomembrane product, because of its high interface friction angle with the cover soil and subgrade soil, will provide a high factor of safety against veneer failure, because of the high interface shear strength and the reduction in the thickness of the saturated cover soil by increased drainage through the integrated drainage net. The drainage capabilities are sufficient to reduce the seepage forces in the cover soil by a factor of 3. But, even without these increased drainage capabilities, the high interface shear strength provides appropriate factors of safety against veneer failure for 100% saturated cover soils.

RELIABILITY AND CONSTRUCTIBILITY

We wanted to present this product to our client, but first we needed to determine if this product is reliable and if there are potential construction problems. The manufacturer provided us with a list of landfills that used this product in their final cover systems. We then interviewed owners, operators, and engineers to determine the response to this product.

The engineers described the product as very efficient and economical. This product is placed in a similar manner to other textured geomembranes, utilizing the same equipment and same manpower. This product has smooth edges for thermal seaming, so that seaming procedures are the same as those for other textured geomembranes.

Thus, placement and seaming are very similar to conventional geomembrane products, except that this product is more difficult to adjust or remove once the product is placed, because of the high frictional characteristics. Difficulties with in-place material adjustments results in a higher material waste percentage, typically due to more trimming. Additional time is also required for

pipe or vent penetrations. Additional time is required to remove studs and spikes and for extrusion welds. Fusion welds can be performed through the studs and spikes, and destructive testing has shown these welds to be stable. Engineers interviewed estimated that 99% of the placement and seaming to be equivalent to conventional geomembrane products, but some additional material may be required to account for waste and a few extra days may be required for penetration welding.

The geotextile that is placed over the drainage studs is handled the same as other geotextiles. The geotextile is pulled over the studs during placement and sewn together at the seams. Those interviewed indicated that there were no problems with walking over the studs during geotextile placement.

The procedures for cover soil placement are the same as those for conventional barrier layers. The soil is placed ahead of the vehicles going up the slope so that the vehicles do not drive directly over the geotextile. It was recommended that the maximum thickness of cover soil be placed at one lift to provide the greatest buffer over the product.

The results of the investigation indicate that the procedures for installation of this product are similar to those for conventional barrier layers. This product has also proven to be reliable and has been recommended by those interviewed.

CONCLUSION

The purpose of this investigation was to determine the minimum requirements for a final cover design based on an infinite slope analysis with parallel seepage forces to achieve appropriate factors of safety against veneer slope failure. If 100% of the cover soil is saturated, the minimum required interface friction angle between the cover soil and the barrier layer, assuming a purely frictional interface, is 45° (see Figure 5). This interface friction requirement is not practical, thus it is necessary to reduce the seepage forces or reduce the required factor of safety. The seepage forces are reduced by adding a drainage net to the barrier layer. With a drainage net that reduces the seepage forces - at a minimum by a factor of 2 (50% saturated soil), the minimum required interface friction angle needed to achieve a factor of safety of 1.5 is 34° . This interface friction angle is practical, and can be achieved with a product that includes a drainage net integrated with a highly textured geomembrane.

This product has been incorporated into a final cover design for a landfill in Florida, with long, continuous 3:1 slopes. This product comes highly recommended by owners and engineers interviewed. This product is thus recommended for final covers on steep slopes to provide high interface friction and reduce seepage forces.

REFERENCES

Giroud, J.P., Bachus, R.C., Bonaparte, R.; "Influence of Water Flow on the Stability of Geosynthetic-Soil Layered Systems on Slopes", Geosynthetics International Special Issue on Design of Geomembrane Applications, 1995, Vol. 2, No. 6.

CONTACT:

Ms. Mickey Pollman
Jones Edmunds & Associates, Inc.
Geotechnical Designer
730 NE Waldo Road
Gainesville, FL 32641
Phone: 352-377-5821
Email: mpollman@jonesedmunds.com

Special Applications

MSW Final Closures Incorporating Structured (Embossed) Geomembranes

Ronald K. Frobel, MSCE, P. E., R.K. Frobel & Associates

INTRODUCTION

Slope failures on final cover systems for municipal solid waste (MSW) cells have been well documented over the past 20 years with many failures of note within the past 3 years. Sliding failures have occurred in spite of known geotechnical reasons for failures and known design methods to avoid slope failures. Many of these failures occur at interfaces with the geosynthetics – most notably at the geomembrane/geotextile interface or geomembrane/soil interface. Early failures in the 1980's prompted manufacturers to develop and provide an alternative geomembrane with a “textured” surface that increases frictional characteristics and thus increases the factor of safety against sliding failures. However, the most common type of “texturing” manufactured by the blown film co-extrusion process (HDPE and LLDPE) has proven to be less than acceptable in both surface frictional values and quality of sheet (inconsistency in asperity height, textured surface and cross roll friction values). Deficiencies in quality and lower than expected asperity height have led to recent slope failures (Sieracke, 2005).

Structured or embossed HDPE and LLDPE geomembranes have been available to the civil engineering community and MSW landfill owners and designers for over 10 years. Their use in final closure designs has been steadily increasing, especially over the past 5 years as owners and designers discover and demand the consistently high quality texture and/or structured characteristics of this type of geomembrane due to the unique manufacturing process which incorporates flat die extrusion and embossed calendars.

This paper will focus on the structured or embossed geomembrane concept and manufacturing process as well as present comparative properties for consideration in design.

SURFACE TEXTURING METHODS FOR HDPE AND LLDPE

The following paragraphs will briefly describe and discuss the two primary surface texture methods in use today in North America. Other methods such as surface impingement are available mostly outside of North America and will not be discussed in this paper.

Structured (Embossed) Geomembrane Texture. During the flat die manufacturing process for geomembranes, hot extruded polymer sheet is run between two counter-rotating hot embossing rollers that contain uniform structural die shapes to form a molded or “embossed” structured or textured surface that is an integral part of the sheet without affecting the core thickness. This method has been in use for over 20 years and was designed to overcome problems of non-uniformity, variable area coverage, variable peaks and valleys, variable thickness and reduction in mechanical properties that is commonly found with the co-extrusion process. Figure 1 is a photo illustrating the production method and Figures 2 and 3 provide examples of the surface texture generated by the flat die molded surface manufacturing process. A major advantage of structuring is the ability to create very different surface textures on the upper and lower

geomembrane sheet surfaces, thus customizing the specific application (ie., drainage on top and aggressive friction surface on the bottom).



Figure 1. Flat Die Calendaring Manufacture (Smooth Sheet Production)



Figure 2. Flat Die Molded Textured Surface (Surface Friction Profile)



Figure 3. Flat Die Molded Structured Surface (Drain Surface Profile)

Coextrusion Geomembrane Texture. During the blown film co-extrusion process, molten polymer is extruded in 2 or 3 layers through concentric ring dies that are up to 10 m in circumference. The outer and inner dies are used to produce layers that can be “textured” or roughened by introducing and allowing nitrogen gas to escape. The texture is formed by the shearing action of the extruder breaking bubbles formed by the cooling of the blowing agent (nitrogen gas) as it expands. This process is known to be highly variable from manufacturer to manufacturer and even within a single roll or across a roll width. Although the texture can not be separated or peeled off, the critical mechanical characteristics of the sheet (ie, tensile stress, strain, tear and multiaxial response) are substantially reduced due to the introduction of peaks and valleys or surface imperfections that are not found on smooth sheet. Additionally, non uniformity of core thickness and even the method used to determine thickness has been questionable and is often a debate in CQA acceptance testing. Figures 4 and 5 provide examples of the surface texture generated by the process.



Figure 4. Co-extruded Surface Texture Light(Blown Film Process)



Figure 5. Co-extruded Surface Texture Medium (Blown Film Process)

COMPARATIVE PROPERTIES FOR DESIGN CONSIDERATIONS

In addition to the noted differences in surface texturing methods and noted inconsistencies from roll to roll or within rolls on co-extruded textured geomembranes as discussed above, the following considerations should be examined during design and ultimate selection of a textured geomembrane.

Potential for Mechanical Properties Reduction. Reduced mechanical properties of a required sheet thickness due to a texturing process such as co-extrusion must be considered, especially for the long term where increasing stresses due to subsidence or localized settlements will occur and affect the out-of-plane (multiaxial) response as well as seam strengths under stress. Reduced tensile strength and strain to rupture under load will also occur due to increased susceptibility to environmental stress cracking again due to the introduction of notches or imperfections caused by the co-extrusion process. Using the flat die extrusion process, the geomembrane mechanical tensile, elongation and other properties are closer to the values of smooth sheet and do not change from roll to roll as imperfections or thickness variations are not introduced during manufacture.

Interaction at the Shear Surface. Depending on the project design requirements (ie., steep slopes, seismic response, construction and service loading, etc) the peak and large displacement (post peak) interface strengths must be taken into consideration. For example, according to Stark and Richardson (2000) and Richardson and Theil (2001), coextruded textured geomembranes exhibit large post peak strength loss against geotextiles due to geotextile fiber tearing, pullout and shear orientation. In addition to geotextile fiber / texture interaction, the texture itself may comb (lay over) causing greatly reduced post peak shear strength (Stark and Richardson, 2000). Embossed surface textures, on the other hand, exhibit higher interface shear strength and lower post peak strength loss at lower normal stresses commonly found in landfill closure designs.

Constructability with Geotextile Surfaces. Some designs require the field placement of a textured geomembrane directly on a geosynthetic clay liner (GCL) or placement of a geonet composite or geotextile directly over the textured geomembrane surface. This requires interfacing a nonwoven geotextile with the textured surface. The “velcro” effect or “hook and loop” adhesion to a co-extruded textured surface is often problematic during field placement and requires very careful positioning or the use of a slip sheet. Embossed geomembrane surfaces, on the other hand, allow positioning of geotextiles and geocomposites without major difficulty. Quantifying of the “hook and loop” phenomenon has been the subject of extensive testing and in particular the effects on interface shear and the textured surface during shear (Hebeler, G. L., et.al., 2005; Giroud, J. P., 2004; Frost, J. D., et. al., 2002).

Geomembranes manufactured with textured surfaces by embossing provide consistent uniform quality texture that will supply the requisite interface shear strength without the detrimental effects of the co-extrusion blown film manufacturing process. Additionally, as regards CQA field testing and laboratory conformance testing, structured or embossed textured geomembranes will provide a consistent value from roll to roll and across the roll width, thus providing requisite design reliability. This is not the case for co-extruded blown film textured geomembranes where “the consistency of the texturing both across the roll and roll to roll should be a concern to the

engineering community..... What good is direct shear testing if the material provided is not consistent with respect to texturing?” (Sieracke, 2005). The following table is a summary of several design considerations that should be addressed when selecting a textured geomembrane to enhance slope stability factors of safety.

Table 1
Summary of Comparative Properties for Design Considerations

<u>Design Consideration</u>	<u>Co-Extruded</u>	<u>Embossed</u>
Consistent Thickness (cross roll)	No	Yes
Consistent Texture (cross roll)	No	Yes
Consistent Asperity Heights	No	Yes
Asperity Heights > 15 mil	No	Yes
Consistent Shear Testing (cross roll)	No	Yes
Affect on Multiaxial Stress-Strain (Settlement/Subsidence)	Yes	No
Texture Combing during Shear	Yes	No
Post Peak Reduction in Shear Strength	Yes	Yes
Easily Placed with Geotextile Surfaces	No	Yes
Increased QC and CQA Costs	Yes	No

Quality Measurements. In order to properly determine the quality and specification conformance of a blown film coextruded texture, multiple locations of discrete measurements must be made using two mechanical test methods, namely ASTM D 5994 “Test Method for Measuring the Core Thickness of a Textured Geomembrane” and GRI Test Method GM 12 “Asperity Measurement of Textured Geomembranes Using a Depth Gage”. Due to the non uniform surface, many discrete locations across a full roll width must be tested and averaged with max and min values. The testing technician tries to obtain the lowest core thickness and the highest asperity height by adjusting measurement locations primarily based on observation. “Both methods have proven to be problematic and have led to numerous conflicts between manufacturer and specifier” (Koerner, G. R. and R. M. Koerner, 2005) Alternative methods to determine these elusive properties have been the subject of several studies and papers (Koerner, G. R. and R. M. Koerner, 2005; Yesiller, N.,2005). Structured or Embossed geomembrane surfaces (textures), on the other hand, are consistent in both core thickness and asperity height due to the manufacturing process. Thus, multiple measurements to determine average or minimum values are not necessary in QC and CQA testing for structured geomembranes.

Large Scale Direct Shear Performance Testing. The interface strength of contact surfaces and in particular interface frictional strength must be determined for the geomembrane / geotextile and geomembrane / soil combinations using project specific geosynthetics, site specific soils materials, expected loading conditions, moisture / density conditions, etc. Mostly, these surface friction determinations are made by experienced personnel in an accredited geosynthetics laboratory using a large scale direct shear box in general accordance with ASTM D 5321 “Standard Test Method for Determining the Coefficient of Soil and Geosynthetic or

Geosynthetic and Geosynthetic Friction by the Direct Shear Method” (ASTM, 2006). This testing has become an essential part of the design process as well as CQA programs that qualify materials for construction. The surface texture consistency is extremely important in this regard and must not change significantly within a roll or from roll to roll. In fact, this has been problematic for co-extruded textures that may be tested only once on a sample from the manufacturer vs what is actually installed in the field and has led to failures due to lower than expected shear strength. If the textured surface of the material actually received in the field is questionable, it is recommended that performance tests be carried out on roll goods that are received on site to verify requisite interface shear properties.

Asperity Height. Additional to the requirement for a consistent textured surface, the minimum value of asperity height must be considered (assuming it can be accurately measured). Current specification requirements call for a minimum of 10 mils and reflects GRI Standard GM 13 and 17. However, 10 mils may be considered insufficient for many applications and should be increased to a minimum of at least 15 mils in order to compensate for known lower values that will be encountered in the co-extruded manufacturing process. Both co-extruded and structured geomembranes can meet the 15 mil minimum.

TYPES OF STRUCTURES OR EMBOSSED TEXTURES

There are generally three types of structured surfaces available to the design engineer for MSW closure applications:

General Slope Applications against soils and geotextiles - 25 mil Asperity Ht.

Aggressive Slope Applications with Integral Drainage – 175 mil Asperity Ht.

For general slope applications on slopes of 3H:1V or less, the embossed textured material (refer to previous figure 2.) provides consistent interface shear values against a variety of soil types. Table 2 illustrates the interface shear values that can be expected with various soil types as well as a non woven geotextile. As with all slope designs, large scale performance testing is encouraged using site specific soils and moisture/loading parameters. Aggressive or steeper slope applications are possible with the structured spike (bottom) surface as shown in figure 6.

Table 2
Representative Interface Shear Values – Embossed Texture
Cap Loading Conditions – ASTM D 5321

Material	Peak	Adhesion	LD	Adhesion	Efficiency
Coarse Sand	34°	65 psf	32°	15 psf	92%
Lean Clay	37°	110 psf	32°	30 psf	97%

Silty Sand	32°	55 psf	28°	10 psf	100%
NW GT	32°	80 psf	17°	80 psf	NA

Notes: P = Peak; LD = Large Displacement; NW GT = Non Woven Geotextile on Geonet Composite
Cap Loading = 250, 500, 1000 psf; Saturated Conditions



Figure 6. Bottom Emposed Structure or Spike Surface

Integral Top Surface Drainage. Structured geomembranes are also manufactured to provide an integral top surface drainage by incorporating a 145 mil stud profile. The top surface of the stud profile is overlain with a non woven geotextile for retention of drainage soil placed on top of the structure. Under normal load, the geotextile will intrude into the drain space as with geonet composites. The transmissivity of the drain layer is similar to geonet composites under cap loading conditions without the requirement for a geonet composite resulting in substantial cost savings per acre. Additionally, the potential for lower than designed interface shear values of a geonet composite against a textured surface is eliminated. The geotextile, once embedded into the stud profile provides for excellent interface shear values against overlying soil with efficiencies greater than 95%. Figure 7 shows a typical structured geomembrane stud profile placed on a cap prior to geotextile and soil cover placement. Based on project specific laboratory conformance testing incorporating site soils, transmissivity values of the drain stud profile with a non woven geotextile and soil/cap loading conditions range from 1.1E-03 to 3.6E-03 m²/s at a gradient of 0.33. Table 3 illustrates transmissivity test values for a cap loading condition after 100 hours testing under load. The non woven geotextile initially intrudes into the drain structure during increasing normal load similar to geonet composites.

Table 3
100 Hour Transmissivity Test Results

8 oz/sy Non Woven Geotextile over 145 mil Drain Stud Profile

Normal Load (psf)	Gradient (i)	Transmissivity (m ² /s)	Flow Rate (gpm)
250	0.25	1.19E-03	1.44
250	0.33	1.11E-03	1.77
250	0.50	9.77E-04	2.36



Figure 7. Structured Drain Profile on a Slope Prior to Geotextile/Cover Soils Placement

SUMMARY

Structured or Embossed HDPE and LLDPE geomembranes are not new to the geosynthetics industry and design engineers and in fact have been in use in a variety of civil engineering applications for over 10 years. Their use in MSW closure applications has been steadily increasing over the past 5 years. The advantages of this type of textured or structured geomembrane are many and include the following:

- Integral texture or structure embossed within the sheet
- Customized texture or structure top and/or bottom sheet surfaces
- Consistent texture, structure and core thickness from roll to roll or within a roll
- Consistent and reliable interface shear properties form roll to roll or within a roll
- Consistent mechanical and multiaxial strain properties
- Steep slope applications potential (aggressive spike profile surface)
- Integral surface drainage potential (drain stud profile surface)
- Cost effective in QCA cost reductions (both field and laboratory)

- Cost effective alternative to geonet composite placed over a textured sheet (structured drain profile)

It must be emphasized that project specific specifications and performance testing regarding required performance characteristics for a textured geomembrane is the design engineer's responsibility. The design engineer must be aware of the differences in the available types of textured materials and develop design specifications and CQA plans that will ultimately satisfy project requirements regardless of the material supplied.

REFERENCES

American Society for Testing and Materials International (ASTM), 2006. ASTM D 5321 "Standard Test Method for Determining the Coefficient of Soil and Geosynthetic or Geosynthetic and Geosynthetic Friction by the Direct Shear Method", Vol 04.13, Geosynthetics, ASTM Annual Book of Standards, ASTM, West Conshohocken, PA

American Society for Testing and Materials International (ASTM), 2006. ASTM D 5994 "Standard Test Method for Measuring the Core Thickness of a Textured Geomembrane", Vol 04.13, Geosynthetics, ASTM Annual Book of Standards, ASTM, West Conshohocken, PA.

Geosynthetic Research Institute (GRI), 2004. GRI Test Method GM 12, "Asperity Measurement of Textured Geomembranes using a Depth Gage", GRI Test Methods and Standards, Geosynthetic Institute, Philadelphia, PA.

Frost, J. D., Evans, T. M., Hebler, G. M. and Giroud, J. P., 2002. "Influence of Wear Mechanisms on Geosynthetics Interface Strengths", Proceedings of the 7th International Conference on Geosynthetics, Nice, France, September, 2002, Vol. 4, pp 1325-1328.

Giroud, J. P., 2004. "Quantitative Analysis of the Impact of Adhesion Between Geomembrane and Geotextile on the Stability of Soil-Geosynthetic Systems on Slopes", J. P. Giroud, Inc Technical Note, 2004.

Hebler, G. L., J. D. Frost, A. T. Myers, 2005. "Quantifying hook and loop interaction in textured geomembrane-geotextile systems", Geotextiles and Geomembranes International Journal, Vol 23, pp 77-105.

Koerner, G. R. And R. M. Koerner, 2005. "Ultrasonic Thickness Testing of Textured Geomembranes", Proceedings Geo-Frontiers 2005, ASCE

Richardson, G. N. And Theil, R. S., 2001. "Interface Shear Strength: Part 1 – Geomembrane Considerations", Geotechnical Fabrics Report, Vol. 19, No.5, IFAI, Roseville, MN, pp. 14-19.

Sieracke, M. D., 2005. "Geosynthetic Manufacturing Concerns from a Consultant's Perspective", Proceedings GRI/NAGS Conference, Las Vegas, December, 2005

Stark, T. D. and Richardson, G. N., 2000. "Flexible Geomembrane Interface Strengths" Geotechnical Fabrics Report, Vol. 18, No. 3, IFAI, Roseville, MN, pp 22-26.

Richardson, G. N. And Theil, R. S., 2001. "Interface Shear Strength: Part 1 – Geomembrane Considerations", Geotechnical Fabrics Report, Vol. 19, No.5, IFAI, Roseville, MN, pp. 14-19.

Yesiller, N., 2005. "Core Thickness and Asperity Height of Textured Geomembranes: A Critical Review", GFR Engineering Solutions, Vol 23, No. 4, IFAI, Roseville, MN, pp. 14-16.

CONTACT:

Ronald Frobel

R.K. Frobel & Associates

1153 Bergen Parkway

Suite M-240

Evergreen, CO 80439

Phone: 303-679-0285

Email: geosynthetics@msn.com

Maximum Protrusion Size under Geomembrane/GCL Composite Liners

D. Narejo, Caro Engineering; E. Kavazanjian, Arizona State University; R. Erickson, GSE Lining Technology, Inc.

ABSTRACT

An empirical design method currently exists for the use of nonwoven needle punched geotextiles as protection materials for high density polyethylene (HDPE) geomembranes. This method was developed by the primary author in conjunction with Drs. Robert Koerner and Ragui Wilson-Fahmy. This paper presents a parallel design method for geotextile-based geosynthetic clay liners (GCLs). Similar to the geotextile test method, the current design procedure is based on quasi-performance and performance tests using hydrostatic puncture method.

Geotextile-based GCLs consist of a clay layer sandwiched between woven and/or nonwoven needlepunched geotextiles. It is assumed that mass per unit area of the geotextile and the clay are the GCL properties of interest with regard to protection performance of GCLs. These two GCL properties are systematically varied over a range of protrusion conditions to develop an empirical relationship between GCL mass per unit area and its protection performance for 60 mil HDPE geomembranes. This relationship shows the influence of both geotextile and clay components to the combined protection performance of GCLs.

1. INTRODUCTION

Composite liners for waste containment facilities typically consist of a high density polyethylene (HDPE) geomembrane underlain by either a compacted clay liner (CCL) or an alternative geosynthetic clay liner (GCL). When under load, HDPE geomembranes are sensitive to point stresses from objects on which they are placed, whether installed with or without an underlying protection material. Much guidance is available regarding proper preparation of the geomembrane subgrade and removal of large soil particles or other sharp protrusions. This is less of a concern for geomembrane/GCL composite liners given the geomembrane is cushioned by the underlying GCL.

A CCL, on the other hand, is typically roller-compacted to “hide” any large-size particles by pushing them below the surface. Even then it is sometimes not possible to meet the subgrade surface requirements for geomembranes. A nonwoven needlepunched geotextile cushion is certainly a viable option to protect the geomembrane from puncture in such cases. Alternatively, a GCL can be placed over the CCL or other soil subgrade to provide necessary protection to the geomembrane. The GCL option has the added advantage of improving the overall quality of the liner system by functioning not only as a protection layer but also as an additional barrier layer.

Construction quality assurance (CQA) of liner systems through leak location survey is becoming increasingly popular and more commonly specified. Published statistics on leak location surveys show that most of the damage to geomembranes occurs during placement of the overlying soil drainage or protection layer. In applications where a geotextile or drainage geocomposite protection layer is placed above the geomembrane, some if not most of the damage to the geomembrane during installation may result from isolated protrusions from objects in the

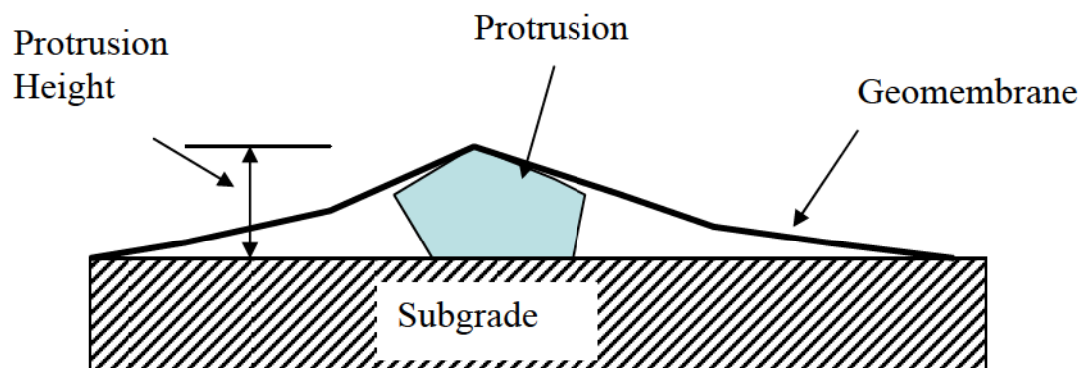
subgrade. This has been confirmed by previous research which demonstrates geomembrane susceptibility to puncture due to isolated protrusions (Narejo, et al., 1996). Placing a GCL between a geomembrane and a soil subgrade with isolated protrusions would not only eliminate most of the damage resulting from the under-layer, but would also improve the overall quality of the liner system. The cost of this additional layer of material can be partially offset by reduced CQA testing and improved leakage performance of the liner system.

The purpose of this paper is to develop recommendations for a maximum size surface protrusion (such as soil, clod, stone, etc.) that should be allowed in a subgrade surface when the geomembrane is protected by an underlying reinforced fabric encased GCL. This information should be useful for project owners and engineers in evaluating the cost of various lining system options and associated subgrade preparation. The data generated in this paper will also help alleviate some of the ambiguity that currently exists on this topic of acceptable subgrade.

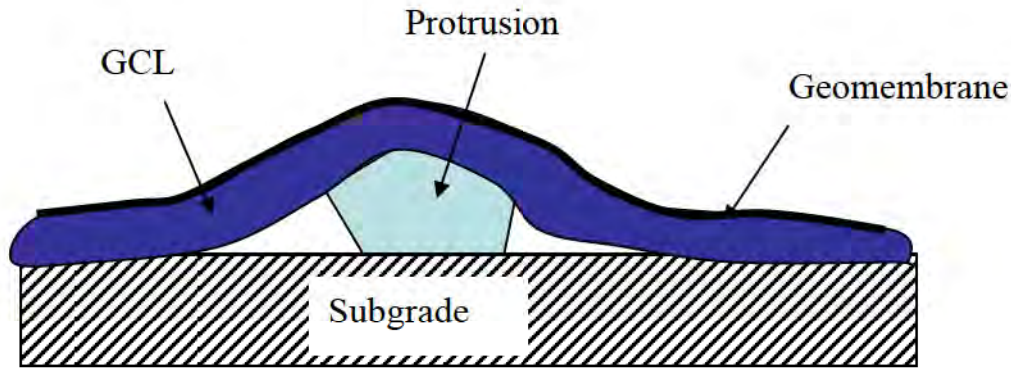
2. TECHNICAL APPROACH

The subgrade is commonly compacted and the surface smooth drum rolled prior to placement of geosynthetics. This essentially has the effect of pushing coarse particles into the subgrade and smoothing the surface so as to blend them in the upper layer of the soil surface. In subgrades with coarse particles, however, it is often not possible to remove all the undesirable larger particles from the surface except by sieving or scarifying the soil followed by re-compaction. Even after scarifying the subgrade surface, however, the surface may be disturbed by equipment or crew traffic during installation whereby freeing additional particles that may potentially damage a geomembrane. Therefore, isolated individual protrusions before or during geomembrane installation is a crucial CQA concern.

Such a hypothetical protrusion is shown in Figure 1(a). As shown in Figure 1(b), when a GCL is installed below the membrane over a subgrade protrusion, the GCL acts as a protective cushion for the geomembrane so as to resist point stresses and greatly decrease potential geomembrane puncture.



(a) Isolated Protrusion on a Prepared Subgrade

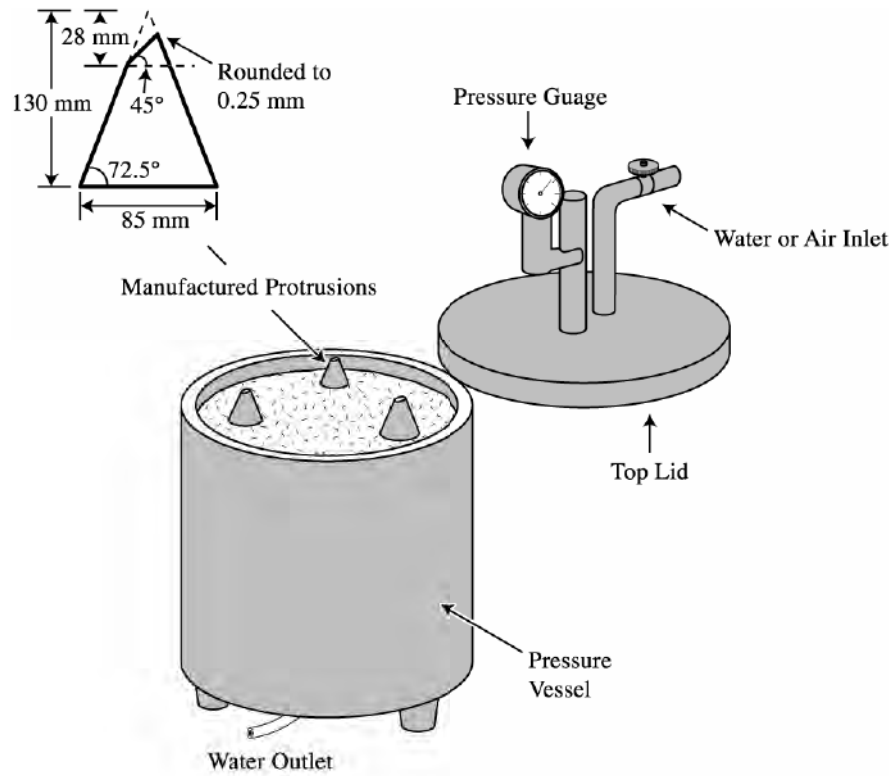


(b) Protection of the Geomembrane with a GCL

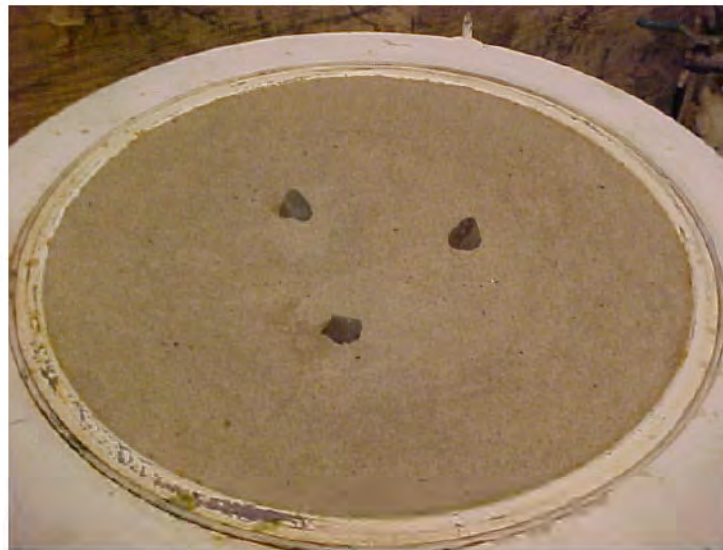
Figure 1 – Illustration of an Isolated Protrusion and Protection using a GCL.

A protrusion can consist of a stone, soil clod, stick or any other sharp or angular object extending above the surface and may generally be greater than 7 mm length or diameter. As shown in Figure 1, with a point overburden stress placed on the geomembrane, the geomembrane is challenged and may ultimately puncture and fail. Given there are limitless varieties of stone shapes and sizes in the field, it would take prohibitively large number of tests to model all the different shapes of protrusions a liner may encounter. Previous research (Hullings & Koerner, 1991; Narejo, et. al., 1996) has shown that a sharp angular stone can be modeled as a truncated cone in a laboratory puncture test. Hullings and Koerner (1991) demonstrated that a truncated cone-shaped protrusion can be used to determine a critical protrusion size below which a geomembrane puncture will not occur, even at very high overburden stresses. Therefore, this same approach for puncture testing was used in this paper to identify the maximum protrusion size that should be allowed below a GCL/HDPE geomembrane composite liner.

Figure 2(a) shows schematics of a truncated cone along with the test setup in accordance with ASTM test method D 5514. A photograph of the test setup prior to placement of a geosynthetic is shown in Figure 2(b). The test procedure is described in detail in the ASTM test method as well as by Hullings & Koerner (1991), and Narejo, et al. (1996). A brief description of the test procedure followed for this testing is provided here for the sake of completeness; however, the reader is encouraged to consult the references for detailed description of the test method.



2(a) – Schematics of Truncated Cone Puncture Setup.



2(b) - A Photograph of Test Setup

Figure 2 – Hydrostatic Truncated Cone Puncture Test.

The tests included placement of the protection material, in this case fabric encased reinforced GCLs, on top of the cones and bedding sand, and anchored over the flanges of the bottom vessel.

The geomembrane, for this testing a 1.5 mm smooth HDPE geomembrane, was placed over the GCL. The top lid (not shown in the figure) was finally placed over the vessel and tightened such that both the protection material and the geomembrane are sandwiched between the flanges. Maximum capacity of the vessel was approximately 700 kPa pressure. Water is introduced from the top side of the geomembrane and pressure incrementally increased into the vessel at the rate of approximately 7 kPa per minute until geomembrane failure occurred or equipment limit was reached. Geomembrane failure was detected digitally via metallic sensors in the cones upon contact with the vessel water passing through the geomembrane puncture. All GCL and geotextile samples were tested at cone heights of 12 mm, 25 mm, 38 mm, and 50 mm. The heights of the cones were varied by adjusting the bedding sand around the cones. All GCLs were tested in as-manufactured moisture content of approximately 10%.

3. GCL AND GEOMEMBRANE PRODUCTS

All tests were performed with a 1.5 mm smooth HDPE geomembrane. The seven GCLs chosen for testing were geotextile-encased reinforced products with a composite structure consisting of a cap nonwoven geotextile, a bentonite clay layer, and a carrier nonwoven or scrim-nonwoven geotextile. The bentonite loading of the samples was varied from 2,470 g/m² up to 4,940 g/m² to evaluate the effect of bentonite mass. All GCL cap/carrier geotextiles were standard 200 g/m² mass for consistency. The specific structure of each of the seven GCLs evaluated is described in Table 1 below.

The structure and mass of the geotextile is expected to influence the protection performance of a GCL. GCLs with bulkier nonwoven needlepunched geotextiles are expected to offer better cushion performance than those with lighter or woven geotextiles. Of the two geotextiles, one facing the protrusion is expected to have a greater influence on protection than the one on the opposite side of the protrusion. As such, protection performance of GCLs is expected to be specific to a particular product unless generic performance criteria covering all the materials are developed through extensive testing.

The use of GCLs as cushion materials should not be confused with their application as low permeability barrier materials. When a GCL is to be used as a cushion for a geomembrane, it may or may not satisfy hydraulic conductivity requirements of a hydraulic barrier. Specifically, the effect of large-size protrusions on hydraulic conductivity of the GCL must be considered. The benefit of a GCL when used as a protection layer is to improve the overall quality of the geomembrane installation by reducing or eliminating puncture of the geomembrane.

Table 1 – Various GCL Products Tested.

GCL Designation	Top Geotextile Type	Bottom Geotextile Type	Total GCL Mass (g/m ²)	Total Geotextile Mass (g/m ²)
A	PP, NW-NP	PP, NW-NP, Scrim Rein, Heat Treated	2541	400
B1	PP, NW-NP	PP, NW-NP, Scrim Rein, Heat Treated	4056	400
B2	PP, NW-NP	PP, NW-NP, Scrim Rein, Heat Treated	4349	400
C1	PP, NW-NP	PP, NW-NP, Scrim Rein,	4740	400

		Heat Treated		
C2	PP, NW-NP	PP, NW-NP, Scrim Rein, Heat Treated	5033	400
C3	PP, NW-NP	PP, NW-NP, Scrim Rein, Heat Treated	4789	400
D	PP, NW-NP	PP, NW-NP	5130	400

4. TEST DATA AND ANALYSIS

Hydrostatic truncated cone puncture tests, as outlined in the previous section, has been used in the past to develop design recommendations for protection of HDPE geomembranes from protrusions with nonwoven needlepunched geotextiles (Narejo, et al., 1996). Consistent with this approach, puncture behavior of an unprotected 1.5 mm smooth HDPE geomembrane is presented in Figure 3. This includes data from this study as well as from Hullings and Koerner (1991) and from Narejo, et al. (1996). The data indicate that as the cone height is decreased, overburden hydrostatic pressure required for puncturing the geomembrane increases. With continued decrease in the cone height, a point is reached below which the geomembrane puncture is not possible at the maximum test pressure (700 kPa for this study).

This point is indicated where the curve becomes asymptotic to the y-axis at a cone height of 10 mm. This is an indication that the maximum size protrusion that should be allowed in the subgrade surface to prevent puncture of the geomembrane should not exceed 10 mm. Applying a typical factor of safety of 1.5 to this value, which includes the uncertainties associated with the protrusion shape, this equates to a maximum allowable protrusion size of 7 mm for a 1.5 mm HDPE geomembrane without any protection. When it is not possible or realistic to ensure that there are protrusions which exceed this value, the geomembrane should be protected by utilizing either a nonwoven needlepunched geotextile, a GCL, or any other suitable cushion material.

The protection behavior of a 1.5 mm smooth HDPE geomembrane with nonwoven needlepunched geotextiles is presented in Figure 4. The nonwoven geotextiles include mass per unit area ranging from 540 g/m² to 680 g/m² which are commonly used as protective cushions. With the added geotextile cushion, the critical cone height has increased from 7 mm to 20 mm. Applying a factor of safety of 1.5, this indicates a maximum protrusion size of 13 mm to prevent geomembrane puncture.

From the data above, if a 1.5 mm smooth HDPE geomembrane is protected by a 540 g/m² nonwoven geotextile, it is very unlikely that the geomembrane will fail due to puncture from subgrade protrusions up to 13 mm. Certainly the use of needlepunched geotextiles is a viable option to protect HDPE geomembranes from puncture from subgrade soils with a certain amount of rocks and protrusions. In some applications, however, such a design is not desirable due to the wicking action of needlepunched geotextiles and increased potential leakage of a geotextile underlying a geomembrane adjacent to a geomembrane puncture. Therefore, the use of an underlying GCL would be a more effective protection option given the sealing and proven hydraulic performance of GCLs underlying geomembranes.

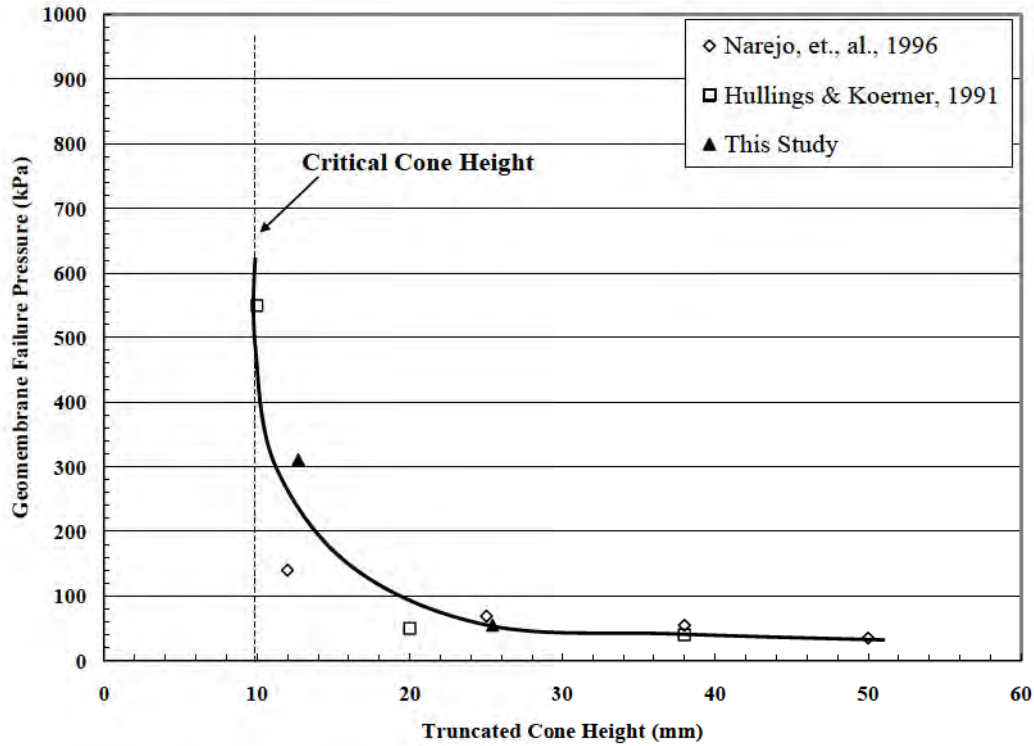


Figure 3 – Truncated Cone Puncture Behavior of Unprotected 1.5 mm HDPE.

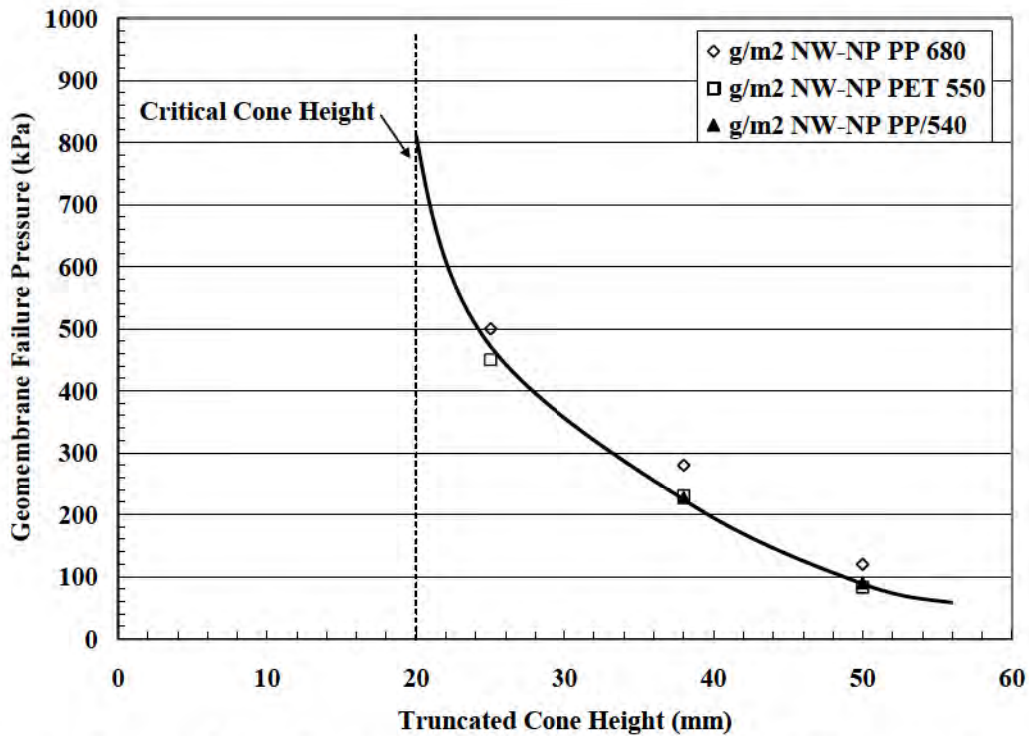


Figure 4 – Truncated Cone Puncture Behavior of 1.5 mm thick HDPE Geomembrane Protected by Nonwoven Needleponched Geotextiles.

Following the puncture testing methodology above, the seven GCLs listed in Table 1 were evaluated for effectiveness in geomembrane puncture protection. Figure 5 presents the puncture behavior of a 1.5 mm HDPE geomembrane protected by the GCLs. The tests were performed with the cap nonwoven geotextiles facing the geomembrane and the carrier geotextiles placed against the cones, consistent with their orientation in the field.

For all GCLs tested, the geomembrane did not puncture to the limit of the equipment (700 kPa) at a cone height up to 25 mm. At a cone height of 38 mm, there was a significant scatter in performance between the GCLs tested. No clear advantage of the increased bentonite mass per unit area of the GCL was indicated at the 38 mm cone height. A relatively light GCL with a total mass of 2,541 g/m² indicated comparable protection for the geomembrane as a GCL with twice its mass of 5,130 g/m². This came as somewhat of a surprise as the authors were expecting an increase in protection performance with an increase in mass per unit area of the GCLs. Thus, more testing is required to confirm the significance of fabric GCL mass and implications with regard to protection layers. It is evident that bentonite migration and thinning associated with the encapsulated bentonite occurred thus negatively affecting the GCL cushioning.

Figure 5 indicates a lower-bound critical cone height of 26 mm for a 1.5 mm smooth HDPE protected by commercially available GCLs with standard cap and carrier 200 g/m² nonwoven and scrim nonwoven geotextiles. Applying a factor of safety of 1.5 to this value, thus accounting for variability in GCL manufacturing and protrusion shapes, a critical cone height and protrusion size of 17 mm is derived.

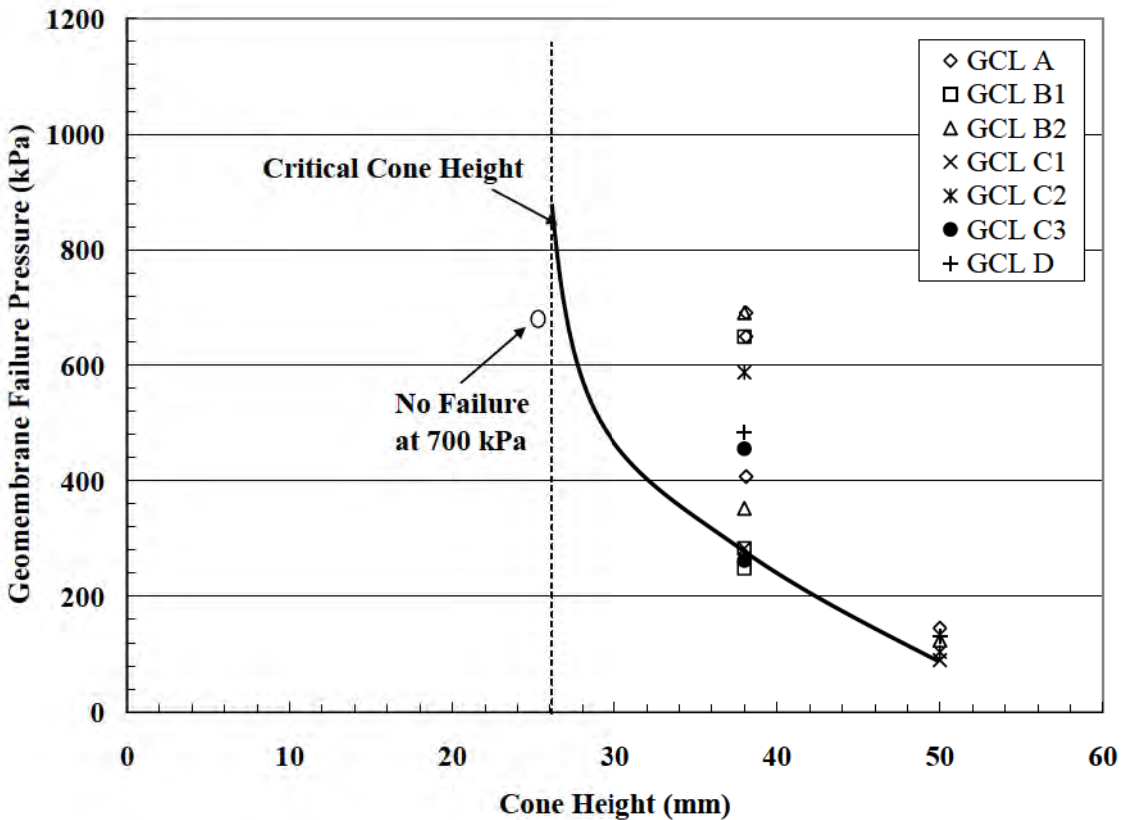


Figure 5 – Truncated Cone Puncture Behavior of 1.5 mm thick HDPE Geomembrane Protected by Various geotextile-based GCLs.

From the above data from a design and CQA perspective, puncture of a 1.5 mm smooth HDPE geomembrane from a subgrade with protrusions less than 17 mm is unlikely when protected by the type of nonwoven/scrim-nonwoven GCLs tested. Comparing this value to a geomembrane alone, the data show an improvement by a factor of $17/7 = 2.4$ times. However, the GCLs tested show only marginally better protection performance than a 540 g/m² nonwoven needlepunched geotextile.

Based on the concept of critical protrusion size or critical cone height, the results indicate that subgrade preparation requirements can be relaxed when GCLs are used under geomembranes. Not only would GCLs reduce potential geomembrane punctures thereby improving CQA of the lining system, but would greatly improve the integrity of the lining system and reduced leakage due to the inclusion of a GCL in intimate contact with the overlying geomembrane and underlying soil subgrade. In geomembrane only applications where it is not possible to achieve the maximum protrusion size of 7 mm extending from the surface of the subgrade, inclusion of a GCL certainly provides a viable alternative by increasing allowable protrusions up to 17 mm

4. BENEFITS TO END USER

Regulations and project specifications generally limit the maximum subgrade soil size that geomembranes can be placed against. In certain cases, it is not possible to achieve these requirements due to either the nature of the existing soil, cost/time associated with scarifying or screening soils, or lack of available alternatives. GCLs provide a mechanism to protect the geomembrane from puncture and improve the quality of the lining system. The added cost of the lining system can be partially offset by the lower CQA costs and improved leakage performance.

The use of a GCL with existing subgrade with relatively poor quality (e.g. high percentage of particles >7 mm) provides flexibility to designers and project owners to comply with project requirements faster and at a lower cost. The puncture test data demonstrates that a GCL with mass as low as 2,541 g/m² can be utilized to provide adequate protection requirements as long as the maximum protrusion size does not exceed 17 mm

5. SUMMARY AND CONCLUSIONS

The test data presented in this paper shows that commercially available fabric encased GCLs can be effectively used to protect HDPE geomembranes from puncture for a protrusion size up to 17 mm. This compares to a maximum size of 7 mm when a geomembrane is not protected by a cushion layer. It is also shown that effective geomembrane protection can be achieved by a GCL with a mass almost 50% less than typical GCLs (e.g. bentonite loading of 2,470 g/m² vs. 4,440 g/m²). Thus, GCLs provide a mechanism for complying with subgrade preparation requirements for projects where this is not possible through other means. The additional cost of utilizing GCLs as protection layers can be partially offset by lower CQA costs and greatly improved leakage performance of the lining system.

6. REFERENCES

Hullings, D and Koerner, R., 1991, "Puncture Resistance of Geomembranes Using a Truncated Cone Test", Geosynthetics '91 Conference, Atlanta, USA, pp. 271-285.

Narejo, D., Koerner, R., and Wilson-Fahmy, R., 1996, "Puncture Protection of Geomembranes, Part II: Experimental", Geosynthetics International, Vol. 3, No. 5., pp. 605-627.

CONTACT:

Dhani Narejo
Caro Engineering
Senior Engineer
10695 Meachen Meadows Trail
Conroe, TX 77302
Phone: 936-321-1956
Email: dnarejo@caroeng.com

RESTORATION OF DISTRESSED SECONDARY MONITORING SYSTEM AT A HAZARDOUS WASTE LANDFILL – REPAIR IMPLEMENTATION

James J. Parsons, P.E., NTH Consultants, Ltd; Jenghwa Lyang, Ph.D., P.E., NTH Consultants, Ltd

ABSTRACT

Distressed secondary riser pipes were discovered at a hazardous waste disposal facility during routine sampling. The riser pipes extended from a secondary sump, up a 10-foot high (vertical) intracell berm, turn 45 degrees through the primary clay and 80 mil geomembrane liner, and extend vertically through approximately 120 feet of hazardous waste to the surface. Video inspection of the 8-inch to 12-inch diameter riser pipes revealed that at four riser locations, the field-fabricated elbows had partially buckled. At one riser location, the vertical portion of the pipe buckled at two points. Investigation of the distressed riser pipes led to a unique and challenging repair approach.

INTRODUCTION

Wayne Disposal, Inc., a subsidiary of EQ The Environmental Quality Company, owns and operates the Site No.2 disposal facility in Belleville, Michigan. The site comprises approximately 400 acres and has landfilled municipal solid waste, industrial hazardous waste, and commingled waste. Current operations include disposal of hazardous waste and waste regulated by the Toxic Substances Control Act (TSCA). The balance of the disposal areas is closed. The facility is currently licensed to landfill 11 million cubic yards of hazardous/TSCA waste.

Master Cell VI is the current active disposal area. The 34-acre cell consists of five subcells designated as A-North, A-South, B, C and D. These cells were constructed during the late 1980's and early 1990's with a typical double composite liner system that includes from the bottom up: a 60 mil secondary HDPE geomembrane liner, one to three layers of secondary drainage net, geotextile, a 5-foot compacted clay liner, an 80 mil primary HDPE geomembrane liner, 12-inch peastone leachate storage layer, geotextile, 12-inch granular drainage layer and a geotextile separation layer.

A network of perforated 6-inch diameter DR 7.3 HDPE pipe comprises the primary leachate collection system.

The secondary leak detection system for subcell D includes a sump and a DR 17 HDPE riser pipe that extends along, and is fully supported by, the sideslope of the cell to ground surface. Each of the remaining subcells incorporates a secondary sump and a DR 17 HDPE riser pipe (Fig.1) that extends approximately 10 vertical feet along a 2 vertical to 1 horizontal slope, then turns within the primary compacted clay layer and extends vertically through approximately 120 feet of waste.

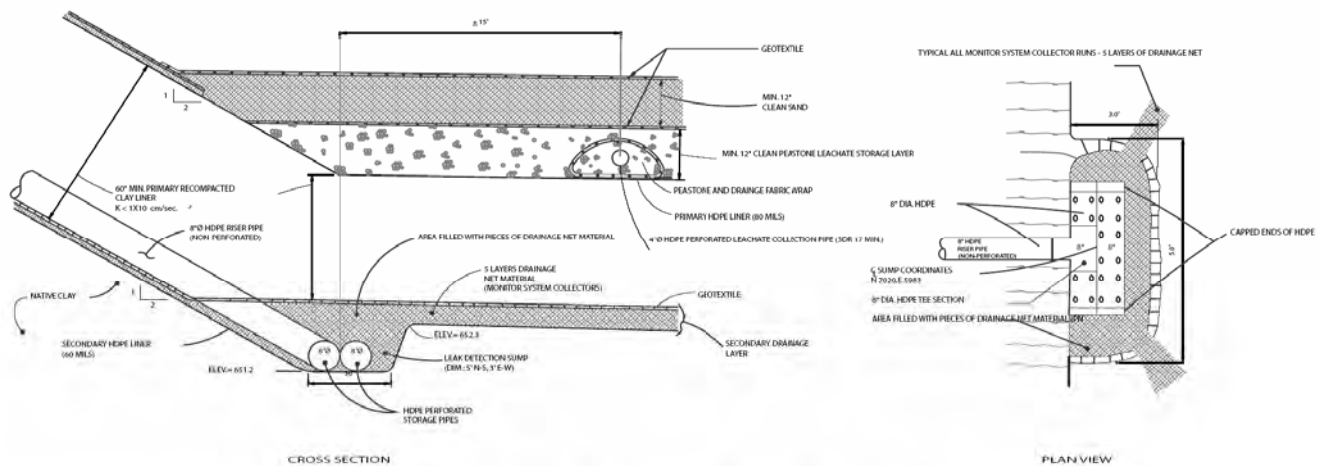


Figure 1. - Typical secondary sump and riser

The vertical portion of the riser pipe is sleeved with a second pipe at a point approximately 10-feet above the primary liner (Fig. 2). The sleeve was designed to reduce downdrag forces imposed upon the riser pipe as waste settlement occurred.

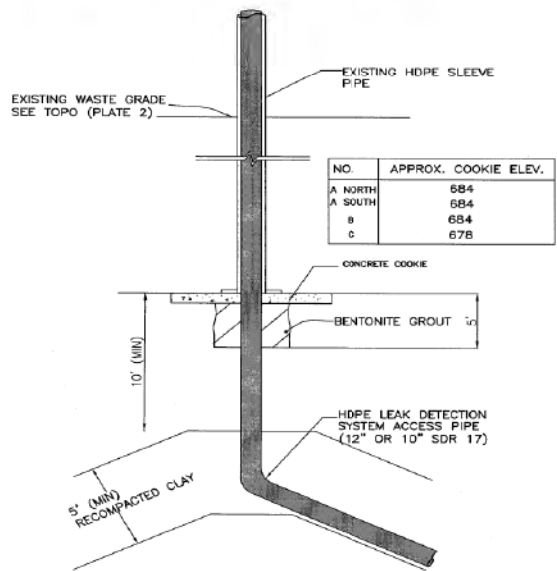


Figure 2. - Protective outer sleeve for riser pipe

In 2002, a vertical expansion of Master Cell VI was constructed. The vertical expansion, designated as subcell E, overfills the existing subcells and extends to the north over the adjacent closed Master Cell V.

THE PROBLEM

The operating permit for the facility requires liquid in the secondary sump to be sampled and pumped dry on a quarterly basis. Water accumulating in the sump is primarily consolidation water from the compacted clay liner and has historically been free of contaminants that may indicate a leak in the primary liner system. Early in 2003, during routine sampling of the secondary sump in subcell B, the pump became stuck during extraction. The pump was eventually retrieved, however the outer pump shield remained inside the riser pipe. In addition, difficulty was encountered extracting the pump from the A-North riser pipe.

Camera inspection of the riser at subcell B was initiated to locate and determine means of retrieving the outer pump shield. A 4-inch diameter pan-and-tilt camera was lowered into the riser pipe and revealed significant deformation of the pipe wall in the field-fabricated elbow within the primary compacted clay liner (Fig. 3). The magnitude of the deformations prevented camera inspection past the elbow.



Figure 3. - Distressed elbow in Subcell B riser

At a depth of approximately 57 feet below the waste surface, the vertical portion of the riser pipe was severely buckled (Fig. 4). Again, this condition prevented camera inspection below the buckled section.

Because
difficult
y was
encount
ered
during
extracti
on of
the
pump
from the
riser at
A-
North,
this pipe
was also
inspecte

All of the risers were subsequently video inspected using a 1-inch diameter push camera to depths of at least 120 feet. At A-North, a second buckled section was observed approximately



five feet below the first. Deformation of the elbow was also noted. At subcells A-

South, B and C, deformation within the elbows was noted but no buckling of the vertical riser pipe was observed. The riser pipe for subcell D, which is the only riser fully supported on the cell sideslope, was undamaged. In addition to the four distressed secondary risers, a primary cleanout riser, critical to the leachate collection system, was damaged.

The impact to the facility operations of potential total failure of the secondary risers could be enormous. Without the ability to sample and test the liquids in the secondary sump, the facility would lose the ability to demonstrate that the liner system has no leaks. Compliance and regulatory constraints could force the facility to severely limit or cease operations.

EVALUATION OF DISTRESSED PIPE

Evaluation of the secondary leak detection riser pipes in Master Cell VI was initiated. The evaluation included a detailed survey of the damaged risers, collection of record photographs, survey notes, inspection reports and other data, as well as structural analysis of the pipe to determine the cause of failure.

The survey included measurements of the depths to each deformation and comparison to record

Fig. 4 – Vertical riser at A-North

survey data. Original construction reports, photographs and surveys were reviewed and collated with measured data and original design calculations. In most cases historic survey data indicated that the horizontal location of the riser pipe at the current waste surface varied from the location of the initial dike penetration significantly, in some cases as much as 50 horizontal feet through the entire 120 foot depth. An observation of the inspection videotapes confirmed sweeps and angular offsets from vertical throughout the lengths of pipes, particularly at welded joints.

Historical photographs from the project records revealed a construction sequence that included fabrication of the HDPE riser pipe from the sloped section of the intra-cell berm, through the

elbow, and the first vertical section of pipe, before the compacted clay layer had been



Figure 5. – A-North riser at tie-in to sub-cell D

the elbow very difficult, if not impossible. Figure 5 shows this sequence at the tie-in between subcell A-North and subcell D.

Figure 6 shows the loose condition of the bedding soil at the reducer and elbow sections.

Other data evaluated included soil boring information and shallow test pits excavated around one of the risers. The original design specified the placement of sand bedding around the vertical portions of the outer protective sleeves, extending around the pipe diameter for 5 feet. The sand bedding was intended to assist in limiting downdrag forces as well as to provide a buffer against waste placement in direct contact with the outer protective pipe. Boring information revealed that the sand bedding was not in place throughout the entire length of the riser. In addition, test pits excavations revealed buried drums in direct contact with the protective sleeve.



Figure 6. - Condition of bedding soil around elbow

constructed.
This sequence made adequate backfilling and structural support below

Structural analysis of the HDPE riser pipes and outer sleeves to resist the forces imposed by lateral and vertical

pressures was completed based on ASTM F1759 – Design of HDPE Manholes for Subsurface Applications. Historic settlement data from settlement plates installed in late 2000 and estimates of settlement based on standard penetration test of the waste were used in the analysis. Settlement analysis suggest that the total waste settlement could be highly differential, varying significantly from place to place and could be as high as 10 to 15 percent under fills of 100 feet or more.

Results of the analysis indicated that the long-term strain in the waste fill could exceed the critical buckling strain of the outer protective sleeves and that the outer sleeves were likely to buckle from waste down drag forces alone at depths of about 50 feet or greater. Load transfer to the inner pipe can occur because the outer sleeve deforms downward from down drag forces and come in contact with the inner pipe at points of angular offset from vertical.

Axial buckling of the inner riser pipe was evaluated for the condition where down drag forces are transferred to the inner pipe installed at an angular offset of 30 degrees from vertical. This condition imposed both an axial load component and a bending load component on the inner pipe. The axial load component was evaluated using ASTM F1759 and the bending component was analyzed using a solution for a beam on an elastic foundation (Hetenyi, 1946). The results showed that the inner riser pipes could fail in axial buckling if down drag forces were transferred to them.

In general, the results of the evaluation concluded that possible poor backfilling below the elbow, lack of sand bedding around the pipe and angular offsets from vertical likely contributed to transfer of down drag forces to the inner pipe causing buckling failure. Other installation defects, such as equipment impact damage or poor waste placement techniques, may have caused or contributed to the observed distress in the pipe.

EVALUATION OF REPAIR METHODS

How do you repair a distressed pipe that terminates in a sump over 120 feet below the surface of a hazardous waste landfill? To answer this, numerous methods were thoroughly evaluated, including:

- Open excavation;
- Sliplining with a smaller pipe and use of micro pumps;
- Pipe bursting technologies;
- Braced excavations;
- Micro-tunneling;
- Directional drilling;
- Conventional tunneling below the landfill
- Internal re-rounding of the pipe followed by structural polymer reinforcing; and
- Drilled access shafts to the sump with complete riser replacement.

The evaluation of the repair methods considered several design challenges. Regulatory oversight by the Michigan Department of Environmental Quality (MDEQ) and the US Environmental

Protection Agency (EPA) would require regulatory approval. Environmental impacts also needed to be considered. Any repair undertaken must be environmentally protective and could not impact the environmentally sensitive secondary leak detection system. Any contamination of the secondary leak detection system could potentially be construed as a leak in the landfill liner system.

The most straightforward solution, and potentially the least costly, was open excavation to the distressed elbows and a direct repair of the riser pipes. This method was not considered desirable because it would require relocation of over 500,000 cubic yards of hazardous waste. Not only was there insufficient permitted area to relocate the waste to, but also would potentially expose the environment to airborne contaminants and undesirable odors. Further, this method would nearly completely disrupt regular site operations.

Cost and risk analysis was completed for most of the options. Three options were considered viable; insertion of a smaller diameter “slipline” pipe with reinforcement of the damaged sections, internal re-rounding with structural reinforcement, and drilling of access shafts for a direct replacement of the damaged sections.

Preliminary evaluation of the slipline option determined that the configuration of the damaged elbow sections combined with length, diameter and capacity of available pumps, prevented this option. Further, the damaged vertical section of the riser at subcell A-North eventually closed completely, preventing even a 1-inch diameter camera to pass. Internal rerounding technology had never been attempted in this application and would require redesign of conventional rerounding equipment and modifications to normal procedures. Drilled access shafts would allow complete replacement of the damaged risers, but required breaching the primary synthetic and clay liners. The owner elected to proceed with development of the rerounding option to occur concurrently with the design of drilled access shafts.

Internal pipe re-rounding is a technology typically applied to horizontal PVC pipe with two-way access. That is, the equipment is inserted into a manhole and is pulled through a length of pipe from a second manhole. To apply this technology to rerounding of the HDPE riser pipes in a vertical orientation with only one-way access limited use of this technology. A contractor was located who had successfully applied rerounding techniques to vertically oriented HDPE pipes.

After several months of research, bench scale trials and equipment modifications, field trials were begun in early 2004 (Fig.7). Field trials successfully rerounded one of the upper deformations of the riser pipe at sub-cell A-North, but failed to make the turn through the deformed elbow section. After numerous unsuccessful attempts at rerounding, the technology was ultimately abandoned.

The shaft accessed repair method became the focus of the repair design effort.



Figure 7. - Field trials of rerounder

SHAFT ASSESSED REPAIR DESIGN

A shaft-accessed repair involved numerous design challenges. The concept would require:

- Drilling through over 120 feet of hazardous waste;
- Accurately excavating to the end of the secondary riser pipes that terminate within a 3-foot by 5-foot sump;
- Put personnel in the shaft to hand excavate through the last 5-feet of hazardous waste;
- Breach the primary 80 mil HDPE geomembrane liner;
- Hand excavate through 5-feet of compacted clay liner;
- Complete the above work at the lowest point in the cell;
- Control leachate and secondary consolidation water;
- Prevent contamination of the secondary leak detection system.

Additional challenges with logistics also needed to be addressed. Regulatory approval was needed to cut a 7-foot diameter hole in the primary containment liner near the low points of the subcells. Drilling a shaft would also require a crane with over 120 feet of boom to be in place on top of the landfill. Because of the proximity to an adjacent major airport, the crane would infringe on FAA and airport management airspace, thereby requiring FAA approvals. And finally, we needed to identify an appropriate contractor to implement the work.

After several meetings with the Environmental Protection Agency, the Michigan Department of Environmental Quality and airport management staff, the draft work plan and conceptual design was approved. With regulatory approval in place, the project team moved forward with addressing the remaining challenges.

Due to the construction complexities and specialty sub-contractor needs of the conceptual repairs, the contractor was solicited early in the final design phase of the project. This

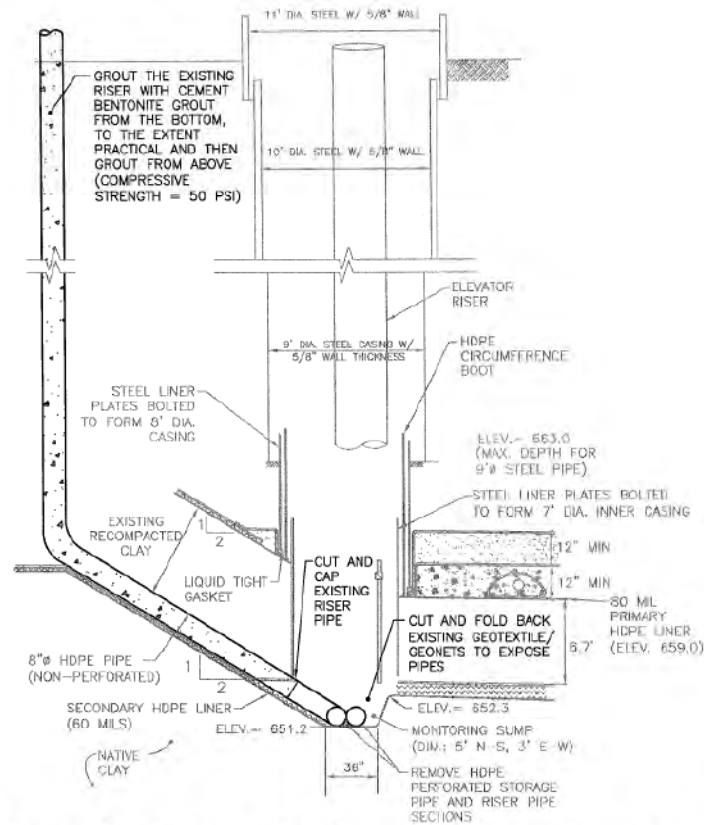


Figure 8. – Design of shaft access to secondary sump

allowed the contractor and major subcontractors to provide input as the final design was developed. Working as a single team, the Owner, designer and contractor provided valuable input in preparation of the final design. Of primary

concern to all parties was the safe execution of work. To this end, the contractor developed a comprehensive Health and Safety Plan to guide each step of the work.

The final repair design was packaged in such a way that a drawing, detailed construction sequence, Quality Assurance requirements, and Health and Safety requirements for each of the anticipated 17 major tasks was presented on it's own sheet relating specifically to that task. This system would allow the team to have easy reference to all pertinent information based upon the current task in progress.

REPAIR IMPLEMENTATION

Construction of the first access shaft was begun for repair of the primary cleanout riser in March of 2006 (Fig 9). This location did not require a breach of the primary liner and would serve as a “dry run” for subsequent shafts.



Figure 9. – Shaft excavation at Cleanout D-14

The shaft was successfully extended through 120 feet of waste and intercepted the leachate collection pipe on the primary geomembrane liner, where a new cleanout riser was installed to the top of the waste (Fig. 10).



Figure 10. – Leachate collection pipe within shaft at D-14

During the shaft design process and even through the start of construction, the design team, including the contractor, had continued to explore options that would avoid the need for penetration of the primary synthetic and clay liners with a shaft. The team had worked extensively with several pump manufacturers to develop or modify a pump that could fit within a small diameter “slipline” pipe and was short enough to extend past the deformed elbows and capable of lifting liquid over 130 feet (air lift pumps could not be used since sampling of the

liquid for volatiles was required). As the shaft at cleanout D-14 was being excavated, the perseverance paid off; a pump manufacturer was able to modify a newly developed pump that met the needs of the project.

A piston driven pump with an outside diameter of 1½-inches, flexible enough to pass through the deformed elbows and capable of lifting the secondary liquid over 130 feet made the “slipline” a viable option again for the secondary risers at sub-cells A-South, B and C. “Sliplining” the distressed secondary risers would avoid the need for breaching the primary liner. With an expedited regulatory approval, the team went forward with an appropriate design. The collapse of the vertical portion of the riser at sub-cell A-North initially was thought to require the use of a shaft accessed repair.

The “slipline” repair methodology included installing 1-inch to 4-inch diameter pipe (the lower 5-feet perforated) inside of the existing 8-inch to 12-inch secondary riser pipes. The annular space was then filled with filter sand to an elevation approximately 5 feet below the damaged elbow sections. A thin “choke” layer of fine sand was placed on the filter sand. High strength, low shrinkage grout was then placed as internal reinforcement through the elbow and to a point approximately 10-feet above the elbow. Because of the limited annular space and the need to assure complete filling of the pipe, as much as 17 cubic feet of filter and choke sand were added one cup at a time through a tremie pipe, washed into place by adding water (Fig. 11).



Figure 11. –Filter sand placement in Riser B

Water added during the filter sand placement operation was pumped out from the bottom to assist settlement of the sand through the elbow and into the storage pipes within the sump.

With cleanout ability restored at cleanout D-14 and pumping capability restored from secondary risers at sub-cells A-South, B and C, attention was turned to the last remaining secondary riser at

sub-cell A-North. At A-North a complete collapse of the vertical riser pipe at a depth of 57 feet below waste surface prevented insertion of a “slipline” pipe. The collapse had also prevented inspection of the deformed lower elbows for over one year, so the condition below the total collapse was unknown.

The decision was made to combine the two successful repair approaches previously used. Install an access shaft to the 57-foot depth, remove the damaged section of pipe, extend the remaining pipe back to waste surface, then install a “slipline” pipe and the piston pump. The first challenge was accurately targeting the shaft location. An inclinometer was used to determine the exact horizontal and vertical location of the collapsed section of pipe. Because the pipe was known to be at roughly a 30 degree angle from vertical, a 9-foot diameter access shaft was selected to provide working room to complete the repair, including butt-fusion welding of a new DR 17 riser pipe to the existing riser, and sweep the new section of pipe back to vertical (Fig. 12).

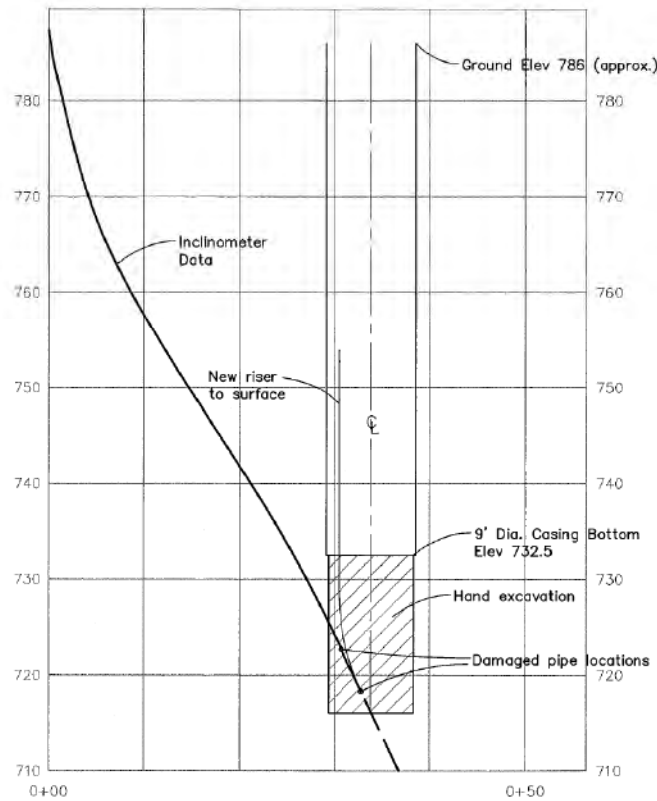


Figure 12 –Access shaft plan at sub-cell A-North

The 9-foot diameter shaft was extended to the collapsed section of the existing riser (Fig. 13), the damaged pipe was removed, and the new vertical riser pipe was installed to waste surface.



Figure 13 –Hand excavation around sub-cell A-North collapsed riser pipe

Once access was restored, video inspection of the lower elbow was completed and revealed that additional deformation of the elbow section had occurred. In fact, difficulty was encountered extending the 1-inch diameter push camera through the elbow. Insertion of several pipes, ranging in diameter from 3-inch down to 1-inch, was attempted. Only the 1-inch diameter pipe could be inserted full depth into the secondary sump. Since the piston pump casing was 1½-inch diameter without a “slipline” pipe, a further redesign of the pumping system was needed.

The pump manufacturer fitted the pump foot valve with a ½-inch diameter suction tube and tested the modified pumping system. Trials showed that the liquid could be lifted through the suction tube the expected 26 vertical feet to the pump foot valve where it was ultimately pumped to the waste surface.

To “slipline” the secondary riser at A-North, a 3-inch diameter DR11 pipe was used. The lower 50 feet was reduced to a 1-inch diameter DR11 pipe with the lower 5-feet perforated section. This allowed the 3-inch diameter pipe to be supported above the deformed elbow and the 1-inch diameter pipe to extend full depth into the sump. The 1½-inch diameter piston pump with 49 feet of suction tube was then threaded into the “slipline” assembly. As with the other slipline repairs, the annular space between the existing 8-inch diameter secondary pipe and the 1-inch diameter “slipline” pipe was filled with filter sand. The deformed elbow was then reinforced with high strength grout. The assemblies as constructed are shown in Figure 14. Upon completion, pumping capability was restored at the secondary sump at a rate of approximately one gallon per minute. This rate is sufficient to pump the secondary sump dry in a single shift and restored sampling capability at sub-cell A-North.

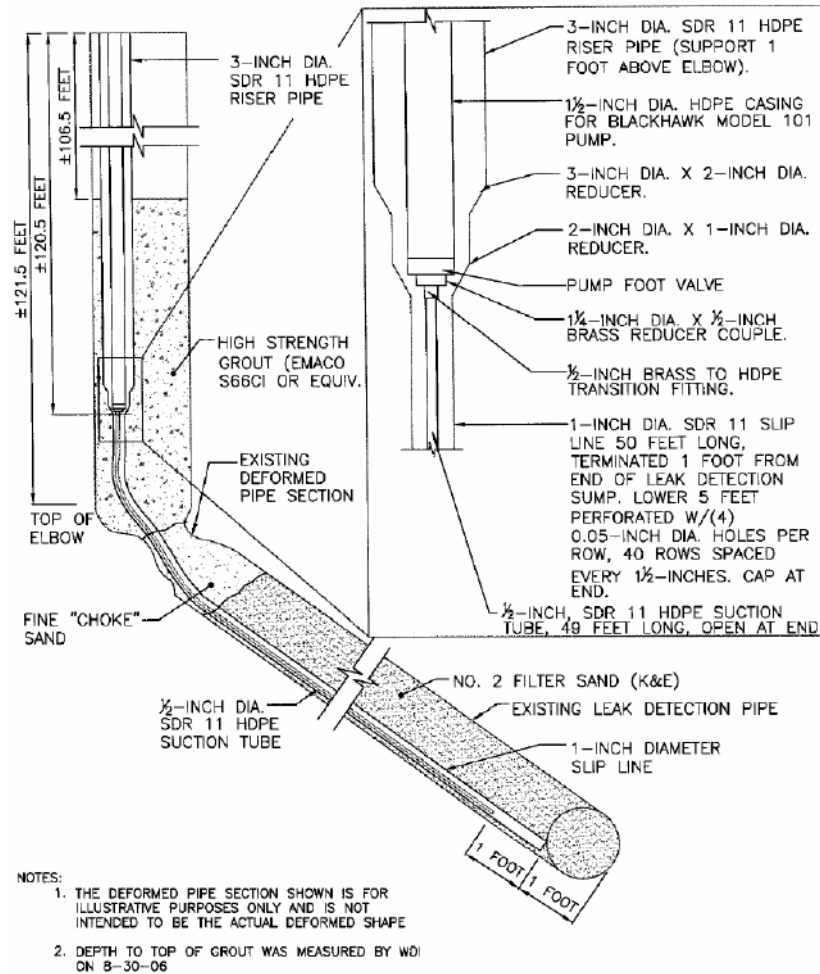


Figure 14 – “Slipline” at sub-cell A-North secondary riser pipe

Conclusion

Failure of riser pipes extending vertically from secondary leak detection sumps could be disastrous to a landfill owner/operator. This paper has presented a case study of a project that restored pumping and sampling capability to a hazardous waste landfill with four distressed secondary risers and one distressed leachate collection system cleanout riser under over 120 feet of hazardous waste. The authors have presented a condensed progression of events that lead to a comprehensive repair design that included excavation through the primary geomembrane and primary clay liners of a hazardous waste landfill.

Diligence on the part of the owner to continue to explore and develop all available options, even as construction began, lead to a non-intrusive repair solution that was preferable to all parties, including the regulatory agencies involved.

ACKNOWLEDGEMENTS

The authors would like to thank the management of Wayne Disposal, Inc. for allowing this case study to be shared. Particular thanks go to Mr. Kerry Durnen, P.E. Director of Operations for Wayne Disposal, Inc. Site No. 2. His attention to detail, willingness to support “out of the box”

approaches, and genuine desire to do the right thing blurred the line between client and consultant.

REFERENCES

Parsons, J., Lyang, J., and Durnen, K (2006) "Restoration Of Distressed Secondary Monitoring System At A Hazardous Waste Landfill" Proceedings of the ASCE 4th Forensics Conference, Cleveland, OH

Simpson Gumpertz & Heger Inc. (2004) Report "Investigation of Distress in Secondary Riser Pipes, Master Cell VI, Wayne Disposal, Inc., Landfill No. 2, Belleville, Michigan". Prepared for NTH Consultants, Ltd.

CONTACT:

James J. Parsons
NTH Consultants Ltd.
38955 Hills Tech Drive
Farmington Hills, MI 48331
Phone: 248-324-5329
Email: jparsons@nthconsultants.com

UNDERSTANDING AND MINIMIZING UNCERTAINTY IN GEOSYNTHETIC TESTING

R. Lacey, P.E., Geotechnics, Inc.

ABSTRACT

This paper describes a procedure for estimating the quality of laboratory test results in terms of test method precision and test result uncertainty. The technique can be used as a tool for resolving inter-laboratory discrepancies and enhancing the overall quality of test methods.

The sampling and testing strategies are governed by the spatially-linked variability characteristics typical of geosynthetics. Noticeable repeating patterns of the material properties as a function of location along the width and length of a roll of material dictate where the individual test specimens are obtained from the source and how they are grouped together to comprise a test sample. Then the necessary sample uniformity is generated without artificially homogenizing the geosynthetic under test. The resulting precision and uncertainty values will then be realistic and applicable to routine conformance test evaluations.

The measurement uncertainty assessment process is demonstrated with a geotextile source material and three test methods: mass per unit area, thickness and grab strength. The geotextile is sampled and tested in accordance with the test methods. Then the results are analyzed with rudimentary control chart statistics in order to calculate and monitor test method precision and uncertainty.

INTRODUCTION

Uncertainty in Geosynthetic Testing encompasses two controversial topics. One is the general uncertainty that we have when we compare a test result to results from another laboratory or to a specification value. The other is the uncertainty there is in the individual test methods themselves, that is, the uncertainty in the process that transforms the sample into a “number”.

Since I just confused myself, I thought it would be appropriate to investigate this “Uncertainty” phenomenon with a Lab Man’s approach. If Measurement Uncertainty is indeed a real attribute of test results, then all we need to do is run some tests. The Measurement Uncertainty should be right there in the data. We just have to extract it.

As it turns out, this extraction process is fairly simple: a typical geosynthetic sample is tested several times, while intelligently controlling the layout of the specimens and the conditions of the tests. The test results are plotted with standard deviation and means control charts to estimate precision and uncertainty.

The precision is the repeatability of the test method. It answers the question, “If I have a test result for a sample, what is the range of values that would result the test were performed again on the same sample?” The uncertainty, on the other hand, is the potential scatter of any individual test result, regardless of the result you might already have on the sample. The uncertainty was in the first test performed, and will be in the second and third tests, etc.

DEVELOPING THE SOURCE SAMPLE

The first step in the Measurement Uncertainty Assessment Process, or “MUAP, is the first step in any routine geosynthetic laboratory procedure; collect a sample of a geosynthetic that is typical of the test method under assessment. Our standards typically specify a one meter by roll width swatch of the material, which we refer to as the “Source sample”. The actual sample may have to be somewhat longer than 1 meter in the machine direction in order to generate the preferred numbers of test results given the individual test specimen sizes. In this example, we are testing a nonwoven geotextile for Mass per Unit Area in accordance with ASTM D 5261, Thickness per D 5199, and Grab Strength per D 4632.

In order to calculate the precision of the test method, the Source sample is tested three consecutive times under repeatability conditions, that is, single operator, single apparatus in a single day. Each of these sets of three test results is referred to as a repeatability unit, or RU. The layout of the test specimens on the Source sample are shown on Figure 1. The tests for the repeatability units were performed on triplicates in the cross machine direction as shown, with Test Results 1, 2 and 3 taken from RU 1, Test Results 4, 5 and 6 from RU 2, etc.

Figure 1

TEST SPECIMEN LAYOUT

RU 1	1	2	3	1	2	3	1	2	3	1	2	3	1	2	3	1	2	3	1	2	3	1	2	3	1	2	3	1	2	3			
RU 2	4	5	6	4	5	6	4	5	6	4	5	6	4	5	6	4	5	6	4	5	6	4	5	6	4	5	6	4	5	6	4	5	6
RU 3	7	8	9	7	8	9	7	8	9	7	8	9	7	8	9	7	8	9	7	8	9	7	8	9	7	8	9	7	8	9	7	8	9
RU 4	10	11	12	10	11	12	10	11	12	10	11	12	10	11	12	10	11	12	10	11	12	10	11	12	10	11	12	10	11	12	10	11	12

Mass per Unit Area

The mass measurements are tabulated in Figure M1 and plotted in Figure M2. A standard deviations control chart is constructed in M3, with the standard deviation of each RU plotted against the RU number. The average of the standard deviations, \bar{s} , is calculated (p units):

$$\bar{s} = \sum s / p = 0.049$$

The upper control limit is:

$$UCLs = B4 * \bar{s} = 2.568 * 0.049 = 0.125$$

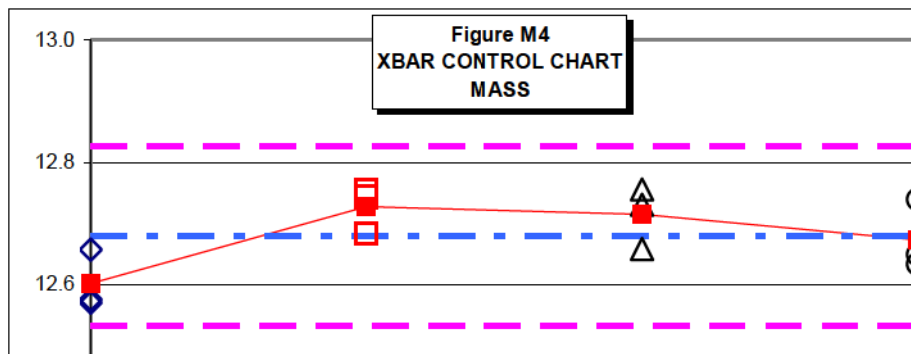
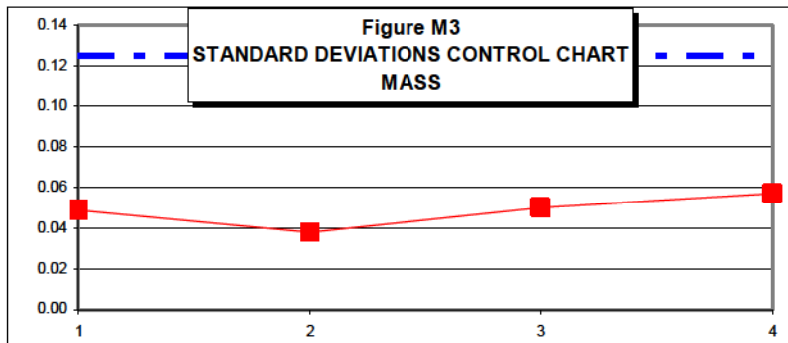
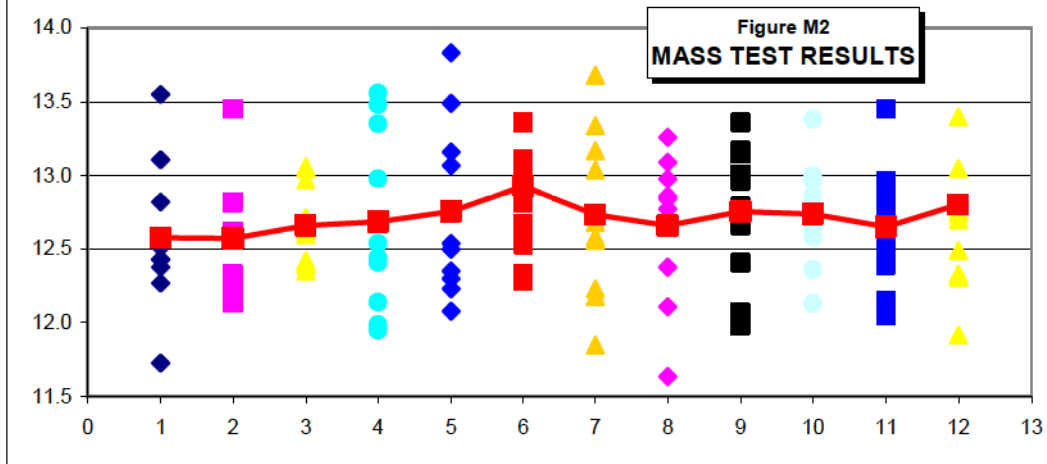
The standard deviations chart does not indicate anything remarkable about the within-unit variations. An estimate of the repeatability standard deviation, or within-lab test method precision, is computed from the average \bar{s} as:

$$sr = \bar{s} / c4 = 0.049 / 0.8862 = 0.055$$

Figure M1
MASS TEST RESULTS

	RU										AVE	MEAN	S.D.
	A	B	C	D	E	F	G	H	I	J			
RU1	12.27	13.55	11.73	12.43	13.11	12.51	12.82	12.38	12.43	12.53	12.58		
	12.33	13.45	12.23	12.56	12.62	12.82	12.13	12.17	12.81	12.59	12.57	12.60	0.049
	12.60	12.97	12.62	12.35	12.42	12.39	12.71	12.41	13.06	13.05	12.66		
RU2	13.56	13.35	11.95	12.54	11.99	12.98	12.41	12.44	12.14	13.48	12.68		
	13.49	13.16	12.23	12.30	12.08	13.07	12.54	12.35	12.50	13.83	12.76	12.73	0.038
	13.36	12.61	12.81	12.33	12.28	12.67	12.99	12.53	13.11	14.57	12.74		
RU3	13.68	13.17	12.58	13.04	12.56	13.34	12.68	12.18	11.85	12.23	12.73		
	13.09	12.77	12.84	12.86	13.26	12.98	12.66	11.64	12.38	12.11	12.66	12.72	0.050
	13.36	12.41	13.17	13.15	12.79	12.66	13.01	11.98	12.07	12.96	12.76		
RU4	12.96	13.00	12.69	13.38	12.13	12.65	12.58	12.36	12.78	12.86	12.74		
	12.73	12.92	12.47	12.96	12.81	12.56	12.15	12.05	12.39	13.45	12.65	12.67	0.057
	14.30	12.70	13.05	12.76	12.33	11.92	12.74	12.31	12.49	13.40	12.63		

AVERAGE: 12.68 0.049



The averages between repeatability units are examined next. First, the grand average of the four units is calculated, which is 12.68. The 3-sigma control limits then are:

$$UCL = 12.68 + 3 * 0.049 = 12.78$$

$$LCL = 12.68 - 3 * 0.049 = 12.58$$

The uncertainty standard deviation is estimated with the standard deviation of the RU averages, that is, the standard deviation of the means control chart, which is 0.057.

Summary of Mass per Unit Area Variability

Condition	Stdev	%CV
Test Method Repeatability	0.055	0.44%
Test Result Uncertainty	0.057	0.45%

Thickness Test Results

The thickness measurements are tabulated in Figure T1 and plotted in Figure T2. The standard deviations control chart is constructed in T3. The average of the RU standard deviations, \bar{s} , is:

$$\bar{s} = \sum s / p = 1.09$$

The upper control limit for the standard deviation chart is:

$$UCLs = B4 * \bar{s} = 2.568 * 1.09 = 2.79$$

Again, the standard deviations chart does not merit further investigation at this point in time. An estimate of the repeatability standard deviation, is computed from the average of the RU standard deviations, s as:

$$sr = \bar{s} / c4 = 1.09 / 0.8862 = 1.39$$

The grand average of the four units is 195.7. The 3-sigma control limits are:

$$UCL = 12.68 + 3 * 195.7 = 199.4$$

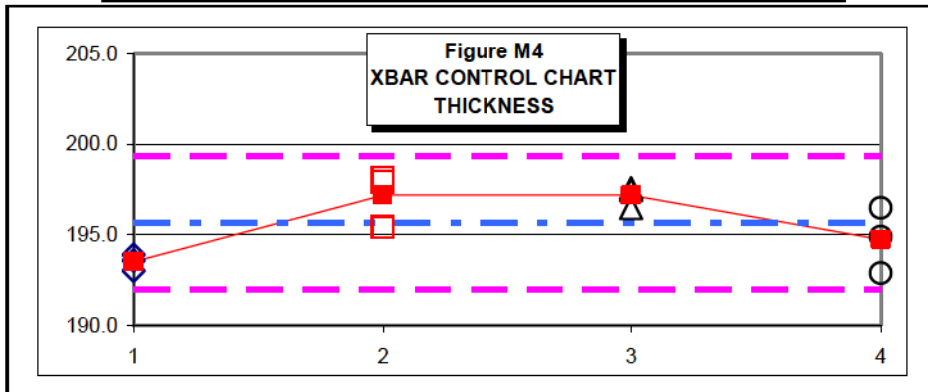
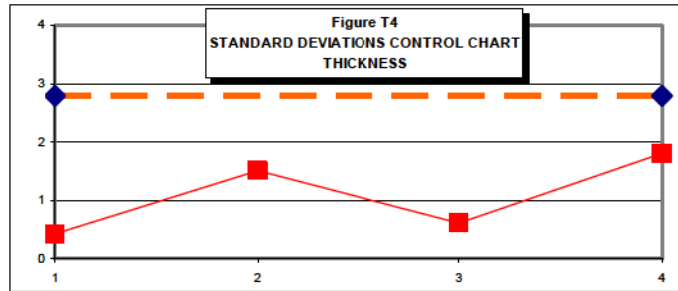
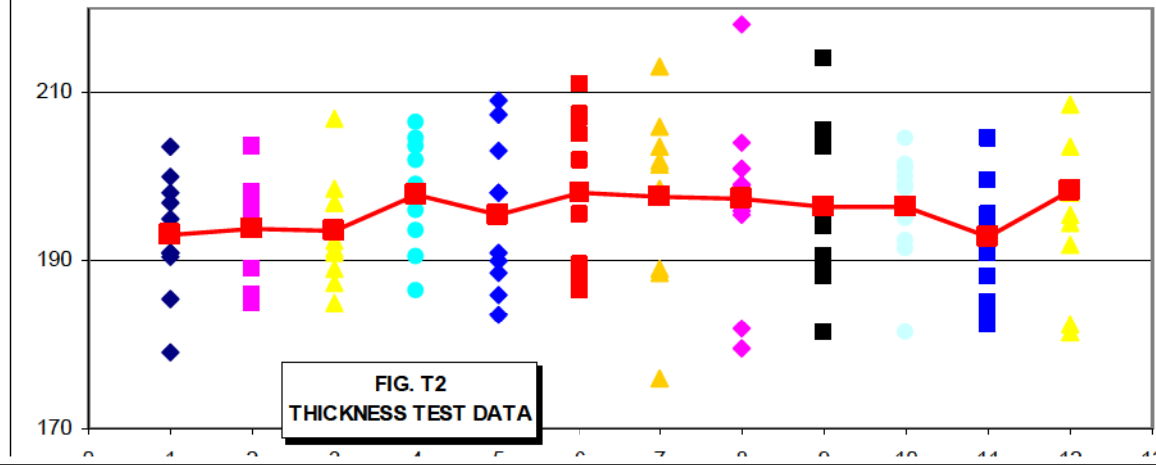
$$LCL = 12.68 - 3 * 195.7 = 192.0$$

The uncertainty standard deviation is the standard deviation of the RU averages, or 1.83.

**Figure T1
THICKNESS TEST RESULTS**

											RU		
	A	B	C	D	E	F	G	H	I	J	AVE	MEAN	S.D.
RU1	179.0	203.5	191.0	200.0	195.0	185.5	197.0	191.0	198.0	190.5	193.05		
	189.0	194.5	197.0	196.0	195.5	194.5	186.0	185.0	203.5	198.0	193.90	193.52	0.431
	191.0	198.5	197.0	192.5	189.0	191.5	207.0	187.5	197.0	185.0	193.60		
	206.5	203.5	199.0	196.0	186.5	197.5	190.5	202.0	193.5	204.5	197.95		
RU2	207.5	203.0	191.0	188.5	186.0	198.0	209.0	190.0	183.5	198.0	195.45	197.18	1.504
	207.5	205.0	202.0	188.0	186.5	189.5	207.0	189.5	195.5	211.0	198.15		
	201.5	213.0	206.0	202.0	188.5	203.5	198.0	198.5	189.0	176.0	197.60		
RU3	179.5	199.0	182.0	199.0	201.0	201.0	195.5	218.0	204.0	196.0	197.50	197.20	0.608
	214.0	194.0	205.5	204.5	190.5	188.0	203.5	194.5	181.5	189.0	196.50		
	199.0	204.5	201.0	195.0	181.5	192.5	191.5	200.0	201.5	198.5	196.50		
RU4	194.5	195.5	191.0	204.5	184.0	185.0	188.0	182.5	199.5	204.5	192.90	194.76	1.803
	230.0	198.0	192.0	198.0	181.5	182.5	208.5	194.5	195.5	203.5	194.89		

AVERAGE: 195.67 1.087



SUMMARY OF THICKNESS TEST METHOD VARIABILITY

Condition	Stdev	%CV
Test Method Repeatability	1.39	0.71%
Test Result Uncertainty	1.83	0.94%

Incidentally, the test method repeatability of 0.71% compares well with the precision statement published in ASTM D 5199, where the lowest repeatability listed of the four materials included in the inter-laboratory study is 3 %.

Grab Strength Test Results

The test data for grab strength is shown in Figures G1 and G2. The standard deviation control chart is presented in Figure G3, and the means control chart in Figure G4.

The repeatability standard deviation for the grab strength results is:

$$sr = \frac{s}{c4} = 8.2 / 0.8862 = 9.2$$

The grand average of the units is 405.7. The 3-sigma control limits are:

$$UCL = 405.7 + 3 * 9.2 = 433.3$$

$$LCL = 405.7 - 3 * 9.2 = 378.0$$

The uncertainty standard deviation for grab strength test results is 5.6.

The individual test result plot as well as the standard deviations control chart show that there might be some change developing in the source sample at RU4. If we are continuing to take samples in the machine direction from the source roll, we should watch for this trend to continue.

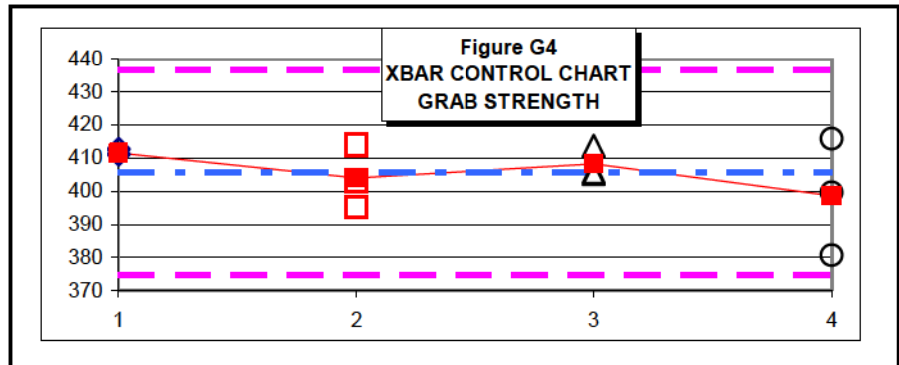
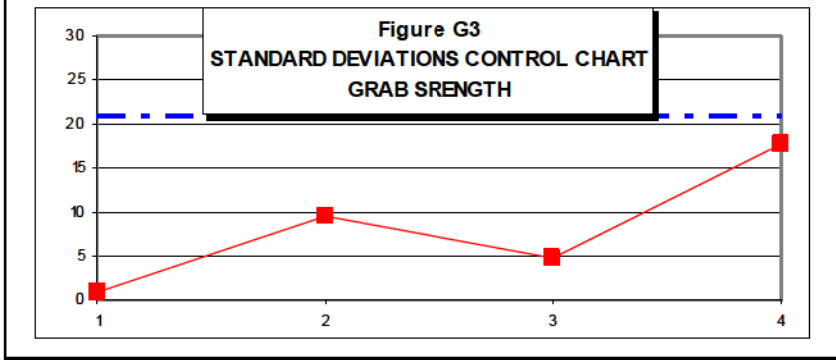
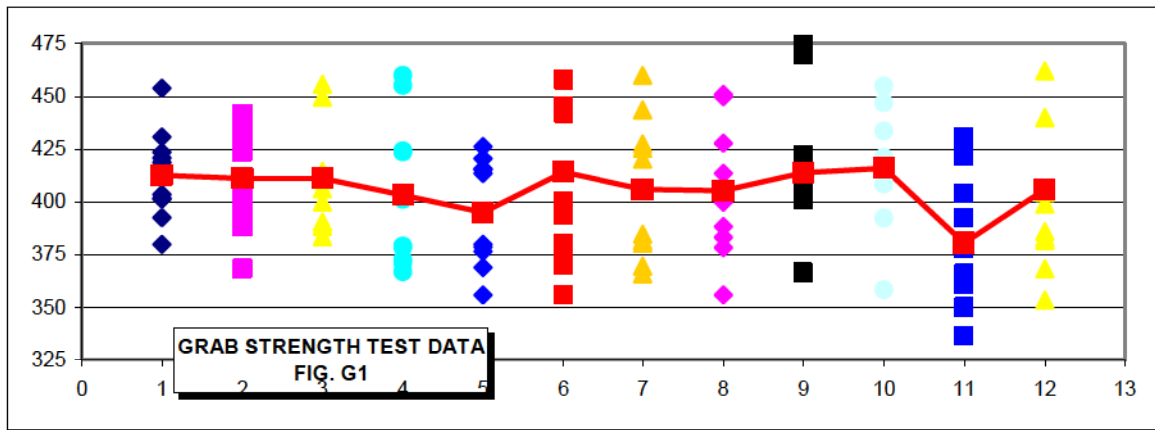
Summary of Grab Strength Test Method Variability

Condition	Stdev	%CV
Test Method Repeatability	9.2	2.3 %
Test Result Uncertainty	5.6	1.4 %

Figure G1
GRAB STRENGTH

												RU		
		A	B	C	D	E	F	G	H	I	J	AVE	MEAN	S.D.
RU1		420.7	453.8	392.5	403.4	418.7	401.5	430.8	401.8	379.9	423.5	412.66		
		423.4	437.4	397.1	368.3	429.8	441.7	388.1	388.8	404.8	432.7	411.21	411.66	0.864
		406.2	449.6	410.4	388.4	390.5	414.3	400.0	383.4	412.9	455.5	411.12		
RU2		459.8	423.6	366.8	379.0	401.0	424.2	378.5	371.1	372.5	455.1	403.16		
		420.6	378.6	355.9	380.0	376.5	413.5	415.7	368.9	415.3	426.3	395.13	404.08	9.449
		457.7	393.4	380.2	355.9	371.1	400.1	444.9	369.8	442.1	524.4	413.96		
RU3		459.8	425.2	381.6	384.6	380.4	443.6	427.5	366.0	369.5	420.1	405.83		
		450.9	427.7	383.2	404.4	449.7	413.4	378.4	355.9	388.3	399.9	405.18	408.22	4.714
		469.7	366.5	366.2	400.9	410.1	408.3	422.2	415.5	403.1	474.0	413.65		
RU4		446.7	417.8	412.6	433.4	413.4	421.2	392.4	358.4	408.2	454.6	415.87		
		430.9	365.8	360.9	365.7	377.9	392.7	336.5	350.3	403.8	421.3	380.58	398.66	17.661
		462.0	386.0	353.4	399.0	368.3	382.8	381.6	404.3	440.0	480.3	399.52		

AVERAGE: 405.66 8.172



REDUCING MEASUREMENT UNCERTAINTY

All of the uncertainty estimates have been confined to “repeatability” conditions. In order to estimate the total uncertainty for the test method in this laboratory, the various influence factors such as operators, apparatus, reagents, environmental conditions, etc. must be varied while performing the RU tests. The total uncertainty would then represent the range of test results that could have been generated on the sample submitted given the normal day-to-day random variations and options in the laboratory system.

Influence factors may cause increases or decreases, or “shifts”, in the test results, without affecting their variance. These shifts are referred to as “systematic effects”. The influence factors also may cause changes in the variability of the test results. These are referred to as “random effects”. Our experience is that the most dominant factors are systematic and cause discrete shifts in the data. An example of a systematic factor would be using excessive grip pressure while performing grab strength tests. This shifts the mean value of the data down due to premature grip-edge ruptures. On the other hand, too low of a grip pressure allows the stronger test specimens to slip in the grips, then gather and snag on the edges of the grips, while the weaker ones behave normally, causing an increase in the overall variance of the data.

Improvements in the quality of the results within a lab will depend on the sensitivity of the individual test method, on the experience and expertise of the personnel, and their proficiency with the measurement uncertainty assessment process.

REPRODUCIBILITY, SHIFT AND DRIFT

In order to determine the variability of test results between laboratories, the MUAP is merely extended in scope. One lab is the designated “Baseline Laboratory, or BL”. The BL distributes consecutive roll width Repeatability Units of the Source sample to the participating laboratories. The Baseline Laboratory retains several bracketing RU samples that span all of the samples distributed.

Then with each lab following the MUAP procedure for repeatability conditions, the between lab reproducibility of the test method as well as the between laboratory uncertainty can be estimated. The interstitial BL results are plotted vs the machine direction to identify possible “drift” of the Source properties across the samples distributed.

The magnitude of discrete “shifts” of the data between the labs, accounting for any identified material property drift, can then be quantified relative to the Baseline Lab as the “reference”. The test method uncertainty of a particular Lab X in the Interlaboratory study would be their uncertainty plus their specific “shift with sign” relative to the BL Lab. This information would be invaluable for resolving Interlaboratory discrepancy issues and would ultimately minimize uncertainty in geosynthetic test results.

CONCLUSION

The measurement uncertainty assessment process is a procedure for calculating test result uncertainty with a single typical geosynthetic sample source. While the statistics are elementary, the effectiveness of the process will depend heavily on the sampling strategy. The key is to preserve the “roll width” natural variations in the individual test determinations, while monitoring the test result drifts in the machine direction due to source material changes. Two immediate applications of this technique include product conformance testing and interlaboratory dispute resolution.

REFERENCES

- Subcommittee E11.20 June 2006 “Standard Practice for Estimating the Uncertainty of a Test Method Using Control Chart Techniques”, Work Item WK3561. (Note: This is not an ASTM standard; it is under consideration within an ASTM technical committee but has not received all approvals required to become an ASTM standard.)
- Ullman, Neil 1997 “Statistics in Standards and Standards Development, Getting to Precision and Bias Course Notes”, PCN #36-023033-00.
- ASTM Committee E-11 on Quality and Statistics 1991 “Manual on Presentation of Data and Control Chart Analysis”, Sixth Edition.
- ASTM D 4632-91 2006 “Standard Test Method for Grab Breaking Load and Elongation of Geotextiles”, Annual Book of ASTM Standards, Volume 4.13.
- ASTM D 5199-01 2006 “Standard Test Method for Determining the Nominal Thickness of Geosynthetics”, Annual Book of ASTM Standards, Volume 4.13.
- ASTM D 5261-92 2006 “Standard Test Method for Measuring Mass per Unit Area of Geotextiles”, Annual Book of ASTM Standards, Volume 4.13.

KEYWORDS

Geosynthetics, Measurement Uncertainty, Precision, Repeatability, Reproducibility, Laboratory Testing, Control Charts

CONTACT:

Rich Lacey

Geotechnics

Phone: 412-823-7600

Email: RLACEY@GEOTECHNICS.NET

Defining the Transmissivity Testing Requirements for Geonets and Composite Drainage Nets

Robert Mackey, P.E. S2L, Incorporated

INTRODUCTION

The primary function of a geonet and composite drainage net (CDN) is to collect and rapidly drain away liquid or gases from a relatively planar area to a collection trench or sump. These products are most frequently used above the geosynthetic barrier layers for bottom liner systems and/or caps for waste containment facilities. For purposes of clarification for the reader unfamiliar with these materials, a CDN is simply a geonet with a geotextile heat bonded to one or both sides of the product. Geonets and CDNs are typically manufactured using a structured high density polyethylene resin core of various thicknesses. The two most common core symmetries are known as bi-planar (2-layers) and tri-planar (3 layers). The bi-planar geonet is a matrix of two series of parallel strands, one series overlaid on top of another series of parallel strands in a crossing pattern (Figure 1). The tri-planar geonet is constructed with a thicker series of parallel strands at its center with two series of thinner parallel strands placed perpendicular to each other, one series above and one series below the center strand (Figure 2). The high porosity of these structured matrixes that allow for the increased liquid flow of the geonets in comparison to conventional granular drainage media.

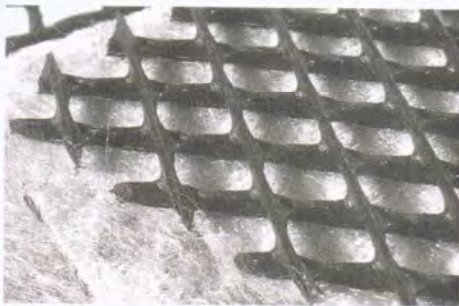


Figure 1. Bi-planar geonet

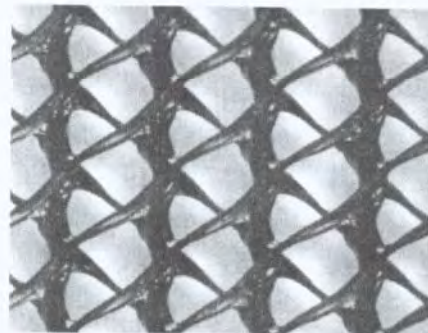


Figure 2. Tri-planar geonet

Each of the above geonets can offer significant benefits over granular media. However, there are limitations to each geonet and CDN that must be considered in their use and testing. There have been numerous papers regarding the design, use and testing of geonets and CDNs. However, these previous papers/presentations may not have addressed all testing requirements and considerations for these products in a step-by-step manner. The author hopes for that this paper will be used as a future reference document by design engineers and those specifying future transmissivity tests for geonets and CDNs.

It should be noted before the discussion proceeds below that there is a successful track record for the use of these products in geosynthetic drainage systems, particularly in leachate collection and leak detection. These products have been installed in at least a thousand sites and continue to demonstrate their suitability to their design function. The additional intent of this paper is to show how appropriate testing procedures can assist the user of these products to qualify and quantify the specific design performance requirements of the geonet/CDN.

DESCRIPTION OF TEST METHOD AND TEST APPARATUS

The test method typically used to determine flow capacity for geonets and CDNs is ASTM D4716-04 "Test Method for Determining the (In-plane) Flow Rate per Unit Width and Hydraulic Transmissivity of a Geosynthetic Using a Constant Head." The apparatus for this test method is relatively simplistic in its design and ability to measure a quantity of flow (Figure 3). By maintaining a constant head during the test and measuring the flow (Q) or rate of discharge from the apparatus, the flow capacity of the product can be determined using the following equation:

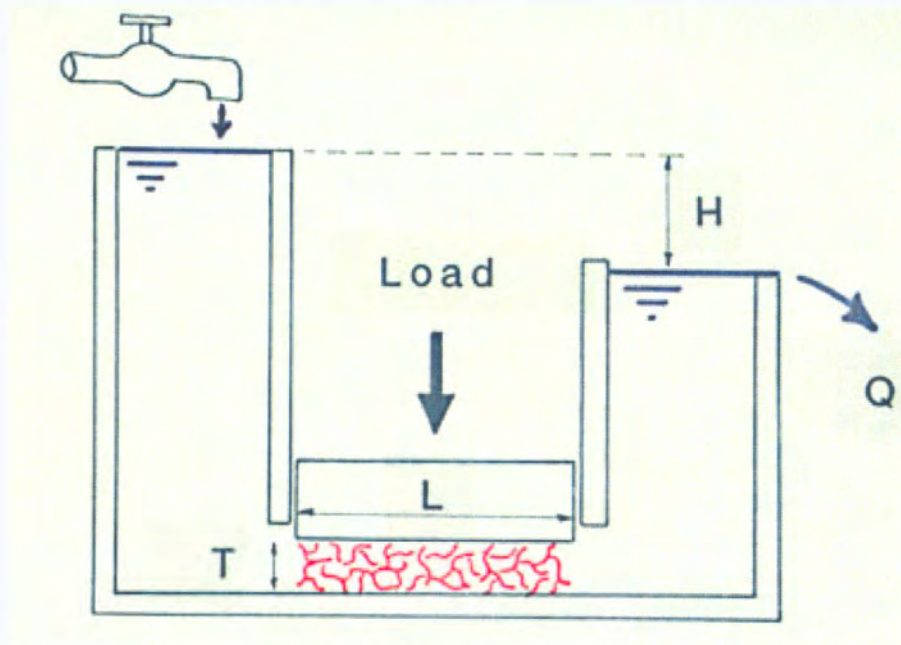


Figure 3. Schematic of the ASTM 4716 apparatus

$$\theta = \frac{Q/B}{i} = \frac{Q/B}{H/L} = kT \quad (1)$$

where:

- θ = transmissivity (m³/sec-m)
(volume per sec per unit width)
- Q = rate of flow (m³/sec)
- B = width of flow (m)
- i = hydraulic gradient
- H = head loss (m)
- L = length of flow (m)
- k = hydraulic conductivity of the sample (m/sec)
- T = thickness of flow

Equation (1) and Figure 3 reflect how the term defining rate of quantity of flow, or transmissivity (θ) is obtained. The use of transmissivity as a term to define the rate of flow is based on the need to quantify the flow rate in relation to the hydraulic gradient in which the product performs. The test apparatus has the ability of accommodating specific design cross-sections within the

apparatus and then applying load(s) to the geonet or CDN, with the load(s) based on design requirements. The normal load is applied vertically across the entire design cross-section, typically by a pneumatic bladder or pneumatic press. The hydraulic gradient for the test is set by adjusting the hydraulic head (H) prior to the start of the test. There is a belief that many apparatus in use have a lower limitation for the hydraulic gradient (i) of 0.1. In truth samples may be tested at hydraulic gradients of less than 0.1, using differential pressure transducers. The importance of testing the specimens at the design-specific hydraulic gradient will be detailed later in this text.

TESTING WITHIN THE PROPOSED DESIGN CROSS-SECTIONS

It cannot be stressed strongly enough that geonets and CDNs should be tested within the proposed design cross-sections, at least during the initial performance testing of the product. The performance of the geonet and CDN can be affected by the intrusion of adjacent materials into the open spaces, or apertures, of the polymeric structure. The amount of intrusion is directly related to the type of material overlying and underlying the geonet and CDN. The manufacturers do a good job quantifying the relative capacity of their products within their marketing documents and material data sheets. Most manufacturers' supply design information which is tested under different (design) conditions as contrasted with the values the manufacturers use for manufacturing quality control. The manufacturer's data (under the 15 minute, stainless steel plate interface) is based on specific conditions for quality control testing to ensure product consistency and do not represent field conditions.

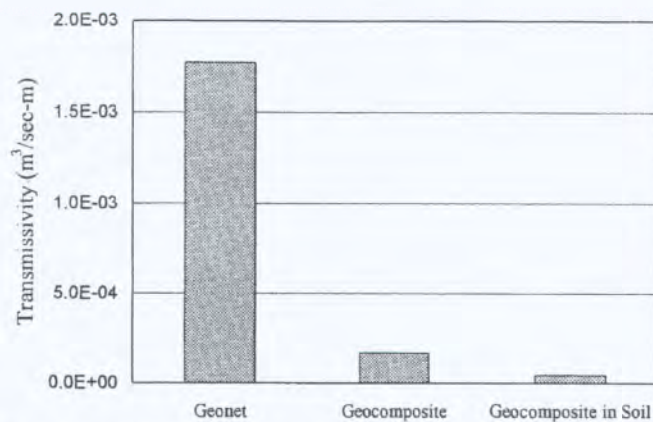


Figure 4. Transmissivity test results for a bi-planar geonet/geocomposite. (normal pressure = 720 kPa, gradient = 1) (Richardson and Zhao 1998)

The flow capacity of the geonet and CDN used in design must be tested under the most representative test conditions of the proposed design. The purpose of this recommendation is to allow those materials above and below the geonet/CDN to intrude into void space of the product. For example, sand placed above the CDN and loaded to design conditions will cause the upper geotextile to intrude into the space between each parallel strand (Figure 4). The degree of intrusion is related to the properties of the geotextile specified for the CDN and the amount of normal load applied to the design cross-section. Please note that the design engineer will need to supply the testing laboratory a sufficient volume of representative soil samples to perform the

number of required tests. The compaction requirements for the soil must also be specified in order to set-up the apparatus to reflect the design conditions. If a geosynthetic clay liner is adjacent to the geonet/CDN, the degree of saturation must be specified along with the load at hydration, prior to placement of the normal load on the design cross-section.

LOADING AND SEATING TIME

Geonets and CDNs are constructed of polymeric material, which can deform under load and over time. This gradual deformation of the polymeric structure is known as “creep.” The rate of deformation or creep is initially rapid, and decreases over time (Figure 5) (Allen 2000). As the degree of creep increases, the thickness of the geonet and CDN reduces; thereby diminishing the porosity or available volume through which the liquid/gases can move through the product. The amount of thickness reduction is dependent on the load placed on the product, density of the resin (lower densities of polyethylene have greater susceptibility to creep), structure of the core, properties of the laminating geotextiles and time.

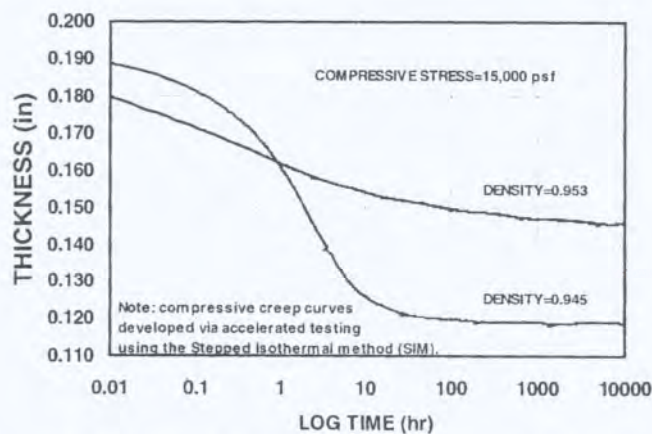


Figure 5. Effect of Density (g/cm^3) on Bi-Planar HDPE Geonet – Long-Term Compression Creep (Allen 2000)

Figure 5 shows that the majority of the creep will occur over the first 100 hours after the design load is applied. Therefore, if the geonet/CDN is subjected to large loads, such as those that occur in leachate collection systems, the design engineer should know the performance of the transmissivity test after the design load has been applied to the design cross-section for 100 hours of seating time. The 100 hour seating time may not be required for geonets or CDNs, for example if they are used for landfill caps that have 0.6 to 1 meter of soil overlaying the product. However, it is recommended that a seating time of at least 1 hour occur prior to running the transmissivity test for the geonet/CDN used for landfill cap designs.

The importance of the 100 hour seating time has been emphasized over the past few years, and this testing requirement can now be found in some State solid waste regulations (e.g. Florida). The requirement of the 100 hour seating time can be a difficult burden for the geosynthetic testing laboratory, which must dedicate test apparatus for over 4 days prior to performing the test. It can also be a burden to those requiring these tests due to the increase in geosynthetic testing cost and length of the testing period prior to the acceptance of the geonet/CDN for a

specific project. With a limited number of transmissivity apparatus available at an individual laboratory, those requiring the 100 hour seating time must allocate a sufficient testing period prior to the start of the construction project in order to obtain the conformance test results. The testing period for transmissivity conformance might be the most significant factor in determining the construction schedule for large projects where numerous conformance tests may be required.

There are potential alternatives to the required 100 hour seating time. The CDN may be compressed to the 100-hour thickness if a thickness vs time relationship has been established. This is called thickness-dependent transmissivity testing (Allen, 2000), instead of load-dependent testing, and requires sufficient previous testing and documentation to demonstrate that the time dependent compression is simulated by immediate compression to desired thickness, and that thickness-dependent flow will produce statistically similar flow measurements as 100 hour seating tests. However, it must be noted that the thickness during or immediately after the transmissivity test can be difficult to measure.

SPECIMENS PER SAMPLE PER TEST

ASTM D4716-04 requires the transmissivity testing of two (2) specimens per sample to obtain an average representative result for the sample of geonet/CDN. Due to how product is manufactured, this requirement is important if one is to obtain an acceptable precision and bias of the reported test result. The geonet structure is manufactured using circular rotating dies that extrude 2 sets of parallel strands (bi-planar) or 3 sets of parallel strands (tri-planar) to generate the desired structure of the product. It is the extrusion process of the geonet that causes a slight variation of the geonet thickness and strand alignment across a product's roll width. The subsequent heat-bonding process to adhere the geotextile to the geonet also causes a slight variation of the CDN thickness across the roll width. The requirement for testing two (2) specimens per sample attempts to average the variability in thickness of the geonet across the roll width. The ability to capture this variability can be seen in the precision and bias statement of the test method (Table 1).

The design engineer should consider variability in transmissivity across the geonet roll when selecting the appropriate safety factor for this engineered component. For example, Table 1 shows a range of intra-laboratory repeatability and inter-laboratory reproducibility of 6.1 to 15.2 percent and 7.3 to 42.6 percent, respectively. Based on the precision and bias statement, the design engineer should be using a safety factor of 1.15 to 1.43 to increase the design transmissivity requirement to account for the following:

limitations of test method,
variability in the ability of various technicians in performing the test,
variability of apparatus within an individual laboratory and between other laboratories,
variability of the specimen thickness and structure across the roll, and
variability of material during production.

If there is a history or concern raised regarding variability across the roll width, the design engineer should consider increasing the number of specimens to three (3) as a method to possibly decrease the variability in the results, and, thereby, lower the necessary safety factor.

Table 1 – Precision of ASTM D4716a

Material	Average l/s·m (gpm/ft)	Repeatability Limit ^b	Reproducibility Limit ^c	95 % Confidence Repeatability Limit	95 % Confidence Reproducibility Limit
Geonet	2.18 (10.5)	7.0 %	7.3 %	19.8 %	20.5 %
Composite I	0.212 (1.02)	10.6 %	21.2 %	29.8 %	59.5 %
Composite II	0.92 (0.443)	15.2 %	42.6 %	44.8 %	125 %
Composite III	0.931 (4.48)	6.1 %	17.1 %	20.7 %	57.8 %

a – Edited from Table 4 of ASTM D4716

b – Intra-laboratory results

c – Inter-laboratory results

Table 1 also indicates that other options to decrease the safety factor for design includes limiting the testing to a highly reputable accredited geosynthetic laboratory, and/or a specific technician, and apparatus. The options to decrease the safety factor(s) are discussed later in the text. However, when comparing the repeatability and reproducibility results of geocomposites, the design engineer’s greatest concern should be in evaluating the variability of the transmissivity test results listed in the manufacturing quality control certificates and from the CQA conformance testing. Significant variability in the thickness and transmissivity of the product is a good indication of poor manufacturing quality control and suspect performance of the product; therefore a need for a higher safety factor with the use of that particular product.

INSTALLATION LAYOUT IMPACT TO FLOW RATE FOR THE GEONET/CDN

As the bi-planar and tri-planar geonets/CDNs have different structures, the flow within these structures is also different. The bi-planar geonet/CDN has a crisscross pattern which inhibits liquid movement in the machine direction and cross-machine direction of the product. The liquid must flow under one strand and then over the next strand to move directly in the machine direction. However, as the bi-planar geonet is rotated to 45 degrees, the liquid no longer has to flow over and under the strands. This issue was noted by Sieracke and Maxson (2001), in which they reported preferential flow patterns within the geonet structures (Figure 6). The design engineer rarely considers the layout of the geonet/CDN in regards of its possible impact to the flow rate capacity of the product and how flow variation may occur due to flow direction and different loads applied to the product. This may not be an issue for landfill cap design in which the roll of geonet/CDN is installed down the slope and flow occurs in the machine direction. However, the layout of geonets/CDNs within leachate collection systems and leak detection systems could have a significant impact.

The typical geonet/CDN layout for a leachate collection or leak detection system is to install the product perpendicular or parallel to the leachate collection lateral. Without considering the actual liquid flow path, the design engineer specifies the geonet/CDN to be tested in the machine, without considering the possible flow in the cross-machine direction or other angles of flow. For example, a typical landfill with a rectangular footprint will the geonet/CDN installed either parallel or perpendicular to the leachate collection lateral. If the bottom liner is sloped 2 percent to the leachate collection lateral and the leachate collection lateral is sloped 1 percent, the angle of liquid flow is approximately 26.6 degrees from the direction of manufacturing (machine direction), if installed perpendicular to the leachate collection lateral. There can be significant changes in flow capacity based on the direction of flow through the geonet/CDN. The design engineer should account for the angle in which the specimen should be cut from the sample and the normal load in order to test the product for its actual flow path across the installed product.

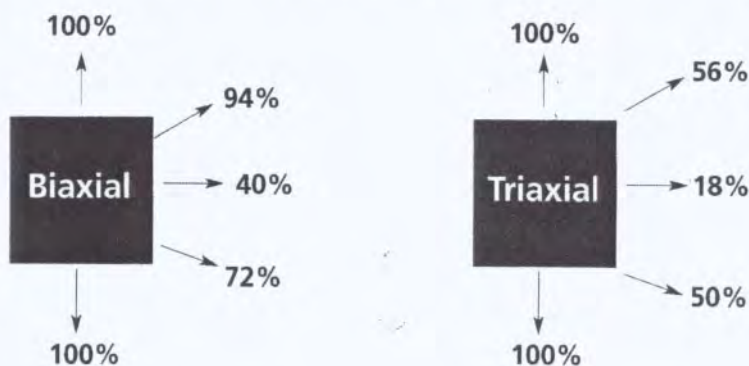


Figure 6. Flow characteristics of commonly used types of geonets (Sieracke and Maxson 2001) with 100% representing the direction of product manufacturing.

The structure of the tri-planar geonet/CDN allows for tremendous flow in the machine direction. However, this tremendous flow rate is greatly reduced as the angle from the machine direction increases, with much less flow in the cross-machine direction. Sieracke and Maxson reported an 82 percent reduction on flow in the cross-machine direction, in comparison to the machine direction. In the cross-machine direction, the flow path is blocked by the thick central core strand. The liquid must flow over or under the much thinner cross strands. If the engineer uses a tri-planar geonet/CDN in the design of the leachate collection or leak detection system, it is critical that the engineer consider the effect the layout of the product will have to the anticipated flow path of the liquid. It should also be noted that although the engineer may need to know the angle from the machine direction in which the specimen may be tested the product, the current test apparatus may not correctly generate an accurate estimate of the product's transmissivity due to edge effects related to test area limitations.

The current apparatus tests the flow capability through a cross-section of the product. It is the large central core of the tri-planar geonet that produces a tremendous flow rate in the machine direction. The central core acts like a series of pipes or channels for the liquid to flow. However, the central strands also inhibit an accurate measurement at angles between 0 and 90 degrees. Depending on the angle in which the specimen is cut from the tri-planar geonet, the flow direction is partially blocked by the central core and forces the liquid to flow under and over these central strands (Figure 7). At 45 degrees, either the upper or lower strand is perpendicular

to the flow and thereby either forces the flow through the compressed geotextile or causes a greater proportion of the liquid to flow to the opposite side of the geonet and along the strands parallel to the intended flow path of the apparatus. Although it might be possible for liquid to continue to flow along the central core, Figure 7 shows that some of these channels are blocked by the sidewalls of the apparatus.

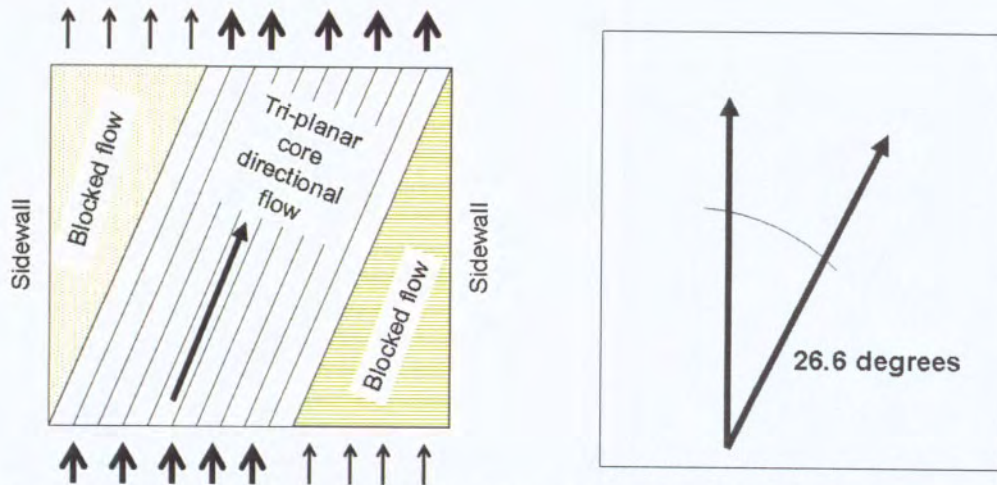


Figure 7. Tri-planar flow pattern caused by the geometry of the geonet structure and sidewalls of test apparatus

Depending on the slope upon which the geonet is installed and the hydraulic head moving the liquid through the structure, the liquid may continue to flow along the central core at a lesser slope within an unconfined structure. Until this issue can be further studied, designers should consider performing the test for the tri-planar geonet/CDN at the slope in which the product is installed, and not the slope in which the liquid wants to flow due to the base grade contours. Using the above example for the geonet/CDN installed perpendicular to the leachate collection lateral with 2 percent slope to the leachate collection lateral and 1 percent slope for the lateral, the slope and angle in which the liquid wants to flow is 2.7 percent and 26.6 degrees, respectively. The tri-planar geonet/CDN should be tested in the machine direction for the 2 percent slope; for this is the direction the liquid is forced to flow within this product.

HYDRAULIC GRADIENT

It is understood that as the hydraulic gradient decreases the transmissivity of a planar geonet/CDN increases. The literature shows that as long as a product is tested at a gradient of 0.1 and the design conditions result in an active hydraulic gradient of less than 0.1, the transmissivity of the product at design conditions will be greater than the transmissivity measured during testing at a hydraulic gradient of 0.1. There is much confusion regarding this phenomenon. In an attempt to clarify this statement it must first be stated that transmissivity is not a quantity of flow per unit time. As stated above, transmissivity is used to define this rate of flow at a specific hydraulic gradient. As the hydraulic gradient increases turbulence within the flow path of the bi-planar geonet structure also increases. Turbulence hinders flow. Thus, as the hydraulic gradient decreases the flow becomes more laminar (less turbulence) and the increased flow relative to gradient occurs. The enormous amount of testing of planar geonets has well served to document

the statement, "as the hydraulic gradient decreases the transmissivity of the planar geonet/CDN increases." However, it is always best to test the product using a gradient as close as possible to the design hydraulic gradient.

The above discussion has led some to recommend laboratory transmissivity testing at a minimum hydraulic gradient of 0.1 as this will result in a "conservative" measurement when actual field conditions dictate a lower hydraulic gradient. This is also based on the acknowledgement that visually observed manometers, used to establish and confirm the hydraulic gradient during the test, are not capable of accurately establishing head differences less than 1.2 inches. Indeed, even the 0.2 portion of a 1.2 inch head difference is challenging to measure and confirm by sight manometers only.

However, this guidance is no longer valid. New technology is now available for use in laboratories to establish and confirm very small differences in head and their related hydraulic gradients. Many laboratories use redundant systems for measuring the hydraulic gradient by employing pressure transducers in the in-flow and out-flow portions of the transmissivity test frame. These transducers are often positioned directly in the manometers. This "electronic" measurement of hydraulic head is yet another gradient indicator for labs to use and becomes very useful when head differences are relatively small. Important in the successful use of these transducers is their appropriate calibration. If soils are used in the transmissivity test profile, fines can sometimes contaminate or "cloud" the test water during testing, changing a calibration established with clean water only. Still, these measurement tools have improved the sensitivity of transmissivity test apparatus with regard to hydraulic gradient and afforded the important use of site specific conditions during testing.

PERMIT REQUIREMENTS VERSUS DESIGN REQUIREMENTS

There is concern regarding the long-term performance of the geonet/CDN under high load for leachate collection and detection systems. Regulators, in particular, appear to be concerned with this aspect of geonet/CDN design. Their concern is appropriate given that the thickness of the geonet/CDN will decrease over time. The reduction in thickness is dependent on the amount of pressure, resin density, product structure and time. However, it is rare that the compressive creep at high loads over time is the governing criteria for selecting a geonet/CDN. The use of the HELP Model shows that the performance requirement for the geonet/CDN is usually the greatest after the first lift of waste is placed in a landfill. This is due to the inability of a small amount of waste to absorb much of the rainfall during the initial operation of the landfill. As more waste is placed to a greater depth in the landfill, the impingement rate to the liner system and the amount of leachate that must be removed from the landfill decreases. The leachate generation rate for the landfill at the highest design loads might be 50 percent to 20 percent that of the initial leachate generation rate.

The design engineer may be required, by regulations, to specify the testing of the geonet/CDN at the maximum load expected for the proposed landfill. However, Figure 4 indicates that the reduction in geonet/CDN thickness after 100 hours of seating time is less than 5 percent. This small reduction in thickness of the geonet is not significant enough to hinder the flow of leachate once the rate of leachate generation declines to 50 to 20 percent of the initial rate. This issue is discussed further later in the text.

The design engineer should specify and test the geonet/CDN to meet transmissivity for two (2) design conditions. The first test should be at the maximum load expected for the geonet/CDN and the result of this test should meet or exceed the transmissivity required to remove leachate during that period of the landfill life. The second test should require the geonet/CDN transmissivity to meet or exceed the maximum leachate generation rate during the life of the landfill and the normal load expected during that period of the landfill life. This second test requirement corresponds to initial waste placement. The design engineer should expect that this requirement may be the controlling criteria for selecting the geonet/CDN.

SELECTION OF REDUCTION FACTORS

The selection of reduction factors (Table 2) should be based on the period of loading, geotechnical conditions, and environmental factors associated with a particular application. The possibility of biological and chemical clogging during the initial placement of waste should be minima, but this possibility will increase over the life of the facility. Since the placement of waste across the base of the landfill occurs over a short period of time prior to placement of subsequent lifts, the reduction factor due to creep should also be based on this same time period. For example, initial waste placement over the drainage layer occurs during first few months of operation. During this initial period of high flow requirements of the geonet/CDN, the possibility of chemical clogging, biological clogging, or long-term creep (i.e. 10,000 hour creep, discussed later in the text) is limited. The selected reduction factors for the geonet/CDN should reflect the initial operational period, and be increased over the life of the landfill.

GRI-GC8 uses the following equation (2) to calculate and specify the allowable equation to specified flow rate (q_{allow}):

$$q_{allow} = q_{100} \left[\frac{1}{RF_{CR} \times RF_{CC} \times RF_{BC}} \right] \quad (2)$$

where:

q_{allow} = allowable flow rate per unit time per unit width (m³/sec-m)

$$(from\ equation\ (1),\ q = \frac{Q}{B})$$

q_{100} = initial flow rate determined under simulated conditions for 100-hour duration

RF_{CR} = reduction factor for creep to account for long-term behavior

RF_{CC} = reduction factor for chemical clogging

RF_{BC} = reduction factor for biological clogging

Table 2 - Range of Clogging Reduction Factors (modified from Koerner, 1998)*

Application	Chemical Clogging (RFCC)	Biological Clogging (RFBC)
Landfill caps	1.0 to 1.2	1.2 to 3.5
Landfill leak detection	1.1 to 1.5	1.1 to 1.3
Landfill leachate collection	1.5 to 2.0	1.1 to 1.3

* This table was reduced in size from the table shown in GRI-GC8

Please note that equation (2) does not include a reduction factor associated with intrusion. GRI-GC8 states, "By simulating site-specific conditions (except for load duration beyond 100 hours and chemical/biological clogging), additional reduction factors such as intrusion need not be explicitly accounted for." The author agrees with this approach. However, the above equation does not take into consideration the variability of the results obtained from ASTM D4716, as stated in the earlier text and as represented by the precision and bias statement. Richardson and Zhao (1998) recommend the use of an additional factor of safety to be included in the above equation to account for various unknowns or uncertainties of the design, such as the variability in the test results. Richardson and Zhao inserted an additional factor of safety of "2" into the equation, thereby doubling the required flow rate and transmissivity of the specified product.

$$q_{allow} = \frac{q_{100}}{2} \left[\frac{1}{RF_{CR} \times RF_{CC} \times RF_{BC}} \right] \quad (3)$$

Although the author agrees with inclusion of this additional safety factor into the equation for q_{allow} , it may be an overly conservative approach. This additional safety factor should reflect the design approach by the engineer and testing requirements for the product. For example, by requiring three specimens per sample for each transmissivity test the variability of the test results may be reduced. The quality of the HELP model runs and assessment/design of the leachate collection system design can further reduce the need for this additional safety factor. The

purpose of this intense review is to reduce the difference between q_{100} and q_{allow} , resulting in a significant financial benefit. Based on the testing requirements, quality of the product and degree of design effort by the engineer, this additional safety factor could be significantly reduced. For example, applying lower factors of safety and lower reduction factors may offer the following:

$$q_{allow} = \frac{q_{100}}{2} \left[\frac{1}{(2.0) \times (2.0) \times (1.3)} \right] = 0.10q_{100}$$

$$q_{allow} = \frac{q_{100}}{1.4} \left[\frac{1}{(1.5) \times (1.5) \times (1.1)} \right] = 0.29q_{100}$$

By testing the geonet/CDN with a 100-hour seating time and calculating the factor of safety and reduction factors for the initial flow requirements during the first lift of waste, the above reflects the ability to specify a material closer to the design flow rate by a factor of greater than "2". In other words, a particular geonet/CDN could be used over twice the distance from the leachate collection lateral, without the need to specify a thicker and more costly product. The difference in the cost between a typical geonet/geocomposite and a higher performance geonet/CDN can be significant for large projects.

The design engineer should apply the appropriate reduction factors and additional safety factors for each significant design condition in order to specify the appropriate transmissivity, such as at maximum load and first lift of waste. Increased testing requirements for the geonets/CDNs should be reviewed as a means of decreasing factors of safety and reduction factors, thereby performing "value engineering" in order to save significant material costs for the project.

LONG-TERM CREEP REDUCTION FACTORS

GRI-GC8 utilizes the work of Giroud, Zhao and Richardson (2000) for determining the effect of long-term creep on the transmissivity of the geonet/CDN. Although the standard recognizes other methods to determine long-term creep, the use of equations 4 and 5 allows the design engineer to calculate the appropriate reduction factors for long-term creep for specific loads and time periods throughout the life of the landfill. A 10,000 hour thickness measure is typically used for this calculation, along with the thickness measurement from the 100-hour seating test. There is no longer a need to always wait for the results from a long-term, 10,000 hour test. An accelerated compressive creep test lasting only a few hours, using the Stepped Isothermal Method (SIM), may be used for this application. SIM allows the proposed geonet/CDN to be tested under a design specific load and the creep reduction factor predicted for a specific design life of the application. SIM is a useful design tool for the prediction of creep; however any results should be supported by long-term creep data from the product's manufacturer.

$$RF_{CR} = \left[\frac{(t_{CO} / t_{original}) - (1 - n_{original})}{(t_{CR} / t_{original}) - (1 - n_{original})} \right]^3 \quad (4)$$

where:

RF_{CR} = reduction factor for creep

$t_{original}$ = original thickness (m)
 t_{CO} = thickness at 100-hours (m)
 t_{CR} = thickness at $\gg 100$ -hours, e.g., at 10,000 hours (m)
 $n_{original}$ = original porosity (see Equation 5)

$$n_{original} = 1 - \frac{\mu}{\rho t_{original}} \quad (5)$$

where:

μ = mass per unit area (kg/m²)
 ρ = density of the formulation (kg/m³)

Note: The above illustration is based on the assumption that the flow is laminar. Flow is typically laminar if the medium conveying the flow is a geonet provided that the hydraulic gradient is small (i.e. ≤ 0.1). Therefore, the illustrated numeric procedure is for the drainage core only and does not apply to composite drainage nets which include geotextiles. (Giroud, et.al.)

However, as previously stated above, the initial placement of waste may only occur within the first few months of landfill operation. The 10,000 hour test reflects approximately 1.1 years of compression. The use of the thickness measurement at 10,000 hour may be overly conservative. It should also be noted that the 10,000 hour test is performed only on the geonet, and tested between two (2) plates. The test reflects the creep of the geonet material under these conditions. The result of this test is then used to determine a creep reduction factor for the geonet or CDN "under design conditions". The author acknowledges that this is the only methodology to calculate long-term creep currently available. With the increased emphasis in evaluating the performance of geonets/CDNs under as close to design conditions as possible, there is a need to obtain a better understanding of actual long-term creep based on actual design scenarios and accounting for possible changes in the geonet due to the process of bonding the geotextile to the geonet and how the geotextile undergoes dimensional changes over time or changes the loading pattern applied to the geonet structure.

SUMMARY

Geonets and composite drainage nets (CDNs) offer significant benefits over granular media. However, the design engineer must be aware of various limitations to the design and testing of these products. Through a greater understanding of the variability that is inherent in the test method and each product, the design engineer can specify the appropriate product to meet the design requirements for the project. Taking steps to limit this variability allows the design engineer to minimize reduction factors and safety factors, thereby specifying a material with reduced transmissivity requirements. Since a greater flow rate requirement for this material usually equates to an increased materials cost, a greater understanding of the transmissivity testing of the products offers the possibility of minimizing the cost for this drainage material. The design engineer must therefore take a step-by-step approach in specifying the test parameters associated with critical design periods for the product. Developing a testing checklist can assist the design engineer in communicating the test parameters to a geosynthetic testing laboratory in order to obtain the necessary results and limit the reduction and safety factors,

which in turn can reduce the cost for this product's use in the design. An example checklist is attached for the reader's use.

ACKNOWLEDGEMENT

The author appreciates the assistance of Sam Allen, TRI/Environmental, Inc., with whom numerous questions were asked, and an abundance of his time was freely given, in order for this author to develop a better understanding of the testing of geonets/CDNs and present them in an appropriate manner.

REFERENCES

Allen S. (2000), "Issues Regarding the Measurement of the Planar Flow of Geocomposite Drains used in Waste Containment Applications", Proceedings from the 5th Annual Landfill Symposium, Solid Waste Association of North America, Austin, Texas, June 2000

ASTM D4716-04, Test Method for Determining the (In-plane) Flow Rate Unit Width and Hydraulic Transmissivity of a Geosynthetic Using a Constant Head, ASTM International, 100 Barr Harbor Drive, PO Box C700, West Conshohocken, PA 19428

Giroud, J.-P., Zhao, A. and Richardson, G. N. (2000), "Effect of Thickness Reduction on Geosynthetic Hydraulic Transmissivity," *Geosynthetics International*, Vol. 7, Nos. 4-6, pp. 433-452.

GRI Standard – GC8 (2001), Determination of the Allowable Flow Rate of a Drainage Geocomposite, Geosynthetic Research Institute, <http://www.geosynthetic-institute.org/grispecs/gc8.pdf>

M. Sieracke and T. Maxson, (2001) "Common sense design with geosynthetic drainage material", Article for *Geotechnical Fabrics Report*, Oct./Nov. 2001, Vol.19, No. 8, pp 22-23

Richardson, G.N., Zhao, A. (1998) "Issues on Geosynthetic Drainage Systems in Landfills." Proc. Of the 12th GRI Conf. on Lessons Learnt from Geosynthetics Case Histories, Philadelphia, pp. 177-196

CONTACT:

Robert Mackey

S2L Incorporated

531 Versailles Drive

Suite 202

Matiland, FL

Phone: 407-475-9163

Email: bmackey@s2li.com

Example Checklist
 For
 Transmissivity Testing (D4716)

Questions:	Test 1	Test 2	Comments
1. What is the product to be tested?			
2. How many specimens per sample?			
3. What is the angle in which to cut the specimen?			
4. What is the design cross-section?			
5. What is the hydraulic gradient?			
6. What is the test normal load?			
7. What is the seating time?			
8. What is the soil compaction?			ASTM Method - ?
9. What is the hydration requirement for the GCL?			

Questions to answer based on the results:

What is the variability of the test results for this specific geonet/CDN?

Are the results sufficient to determine the necessary reduction factors and safety factors?

What is the thickness of the geonet/CDN prior to testing and at the end of the test?

Would increasing the normal load applied to the geonet/CDN to obtain the desired thickness save time and cost for additional testing?

Is a 10,000 hour creep test data required?

NAGS Student Paper Competition

Development of a low altitude aerial photogrammetry technique to quantify geomembrane wrinkles

M. J. Chappel, Graduate Student, GeoEngineering Centre at Queen's-RMC Queen's University; R. W. I. Brachman, Assistant Professor, GeoEngineering Centre at Queen's-RMC Queen's University; W. A. Take, Assistant Professor, GeoEngineering Centre at Queen's-RMC Queen's University; R. K. Rowe, Vice Principal (Research) and Professor, GeoEngineering Centre at Queen's-RMC Queen's University

ABSTRACT

A low altitude air photo system has been developed to quantify the geometry of geomembrane (GM) wrinkles at a large scale. Wrinkles which are caused mostly by solar heating and expansion are of particular interest for high-density polyethylene (HDPE) geomembranes. It is important to improve wrinkle quantification because wrinkles may lead to greater leakage through the geomembrane if a hole is at or near a wrinkle. Wrinkles also result in greater local tensile strains in the geomembrane.

A low altitude aerial photogrammetry technique to quantify geomembrane wrinkles is presented. The system consists of a Digital Single Lens Reflex (DSLR) camera, with remote infrared shutter control mounted on a tethered helium blimp. This system allows the operator to obtain clear, accurate near-vertical air photos.

The wrinkle geometry is analyzed from the low altitude air photos using the digital image processing capabilities and custom functions in Matlab. This allows the user to geometrically correct images; stitch images of parts of a site together into a single image; and select and quantify wrinkle geometry from the image of the site. Preliminary results on the length, connectivity and frequency of wrinkles are presented.

INTRODUCTION

Calculations commonly used to estimate leakage through composite liners typically assume that there is intimate contact between the geomembrane and the compacted clay liner or the geosynthetic clay liner beneath it. This contact restricts the horizontal flow of leachate between the two barriers in a low transmissivity interface zone. Wrinkles (also referred to as waves) substantially increase the potential leakage through a hole in the geomembrane when it coincided with a wrinkle (Rowe, 2005). They also increase the tensile strains in the geomembrane when covered and buried beneath waste (Gudina and Brachman, 2006). The wrinkles in high-density-polyethylene (HDPE) geomembranes predominantly form due to material expansion by heating from the sun.

Rowe et al. (2004) reported the distribution of wrinkles on the base of one particular landfill cell during construction. These wrinkles were randomly distributed with no discernable patterns, thus making it challenging to quantify their length and spacing. Wrinkles developed at, and

parallel to, the geomembrane seams as well at locations both perpendicular and inclined to the seams. The longest wrinkle was at least 17 m and may have extended the entire length of the cell (≈ 40 m). The shortest wrinkle was roughly 1 m long and the minimum spacing between wrinkles was about 0.5 m. The wrinkles inclined to the seams appeared to be connected to the long wrinkles at each seam. Such a distribution of wrinkles would provide an extensive preferential pathway for liquid migration beneath the geomembrane if there were any holes in the geomembrane at any point on the interconnected wrinkles.

Pelte et al. (1994) reported field observations of wrinkles for 1.5 mm thick black HDPE geomembrane overlying clay in a 30 m by 30 m cell in a landfill in France. They observed that major wrinkles occurred parallel to the length of the geomembrane roll at the location of seams, and also perpendicular to the seam direction. They reported large wrinkles between 0.05 to 0.1 m high and 0.2 to 0.3 m wide, and had a spacing of 4 to 5 m and appeared to extend across a significant width of the cell. They also noticed small wrinkles (less than 0.05 m high and 0.2 m wide) occurred perpendicular to the seams.

Touze-Foltz et al. (2001) quantified wrinkles in a 2 mm thick HDPE geomembrane over compacted clay using a photogrammetric technique. Wrinkle heights varied between 0.05 and 0.13 m, wrinkle widths between 0.1 and 0.8 m, spacing between wrinkles from 0.3 and 1.6 m, while the length of wrinkles was less than 4 m with most wrinkles 1-2 m long. The size of installation was only 7.5 m by 7.5 m, and consequently most likely limited the length of wrinkle that could form. However, the technique of Touze-Foltz et al. (2001) represents a very useful way of quantifying wrinkles at larger sites.

The objective of this paper is to present the details of the development of a low altitude air photogrammetry system to quantify the geometry of geomembrane (GM) wrinkles at a large scale. Details of the equipment used for obtaining the photos, the method of acquiring the photos, digital wrinkle analysis and the photo calibration are presented. Preliminary results from a large geomembrane installation are presented.

LOW ALTITUDE AERIAL PHOTOGRAPHY EQUIPMENT

The system consists of a Digital Single Lens Reflex (DSLR) camera with remote infrared shutter control, attached to a tethered helium blimp (Figures 1 and 2). A Canon 5D DSLR camera is used for this application. It has a 13.3 megapixel complementary metal oxide semiconductor (CMOS) that measures 35.8 mm by 23.9 mm. The high density of pixels allows a greater resolution than cameras with a lower pixel count. The area of the CMOS is very close to the format of a film 35 mm SLR camera, which permits the use of the full focal length of a lens, unlike most DSLR cameras.

The blimp stability is a function of both the blimp size and wind speed. The blimp is 6.4 m long by 2.1 m diameter, which optimizes platform stability and ease of handling on the ground. The wind speed at ground level is greater and less predictable because there are many localized currents due to uneven ground surface and differential heating. At an elevation of about 60 m, the wind speed is more constant. Thus a flying elevation of approximately 60 m is used in this

study for the best possible stability. The blimp can lift 4.8 kg, and requires a 15 kg anchor. Since the blimp is streamlined and has tailfins, it will always orient itself into the wind. This prevents the blimp from becoming a large kite, and reduces the lifting or dragging the anchor in high winds; higher winds result in more side-to-side movements, as well as a decrease in altitude as the blimp blows downwind. Increased camera motion must be accommodated by a higher shutter speed although this reduces the resolution of the image.



Figure 1 Photograph showing blimp equipped with a digital camera used to obtain images of geomembrane wrinkles.

LOW ALTITUDE AERIAL PHOTOGRAMMETRY TECHNIQUE

This blimp and camera system allows the operator to take clear, accurate near-vertical air photos by optimizing the following variables: altitude of the camera, focal length of the lens, resolution of the image, field of view (or ground coverage), and number of images required to capture the site.

The altitude of the camera is controlled by the length of the blimp tether. The control over the altitude of the camera using this method should be considered nominal, as the true height of the blimp, and therefore the camera, is ultimately controlled by the wind speed and direction. The wind direction affects the direction of the blimp, because the blimp will always point into the wind, and a greater wind speed will push the blimp downwind, and decrease the altitude. If the blimp moves in the air with gusts of wind, then the angle of the camera with respect to the

ground will also change. The choice of nominal camera altitude is particularly important as the scale, S , of a captured photo is determined by the ratio of the focal length, f , of the camera lens to the altitude, A , of the camera. In the present study, the focal length of the camera is 0.050m and the nominal camera elevation is 60m, leading to a scale factor of 0.050/60, or 1:1200.

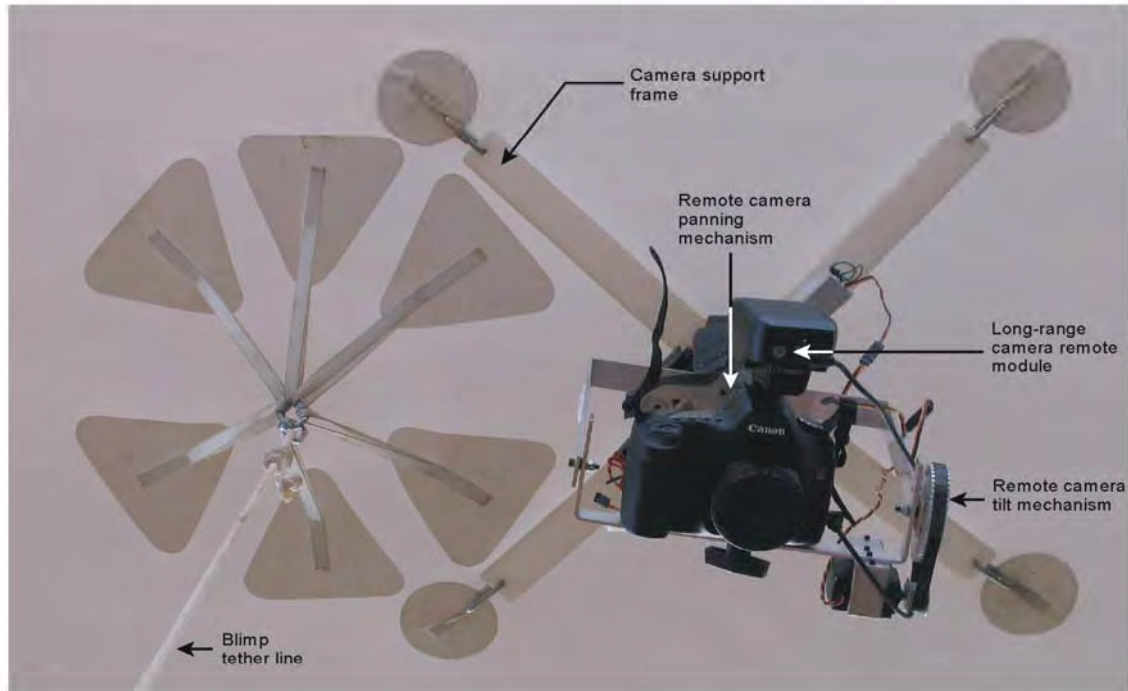


Figure 2 Photograph showing digital camera mounted to the underside of the blimp.

At a given blimp altitude, changing the focal length of the lens allows the user to change the object-space resolution and the ground coverage (i.e. field of view) of the photo. The object-space resolution describes the effective size in real-world units (i.e. mm) of a single pixel. This resolution can be calculated by considering a simple pin-hole camera model in which:

$$\text{ground coverage}(m) = \frac{\text{altitude}(m) \times \text{CMOS sensor width}(mm)}{\text{focallength}(mm)}$$

Thus, for the same camera orientation the object-space resolution of the images will be the ground coverage / number of pixels in the CMOS sensor. Whereas a shorter focal length will take wider angle photos and enable greater land coverage, this will be at the expense of the object-space resolution of the image and increased lens distortion. The resolution and image quality of the photo is very important, because the system must have sufficient resolution to define wrinkles of a few centimetres in height at a camera elevation of 60 m. For image collection, a 50 mm lens is the optimal size to maximize land coverage per photo (19.1m x 28.6m) while still maintaining the precision needed to detect small wrinkles. The 50 mm lens at 60 m above the ground results in a theoretical resolution of 1 pixel = 5 mm on the ground. This can commonly be achieved in the field under good conditions. Photos for analysis are taken as

close as possible to vertical. This minimises the image transformation errors when correcting the projection of the image.

During data collection, there is a theoretical minimum number of photos required to cover the entire field site. In practice, since the photo content and quality are initially unknown, with an unknown camera location, hundreds of photos must be taken to choose the best set of images required to produce a single image of the entire GM.

XY PLANE WRINGLE GEOMETRY ANALYSIS

The black GM reflects enough light that the wrinkles are easily delineated by the contrast difference between the wrinkle reflecting the sunlight and the flat black of the non-reflecting flat portions. The wrinkles are linear white features on the black geomembrane (Figure 3).

The wrinkle geometry is determined by manipulating and analyzing the low altitude air photos with the image processing features and custom functions developed with Matlab. For this analysis, a single large image of the GM area is created from a selection of photos that cover the entire area to allow the analysis of the full area.

The wrinkles are subsequently located and quantified. The user digitally selects the wrinkles and the continuity of the linear features. The vectors created are located by a Matlab function which determines the geometric wrinkle properties of interest: length, connectivity and frequency, as well as the hydraulic connectivity.



Figure 3 Air photo of geomembrane installation. 1.5 mm smooth HDPE; Camera elevation 65 m; Latitude 43°16' N; Air temperature 28°C; 1:20 pm Aug 18 2006

CALIBRATION OF IMAGES

Calibration is achieved by using the surveyed control points (CPs) as known points in the photos of the GM. This allows the photos to be geometrically corrected and stitched together to create one large image of the entire GM with a known scale. The scale chosen is one pixel represents 10 mm on the ground, which is a lower resolution than the original photo with one pixel representing 5 mm on the ground. This reduces the file size of the large image, and simplifies further measurements and quantification.

To develop an image of the entire GM area, a grid of labelled CPs every 10 m were drawn and labelled on the geomembrane. The spacing of 10 m ensures that there will always be many CPs in each picture. Each CP is marked on the GM by an “X” and is labelled with a grid coordinate. These ground control points are surveyed using a total station, and are visible in the photos. By connecting the grid locations of the CPs to the markings in the photos, the user can determine the orientation and scale of the objects in the photo in real world units. This also allows the user to further quantify the images.

Geometrically corrected images are created from the original photographs, using the known locations of the CPs. The individual images are then digitally stitched together to create one large image of the site, once again by utilizing the actual surveyed location of the CPs.

In a vertical air photo, there is geometric distortion due to three dimensional objects being projected on a two dimensional plane. This distortion results in a change in scale between the centre of the photo and the edges. In a geometrically corrected image, this distortion is eliminated by determining the three dimensional coordinates of objects of several points in each photo. This correction is completed by the user manually choosing the points on the digital photo and inputting relative coordinates into a custom Matlab function.

After photos have been geometrically corrected, the grid of CPs can be used to stitch all of the geometrically corrected images of the field site. This creates one large image with a scale of 1 pixel represents 1 cm.

PRELIMINARY RESULTS

The air photo shown in Figure 3 was obtained during installation of a 1.5 mm thick, smooth HDPE geomembrane. The site was at a latitude 43°16' N and the image was captured at 4:09 pm on August 17, when the air temperature was 24°C. The camera was at an elevation of 60 m.

Wrinkles parallel, perpendicular and inclined to the geomembrane panels are visible in Figure 3. There were at least 76 wrinkle features identified over the 1172 m² area capture in this image. If extrapolated, this represents nearly 650 wrinkles per hectare. The minimum wrinkle length was 0.5 m, maximum wrinkle length was 29 m. Sixty-eight percent of the wrinkles had lengths

between 1-5 m, while 9% has lengths between 20-30 m. At many locations, it appears that adjacent wrinkles may be interconnected as they intersect and join each other and thus the length of hydraulically connected wrinkles is much greater than the maximum wrinkle length.

SUMMARY

High resolution, digital images have been successfully used to capture wrinkle formation in geomembrane liners. Following photogrammetric principles, the altitude of the camera platform (in this case, a 6.4 m long blimp), the camera lens, the land coverage, and the resolution of the photos have been optimized to yield images of sufficient quality to define the spatial orientation of wrinkles over large areas. The wrinkles are analyzed using the image processing toolbox in Matlab, as well as custom functions. The photos are calibrated and connected together to create one large image of a GM installation. Work is currently ongoing to gather and analyse wrinkle image data from different field installations to better quantify the process of wrinkle formation in geomembrane liners.

ACKNOWLEDGEMENTS

This study was financed by the Natural Sciences and Engineering Research Council of Canada (NSERC). The authors are grateful to their industrial partners, Solmax International, Terrafix Geosynthetics Inc, Ontario Ministry of Environment, Gartner Lee Ltd, AMEC Earth and Environmental, Golder Associates Ltd., and CTT group.

Corresponding author: R.W.I. Brachman; brachman@civil.queensu.ca; Phone: (613) 533-3096

REFERENCES

- Gudina, S. and Brachman, R.W.I. 2006. Physical Response of Geomembrane Wrinkles Overlying Compacted Clay, *Journal of Geotechnical and Geoenvironmental Engineering*, **132**(10): 1346-1353.
- Pelte, T., Pierson, P. and Gourc, J.P.(1994) Thermal analysis of geomembranes exposed to solar radiation, *Geosynthetics International*, 1(1): 21-44.
- Rowe, R.K. (2005) "Long-Term Performance of Contaminant Barrier Systems", 45th Rankine Lecture, *Geotechnique*, **55** (9): 631-678.
- Rowe, R.K., Quigley, R.M., Brachman, R.W.I., and Booker, J.R. 2004. *Barrier Systems for Waste Disposal Facilities*, Taylor & Francis / Spon, London, U.K., 579 p.
- Touze-Foltz, N., Schmittbuhl, J., and Memier, M. (2001) Geometric and spatial parameters of geomembrane wrinkles on large scale model tests, in *Proceedings of Geosynthetics 2001*, Portland, USA, pp. 715-728.

CONTACT:

Melissa Chappel

GeoEngineering Centre at Queen's-RMC

Civil Engineering, Queen's University

Kingston, Ontario

CANADA

Phone: 613-533-6000 ext. 77142

Email: chappel@civil.queensu.ca

ASSESSMENT OF GEOTEXTILE FILAMENT PROPERTIES AND SIZE VARIATIONS DURING INTERFACE SHEARING

Duhwan Kim, and J. David Frost, Georgia Institute of Technology

ABSTRACT

The shear induced micro-mechanical interaction of geotextile filaments and geomembrane surface texture elements have been quantified using needle punched nonwoven geotextiles in combination with a coextruded HDPE geomembrane. The tensile properties of single filaments from three geotextiles were determined using an advanced optical experimental setup. The change in filament diameter was monitored at different tensile strain levels, using a helium neon gas reflectometer. A sample preparation method of epoxy resin impregnation followed by optical image analysis was applied to allow the sensitive geotextile microstructure at different stages of interface shear loading to be observed. The variations in filament size distributions were quantitatively evaluated under various boundary conditions. The filaments at strain levels corresponding to peak shear resistance showed the largest change in diameter and indicated that 50 % of the filaments were smaller than $27 \mu m$ at a normal stress of 100 kPa. In contrast, for compressed but unsheared specimens under the same normal stress, the corresponding filament diameter was $32 \mu m$.

INTRODUCTION

During the past few decades, various manufacturing methods have been developed to produce textiles suitable for geotechnical engineering applications. Needle punched nonwoven (NPNW) geotextiles are amongst the more common geotextiles used in various field applications. NPNW geotextiles consist of spatially curved filaments that are often assumed to be randomly oriented and isotropically distributed. Due to difficulties in direct observation, the micromechanical behavior of the internal geotextile structure has received limited attention. In this study, the effects of interface shearing against geomembranes on the geotextile microstructure is discussed in terms of tensile stress-strain-diameter response of the filaments as a function of boundary load conditions.

TENSILE PROPERTIES OF SINGLE GEOTEXTILE FILAMENTS

Most previous studies into the interaction between geotextiles and geomembranes have been limited to mechanical responses from large-scale perspectives. For example, Frost and Lee (2001) investigated the role of geomembrane textures on the evolution of interface friction against NPNW geotextiles, and quantified the degree of wear of geomembrane surface textures in terms of surface roughness parameters. Similarly, while Hebel et al. (2005) studied geotextile-geomembrane behavior in terms of "hook and loop" interaction, their experimental efforts focused on global rather than filament level response. It is obvious that the interface resistance is determined by the combined response of textures and filaments, however the sensitive unbonded nature of the filaments in nonwoven geotextiles have rendered the direct measurement of shear induced changes in their structure impractical to date.

The sample preparation and image analysis techniques used in this study enable the internal structure at geotextile-geomembrane interfaces to be observed (Kim and Frost, 2005; 2006). In order to quantitatively analyze the localized interlocking between geotextile filaments and geomembrane texture elements, the ability to characterize the tensile properties of single filaments is essential. Tensile testing with single filaments is also potentially useful for designing new products and for predicting material durability.

Various techniques have been developed to characterize the tensile properties of single filaments and fibers. Typical test methods can be categorized into two types: (1) constant-rate-of-elongation (CRE) tests (Hindman, 1948); (2) constant-rate-of-loading (CRL) tests (Krais, 1928; de Meulemeester and Nicoloff, 1936). Due to creep effects, the two methods are known to provide different results if the stress-strain responses are non-linear. It is known that the CRE method shows higher strength values at low strain and lower values at large strain because of the greater amount of cumulative creep (Morton and Hearle, 1993). Specific test procedures and analysis methods are described in ASTM D 3822 and D 3379.

Even for natural fibers with low homogeneity and isotropy, fiber diameter or fineness, is known to be an important parameter that influences various physical properties of fibers and textiles including stiffness, torsional rigidity, reflection of light, absorption of liquids, vapors, cohesion, and twist (Morton and Hearle, 1962; 1993). One of the most popular and traditional methods of measuring a fiber diameter is to use the projected surface image under a microscope. If the fiber has an oval cross sectional shape, this method is achieved by dispersing a fiber 0.8 mm long in a suitable mounting medium and then observing the specimen in random directions. Other methods include the gravimetric (ASTM, 1954), air-flow (Lord, 1955), and vibroscope methods (Gonsalves, 1947).

Materials Tested

Materials used in this study include two polypropylene (PP) geotextiles, one polyethylene (PE) geotextile, and a textured HDPE geomembrane that are all widely used in practice. The geotextiles are needle punched nonwoven types and their physical properties are listed in Table 1.

Table 1. Physical properties of the geotextiles.

Type	Mass per unit area ¹ (g/m ²)	Tensile properties ²		Puncture strength ³ (N)	Trapezoidal tear strength ⁴ (N)	Apparent opening size ⁵ (mm)
		σ_v (N)	ϵ_v (%)			
NPNW PP ⁶	270	955	50	525	420	0.180
NPNW PP	405	1,420	50	835	555	0.150
NPNW PE ⁷	271	1,023	60	444	356	0.210

Notes: ¹ASTM D 5216; ²ASTM D 4632; ³ASTM D 4833; ⁴ASTM D 4632; ⁵ASTM D 4751; ⁶Polypropylene; ⁷Polyethylene. Data from manufacturers literature.

Table 2. Physical properties of the geomembrane.

Type	Thickness ¹ (mm)	Density ² (g/cm ³)	Tensile Properties ³			
			σ_v (N/mm) ⁴	σ_b (N/mm)	ϵ_v (%)	ϵ_b (%)
Textured HDPE	1.5	0.94	16	23	13	150

Notes: ¹ASTM D 5199; ²ASTM D 1505; ³ASTM D 1603; ⁴N/mm-width. σ_y =stress at yield; σ_b =stress at break; ϵ_y =strain at yield; ϵ_b =strain at break. Data from manufacturers literature.

The geomembrane has a nominal thickness of 1.5 mm and yield tensile strength of 16 N/mm-width. It has a carbon black content of 2% and surface texture that is generated by the coextruding process. The surface roughness profile of the geomembrane measured using a stylus profilometer indicates that the sample is categorized as a moderately textured geomembrane based on the description proposed by Dove and Frost (1996). Detailed information about the selected geomembrane is shown in Table 2.

Experimental Setup and Test Method

Tensile properties of single geotextile filaments were measured using an experimental device at the Georgia Institute of Technology for measuring and recording the stress-strain response of filaments. The device had a force resolution of 0.0002 grams, maximum force of 35 N (3500 gram-force), and strain resolution of 1×10^{-6} mm. A single fiber is centerline mounted using glue on a paper tab that has a slot at the center. Figure 1a presents a schematic diagram of a mounted specimen. The filament-mounted tab is gripped with a set of stationary jaws (Figure 1 b) and then strained until the specimen is exposed to a small load less than one tenth of gram-force (Figure 1c). The tab is initially pulled using delicate control of the tensile force to ensure the axial alignment of the filament specimen. After applying this initial force, the paper tab is cut gently at the middle points of either side, ensuring that the force applied to the filament does not exceed the allowable variation range. The gage length (net measurement length of the filament) is 25 mm, and the extension rate is controlled to a constant value of 0.1 mm/sec. Data are collected at the rate of 10 points per second (100 points per 1 mm extension). All other sample preparation and measurements are conducted based on the procedures described in ASTM D 3379.

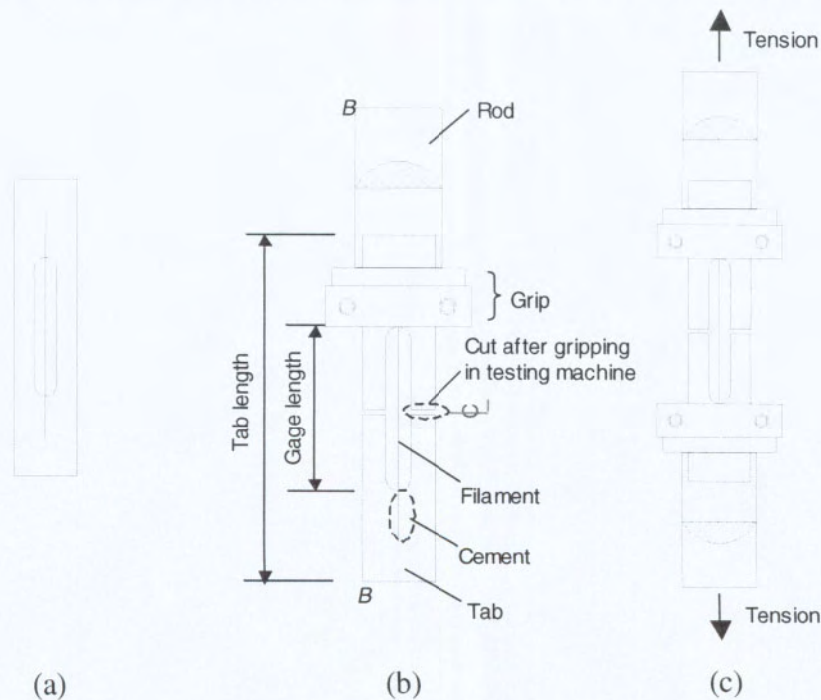


Figure 1. Specimen mounting method of a single filament: (a) tab and filament, (b) tab and filament in grip; (c) testing configuration.

Observing the change of filament diameter under tensile strain is required in order to be able to evaluate the subsequent shear induced change of filament sizes. Observing the surface image of a filament under a microscope is a widely used method to acquire the nominal diameter in practice. However, maintaining the required optical focus on a filament during tension testing is very difficult. This is because an optical microscope usually does not satisfy the two requirements for focusing at the same time: (a) a large range of measurement depth; (b) sufficient reflection of the light from the filament surface into the eyepiece of the microscope. Delicate focusing is essential to quantitatively and accurately measure the changing diameter of a filament in space and has technical limitations with conventional methods.

To overcome such measurement difficulties, the diameters (d) of single filaments were monitored at various strain levels using a helium neon gas deflectometer. This method is based on Bragg's law of diffraction (1913) as shown in equation 1.

$$d = \frac{m\lambda D}{\Delta y} \quad (1)$$

where, λ is the wavelength of the laser beam, D is the distance between the filament and the image wall that the deflected lights reach, Δy is the interval of the reflected light element in which the center and n th bright zone of the reflected light image are measured, and m is a constant determined by the interval of the bright span of the reflected image.

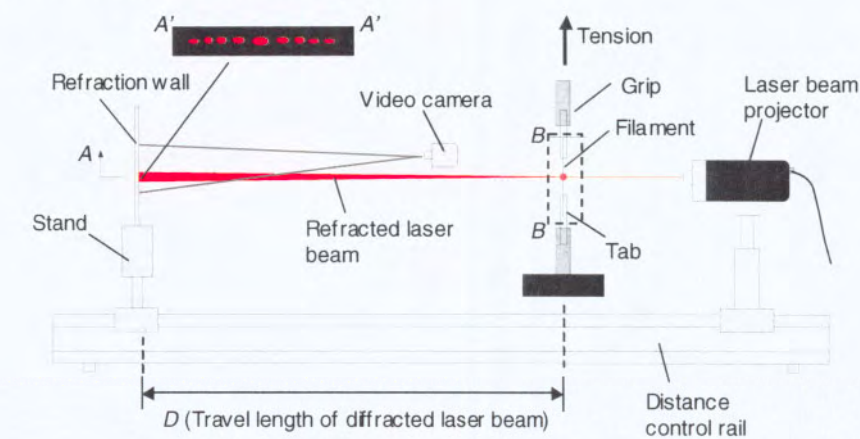
Figure 2 shows a schematic diagram of the experimental setup that includes a deflectometer and tensile strength facilities. For example, if the nearest bright point from the center image is selected among the detected points then m is set as 0.5. Similarly, m is 1.0 and 1.5 for the second and third points of bright zone. Helium neon gas which has a wavelength of 632.8 nm is used for the test. An important advantage of this method, particularly in this study was that the measurements could be conducted during the tensile straining of filaments by recording the reflected beam images on the wall with a video camera.

Measurement Parameters

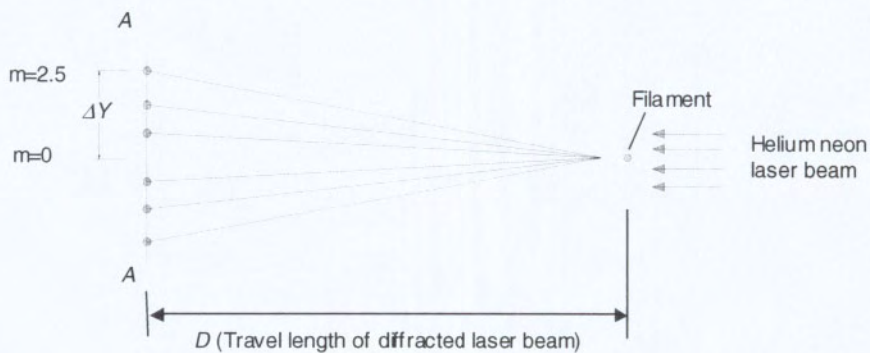
The tensile behavior of single fibers and filaments can be expressed using various quantitative descriptors. The definitions and terminology illustrated in ASTM are summarized below (ASTM D 123, D3822, D3379), where tex is a unit of linear density that is equal to the mass in grams of a 1,000 meter long fiber. Denier (den) is another unit of linear density that is equal to the mass in grams of a 9,000 meter long fiber. Other definitions include:

- Breaking force, BF (mN or gf): maximum force applied to a fiber to carry the fiber rupture.
- Breaking tenacity, BT (gf/den): tenacity at breaking force.
- Breaking toughness, BTO ($joule/den$): energy absorbed to a specimen until rupture.
- Chord modulus, CM (cN/tex or gf/den): ratio of the change in stress to the change in strain between two specified points on a stress-strain curve.

- Elongation at peak, $EP(\%)$.
- Initial modulus, IM (cN/tex or gf/den): ratio of the change in stress to the change in strain of the initial straight portion of the stress-strain curve.
- Linear density, LD (tex or $denier$): mass per unit length.
- Tangent modulus, TM (cN/tex or gf/den): the ratio of change in stress to change in strain derived from the tangent to any point on the stress-strain curve of a tensile test.
- Tenacity (specific stress), TN (gf/den): tensile stress expressed as force per unit linear density of the unstrained specimen.
- Tensile stress at specific elongation, $TSSE$ (cN/tex).
- Toughness (work per unit volume; work per unit mass; work of rupture), TO ($Joules/gf/kilometer$): capacity of a material to absorb energy required to a strain.
- Yield point, YP ($\%$): the point beyond which work is not completely recoverable and permanent deformation takes places.



(a)

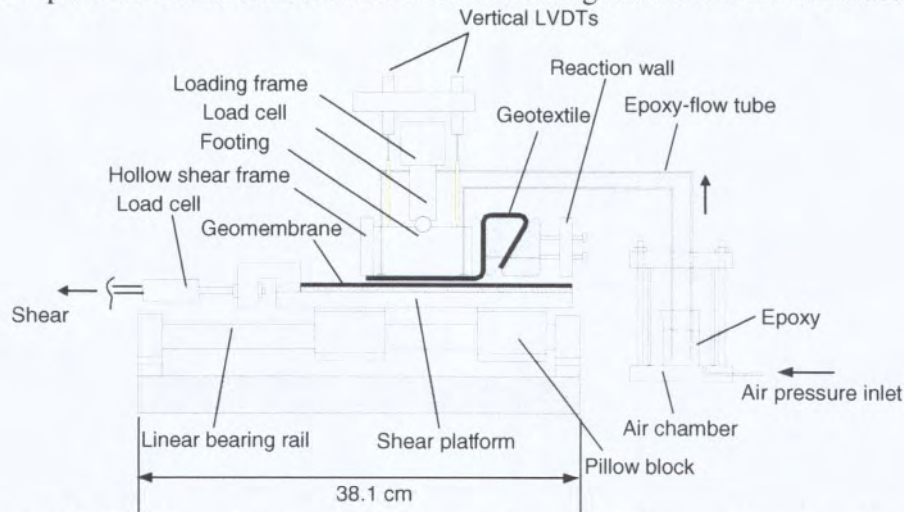


(b)

Figure 2. Schematic diagram of filament property measurement: (a) experimental setup (side view); (b) Bragg's law of diffraction (plan view).

SHEAR RESPONSE OF GEOTEXTILE-GEOMEMBRANE INTERFACES

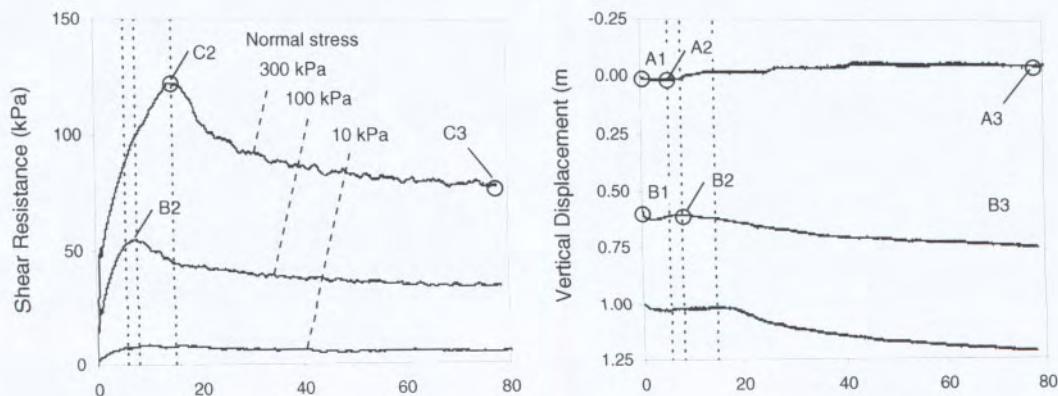
The shear failure of geotextile-geomembrane interfaces in the field is known to be accompanied with excessive internal strain of the geotextiles (Mitchell and Seed, 1990; Seed and Mitchell, 1990; Villard et al., 1999). In order to model such a mechanism, a new shear device was used in this study as shown in Figure 3. A geomembrane specimen, 200 mm wide by 290 mm long, is positioned on a platform mounted on a set of linear bearing rails with the manufacturing machine



direction parallel to the shear direction. The geotextile is folded around wedge-shaped plates on the leading edge of the hollow shear frame and secured by pressure fastening the wedges to a reaction wall, while the shear frame is held in a plane above the platform base by two rigid shafts installed on either side of the shear platform so that error caused by the contact between the shear box and geomembrane is avoided. (Kim and Frost, 2005).

Figure 3. Schematic diagram of the interface shear device (Kim and Frost, 2005).

Typical results of interface shear resistance using geotextile A and the textured geomembrane are shown in Figure 4a. The corresponding vertical displacements that occurred during the initial compression and shear displacements are illustrated in Figure 4b. The specimen showed a dilation under a low normal stress of 10 kPa (A3 in Figure 4b) during shearing while the samples at 100 kPa and 300 kPa resulted in residual settlements after the peaks due to filament rearrangement and the localized filament-texture interactions.

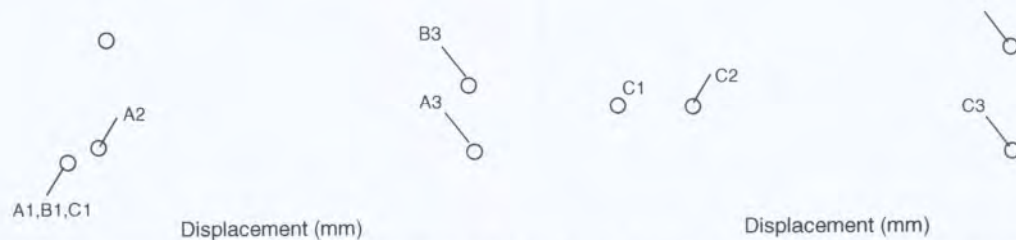


(a)

(b)

Figure 4. Interface shear response of the geotextile against a moderately textured geomembrane: (a) shear resistance; (b) vertical displacement.

DIGITAL IMAGE ANALYSIS



The geotextile-geomembrane layered specimens were encapsulated by low-viscosity epoxy resin at compressed/sheared states as shown in Figure 4. The initial unsheared compressed states of the specimens are marked as A1, B1, and C1 for normal stress states of 10, 100, and 300 kPa, respectively. Specimens were also prepared at peak strain (A2, B2, and C2), and at pseudo residual states (A3, B3, and C3) corresponding to displacements of about 80 mm.

The flow of epoxy resin into the geotextile pores was controlled using constant air pressure of 7 kPa (Figure 3). The selected epoxy resin is known to have appropriate properties for sensitive sample preservation satisfying critical requirements including optical clarity, hardness, bonding strength, and low volume change (Jang et al., 1999). The specimens were cured at room temperature for 24 hours. After being cured, the specimens were sectioned as appropriate to observe the internal structure of the filament-texture interfaces under a digital optical microscope. The tri-sector sampling method (Gokhale and Drury, 1994) was applied to the compressed specimens to obtain representative 3-D information from the section images (Figure 5a). In order to identify the effects of shear on the geotextile microstructure, two orthogonal viewing planes (Vaughan, and Brown, 1996) were observed including the shear surfaces (face I) and the cross-shear surfaces (face II) of the specimens as illustrated in Figure 5b.

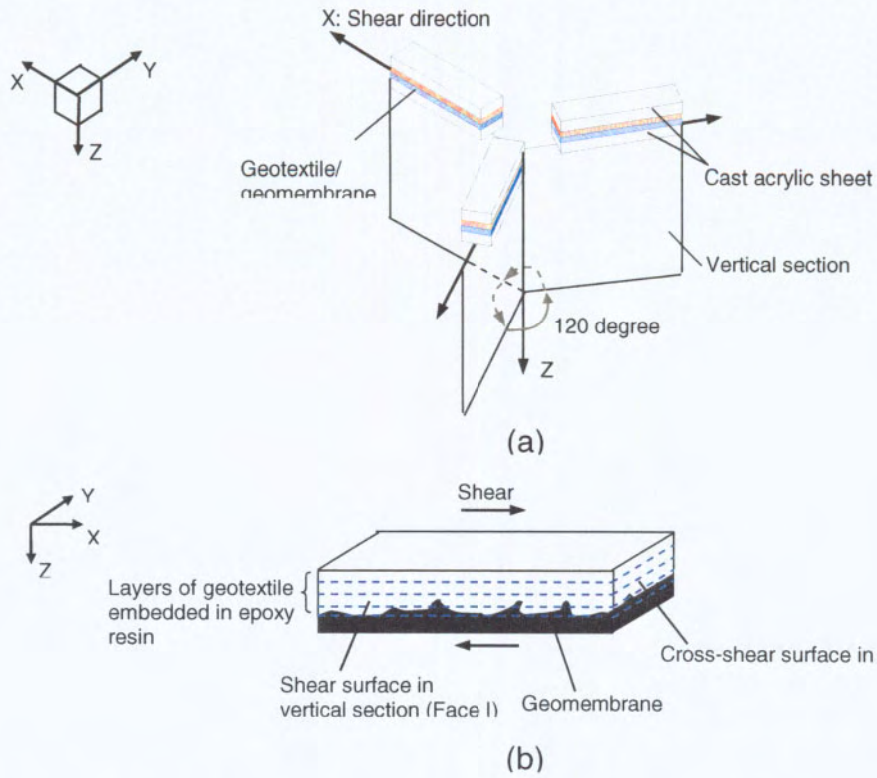


Figure 5. Sampling methods: (a) tri-sector sectioning method used for compressed specimens; (b) orthogonal viewing planes method used for sheared specimens.

TEST RESULTS

Tensile Behavior of Geotextile Filaments

The typical tensile behavior of single geotextile filaments is shown in Figure 6. The tensile force versus strain had a nonlinear elasto-perfect plastic form for the two PP geotextiles, resulting in nearly constant resistances after peak until they reached rupture at elongations of 62% and 57%, respectively (Figure 6a). The change of filament diameter is also shown as a function of displacement (Figure 6b). The diameter of the filament from geotextile A decreased rapidly under initial tensile loading and the slope of the stress-strain curves changed with the axial tensile strain. The filament from geotextile B resulted in a similar trend of stress-strain response and constant decrease of diameter with tensile force. The filament from geotextile C made from polyethylene demonstrated a different response. Its initial modulus was relatively high and then decreased at an elongation of about 0.5 mm. This specimen resulted in a constant increase of tensile force until the break point without yielding. Parameters obtained from the tests are summarized in Table 3. Geotextile A was selected for further study using image analysis techniques since it had a relatively large filament thickness and showed a large and constant rate of change of diameter with tensile strain (i.g., about $15 \mu\text{m}$ or 35% strain at failure).

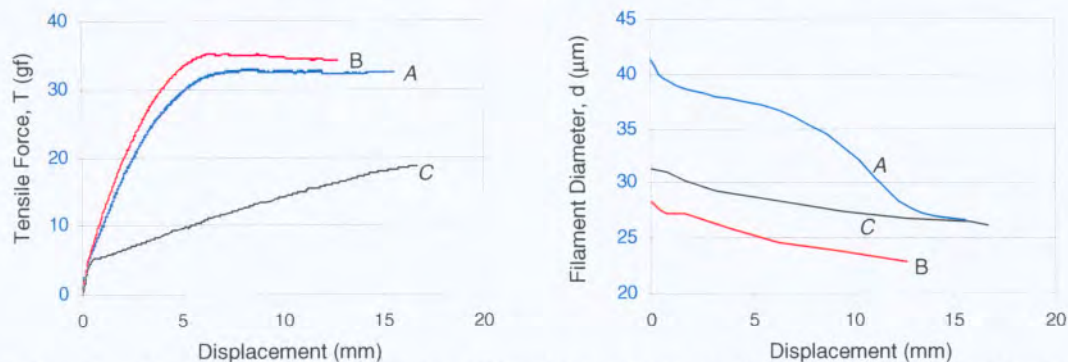


Figure 6. Tensile behavior of single filaments: force-strain-diameter relation: (a) force-displacement; (b) diameter-displacement.

Table 3. Tensile properties of single filaments of NPNW geotextiles.

Property	Geotextile		
	A	B	C
Breaking force, BF (gf)	33.0	35.3	18.7
Breaking tenacity, BT (gf/den)	28.9	66.2	28.5
Breaking toughness, BTO (joules/den)	383	696	204
Chord modulus, CM (gf/den-mm)	5.3	12.9	1.9
Elongation at peak, EP (%)	62.3	51.1	66.7
Initial Diameter, d (μm)	41.3	28.3	31.2
Initial modulus, IM (gf/den-mm)	342	750	667
Linear density, LD (denier)	1.145	0.533	0.656
Tangent modulus, TM (gf/den-mm)	13.7	30.0	26.7
Yield point, YP (%)	28.0	26.5	3.3

Filament Size Distribution

Synthetic fibers can have various cross section shapes such as three-lobal, three-sided, round and hollow. Other forms include four-, five-, or multi-lobal, and ribbon-shaped. In textile and fiber engineering fields, fibers with a certain cross section shape are often selected to obtain the required visual effect and performance. For example, hollow fibers are often used since they present more volume and increased stiffness compared to their mass per unit volume (Lunenschloss and Albrecht, 1985). Geotextile A which was selected for additional image analysis in this study had cross-sections of semi-round shape (Figure 7) so that the filament size could be expressed in terms of the width orthogonal to the longest length of the sectioned filament features.

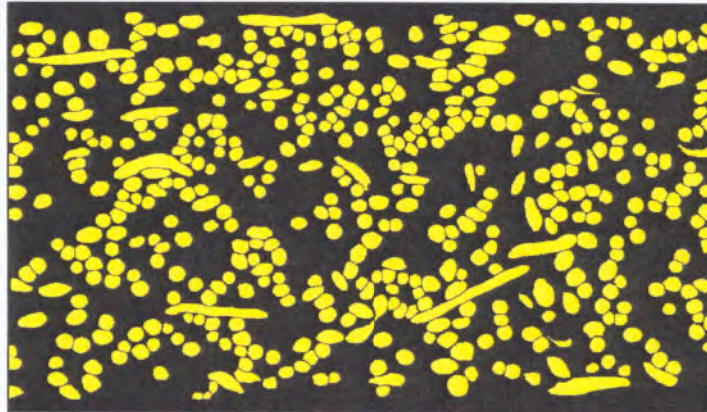


Image size: 1.993 mm (W) x 1.144 mm (H)
 Loading: compression to 300 kPa
 Filament area fraction: 0.331

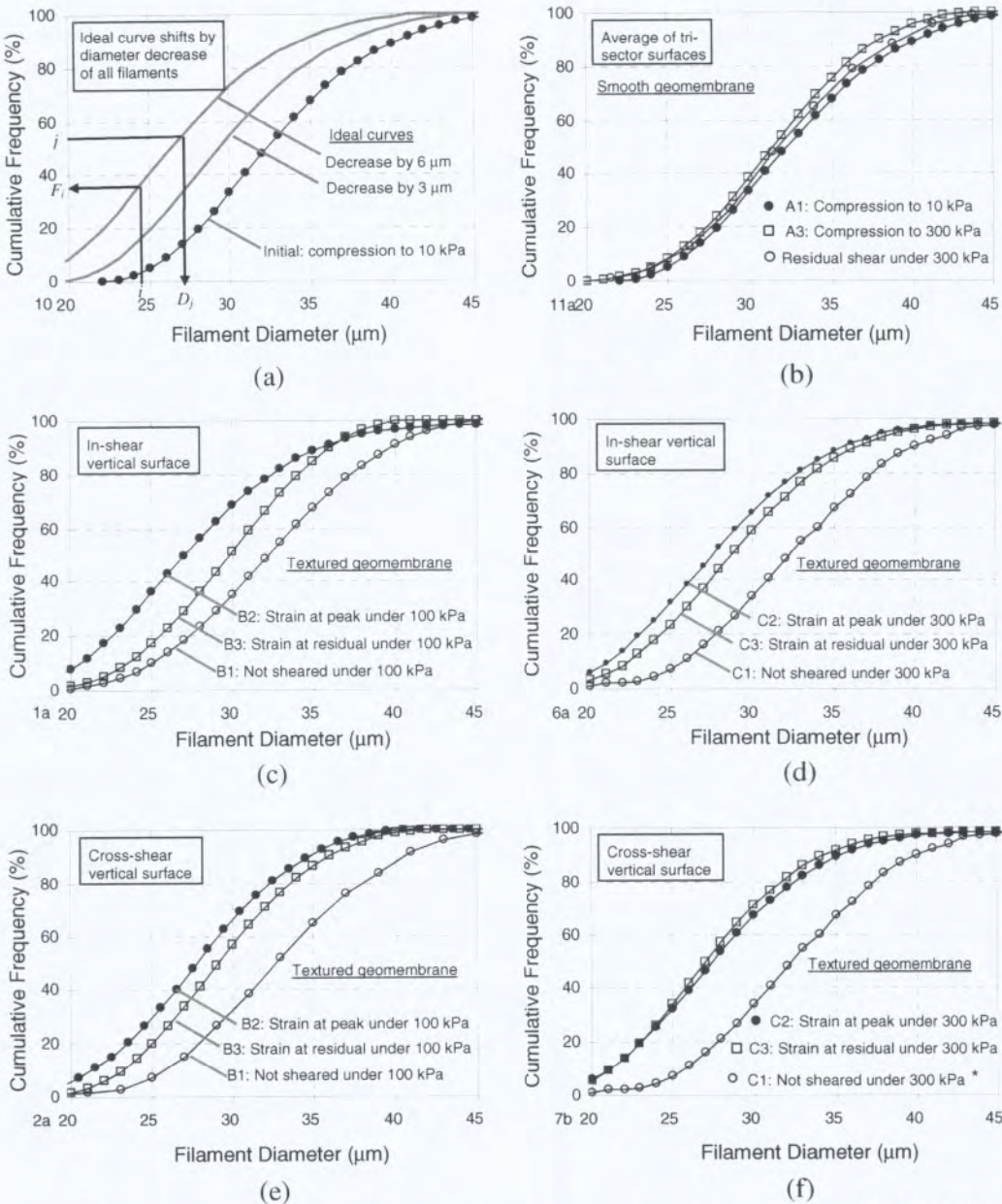
Figure 7. Cross section view of a NPNW geotextile.

Results of the filament size distribution obtained from the vertical sections of the specimens are illustrated in Figure 8. The distribution of initial filament sizes at low normal stress of 10 kPa (A1 in Figure 4) is shown in Figure 8a. Theoretical curves shifted by decrease of filament size by 3 and 6 μm were also illustrated where all the filament sizes are assumed to decrease in the same ratio. Symbol F_i defines herein a cumulative percent frequency of filaments smaller than $i \mu\text{m}$ in diameter. Similarly, D_j indicates a filament diameter corresponding to cumulative frequency of $j\%$.

Figure 8b shows the effect of normal stress on filament size distribution. A slight decrease of about 1 μm is found for the diameter corresponding to the 50% cumulative frequency of filaments (D_{50}). The cumulative frequency of filaments smaller than 40 μm increased by 7% as the load increased from 10 to 300 kPa. This relatively small difference is considered to be a result of pulling of filaments as the geotextile strains in the horizontal direction under increased vertical normal loading.

Figure 8c presents the change of filament size due to shear against the textured geomembrane. The data were obtained from the shear surface (face I in Figure 5) under a normal stress of 100 kPa. The filament size corresponding to 50% frequency (D_{50}) decreased by about 6 μm at the

peak stain. At pseudo residual displacement, the value of D_{50} had recovered by $3 \mu m$, but was still smaller than the initial value at a normal stress of 100 kPa by about $3 \mu m$. At both the peak and residual shear states, 90% of filaments remained smaller than $37 \mu m$. The filaments under 300 kPa had slightly smaller diameters compared to the specimens under 100 kPa (Figure 8d). A relatively small change of filament size of about $1.5 \mu m$ was found after peak as the specimen was displaced to pseudo residual state of 80 mm. This lower amount of recovery after peak shear



is considered as a result of the higher contact stress at the interlocking points between the deformed geomembrane textures and more densely compressed filaments.
 Figure 8. Results of filament size distribution measured from vertical sections with various boundary conditions: (a) normal stress on a smooth geomembrane with theoretical curves; (b)

effect of normal stress; (c) and (d) effects of shear on a textured geomembrane-shear surface (I); (e) and (f) effects of shear on a textured geomembrane: cross-shear surface (II).

Friction is typically divided into two components: sliding and deformation (Bowden, 1952). The relatively small change in the distribution of filament sizes against a smooth geomembrane as shown in Figure 8b indicates a typical sliding friction response while the dominant change at different load stages (Figure 8d) suggests a deformation friction in which the geomembrane surface deforms and geotextile filaments strain.

The results from the counter shear surfaces (face II in Figure 5) which is orthogonal to the shear direction are illustrated in Figure 8e and f. A lower frequency of filaments smaller than $50\ \mu\text{m}$ (F_{50}) was found at peak strain under 100 kPa compared to the result from the shear surface (face I). A small change was found after peak strain with the value of D_{50} increasing to $29\ \mu\text{m}$. Similar to the results from the in-shear surface in Figure 8d, the change of distribution after peak strain was smaller for specimens at the higher normal stress of 300 kPa (Figure 8f). When compared to the changes in single filament diameters measured using the helium neon gas deflectometer, the observed changes in diameter under normal and shear loading suggest that tensile forces in individual filaments may be approaching yield loads at peak.

CONCLUSIONS

The tensile properties of filaments in needle-punched nonwoven geotextiles were measured through an experimental program and quantified in terms of the stress-strain-diameter response as well as other quantitative parameters. The experimental setup using a helium neon deflectometer enabled tracking of the complete tensile response of filaments as a function of shear displacement. Using digital image analysis techniques, the change of filament size during interface shearing was quantified. The interface shearing of a needle-punched non-woven geotextile against a textured geomembrane resulted in distinct reduction of filament size distribution. The maximum change of filament diameter was observed at peak shear. The test results showed the impact of the concentrated normal stress and micromechanical interlocking between the geomembrane textures and geotextile filaments during interface shearing.

This study resulted in a number of findings of importance to practitioners. A method to enable changes in geotextile filament diameter under different boundary load conditions was developed and implemented. Use of this method can lead to a better understanding of the long-term behavior of geosynthetics. As field applications involving geotextiles result in larger loads being transmitted to interfaces, understanding not only how the geotextile sheet is behaving but what tensile force individual filaments within the geotextile are being subjected to becomes increasingly important. Manufacturers can also use this insight to implement processes that can produce filaments that lead to enhanced long-term performance of geotextiles.

REFERENCES

- Bowden, F. P. (1952) "Introduction to the Discussion: The Mechanism of Friction," Proceedings of the Royal Society of London. Series A, Mathematical and Physical Sciences, Vol. 212(1111), pp. 440-449.

- De Meulemeester, D. and I. Nicoloff (1936) "Stress-extension recording dynamometer for textile fibres," *Textile Institute Journal*, Vol. 27(3), pp. 84-87.
- Dove, J. E., and Frost, J.D. (1996) "A Method for Measuring Geomembrane Roughness," *Geosynthetics International*, Vol. 3, pp. 369-392.
- Frost, J.D., and Lee, S.W. (2001) "Microscale Study of Geomembrane-Geotextile Interactions," *Geosynthetics International*, Vol. 8, No. 6, pp. 577-597.
- Hindman, H. (1948) "Instron tensile tester," *American Society of Mechanical Engineers-Advance Papers*, Vol. 48, A-68, 3p.
- Gokhale, A.M., and Drury, W.J. (1994) "Efficient Measurement of Microstructural Surface Area Using Trisector," *Metallurgical and Materials Transactions A*, Vol. 25A, pp. 919-928.
- Gonsalves, V. E. (1947) "Determination of denier and strength of single filaments by vibroscope and Heim tensile tester," *Textile Research Journal*, Vol. 17(7), pp. 369-375.
- Hebeler, G. H., Frost, J.D., and Myers, A.T. (2005) "Quantifying Hook and Loop Interaction in Textured Geomembrane-Geotextile Systems," *Geotextiles and Geomembranes*, Vol. 23(1), pp. 77-105.
- Jang, D. J., Frost, J.D., and Park, J.Y. (1999) "Preparation of Epoxy Impregnated Sand Coupons for Image Analysis," *Geotechnical Testing Journal*, GTJODJ, Vol. 22(2), pp. 147-158.
- Kim, D., and Frost, J.D., (2005) "Multi-Scale Assessment of Geotextile-Geomembrane Interaction," *NAGS 2005/GRI 19 Conference*, Las Vegas, USA, 8p.
- Kim, D., and Frost, J.D. (2006) "[Microscopic Investigation of Geotextile-Geomembrane Interface](#)," *Special Issue of Geosynthetics International* (Accepted).
- Krais, P. (1928) "The tensile testing of single fibres," *Textile Institute Journal*, Vol. 19(1), pp. 32-36.
- Lunenschloss, J. and Albrecht, W. (1985) *Non-Woven Bonded Fabrics*, translator: Hock, J.; translation editor, Sharp, D., Ellis Horwood, 549p.
- Lord, E. (1955) "Air flow through plugs of textile fibres (1)," *Journal of Textile Institute*, Vol. 46(3), pp. 191-213.
- Mitchell, J. K., Seed, R.B., and Seed, H.B. (1990) "Kettleman Hills Waste Landfill Slope Failure. I: Liner System Properties," *Journal of Geotechnical Engineering*, Vol. 116(4), pp. 647-668.
- Morton, W.E., and Hearle, J.S.W. (1962) *Physical Properties of Textile Fibres*, Manchester & London, The Textile Institute, Butterworths, 1st Edition, 608p.

- Morton, W.E., and Hearle, J.S.W. (1993) Physical Properties of Textile Fibres, Manchester & London, The Textile Institute, Butterworths, 3rd Edition, 725p.
- Park, Y. (2006) Personal Communication, Florida State University, FL.
- Seed, R. B., Mitchell, J.K., and Seed, H.B. (1990) "Kettleman Hills Waste Landfill Slope Failure, Failure. II: Stability Analysis," Journal of Geotechnical Engineering, Vol. 116(4), pp. 669-690.
- Vaughan, N.P. and R.C. Brown (1996) "Observations of the microscopic structure of fibrous filters," Filtration and Separation, Vol. 33(8), pp. 741-748.
- Villard, P., J. P. Gourc, et al. (1999) "Analysis of geosynthetic lining systems (GLS) undergoing large deformations," Geotextiles and Geomembranes, Vol. 17(1), pp. 17-32.

CONTACT:

Duhwan Kim
Georgia Institute of Technology
210 Technology Circle
Savannah, GA 31407
Phone: 404-610-5700
Email: duhwan.kim@ce.gatech.edu

Effect of Wet-Dry Cycles on Capillary Break Formation in Geosynthetic Drainage Layers

John S. McCartney, The University of Texas at Austin; Jorge G. Zornberg, The University of Texas at Austin

ABSTRACT

This study investigates the impact of wet-dry cycles on the formation of a capillary break at the interface between a compacted clay layer and a geosynthetic drainage layer. To highlight the importance of this issue in practice, field monitoring data from a vegetated landfill test cover is presented showing how the behavior of the cover was altered by the capillary break effect. The landfill cover, consisting of a 1.17-m thick low plasticity clay layer over a geosynthetic drainage layer, experienced an increase in available moisture storage due to the capillary barrier effect. Negligible amounts of water were observed to flow from the soil into the geosynthetic drainage layer during a six year period. To interpret this behavior, two infiltration/evaporation column tests were performed on compacted clay underlain by geosynthetic drainage layers. A 1.35 m-long soil column was used to infer moisture and suction profiles during wetting and drying from the surface. The results indicate formation of a capillary break during infiltration and limited moisture removal during evaporation. A 0.125 m-long soil column was used to investigate the influence of wet-dry cycles on the formation of a capillary break. The capillary break effect was observed to occur during repeated wetting cycles, with breakthrough occurring at the same suction value on each cycle. These results indicate that a capillary break effect can be used in landfill covers to provide an increase in moisture storage during wet seasons if adequate moisture is removed from the interface during dry seasons.

INTRODUCTION

Geosynthetic drainage layers consisting of a geonet sandwiched between two nonwoven geotextiles are often used to provide drainage of water from soil profiles. Geotechnical applications involving geosynthetic drainage layers include leachate collection and leak detection systems in landfills, drainage components of lysimeters for performance evaluation of alternative landfill covers, sub-base separation systems in roadways, and drainage systems for mechanically stabilized earth walls. When saturated, the permittivity and transmissivity of geosynthetic drainage layers are typically higher than that of the soil being drained, and do not have a significant impact on the flow of water through the system. The behavior of a saturated system can be characterized using only the hydraulic conductivity values of the soil and geosynthetic drainage layer. When the system is slightly unsaturated (e.g., when suction value at the interface is between 1 kPa and 10 kPa), geosynthetic layers are practically non-conductive to water while in this range most fine-grained soils have hydraulic conductivity close to their saturated value. Depending on the soil, the geosynthetic drainage layer may have a significant impact on the flow of water through an unsaturated system.

Hydraulic properties that are useful to interpret the interaction between unsaturated soils and geosynthetics include the water retention curve (WRC) and the hydraulic conductivity function (K-function). Due to their uniform and relatively large pore size, nonwoven geotextiles will retain water at saturation until the suction applied to a boundary of the geotextile increases to

about 1 kPa, at which point air enters the geotextile and water drains. This suction value is referred to as the air-entry suction. For imposed suctions slightly greater than the air-entry suction, a sharp decrease in moisture content from full saturation to residual water retention has been observed (Stormont et al. 1997; Morris 2000; Stormont and Morris 2000; Knight and Kotha 2001; McCartney et al. 2005; Bouazza et al. 2006). At residual water retention, the hydraulic conductivity of a nonwoven geotextile predicted from the shape of the WRC using the van Genuchten-Mualem model (1980) is less than 10-11 m/s. Measurements of the K-function for unsaturated geotextiles were made by Morris (2000) and Stormont et al. (2001), and indicate that the van Genuchten-Mualem model is acceptable for prediction of the K-function shape.

The contrast in hydraulic conductivity between nonwoven geotextiles and unsaturated clay has been shown to cause a capillary barrier effect (Henry and Holtz 2001; McCartney et al. 2005; Iryo and Rowe 2005). A capillary break effect occurs when water will not flow across the interface between a fine grained material (e.g., clay) and an underlying dry, coarse grained material (e.g., a nonwoven geotextile). The water in the small pores of the fine-grained material must increase in pressure in order to displace air in the larger pores of the coarse-grained material. This effect prevents a measurable amount of water from flowing from a clay layer into a geotextile until the suction at their interface is reduced to a critical value. This critical suction is referred to as the water entry or breakthrough suction. The capillary barrier effect also causes an increase in moisture storage of the clay, in excess of the volume that would be stored during flow under a unit hydraulic gradient (i.e., water flow driven by self-weight).

This study investigates the hydraulic interaction between unsaturated, low plasticity, compacted clay and a geosynthetic drainage layer. To highlight the motivation of this research, monitoring results are presented from an evapotranspirative landfill test cover in which the interaction between a geosynthetic drainage layer and an unsaturated soil played an important role in the behavior of the cover. An experimental study in the laboratory was conducted to interpret the capillary break effect in soil-geosynthetic columns during cycles of infiltration and evaporation. The results from the column tests are used to interpret the behavior noted in the field monitoring results under controlled conditions, and provide guidance on the use (or prevention) of the capillary break in unsaturated soils and geosynthetic drainage layers.

MOTIVATION: GEOSYNTHETICS IN EVAPOTRANSPIRATIVE COVERS

An evapotranspirative landfill cover consists of a hydraulic barrier consisting of a vegetated, compacted clay layer placed atop waste. The cover functions by storing infiltrated water in the soil until it may be subsequently removed by evapotranspiration, which prevents percolation of water into underlying waste (Zornberg and McCartney 2006). An evapotranspirative landfill test cover, consisting of a 1.17-m-thick monolithic layer of low plasticity clay atop a geosynthetic drainage layer, was constructed in 1997 to investigate the behavior of this system under atmospheric boundary conditions. The system is underlain by a 60-mil geomembrane placed on a 3% grade in order to collect the water that passes through the system (referred to as percolation). The combination of a geosynthetic drainage layer and geomembrane is referred to as a lysimeter. The soil was vegetated with Cheatgrass, a local plant with a rooting length of 0.5 m (less than the thickness of the cover). A schematic of the cover is shown in Figure 1. The cover was instrumented with a weather station to measure precipitation, air temperature, and wind speed. The cover also has a vertical nest of 6 horizontally-oriented water content

reflectometer (WCR) probes, which are used to infer the volumetric moisture content. The depth of each probe is shown in Figure 1. More information on WCR probes can be found in McCartney and Zornberg (2006). The test cover was monitored until 2003.

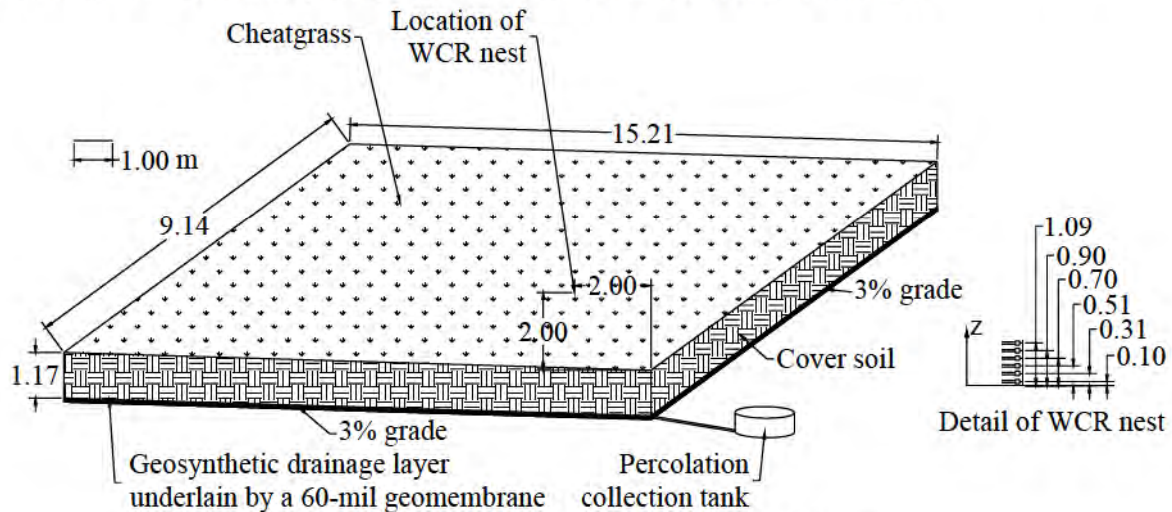


Figure 1: Schematic of the landfill test cover

An important finding from the monitoring program was that the percolation collected from the lysimeter was negligible (less than 0.1% of the precipitation). However, investigation of the moisture content profiles inferred using the WCR probes indicated that infiltration fronts reached the base of the cover during significant rainfall events. For example, the moisture content profiles shown in Figure 2(a) illustrate the migration of a wetting front through the cover during a particularly wet spring season. The infiltration front progressed through the cover at a moisture content of 20%, but after reaching the base the moisture content near the geosynthetic drainage layer increased to approximately 28%. This observation indicates that ponding of water occurred about the geosynthetic drainage layer, which is evidence of a capillary break effect. Also, a small volume of percolation was collected at the end of May 1999, indicating that breakthrough occurred after ponding was observed. The original intent of the geosynthetic drainage layer was to facilitate collection of the percolation, not to impact the hydraulic performance of the cover. However, the final design of the cover incorporated a geosynthetic drainage layer to cause a capillary break and to provide separation of the cover soil from the waste. Another important finding from the moisture profiles is that the cover “recovered” after ponding occurred. Specifically, the soil dried over the course of six months due to a combination of evapotranspiration and lateral drainage, as shown in Figure 2(b). More importantly, ponding and recovery trends were observed to occur on two other occasions during the monitoring period.

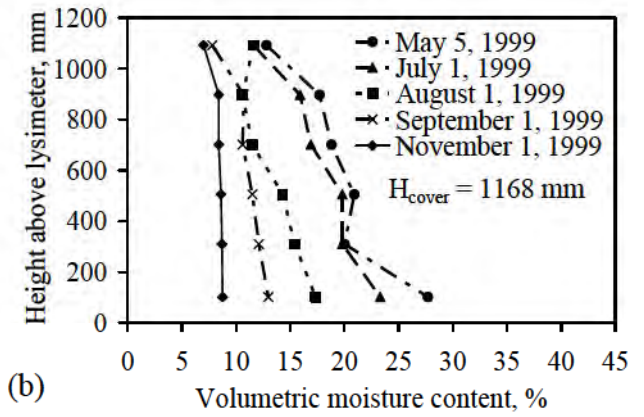
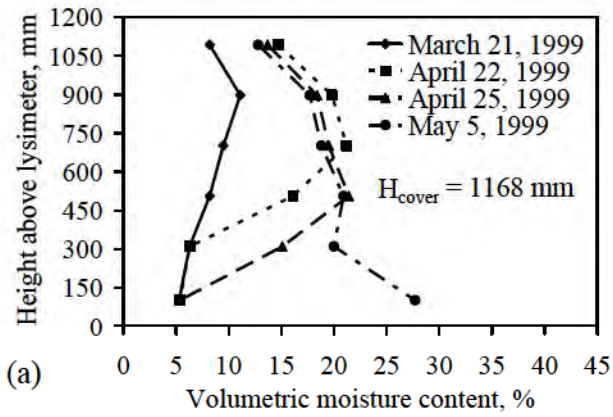


Figure 2: Moisture content profiles: (a) Wet season; (c) Dry season

MATERIALS

Geosynthetic Drainage Layer

The geosynthetic drainage layer used in the laboratory component of this study is a GSE Fabrinet[®] geocomposite, which is composed of a 200-mil geonet sandwiched between two 6 oz/yd² nonwoven geotextiles (GSE 2004). The thickness of the geocomposite as a whole is 12.5 mm. The porosity of a nonwoven geotextile is necessary to calculate its degree of saturation from measured values of gravimetric moisture content. The nonwoven geotextile components of the geocomposite have a thickness t of 2.56 mm, a mass per unit area μ of 20 kg/m², and a fiber density ρ_f of 910 kg/m³. The porosity of the nonwoven geotextile was calculated to be 0.99 using the following expression (Koerner 2005):

$$\eta = 1 - \frac{\mu}{t\rho_f} \quad (1)$$

Compacted Clay

The low plasticity clay (CL) used in this study has a specific gravity of 2.71, an average plasticity index of 12, and an average liquid limit of 27. The same soil used in the field study was used in the laboratory tests. The specified range of relative compaction in the field was 70 to 80% of the maximum standard proctor dry density (1902 kg/m³). In the laboratory and field, the clay was compacted at the optimum water content of 11.5%. The compaction energy was controlled in the field using a lightweight roller, and was controlled in the laboratory using a piston compactor.

Hydraulic Properties

The hanging column and pressure plate methods (Wang and Benson 2004) were used to define drying-path WRCs for the nonwoven geotextile component of the geosynthetic drainage layer and for specimens of the clay at relative compactations of 70% and 80%. The WRC results shown in Figure 3(a) indicate that the nonwoven geotextile drains from saturation to residual conditions at a suction value of 0.2 kPa, while the clay drains gradually. The density has only a slight impact on the WRC of the clay. The hydraulic conductivity of saturated soil and geosynthetic drainage layer specimens was assessed using a flexible-wall permeameter. The specimens were back-pressure saturated with tap water as the permeating fluid. An effective stress of 7 kPa was used, along with an average hydraulic gradient of 2.0. The K-functions shown in Figure 3(b) for the different materials were predicted from the WRC using the van Genuchten-Mualem model (1980). The hydraulic conductivity of the geotextile is higher than that of the clay when saturated, but is lower for suction values greater than 2 kPa.

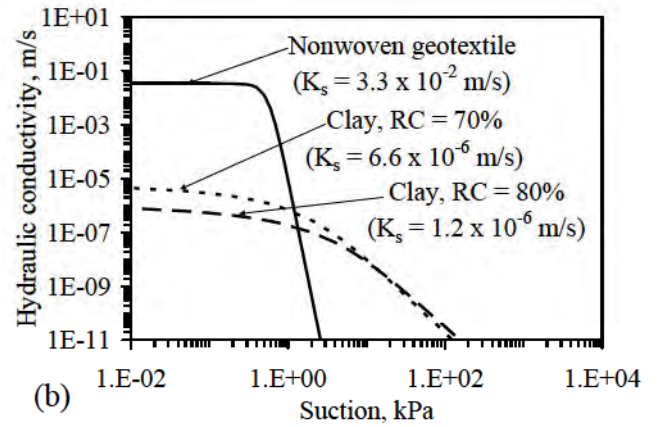
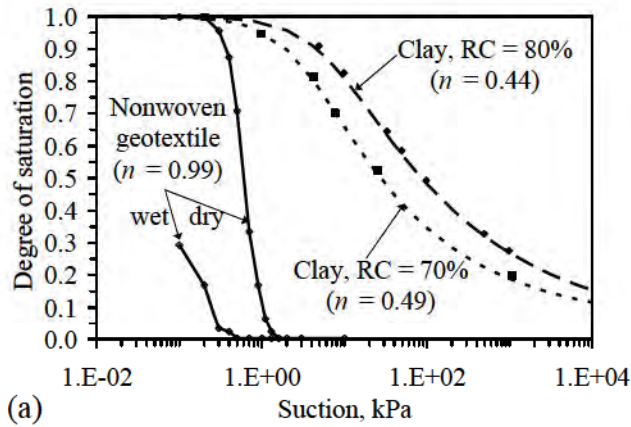


Figure 2: Hydraulic properties; (a) Water retention curves and porosities; (b) Predicted K-functions

LABORATORY TESTING PROGRAM

Soil Profiles

To investigate the behavior noted in the field program in a controlled setting, two soil-geosynthetic profiles were constructed in 203-mm diameter cylindrical columns. The columns are clear PVC tubes mounted with an “o”-ring seal onto a perforated acrylic disc, supported by a wooden platform. Tensioned wires were used to confine the tubes to the acrylic disc. Profile A is a 1350-mm-thick clay layer placed at a relative compaction of 70% above a geosynthetic drainage layer. The thickness of the soil in Profile A allows full-scale simulation of the moisture content and suction profiles in an evapotranspirative cover. Profile B is a 125-mm-thick clay layer placed at a relative compaction of 80% above a geosynthetic drainage layer. This profile is used to investigate the influence of wet-dry cycles on capillary break formation.

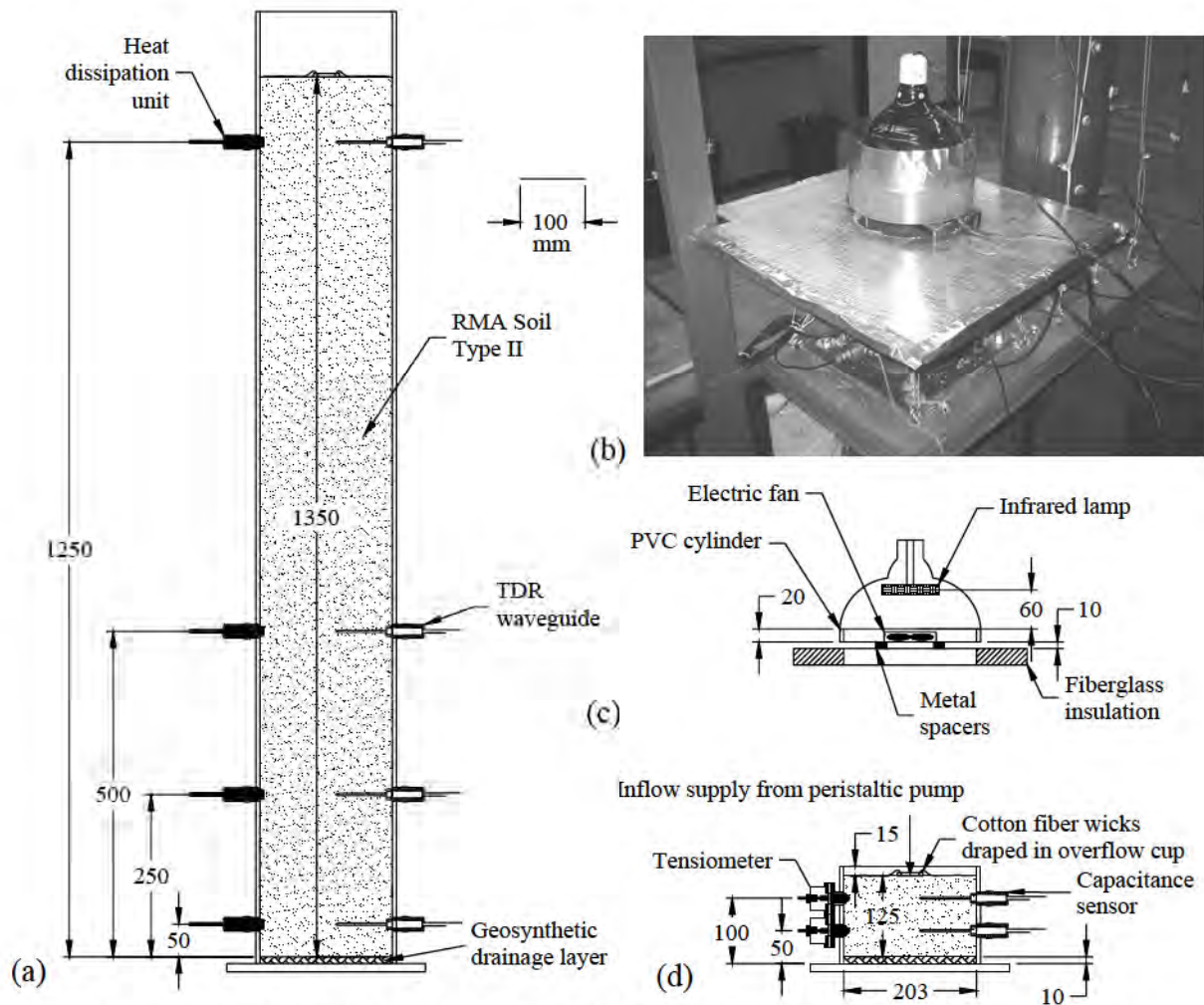


Figure 4: (a) Schematic of Profile A; (b) Picture of Evaporation setup for Profile B; (c) Schematic of Evaporation setup; (d) Schematic of Profile B

The profiles are shown in Figure 4. During infiltration, water is supplied to a reservoir on the surface of the soil profile via a peristaltic pump. The water is then distributed from the reservoir to the soil surface using a system of cotton fiber wicks. Outflow was measured using a tipping

bucket rain gauge mounted below the acrylic disc. During evaporation, an infrared lamp and a fan were used to induce drying from the soil surface, shown in Figure 4(c). This approach was not intended to replicate the actual energy supplied to the soil surface in the field to cause evaporation. Instead, this approach was used to provide a simple, yet controlled means of inducing drying of the soil. A sheet of fiberglass insulation with a hole having the same diameter as the column was placed on top of the column to limit heating of the column sides.

Monitoring System

Volumetric moisture content profiles in the columns were inferred using time domain reflectometry (TDR) and capacitance probes. The MiniTRASE[®] TDR system, developed by SoilMoisture, Inc. was used in Profile A, while ECH₂O-TE[®] capacitance probes, developed by Decagon, Inc., were used in Profile B. The ECH₂O-TE[®] probes also measure temperature and electrical conductivity. For calibration, the probes were embedded horizontally in clay specimens having a range of compaction moisture contents. The calibration relationships for two relative compactions obtained at room temperature are presented in Table 1. Linear relationships were obtained between the inferred quantities (dielectric permittivity for TDR and raw moisture content for the ECH₂O-TE[®]) and actual volumetric moisture content values for the range of compaction conditions in the calibration program.

Table 1: Calibration equations for moisture content monitoring systems

System	Relative compaction (%)	Moisture content range (%)	Equation
TRASE TDR	70	10 to 49	$\theta_a = 14.9K_a^{0.5} - 23.4$
	80	8 to 44	$\theta_a = 12.0K_a^{0.5} - 17.0$
ECH ₂ O-TE	70	10 to 49	$\theta_a = 1.1\theta_i - 3.9$
	80	8 to 44	$\theta_a = 0.9\theta_i - 0.3$

θ_a = Actual volumetric moisture content

θ_i = Inferred volumetric moisture content

K_a = Inferred dielectric permittivity

Suction was measured using heat dissipation units (HDUs) in Profile A and using flushing tensiometers in Profile B. HDUs infer suction by measuring the change in temperature of a low-air entry ceramic in contact with the clay during an imposed heat pulse (Flint et al. 1999). For the same heat pulse, the temperature change for a dry ceramic will be greater than for a wet ceramic because of variation in the ceramic's thermal conductivity with water content. As the suction between the soil and ceramic is continuous, the temperature response can be correlated with the suction in the ceramic, providing a soil-independent calibration. The HDUs were calibrated using the method described by Flint et al. (1999), and the same calibration equation used in that study was used in this study. The HDUs were found to be useful for measurement of suction values greater than 20 kPa. Tensiometers are a commonly used approach to directly measure suction. A miniature pore pressure transducer is used to monitor changes in pressure inside a water reservoir in hydraulic contact with the soil through a high-air entry ceramic (Ridley and Burland 1995). As a soil dries, water is drawn from the reservoir through the ceramic, causing a negative pressure in the reservoir. The tensiometers used in this study were

designed for this project, and include flushing ports. The flushing ports aid in initial saturation of the ceramic and removal of air bubbles in the case that cavitation occurs. The tensiometers were calibrated by applying pressures ranging from -100 to 100 kPa to the transducer. These tensiometers are useful for measurement of suction values less than 200 kPa.

Profile Preparation

The soil was placed into the columns in 25 mm lifts using a piston compactor. An relative compaction of 70% was obtained using a pressure of 10 psi and a 40-mm diameter piston and a relative compaction of 80% was obtained using a pressure of 15 psi and a 40-mm diameter piston. The walls of the cylinder were greased to minimize side-wall leakage. The sensors were placed at the elevations noted in Figures 4(a) and 4(d). The moisture content sensors and HDUs were placed in the middle of lifts during compaction, shown in Figure 5(a), while the tensiometers were screwed into the column after compaction, as shown in Figure 5(b).

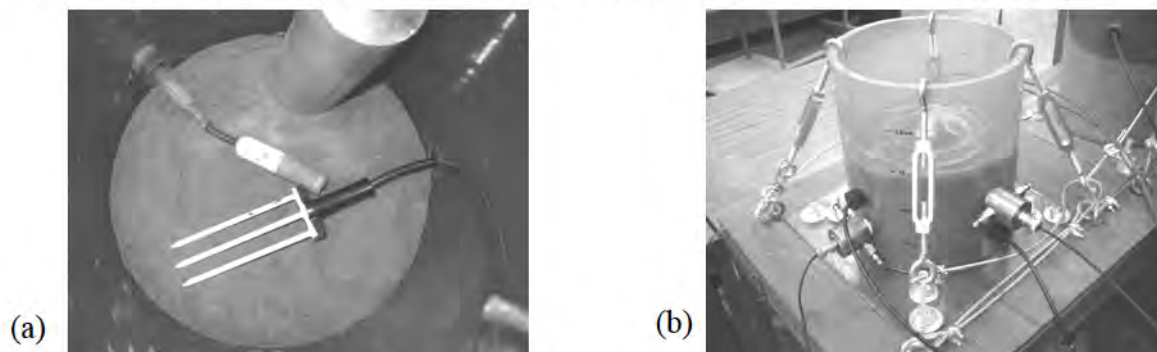


Figure 5: (a) Soil profile A during compaction; (b) Soil profile B after compaction

Test Procedures. The infiltration stages involved imposing a steady flow rate, measuring the volumetric moisture content and suction changes with time as the wetting front progresses through the soil. An infiltration stage was completed when the outflow discharge velocity was the same as the inflow discharge velocity. The soil surface was covered to maintain a constant relative humidity (~96%) during infiltration. The evaporation stages involved measurement of the surface temperature and relative humidity as well as internal profiles of temperature, moisture content, and suction. The geometry, soil conditions, stage duration, and boundary conditions are summarized in Table 2. The stage names include the profile name, the cycle number, and the stage type (i for infiltration or e for evaporation). The infiltration rates were selected to be less than the hydraulic conductivity of the clay when saturated. The suction at the soil surface was inferred from the relative humidity using the equation in Table 2.

Table 2: Details of the laboratory column testing program

Profile name	Length (mm)	Relative compaction (%)	Compaction water content (%)	n	$K_{s,system}$ (m/s)	Stage name	Stage description	Duration (hrs)	Infiltration rate (m/s)	Evaporation surface suction (kPa)
A	1350	70	11.5	0.49	6.20E-06	A1(i-1)	Infiltration	2423	3.4E-09	N/A
						A1(i-2)	Infiltration	683	6.5E-08	N/A
						A1(e)	Evaporation	2179	N/A	3.0E+05
						A2(i)	Infiltration	819	3.4E-08	N/A
						A2(e)	Evaporation	857	N/A	3.0E+05
B	125	80	11.5	0.44	1.20E-06	B1(i)	Infiltration	135	8.0E-09	N/A
						B1(e)	Evaporation	101	N/A	3.0E+05
						B2(i)	Infiltration	93	8.0E-09	N/A
						B2(e)	Evaporation	174	N/A	3.0E+05
						B3(i)	Infiltration	596	8.0E-09	N/A

Note: N/A is not applicable

$$\text{Boundary Suction} = -\frac{\rho_w RT}{M_w} \ln\left(\frac{R_h}{100\%}\right)$$

where ρ_w = water density, R = universal gas constant, T = temperature in K,
 M_w = molecular mass of water vapor, and R_h = relative humidity in percent

RESULTS

Profile A

The inflow and outflow data in Profile A during the infiltration stages are shown in Figure 6(a). The amount of moisture leaving the columns during the evaporation stages was not measured. The progress of the wetting front shown in Figure 6(b) indicates that the initial wetting front reached the base of the profile in 1400 hrs, even though capillary breakthrough did not occur until 1874 hrs. Less time was required to cause capillary breakthrough during infiltration Stage A2(i). This occurred because the moisture removed during evaporation Stage A1(e) was not sufficient to return the soil profile to its original moisture content. Accordingly, infiltration and evaporation Stages A2(i) and A2(e) are not discussed in this paper.

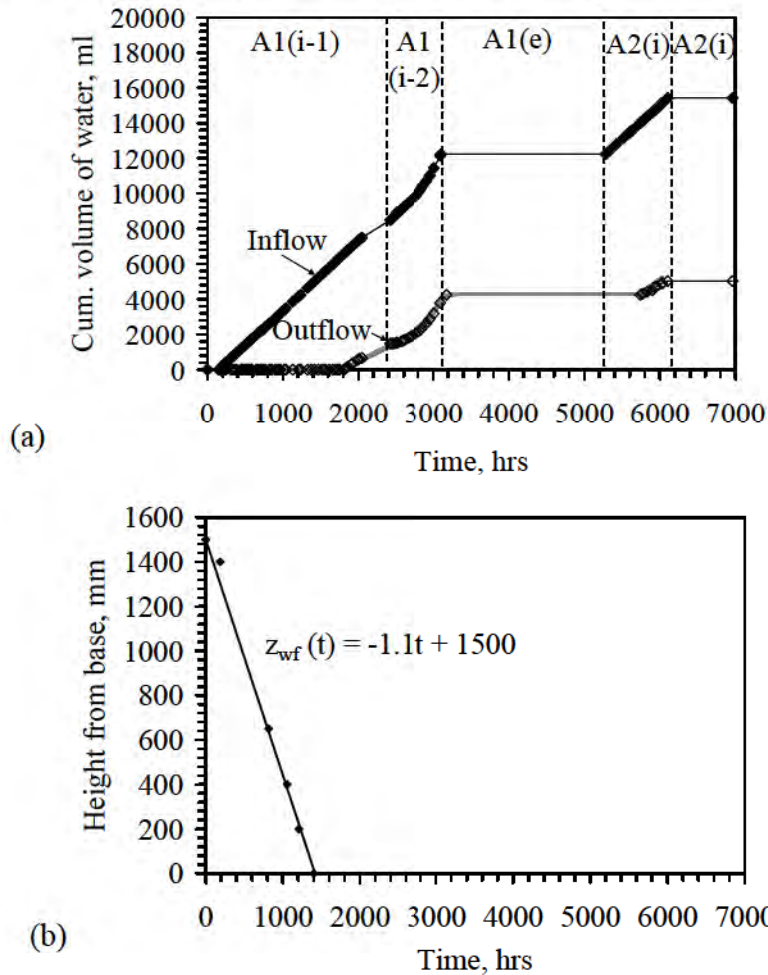
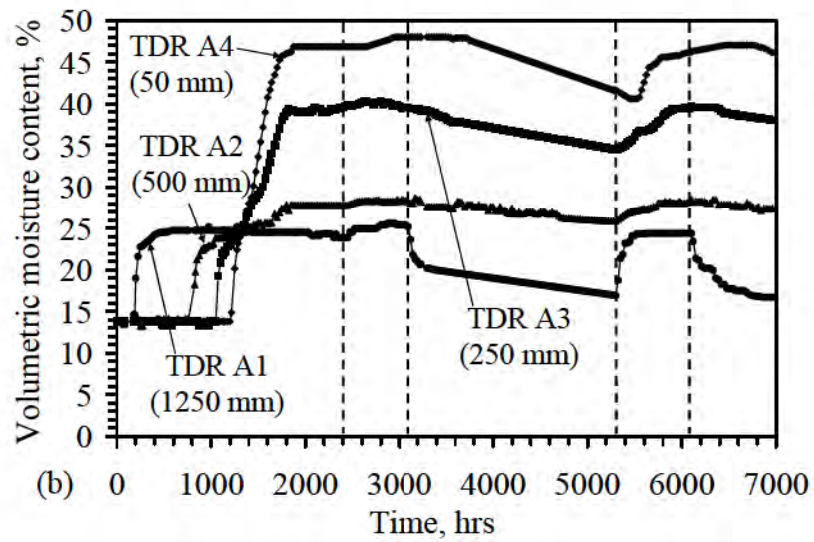
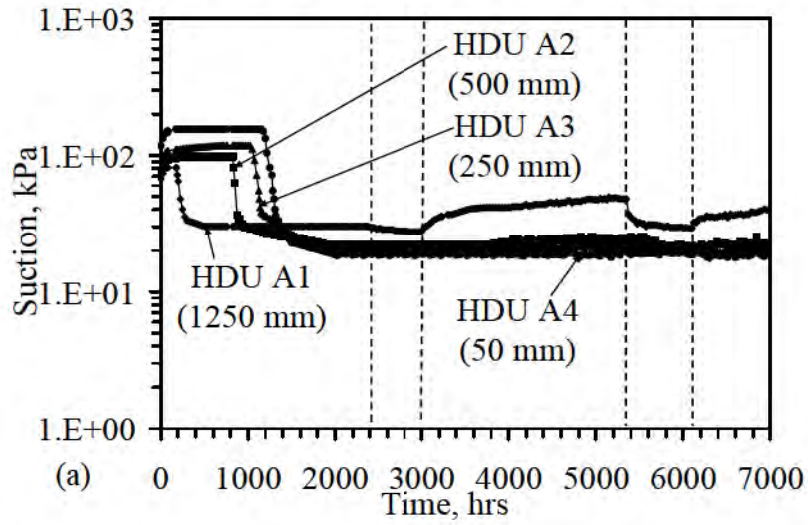


Figure 6: Profile A: (a) Cumulative inflow and outflow; (b) Initial wetting front

The suction time series for Profile A are shown in Figure 7(a). The HDUs were responsive to changes in suction during the initial infiltration stage. During this stage, HDU A1 shows a drop in suction from a value of approximately 100 kPa to 30 kPa. As the infiltration passes through the soil profile, the other HDUs showed subsequent drops in suction to approximately 20 kPa. The HDUs are not able to measure suction values less than 20 kPa, so the suction in the bottom portion of the profile after 2000 hrs is not certain. However, the upper HDU shows a decrease in

suction during Stage A1(i-2), and an increase in suction from 30 kPa to 49 kPa during Stage A1(e). The evaporation front did not progress to the depths of the lower HDUs.



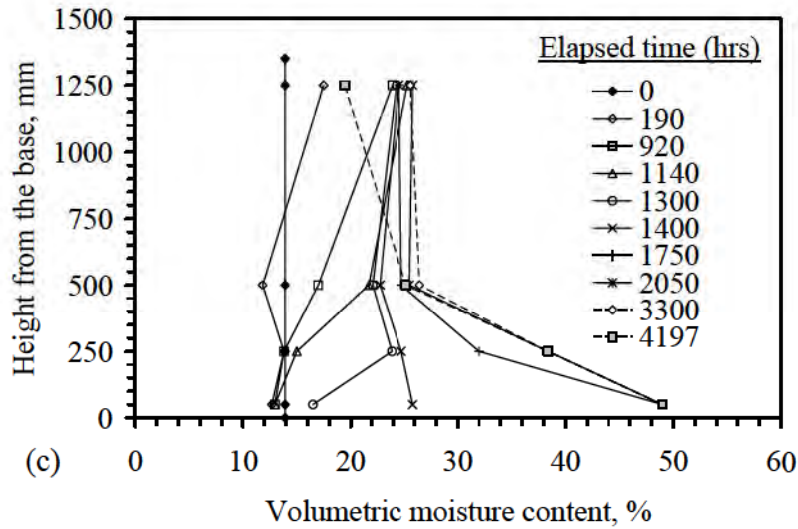


Figure 7: Profile A: (a) Suction; (b) Moisture content; (c) Moisture content profiles

The moisture content time series shown in Figure 7(b) indicate progression of the infiltration front through the soil profile during Stage A1(i-1) at a moisture content of 24%. Unlike the suction time series, the moisture content data allows closer investigation of the behavior of the soil profile after the infiltration front reaches the base of the profile. Specifically, an increase in moisture content from 24% to 47% occurred after the wetting front reached the base of the profile (TDR A4, $z = 50$ mm). TDR A3 ($z = 250$ mm) and TDR A2 ($z = 500$ mm) also showed increases in moisture content (although less significant), while TDR A1 ($z = 1250$ mm) did not show an increase in moisture content. The moisture content at the base of the profile was close to saturation when capillary breakthrough occurred at $t = 1824$ hrs. The moisture profiles with depth during Stage A1(i-1), shown in Figure 7(c), indicate that ponding occurred in the profile. The shapes of these profiles are similar to those from the field study shown in Figure 2(a). The moisture content profiles during Stage A1(i-1) indicate that the capillary break effect was the cause of the accumulation of water at the base of the covers observed in Figure 2(a).

During the first evaporation stage ($t = 3100$ hrs), the moisture content near the surface of the profile ($z = 1250$ mm) decreases from 24% to 20% during the first 100 hrs of evaporation, followed by a more gradual decrease to 16% over 3 months. HDU A1 indicates that the suction at this depth also increased to 49 kPa during this stage. Slight decreases in moisture content were also noted at the depths of the other TDR waveguides during this stage. However, these decreases were most likely due to gravity drainage, not evaporation. Measurements of moisture content obtained by gravimetric sampling indicate that the drying front progressed only 700 mm into the cover (*i.e.*, $z = 650$ mm) during the 3 month-long Stage A1(e). The field data in Figure 2(b) showed a uniform decrease in moisture content throughout the depth of the cover during 7 months. Differences in the rates and depths of drying in the field and laboratory are due to differences in the energy supplied to the soil to cause evaporation, as well as due to the added contributions of transpiration and lateral drainage to moisture removal in the field.

Profile B

Inflow and outflow during the different stages for Profile B are shown in Figure 8(a). Three infiltration stages were conducted to evaluate the formation of a capillary break during infiltration. The intermediate evaporation stages were used to dry the soil profile. The infiltration stages were stopped when steady-state flow was observed, while the evaporation stages were stopped when the moisture content in the top of the profile reached the initial value.

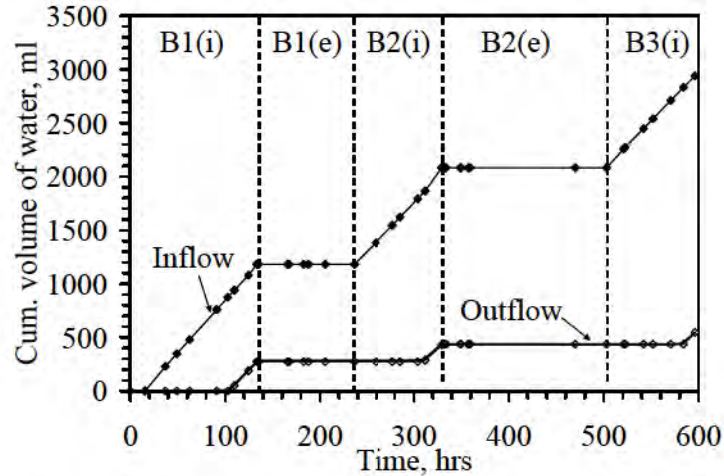


Figure 8: Cumulative inflow and outflow in Profile B

The changes in temperature and relative humidity at the surface are shown in Figure 9(a), and changes in temperature at the depths of the capacitance sensors are shown in Figure 9(b). The infrared lamp led to an increase in surface temperature from 23 to 44 °C and a decrease in surface relative humidity from 96 to 13%. This corresponds to a steady-state suction boundary condition at the surface of 3×10^5 kPa. The temperature in the soil increased significantly during early stages of evaporation, but reached a steady-state profile after 40 hrs of evaporation.

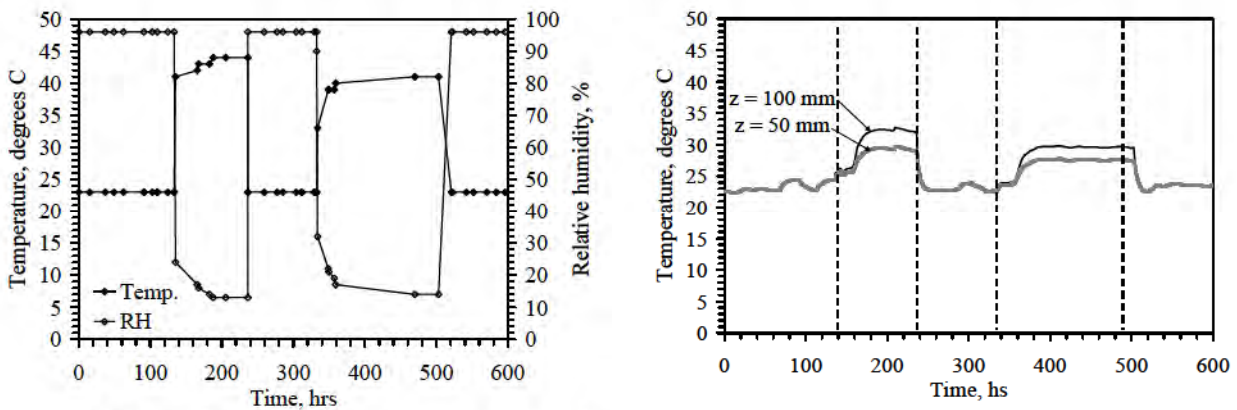


Figure 9: (a) Surface temperature and relative humidity; (b) Internal temperature

The bottom boundary in Profile B (i.e., the geosynthetic drainage layer) has a significant effect on the suction and moisture content profiles in the soil due to its short length. Accordingly, this profile is useful to investigate the impact of the interface on the soil. The suction time series for Profile B are shown in Figure 10(a). The tensiometers are able to measure suction values less than 20 kPa, so they were more useful than the HDUs in interpreting the suction at capillary breakthrough. However, the tensiometer at a height of 100 mm was affected by vibrations from the fan, so it does not yield reliable results at low suctions. The tensiometer at a height of 50 mm was assumed to be representative of the suction at the interface. During Stage B1(i), the tensiometers were equilibrating with the initial suction in the soil when the infiltration front passed their locations. Although they had not fully equilibrated with the initial suction after about 25-45 hours, the tensiometers showed a smooth decrease in suction that is consistent with trends in moisture content measured using the capacitance sensors. The initiation of outflow (i.e., capillary breakthrough) for each infiltration stage is denoted in Figure 10(a) with arrows. Breakthrough occurred in Stage B1(i) after 104 hrs, at a suction of 3.64 kPa. After breakthrough, the tensiometers showed further decreases in suction. After reaching steady state outflow, evaporation was started. Suction increased asymptotically with time during Stage B1(e), and Tensiometer B-1 approached the suction value measured before the first infiltration front passed through the profile. After this point, infiltration was started again. Despite different durations of the evaporation stages evaluated for this profile (and corresponding differences in moisture removal), breakthrough occurred at approximately the same suction.

The moisture content time series for Profile B are shown in Figure 10(b). In general, the trends in moisture content measured using the capacitance sensors are consistent with the trends in suction measured using the tensiometers. The moisture content of the wetting front is indicated by the first bend in the moisture content time series after infiltration starts (point A). The moisture content at the wetting front is approximately 24% for each infiltration stage. Unlike the moisture content time series for Profile A, the upper portion of the profile did not remain at the moisture content of the wetting front due to the shorter height of this column. Instead, the moisture content of the entire profile increased. This is because ponding of water above the geosynthetic drainage layer affected the entire height of the profile. Capillary breakthrough occurred at a moisture content of 40%, slightly after the second bend in the moisture content time series (point B). A significant decrease in moisture content from 43% to 25% occurred during the first 20 hrs of drying in Stage B1(e). A less significant decrease in moisture content from 25% to 21% was observed over the next 80 hrs of drying. The imposed suction boundary condition caused a gradient in moisture content (and suction) with height in the specimen. Based on the value of moisture content at $z = 50$ mm after 240 hrs of testing, it is likely that the moisture content at the soil-geosynthetic interface did not return to its original value. However, after subsequent wetting in Stages B2(i) and B3(i), the moisture content at breakthrough was similar to that observed during Stage B1(i).

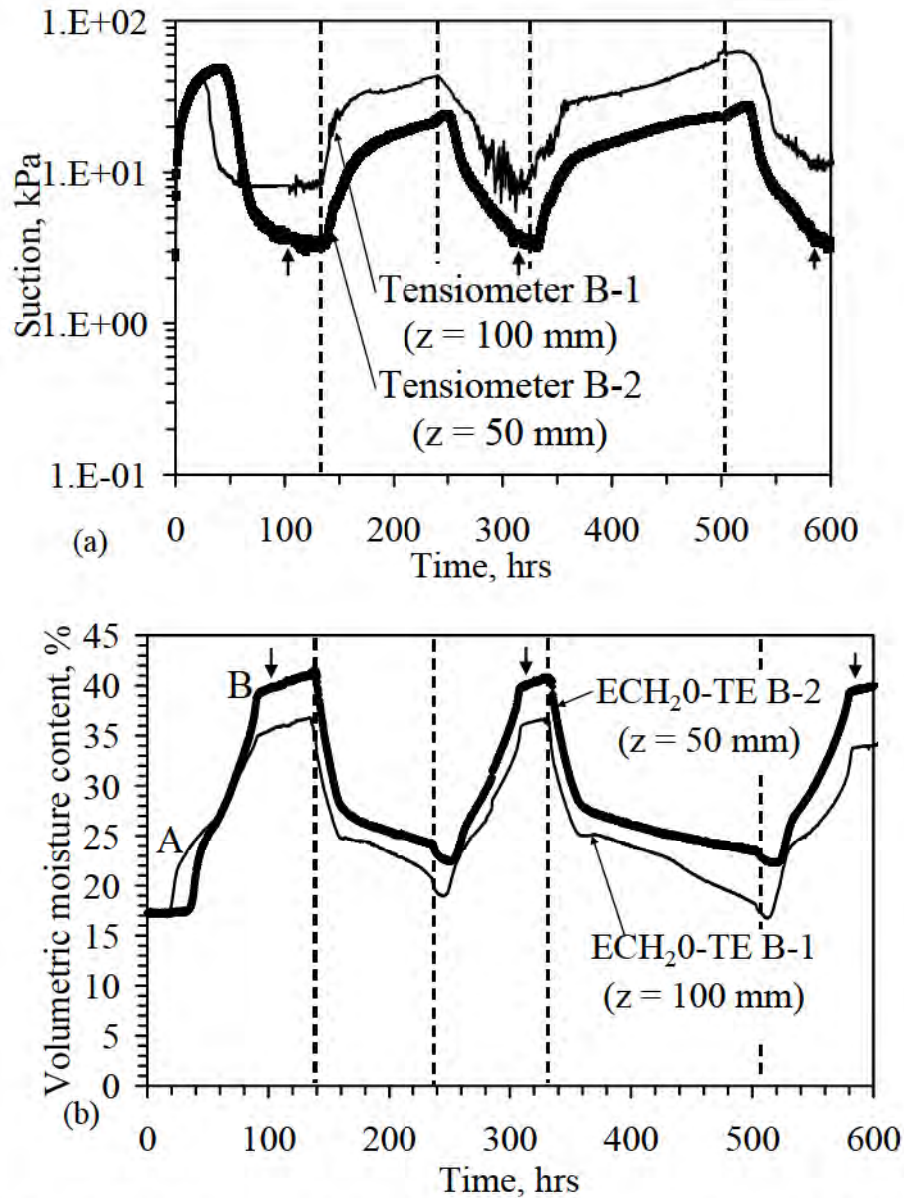


Figure 10: Profile B: (a) Suction; (b) Moisture content (Arrows denote breakthrough)

After the evaporation boundary condition was removed (i.e., at $t = 240$ hrs), the capacitance sensors tended to show a decrease in moisture content. This was attributed to temperature effects. These temperature effects altered both the suction and moisture content measurements, and tended to be more relevant during the evaporation stages (under a surface temperature of 40°C). A third evaporation stage was conducted for Profile B (outside the scope of this study) to help shed light into the temperature dependence of the sensors. During this extra stage, the temperature was cycled with time by shutting the infrared lamp on and off, as shown in Figure 11(a). The corresponding changes in suction and moisture content are shown in Figure 11(b). At high temperatures, the suction is 8% greater than at room temperature, and moisture content is 5% smaller than at room temperature. Nonetheless, as the main interest of this study is the behavior of the soil near the interface during infiltration (i.e., capillary breakthrough), the

measurements of the sensors during evaporation are deemed acceptable. During infiltration, the system is at room temperature, so the error in the suction and moisture content is the same as the error obtained during the calibration program, approximately 0.1%.

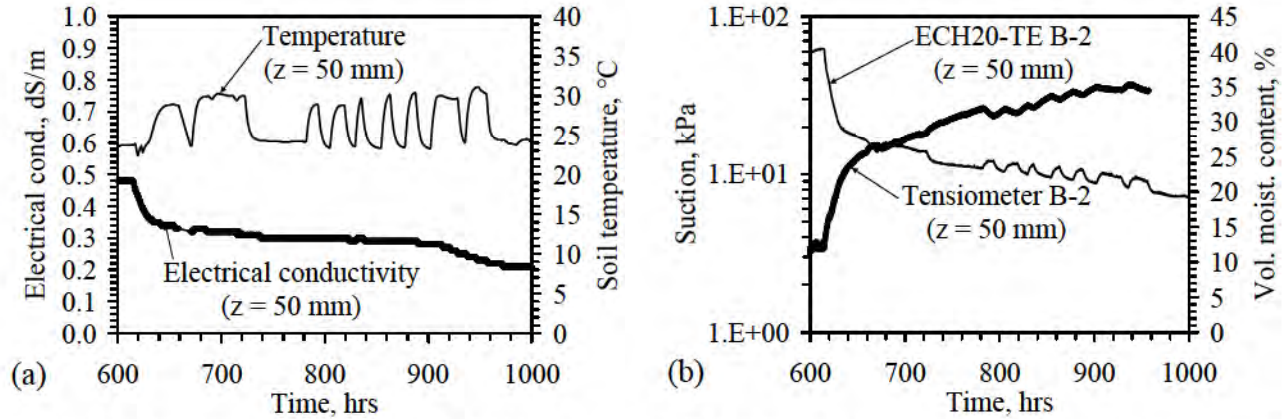


Figure 11: Temperature effects: (a) Temperature and EC; (b) Moisture content and suction changes

DISCUSSION

The results obtained during the infiltration and evaporation stages for Profiles A and B are summarized in Table 3. The results from the two profiles can be compared in spite of their differences in density and length. The moisture content and suction at the infiltration front are similar (24% and 20 to 30 kPa, respectively) as the inflow rates applied to the profiles are similar. Also, breakthrough occurred at a similar degree of saturation (94%) for both profiles. The breakthrough suction for each wet/dry cycle in Profile B is approximately 3.7 kPa. These values are consistent with the transition of the geotextile WCR from residual conditions to saturated conditions [Figure 3(a)]. This signifies that the WCRs can be used to estimate the breakthrough suction for unsaturated soil-geosynthetic system. The speed of the wetting fronts tended to increase with time because the profiles had not returned to their original moisture content after the end of each evaporation stage. Similar conclusions can be made about the time required to reach steady-state infiltration. The speed of the evaporation front in Profile B was calculated from the difference between times at which the capacitance sensors responded to the evaporation boundary condition. The calculated speeds were similar for both evaporation stages in Profile B. The evaporation fronts in Profile A only passed 500 to 700 mm into the profile, so a speed was not calculated. A capillary break effect was not obvious during Stage A2 in Profile A.

Table 3: Summary of column test results

Column name	Wet-dry cycle	Depth of evaporation front (mm)	Speed of wetting front (m/s)	Suction at wetting front (kPa)	Moisture content at wetting front (%)	Time until steady state infiltration (hrs)	Breakthrough suction (kPa)	Breakthrough moisture content (%)	Speed of evaporation front (m/s)
A	A1	700	2.7E-07	30.1	24.7	1874	?	46.2	?
	A2	500	1.0E-06	29.6	24.4	453	?	45.6	?
B	B1	125	9.6E-07	21.1	24.3	105	3.64	40.2	3.5E-06
	B2	125	1.5E-06	25.0	24.1	75	3.74	40.5	3.1E-06
	B3	125	1.8E-06	25.8	24.2	83	3.64	39.6	N/A

The transient WRCs for Profile B, shown in Figures 12(a) and 12(b), were obtained from the capacitance sensor and tensiometer data. The left-most point on the WRCs at $z = 50$ mm are similar for both cycles, corresponding to breakthrough. The wetting and drying paths follow the shape of the drying-path WRC obtained for the clay with a relative compaction of 80% [see Figure 3(a)]. This has practical significance, because it is common to obtain only the drying WRC in practice. Accordingly, this indicates that the breakthrough suction for a soil-geosynthetic drainage layer interface may be estimated using only the drying-path WRCs. The drying path WRC is the most commonly obtained information for unsaturated soils. Hysteresis is not significant (except at $z = 100$ mm in Cycle 1, likely due to errors in the tensiometer near saturation), and less hysteresis is observed in Cycle 2 than in Cycle 1.

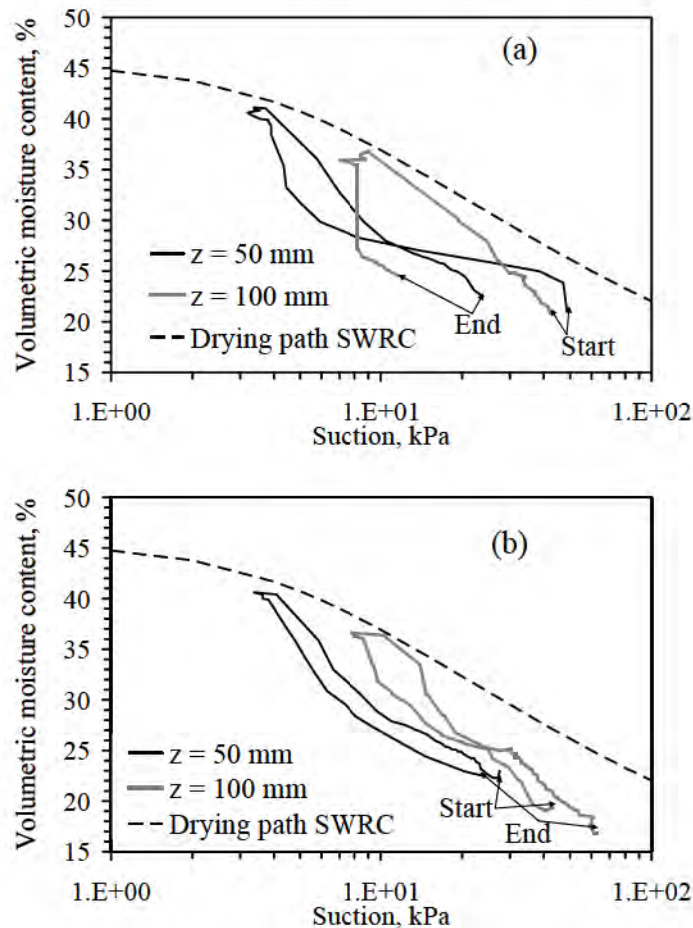


Figure 12: Transient WRCs for Profile B: (a) Cycle 1; (b) Cycle 2

CONCLUSIONS

The results of this study indicate that the capillary break effect is the cause of moisture accumulation above the interface between an unsaturated soil and a geosynthetic drainage layer observed in the field. Further, during infiltration after repeated wet-dry cycles, capillary breakthrough occurred at the same suction and moisture content. This finding implies that landfill cover systems using geosynthetic drainage layers, like the test cover described herein, can rely on the capillary break effect to provide additional moisture storage during significant storms. However, this also implies that drainage systems for retaining walls or roadways may need to approach saturation before functioning as drains. This may have implications on stability and deformations. Comparison of the results from Profiles A and B indicate that the repeated effectiveness of a capillary break relies on removal of water from the soil-geosynthetic interface. Landfill covers with a capillary break should be designed to either promote lateral drainage from the base of the cover, or to facilitate evapotranspiration through the use of plants.

ACKNOWLEDGEMENTS

Funding was provided by the NSF under Grant CMS-0401488. This support is gratefully appreciated.

REFERENCES

- Bouazza, A., Nahlawi, H., Kodikara, J., and Delage, P. (2006). "Water retention curves of a non woven polyester geotextile." *UNSAT'06*. ASCE Geotech. Sp. Pub. 147(2):1651-1658.
- Flint, A.L., Campbell, G.S., Ellet, K.M., and Calissendorff, C. (2002). "Calibration and temperature correction of heat dissipation matric potential sensors." *SSSA*. 66:1439-1445.
- GSE, Inc. (2004). "GSE Fabrinet Geocomposite – Product Data Sheet." Houston, TX.
- Henry, K.S. and Holtz, R.D. (2001). "Geocomposite capillary barriers to reduce frost heave in soils." *Can. Geotech. J.* 38:678-694.
- Iryo, T. and Rowe, R.K. (2005) "Infiltration into an embankment reinforced by nonwoven geotextiles" *Can. Geotech. J.* 42(4):1145-1159.
- Lu, N. and Likos, W. (2004). *Unsaturated Soil Mechanics*. John Wiley and Sons. New York.
- Knight, M.A. and Kotha, S.M. (2001). "Measurement of Geotextile-Water Characteristic Curves Using a Controlled Outflow Capillary Pressure Cell." *Geosyn. Int.*, 8(3):271-282.
- Koerner, R.M. (2005). *Designing With Geosynthetics*. 5th Edition. Prentice Hall, NJ.
- McCartney, J.S., Kuhn, J.A., and Zornberg J.G. (2005). "Geosynthetic drainage layers in contact with unsaturated soils." *16th ISSMGE*. 12-16 Sept. Osaka, Japan.
- McCartney, J.S., and Zornberg, J.G. (2006). "Correction of Lightning Effects on Water Content Reflectometer (WCR) Soil Moisture Data." *Vadose Zone J.* 5:673–683.
- Zornberg, J.G. and McCartney, J.S. (2006). "Chapter 34: Evapotranspirative Cover Systems for Waste Containment." *Handbook of Groundwater Eng, Vol. 2*. CRC Press. Boca Raton.
- Ridley, A.M. and Burland, J.B. (1995). "A pore pressure probe for the in-situ measurement of soil suction". *Proc. Of Conf. on Advances in Site Investigation Practice*. I.C.E., London.
- Stormont, J.C., Henry, K.S. and Evans, T.M. (1997). "Water retention functions of four nonwoven polypropylene geotextiles." *Geosyn. Int.* 4(6):661-672.
- Stormont, J.C. and Morris, C.E. (2000). "Characterization of unsaturated nonwoven geotextiles." *Advances in Unsaturated Geotechnics*. ASCE Geotech. Sp. Pub. 99:153-164.
- Stormont, J. C., Ray, C., and Evans, T. M., (2001). "Transmissivity of a Nonwoven Polypropylene Geotextile Under Suction," *Geotech. Test. J.* 24(2):164–171.
- van Genuchten, M. (1980). "A closed-form equation for predicting the hydraulic conductivity of unsaturated soils." *SSSA*. 44:892-898.

CONTACT:

John McCartney

The University of Texas at Austin

Department of Civil, Architectural, and Environmental Engineering

1 University Station

Austin, TX 78712-0280

Phone: 512-232-3595

Email: jmccartney@mail.utexas.edu.

Disclaimer: The opinions expressed and the data provided during Geosynthetics 2007 and the published Proceedings are those of the author(s) and/or presenter(s) and do not necessarily represent the opinions of the Industrial Fabrics Association International (IFAI) or any of its subsidiaries or divisions. Papers contained in these proceedings are the unedited, original work of each author. For permission to reprint any paper or presentation material in these proceedings, please contact the authors directly or the IFAI Bookstore Manager, 1801 County Road B West, Roseville, MN 55113-4061 USA.